The Shear Strength of Granular Soils under the Influence of Vibration

by

Karen Taslagyan

A thesis submitted in partial fulfillment of the requirements for the degree of

Doctor of Philosophy

in

Geotechnical Engineering

Department of Civil and Environmental Engineering

University of Alberta

Abstract

For some geotechnical design projects where soils are exposed to vibration, it becomes necessary to evaluate the strength and deformation characteristics of the soil under existing and/or anticipated vibrations. If large displacements are anticipated, the design of an earth structure, such as an earth or tailing dam, has to take into account the residual shear strength characteristics of the soils that underlie or/and constitute the structure. In this case, if the soil is subjected to vibration, depending on the magnitude of the vibrations, it may undergo some loss of strength, thus resulting in excessive deformation and compromising the stability of the structure. Therefore, it is of paramount importance to predict and consider the effects of vibrations on the residual strength of soils; that is, the effect of vibration on the critical state, a unique state independent of the initial density (void ratio) of the soil that can be reached upon sufficiently large shear deformations.

This thesis presents a summary of an experimental program performed to investigate the influence of vibration on the strength and deformation characteristics of dry granular media with no cementation bonds. A new vibrating direct shear apparatus is designed and built to evaluate the mentioned characteristics under a wide range of vibrational accelerations. The apparatus is used throughout the research project to investigate the behavior of dry granular materials at their residual strength states under the influence of vibration with different intensities. The impact of vibration on the overburden (normal) stress and the peak strength of granular materials is evaluated. Experiments have also been conducted to study the post-vibration behavior of granular materials, as well as the particle shape effect on the strength loss and deformations of the granular media during vibration. Finally, the behavior of the shear zone in the granular

materials before, during and after the application of vibration at the pre-peak and residual strength states is investigated.

About 200 samples of different granular materials have been tested by using the new vibrating direct shear apparatus with different testing modes, procedures, normal stresses and vibration intensities. A number of plots are presented that show the behavior of the granular materials under the impact of vibration in different testing conditions. The Mohr-Coulomb equation for granular materials has been modified to account for the effect of vibrational fluidization. A new pattern of the shear zone in granular media is provided, which outlines the deformation and shear resistance before, during and after the application of vibration.

Acknowledgements

First of all, I would like to thank my supervisor, Professor Dave H. Chan, for his invaluable support and guidance throughout the whole course of this research. Professor Chan has always found the time to kindly share his knowledge and inspire new ideas. I also want to extend my gratitude to my co-supervisor, Professor Norbert R. Morgenstern, for his important comments and suggestions on the research project. The discussions with Professor Morgenstern have always been encouraging and stimulating.

Many thanks to Christine Hereygers, Steve Gamble and Chris Krath for their assistance in building the laboratory apparatus used in this research.

The financial support for this project was provided by the Natural Science and Engineering Council of Canada (NSERC Postgraduate Scholarship) and the Alberta Innovates Technology Futures (Graduate Student Scholarship).

Special thanks to my family and friends for their endless help and motivation.

Table of Contents

List of Figures

List of Tables

1. Chapter 1: Introduction

1.1 Statement of Problem

Granular soils are frequently exposed to vibrations due to earthquakes, blasting, construction operations, machinery and vehicle traffic. The strength behavior of a soil during vibration not only depends on the vibration characteristics, such as acceleration, frequency and amplitude, but also on the physical properties of the soil, such as moisture content, grain size distribution, particle shape, dry density or void ratio, cohesion and internal friction angle, as well as the density and mineralogy of the soil particles.

There are two important aspects that contribute to the unique properties of granular materials: ordinary temperature plays no role on their mechanical behaviour, and the interactions between grains are dissipative because of static friction and the inelasticity of collisions (Jaeger et al., 1996). Granular material can behave like solids, fluids and even gas under different conditions. When sufficient energy is supplied to a granular material in a vibrating system, the granular material can exhibit fluid-like behavior. This transition from a solid state to a liquid state (fluidization) takes place when vibrational acceleration, a, exceeds a certain critical value. When granular materials are subjected to strong enough vibration intensities, various phenomena, such as compaction, mixing, localized excitations, convective flow, size segregation and surface wave formation, can be observed. Although the above mentioned processes have been well investigated, it should be mentioned that there are very few, if any, studies done on the effect of normal stress on the vibrational fluidization of granular materials.

If large displacements are anticipated, the design of an earth structure, such as an earth or tailing dam, has to take into account the residual shear strength characteristics of the soils that underlie or/and constitute the structure. In this case, if the soil is subjected to vibration, depending on the magnitude of the vibrations, it may undergo some loss of strength, thus resulting in excessive deformation and compromising the stability of the structure. Therefore, it is of paramount importance to predict and consider the effects of vibrations on the residual strength of soils.

Despite the knowledge gained on this issue in the last few decades, there is still a lack of understanding on the mechanism of particle interactions and shear deformation due to vibration. Therefore, there is a need to study the shear strength and deformation behavior of soils due to vibration. In particular, it is specifically interesting to determine the effect of vibration on the residual shear strength of soils, that is, the effect of vibration on the critical state, which is a unique state independent of the initial density (void ratio) of soil that can be reached upon sufficiently large shear deformations.

The strength of a granular material is determined by the strength characteristics of the material at the shear zone/band defined by a certain combination of boundary conditions and the mechanical properties of the material. Therefore, to better understand the mechanism of the strength loss of granular materials, it is important to investigate the stress and deformation characteristics of the shear zone during its initiation and propagation through the granular media. The thickness of the shear zone is usually 8 to 10 times the mean grain diameter (Roscoe, 1970; Muhlhaus and Vardoulakis, 1987; Bardet and Proubet, 1992).

Direct shear testing (used in this research project) has successfully been used to evaluate the shear strength characteristics of soils for many decades. Despite some of the disadvantages of

the testing, such as lack of control of pore pressure, failure at predefined planes and non-uniform stress conditions in the tested samples, it is one of the most common shear strength evaluation tests used in geotechnical laboratories. The popularity of direct shear testing arises from the simplicity of the setup and ease of testing procedures.

1.2 Research Objectives

The main objectives of the research project are as follows.

1. Design and build a laboratory apparatus and develop a testing methodology that can be used to investigate the effect of vibration on the shear strength characteristics of granular materials at different strength states, normal (confining) stresses and vibrational accelerations.
2. Investigate the behavior of granular materials at their residual strength states under the influence of vibration with different intensities.
3. Investigate the impact of vibration on the normal (overburden) stress and determine the amount of strength loss of the granular materials due to the normal stress changes when subjected to vibrations of different acceleration values.
4. Evaluate the post-vibration behavior of granular materials.
5. Investigate the impact of vibration on the peak strength of dense granular materials by subjecting them to vibration at pre-peak states.
6. Determine the particle size and shape effect on the behavior of the granular materials subjected to vibration.
7. Investigate the behavior of the shear zone in the granular materials before, during and after the application of vibration at the pre-peak and residual strength states.

8. Use the experimental results to develop a comprehensive framework of the behavior of granular materials during and after vibration.

The developed framework will relate all of the mentioned experimental results and reveal the mechanism of the strength behavior of granular soils during and after vibration. The framework will be used to develop a constitutive model for granular materials subjected to vibration. This will make it possible to more accurately predict the strength loss, as well as compression and shear deformations of granular soils for the anticipated or existing vibrations.

The framework will allow for a more realistic and reliable design of structures on/in granular soils subjected to vibration. Of special interest will be the contribution of the research data to improve design and stability analyses of tailing dams in seismically active areas. It is also anticipated that the research project will assist towards a better understanding of the extreme mobility of big rock avalanches.

1.3 Scope of the Thesis

The following steps have been carried out to achieve the research project objectives.

- A new vibrating direct shear apparatus is built. The apparatus has been designed and built to investigate the effect of vibration on soils at different strength states, especially at the critical state, as well as to evaluate the impact of vibration on the deformation properties of soil under different normal, shear and vibrational loading conditions. The new apparatus represents a modification of the conventional WYKEHAM FARRANCE direct shear apparatus, such that

soil samples can be tested in both strain and stress controlled modes under different vibrational frequencies, amplitudes and accelerations.

- Experiments have been carried out on granular materials at relatively low vibrational accelerations. The materials are tested in the strain-controlled mode at different vibration intensities and normal stresses to investigate the effect of vibration on the residual strength and deformation characteristics of the tested materials. The particle shape effect on the strength loss during vibration is evaluated, as well as the impact of vibration on the normal (overburden) stress that acts on the samples.
- Experiments are implemented on granular materials at relatively high vibrational accelerations. To investigate the mechanism of the vibrational fluidization of dry granular media, three different types of granular materials are tested by using the vibrating direct shear apparatus at greater vibrational accelerations. The effects of normal stress and vibrational acceleration on the shear strength characteristics and the fluidization of granular media are evaluated.
- Experiments that focus on the behavior of the shear zone in granular materials subjected to vibrations are carried out. The behavior of the shear zone before, during and after the application of vibration is investigated at the pre-peak and residual strength states of two different granular materials. The effects of the particle shape, normal (confining) stress and vibrational acceleration on the shear zone are also studied.

1.4 Organization of the Thesis

This thesis has been prepared in a paper-based format. A brief outline of the main chapters are provided below.

Chapter 3 is a description of the setup and testing procedures of the new vibrating direct shear apparatus that is designed and built to evaluate the strength and deformation characteristics of soils under a wide range of vibrational accelerations. The results of two sets of sand samples tested in stress and strain controlled modes are provided, which prove the workability and reliability of the new apparatus.

Chapter 4 is a summary of the test results of eighty samples from four different granular materials which are tested with the new vibrating direct shear apparatus at four normal stresses and different vibrational accelerations. Strength loss vs. vibration acceleration plots at different normal stresses, as well as the peak, residual and vibro-residual shear strengths obtained for the four granular materials at different intensities of vibration, are provided. The results show the effect of vibration on the critical state of the dry granular media; particularly, a reduction in the residual friction angles of the tested materials with an increase in the intensity of vibration. The effect of particle shape on the strength loss due to vibration and the effect of vibration on the normal stress are also discussed.

Chapter 5 is a summary on the experiments conducted to investigate the vibrational fluidization of granular media. The test results of sixty samples from three different granular materials which are tested by using the modified direct shear apparatus at six normal stresses and a wide range of vibration accelerations are provided. The peak, residual and vibro-residual shear strength envelops obtained for the tested materials at different vibration intensities are presented.

It is shown that an increase in vibration intensity reduces the friction angle of the granular materials, and increases the value of the normal stress, the *vibro-fluidizational limit*, below which, the granular material is fluidized. The particle shape effect on strength loss due to vibration is demonstrated, as well as a reduction in friction angle and increase in vibro-fluidizational limit with an increase in vibration acceleration.

An outline of the results of the laboratory experiments conducted with glass beads and sand by using the modified vibrating direct shear apparatus and different testing procedures is provided in Chapter 6. The behavior of the shear zone in the granular materials before, during and after the application of vibration at the pre-peak and residual strength states is discussed. Three zones are identified in a sheared granular material: *A* – zone unaffected by the shear of the granular media, *B* – the shear zone portion that has been developed due to the shear of the material, but does not contribute to the critical state of a thinner shear zone, *C,* at which the actual shear takes place. Also, the shear strength and deformation characteristics of the granular materials affected by vibration at their pre-peak and residual strength states are presented and discussed.

1.5 References

Bardet, J. P., and Proubet, J. (1992). "Shear-Band Analysis in Idealized Granular Material". J. Eng. Mech., 118, pp. 397-415.

Jaeger, H. M., Nagel, S. R. and Behringer, R. P. (1996). Granular solids, liquids, and gases. Rev. Mod. Phys. 68, 1259

Muhlhaus, H. B., and Vardoulakis, I. (1987). "The thickness of shear bands in granular materials." Geotechnique, 37, pp. 271-283.

Roscoe, K. H. (1970). "Tenth Rankine lecture: The influence of strains in soil mechanics", Geotechnique, 20, pp. 129-170.

2. Chapter 2: Literature Review

Granular soils are often exposed to vibrations that are natural and human-made in origin. Examples of vibration types include earthquakes, blasting, machinery, vehicle traffic and wind. Depending on their intensity, vibrations may result in partial or complete strength loss, which would lead to significant deformation of soils.

There are two important aspects that contribute to the unique properties of granular materials: ordinary temperature plays no role on their mechanical behaviour, and the interactions between grains are dissipative because of static friction and the inelasticity of collisions (Jaeger et al., 1996). Granular material can behave like solids, fluids and even gas under different conditions. When sufficient energy is supplied to a granular material in a vibrating system, the granular material can exhibit fluid-like behavior. This transition from a solid state to a liquid state (fluidization) takes place when vibrational acceleration, a, exceeds a certain critical value. For example, when vibration is applied in the vertical direction, fluidization takes place at an a that is greater than 1 g (Huan, 2008). Further increases in the vibration acceleration changes the behavior of the granular material to that of a gas. Jaeger et al. (1996) described the three aforementioned states of granular materials.

When granular materials are subjected to strong enough vibration intensities, various phenomena, such as compaction (e.g. Barkan (1962), Ayer and Soppet (1965/1966)), swelling (e.g. Poschel and Rosenkranz (1998)), mixing (e.g. Alexeev et al. (2000)), localized excitations (e.g. Umbanhowar et al. (1996), Tsimring and Aranson (1997)), convective flow (e.g. Laroche et al. (1989), Evesque and Rajchenbach (1989), Gallas et al. (1992), Pak et al. (1995) and Huan (2008)), Bourzutschky and Miller (1995), Wassgren (1997) and Liffman et al. (1997)), size

segregation (e.g. Knight et al. (1993), Cooke et al. (1996) and Alexeev et al. (2000)) and surface wave formation (e.g. Pak and Behringer (1993), Melo et al., (1993 and 1995), Clement et al. (1996), Brone and Muzzio (1997), and Mujica and Melo (1998)) can be observed. Although the above mentioned processes have been well investigated, there are very few, if any, studies done on the effect of normal stress on the vibrational fluidization of granular materials.

Richards et al. (1990) proposed the concept of "dynamic fluidization" which takes into consideration the effect of earthquake accelerations on dry granular soils. The imposed accelerations at some critical level change the state of the soil, which causes general plastification, such that the soil becomes, in a sense, an anisotropic fluid. They assumed that the main trigger of the fluidization is the inertial forces that act between the particles of a granular soil. They showed that fluidization mainly depends on horizontal and not vertical accelerations. Another distinguishing feature of fluidization is that when it occurs, flow takes place, if at all, in finite increments rather than continuously, with increments that correspond to the acceleration pulses of an earthquake above a critical value (Richards et al., 1990).

Other researchers who investigated the vibro-fluidization of granular materials are Savage (1988), Fauve et al. (1989), Doudy et al. (1989), Zik et al. (1992), Lan et al. (1995), Warr et al. (1995), Goldstein et al. (1995), Luding (1995), Ristow et al. (1997), Tennakoon et al. (1998), Falcon et al. (1999), Sunthar et al. (2001), Moon et al. (2004) and Gotzendorfer et al. (2006).

There has been significant progress in understanding the effects of vibration on the strength and deformation properties of soils since the first half of the last century (Housner, 1954, 1959; Barkan, 1962; Richart, 1970; Seed and Idriss, 1982, 1983; Idriss and Boulanger, 2008). A number of different experiments with vibration application have been conducted on cohesive and cohesionless soils that generated valuable data which have led to some important conclusions

(Savchenko, 1958; Pyke et al., 1975; Robertson and Campanella, 1985, 1986; Wartman et al., 2005; Meehan et al., 2008). All of these findings significantly help to improve the design of different structures subjected to dynamic loads (Barkan, 1962; Seed, 1966; Richart, 1970; Seed and Idriss, 1982; Das, 2011; Sangroya and Choudhury, 2013).

Pokrovsky et al. (1934) were the first to experimentally investigate the influence of vibrations on the internal friction of sand and showed that the coefficient of internal friction decreases with an increase in the kinetic energy of vibration. These results were later supported by experiments performed by Barkan (1962). Nowadays, there are different types of laboratory apparatuses to measure the strength properties of soils under vibrational loads. Depending on the design and technical characteristics, each of the tests has its advantages and limitations in simulating field conditions. The following are some examples of the above mentioned techniques and the investigations performed by using these techniques.

Levshinsky designed a stress-controlled vibrating shear apparatus that generates cyclic shear loads (horizontal vibration) on soil samples. It was later used by Preobrazhenskaya and Savchenko in 1958 to determine the shearing strength of soils with vibration (from Meschyan, 1992). Youd (1970) investigated shear strength reduction and density changes of granular materials under vibration by mounting a direct shear apparatus onto a shaker table. Some examples of work done with the use of shaking table tests are that by Arango and Seed (1974), Wartman et al. (2005), and Toyota et al. (2004), who used the technique to investigate vibration induced deformations in slopes. Meschyan and Badalyan modified a stress-controlling torsional shear apparatus into a stress-controlling vibrating torsional shear apparatus that allows the testing of thin cylindrical samples under vibrational torsional shear loads generated by a vibrator (Meschyan, 1978). Melosh et al. (1995) built a rotational viscometer to quantitatively investigate

the relationship between stress and strain rate in a bucket of strongly vibrated dry, fine sand. A similar setup, with the use of a penetrating cone instead of a sanding drum (Melosh et al., 1995), was used to evaluate the strength of soils under vibration (Kutergin, 1989). Shibata et al. (1970), who conducted experiments on sand, used a vibrating triaxial apparatus.

Of special interest is the effect of vibration on the critical state (residual shear strength) of granular soils, a unique state independent of the initial density (void ratio) of soil that can be reached upon sufficiently large shear deformations. There is very little research done in this regard, an example of which is the work done by Youd (1968), who experimentally investigated the effect of vibration on the critical state of granular media and found that both the shear strength and void ratio are reduced by vibration.

The strength of a granular material is determined by the strength characteristics of the material at the shear zone/band defined by a certain combination of boundary conditions and the mechanical properties of the material. Therefore, to better understand the mechanism of the strength loss of granular materials, it is important to investigate the stress and deformation characteristics of the shear zone during its initiation and propagation through the granular media. The thickness of the shear zone is usually 8 to 10 times the mean grain diameter (Roscoe, 1970; Muhlhaus and Vardoulakis, 1987; Bardet and Proubet, 1992).

Some examples of the numerous studies carried out on the shear zone in granular media are provided below.

Bardet and Proubet (1992) investigated the emergence, inclination, and thickness of shear bands in idealized granular materials and showed that they are similar to those of real materials. Aidanpaa et al. (1996) used a torsional shear cell to study the shear layers of uniform spheres, and observed that the shear zone thickens and dilates with an increase in the shear speed,

accompanied by a transition from a single layer to many layers of shearing. Bora (1984) experimentally investigated the shear failure mechanism in granular materials, and found that the friction angle is dependent on effective confining contact stress within a dilative range regardless of the drainage conditions and amount of particle crushing. Frost et al. (2002) studied the shear failure behavior of granular–continuum interfaces on a selection of sand–continuum material interfaces and through the use of discrete element modeling. Borja (2003) used a geological and mathematical framework to classify deformation patterns in granular media. Frost et al. (2004) evaluated the interface behaviour of granular soils by carrying out physical and numerical experiments. Rechenmacher (2005) evaluated local displacements and strains that are associated with shear band growth and evolution in sands by testing the plane strain with the use of digital image correlation (DIC). The magnitude of the shear and rotational strains was found to vary along the length of the shear bands, which lends support to the idea of fluctuating buildup and collapse of the "force chains". Alshibli and Alramahi (2006) investigated the evolution of local strains during the shearing of particles of a granular material, and showed that when compared to particle sliding, rotation is imperative in the shearing resistance of granular materials. Abriak and Caron (2006) conducted an experimental study of shear in granular media, and showed that granular media behavior depends on the local friction (grain–grain friction). Sadrekarimi (2008) studied the shearing behavior of loose and dense sands by implementing constant volume ring shear tests. Widulinski et al. (2010) performed comparative modeling of shear localization in granular bodies with the finite and discrete element methods (FEM and DEM). Liu (2010) conducted laboratory experiments and numerical simulations to investigate the failure characteristics and micro-mechanical behaviors of granular soil slopes. Cox and Budhu (2010) studied the grain shape of granular materials, and through the use of light microscopy,

determined that there are several grain shape parameters. They then related these parameters to the dilatancy of the granular materials. Mesarovic et al. (2013) analyzed the changes in the topology of a granular assembly during deformation by using the graph theory and showed that the elementary mechanism of diffuse deformation consists of intermittent flips, an increasing number of which directly stems from dilatancy, as well as that shear band formation is associated with the massive rolling of particles.

Direct shear testing has successfully been used to evaluate the shear strength characteristics of soils for many decades. Despite some of the disadvantages of the testing, such as lack of control of pore pressure, failure at predefined planes and non-uniform stress conditions in the tested samples, it is one of the most common shear strength evaluation tests used in geotechnical laboratories these days. The popularity of direct shear testing arises from the simplicity of the setup and ease of testing procedures.

Many researchers have studied the applicability and limitations of direct shear testing through experimental investigations and numerical modelling. One of the more early studies on direct shear testing through the use of finite element analysis was performed by Potts et al. (1987). They demonstrated that, despite the strongly non-uniform stresses and strains in the shear box before failure, strains and stresses in the final failure zone are surprisingly uniform. Liu et al. (2005) investigated the interface friction through direct shear tests. Two improvements were made to reduce the friction of the sample material at the inner surface of the upper shear box, which caused the real shear strength to increase for a dense sample and decrease for a loose sample. Bagherzadeh-Khalkhali and Mirghasemi (2009) performed numerical modeling and experiments by using direct shear testing to study its suitability and limitations for testing coarse-grained soils. Li and Aydin (2010) investigated the fluctuations in vertical displacement and

shear stress with different sized glass beads during direct shearing. Nam et al. (2011) used multistage direct shear tests to determine the shear strength of unsaturated soils, which allowed the matric suction to be independently controlled, and compared the results with samples which underwent conventional direct shear testing. Härtl and Ooi (2011) investigated, through direct shear tests, how particle shape and interparticle friction would influence bulk friction by using DEM. They showed that packing density has less influence than particle interlocking on the bulk friction. Kang et al. (2012) performed 3D discrete element simulations in conjunction with image processing of the pore geometry to determine the pore size distribution and orientation in dilative and contractive assemblies in direct shear testing.

Despite the knowledge obtained on this topic in the last few decades, there is still a lack of understanding on the mechanism of particle interactions and shear deformation due to vibration. Therefore, granular media strength and deformation behavior under the impact of vibration warrants further research work.

3. Chapter 3: A Direct Shear Apparatus with Vibrational Loading

3.1 Abstract

For some geotechnical design projects where soils are exposed to dynamic loads (vibration), it becomes necessary to evaluate the strength and deformation characteristics of the soil under existing and/or anticipated vibrations. In order to investigate the effect of the vibrations on the strength and deformation properties of soils, representative samples should be collected and tested in laboratories and subjected to vibration of expected magnitudes. In this case, it is important that the laboratory equipment used is able to simulate field conditions as close as possible to provide the necessary parameters that can successfully be used in the design. A vibrating direct shear apparatus has been developed based on the conventional direct shear apparatus to evaluate the strength and deformation characteristics of soils (granular and cohesive) under a wide range of vibrational accelerations and frequencies. The apparatus makes it possible to test soils in both stress and strain controlled modes. The design of the apparatus is such that it allows modification of the most commonly used direct shear apparatuses into vibrating ones. The new apparatus has been built and tested to prove its workability and reliability.

3.2 Introduction

Soils are frequently exposed to dynamic loads (vibrations) due to natural and human-made causes. Examples of vibration types include earthquakes, blasting, machinery and vehicle traffic. Depending on their intensity, vibrations may result in partial or complete strength loss, which leads to significant deformation of soils. Of specific interest is the effect of vibration on the critical state (residual shear strength) of soils, a unique state independent of the initial density (void ratio) of the soil that can be reached upon sufficiently large shear deformations.

Pokrovsky et al. (1934) were the first to experimentally investigate the influence of vibrations on the internal friction of sand and showed that the coefficient of internal friction decreases with an increase in the kinetic energy of vibration. These results were later supported by experiments performed by Barkan (1962). Nowadays, there are different types of laboratory apparatuses to measure the strength properties of soils under vibrational loads. Depending on the design and technical characteristics, each of the tests has its advantages and limitations in simulating field conditions. The following are some examples of the above mentioned techniques and the investigations performed by using these techniques.

Levshinsky designed a stress-controlled vibrating shear apparatus that generates cyclic shear loads (horizontal vibration) on soil samples. It was later used by Preobrazhenskaya and Savchenko in 1958 to determine the shearing strength of soils with vibration (from Meschyan, 1992). Youd (1970) investigated shear strength reduction and density changes of granular materials under vibration by mounting a direct shear apparatus onto a shaker table. Some examples of work done with the use of shaking table tests are that by Arango and Seed (1974), Wartman et al. (2005), and Toyota et al. (2004), who used the technique to investigate vibration induced deformations in slopes. Meschyan and Badalyan modified a stress-controlling torsional

shear apparatus into a stress-controlling vibrating torsional shear apparatus that allows the testing of thin cylindrical samples under vibrational torsional shear loads generated by a vibrator (Meschyan, 1978). Melosh et al. (1995) built a rotational viscometer to quantitatively investigate the relationship between stress and strain rate in a bucket of strongly vibrated dry, fine sand. A similar setup, with the use of a penetrating cone instead of a sanding drum (Melosh et al., 1995), was used to evaluate the strength of soils under vibration (Kutergin, 1989). Shibata et al. (1970), who conducted experiments on sand, used a vibrating triaxial apparatus.

It should be mentioned that presently, there are very few, if any, laboratory equipment that can be used to determine the effect of vibration on soil at different states, especially at the critical state, as well as to evaluate the impact of vibration on the deformation properties of soil under different normal, shear and vibrational loading conditions.

A vibrating direct shear apparatus has been designed and built that meets the requirements mentioned above. The new apparatus represents a modification of a conventional WYKEHAM FARRANCE direct shear apparatus, such that soil samples can be tested in both strain and stress controlled modes under different vibrational frequencies, amplitudes and accelerations. One of the main advantages of this apparatus is that vibration can be applied at the residual state. Also, the modifications can easily be implemented in most existing direct shear apparatuses in conventional geotechnical laboratories.

The changing of a conventional direct shear apparatus into a vibrating direct shear apparatus requires the placement of an actuator between the top half of the shear box and the load cell to apply shear loading onto the sample as shown in Fig. 3.1. The actuator generates vibration in the horizontal (shear) direction by horizontally expanding and contracting, and induces vibration on the top half of the shear box. The actuator can be electromagnetic,

piezoelectric or pneumatic. By using a control panel connected to the actuator, the frequency and force of vibrations can be changed. To measure acceleration, frequency and amplitude of vibrations, an accelerometer is attached to the top half of the shear box. To measure the acceleration, frequency and amplitude of vibrations in the vertical direction, another accelerometer is attached to the top of the loading plate which is subjected to a normal load. The readings can be recorded by using an oscilloscope, data-logger or a PC.

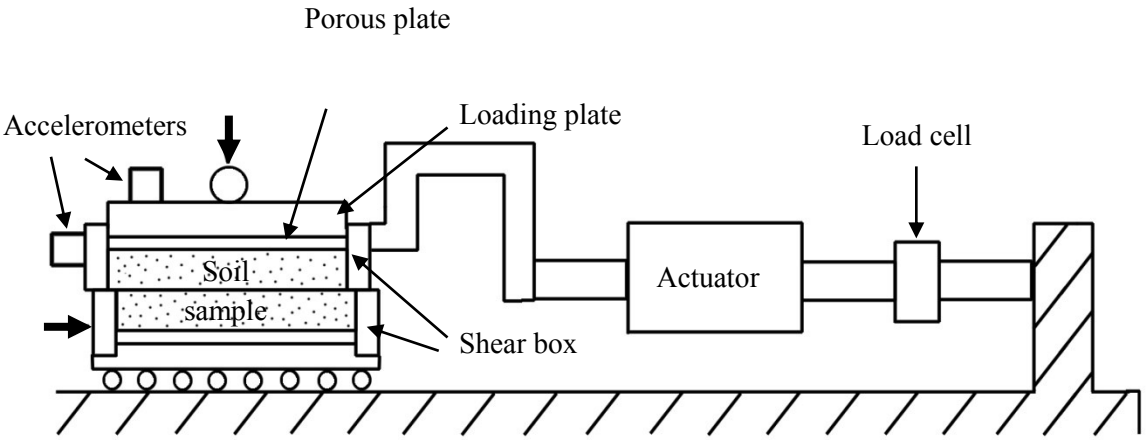

Figure 3.1 Schematic of the vibrating direct shear apparatus

3.3 Strain controlled vibrating direct shear apparatus

Presently, most direct shear apparatuses use a load cell to measure the shearing resistance of a soil (see Fig. 3.2a). However, there are some that still use a proving ring, as shown in Fig. 3.2b. Modifications can be made in both types of devices that use a load cell and/or a proving ring. There are advantages and limitations in both cases. A proving ring allows more compression under loading and therefore enables the actuator to apply larger amplitudes of vibration onto the sample. A load cell delivers high stiffness which requires a larger actuator.

In strain controlled testing with a load cell, see Fig. 3.3a, the long shafts (4) that are attached to the force transducer (5) must be replaced with shorter shafts (14) to accommodate the actuator (13), which is mounted between the shear box (3) and the load cell (5). Depending on the testing conditions, an additional load cell can be placed between the control panel (1) and the shear box (3) in order to measure the shear load which is less affected by the actuator (13).

In order to modify the strain controlled direct shear apparatus (Fig. 3.2b) into a strain controlled vibrating direct shear apparatus with a proving ring for shear load measurement (Fig. 3.3b), the main body of the direct shear apparatus (7) has to be extended with an extension (15) for sufficient space to accommodate the location of the actuator (13) between the shear box (3) and the proving ring (12).

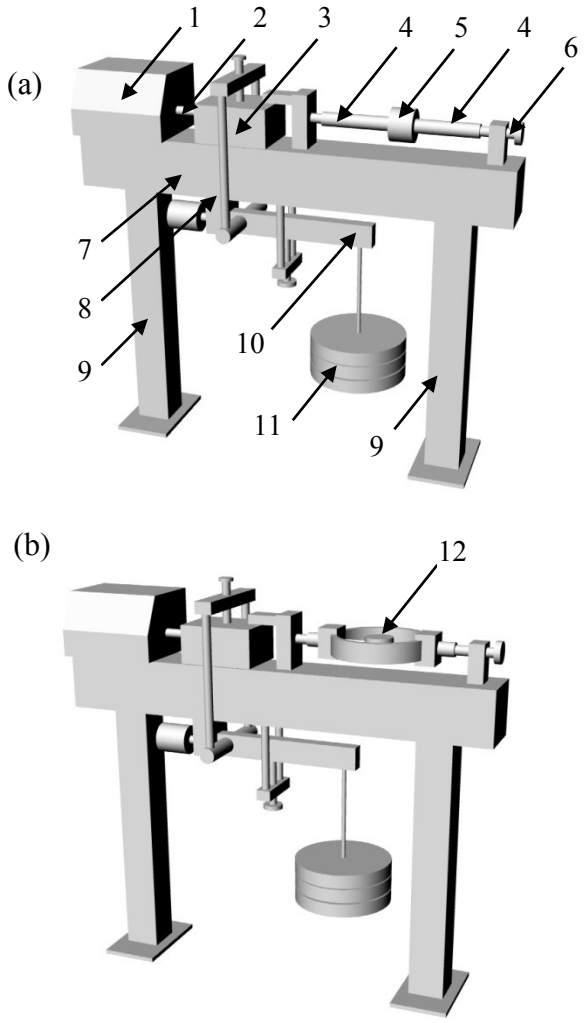

Figure 3.2 (a) – Conventional strain controlled direct shear apparatus with load cell & (b) – with proving ring.

Dial gages (or LVDTs) that measure vertical and shear displacements are not shown for simplicity. 1 – Control panel of the direct shear apparatus; 2 – Shaft that pushes the shear box (3); 3 – Shear box with soil sample; 4 – Shaft attached to load cell (5); 5 – Load cell that measures the shear force; 6 – Screw for zero setting of shear load before starting a test; 7 – Main body of the direct shear apparatus; 8 – Frame that transfers normal load to the soil sample (3); 9 – Legs of the direct shear apparatus that support the main body (7); 10 – Lever that provides

normal load to the soil sample; 11 –Weights to apply the normal load; 12 – Proving ring to measure the shear force.

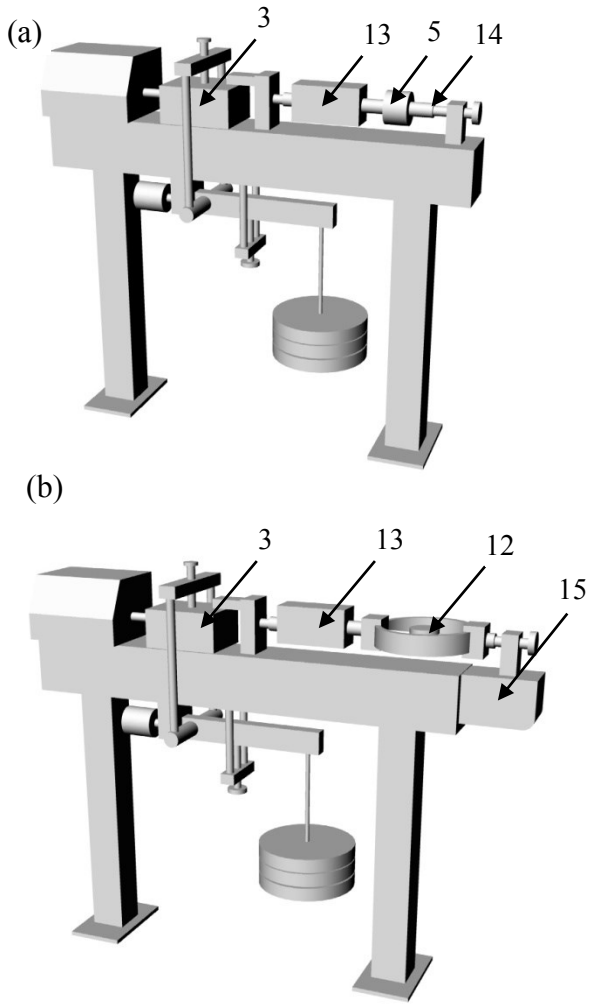

Figure 3.3 (a) – Strain controlled vibrating direct shear apparatus with load cell and (b) – with proving ring.

13 – Actuator that generates vibrations; 14 – Short shaft attached to the load cell (5); 15 – Extension of the main body (7) in Fig. 3.2 of the direct shear apparatus to accommodate the proving ring.

A photograph of the prototype of the strain controlled vibrating direct shear apparatus is shown in Fig. 3.4. Note that both the proving ring and a load cell (on the right hand side of the proving ring) are used together for this apparatus, as well as another load cell is placed on the left hand side of the shear box.

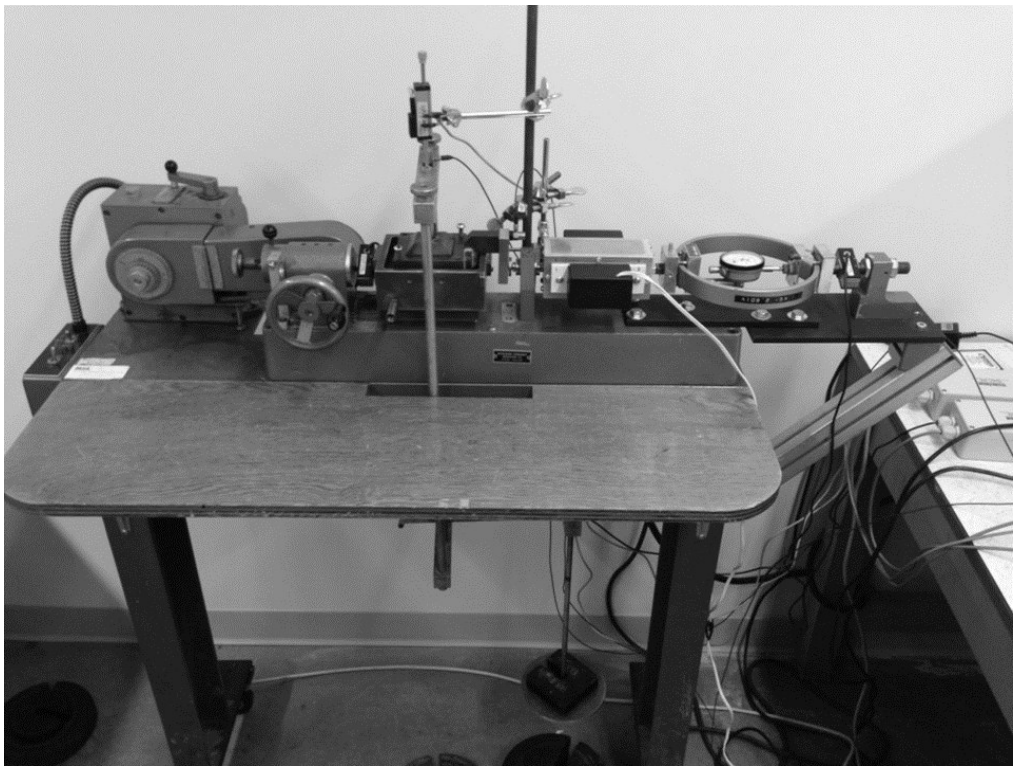

Figure 3.4 Prototype of the strain controlling vibrating direct shear apparatus

3.4 Stress controlled vibrating direct shear apparatus

In stress controlled testing, two pulley (17) carrying cables (16) are placed at the corners of the main body (7) on both sides of the zero setting screw (6) (see Fig. 3.5a). One end of the cables (16) is attached to the hanger (18) that carry the weights (19) and the other end is attached to two pins (20) mounted on both sides of the bottom half of the shear box (3). In this case, the control panel (1) of the direct shear apparatus is not used and the bottom half of the shear box (3) is disconnected from the shaft (2), thus preventing movement during the testing. The bottom half of the shear box (3) is moved by the shear load generated by the weights (19) placed on the hanger (18) (see Fig. 3.5a). Fig. 3.5b shows a schematic of a modified stress controlling vibrating direct shear apparatus with both a proving ring and a load cell. A photograph is shown in Fig. 3.6.

In this modification, the actuator (13) generates vibration shear loads, which, depending on the intensity of the vibration and the shear load, may cause shear deformation or failure of the soil.

(a)

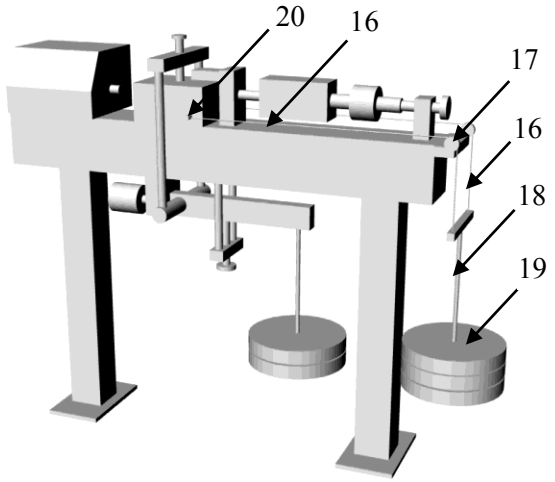

(b)

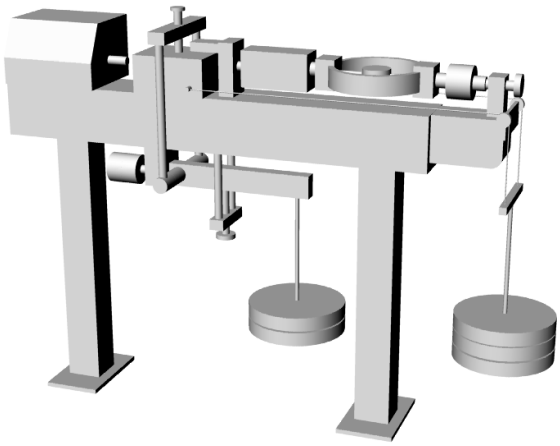

Figure 3.5 (a) – Stress controlling vibrating direct shear apparatus with a load cell and (b) – with a proving ring.

16 – Cable that transfers shear loads to the sample by pulling the bottom half of the soil sample; 17 –Pulley carrying cable (16); 18 – Hanger attached to cables (16) and carrying the weights (19); 20 – Pins mounted to the shear box (3) in Fig. 3.3 that connect to the cables (16).

A photograph of the prototype of the stress controlling vibrating direct shear apparatus is given in Fig. 3.6. Note that both the proving ring and load cell (on the right hand side of the proving ring) are used. Also, the shear box is disconnected from the gearbox shaft. An additional dial gauge is used to measure shear deformation.

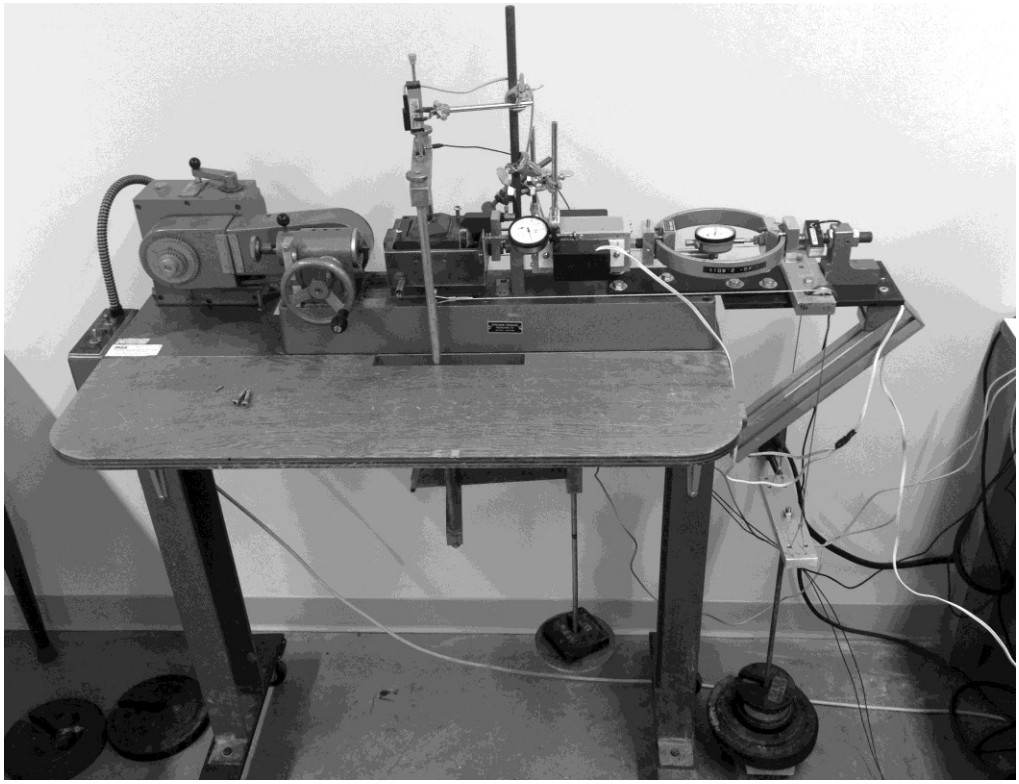

Figure 3.6 Prototype of stress controlling vibrating direct shear apparatus.

3.5 Testing of the Apparatus

3.5.1 Strain Controlled Testing Mode

To determine the workability of the strain controlled vibrating direct shear apparatus, dry fine sand samples that were angular in shape were tested to obtain both static and dynamic shear strength characteristics. A picture of a representative sample taken by a microscope and the particle size distribution of the tested material are provided in Figs. 3.7 and 3.8, respectively. The density of the sand ρ = 1.46 g/cm^3, density of solids ρ_s = 2.65 g/cm^3 and void ratio e = 0.815. The size of the shear box was 60 mm x 60 mm x 32 mm (W x L x H) and loading was applied at a shear rate of 0.61 mm/min under eight normal stresses (8.4, 23.2, 36.3, 50, 77.3, 118.2, 159.1 and 200 kPa). After reaching the residual shear strength, the samples were subjected to vibration (frequency = 140 Hz; horizontal acceleration ≈ 0.4 g; vertical acceleration ≈ 0.15 g) and changes in shearing resistance (dubbed "vibro-residual strength" here) were recorded. Two linear variable differential transformers (LVDTs) were used to measure the vertical and horizontal displacements, two load cells to measure the shear resistance of the samples at the bottom and top halves of the shear box, and two uniaxial accelerometers to measure the vertical and horizontal vibration accelerations of the samples (see Fig. 3.4). Measurements were taken at a frequency of 1 kHz by using the NI CompactDAQ System, which was connected to a computer that logged the data with NI LabVIEW software (National Instruments). The test results are shown in Table 3.1 and Fig. 3.9.

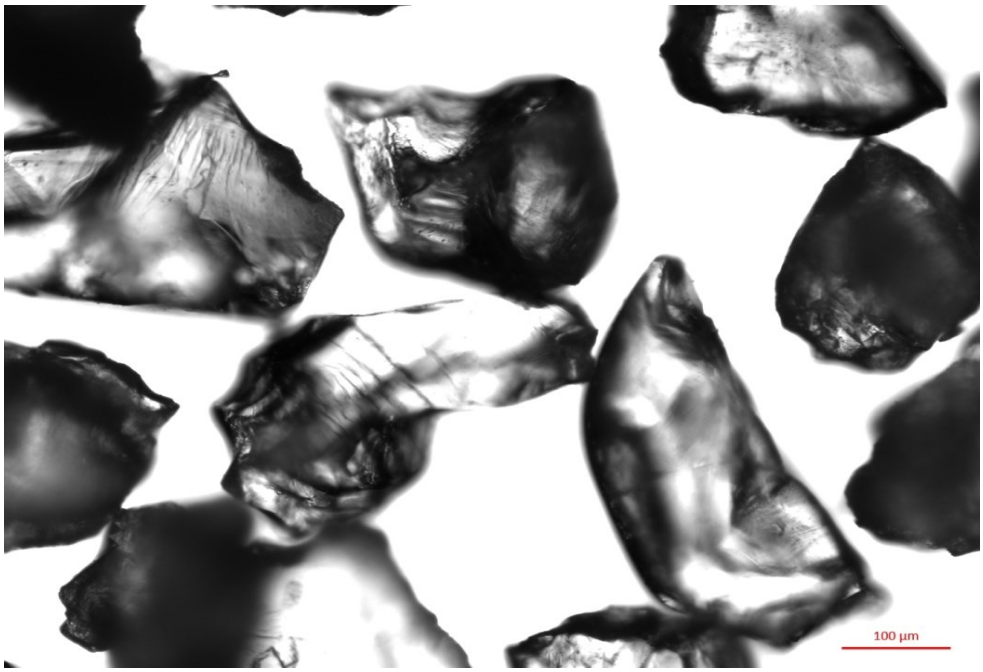

Figure 3.7 Photograph of sand taken by using a microscope

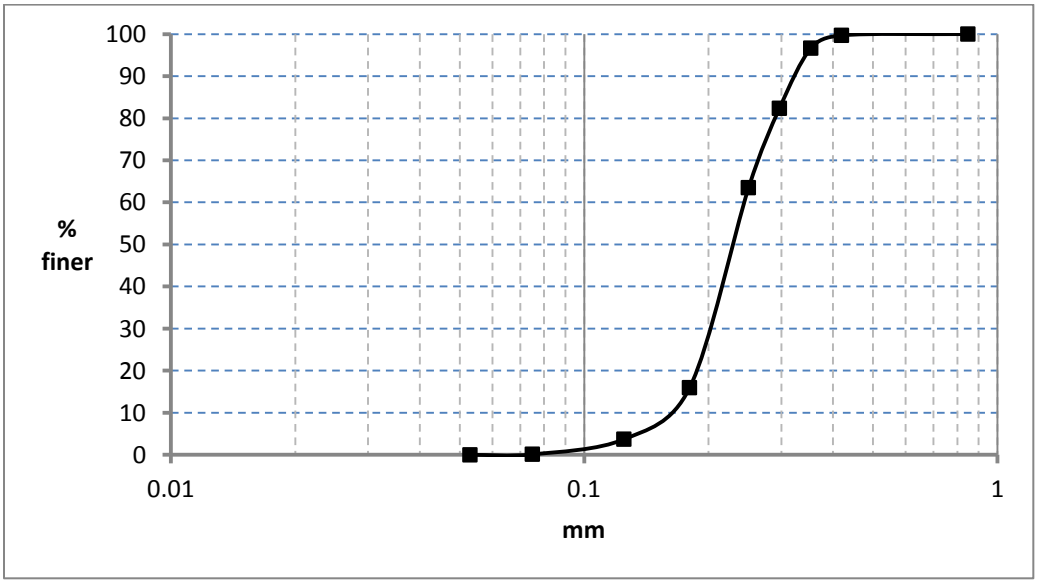

Figure 3.8 Particle size distribution of the tested sand samples

Table 3.1 Measured peak, residual and vibro-residual strengths of sand samples

Sample #	Normal stress σ (kPa)	Peak strength τ_p (kPa)	Residual strength τ_f (kPa)	Vibro-residual strength τ_{fd} (kPa)
1	8.4	15	11	5
2	23.2	30	21	14
3	36.3	38	29	21
4	50	51	37	30
5	77.3	78	56	43
6	118.2	106	80	61
7	159.1	148	113	91
8	200	173	134	110
Friction angle		40^0	33^0	29^0

As shown in Table 3.1 and Fig. 3.9, vibration reduces the residual friction angle by about 4^0 and cohesion[1] by about 4.5 kPa. An example of the typical plots of shear resistance, vertical deformation, and horizontal and vertical accelerations are shown in Fig. 3.10. From the shear resistance plot, it is seen that vibration causes the residual shear strength to drop to the vibro-residual strength. When vibration is stopped, the residual strength returns to the pre-vibration value. This means that the decrease in residual strength is temporary and only occurs during the application of vibration. Note that the normalized displacement in the plots of Fig. 3.10 is defined as $\Delta d/L$, where Δd is the horizontal displacement and L is the initial length of the specimen.

[1] Note that this is not real cohesion since sand has zero cohesion. The cohesion intercept is due to assumption that a straight line can be used to approximate the shear strength envelop. The actual shear strength envelop is non-linear, especially at low stress, due to particle interlocking and dilation.

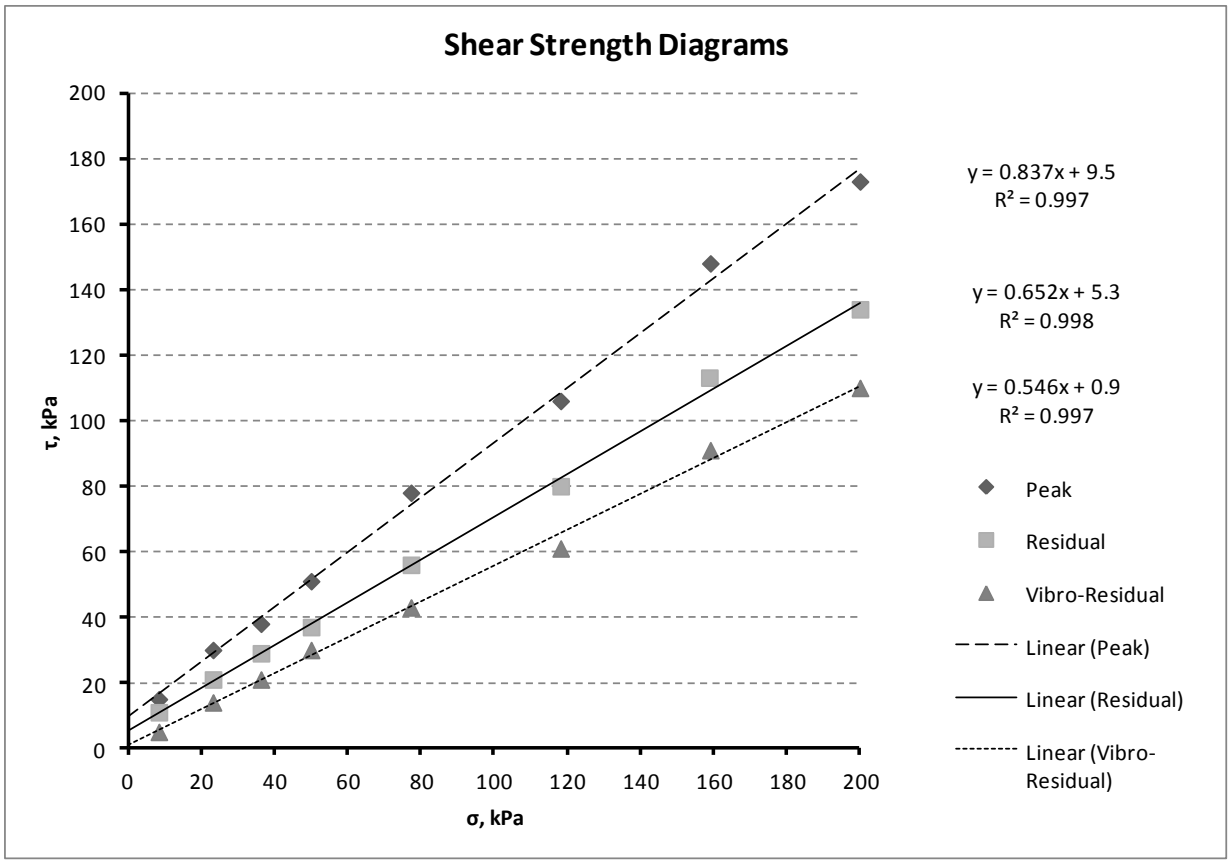

Figure 3.9 Static and dynamic shear strength envelops of sand

Depending on the objective of the laboratory testing program, soil samples can be subjected to vibration at different states (pre-peak, at peak, post-peak and residual states). Also depending on the technical characteristics of the actuator, the acceleration, amplitude and frequency can be changed in order to simulate existing or expected field conditions.

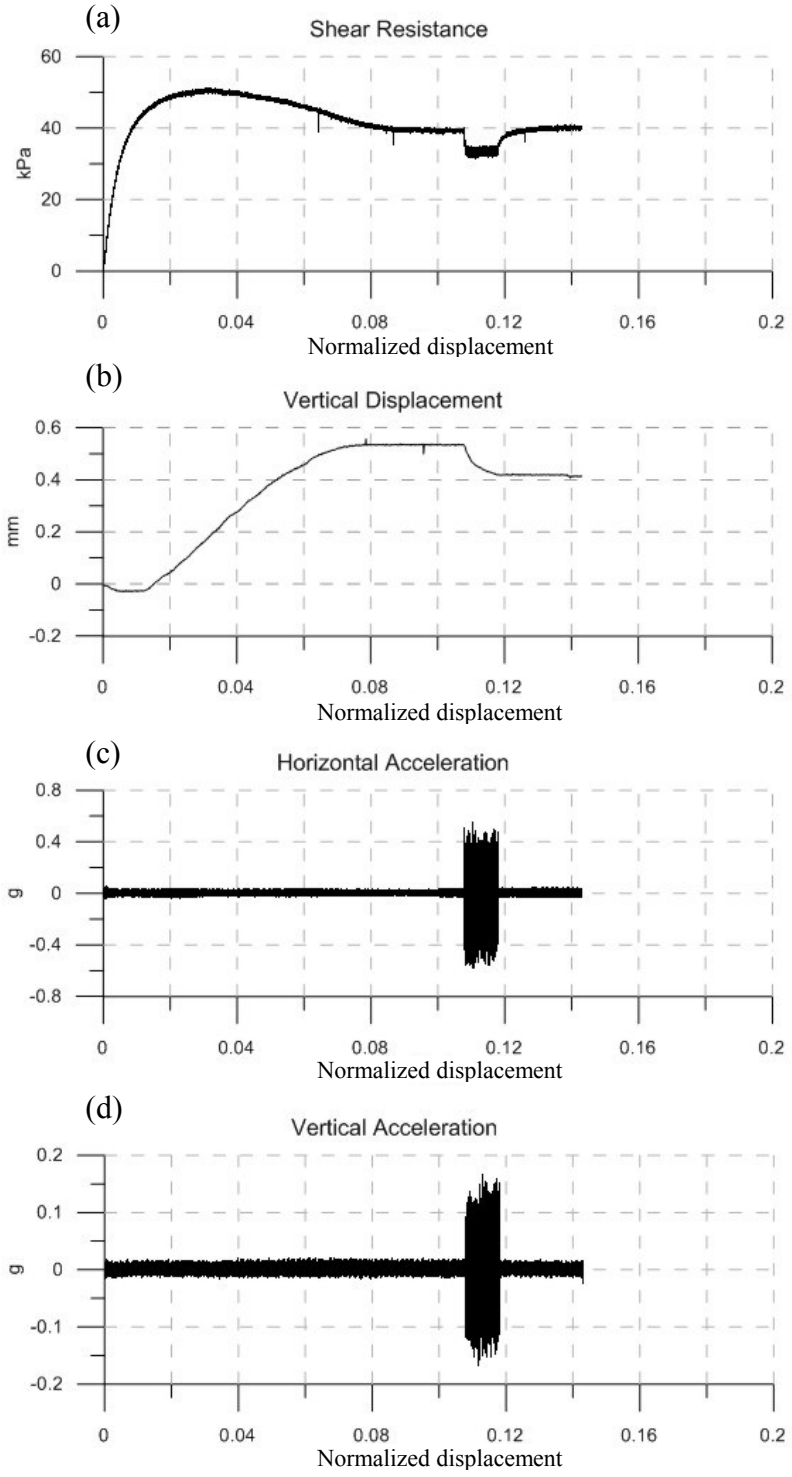

Figure 3.10 Shear stress (a), vertical displacement (b), and horizontal (c) and vertical (d) acceleration responses versus normalized horizontal displacement of sand under a normal stress of 50 kPa.

3.5.2 Stress Controlled Testing Mode

To verify the workability of the stress controlled vibrating direct shear apparatus, five dry sand samples were tested at a normal stress of 50 kPa. The samples were subjected to a shear stress equal to 50%, 60%, 70%, 80% and 90% of the static shear strength (τ) determined at a normal stress of 50 kPa. After being loaded with the appropriate shear load, the samples were subjected to vibration (frequency = 140 Hz; horizontal acceleration $\approx$ 0.4 g; vertical acceleration $\approx$ 0.15-0.2 g) and the shear deformations of the samples were recorded. The results are shown in Fig. 3.11.

As seen in Fig. 3.11, depending on the magnitude of the shear load, the samples experience different shear deformations due to vibration. It is seen that the samples fail at 0.9 τ while the soil would undergo shear deformations at different rates for the other tests.

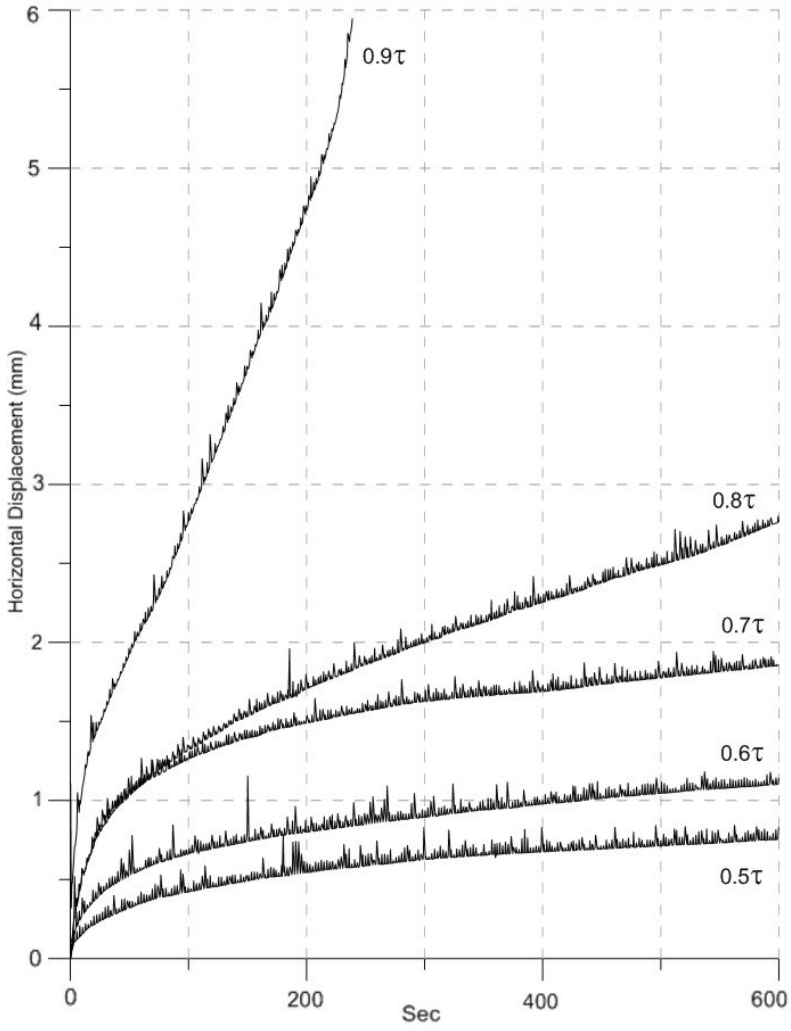

Figure 3.11 Displacement and time response of stress controlled direct shear testing with vibration at different levels of peak stresses with normal stress of 50 kPa

Typical plots of the shear resistance, vertical and horizontal (shear) deformations, as well as horizontal and vertical accelerations versus time are shown in Fig. 3.12. There is some "noise" in the horizontal (shear) deformation plots which is due to the technical characteristics of the LVDT used to measure the shear displacement of the samples and the frequency of the data logging relative to the output signal frequency of the sensor.

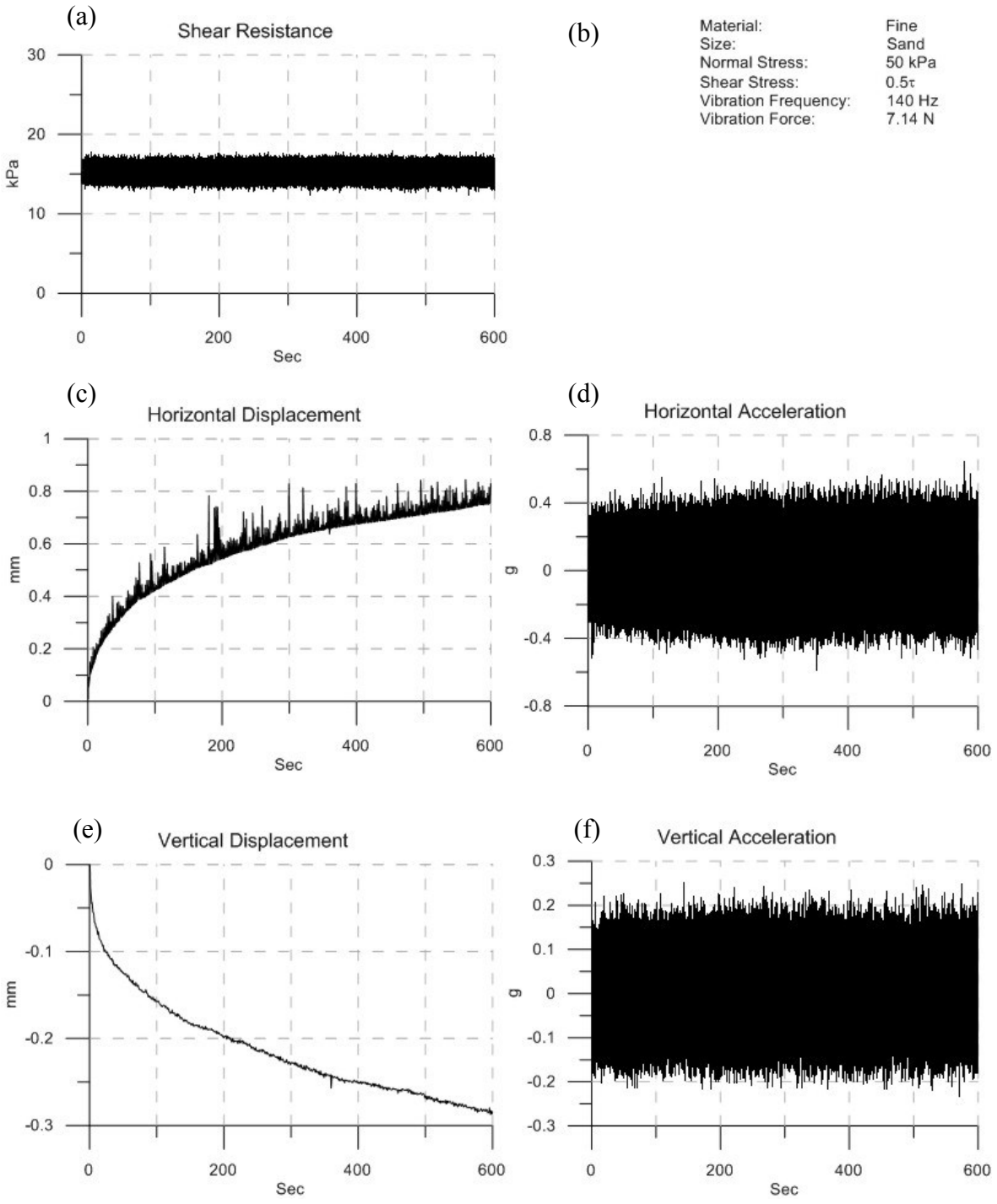

Figure 3.12 Shear stress (a), horizontal (c) and vertical displacement (e), horizontal (d) and vertical (f) acceleration responses versus time of sand in stress controlled tests at 50 kPa normal stress and shear stress equal to 50% of the static shear strength

3.6 Conclusions

The simple design of the vibrating direct shear apparatus discussed here makes it possible to apply modifications to most of the existing direct shear (and simple shear) apparatuses that are readily available in many geotechnical laboratories. Prototypes for a stress and strain controlled vibrating direct shear apparatus have been built and tested. The new apparatus has been proven in terms of its workability and efficiency in studying the vibrational responses of sand.

The new vibrating direct shear apparatus can be successfully used to determine the strength and deformation characteristics of fine and granular soils (up to the size of coarse sand) under different accelerations and frequencies of vibration. Depending on the testing mode (strain or stress controlled) the characteristics of soils can be determined under drained conditions at different shear rates, normal and shear stresses, as well as different stress states.

3.7 References

Arango, I. and Seed, H. B. (1974). "Seismic stability and deformation of clay slopes." J. Geotech. Engrg. Div., 100(2), pp. 139–156.

Barkan, D. D. (1962). "Dynamics of Basis and Foundations". Translated from Russian by L. Drashevska, New York, McGraw-Hill, 434 p.

Kutergin, V. N. (1989). The property change patterns of clayey soils under vibration. (in Russian) Moscow: Nauka, 143 p.

Melosh, H. J. and Girdner K. K. (1995). Rheology of vibrated granular materials: Application to long-runout landslides, EOS, 76.

Meschyan, S. R. (1978). "Short-term and long-term strength of clayey soils". (in Russian) Moscow, Nedra, 207 p.

Meschyan, S. R. (1992). "Rheological processes in clayey soils". (in Russian) Yerevan, "Hayastan", 395 p.

National Instruments website: http://www.ni.com/labview/ (accessed in September, 2013)

Pokrovsky, G. I., Ehrlich, A. A., Laletin, N. V. and Lush, F. A. (1934). New Methods of Investigation of the Compressibility and Internal Friction in Soils. Vestnik Voyenno-Inzhenernoy Akademii RKKA, no. 6.

Shibata, T. and Yukitomo, H. (1970). Shear strength of sand under a vibrating load. Bulletin of the Disaster Prevention Research Institute, 19(3): pp. 27-37.

Toyota, H., Towhata, I., Imamura, S. and Kudo, K. (2004). "Shaking Table Tests on Flow Dynamics in Liquefied Slope", Soils and Foundations, Vol. 44, No. 5, pp. 67 – 84.

Youd, L. T. (1970). Densification and Shear of Sand during Vibration. ASCE, Journal of the Soil Mechanics and Foundations Division, Vol. 96, No. 3, May/June 1970, pp. 863-880.

Wartman, J., Seed, R. B. and Bray, J. D. (2005). "Shaking table modeling of seismically induced deformations in slopes." J. Geotech. Geoenviron. Eng., 131(5), pp. 610–622.

4. Chapter 4: Effect of Vibration on the Critical State of Dry Granular Soils

4.1 Abstract

In order to investigate the effect of vibration on the critical state of dry granular soils, eighty samples from four different granular materials are tested at four normal stresses under different vibrational frequencies and accelerations. The experiments are performed on a modified vibrating direct shear apparatus with vibrational loading in the horizontal (shear) direction. Strength loss vs. vibration acceleration plotting at different normal stresses, as well as that for the peak, residual and vibro-residual shear strengths, have been carried out for the four granular materials at different intensities of vibration. It has been determined that an increase in the intensity of vibration reduces the friction angle of the granular materials. The effect of particle shape on the strength loss due to vibration has been observed, as well as the effect of vibration on normal stress.

4.2 Introduction

Granular soils are frequently exposed to vibrations due to earthquakes, blasting, construction operations, machinery and vehicle traffic. The strength behavior of a soil during vibration not only depends on the vibration characteristics, such as acceleration, frequency and amplitude, but also on the physical properties of the soil, such as moisture content, grain size distribution, particle shape, dry density or void ratio, cohesion and internal friction angle, as well as the density and mineralogy of the soil particles.

There has been significant progress in understanding the effects of vibration on the strength and deformation properties of soils since the first half of the last century (Housner, 1954, 1959; Barkan, 1962; Richart, 1970; Seed and Idriss, 1982, 1983; Idriss and Boulanger, 2008). A number of different experiments with vibration application have been conducted on cohesive and cohesionless soils that generated very valuable data which have led to some important conclusions (Savchenko, 1958; Pyke et al., 1975; Robertson and Campanella, 1985, 1986; Wartman et al., 2005; Meehan et al., 2008). All of these findings significantly help to improve the design of different structures subjected to dynamic loads (Barkan, 1962; Seed, 1966; Richart, 1970; Seed and Idriss, 1982; Das, 2011; Sangroya and Choudhury, 2013).

Despite the knowledge gained on this issue in the last few decades, there is still a lack of understanding on the mechanism of particle interactions and shear deformation due to vibration. Therefore, there is a need to study the shear strength and deformation behavior of soils due to vibrations. In particular it is specifically interesting to determine the effect of vibration on the residual shear strength of soils, that is, the effect of vibration on the critical state, a unique state independent of the initial density (void ratio) of the soil that can be reached upon sufficiently large shear deformations.

If large displacements are anticipated, the design of a structure, such as an earth or tailing dam, has to take into account the residual shear strength characteristics of the soils that underlie or/and constitute the structure. In this case, if the soil is subjected to vibration, depending on the magnitude of the vibrations, it may undergo some loss of strength, thus resulting in excessive deformation and compromising the stability of the structure. Therefore, it is of paramount importance to predict and consider the effects of vibrations on the residual strength of soils.

4.3 Previous Studies on Vibrational Loading on Soils

There are two important aspects that contribute to the unique properties of granular materials: ordinary temperature plays no role on their mechanical behaviour, and the interactions between grains are dissipative because of static friction and the inelasticity of collisions (Jaeger et al., 1996). Pokrovsky (1934) was the first to experimentally investigate the influence of vibration on the internal friction of sand. He showed that the coefficient of internal friction depends on the kinetic energy of vibration. As the energy increased, the coefficient decreased, thus approaching a value that was 25% to 30% smaller than that observed before vibration. These results were later supported by experiments performed by Barkan (1962), who tested sand at a vibration frequency of 140 sec^{-1} and amplitude of 0.5 - 0.15 mm. It was concluded that vibration has considerable effects on the shearing resistance of soil and the internal friction is lower than the static friction during vibration. Increase in acceleration will decrease the internal friction, which asymptotically approaches to a limit value, depending on the properties of the soil. Analogous experiments conducted on sand with a moisture content of 10% to 12 % showed that the moist sand subjected to vibration has a smaller decrease in the internal friction than dry sand. This was attributed to the capillary forces between the soil particles with a moisture content of 10% to 12%.

Additional confirmation of the above observations was provided by Savchenko (1958) who revealed that at a constant vibrational frequency, the coefficient of the internal friction of sand continuously decreases as the amplitude increases. The dependence of tan φ on the frequency of vibration is more complicated, and as the test results showed, there exist frequency ranges that correspond to small and large changes in tan φ of sand. Savchenko (1958) also tested two sets of medium grained sand at different moisture contents (2 – 24 %), constant vibration amplitude of

0.35 mm and two vibration frequencies of 144 sec^{-1} and 250 sec^{-1}, respectively. For both sets of samples, the largest decrease in tan φ was observed at approximately a moisture content of 13% (Barkan, 1962). Barkan (1962) concluded that the principal vibration parameter which determines the effect of vibrations and shocks on the compaction of soils is the acceleration, or rather, the inertial force, which acts on the soil particles during vibration. Metcalfe et al. (2002) and Huan (2008) also confirmed that dimensionless acceleration $\Gamma=A\omega^2/g$ is a key vibration parameter, where A is the vibration amplitude, ω is the frequency and g is the gravitational acceleration.

To study the influence of particle size on the effect of vibration, Savchenko (1958) conducted experiments on four different sizes of sand at vibrational frequencies of 144 sec^{-1} and 250 sec^{-1} and a constant vibration amplitude of 0.35 mm. The results revealed that the effect of vibration on internal friction in sand is directly proportional to the diameter of the sand grains (Barkan, 1962). On the other hand, Maslov (1959) performed a series of experiments on sands and concluded that vibration does not cause any changes in the coefficient of the internal friction of sand, and that the changes in its shear resistance are due to a decrease in the normal stress caused by vibration. Shibata and Yukitomo (1969) carried out triaxial vibrating tests under drained conditions. The results revealed that the dynamic strength increases with increases in the density of sand, and that the influence of vibration frequency on the strength of sand is rather remarkable; higher frequency indicates lower shear strength.

An interesting concept of "dynamic fluidization" was proposed by Richards et al. (1990). They took into consideration the effect of earthquake accelerations on dry granular soils. They hypothesized that the imposed accelerations at some critical level change the state of the soil, which causes general plastification, such that the soil becomes, in a sense, an anisotropic fluid.

They assumed that the main trigger of the fluidization is the inertial forces that act between the particles of a granular soil. They showed that fluidization mainly depends on horizontal and not vertical accelerations. Another distinguishing feature of fluidization is that when it occurs, flow takes place, if at all, in finite increments rather than continuously, with increments that correspond to the acceleration pulses of an earthquake above a critical value (Richards et al., 1990).

The authors distinguished three stages of dynamic fluidization: initial, intermediate and general. Initial fluidization is recognized as a threshold, above which, significant loss of soil shearing resistance may occur. For a dry sand in its neutral condition, the K_o initial fluidization takes place at $\Gamma<0.3$ and at even lower values for soils with a smaller friction angle. For saturated loose granular soils, it is postulated that the initial fluidization will initiate liquefaction because of collapse of the soil structure under shear flow. At the intermediate stage of dynamic fluidization, the soil continues to lose its shearing resistance and provides support of the external loads from internal shearing generated by the inertial forces. When the soil reaches the general stage of dynamic fluidization, its shear strength is mobilized based on a broad range of orientations, and the soil within these orientations behaves like a viscous fluid (Richards, 1970).

Youd (1968) performed laboratory experiments by mounting a direct shear apparatus onto a shaking table to show the effects of vibration on the shear strength and void ratio of dry granular materials. It was concluded that each vibratory equilibrium void ratio[2] is also the critical void ratio when the sample is sheared under the same vibration. The critical void ratio and coefficient of internal friction were both considerably reduced during vibration.

[2] Vibratory equilibrium void ratio is defined as the ultimate minimum void ratio for a sample densified at a particular vibration.

Of special interest are the theories of "mechanical fluidization" (Davies, 1982) and "acoustic fluidization" (Melosh, 1979) which attempt to explain the large runout distance of big rock avalanches. The essence of mechanical fluidization is the concept that high energy input into a granular mass causes high impulsive contact pressure between individual grains such that they become statistically separated and the mass dilates. The internal shearing resistance is thereby reduced as shown by Bagnold (1954) and Bjerrum et al. (1961), and the mass may flow under gravity when dilated. The high relative velocity between the base of the high-speed debris flow and the bedding material of the flow channel causes high speed shearing with high energy, which results in dilation as shown by Bagnold (1954) for a granular material subjected to unidirectional shearing (Davies, 1982). On the other hand, Hungr (1981) conducted high velocity ring shear tests and did not observe any effects of "mechanical fluidization". Several types of materials were tested, including two sizes of relatively coarse sand, mixtures of sand and rock flour, polystyrene beads and sand in water, under different velocities and normal stresses. All of the materials showed straight linear residual strength envelopes with zero cohesion and unique angles of residual friction, which were minimally influenced by the shearing speed (Hungr, 1981).

The acoustic fluidization theory proposed by Melosh (1979) is another attempt to explain the large runout distance of sturzstroms observed on earth, as well as on the moon and Mars. Based on this theory, a thin layer of material can be fluidized by strong enough sound waves at the bottom interface of moving debris, if its volume is large enough to retain enough acoustic energy to maintain fluidization. An important aspect of the flow process is that sound (acoustic energy) is created as debris moves, and that the sound must have short wave-lengths compared to the dimensions of the fluidized rock debris. Melosh (1996) also suggested that the overburden

pressure in some of the faults can be relieved by acoustic fluidization and allow pressure to slide at a low average stress (Melosh, 1979). Later, Sornette and Sornette (2000) found inconsistency in Melosh's theory of acoustic fluidization in explaining fault motion which nulls the results, and although they provided alternatives, they also indicated that the significance of acoustic fluidization remains questionable.

As evident from the studies summarized above, there is currently no comprehensive model that can fully explain the mechanism of the effect of vibrations on the shear strength characteristics of soils. Moreover, some of the findings seem to contradict each other. Therefore, the shear strength characteristics of soils under the influence of vibration remains open for further studies.

4.4 Testing Equipment and Procedures

In order to investigate the effects of vibration on the residual shear strength of granular material, a direct shear apparatus was modified into a vibrating direct shear apparatus as shown in Figs. 4.1 and 4.2. The modifications include installation of an electromagnetic actuator (11) between the proving ring (3) and the shear box (2), as well as two load cells (10 and 12) to measure the shear forces at the top and bottom halves of the shear box (2). An extension (13) of the main body (5) is installed to accommodate the actuator (11). The actuator (11) consists of two electromagnets, and the frequency and force can be changed by using a control panel. The vibration generated by the actuator is in the horizontal shearing direction.

The measuring equipment consisted of two linear variable differential transformers (LVDTs) that measured the vertical and horizontal displacements, two load cells (10 and 12),

and two uniaxial accelerometers that measured the vertical and horizontal vibration accelerations on the soil samples. One of the accelerometers was placed on top of the loading plate (measured vertical vibration accelerations), and the other accelerometer was attached to the top half of the shear box in the direction of the shear (measured horizontal vibration accelerations). The output signals were acquired by using the NI CompactDAQ System, which was in turn, connected to a PC that logged the data with NI LabVIEW software.

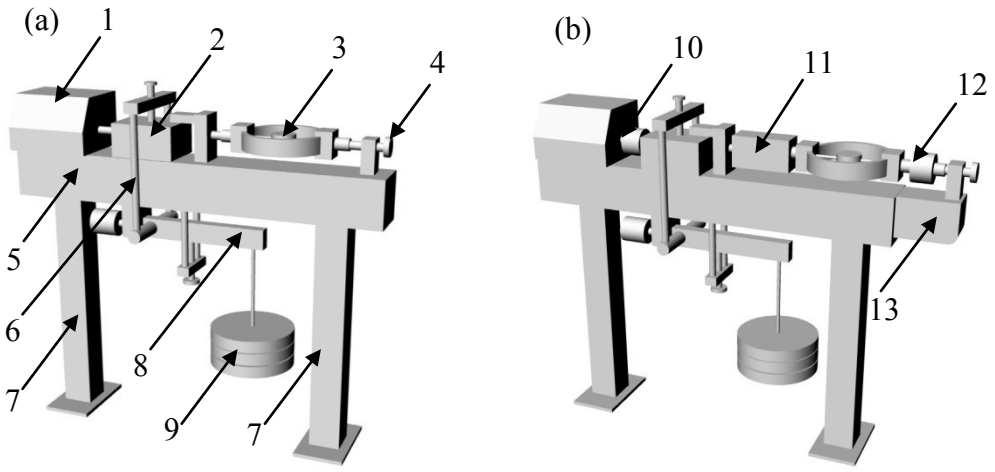

Figure 4.1 (a) – Strain controlled direct shear apparatus and (b) – modified strain controlled vibrating direct shear apparatus.

1 – Control panel of the direct shear apparatus; 2 – Shear box with a soil sample; 3 – Proving ring; 4 – Screw for zero setting of shear load before starting a test; 5 – Main body of the direct shear apparatus; 6 – Frame that transfers normal load to the soil sample placed in the shear box (2); 7 – Legs of the direct shear apparatus that supports the main body (5); 8 – lever that provides a normal load to the soil sample; 9 – Weights that define a normal load on the soil sample; 10 – Load cell; 11 –Actuator; 12 – Load cell; and 13 – Extension of the main body (5) of the direct shear apparatus.

The testing procedures were carried out in accordance with ASTM D3080/D3080M (Standard Test Method for Direct Shear Test of Soils Under Consolidated Drained Conditions), with additional vibration applied for a short period of time at the pre-peak and residual strength states. Depending on the objective of the test, vibrations were applied while the sample was being sheared, as well as when shearing was terminated. The frequency and force of the vibrations were adjusted to the required magnitude and kept constant for the set of soil samples tested.

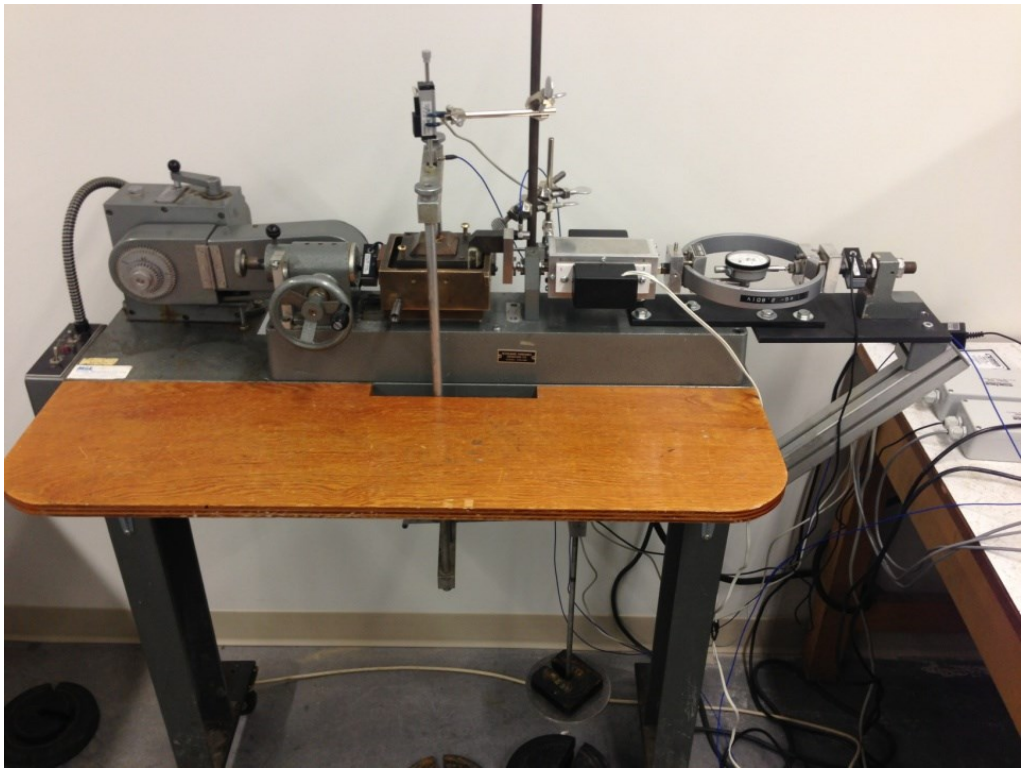

Figure 4.2 Photograph of the modified direct shear apparatus

4.5 Tested Materials

To evaluate the effect of vibration on the residual strength of granular material, four different dry granular materials (a total of 80 samples) were tested. The materials were 0.1 mm and 0.55 mm glass beads, as well as fine and coarse sands. These materials were selected to investigate the effect of particle shape and size on the vibro-residual strength characteristics at different vibrational accelerations. Particularly, different glass bead sizes (0.1 and 0.55 mm) were chosen to determine how the different inertial forces (due to different sized particles), generated among the particles through vibration, contributed to the vibro-residual strength. On the other hand, coarse sand (well-rounded) and fine sand (angular) samples were chosen in addition to the glass beads in order to evaluate the effect of particle roundness on the vibro-residual strength of the materials, particularly to observe the influence of particle friction during the induced vibration.

The samples (6 cm x 6 cm x 3.2 cm (W x L x H) in size) were tested under normal stresses of 23, 50, 118 and 200 kPa in strain-controlled mode at a shear rate of 0.61 mm/min. A vibration frequency of 140 Hz was used for all of the samples. From each type of granular material, five sets of samples (four samples in each set) were tested at five different vibration intensities. The maximum impact forces of the actuator electromagnets were 1.61, 3.22, 3.71, 5.18 and 7.14 N. Note that these impact forces are the designed forces provided by actuator. The actual impact forces may vary during the testing. They were measured by the accelerometers and load cell. All of the data were recorded at a rate of 1 kHz.

The vibration frequency value used in the text (140 Hz) was set by the control panel of the actuator, and double-checked by the observation of the recorded horizontal vibration acceleration sine wave, where it corresponded to the acceleration peaks. It should be mentioned that there is also vibration noise present in the recorded horizontal acceleration plots that has different

frequencies. The vibration noise is the secondary vibration frequency that is combined with the recorded primary frequency at low frequency level. Although these secondary vibration frequencies have not been analyzed and only the frequency corresponding to the peak acceleration values has been used for simplicity, it is realised that they shouldhave some effects on the measured strength and deformation characteristics of the tested materials.. To filter this noise effect a Fast Fourier transform analysis can be done.

The physical characteristics of the tested materials are provided in Table 4.1. The particle size distributions of the four materials are given in Fig. 4.3. Representative samples of the materials were examined under a microscope to determine the shape of the particles (see Figs. 4.4a, 4.4b, 4.4c, and 4.4d). It is seen in Fig. 4.4a that the 0.1 mm glass beads are not round with irregular shape grains and some are smaller than 0.1 mm. Therefore the "0.1 mm glass beads" should be treated like a mixture of fine sand sized 0.1 mm and smaller. The 0.55 mm glass beads are basically the ideal spherical shape, see Fig. 4.4b. From Figs. 4.4c and 4.4d, it can be seen that the fine sand particles have an angular shape and the coarse sand is well rounded. The shear strength diagrams and the residual friction angles of the four materials are shown in Fig. 4.5.

Table 4.1 Physical characteristics of the glass beads and sands

Material	ρ_s	ρ	**e**	**n**
Glass Beads 0.1 mm	2.65	1.49	0.779	0.438
Glass Beads 0.5 mm	2.65	1.566	0.692	0.409
Fine Sand	2.65	1.46	0.815	0.449
Coarse Sand	2.65	1.755	0.510	0.338

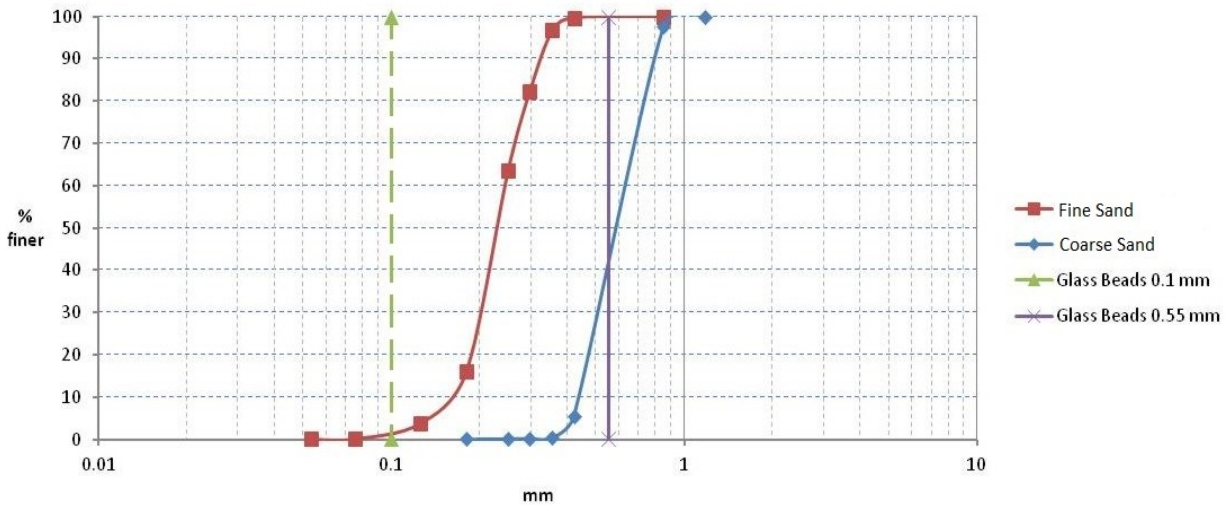

Figure 4.3 Particle size distribution of the tested materials

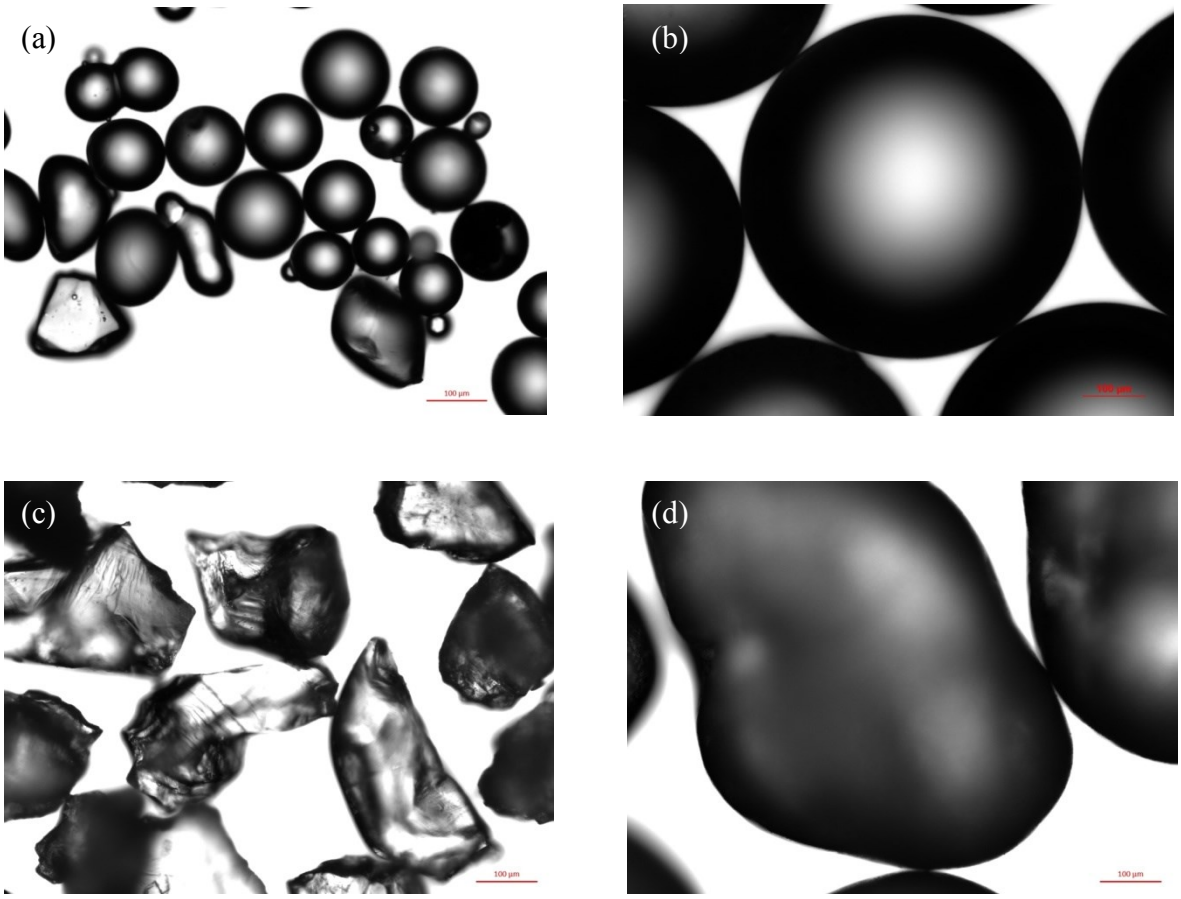

Figure 4.4 Pictures of the glass beads and sand under a microscope at magnification of 50x. (a) 0.1 mm glass beads; (b) 0.55 mm glass beads; (c) fine sand; and (d) coarse sand

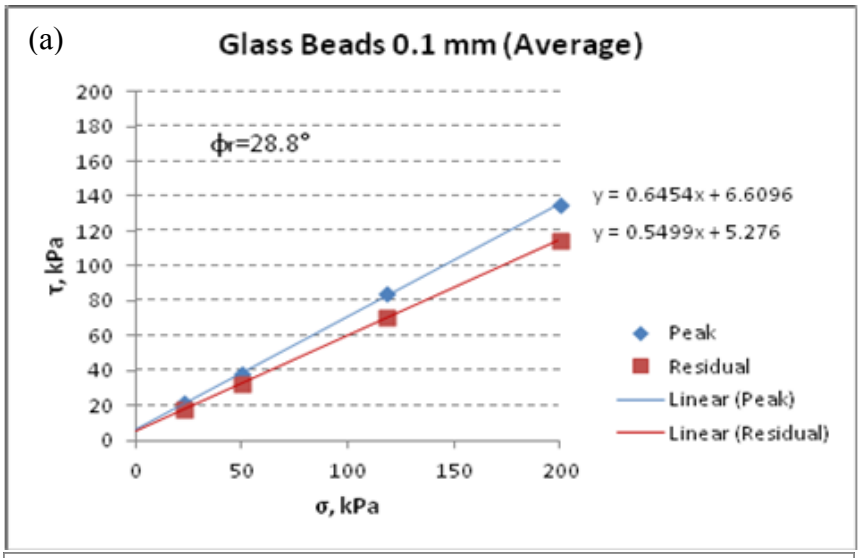

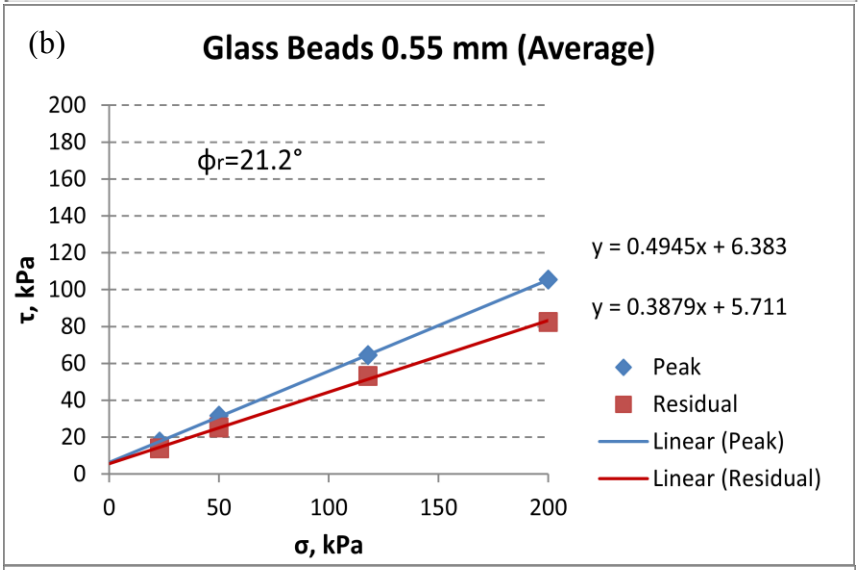

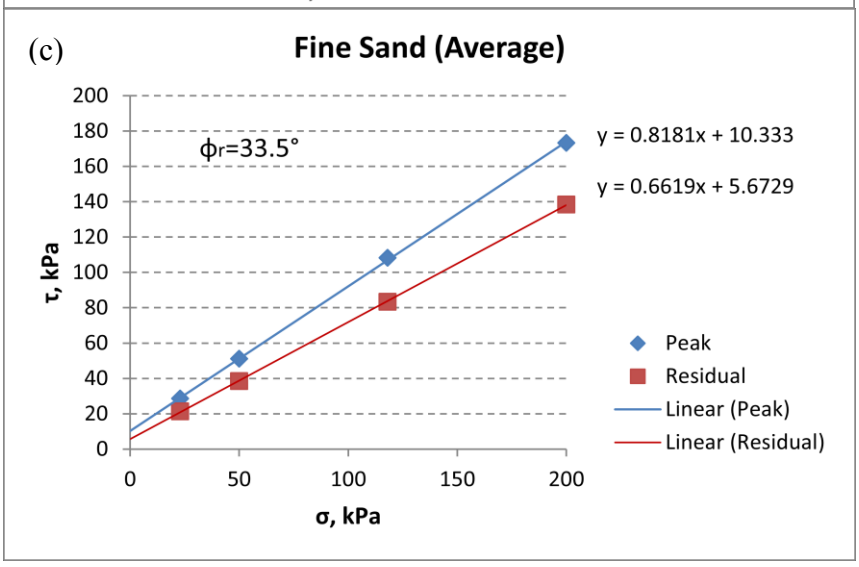

(Continued on the next page)

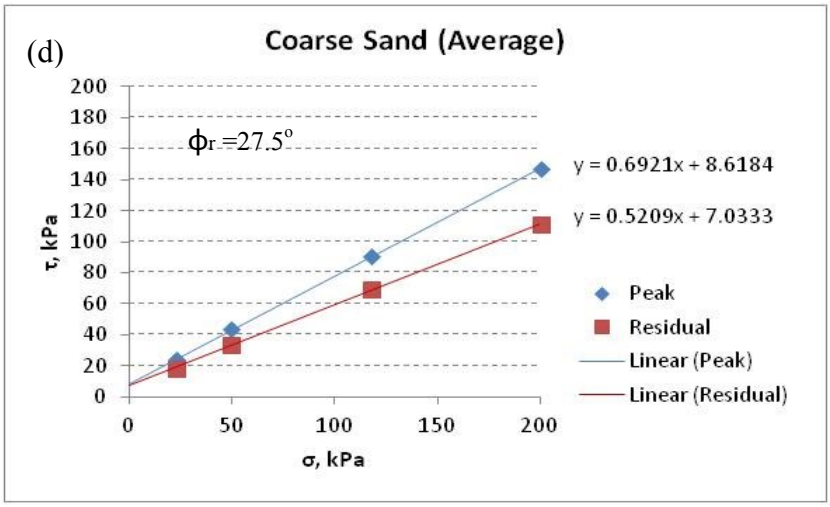

Figure 4.5 Shear strength diagrams of 0.1 mm glass beads (a), 0.55 mm glass beads (b), fine sand (c) and coarse sand (d).

4.6 Test Results under Vibration

A summary of the test results for the 0.1 mm and 0.55 mm glass beads, and the fine and coarse sands are given in Tables 4.2, 4.3, 4.4 and 4.5, respectively. Fig. 4.6 shows a typical plot of shear stress, vertical displacement, horizontal and vertical accelerations versus the normalized displacement of fine sand. The shearing resistance of the material was measured by using a load cell mounted at the top half of the shear box (see Fig. 4.1b (12)). Vertical displacements were measured from an LVDT attached to the loading plate of the shear box. Horizontal and vertical accelerations were obtained from an accelerometer attached to the top half of the shear box in the direction of shearing and a second accelerometer that measured the vertical accelerations of the loading plate, respectively. All of the data except for vertical displacement were collected at a rate of 1 kHz. Due to the technical characteristics of the LVDT, vertical displacements were measured at a rate of 2 Hz filtered from the original rate of 1 kHz.

As seen in Fig. 4.6, vibration is applied when the soil reaches the critical state. The shear resistance plot shows that during vibration, there is an immediate strength loss, $\Delta\tau$, for the residual to vibro-residual states. It is believed that the strength loss occurs in a very short time, probably in a few milliseconds. The vibro-residual strength remains practically constant during vibration. When vibration is terminated, the shear strength of the material gradually increases and reaches the residual quasi-static strength value. Note that the normalized displacement in Figs. 4.6 and 4.7 is defined as $\Delta d/L$, where Δd is the horizontal displacement and L is the initial length of the specimen.

All of the samples have experienced contraction and decrease in volume, due to vibration as shown in the vertical displacement plot in Fig. 4.6. It is seen that contraction takes place during vibration and the volume change is permanent or plastic. The initial volume before vibration cannot be restored when vibration stops.

An example of the effect of an increase in horizontal vibration acceleration on the residual shear strength of fine sand is provided in Fig. 4.7 (a, b and c), which shows the plots of fine sand samples tested at vibration forces of 3.71, 5.18 and 7.14 N of the electromagnets and horizontal accelerations of 0.27, 0.37 and 0.47 g, respectively. The example demonstrates that at a constant normal stress (118 kPa) and vibration frequency, an increase in vibration acceleration by 0.1 g results in greater strength loss.

The strength loss process can be briefly outlined in the following way: when vibration is applied to a sample of granular material sheared at its residual strength state, momentary loss of contacts between the grains takes place at the shear zone. This disturbs the stress chains in the sample, thus causing reduction in shear resistance. It should also be stated that since the amplitude of vibration is much smaller than the diameter of grains comprising the most of the

tested materials, the movement of particles in the shear zone can be combination of rotational and translational motions.

The peak, residual and vibro-residual shear strength envelops of the 0.1 and 0.55 mm glass beads, as well as fine and coarse sand for five different vibration forces are shown in Figs. 4.8, 4.9, 4.10 and 4.11, respectively. The peak, residual and vibro-residual friction angles of the four materials are given in Tables 4.6, 4.7, 4.8 and 4.9. As seen in Figs. 4.8 to 4.11 and acceleration values in Tables 4.2 to 4.5, increase in the vibration force results in an increase of the vertical and horizontal accelerations and amplitudes (not provided in Tables 4.2 to 4.5), which in turn, results in a greater loss in the residual strength at a given normal stress. From the tables and figures, it is seen that vibration reduces the residual friction angle.

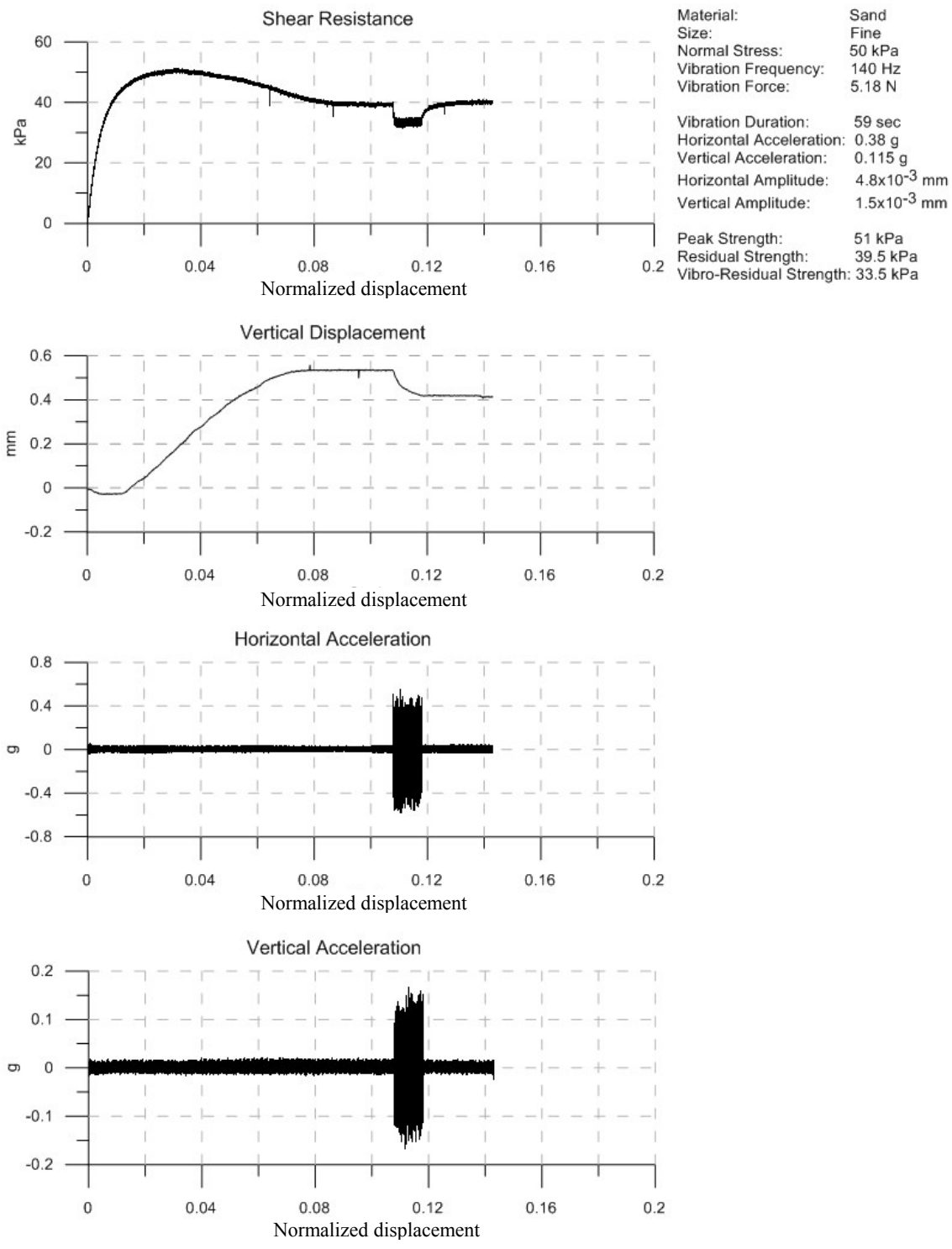

Figure 4.6 Shear stress, vertical displacement, horizontal and vertical accelerations versus normalized displacement of fine sand subjected to a normal stress of σ=50 kPa, vibration frequency of 140 Hz and vibration force of 5.18 N.

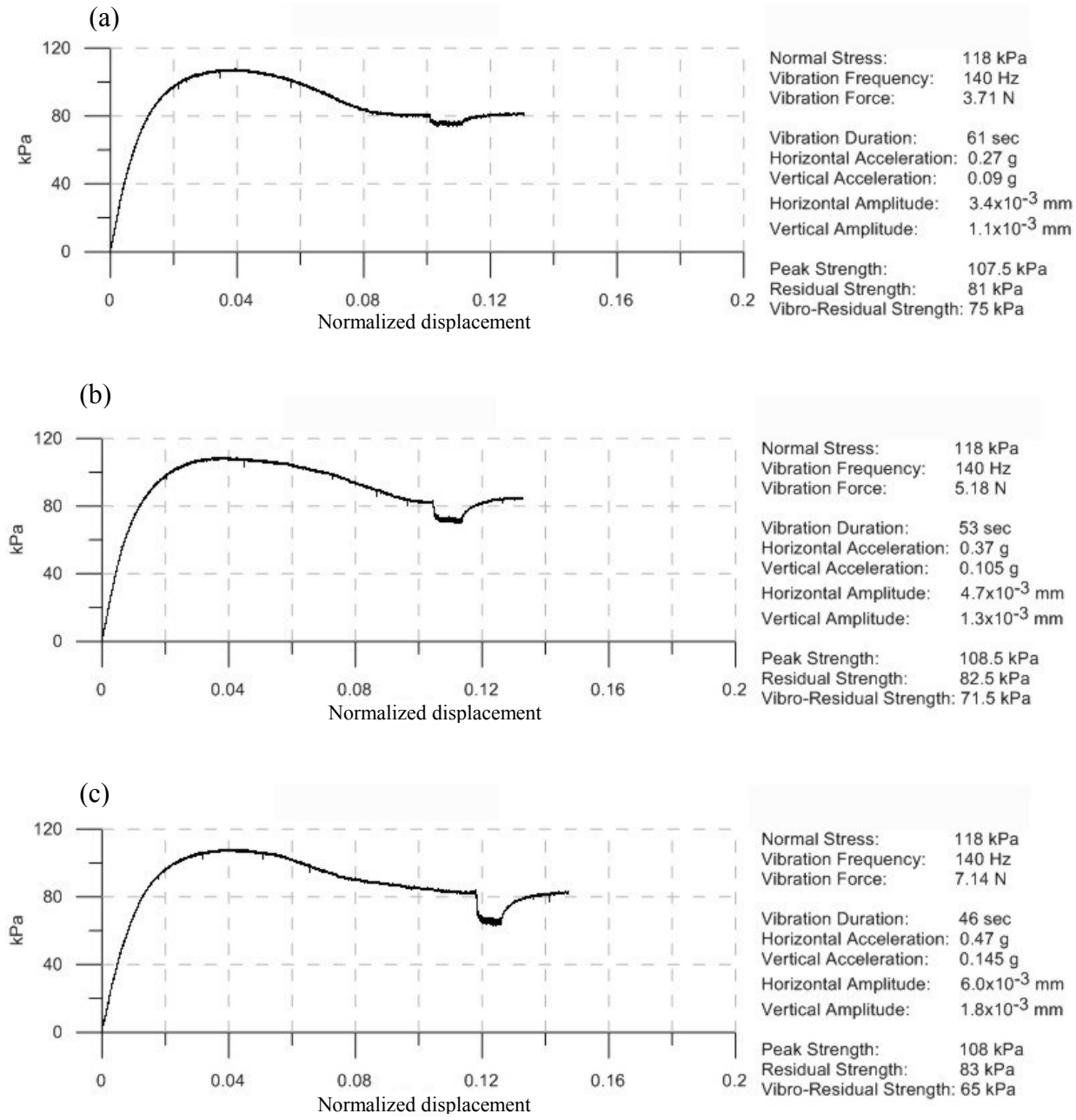

Figure 4.7 Shear stress plots of three fine sand samples tested at normal stress of 118 kPa and different vibration accelerations

Table 4.2 Test results of 0.1 mm glass beads

Force N	Normal Stress σ kPa	Peak Strength τ_p kPa	Residual Strength τ_f kPa	Vib.-Res. Strength τ_{fd} kPa	Vertical Acceleration g	Horizontal Acceleration g	Strength Loss $\Delta\tau$ kPa
1.61	**23**	21	19.5	18	0.03	0.1	1.5
	50	38.5	35	33	0.03	0.11	2
	118	82.5	71	68	0.04	0.12	3
	200	137.5	113	109.5	0.04	0.12	3.5
3.22	**23**	21	16.5	15	0.09	0.22	1.5
	50	38.5	29	26.5	0.08	0.23	2.5
	118	83.5	67	63	0.07	0.22	4
	200	135.5	114	108	0.065	0.2	6
3.71	**23**	21	18	15.5	0.075	0.25	2.5
	50	38	31.5	28	0.09	0.28	3.5
	118	85.5	70	65	0.08	0.24	5
	200	132	111.5	105	0.07	0.23	6.5
5.18	**23**	21.5	17	14	0.11	0.42	3
	50	38	32.5	26	0.11	0.38	6.5
	118	84	73	63	0.105	0.325	10
	200	136	121	108	0.09	0.3	13
7.14	**23**	22	17	13	0.14	0.5	4
	50	39.5	36	26.5	0.13	0.43	9.5
	118	83.5	73	56	0.15	0.43	17
	200	135	115	94	0.13	0.38	21

Table 4.3 Test results of 0.55 mm glass beads

Force N	Normal Stress σ kPa	Peak Strength τ_p kPa	Residual Strength τ_f kPa	Vib.-Res. Strength τ_{fd} kPa	Vertical Acceleration g	Horizontal Acceleration g	Strength Loss $\Delta\tau$ kPa
1.61	**23**	17.5	13.5	12.5	0.04	0.11	1
	50	32	25.5	24	0.035	0.11	1.5
	118	69	55.5	53.5	0.035	0.08	2
	200	111	82	79	0.035	0.09	3
3.22	**23**	17	14	12.5	0.07	0.175	1.5
	50	30.5	24.5	22.5	0.07	0.175	2
	118	65	51.5	47.5	0.07	0.175	4
	200	101	84	78	0.07	0.17	6
3.71	**23**	18	14	11.5	0.1	0.28	2.5
	50	32	25.5	22.5	0.085	0.23	3
	118	64	54	48.5	0.09	0.23	5.5
	200	103	82	73	0.085	0.23	9
5.18	**23**	17	14	10.5	0.105	0.325	3.5
	50	31	25.5	21	0.105	0.325	4.5
	118	62.5	51.5	43	0.105	0.325	8.5
	200	106	81	68	0.09	0.325	13
7.14	**23**	18	13.5	9	0.16	0.46	4.5
	50	32.5	25	19	0.16	0.46	6
	118	61.5	53	42	0.16	0.42	11
	200	106	83	66.5	0.14	0.43	16.5

Table 4.4 Test results of fine sand

Force N	Normal Stress σ kPa	Peak Strength τ_p kPa	Residual Strength τ_f kPa	Vib.-Res. Strength τ_{fd} kPa	Vertical Acceleration g	Horizontal Acceleration g	Strength Loss $\Delta\tau$ kPa
1.61	**23**	27	21	19.5	0.045	0.15	1.5
	50	53.5	40	38	0.045	0.12	2
	118	110	87.5	85.5	0.05	0.12	2
	200	178.5	139	137	0.045	0.11	2
3.22	**23**	26.5	20.5	17.5	0.1	0.26	3
	50	49	38.5	35	0.1	0.27	3.5
	118	107.5	83	77.5	0.09	0.27	5.5
	200	170.5	137.5	131	0.07	0.23	6.5
3.71	**23**	30	22	18.5	0.09	0.25	3.5
	50	51.5	37	33.5	0.1	0.27	3.5
	118	107.5	81	75	0.09	0.27	6
	200	169	143	134.5	0.08	0.25	8.5
5.18	**23**	29.5	22	17.5	0.1	0.37	4.5
	50	51	39.5	33.5	0.115	0.38	6
	118	108.5	82.5	71.5	0.105	0.37	11
	200	171	134	121	0.1	0.32	13
7.14	**23**	30	21	14.5	0.17	0.5	6.5
	50	50.5	37.5	27.5	0.155	0.49	10
	118	108	83	65	0.145	0.47	18
	200	177	138	116	0.145	0.45	22

Table 4.5 Test results of coarse sand

Force N	Normal Stress σ kPa	Peak Strength τ_p kPa	Residual Strength τ_f kPa	Vib.-Res. Strength τ_{fd} kPa	Vertical Acceleration g	Horizontal Acceleration g	Strength Loss $\Delta\tau$ kPa
1.61	**23**	25	18.5	17	0.045	0.12	1.5
	50	42	34.5	33	0.04	0.12	1.5
	118	88.5	67.5	66	0.045	0.1	1.5
	200	145	108.5	106.5	0.04	0.1	2
3.22	**23**	24.5	18.5	16.5	0.075	0.2	2
	50	43	34	31.5	0.065	0.2	2.5
	118	89	67.5	64.5	0.07	0.19	3
	200	145.5	111	107	0.07	0.18	4
3.71	**23**	24	18.5	16	0.085	0.23	2.5
	50	44.5	33.5	30.5	0.075	0.22	3
	118	93.5	70	66.5	0.075	0.21	3.5
	200	148.5	116	111	0.075	0.2	5
5.18	**23**	24	18	14.5	0.12	0.35	3.5
	50	43	34.5	29.5	0.09	0.33	5
	118	91.5	71	65.5	0.1	0.28	5.5
	200	148	110	102	0.08	0.28	8
7.14	**23**	23.5	18	12	0.2	0.59	6
	50	44.5	32	25.5	0.145	0.4	6.5
	118	91	68.5	59	0.135	0.39	9.5
	200	147	109	95	0.1	0.39	14

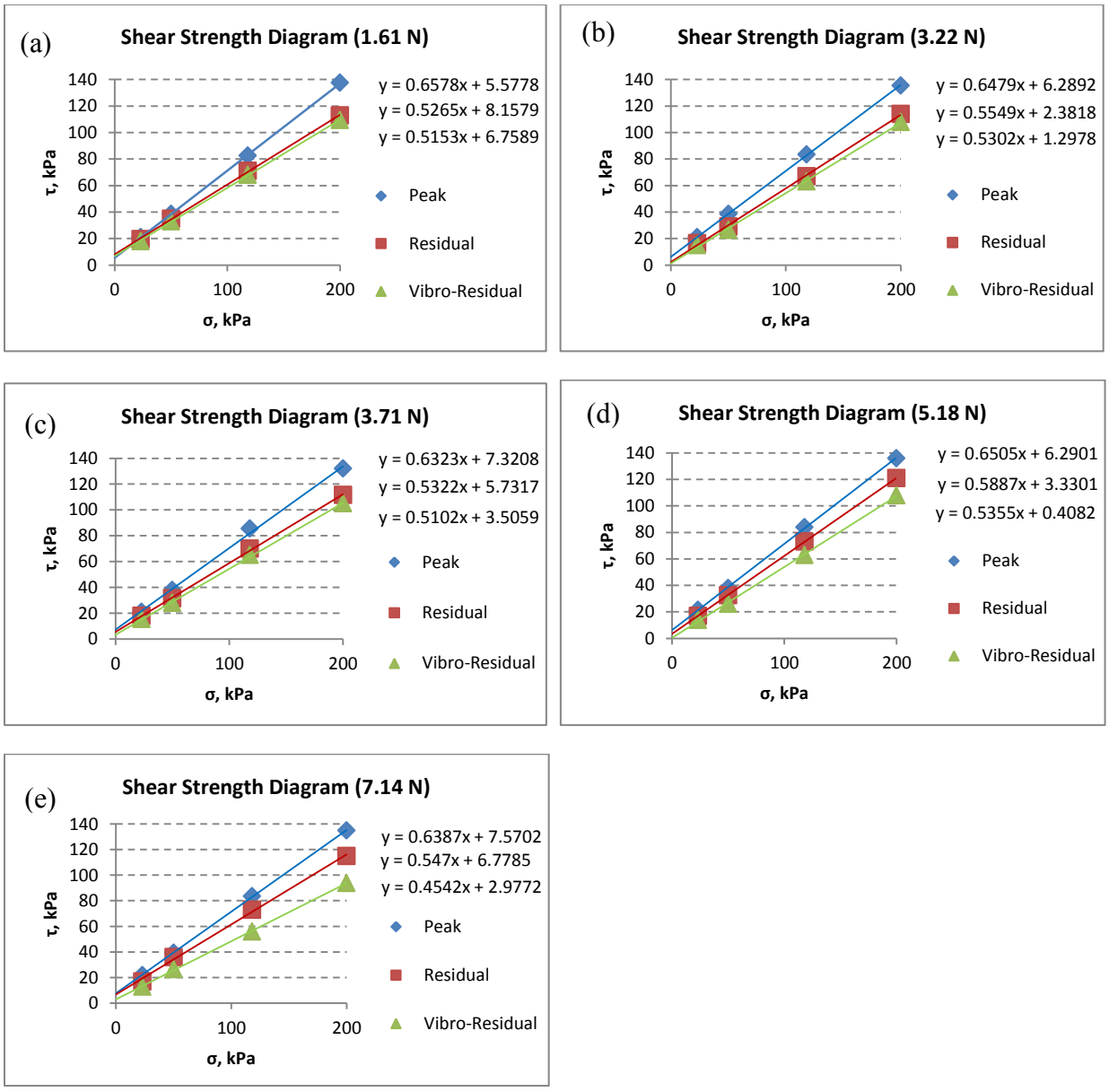

Figure 4.8 Shear strength envelops of 0.1 mm glass beads tested at: (a) vibration force of 1.61 N; (b) vibration force of 3.22 N; (c) vibration force of 3.71 N; (d) vibration force of 5.18 N and (e) vibration force of 7.14 N.

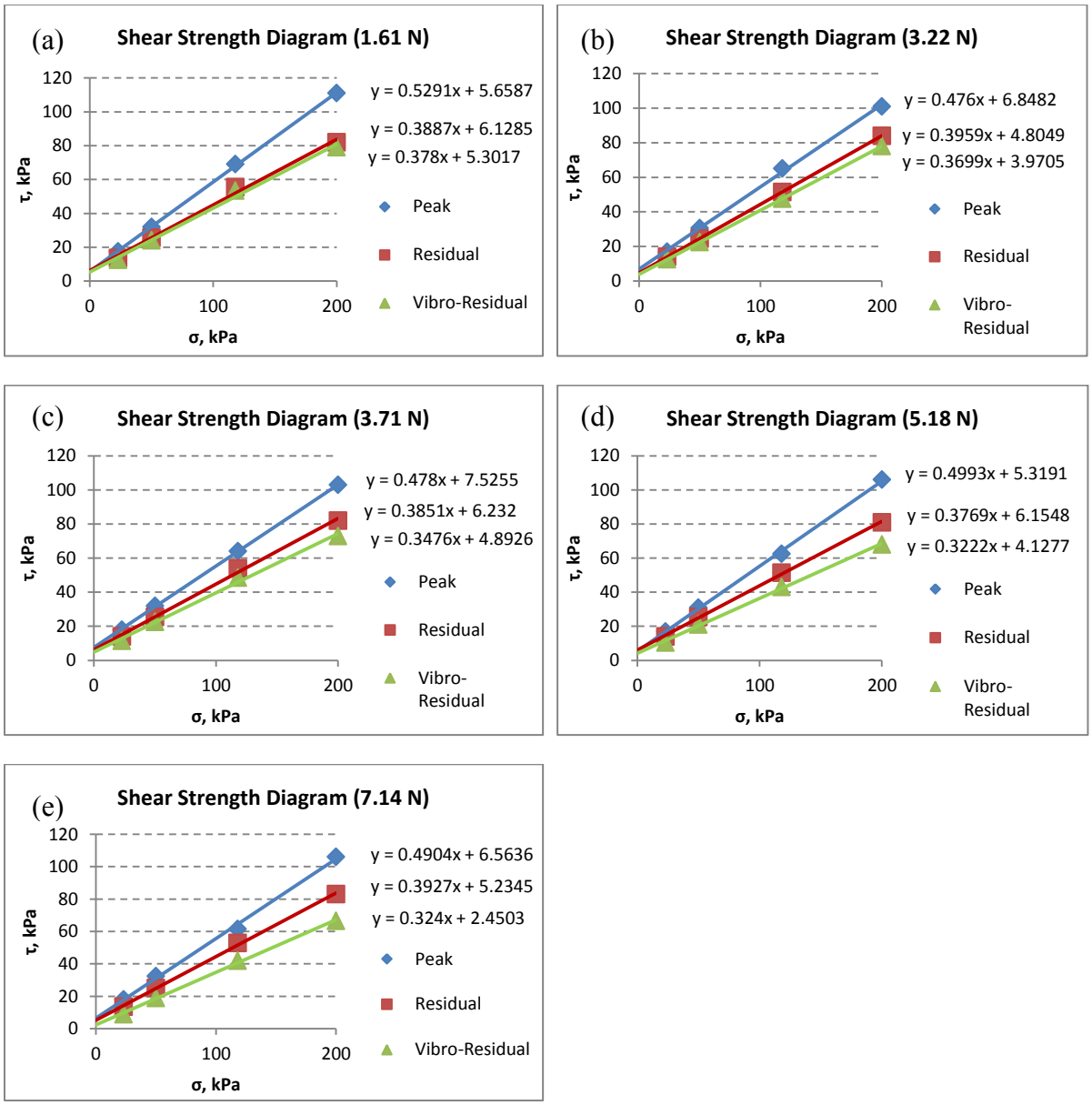

Figure 4.9 Shear strength diagrams of 0.55 mm glass beads tested at: (a) vibration force of 1.61 N; (b) vibration force of 3.22 N; (c) vibration force of 3.71 N; (d) vibration force of 5.18 N and (e) vibration force of 7.14 N.

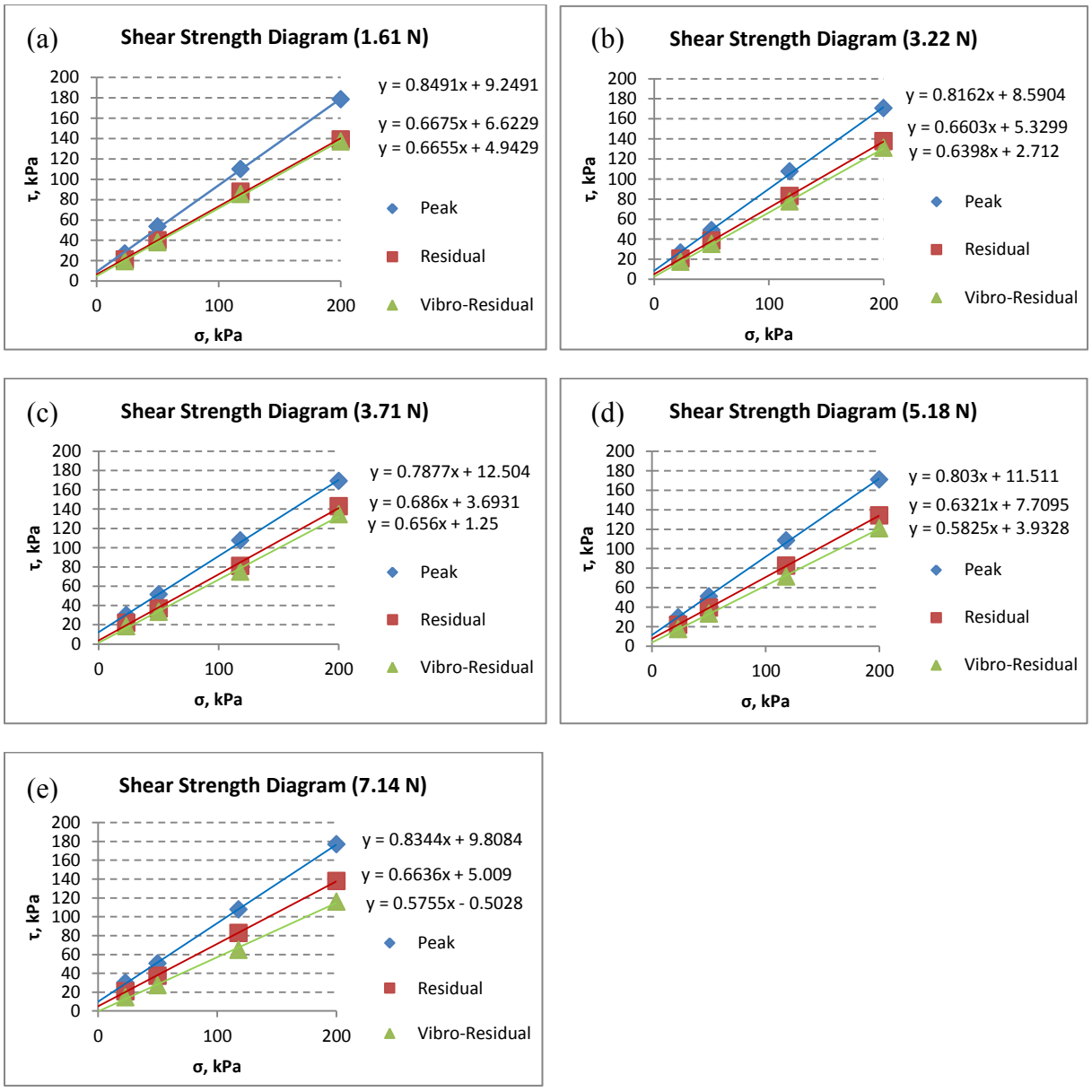

Figure 4.10 Shear strength diagrams of fine sand tested at: (a) vibration force of 1.61 N; (b) vibration force of 3.22 N; (c) vibration force of 3.71 N; (d) vibration force of 5.18 N and (e) vibration force of 7.14 N.

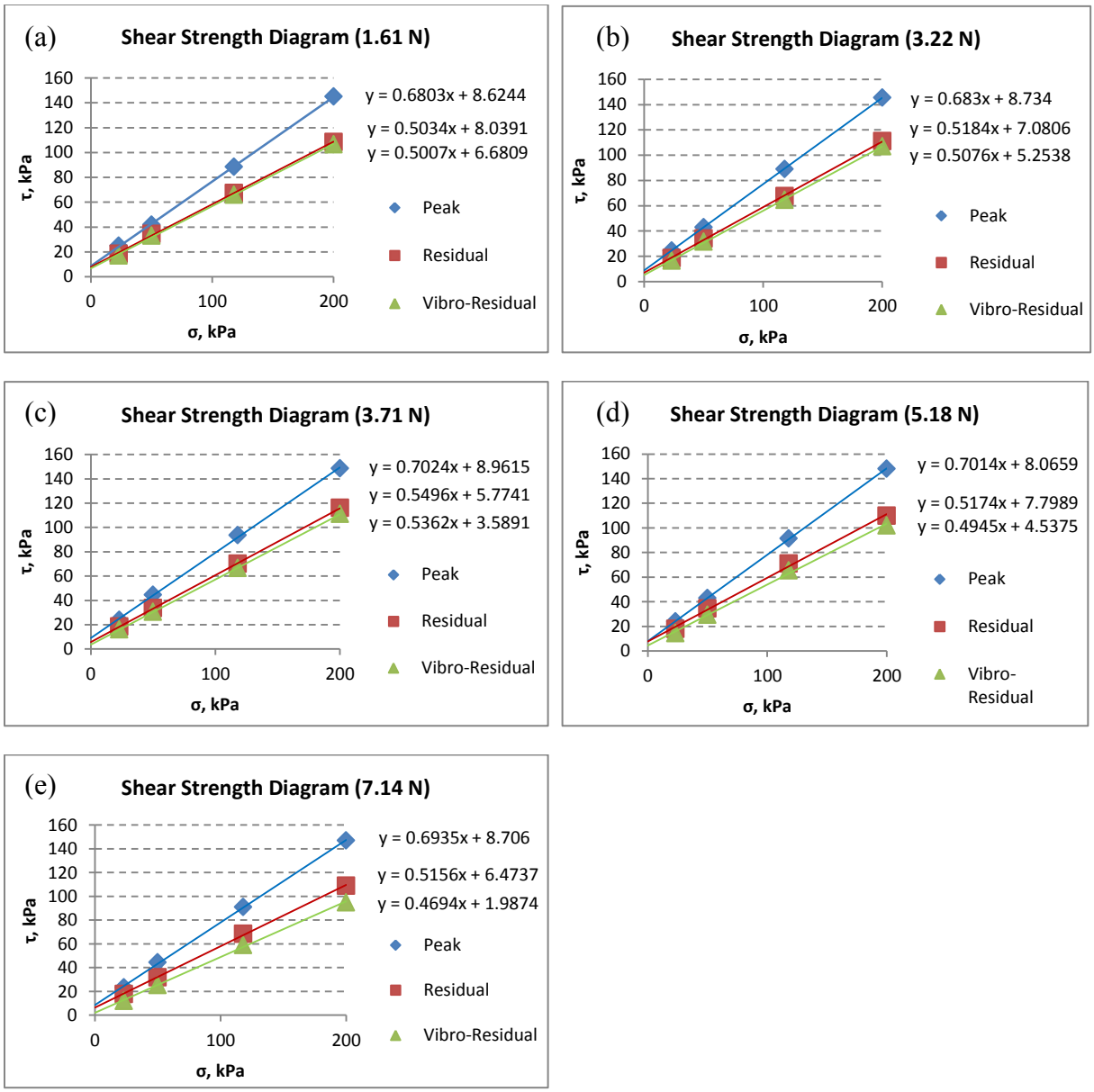

Figure 4.11 Shear strength diagrams of coarse sand tested at: (a) vibration force of 1.61 N; (b) vibration force of 3.22 N; (c) vibration force of 3.71 N; (d) vibration force of 5.18 N and (e) vibration force of 7.14 N.

Table 4.6 Friction angles of 0.1 mm glass beads.

Force (N)	ϕ (°)		
	Peak	Residual	Vibro-residual
1.61	33.3	27.8	27.3
3.22	32.9	29	27.9
3.71	32.3	28	27
5.18	33	30.5	28.2
7.14	32.6	28.7	24.4

Table 4.7 Friction angles of 0.55 mm glass beads

Force (N)	ϕ (°)		
	Peak	Residual	Vibro-residual
1.61	27.9	21.2	20.7
3.22	25.5	21.6	20.3
3.71	25.5	21.1	19.2
5.18	26.5	20.7	17.9
7.14	26.1	21.4	17.9

Table 4.8 Friction angles of fine sand

Force (N)	ϕ (°)		
	Peak	Residual	Vibro-residual
1.61	40.3	33.7	33.6
3.22	39.2	33.4	32.6
3.71	38.2	34.5	33.3
5.18	38.8	32.3	30.2
7.14	39.8	33.6	29.9

Table 4.9 Friction angles of coarse sand.

Force (N)	ϕ (°)		
	Peak	Residual	Vibro-residual
1.61	34.2	26.7	26.6
3.22	34.3	27.4	26.9
3.71	35.1	28.8	28.2
5.18	35	27.4	26.3
7.14	34.7	27.3	25.1

4.6.1 The Effect of Strength Loss Due to Changes in Normal Stress Caused by Vibration

Changes in the shearing resistance can be due to changes in the normal stress during vibration, per Maslov (1959). In this study, vertical acceleration is measured to calculate the normal stress that acts on a sample during vibration. From Newton's second law of motion (F = m a), when the vertical acceleration of the loading plate and the mass that acts on the loading plate are known, the force due to vibration can be calculated. By using the area (A) of the sample, the reduction in normal stress can be calculated from $\Delta\sigma = F/A$. If the $\Delta\sigma$ value is known and the residual shear strength diagram (equation) of the material is used, the strength loss $\Delta\tau`$ due to reduced normal stress $\Delta\sigma$ is obtained.

The measured total residual strength loss $\Delta\tau$ and the calculated residual strength loss $\Delta\tau`$ due to normal stress reduction caused by vibration are provided in Figs. 4.12 to 4.15, where $\Delta\tau$ is equal to the total strength loss, $\Delta\tau`$ is the strength loss due to reduction in normal stress σ, for samples tested at normal stresses of σ = 23, 50, 118 and 200 kPa, denoted by 1, 2, 3 and 4 respectively in the figures.

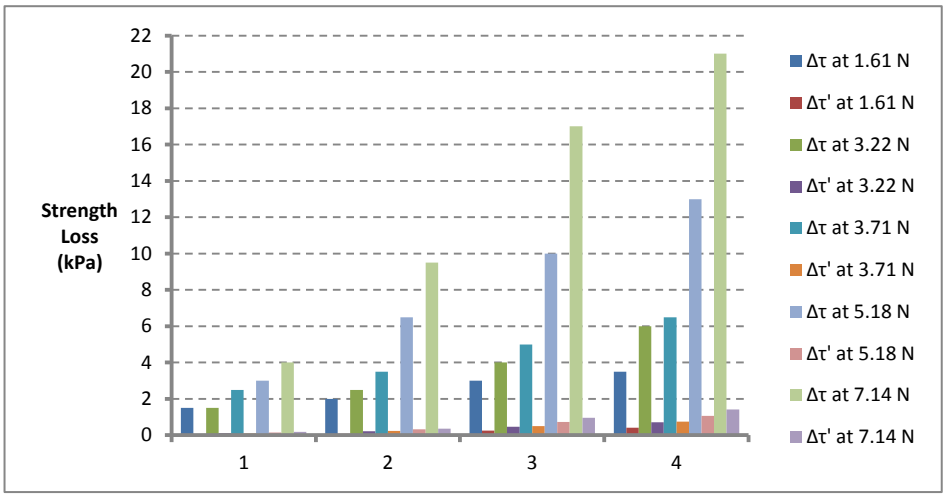

Figure 4.12 Total strength loss and strength loss due to reduced normal stress for 0.1 mm glass beads.

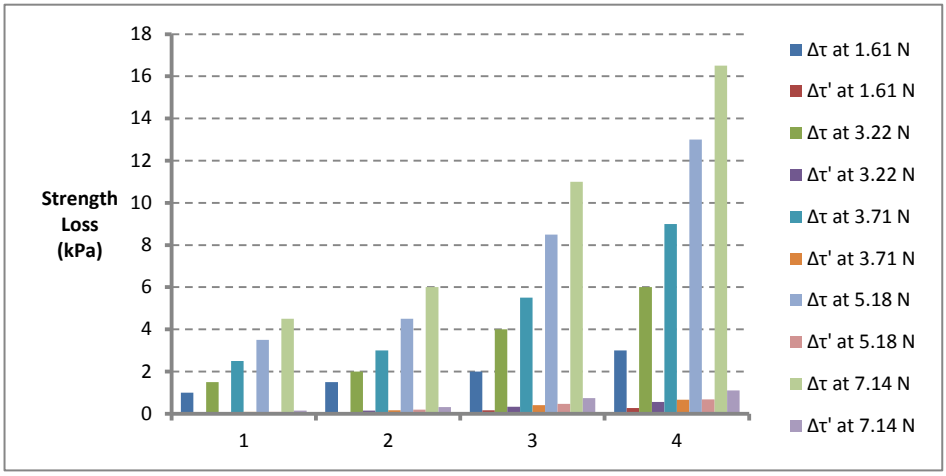

Figure 4.13 Total strength loss and strength loss due to reduced normal stress for 0.55 mm glass beads.

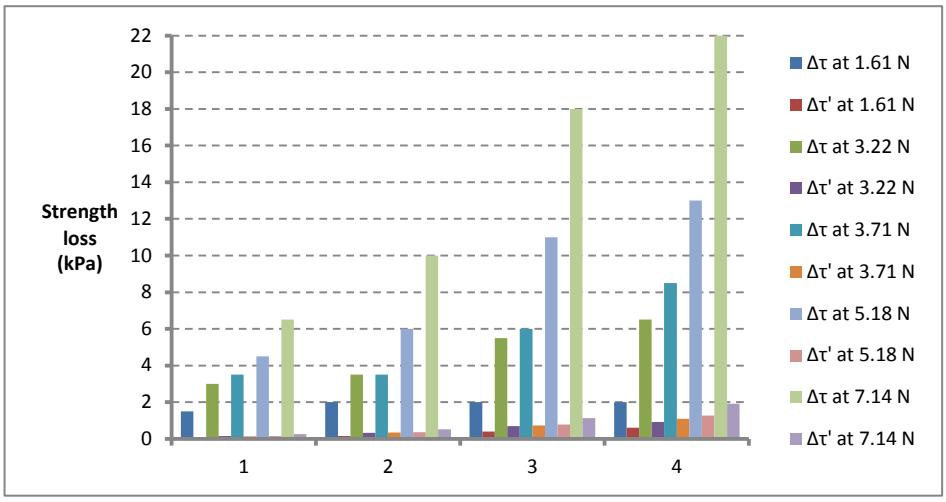

Figure 4.14 Total strength loss and strength loss due to reduced normal stress for fine sand.

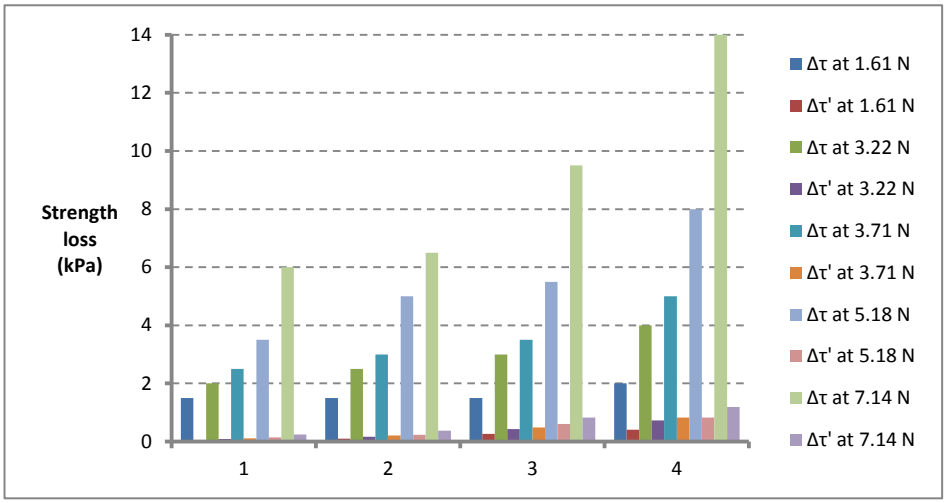

Figure 4.15 Total strength loss and strength loss due to reduced normal stress for coarse sand.

As seen in Figs. 4.12 to 4.15, the residual strength loss $\Delta\tau`$ due to a reduction in normal stress $\Delta\sigma$ caused by vibration for all of the materials is very small compared to the total strength loss $\Delta\tau$. Therefore, it can be concluded that although there is some reduction in normal stress due to vibration, the contribution to the loss in residual strength is minimal and the strength loss is mainly due to the material fluidization.

4.6.2 The Effects of Acceleration on Residual Strength Loss

Based on the data from Tables 4.2 to 4.5, the total residual strength loss is plotted against horizontal acceleration for the 0.1 mm and 0.55 mm glass beads, and fine and coarse sands, and the results are shown in Figs. 4.16 to 4.19. As seen in Figs. 4.16, 4.18 and 4.19, the effect of horizontal acceleration on the strength loss for the 0.1 mm glass beads, and fine and coarse sands is nonlinear under higher normal stresses of 50, 118 and 200 kPa. The relationship is practically linear at a low normal stress of σ = 23 kPa. Also, the plots become more nonlinear with an increase in the normal stress from 50 to 200 kPa. On the other hand, Fig. 4.17 shows that the relationship between strength loss and horizontal acceleration for the 0.55 mm glass beads is practically linear under all normal stress values (23, 50, 118 and 200 kPa). This can probably be explained by the absence of irregular shape particles in this material (see Fig. 4.4b). It was discussed earlier that the 0.1 mm glass beads are not round, but consisted of angular and irregular particles. This can be considered parallel to a mixture of fine angular sand and glass beads with a size up to 0.1 mm in diameter.

As mentioned above, the irregular shape of the particles that comprised the tested 0.1 mm glass beads, and fine and coarse sands, results in nonlinearity of horizontal acceleration vs. residual strength loss at higher normal stresses (50, 118 and 200 kPa). It is apparent from Figs.

4.16, 4.18 and 4.19 that unlike the plots of the samples tested at a normal stress of 23 kPa, the samples tested at higher normal stress values demonstrate less strength loss at low horizontal accelerations than they would if their plots were linear. This phenomenon can be explained by the additional friction among particles due to their irregular shape. The irregular shape of the particles generates greater shear resistance during their rotational and translational motions induced by relatively low vibration intensities.

On the other hand, the 0.55 mm glass beads practically have a round shape and unlike the other materials, they do not generate additional friction due to the irregular shape of the grains. Here, the round shape of the particles results in a linear pattern of the horizontal acceleration vs. residual strength loss at all normal stress values (23, 50, 118 and 200 kPa) as seen in Fig. 4.17.

It should also be noted that at higher horizontal acceleration, the strength loss of the 0.1 mm glass beads, and the fine and coarse sand samples notably increases. This implies that there is a certain value of the horizontal acceleration, above which, the effect of the irregular shape of the particles becomes insignificant.

Figs. 4.16 to 4.19 show estimates of strength loss due to vibration for different normal stresses and accelerations.

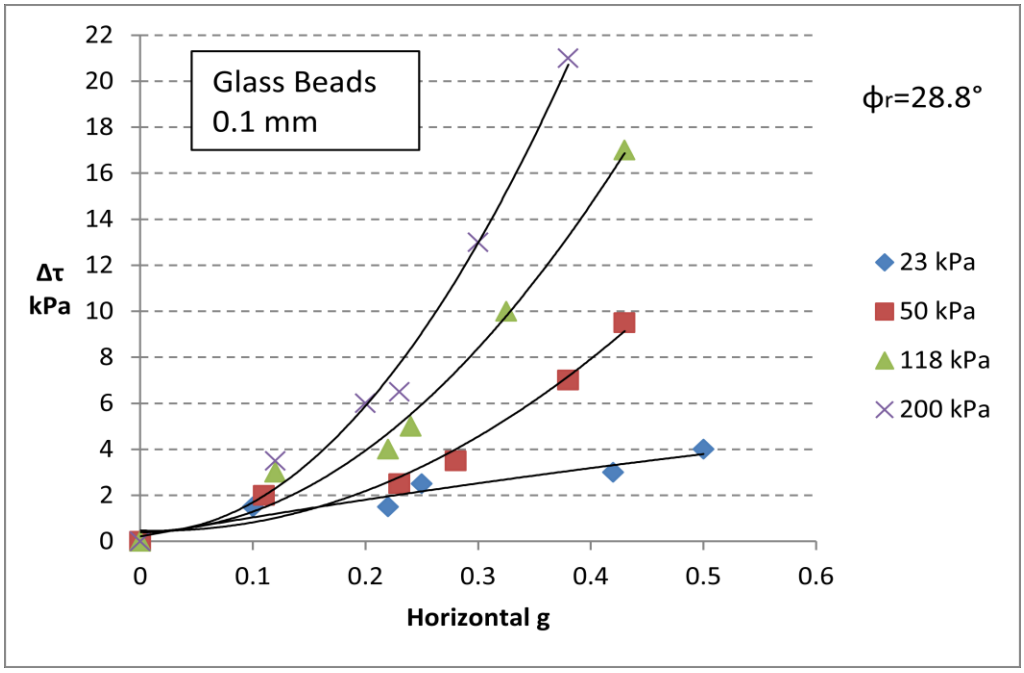

Figure 4.16 Total strength loss vs. horizontal acceleration of 0.1 mm glass beads

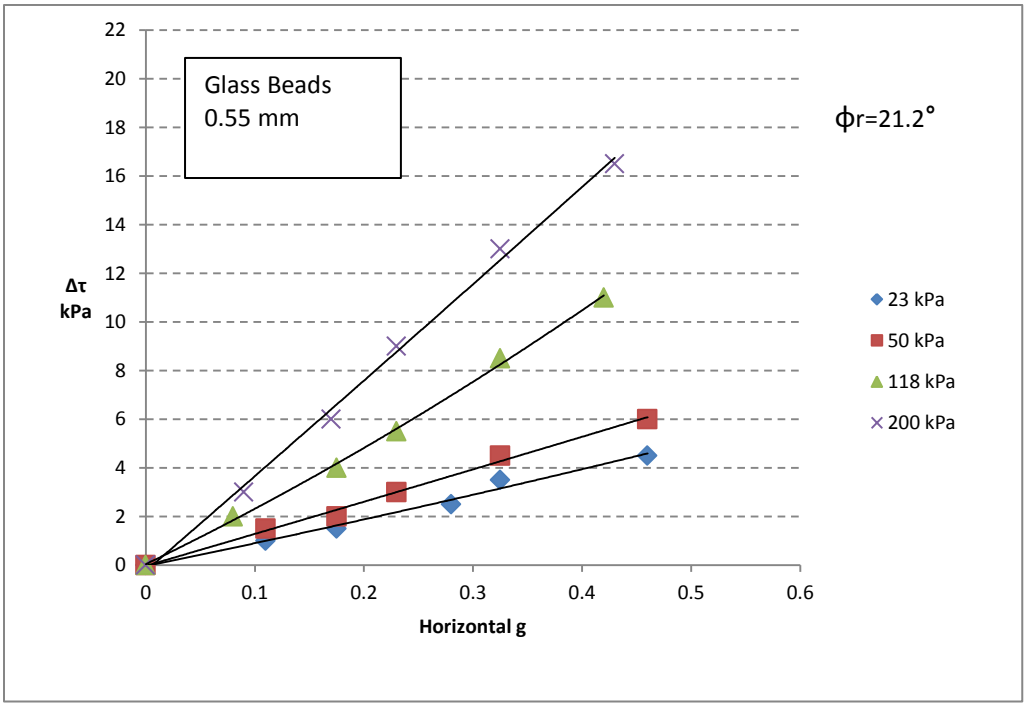

Figure 4.17 Total strength loss vs. horizontal acceleration of 0.55 mm glass beads

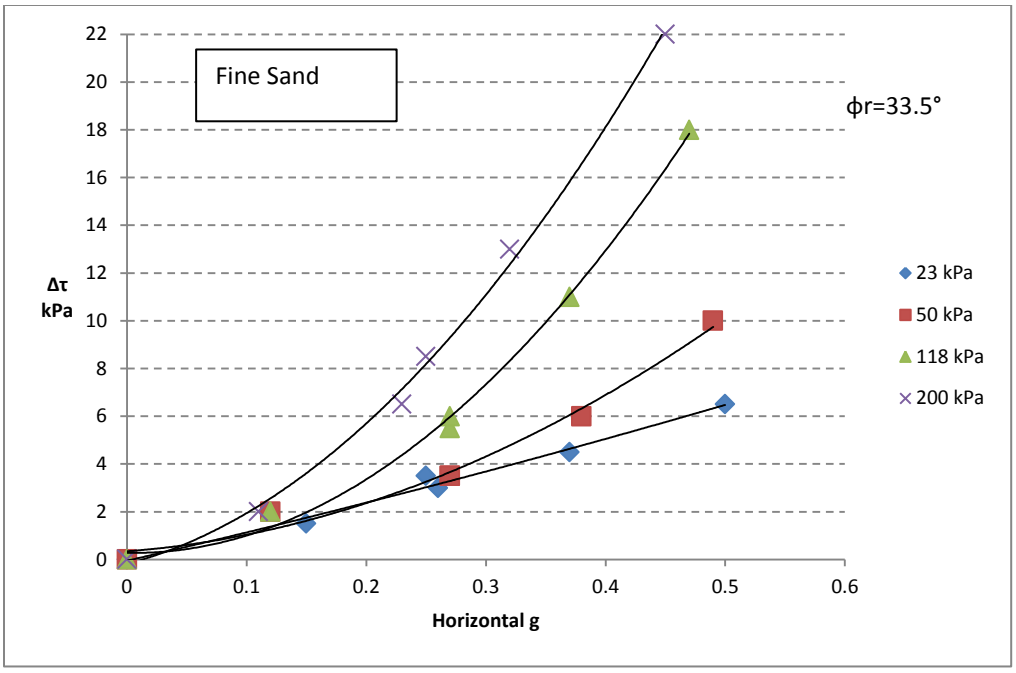

Figure 4.18 Total strength loss vs. horizontal acceleration of fine sand

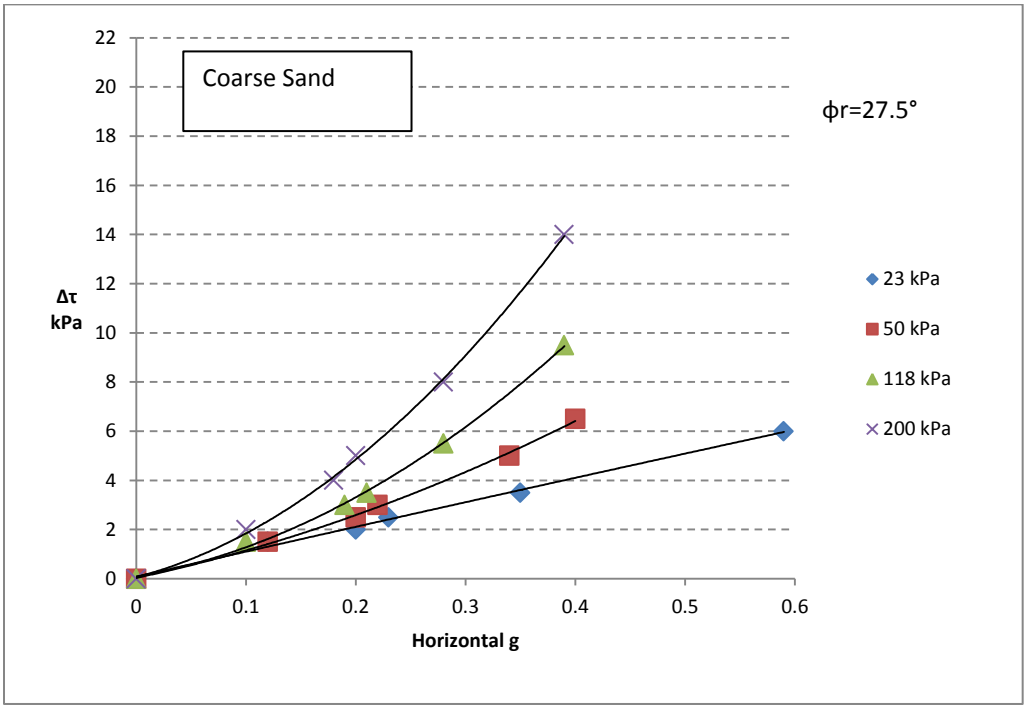

Figure 4.19 Total strength loss vs. horizontal acceleration of coarse sand

4.7 Conclusions

A new experimental technique and apparatus have been introduced in this paper to study the effect of vibration on the critical state strength of granular material. If the material is subjected to vibration after reaching the critical state, there is a decrease in volume and shearing resistance of the material. A decrease in volume implies compaction and a denser state, which usually lead to higher shear strength under static conditions. However, the shearing resistance of the material is reduced during vibration. Based on the test results of the 0.1 and 0.55 mm glass beads and the fine and course sands, the following conclusion can be made.

1. Upon application of a sufficiently strong vibration at the critical strength state of a granular material, an immediate strength loss takes place for the residual to vibro-residual strengths, after which the vibro-residual strength remains practically constant during vibration.
2. Vibration does not have any permanent post-vibrational effects on the residual strength of granular material, provided that there is sufficient shear displacement of the material after termination of the vibration.
3. Initially dense or loose granular material compresses when vibration is applied at its critical strength state.
4. At a constant vibration frequency, an increase in vibration force results in an increase in the vertical and horizontal vibration accelerations and amplitudes, which in turn, results in a greater residual strength loss at the given normal stress.
5. Sufficiently strong vibration reduces the residual friction angle; that is, the magnitude of the residual strength loss increases with an increase in the normal stress.
6. The residual strength loss $\Delta\tau`$ due to the normal stress reduction caused by vibration for all of the granular materials tested is small compared to the total loss in residual strength $\Delta\tau$.

Therefore, it can be concluded that although normal stress reduction caused by vibration (in the given range of accelerations) contributes to residual strength loss, the strength loss is mainly due to material fluidization.

7. For a given test condition, the relationship between the residual strength loss and horizontal acceleration is nonlinear for irregularly shaped particles. The nonlinearity increases with an increase in confining (normal) stress.
8. For a given test condition, the relationship between the residual strength loss and horizontal acceleration is linear for glass beads (0.55 mm) with spherical shape particles under all normal stresses tested.

4.8 References

Bagnold, R. A. (1954). "Experiments on the Gravity-Free Dispersion of Large Solid Spheres in a Newtonian Fluid Under Shear". Proc. Royal Soc. London 225. pp. 49–63.

Barkan, D. D. (1962). "Dynamics of Basis and Foundations". Translated from Russian by L. Drashevska, New York, McGraw-Hill, 434 p.

Bjerrum, L., Kringstad, S. and Kummeneje, O. (1961). "The Shear Strength of a Fine Sand". Proc. 5th Int. Conf. Soil Mech. and Found. Eng. pp 29–37.

Bougie, J. L. (2004) Continuum Simulations of Fluidized Granular Materials. The University of Texas, Austin.

Das, B. M. (2011). "Principles of Soil Dynamics", Second Edition. Cengage Learning, 563

Davies, T. R. H. (1982). “Spreading of Rock Avalanche Debris by Mechanical Fluidization”. Rock Mechanics 15; Springer-Verlag, pp. 9-24.

Housner, G. W. (1954). “Geotechnical problems of destructive earthquakes”. Geotechnique, December.

Housner, G. W. (1959). “Behavior of structures during earthquakes”. Journal of the Engineering Mechanics Division, ASCE, 85, No. EM-4.

Huan, C. (2008) NMR Experiments on Vibrofluidized and Gas Fluidized Granular Systems. PhD Thesis, University of Massachusetts Amherst.

Hungr, O. (1981). “Dynamics of Rock Avalanches and Other Types of Slope Movements”. PhD Thesis, University of Alberta, 506 p.

Idriss, I. M. and Boulanger, R. W. (2008). “Soil liquefaction during earthquakes”. Earthquake Engineering Research Institute, Oakland, California.

Ingale, R. A. (2008). Dynamics of vibrated granular matter. PhD Thesis, The City University of New York.

Jaeger, H. M., Nagel, S. R. and Behringer, R. P. (1996). Granular solids, liquids, and gases. Rev. Mod. Phys. 68, 1259.

Youd, L. T. (1968) Reduction of critical void ratio during steady-state vibration. International symposium on wave propagation and dynamic properties of earth materials, Albuquerque, N. Mex., 1967, Proc.

Maslov, N. N. (1959). “Stability Conditions of Saturated Sands”. (Russian: Usloviya Ustoychivosti Vodonasishennikh Peskov). M. – L. Gosenergoizdat. 328 p.

Meehan, C. L., Boulanger, R. W., and Duncan, J. M. (2008). "Dynamic Centrifuge Testing of Slickensided Shear Surfaces", Journal of the Geotechnical Engineering Division, American Society of Civil Engineers (month), Vol. 134, No. 8, pp. 1086-1096

Melhus, M. F. (2011). Effects of Noise and Vibration on the Solid to Liquid Fluidization Transition in Small Dense Granular Systems under Shear. PhD Thesis. Northwestern University, Evanston, Illinois.

Melosh, H. J. (1979). “Acoustic Fluidization: A New Geologic Process?” Journal of Geophysical Research, v. 84: pp. 7513-7520.

Melosh, H. J. (1996). Dynamical weakening of faults by acoustic fluidization, Nature, 379, pp. 601-606.

Metcalfe, C., Tennakoon, S. G. K., Kondic, L., Schaeffer, D. G. and Behringer, R. P. (2002). Granular Friction, Coulomb Failure, and the Fluid-Solid Transition for Horizontally Shaken Granular Materials. Physical Review E - Statistical, Nonlinear, and Soft Matter Physics.

Pokrovsky, G. I., Ehrlich, A. A., Laletin, N. V. and Lush, F. A. (1934). New Methods of Investigation of the Compressibility and Internal Friction in Soils. Vestnik Voyenno-Inzhenernoy Akademii RKKA, no. 6.

Pyke, R., Seed, H. B. and Chan, C. K. (1975). “Settlement of sands under multidirectional shaking”. Journal of Geotechnical Engineering Division, ASCE, 101, GT-4, pp.379-398.

Richards, R., Jr., Elms, D. and Budhu, M. (1990). "Dynamic Fluidization of Soils." Journal of Geotechnical Engineering, 116(5), pp. 740–759.

Richart, F. E. (1970). "Vibrations of Soils and Foundations". Prentice-Hall, 414 p.

Robertson, P. K. and Campanella, R. G. (1985). "Liquefaction potential of sands using the CPT". Research Report R69-15, Dept. of Civil Engineering, Massachusetts Institute of Technology, Cambridge, Mass.

Robertson, P. K. and Campanella, R. G. (1986). "Estimating liquefaction potential of sands using the flat plate dilatometer". Geotechnical Testing Journal, 9, No. 1, pp. 38-40.

Sangroya, R. and Choudhury, *D.* (2013). "Stability Analysis of Soil Slope Subjected to Blast Induced Vibrations Using FLAC3D", Geo-Congress 2013, pp. 472-481

Savchenko, I. A. (1958). "Effect of Vibrations on Internal Friction in Sand". Symposium, Soil Dynamics, Moscow, Gosstroiizdat, No. 2.

Seed, H. B. (1966). "A method for earthquake resistant design of earth dams". Journal of the Soil Mechanics and Foundation Division, ASCE, 92, No. SM-1, pp. 13-41.

Seed, H. B. and Idriss, I. M. (1982). Ground motions and soil liquefaction during earthquakes. Monograph series, Earthquake Engineering Research Institute, Berkeley, California.

Seed, H. B. and Idriss, I. M. (1983). Evaluation of liquefaction potential using field performance data. Journal of Geotechnical Engineering, ASCE, 109, No. 3, pp. 458-482.

Shibata, T. and Yukitomo, H. (1969). "Liquefaction Process of Sand during Cyclic Loading". Soils and Foundations, Vol. 3, pp. 54-69.

Sornette, D. and Sornette, A. (2000). "Acoustic Fluidization for Earthquakes?". Bulletin of the Seismological Society of America, 90, 3, pp. 781-785.

Wartman, J., Seed, R. B. and Bray, J. D. (2005). "Shaking table modeling of seismically induced deformations in slopes." J. Geotech. Geoenviron. Eng., 131(5), pp. 610–622.

Wassgren, C. R. (1997). Vibration of granular materials. PhD Thesis, California Institute of Technology, Pasadena, California.

5. Chapter 5: Vibrational Fluidization of Granular Media

5.1 Abstract

To investigate the vibrational fluidization of granular media, sixty samples of three different granular materials are tested at six normal stresses and a wide range of vibration accelerations. The experiments are conducted on a modified vibrating direct shear apparatus, where vibration is horizontally applied in the direction of shear. The peak, residual and vibro-residual shear strength envelops are obtained for the tested materials at different vibration intensities. It has been determined that increasing vibration intensity reduces the friction angle of the granular materials, as well as increases the value of the normal stress, σ_f, below which, the granular material is fluidized. The particle shape effect on strength loss due to vibration has also been observed, and a reduction in the friction angle and increase in the σ_f with an increase in vibration acceleration are found.

5.2 Introduction

There are two important aspects that contribute to the unique properties of granular materials: ordinary temperature plays no role on their mechanical behaviour, and the interactions between grains are dissipative because of static friction and the inelasticity of collisions (Jaeger et al., 1996). Granular material can behave like solids, fluids and even gas under different conditions. When sufficient energy is supplied to a granular material in a vibrating system, the granular material can exhibit fluid-like behavior. This transition from a solid state to a liquid state (fluidization) takes place when vibrational acceleration, *a*, exceeds a certain critical value.

For example, when vibration is applied in the vertical direction, fluidization takes place at an *a* that is greater than 1 g (Huan, 2008). Further increases in the vibration acceleration changes the behavior of the granular material to that of a gas. Jaeger et al. (1996) described the three aforementioned states of granular materials.

When granular materials are subjected to strong enough vibration intensities, various phenomena, such as compaction (e.g. Barkan (1962), Ayer and Soppet (1965/1966)), swelling (e.g. Poschel and Rosenkranz (1998)), mixing (e.g. Alexeev et al. (2000)), localized excitations (e.g. Umbanhowar et al. (1996), Tsimring and Aranson (1997)), convective flow (e.g. Laroche et al. (1989), Evesque and Rajchenbach (1989), Gallas et al. (1992), Pak et al. (1995) and Huan (2008)), Bourzutschky and Miller (1995), Wassgren (1997) and Liffman et al. (1997)), size segregation (e.g. Knight et al. (1993), Cooke et al. (1996) and Alexeev et al. (2000)) and surface wave formation (e.g. Pak and Behringer (1993), Melo et al., (1993 and 1995), Clement et al. (1996), Brone and Muzzio (1997), and Mujica and Melo (1998)) can be observed. Although the above mentioned processes have been well investigated, there are very few, if any, studies done on the effect of normal stress on the vibrational fluidization of granular materials.

Richards et al. (1990) proposed the concept of "dynamic fluidization" which takes into consideration the effect of earthquake accelerations on dry granular soils. The imposed accelerations at some critical level change the state of the soil, which causes general plastification, such that the soil becomes, in a sense, an anisotropic fluid. They assumed that the main trigger of the fluidization is the inertial forces that act between the particles of a granular soil. They showed that fluidization mainly depends on horizontal and not vertical accelerations. Another distinguishing feature of fluidization is that when it occurs, flow takes place, if at all, in

finite increments rather than continuously, with increments that correspond to the acceleration pulses of an earthquake above a critical value (Richards et al., 1990).

Other researchers who investigated vibro-fluidization of granular materials are Savage (1988), Fauve et al. (1989), Doudy et al. (1989), Zik et al. (1992), Lan et al. (1995), Warr et al. (1995), Goldstein et al. (1995), Luding (1995), Ristow et al. (1997), Tennakoon et al. (1998), Falcon et al. (1999), Sunthar et al. (2001), Moon et al. (2004) and Gotzendorfer et al. (2006).

The objective of the conducted laboratory experiments outlined below is to investigate the effect of vibration intensity, normal (confining) stress and particle shape on the fluidization phenomenon of dry granular media. The following series of tests is a continuation of an experimental program conducted earlier with the use of similar testing equipment and procedures.

5.3 Testing Equipment and Procedures

In order to investigate the vibrational fluidization of granular materials, a direct shear apparatus was modified into a vibrating direct shear apparatus (Taslagyan et al., 2014[1]) as shown in Figs. 5.1 and 5.2. The modifications include installation of an electromagnetic actuator (11) between the proving ring (3) and the shear box (2), as well as two load cells (10 and 12) for shear force measurement at the top and bottom halves of the shear box (2). An extension (13) is added to the main body (5) to accommodate all of the additional components. The actuator (11) has two electromagnets, which generate vibrations in the horizontal shearing direction. The frequency and intensity of the vibrations were controlled by using a control panel (not shown in Fig. 5.1).

The measuring equipment consisted of two linear variable differential transformers (LVDTs) that measured the vertical and horizontal displacements, two load cells (10 and 12),

and two uniaxial accelerometers that measured the vertical and horizontal vibration accelerations on the soil samples. One of the accelerometers was placed on top of the loading plate (measured vertical vibration accelerations), and the other accelerometer was attached to the top half of the shear box in the direction of the shear (measured horizontal vibration accelerations). The output signals were acquired by using the NI CompactDAQ System, which was in turn, connected to a PC that logged the data with NI LabVIEW software.

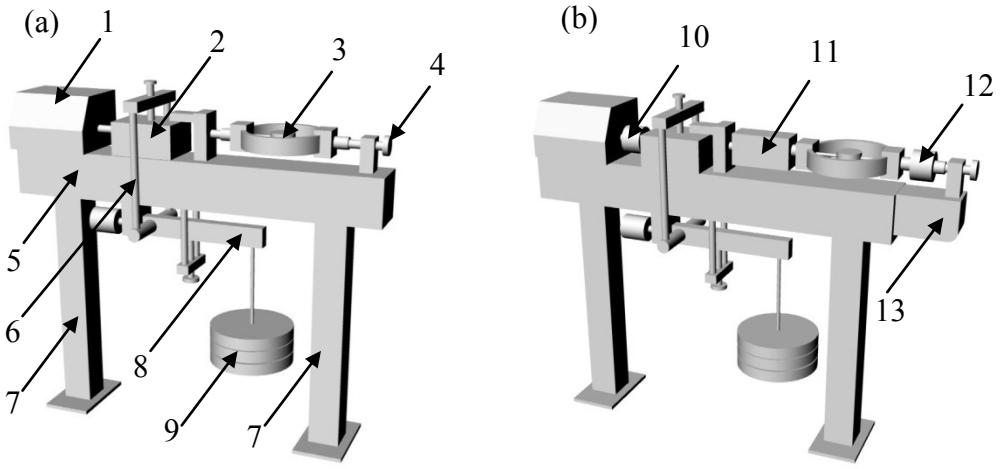

Figure 5.1 (a) – Strain controlled direct shear apparatus (LVDTs that measured the vertical and shear displacements are not shown for simplicity) and (b) – modified strain controlled vibrating direct shear apparatus.

1 – Control panel of the direct shear apparatus; 2 – Shear box with a soil sample; 3 – Proving ring; 4 – Screw for zero setting of shear load before starting a test; 5 – Main body of the direct shear apparatus; 6 – Frame that transfers normal load to the soil sample placed in the shear box (2); 7 – Legs of the direct shear apparatus that supports the main body (5); 8 – lever that provides a normal load to the soil sample; 9 – Weights that define a normal load on the soil sample; 10 –

Load cell; 11 –Actuator; 12 – Load cell; and 13 – Extension of the main body (5) of the direct shear apparatus.

The testing procedures were carried out in accordance with ASTM D3080/D3080M (Standard Test Method for Direct Shear Test of Soils Under Consolidated Drained Conditions), with additional vibration applied for a short period of time at the pre-peak and residual strength states. Depending on the objective of the test, vibrations were applied while the sample was being sheared, as well as when shearing was terminated. The frequency and force of the vibrations were adjusted to the required magnitude and kept constant for the set of soil samples tested.

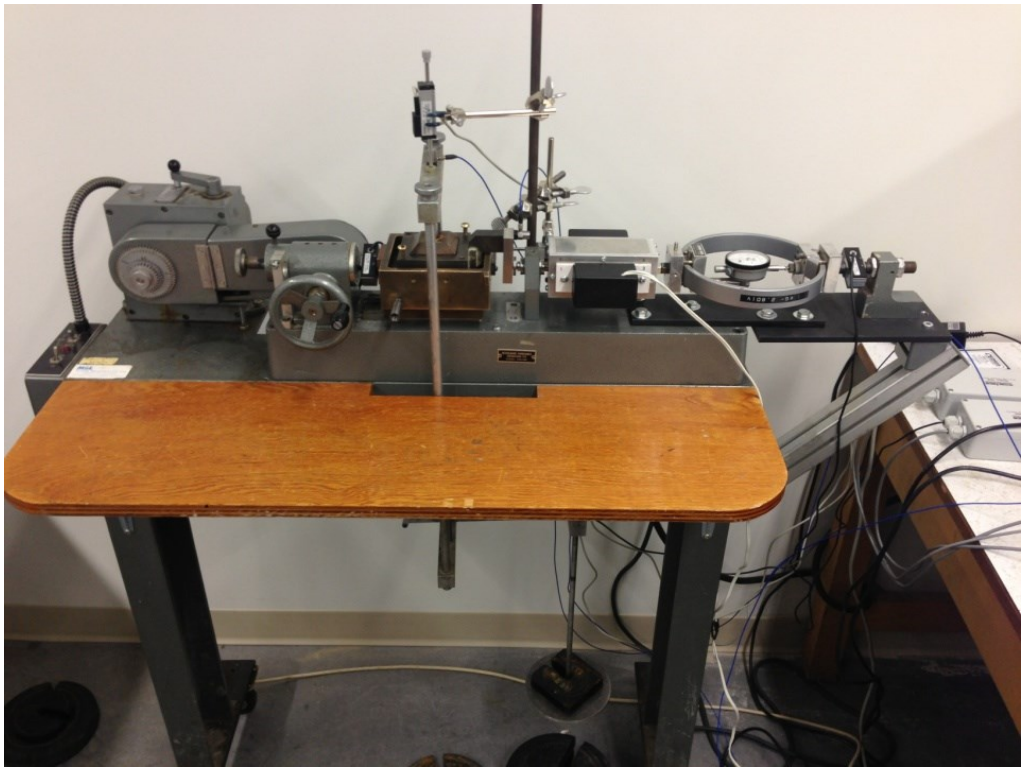

Figure 5.2 Modified direct shear apparatus.

5.4 Tested Materials

In order to investigate the effect of vibrating on the shear zone in granular materials, three different dry granular materials (a total of 60 samples) were tested on the modified direct shear apparatus. The tested materials were 0.55 mm glass beads, as well as fine and coarse sands. The samples filled a shear box with dimensions of 6 cm x 6 cm x 3.2 cm (W x L x H), after which, a constant compaction effort was applied to the samples which brought them to a dense state and similar density. The samples were tested at normal stresses of 8, 23, 36, 50, 118 and 200 kPa in strain-controlled mode at a shear rate of 0.61 mm/min. The vibration frequency was 60 Hz for all of the samples that were being tested. Four sample sets of the 0.55 mm glass beads (six samples each), as well as three sample sets of the fine and coarse sand were tested at different vibration intensities. The sensor data were logged at a frequency of 1 kHz.

The highest normal stress did not exceed 200 kPa to avoid grain crushing. Low normal stresses (8, 23 and 36 kPa) were used to obtain realistic experimental evidence of material fluidization at low normal (confining) stresses.

The physical characteristics of the tested materials are provided in Table 5.1. The particle size distributions of the three materials are given in Fig. 5.3. Representative samples of the materials were observed under a microscope to determine the shape of the particles (see Figs. 5.4a, 5.4b and 5.4c). As can be seen in the photographs in Fig. 5.4a, the 0.55 mm glass beads have a practically ideal spherical shape. From Figs. 5.4b and 5.4c, it can be concluded that the fine sand particles have an angular shape and the coarse sand is well rounded.

Table 5.1 Physical characteristics of the tested materials.

Material	ρ_s	ρ	e	n
Glass Beads	2.65	1.566	0.692	0.409
Fine Sand	2.65	1.460	0.815	0.449
Coarse Sand	2.65	1.755	0.510	0.338

The three materials were chosen because of their different particle shapes in order to investigate the particle shape effect on the vibrational fluidization of granular materials. A material with round and angular particle shape was selected to obtain a wide range of residual friction angles (φ_r from 21.2^o to 32.2^o), and the well rounded coarse sand (with φ_r = 29.7^o) was chosen as a material with an intermediate friction angle to determine the reliability of the approximation of the experimental results for granular materials which have a residual friction angle in the range of 21.2^o to 32.2^o.

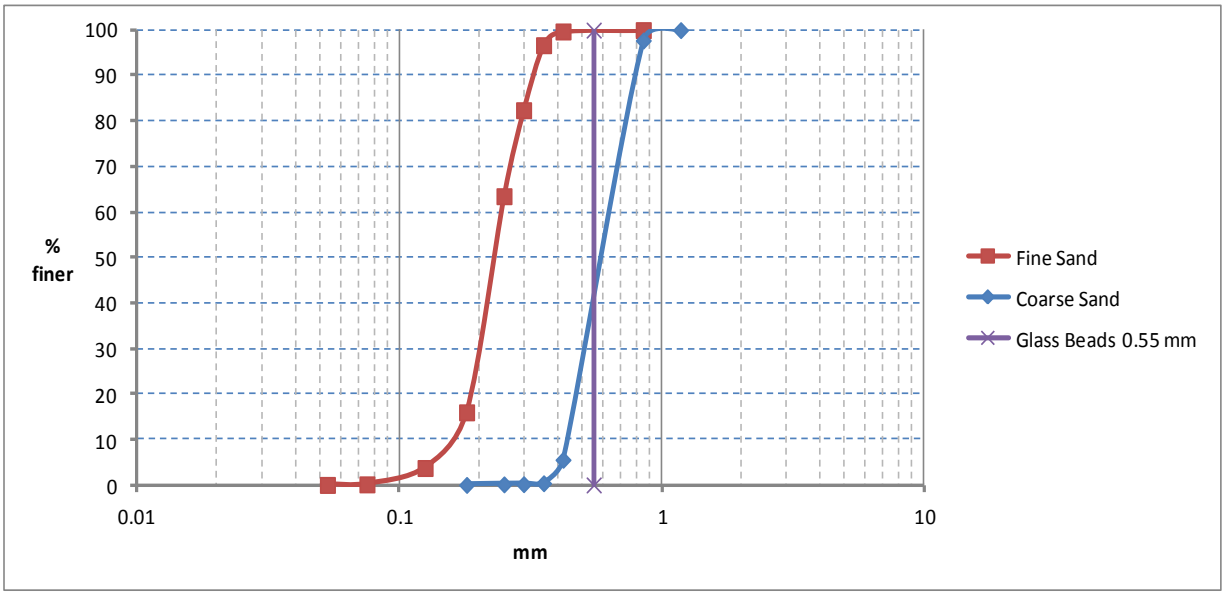

Figure 5.3 Particle size distribution of the tested materials.

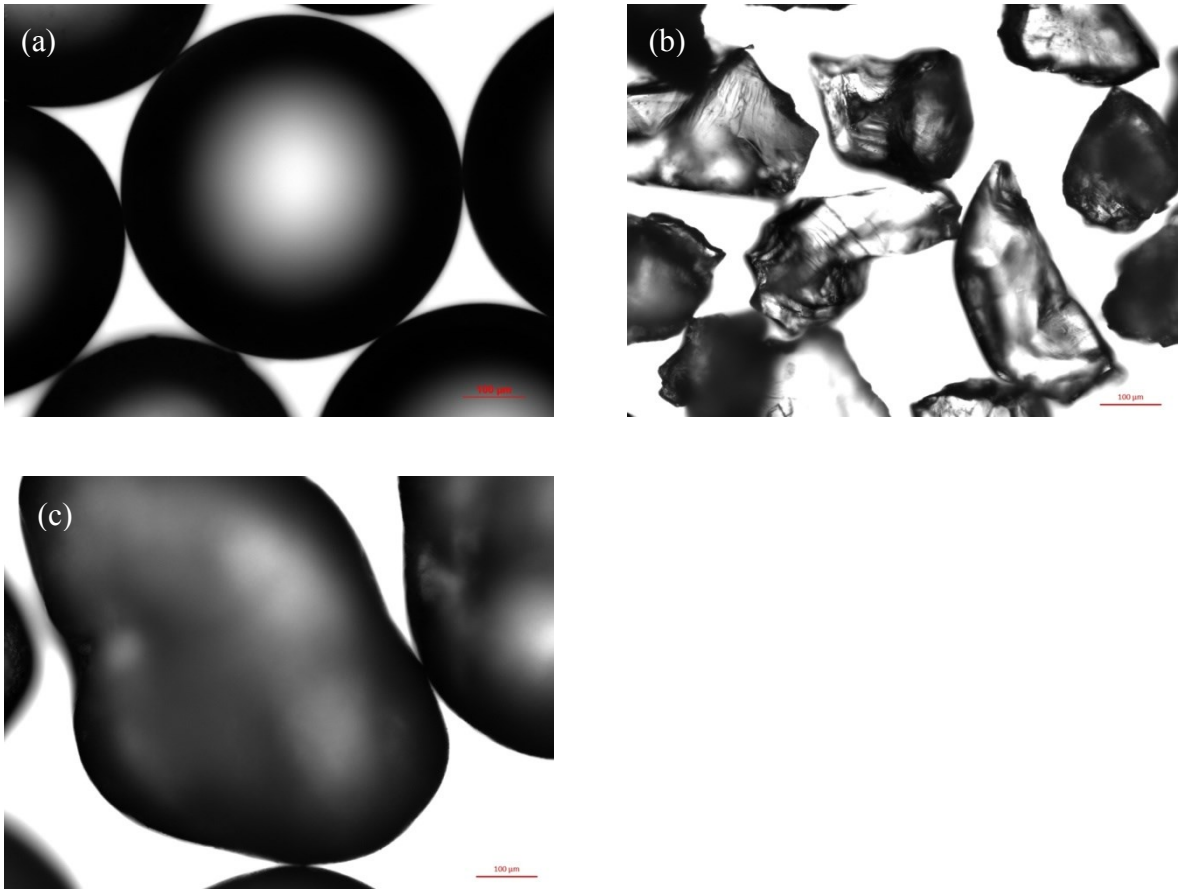

Figure 5.4 Photographs of the glass beads and sand samples under a microscope at magnification of 50x. (a) - 0.55 mm glass beads; (b) - fine sand; and (c) - coarse sand

(scale bar on the right bottom corner is 0.1 mm in length)

5.5 Test Results

The results of the laboratory experiments conducted on the glass beads, and fine and coarse sands are summarized in Tables 5.2, 5.3 and 5.4, respectively, where $\Gamma_{h\text{-}av}$ is the average relative horizontal acceleration, σ is the normal stress, τ_p is the peak strength, τ_r – residual strength, τ_{rv} – vibro-residual strength, Γ_h –relative horizontal acceleration, Γ_v –relative vertical acceleration, and $\Delta\tau$ – strength loss for the residual to the vibro-residual strengths.

The relative acceleration, Γ, mentioned above, is a dimensionless parameter and defined as:

$$\Gamma = A\omega^2/g \qquad [1]$$

where A is the vibration amplitude, ω is the vibration frequency and g is the gravitational acceleration.

The values given in Tables 5.2, 5.3 and 5.4 were taken from the plots of the sensor readings. An example of such is provided in Fig. 5.5. The shear resistance plots were obtained from the load cell that measured the shear force at the top half of the shear box (see Figs. 5.1 (b) – 12). The vertical displacement plots were constructed from the measurements of an LVDT located on the loading plate of the shear box. The horizontal and vertical acceleration plots were created from an accelerometer that measured the horizontal accelerations at the top half of the shear box in the direction of shear, and a second accelerometer that measured the vertical accelerations of the loading plate, respectively.

All of the data, except for vertical displacement, were collected at a frequency of 1 kHz. Due to the technical characteristics of the LVDT, vertical displacements were plotted based on 2 Hz data filtered from the original 1 kHz records.

As seen in Fig. 5.5, vibration is applied when the samples have reached their residual strength. The shear resistance plot shows that upon the application of vibration, an immediate strength loss of shearing resistance $\Delta\tau$ takes place for the residual to the vibro-residual strengths. When vibration is terminated, the strength of the sample gradually increases and reaches the residual strength value. All of the tested samples experienced compression (compaction) due to vibration (e.g. see Figs. 5.5, 5.11 – 5.19). Note that the normalized displacement in the plots of Figs. 5.5, 5.11 – 5.19 is defined as $\Delta d/L$, where Δd is the horizontal displacement and L is the initial length of the specimen.

The peak, residual and vibro-residual shear strength diagrams of the glass beads, as well as those of the fine and coarse sand samples tested at different vibration intensities, are provided in Figs. 5.6 (a, b, c, d), 5.7 (a, b, c) and 5.8 (a, b, c), respectively. The residual and vibro-residual friction angles of the three materials tested at different vibration intensities are given in Table 5.5.

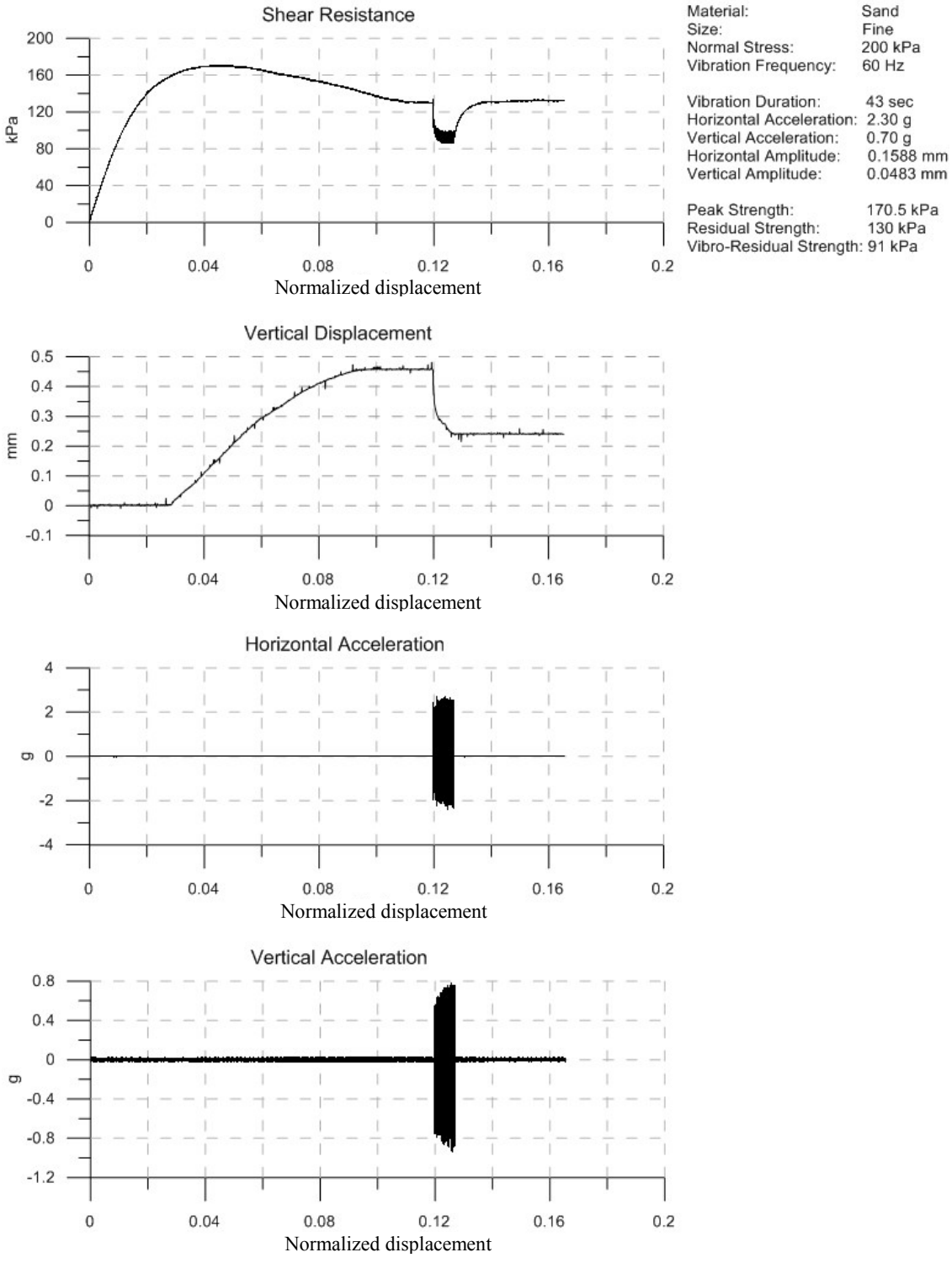

Figure 5.5 An example of test results of a fine sand sample tested at σ=200 kPa, ω=60 Hz and Γ_h=2.3.

Table 5.2 Test results of glass beads.

$\Gamma_{h\text{-}av}$	σ	τ_p	τ_r	τ_{rv}	Γ_h	Γ_v	$\Delta\tau$
0.44	**8**	8	6	2	0.4	0.04	4
	23	16	12.5	7	0.55	0.08	5.5
	36	22	19	12.5	0.35	0.15	6.5
	50	29	24	17	0.5	0.15	7
	118	63.5	53	38	0.44	0.13	15
	200	107	85	66	0.4	0.11	19
1.38	**8**	8	6	0	1.55	0.3	6
	23	16	12.5	4	1.4	0.2	8.5
	36	23	18.5	6.5	1.55	0.2	12
	50	30	24	10	1.4	0.18	14
	118	65.5	54.5	32	1.2	0.42	22.5
	200	107	91	58	1.2	0.35	33
2.12	**8**	8	6	0	2.2	0.45	6
	23	16	13	1	2	0.32	12
	36	24	19	4.5	2.2	0.32	14.5
	50	29.5	23	8	2.1	0.22	15
	118	65	54	26	2.2	0.41	28
	200	107	88	53	2	0.41	35
3.40	**8**	8	6	0	3.5	0.38	6
	23	17	13	0	3.5	0.7	13
	36	24	19	0	3.4	0.9	19
	50	31	25	4	3.4	0.75	21
	118	63	50	17	3.3	0.75	33
	200	106	86	40	3.3	0.65	46

It is apparent from Figs. 5.6, 5.7 and 5.8 that increasing of vibration intensity results in a reduction of the residual friction angle of all the materials. From these figures, it can also be seen that besides reducing the friction angles of the materials, vibration results in the intersecting of the shear strength envelop with the normal stress axis at the non-zero *vibro-fluidizational limit*, σ_f, which increases with an increase in the vibration intensity. This implies that at a given vibration acceleration, a granular material can fluidize at normal stresses up to the σ_f value, and above the σ_f value, remains in the solid state, but has a smaller friction angle (vibro-residual friction angle, φ_{vr}) than the residual one, φ_r. Thus, Coulomb's equation for dry granular material, $\tau = \sigma \tan \varphi$, can be written as:

$$\tau = (\sigma - \sigma_f) \tan \phi_{vr} \qquad \text{if } \sigma > \sigma_f \qquad [2]$$

$$\tau = 0 \qquad \text{if } \sigma \leq \sigma_f$$

where τ – shear stress, σ – normal stress, σ_f – vibro-fluidizational limit (intersection point of the vibro-residual shear strength with the normal stress axis), and φ_{vr} –friction angle of vibro-residual strength.

Alternatively, the σ_f parameter can be expressed as:

$$\sigma_f = \tau/\tan\phi_{vr} + \sigma \qquad \text{where } \sigma > \sigma_f \qquad [3]$$

Table 5.3 Test results of fine sand.

$\Gamma_{h\text{-}av}$	σ	τ_p	τ_r	τ_{rv}	Γ_h	Γ_v	$\Delta\tau$
0.42	**8**	12.5	9	5	0.43	0.07	4
	23	25	19	14.5	0.43	0.14	4.5
	36	36.5	26.5	22.5	0.4	0.13	4
	50	46	37.5	32.5	0.41	0.13	5
	118	103	81	71.5	0.43	0.18	9.5
	200	166	130	118.5	0.4	0.08	11.5
2.42	**8**	13	9.5	0	2.5	0.22	9.5
	23	25	20.5	8	2.5	0.4	12.5
	36	35.5	31	14	2.6	0.58	17
	50	46.5	37.5	19.5	2.3	0.4	18
	118	102.5	83.5	51	2.3	0.75	32.5
	200	170.5	130	91	2.3	0.7	39
4.25	**8**	13.5	9.5	0	3.5	0.4	9.5
	23	24	20	0	3.9	0.65	20
	36	39.5	30	5	4	0.85	25
	50	46	34.5	8	4.5	0.7	26.5
	118	112.5	87	38	4	0.7	49
	200	178	128	62	4.5	1.3	66

Table 5.4 Test results of coarse sand.

$\Gamma_{h\text{-}av}$	σ	τ_p	τ_r	τ_{rv}	Γ_h	Γ_v	$\Delta\tau$
0.44	**8**	11	7.5	1.5	0.44	0.04	6
	23	21.5	16.5	9.5	0.47	0.08	7
	36	30	25	19	0.47	0.1	6
	50	40.5	32	22.5	0.46	0.15	9.5
	118	88	71	62.5	0.42	0.15	8.5
	200	144	119	97	0.4	0.21	22
2.50	**8**	11	8	0	2.3	0.52	8
	23	21	16	0	2.6	0.52	16
	36	29.5	24	7	2.7	0.49	17
	50	39.5	31.5	11	2.8	0.49	20.5
	118	88	71.5	36	2.3	0.52	35.5
	200	141.5	117.5	76	2.3	0.75	41.5
4.28	**8**	10.5	8	0	4.6	1.1	8
	23	21	17	0	4.2	1.1	17
	36	31	24.5	0	4.1	1.2	24.5
	50	40	32.5	4	4.5	0.8	28.5
	118	89	71	27.5	4.2	1	43.5
	200	145.5	115.5	52	4.1	1.4	63.5

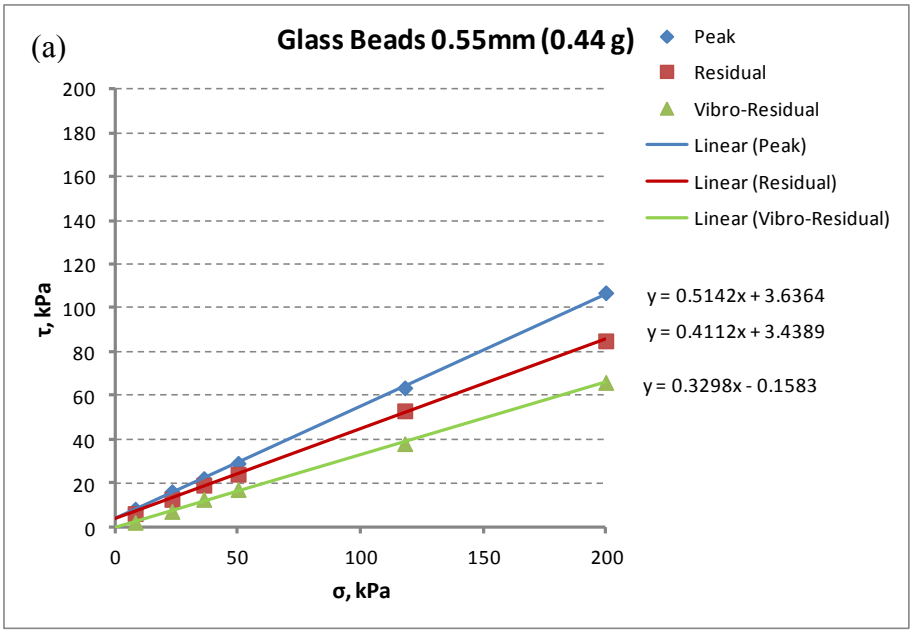

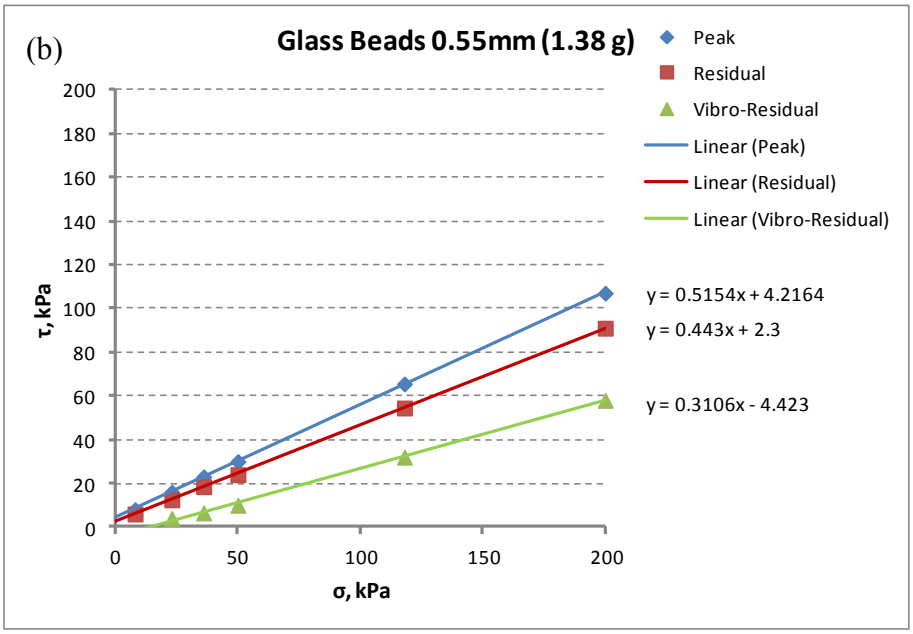

(Continued on the next page)

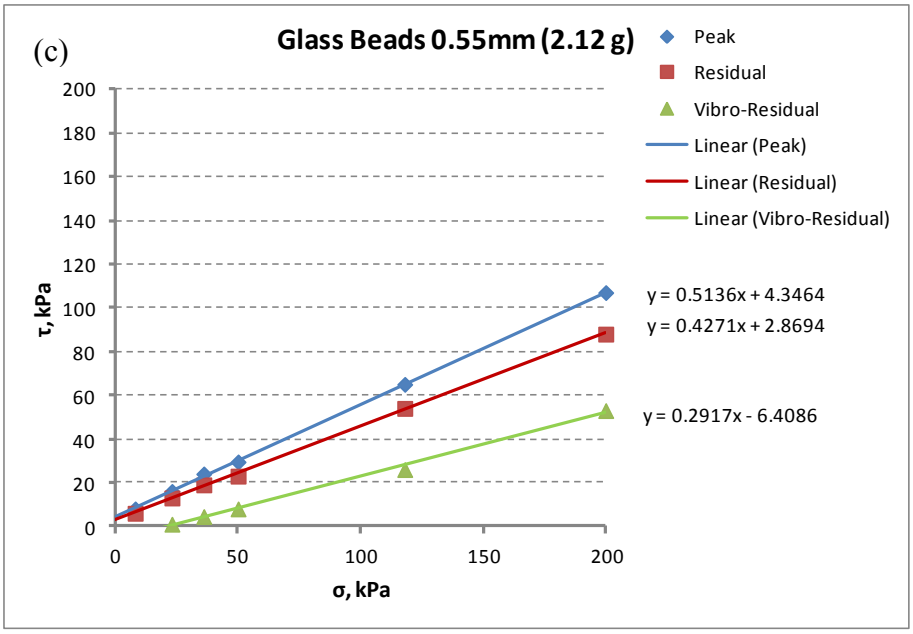

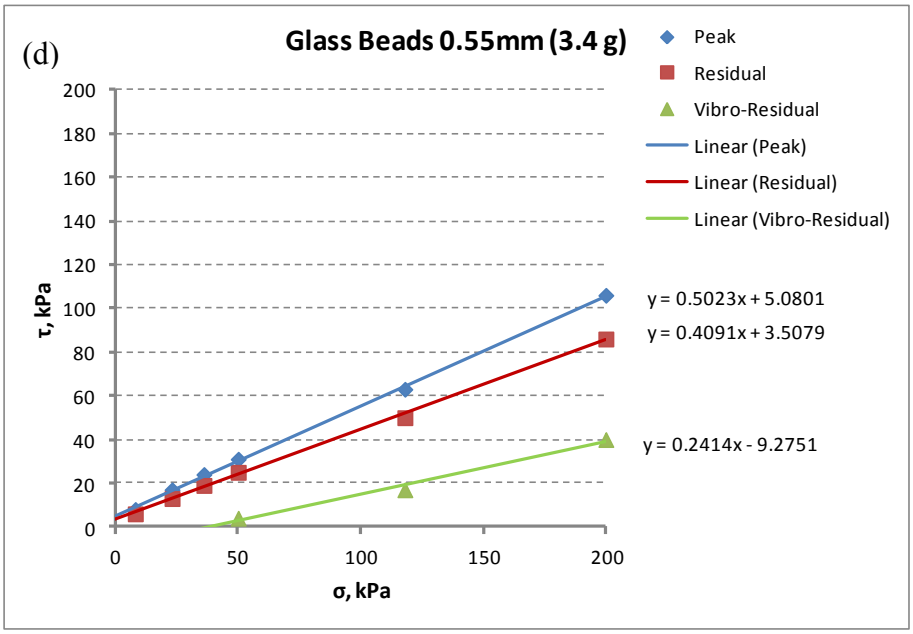

Figure 5.6 Shear strength diagrams of glass beads tested at (a) - Γ_h=0.44, (b) - Γ_h=1.38, (c) - Γ_h=2.12 and (d) - Γ_h=3.4.

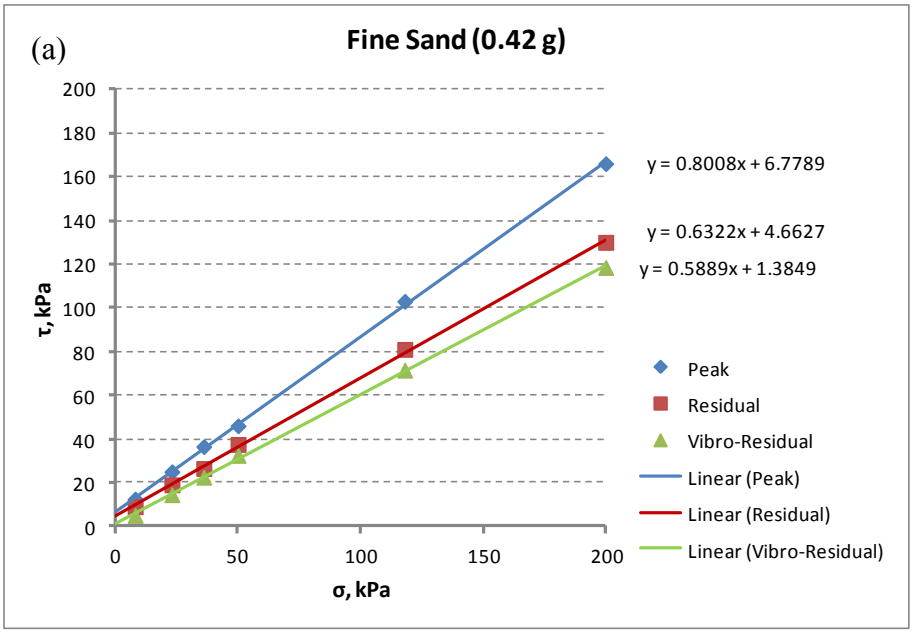

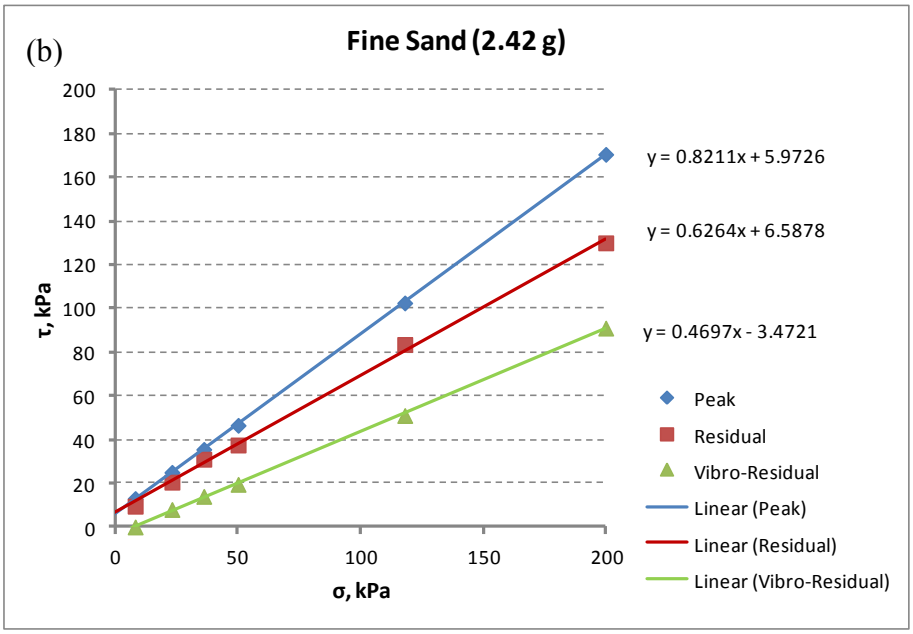

(Continued on the next page)

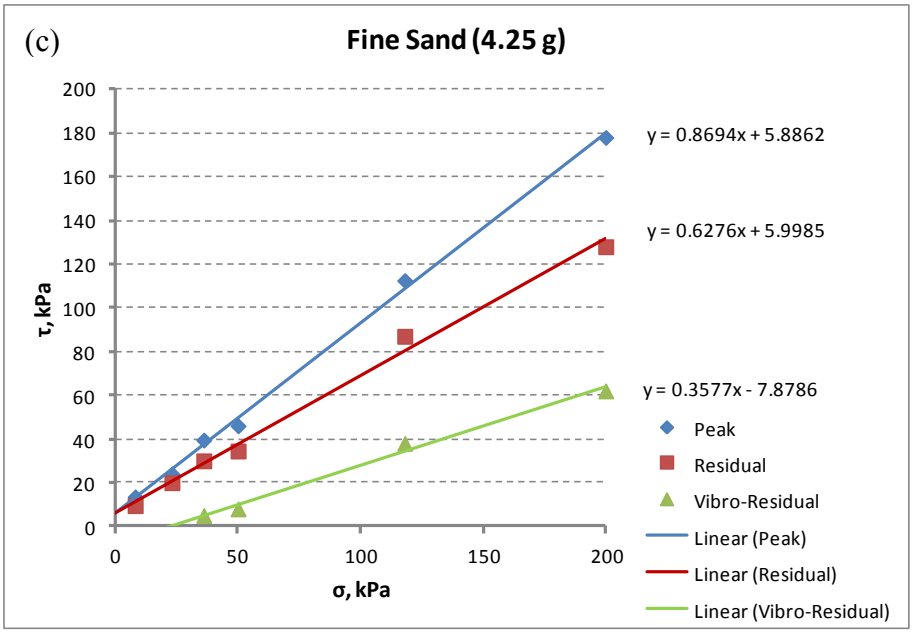

Figure 5.7 Shear strength diagrams of fine sand tested at (a) - Γ_h=0.42, (b) - Γ_h=2.42 and (c) - Γ_h=4.25.

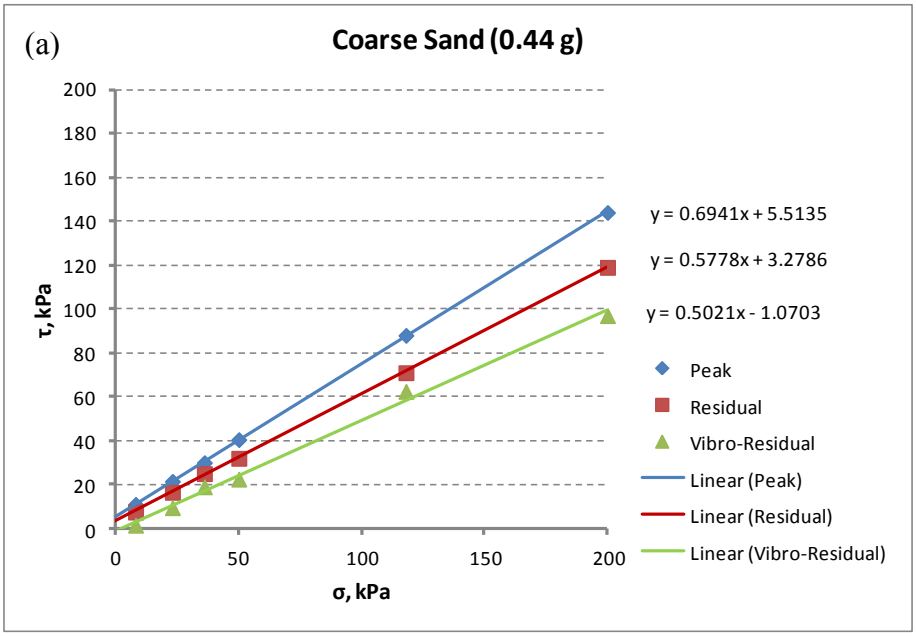

(Continued on the next page)

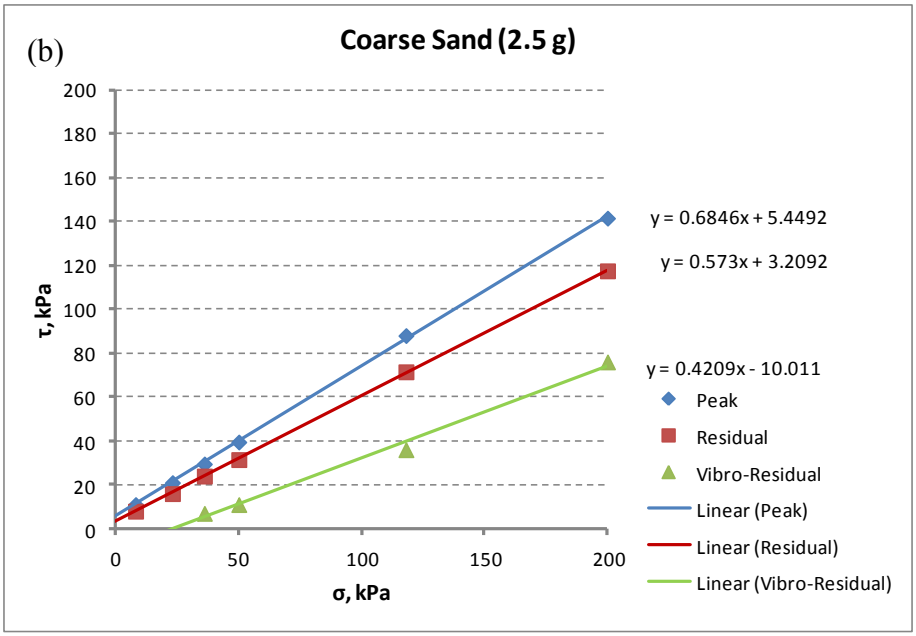

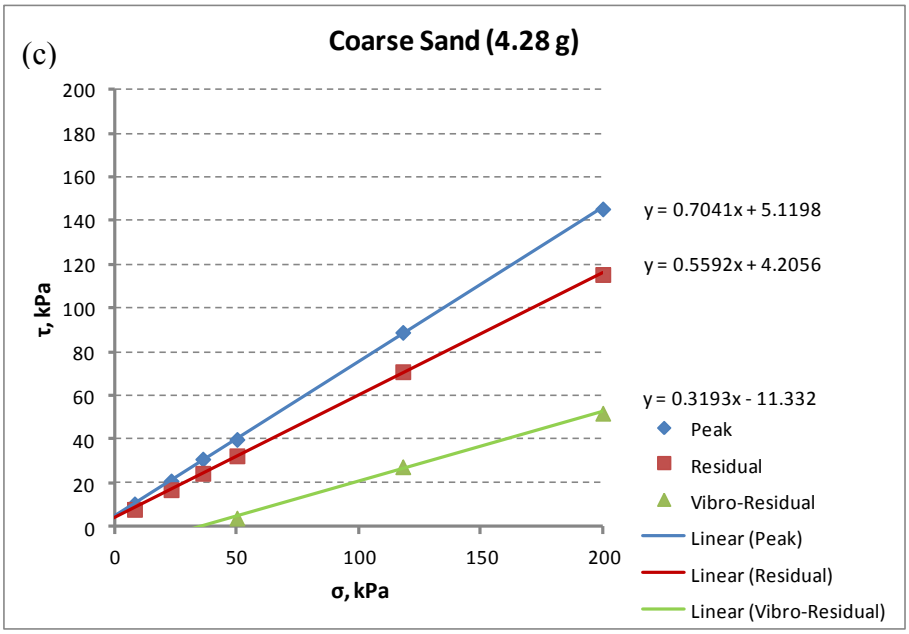

Figure 5.8 Shear strength diagrams of coarse sand tested at (a) - Γ_h=0.44, (b) - Γ_h=2.5 and (c) - Γ_h=4.28.

Evidence of the presence of both a vibro-fluidizational limit, σ_f, and a reduced friction angle due to vibration can possibly be explained by the bifurcation process that takes place during sufficiently strong vibrations, which results in the fluidization of the top layer of a granular material, while the bottom layer remains in a solid state. This phenomenon was described in detail by Metcalfe et al. (2002), who performed experiments on granular materials by subjecting them to horizontal vibrations and concluded that normal stress has a significant impact on the thickness of the vibro-fluidized layer of the granular media.

Table 5.5 Friction angles and normal stress axis intersection values of the shear strength diagrams for the three granular materials tested at different vibration intensities.

Material	$\Gamma_{h\text{-}av}$	ϕ (^{0})	σ_f (kPa)
Fine Sand	0	32.2	0
	0.42	30.5	7.4
	2.42	25.1	19.6
	4.25	19.7	38.1
Coarse Sand	0	29.7	0
	0.44	26.7	2.1
	2.50	22.8	23.8
	4.28	17.7	35.5
Glass Beads	0	21.2	0
	0.44	18.3	9.7
	1.38	17.3	24
	2.12	16.3	32.4
	3.40	13.6	51

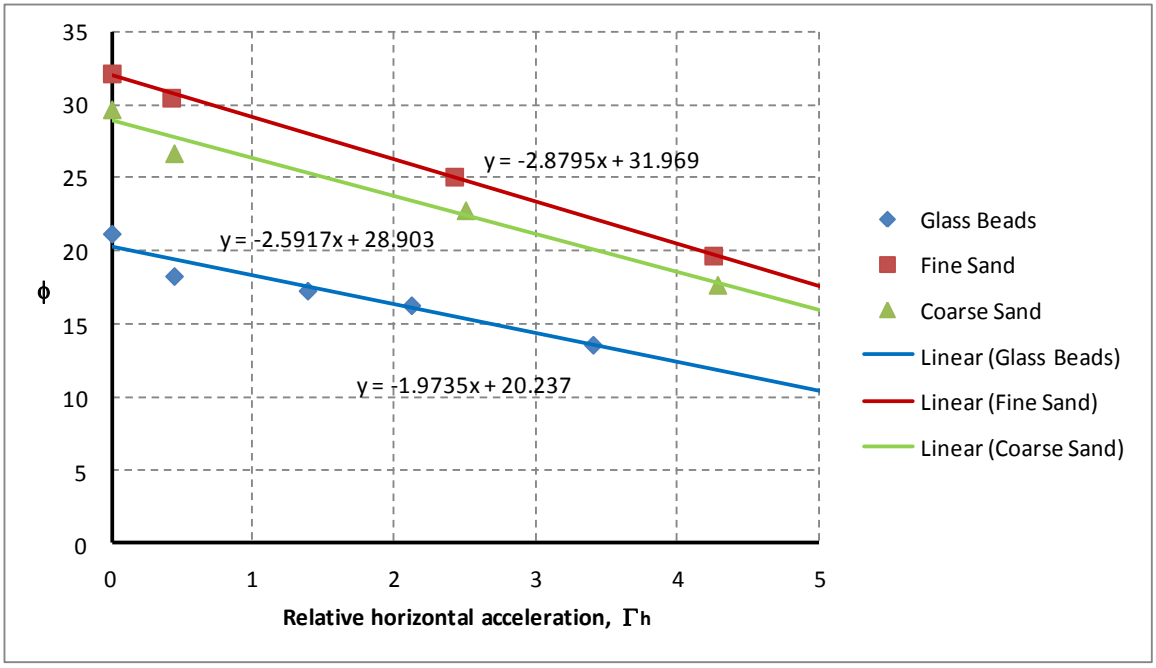

Figure 5.9 Friction angles of the tested materials at different vibration intensities.

The final results provided in Table 5.5 are graphically presented in Figs. 5.9 and 5.10. It is seen from Fig. 5.9 that the reduction of the residual friction angles of the tested granular materials with an increase in vibration intensity is practically linear. The only noticeable deviation from the linear pattern of the ϕ vs. Γ_h relationship is observed at a Γ_h value of less than 1. It is also apparent that the plot of the well rounded coarse sand correlates well with those of the angular fine sand and glass beads. This means that the plots presented in Fig. 5.9 can be used for the approximation of the residual friction angle changes of sand sized dry granular materials (which have a residual friction angle that ranges from 21^o to 32^o) when subjected to vibration in the given range of horizontal acceleration values.

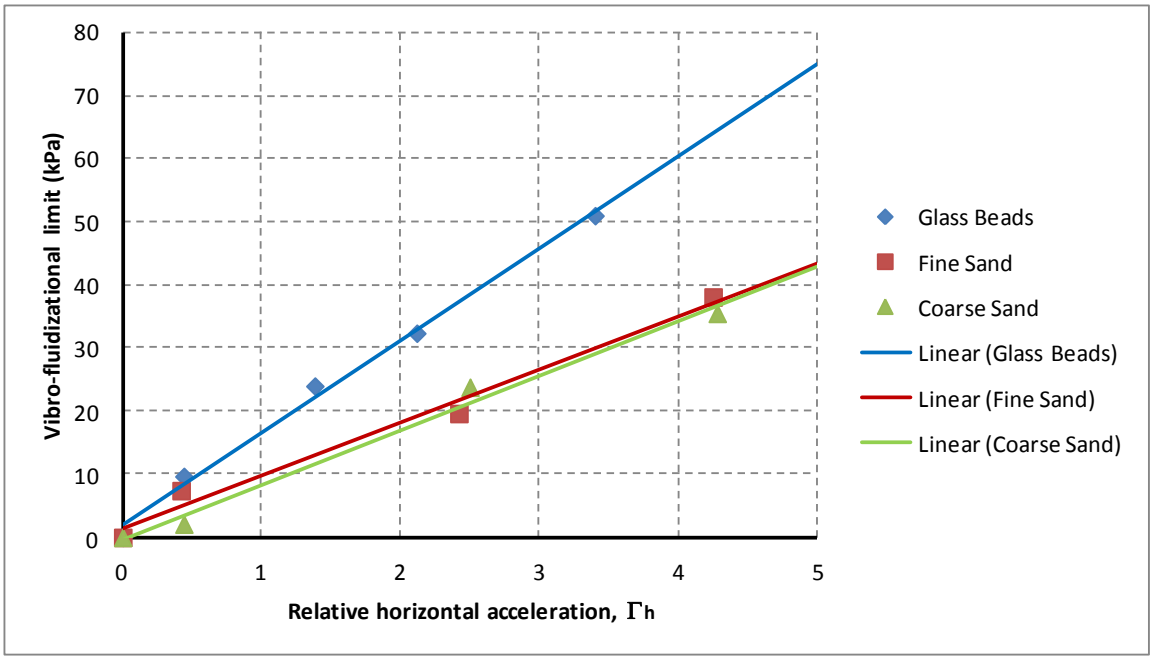

Figure 5.10 σ_f values at different vibration intensities. (Note that $\sigma_f = 0$ at $\Gamma_h = 0$. These points represent a static condition).

As shown in Fig. 5.10, the plots of the σ_f vs. Γ_h relationship for all of the tested materials are linear. At a given vibration intensity, the glass beads have a greater σ_f magnitude than the coarse and fine sands, the plots of which practically coincide. It can be assumed that there is a certain level of roundness, above which the σ_f vs. Γ_h plot will shift from that of the coarse and fine sand to the one of the glass beads.

Since vibration generated by the actuator is in the horizontal (shear) direction, the main parameter that defines vibration intensity used in this work is horizontal acceleration. The vertical accelerations measured on the loading plate are generated due to the horizontal vibrations and their magnitude depends on the boundary conditions and the materials tested. That

is why the Γ_v values provided in Tables 5.2, 5.3 and 5.4 are somewhat random at given $\Gamma_{h\text{-}av}$. Despite this fact, it is apparent from Tables 5.2, 5.3 and 5.4 that the Γ_v values generally increase with an increase in the magnitude of the horizontal acceleration (Γ_h). Therefore, it should be mentioned that although vertical accelerations are not used in the data analysis in this paper, they contribute to the strength loss of the tested materials, and show a well defined trend of their magnitude change which is related to the horizontal acceleration intensity.

Below are some examples that show the effect of vibration intensity on the shearing resistance and compressive deformations of the glass beads. Figs. 5.11, 5.12, 5.13 and 5.14 show the test results of glass bead samples tested at a normal stress of 200 kPa and Γ_h equal to 0.4, 1.2, 2 and 3.3, respectively. It can be seen that an increase in the horizontal vibration acceleration results in not only greater strength loss, but also greater compression deformations. Note that at high vibration intensities (Figs. 5.13 and 5.14) excessive vibro-compaction of the samples leads to post-vibrational peaks, which with further shear deformation, decrease to the residual strength. It can also be seen that after sufficiently strong vibration, the development of post-vibrational peak strength is accompanied with post-vibration dilation (see Figs. 5.14 – 5.19). On the other hand, the shear resistance plots of the fine and coarse sands do not show any post-vibrational peaks at high normal stress values (σ = 118 kPa and 200 kPa), which can be explained by the irregular shape of the grains that did not allow the samples to undergo sufficient compaction at high confining stresses, even at horizontal vibration accelerations greater than $\Gamma_h > 4$.

The irregular pattern of the shear resistance plots at the post-peak strength state (see Figs. 5.11, 5.12, 5.13 and 5.14) is due to the arranged alignment of the glass beads on the shear surface that takes place when the tested samples approach their residual strength. When the glass beads

which have an arranged alignment snap over each other, a sudden decrease in the shearing resistance takes place, after which, the shear stress starts to increase until it reaches its residual value. This phenomenon has only been observed for glass beads at higher normal stresses, σ = 118 kPa and 200 kPa (see Fig. 5.5 for comparison purposes).

The effect of normal (confining) stress on the strength and deformation characteristics of granular materials subjected to similar vibration intensities (horizontal vibration accelerations) can be seen in Figs. 5.14 – 5.19. The greatest compressive deformations induced by vibration are observed at the lowest normal stress, σ = 8 kPa. An increase in normal stress from 8 to 200 kPa leads to a reduction in compression. This phenomenon is also apparent from the magnitude of the post-vibrational peak of the shear resistance plots. Higher normal stress means lower post-vibrational peak. Therefore, the mechanism here is similar to the initial dilation of the tested samples, where the dilation magnitude reduces with an increase in normal stress (see Figs. 5.14 – 5.19).

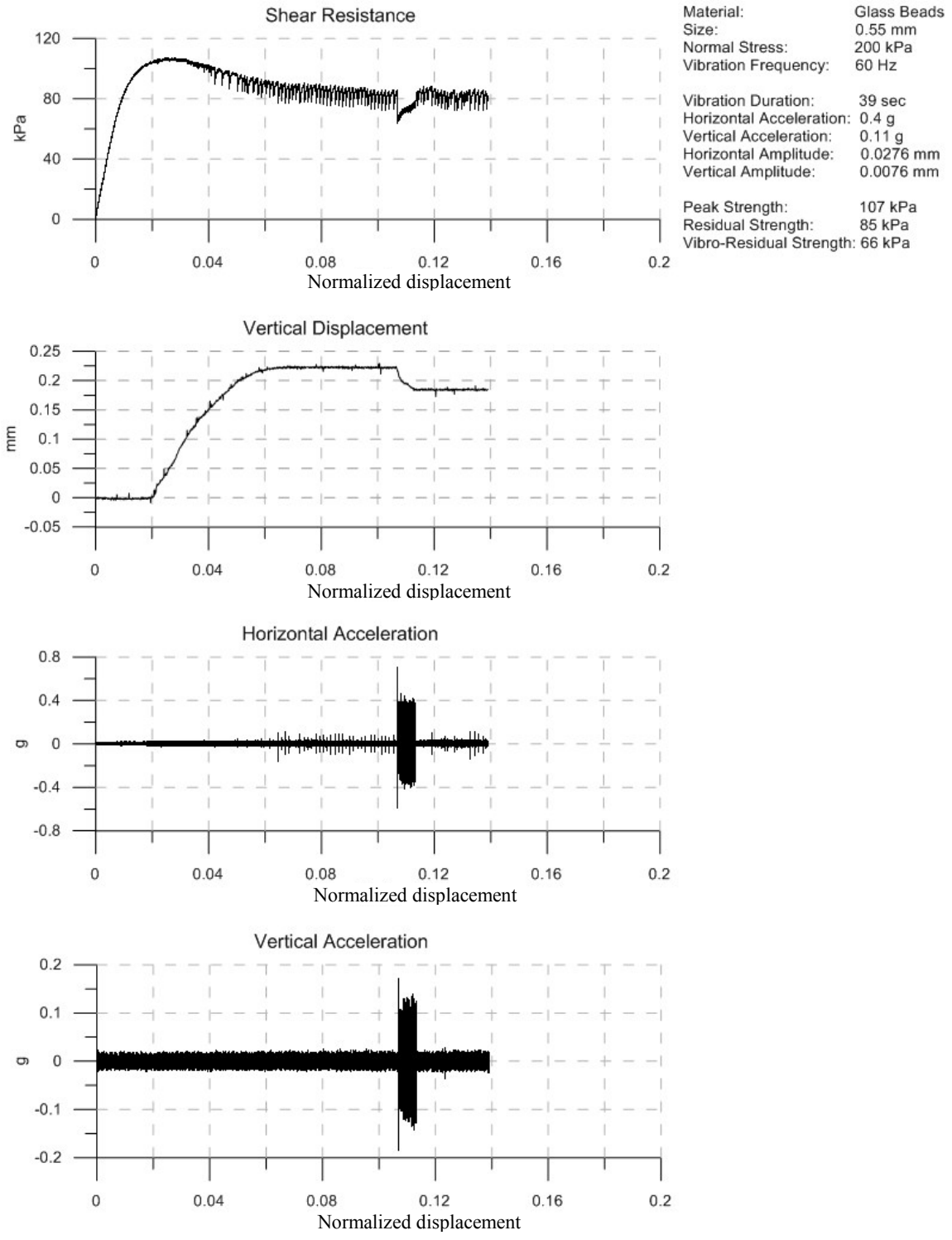

Figure 5.11 Effect of vibration on the strength loss and compressive deformation of glass bead samples tested at $\Gamma_h = 0.4$.

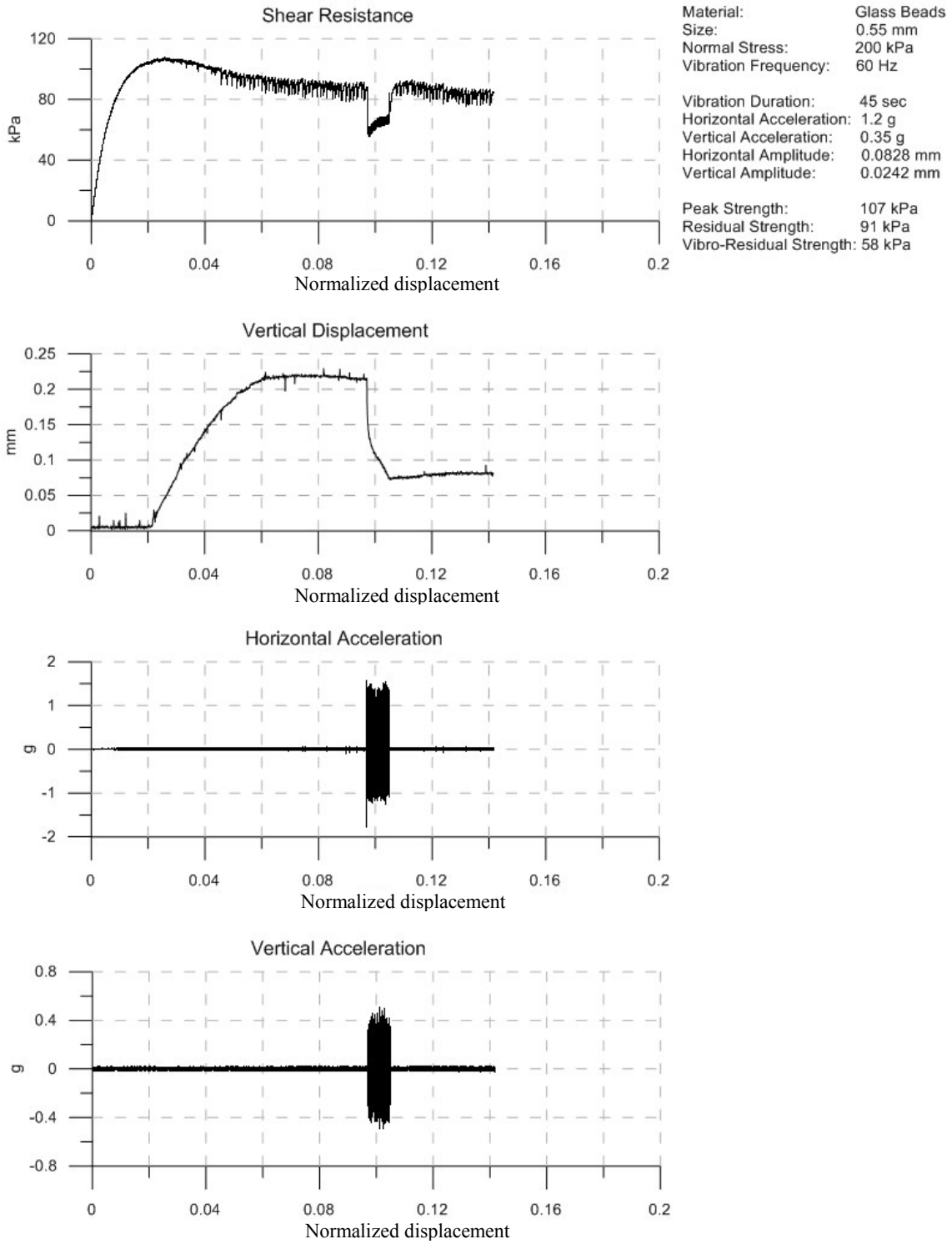

Figure 5.12 Effect of vibration on the strength loss and compressive deformation of glass bead samples tested at $\Gamma_h = 1.2$.

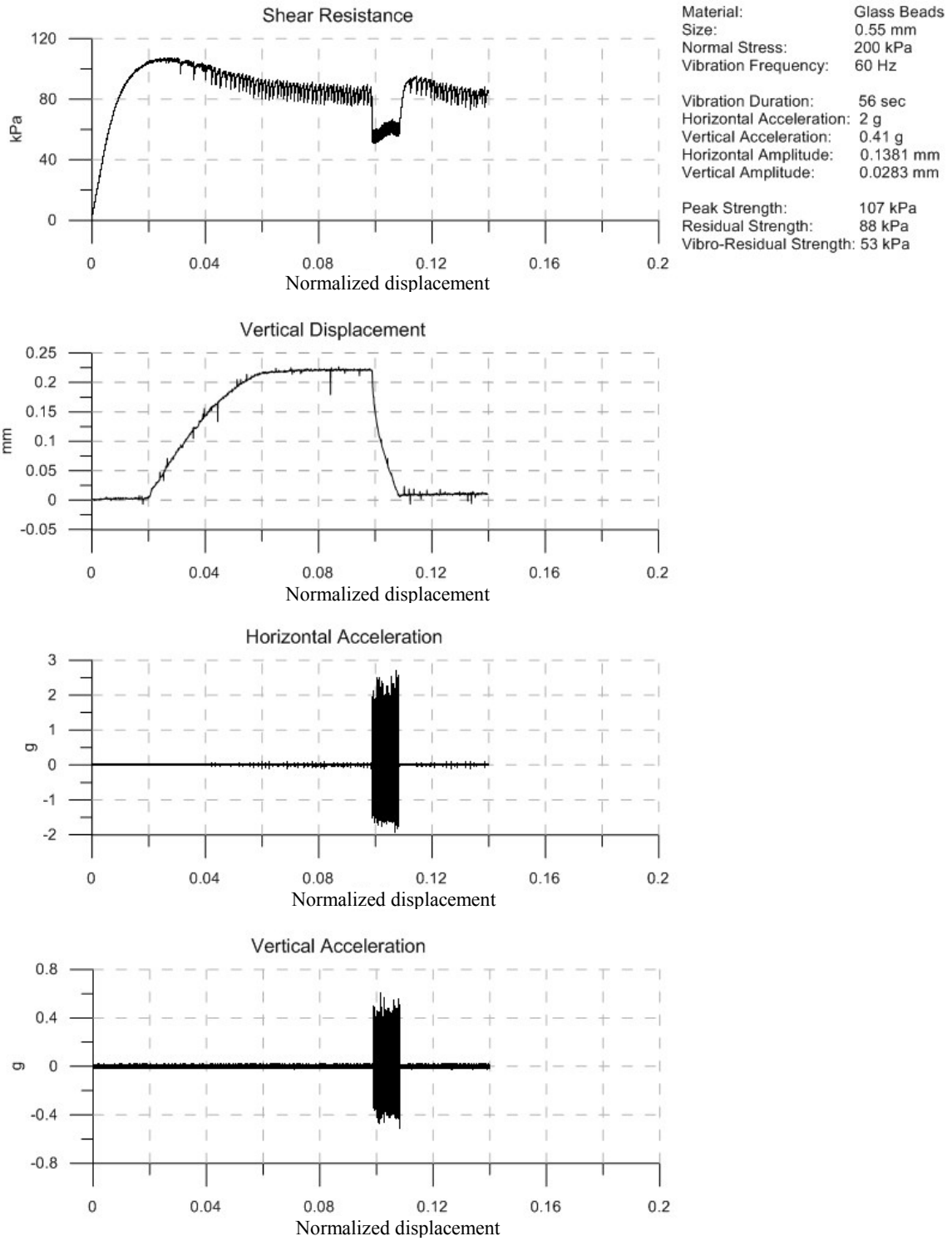

Figure 5.13 Effect of vibration on the strength loss and compressive deformation of glass bead samples tested at $\Gamma_h = 2$.

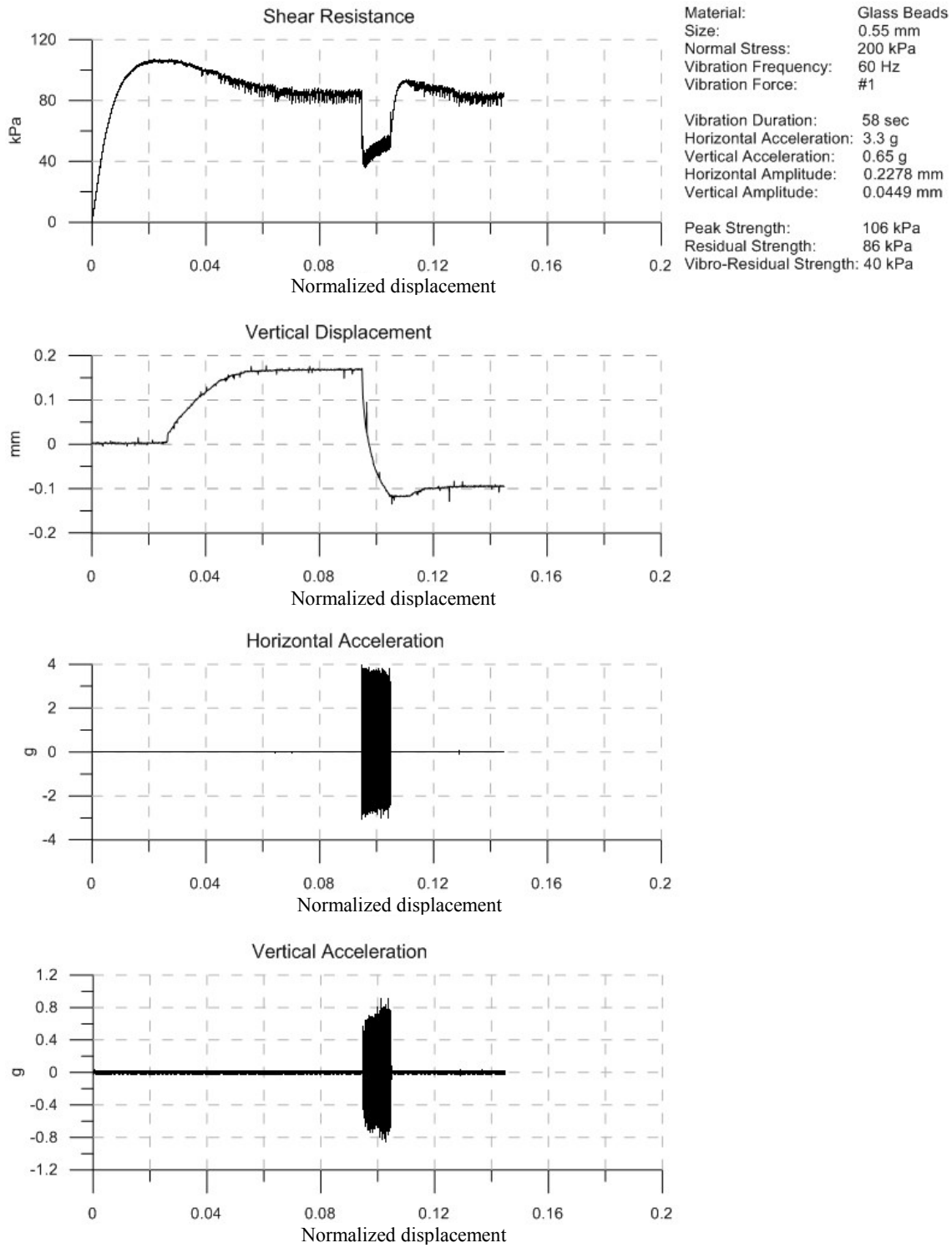

Figure 5.14 Effect of vibration on the strength loss and compressive deformation of glass bead samples tested at $\Gamma_h = 3.3$.

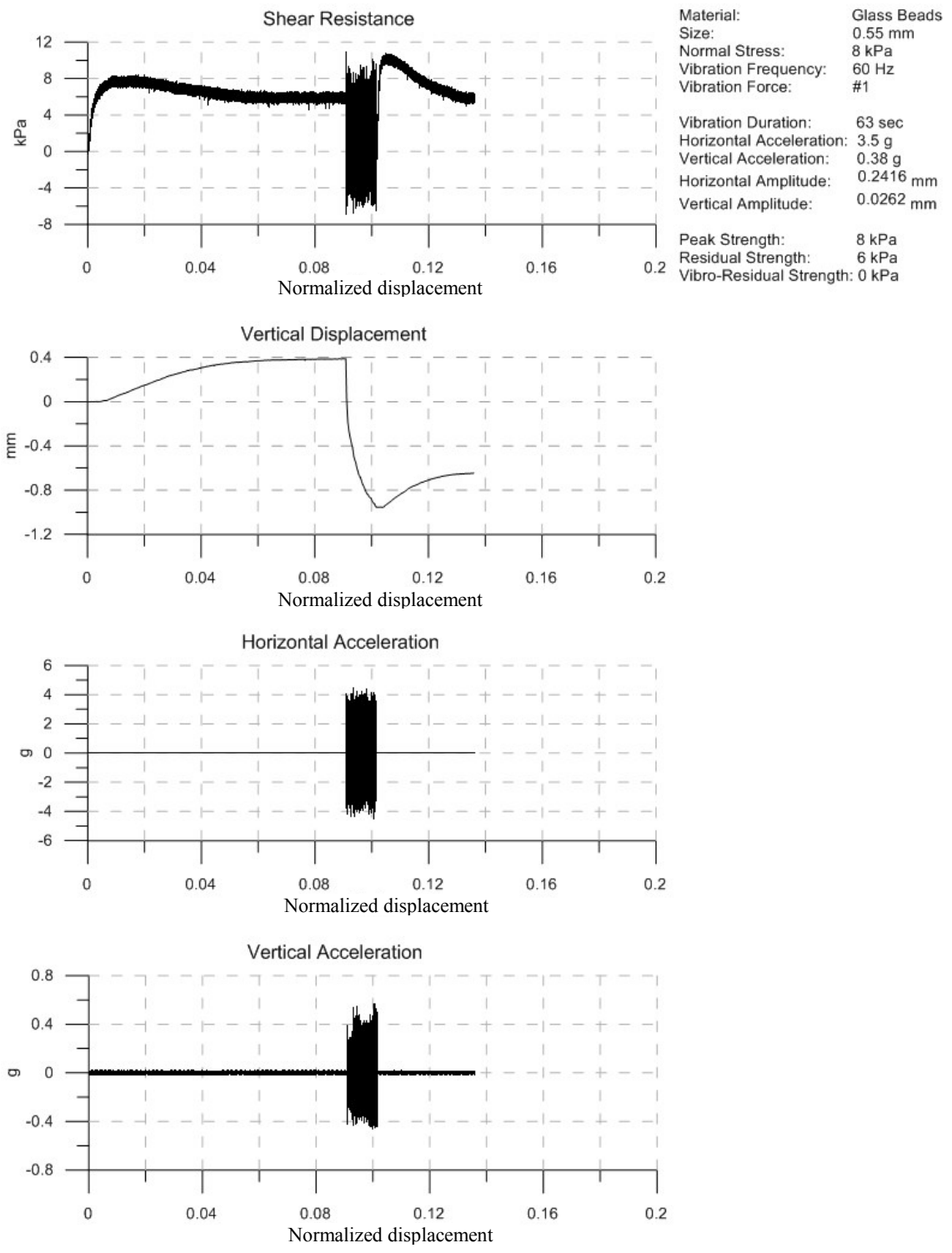

Figure 5.15 Effect of normal stress on post-vibrational strength and compressive deformation of glass beads tested at σ = 8 kPa.

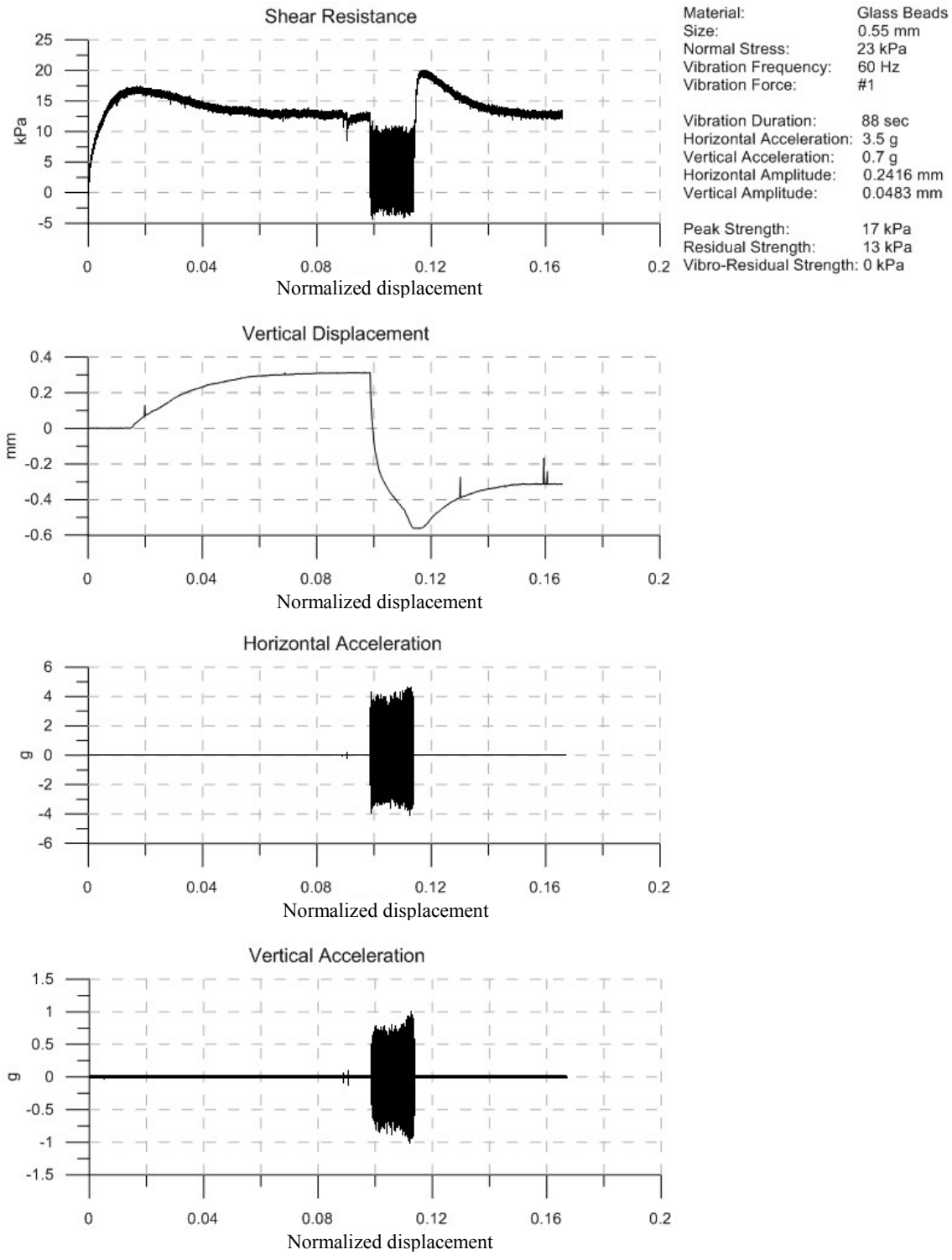

Figure 5.16 Effect of normal stress on post-vibrational strength and compressive deformation of glass beads tested at σ = 23 kPa.

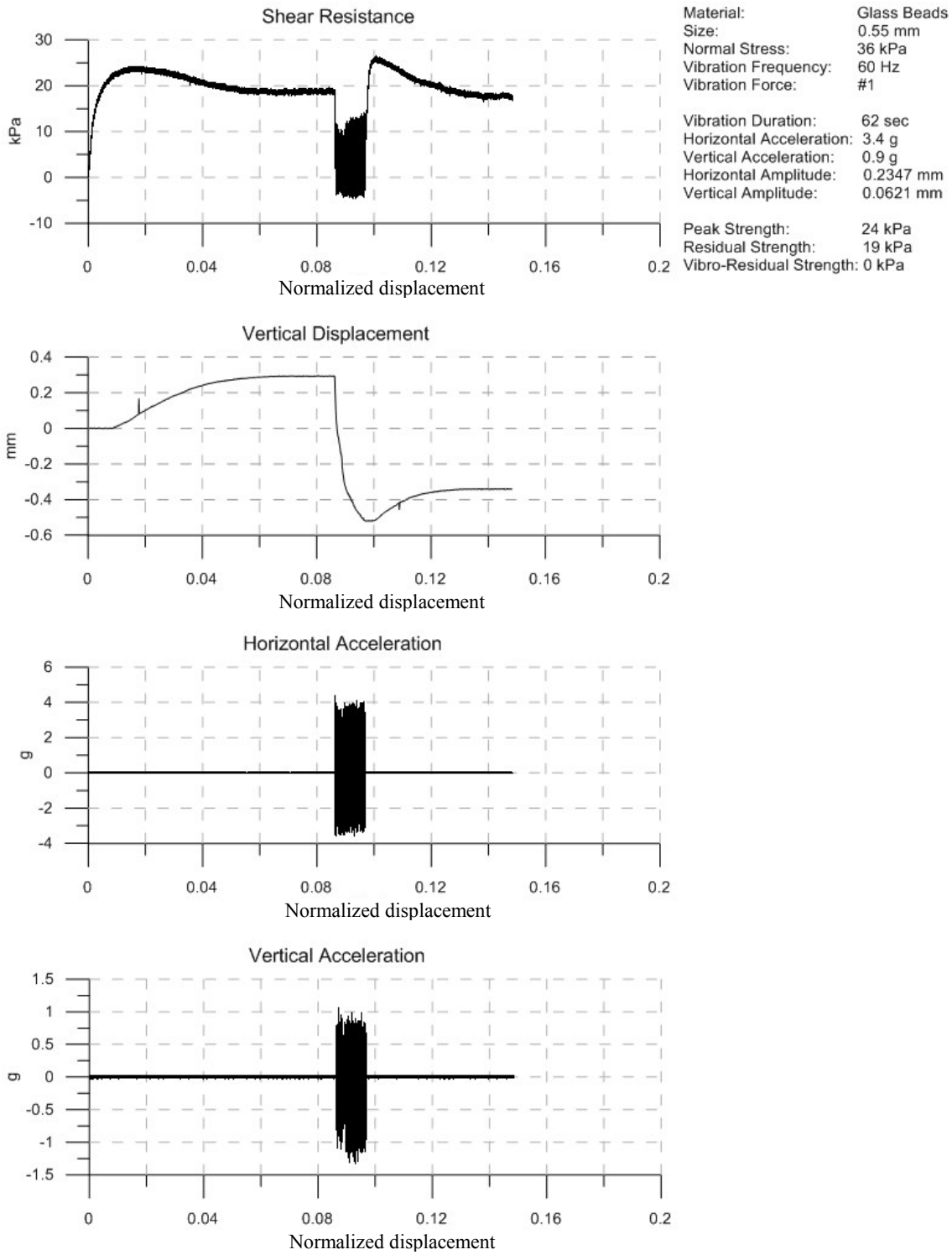

Figure 5.17 Effect of normal stress on post-vibrational strength and compressive deformation of glass beads tested at σ = 36 kPa.

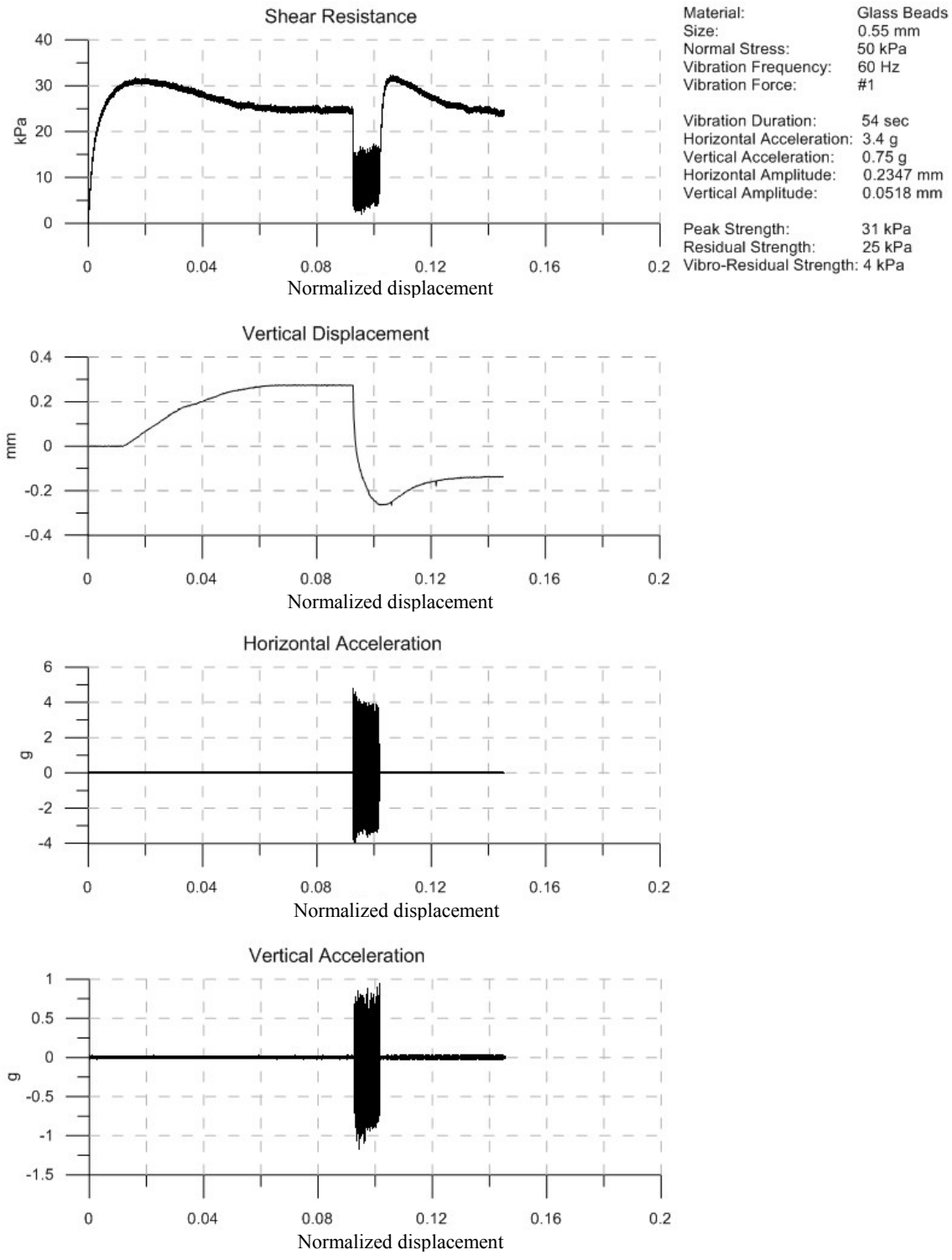

Figure 5.18 Effect of normal stress on post-vibrational strength and compressive deformation of glass beads tested at σ = 50 kPa.

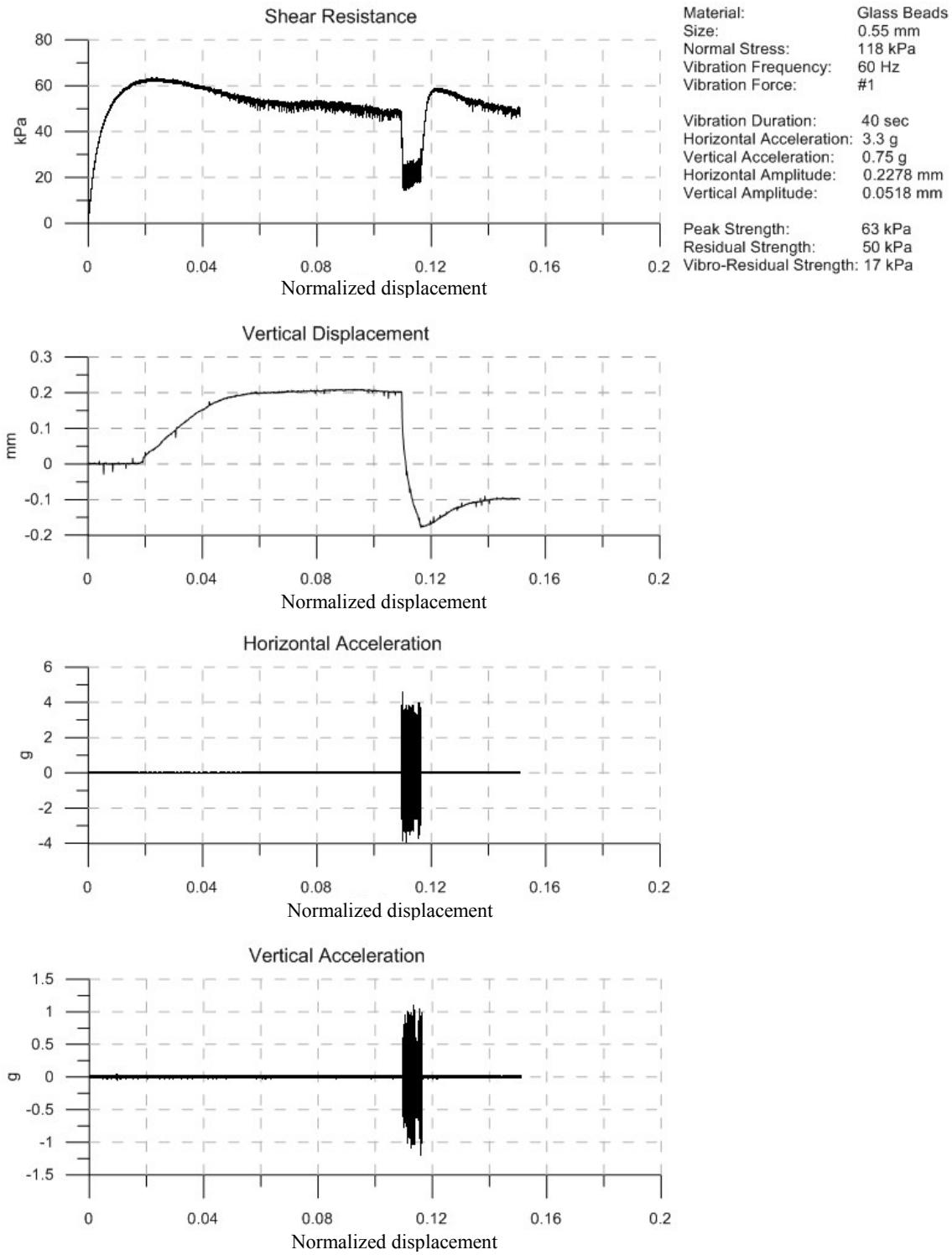

Figure 5.19 Effect of normal stress on post-vibrational strength and compressive deformation of glass beads tested at σ = 118 kPa.

On the other hand, as seen from Figs. 5.14, 5.18, and 5.19, the magnitude of the shear strength loss due to vibration increases with an increase in the normal stress, which in turn, defines the friction angle reduction from the residual to the vibro-residual value.

Figs. 5.14 – 5.19 show that strong vibrations (Γ_h = 3.3 to 3.5) bring the samples to a denser state than their state prior to testing. It is also seen that compression caused by vibration is greater than dilation due to the shearing of the samples. This results in well defined post-vibrational peaks in the shear resistance plots.

As mentioned earlier, the development of post-vibrational peak strength is accompanied with post-vibration dilation. It is apparent from Figs. 5.14 to 5.19 that the magnitude of post-vibration dilation is smaller than the initial dilation of the samples. Therefore, it can be concluded that post-vibration dilation is caused by the expansion of the shear zone of the samples, while the difference between the initial and post-vibration dilation is due to the compression of the material beyond the shear zone.

It can also be seen that some of the samples showed an increase in shear resistance during vibration (e.g. Fig 5.14), which can be explained by the ongoing densification of the shear zone material.

The experimental results mentioned above can contribute to a better understanding of long run-out distance of large rock avalanches. The attempts to explain this phenomenon were made by Melosh (1979) and Davies (1982). It has been observed that the run-out distance of large rock avalanches depends on their volume, such that the larger volume of an avalanche results in longer run-out distance.

The evidence that sufficiently strong vibration decreases the friction angle of a granular material from residual to vibro-residual value, such that greater vibration intensity results in lower vibro-residual friction angle, correlates well with the concepts of "acoustic fluidization" (Melosh, 1979) and "mechanical fluidization" (Davies, 1982) attempting to explain the long run-out distances of large rock avalanches: the resistance of granular media at the shear interface is affected by the vibration generated by the collisions of the avalanche material with the stationary base, such that larger volume of a rock avalanche having greater kinetic energy generates greater vibration intensity, which will, in turn, result in a longer run-out distance of the rock avalanche.

5.6 Conclusions

Based on the physical observations of the mechanical response of sand and glass beads under vibrational shearing, the following conclusion can be made.

1. Upon vibration application, an immediate strength loss of the granular material takes place from the residual to vibro-residual strengths. If the granular material experiences sufficient shear deformation after the termination of vibration, its strength reaches the residual strength value.
2. All of the tested samples have experienced compression (compaction) due to the applied vibration. An increase in the horizontal vibration acceleration results in greater compression deformation.
3. An increase in the vibration intensity results in a reduction of the residual friction angle of all the tested granular materials.

4. Besides reducing the friction angles of the tested materials, vibration causes the intersecting of the shear strength envelop with the normal stress axis at a certain vibro-fluidizational limit value, σ_f, which increases with an increase in vibration intensity. This implies that at a given vibration acceleration, a granular material can fluidize at normal stresses up to the σ_f value, and above this σ_f value, remains in a solid state. However, the granular material has a smaller friction angle (vibro-residual friction angle, φ_{vr}) than the residual friction angle, φ_r. Thus, the Coulomb's equation for dry granular material, $\tau = \sigma \tan \varphi$, can be written as: $\tau = (\sigma + \sigma_f) \tan \varphi_{vr}$.
5. The reduction of the residual friction angles of the tested granular materials with an increase in vibration intensity is practically linear. The only noticeable deviation from the linear pattern of the φ vs. Γ_h relationship is observed at a Γ_h value less than 1.
6. The φ vs. Γ_h plots can be used for the approximation of changes in the residual friction angle of sand sized dry granular materials (with residual friction angles from 21^o to 32^o) when subjected to vibration in the given range of the horizontal acceleration values ($0 < \Gamma_h < 4.5$).
7. The plots of the σ_f vs. Γ_h relationship for all of the tested materials are linear. At a given vibration intensity, the glass beads have a greater σ_f magnitude than the coarse and fine sands, the plots of which coincide. It can be assumed that there is a certain level of roundness, above which, the σ_f vs. Γ_h plot will shift from that of the coarse and fine sand to the one of the glass beads.
8. Excessive vibro-compaction of the samples leads to post-vibrational peaks, which with further shear deformation, decreases to the residual strength. The development of post-vibrational peak strength is accompanied with post-vibration dilation.

9. The shear resistance plots of the fine and coarse sands, unlike that of the glass beads, do not show any post-vibrational peaks at high normal stress values (σ = 118 kPa and 200 kPa), which can be explained by the irregular shape of the grains that did not allow the samples to undergo sufficient compaction, even at horizontal vibration accelerations greater than $\Gamma_h > 4$.
10. The largest compressive deformation of the granular materials induced by vibration is observed at the lowest normal stress, σ = 8 kPa. An increase in the normal stress from 8 to 200 kPa leads to compression reduction. This phenomenon is also apparent from the magnitude of the post-vibrational peak of the shear resistance plots. A higher normal stress means a lower post-vibrational peak.
11. It appears that the essence of acoustic fluidization, which attempts to explain the large runout distance of big rock avalanches (Melosh, 1979), and vibrational fluidization observed in the above mentioned experiments, is the same: the resistance of granular media at the shear interface is affected by the vibration generated by the collision of the grains.

5.7 References

Alexeev, A., Royzen, V., Dudko, A., Goldshtein, A. and Shapiro, M. (2000). "Mixing and Segregation in Vertically Vibrated Granular Layers". Solid Mechanics and Its Applications, Volume 81, 2000, pp 129-139

Ayer, J. E. and Soppet, F. E. (1965/1966): Vibratory Compaction, Part I: Compaction of Spherical Shapes and Part II: Compaction of Angular Shapes. J. Am. Ceramic Soc. 48, 180-183 and 49, 207-210.

Barkan, D. D. (1962). "Dynamics of Basis and Foundations". Translated from Russian by L. Drashevska, New York, McGraw-Hill, 434 p.

Bourzutschky, M. and Miller, J. (1995): "Granular" Convection in a Vibrated Fluid. Phys. Rev. Lett. 74, 2216-2219.

Brone, D. and Muzzio, F. J. (1997). Size segregation in vibrated granular systems: A reversible process. Phys. Rev. E. 56[1], pp. 1059-1063.

Clement, E., Vanel, L., Rajchenbach, J. and Duran, J. (1996). Pattern formation in a vibrated granular layer. Phys. Rev. E, 53, 2972-2975.

Cooke, W., Warr, S., Huntley, J. M. and Ball R. C. (1996). "Particle size segregation in a two-dimensional bed undergoing vertical vibration", Phys. Rev. E, 53, 2812.

Doudy, S., Fauve, S. and Laroshe, C. (1989). Subharmonic instabilities and defects in a granular layer under vertical vibrations. Europhys. Lett., 8[7], 621

Evesque, P. and Rajchenbach, J. (1989). "Instability in a sand heap", Phys. Rev. Lett., 62, 44.

Falcon, E., Wunenburger, R., Evesque, P., Fauve, S., Chabot, C., Garrabos, Y. and Beysens, D. (1999). Cluster formation in a granular medium fluidized by vibrations in low gravity. *Phys. Rev. Lett.*, 83:440.

Fauve, S., Douady, S. and Laroche, C. (1989): Collective behaviours of granular masses under vertical vibrations. J. Physique C3, 187-191.

Gallas, J. A. C., Herrman, H. J. and Sokolowski, S. (1992): Convection Cells in Vibrating Granular Media. Phys. Rev. Lett. 69, 1371-1374.

Goldshtein, A., Shapiro, M., Moldavsky, L. and Fichman, M. (1995). Mechanics of collisional motion of granular materials. 2. Wave propagation through vibrofluidized granular layers. J. Fluid Mech., 287, p. 349

Gotzendorfer, A., Tai, C., Kruelle, C. A., Rehberg, I. and Hsiau, S. S. (2006), `Fluidization of a vertically vibrated two-dimensional hard sphere packing: A granular meltdown', Phys. Rev. E 74, 011304.

Huan, C. (2008) NMR Experiments on Vibrofluidized and Gas Fluidized Granular Systems. PhD Thesis, University of Massachusetts Amherst.

Jaeger, H. M., Nagel, S. R. and Behringer, R. P. (1996). Granular solids, liquids, and gases. Rev. Mod. Phys. 68, 1259

Knight, J. B., Jaeger, H. M. and Nagel, S. R. (1993). "Vibration-induced size separation in granular media: the convection connection", Phys. Rev. Lett., 70, 3728.

Lan, Y. and Rosato, A. D. (1995). "Macroscopic behavior of vibrating beds of smooth inelastic spheres", Phys. Fluids, Vol. 7, No. 8, pp. 1818-1831.

Laroche, C., Douady, S. and Fauve, S. (1989): Convective Flow of Granular Masses under Vertical Vibration. J. Physique 50, 699-706.

Liffman, K., Metcalfe, G. and Cleary, P. (1997): Convection due to horizontal shaking. in: (Behringer and Jenkins (1997)). 405-408.

Luding, S. (1995). Granular materials under vibration: simulations of rotating spheres. *Phys. Rev. E*, 52:4442.

Melo, F., Umbanhowar, P. and Swinney, H. L. (1993). "Transition to parametric wave patterns in a vertically oscillated granular layer", Phys. Rev. Letts., 72, 172.

Melo, F., Umbanhowar, P. and Swinney, H. L. (1995). "Hexagons, kinks, and disorder in oscillated granular layers", Phys. Rev. letts., 75, 3838.

Melosh, H. J. (1979). "Acoustic Fluidization: A New Geologic Process?" Journal of Geophysical Research, v. 84: pp. 7513-7520.

Metcalfe, C., Tennakoon, S. G. K., Kondic, L., Schaeffer, D. G. and Behringer, R. P. (2002). Granular Friction, Coulomb Failure, and the Fluid-Solid Transition for Horizontally Shaken Granular Materials. Physical Review E - Statistical, Nonlinear, and Soft Matter Physics.

Moon, S. J., Swift, J. B., and Swinney, H. L. (2004). Role of friction in pattern formation in oscillated granular layers. *Phys. Rev. E*, 69(031301):1.

Mujica, N. and Melo, F. (1998). Solid-liquid transition and hydrodynamic surface waves in vibrated granular layers. *Phys. Rev. Lett.*, 80:5121.

Pak, H. K. and Behringer, R. P. (1993). "Surface waves in vertically vibrated granular materials", Phys. Rev. Lett. 71, 1832

Pak, H. K., Van Doorn, E. and Behringer, R. P. (1995). "Effects of ambient gases on granular materials under vertical vibration", Phys. Rev. Lett., 74, 4643.

Poschel, T. and Rosenkranz, D. E. (1998). Experimental study of horizontally shaken granular matter – the swelling effect. Lecture Notes in Physics, Volume 503, 1998, pp 96-109

Richards, R., Jr., Elms, D. and Budhu, M. (1990). ”Dynamic Fluidization of Soils.” Journal of Geotechnical Engineering, 116(5), pp. 740–759

Ristow, G. H., Strasburger, G. and Rehberg, I. (1997). Phase diagram and scaling of granular materials under horizontal vibrations. *Phys. Rev. Lett.*, 79(5):833.

Savage, S. B. (1988). Streaming motions in a bed of vibrationaly fluidized dry granular material. *J. Fluid Mech.*, 194:457.

Sunthar, P. and Kumaran, V. (2001). Characterization of the stationary states of a dilute vibrofluidized granular bed. *Phys. Rev. E*, 64:041303.

Tennakoon, S. G. K. and Behringer, R. P. (1998). Vertical and horizontal vibration of granular materials: Coulomb friction and a novel switching state. *Phys. Rev. Lett.*, 81(4):794–797.

Tsimring, L. and Aranson, I. (1997). Localized and cellular patterns in a vibrated granular layer. Phys. Rev. Lett., 79(2):213–216.

Umbanhowar, P. B., Melo, F. and Swinney, H. L. (1996). “Localized excitations in a vertically vibrated granular layer”, Nature (London) 382, 793

Warr, S., Huntley, J. M. and Jacques, G. T. H. (1995): Fluidization of a two-dimensional granular system: Experimental study and scaling behavior. Phys. Rev. E, 52, 5583-5595.

Wassgren, C. R. (1997). Vibration of granular materials. PhD Thesis, California Institute of Technology, Pasadena, California.

Zik, O., Stevans, J. and Rabin, Y. (1992). “Mobility of a sphere in vibrated granular media”, Europhys. Lett., Vol. 17, No. 4, pp. 315-319.

6. Chapter 6: Effect of Vibration on the Shear Zone in Dry Granular Materials

6.1 Abstract

The following paper outlines the results of laboratory experiments conducted on glass beads and sand by using a modified vibrating direct shear apparatus. The behavior of the shear zone in the granular materials before, during and after the application of vibration is investigated at the pre-peak and residual strength states. Three zones are identified in the sheared granular material: *A* – the zone that is unaffected by the shear of the granular media, *B* – the shear zone portion that has been developed due to the shear of the material, but does not contribute to the critical state of the thinner shear zone *C,* at which the actual shear takes place. Also, the shear strength and deformation characteristics of the granular materials affected by vibration at their pre-peak and residual strength states are presented and discussed.

6.2 Introduction

The strength of a granular material is determined by the strength characteristics of the material at the shear zone/band defined by a certain combination of boundary conditions and the mechanical properties of the material. Therefore, to better understand the mechanism of the strength loss of granular materials, it is important to investigate the stress and deformation characteristics of the shear zone during its initiation and propagation through the granular media. The thickness of the shear zone is usually 8 to 10 times the mean grain diameter (Roscoe, 1970; Muhlhaus and Vardoulakis, 1987; Bardet and Proubet, 1992).

Some examples of the numerous studies on shear zones in granular media are provided below.

Bardet and Proubet (1992) investigated the emergence, inclination, and thickness of shear bands in idealized granular materials and showed that they are similar to those of real materials. Aidanpaa et al. (1996) used a torsional shear cell to study the shear layers of uniform spheres, and observed that the shear zone thickens and dilates with an increase in the shear speed, accompanied by a transition from a single layer to many layers of shearing. Bora (1984) experimentally investigated the shear failure mechanism in granular materials, and found that the friction angle is dependent on effective confining contact stress within a dilative range regardless of the drainage conditions and amount of particle crushing. Frost et al. (2002) studied the shear failure behavior of granular–continuum interfaces on a selection of sand–continuum material interfaces and through the use of discrete element modeling. Borja (2003) used a geological and mathematical framework to classify deformation patterns in granular media. Frost et al. (2004) evaluated the interface behaviour of granular soils by carrying out physical and numerical experiments. Rechenmacher (2005) evaluated local displacements and strains that are associated with shear band growth and evolution in sands by testing the plane strain with the use of digital image correlation (DIC). The magnitude of the shear and rotational strains was found to vary along the length of the shear bands, which lends support to the idea of fluctuating buildup and collapse of the "force chains". Alshibli and Alramahi (2006) investigated the evolution of local strains during the shearing of particles of a granular material, and showed that when compared to particle sliding, rotation is imperative in the shearing resistance of granular materials. Abriak and Caron (2006) conducted an experimental study of shear in granular media, and showed that granular media behavior depends on the local friction (grain–grain friction). Sadrekarimi (2008)

studied the shearing behavior of loose and dense sands by implementing constant volume ring shear tests. Widulinski et al. (2010) performed comparative modeling of shear localization in granular bodies with the finite and discrete element methods (FEM and DEM). Liu (2010) conducted laboratory experiments and numerical simulations to investigate the failure characteristics and micro-mechanical behaviors of granular soil slopes. Cox and Budhu (2010) studied the grain shape of granular materials, and through the use of light microscopy, determined that there are several grain shape parameters. They then related these parameters to the dilatancy of the granular materials. Mesarovic et al. (2013) analyzed the changes in the topology of a granular assembly during deformation by using the graph theory and showed that the elementary mechanism of diffuse deformation consists of intermittent flips, an increasing number of which directly stems from dilatancy, as well as that shear band formation is associated with the massive rolling of particles.

Direct shear testing has successfully been used to evaluate the shear strength characteristics of soils for many decades. Despite some of the disadvantages of the testing, such as lack of control of pore pressure, failure at predefined planes and non-uniform stress conditions in the tested samples, it is one of the most common shear strength evaluation tests used in geotechnical laboratories these days. The popularity of direct shear testing arises from the simplicity of the setup and ease of testing procedures.

Many researchers have studied the applicability and limitations of direct shear testing through experimental investigations and numerical modelling. One of the more early studies on direct shear testing through the use of finite element analysis was performed by Potts et al. (1987). They demonstrated that, despite the strongly non-uniform stresses and strains in the shear box before failure, strains and stresses in the final failure zone are surprisingly uniform. Liu et al.

(2005) investigated the interface friction through direct shear tests. Two improvements were made to reduce the friction of the sample material at the inner surface of the upper shear box, which caused the real shear strength to increase for a dense sample and decrease for a loose sample. Bagherzadeh-Khalkhali and Mirghasemi (2009) performed numerical modeling and experiments by using direct shear testing to study its suitability and limitations for testing coarse-grained soils. Li and Aydin (2010) investigated the fluctuations in vertical displacement and shear stress with different sized glass beads during direct shearing. Nam et al. (2011) used multistage direct shear tests to determine the shear strength of unsaturated soils, which allowed the matric suction to be independently controlled, and compared the results with samples which underwent conventional direct shear testing. Härtl and Ooi (2011) investigated, through direct shear tests, how particle shape and interparticle friction would influence bulk friction by using DEM. They showed that packing density has less influence than particle interlocking on the bulk friction. Kang et al. (2012) performed 3D discrete element simulations in conjunction with image processing of the pore geometry to determine the pore size distribution and orientation in dilative and contractive assemblies in direct shear testing.

Of special interest is the effect of vibration on the shear zone in granular media (Youd, 1968). In this work, the deformation and strength characteristics of two granular materials with different grain shapes are experimentally investigated by applying vibration at their pre-peak and residual strength states. The post-vibrational strength and volumetric changes of the materials are also evaluated, as well as a case in which the materials are sheared over a smooth glass surface. The laboratory experiments are performed on a modified vibrating direct shear apparatus, the description of which together with the test results will be provided in the following sections.

6.3 Testing Equipment and Procedures

A modified vibrating direct shear apparatus was used to conduct the laboratory experiments (see Figs. 6.1 and 6.2). The modifications included the installation of an electromagnetic actuator (11) between the shear box (2) and proving ring (3), as well as two load cells (10 and 12) for shear force measurement at the top and bottom halves of the shear box (2). An extension (13) was added to the main body (5) to accommodate all of the mentioned components. The actuator (11) incorporated two electromagnets, which generate vibrations in the horizontal shearing direction. The frequency and intensity of vibrations were controlled by a control panel (not shown in Fig. 6.1).

The measuring equipment consisted of two linear variable differential transformers (LVDTs) that measure vertical and horizontal displacements, two load cells (10 and 12), and two uniaxial accelerometers that measure the vertical and horizontal vibration accelerations on the soil samples. One of the accelerometers was placed on top of the loading plate (measured vertical vibration accelerations), and the other accelerometer was attached to the top half of the shear box in the direction of the shear (measured horizontal vibration accelerations). The output signals were acquired by using the NI CompactDAQ System, which was in turn, connected to a PC that logged the data with NI LabVIEW software.

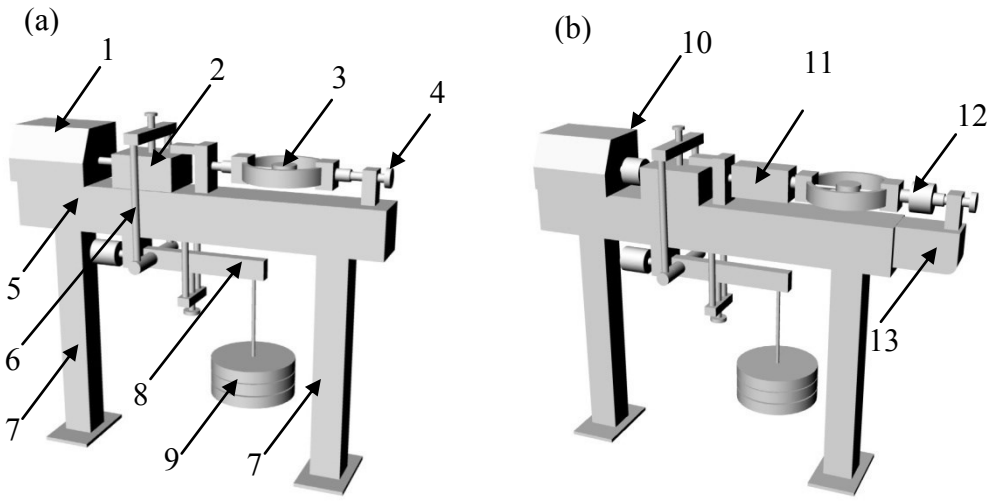

Figure 6.1 (a) – Strain controlled direct shear apparatus and (b) – modified strain controlled vibrating direct shear apparatus.

1 – Control panel of the direct shear apparatus; 2 – Shear box with a soil sample; 3 – Proving ring; 4 – Screw for zero setting of shear load before starting a test; 5 – Main body of the direct shear apparatus; 6 – Frame that transfers normal load to the soil sample placed in the shear box (2); 7 – Legs of the direct shear apparatus that supports the main body (5); 8 – lever that provides a normal load to the soil sample; 9 – Weights that define a normal load on the soil sample; 10 – Load cell; 11 –Actuator; 12 – Load cell; and 13 – Extension of the main body (5) of the direct shear apparatus (LVDTs that measured the vertical and shear displacements are not shown for simplicity).

The testing procedures were carried out in accordance with ASTM D3080/D3080M (Standard Test Method for Direct Shear Test of Soils Under Consolidated Drained Conditions), with additional vibration applied for a short period of time at the pre-peak and residual strength states. Depending on the objective of the test, vibrations were applied while the sample was being sheared, as well as when shearing was terminated. The frequency and force of the

vibrations were adjusted to the required magnitude and kept constant for the set of soil samples tested.

Each of the tested samples generated a set of plots, such as those provided in Figs. 6.6, 6.8 and 6.10. As seen from the figures, each plot set consists of four plots: shear resistance vs. normalized displacement, vertical displacement vs. normalized displacement, horizontal acceleration vs. normalized displacement and vertical acceleration vs. normalized displacement, as well as a short outline on the right hand side related to the type of material tested, normal stress, and vibration and material strength properties.

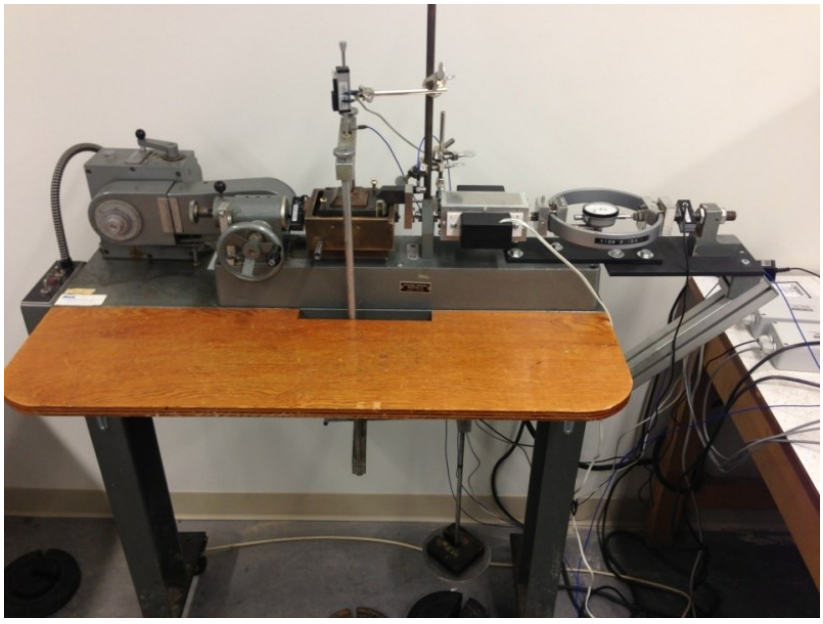

Figure 6.2 Modified direct shear apparatus.

6.4 Tested Materials

In order to investigate the effect of vibrating on the shear zone in granular materials, two different dry granular materials (40 samples) were tested on the modified direct shear apparatus. The tested materials were 0.55 mm glass beads and fine sand samples. The two materials were chosen with different particle shapes in order to investigate the particle shape effect on the shear zone of the granular materials under vibration. The samples filled a shear box with dimensions of 6 cm x 6 cm x 3.2 cm (W x L x H), after which, a constant compaction effort was applied to the samples which brought them to a dense state and similar density. Some of the samples were tested in the loose state, which was achieved by pouring the granular materials through a narrow neck funnel, and no consequent compaction. The samples were tested at normal stresses of 8, 23, 36, 50, 118 and 200 kPa in strain-controlled mode at a shear rate of 0.61 mm/min. The highest normal stress did not exceed 200 kPa to avoid grain crashing. The vibration frequency was 140 Hz, and the force of the actuator electromagnets was set at 7.14 N and kept constant to generate the same vibration intensity for all of the samples tested. The sensor data were logged at a frequency of 1 kHz.

The physical characteristics of the tested materials are given in Table 6.1, where ρ_s – is the density of the solids, ρ – bulk density, e – void ratio, n – porosity and φ_r – residual friction angle. The particle size distributions of the four materials are given in Fig.6.3. Representative samples of the materials were observed under a microscope to determine the shape of the particles (see Figs.6.4a and 6.4b). As can be seen in the photographs in Figs. 6.4a and 6.4b, the 0.55 mm glass beads have a practically ideal spherical shape, and the fine sand particles have an angular shape.

Table 6.1 Physical characteristics of the tested materials.

Material	ρ_s	ρ	e	n	ϕ_r
Glass Beads	2.65	1.566	0.692	0.409	21.9^0
Fine Sand	2.65	1.460	0.815	0.449	31.5^0

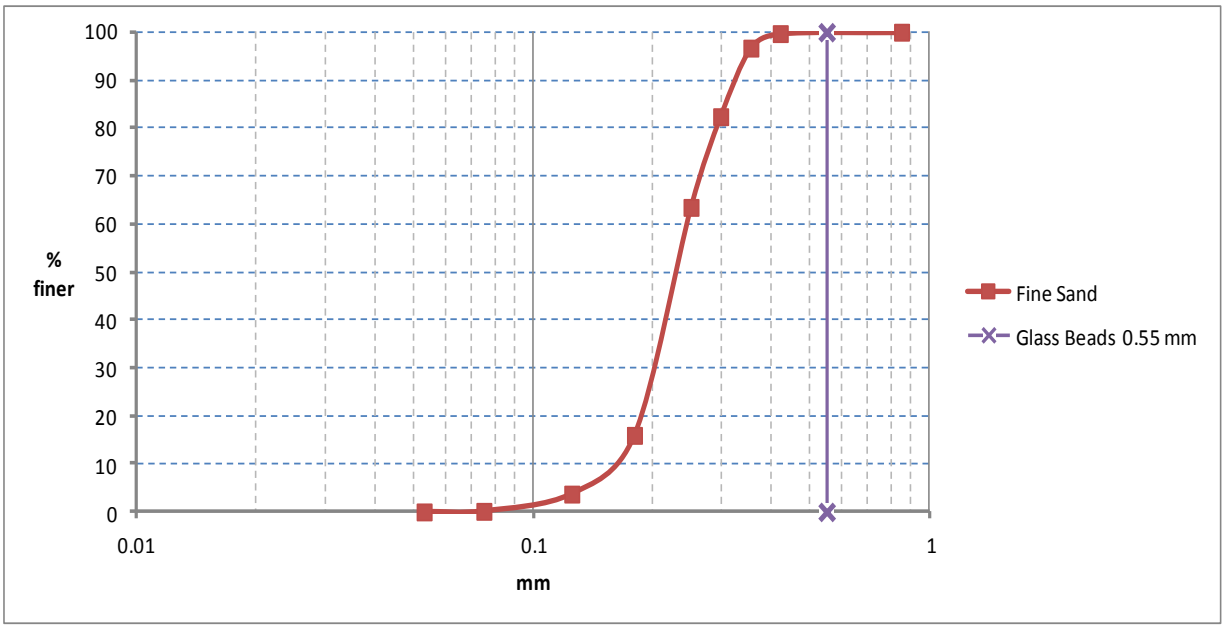

Figure 6.3 Particle size distribution of the tested materials.

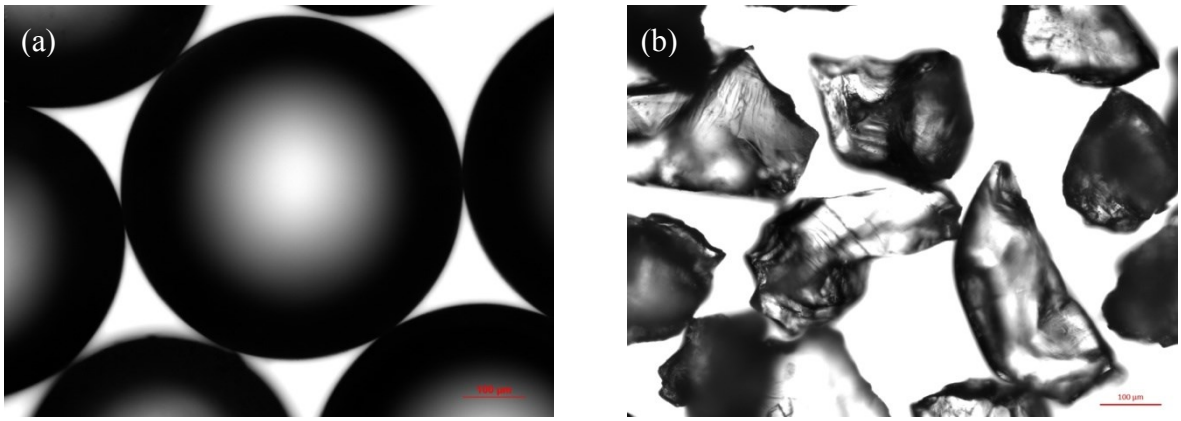

Figure 6.4 Photographs of the glass beads and sand samples under a microscope at magnification of 50x. (a) 0.55 mm glass beads and (b) fine sand.
(scale bar on the right bottom corner is 0.1 mm in length)

6.5 Test Results

6.5.1 Pre-Peak and Residual Strength States of Granular Materials under Vibration

Four samples of the 0.55 mm glass beads and four samples of the fine sand were tested to investigate the effect of vibration on their pre-peak and residual strengths and deformation properties. Vibration of the same intensity was applied for 15 sec while the samples were being sheared both at pre-peak and residual strength states. The test results are summarized in Table 6.2 and Figs. 6.5a and 6.5b. The relative acceleration (horizontal and vertical), Γ, given in Table 6.2, is a dimensionless parameter and defined as: $\Gamma = A\omega^2/g$, where A is the vibration amplitude, ω is the vibration frequency and g is the gravitational acceleration.

Table 6.2 Shear strengths and strength losses at pre-peak and residual strength states for 0.55 mm glass beads and fine sand.

Material	Normal Stress σ kPa	Peak Strength τ_p kPa	Residual Strength τ_r kPa	Vib.-Res. Strength τ_{vr} kPa	Residual Strength Loss $\Delta\tau$ kPa	Pre-Peak Strength Loss $\Delta\tau_p$ kPa	Horizontal Acceleration Γ_h	Vertical Acceleration Γ_v
0.55 mm Glass Beads	23	18	14	9	5	4	0.42	0.13
	50	31.5	26	18	8	4	0.41	0.13
	118	68.5	55.5	44.5	11	4	0.41	0.14
	200	110.5	85	69	16	3	0.40	0.13
Fine Sand	23	29	22.5	16	6.5	7.5	0.48	0.14
	50	51	38.5	31	7.5	6	0.48	0.14
	118	105.5	90	71	19	6.5	0.46	0.14
	200	164	134	119	15	8	0.42	0.14

As can be seen from Table 6.2, vibration of the glass bead samples at the pre-peak strength state does not affect their peak strength. The magnitude of the pre-peak strength loss was practically the same (≈4 kPa) for all normal stresses and smaller (especially at high normal stresses) than the strength loss at the residual strength state.

The same pattern of strength loss was observed in the case of the fine sand samples, with the exception that the pre-peak strength loss was somewhat greater (the horizontal accelerations as well) than that of the 0.55 mm glass beads, and ranged from 6 to 8 kPa. The peak strength was also not affected by vibration.

It is assumed tough that vibration of a greater intensity, capable of causing compaction of the materials, would densify the samples, which would in turn, result in an increase in their peak strength.

It is seen from Figs. 6.5a and 6.5b that vibration reduces the residual friction angle values of the tested glass beads and fine sand. Note that this is not real cohesion since granular materials have zero cohesion. The cohesion intercept is due to the assumption that a straight line can be used to approximate the shear strength envelop. The actual shear strength envelop is non-linear, especially at low normal stresses, due to particle interlocking and dilation.

Two examples of the fine sand and glass bead samples tested at a normal stress of 50 kPa are provided in Figs. 6.6 and 6.7, respectively. The vertical displacement plots in Figs. 6.6 and 6.7 show no deformation during pre-peak vibration. The only exception from the eight samples of the glass beads and sand is a fine sand sample tested at a normal stress of 23 kPa, where the sample experiences compressive deformation at the pre-peak strength state. It has to be mentioned that all 40 tested samples (both types of materials) demonstrated compressive deformations upon application of vibration at the residual strength state. Note that the normalized displacement in the plots of Figs. 6.6, 6.7, 6.14 and 6.15 is defined as $\Delta d/L$, where Δd is the horizontal displacement and L is the initial length of the specimen.

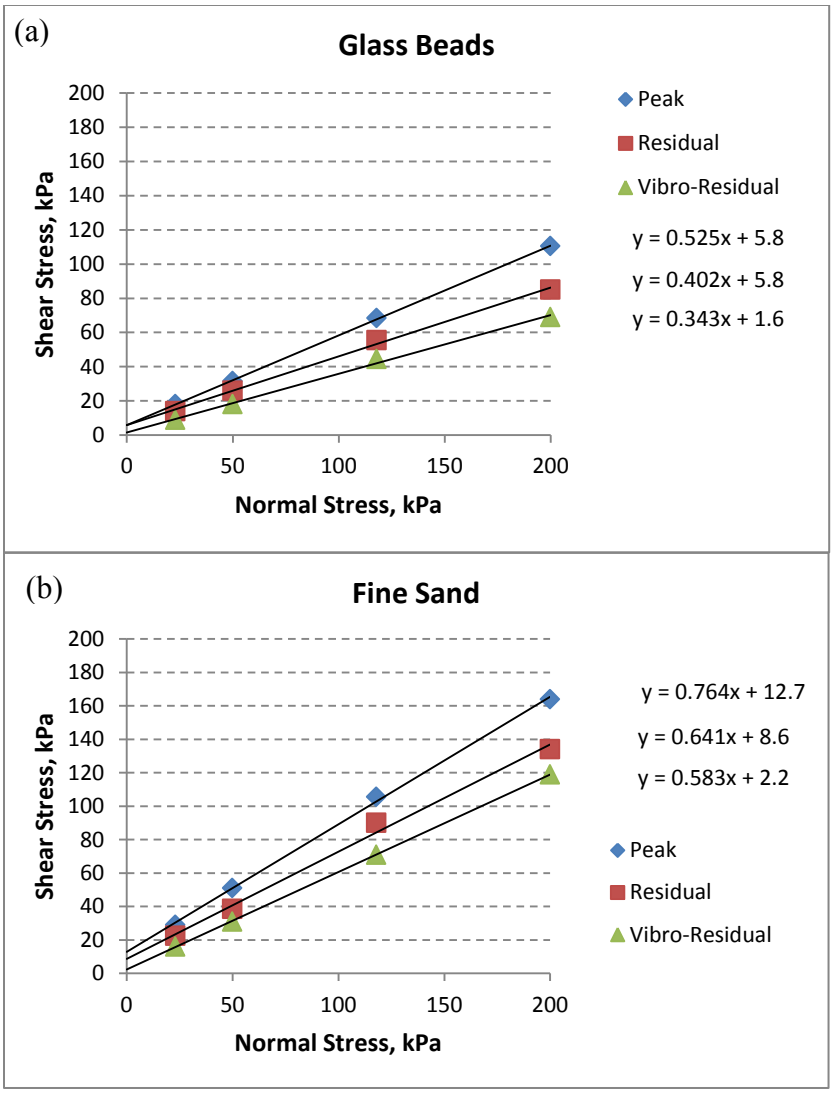

Figure 6.5 Shear strength diagrams of 0.55 mm glass beads (a) and fine sand (b).

The compressive deformation and relatively high value of strength loss at the pre-peak strength state of the fine sand sample tested at a normal stress of 23 kPa showed that compression of the fine sand at the given vibration intensity can take place only at low normal stresses. High normal stresses prevent the sand particles from sliding along each other during vibration at the pre-peak strength state.

In comparing the vertical deformation plots of the 0.55 mm glass beads and fine sand samples, the absence of compressive deformations due to vibration at the pre-peak strength state of the glass bead sample tested at a normal stress of 23 kPa can be explained by the difference in the particle shape of the glass beads (spherical) and the fine sand (angular) as shown in Figs. 6.4a and 6.4b.

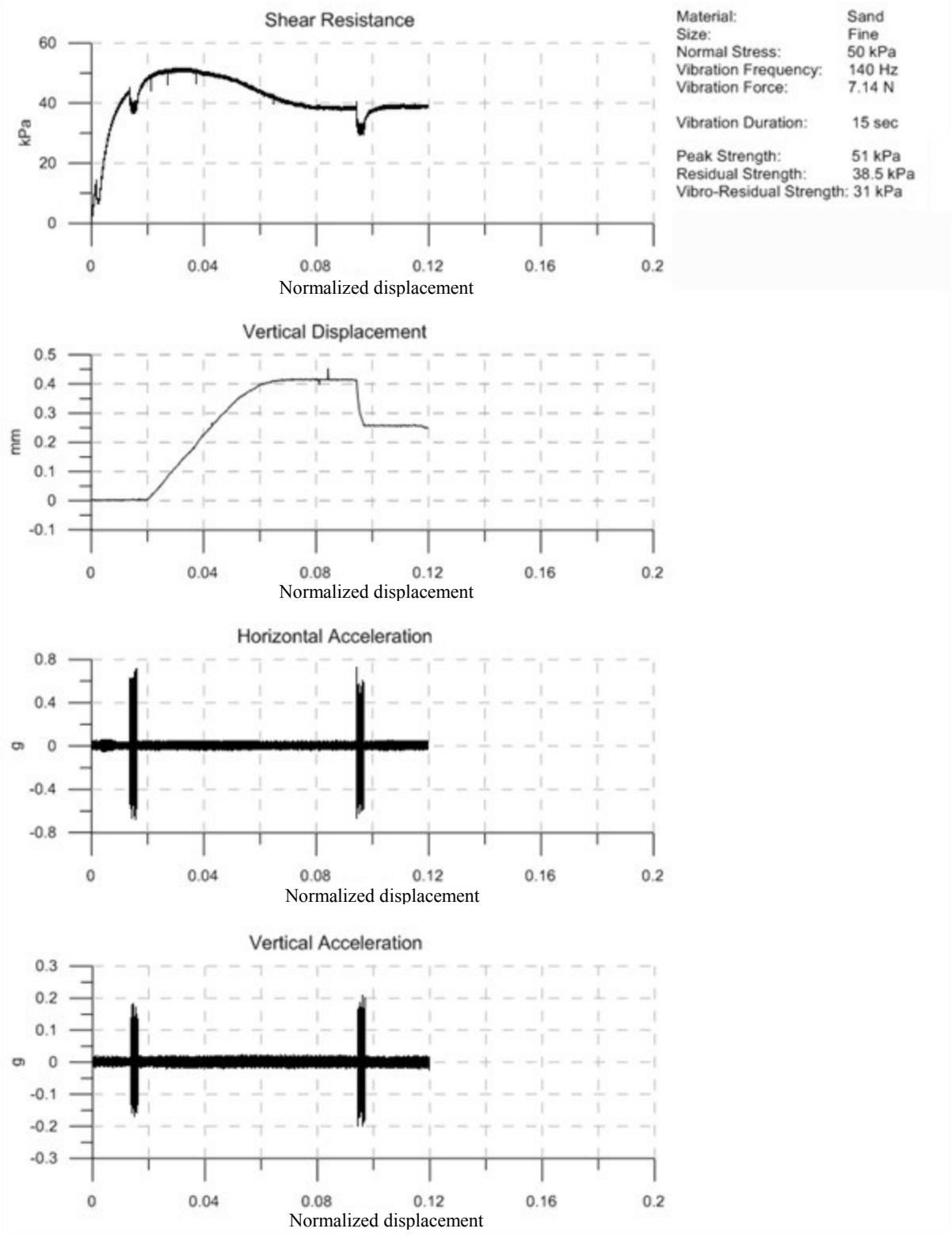

Figure 6.6 Vibration of fine sand at pre-peak and residual strength states.

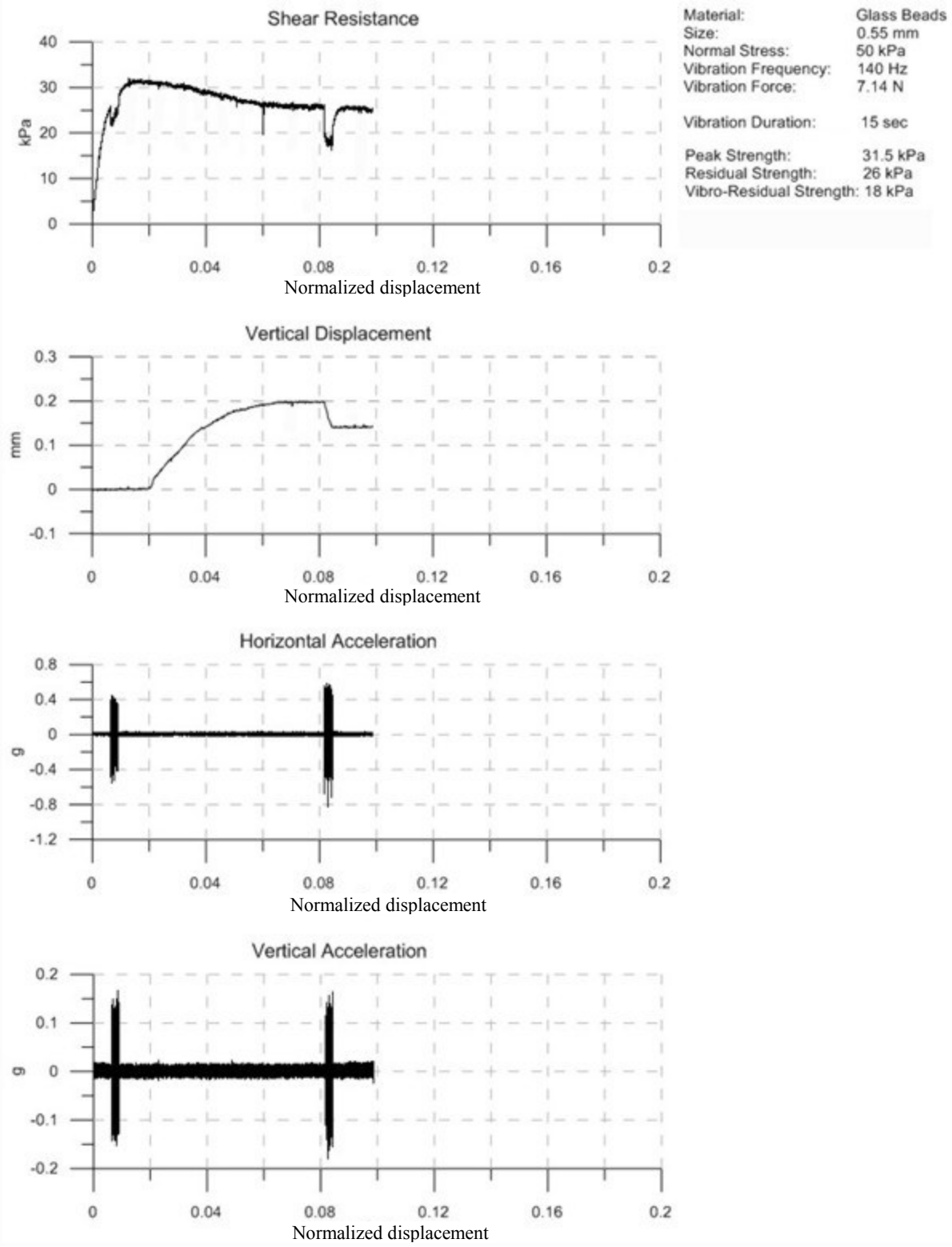

Figure 6.7 Vibration of 0.55 mm glass beads at pre-peak and residual strength states.

It is interesting to note that vibration at the residual strength state densifies the samples, thus decreasing their void ratio to a certain e value that stays constant after vibration termination, so that $e < e_{critical}$. This should lead to a strength level greater than the residual strength, but in fact, strength reaches the critical state (residual strength) and remains the same at a constant e value, as can be seen in Figs. 6.6 and 6.7. This phenomenon can possibly be explained in the following way: A dense granular material sample dilates when it is sheared, thus developing a shear zone. The thickness of this shear zone reaches a certain maximum value, which is greater than the actual shear zone thickness required for the sample to remain at the critical state. Since the material in the shear zone is looser than in the rest of the sample, vibration causes compression of the shear zone portion which no longer contributes to the developed critical state.

It is assumed that the absence of post-vibrational vertical deformations (dilation) can be attributed to the shearing that takes place when the vibration is applied. The ongoing shear deformations keep the actual shear zone at its critical state void ratio ($e_{critical}$) during vibration, thus preventing any further post-vibrational vertical deformations. It is also assumed that if a sample was subjected to the same intensity of vibration at the critical state, while not being sheared, the vibration would densify the actual shear zone to a certain void ratio ($e < e_{critical}$). This would increase the magnitude of compression induced by vibration, thus resulting in dilation with further shearing of the sample.

In other words, the post-vibration dilation of a granular material depends on the vibration intensity and the shear rate of the test. This means that post-vibration dilation can be caused not only by the termination of shearing during vibration, but also an increase in vibration intensity and lowering of the shear rate of the test.

6.5.2 Post-Vibrational Strength and Volumetric Changes of Granular Materials

As a result of the observations mentioned above, additional experiments were performed in order to investigate the impact of vibration on the post-vibrational strength and volumetric change characteristics of granular materials. These were particularly carried out to demonstrate and prove the assumption that the shear zone thickness in granular materials consists of two parts/zones: one that develops before the material reaches the critical state and the second (thinner than the initially developed thickness of the shear zone) that keeps the material in the critical state, so that the first part/zone does not contribute to the critical state maintained by the second thinner zone. A schematic drawing of the mentioned shear zone formation in a granular material is given in Fig. 6.8, where A denotes the zone unaffected by the shear of the granular medium, B is the shear zone portion that has been developed due to the shear of the material, but does not contribute to the critical state of shear zone C, at which the actual shear takes place.

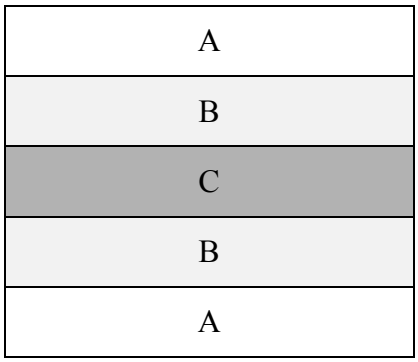

Figure 6.8 Schematic cross-section of the shear zone in a granular material.

Two materials, fine sand and 0.55 mm glass beads, were tested in dense and loose states for this purpose. The vibration applied at the residual strength state had a frequency of 140 Hz and vibration force of 7.14 N.

Dense samples were prepared in the same way as all of the previously tested samples, by filling the shear box with a certain amount of material and compacting the material. The loose samples were prepared by slowly filling the shear box with the granular material through a narrow neck funnel, with no consequent compaction, in order to achieve the loosest possible state. A total of 24 samples were tested: 12 samples of fine sand and 12 samples of 0.55 mm glass beads. Six samples of each material, in dense and loose states, were tested at normal stress values of 8, 23, 36, 50, 118 and 200 kPa. Unlike the previously tested samples, these samples were not sheared during the application of vibration, that is, shearing was terminated before and started after vibration. This was done to allow the shear zones B and C (see Fig. 6.8) to compress equally, so that the void ratio (or density) of the sample at the shear zone is not affected by shearing during the vibration. Four examples of the tests conducted on dense and loose 0.55 mm glass beads and fine sand at a normal stress of 23 kPa are given in Figs. 6.9 – 6.12.

After termination of vibration, the samples of dense fine sand tested at normal stresses of 8 and 23 kPa demonstrated dilation and shear resistance greater than those at the residual strength state. Then after a certain amount of shear deformation, the vertical displacement of the samples reached a constant value which was also the case for the shear resistance while approaching the residual strength value. The sample tested at σ=36 kPa did not demonstrate any changes in post-vibrational vertical displacement. On the other hand, the samples tested at σ=50, 118 and 200 kPa after some of the shear deformations started to compress, and higher normal stresses resulted in greater compression. This was probably due to some tilting of the loading plate, which usually

takes place in direct shear testing when shearing granular material at relatively high normal stresses, especially at high shear displacements.

In the case of the dense 0.55 mm glass beads (note that vibration was applied twice to the samples tested at σ=23, 36, 50 and 118 kPa), the samples that demonstrated post-vibration dilation and strength increase were those tested at σ=8, 23 and 36 kPa. The samples tested at normal stresses of 50a and 118 kPa had no post-vibrational vertical deformation changes, and the sample tested at σ=200 kPa showed some compression close to the end of the shear test.

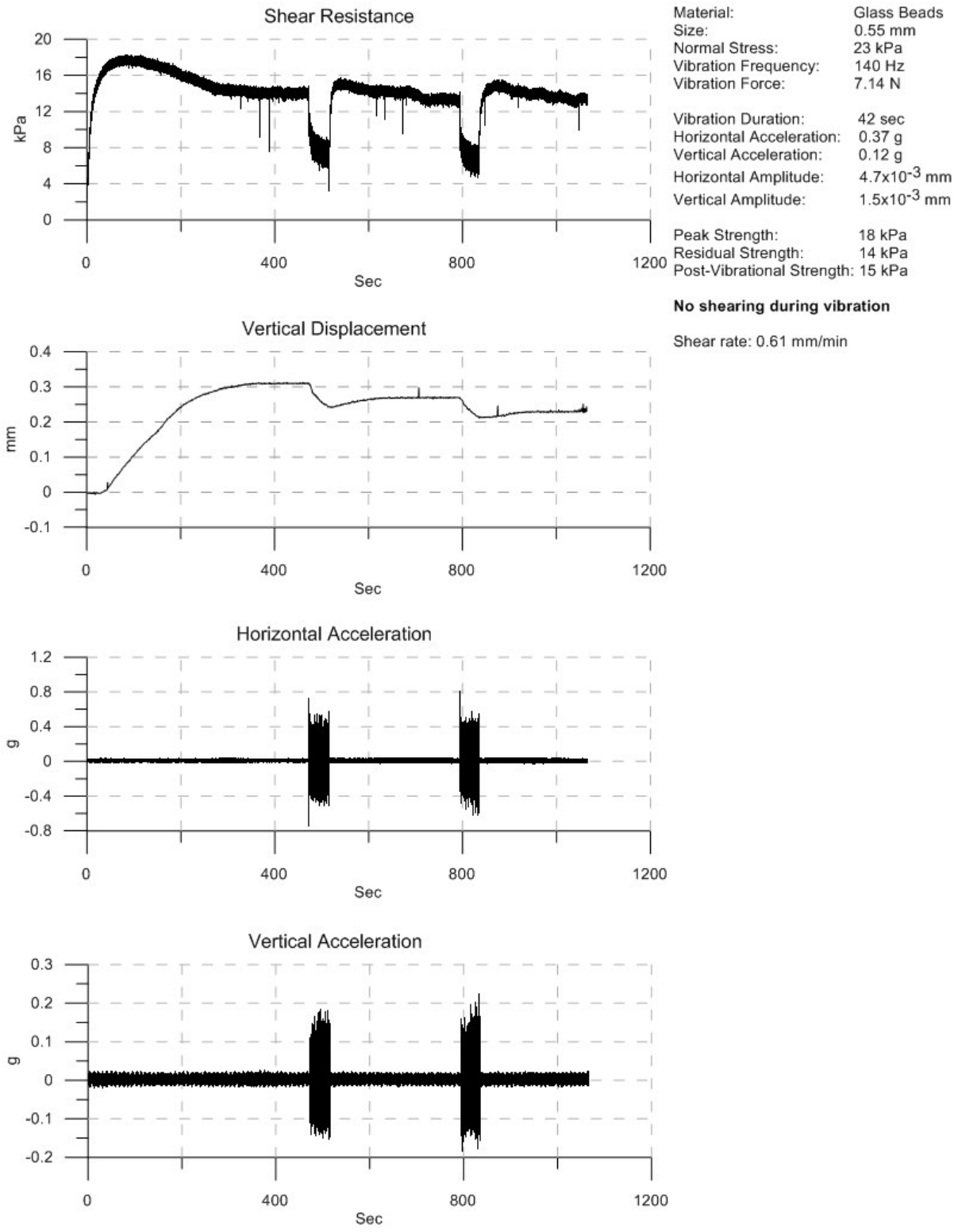

Figure 6.9 Test results of dense 0.55 mm glass beads tested at σ = 23 kPa.

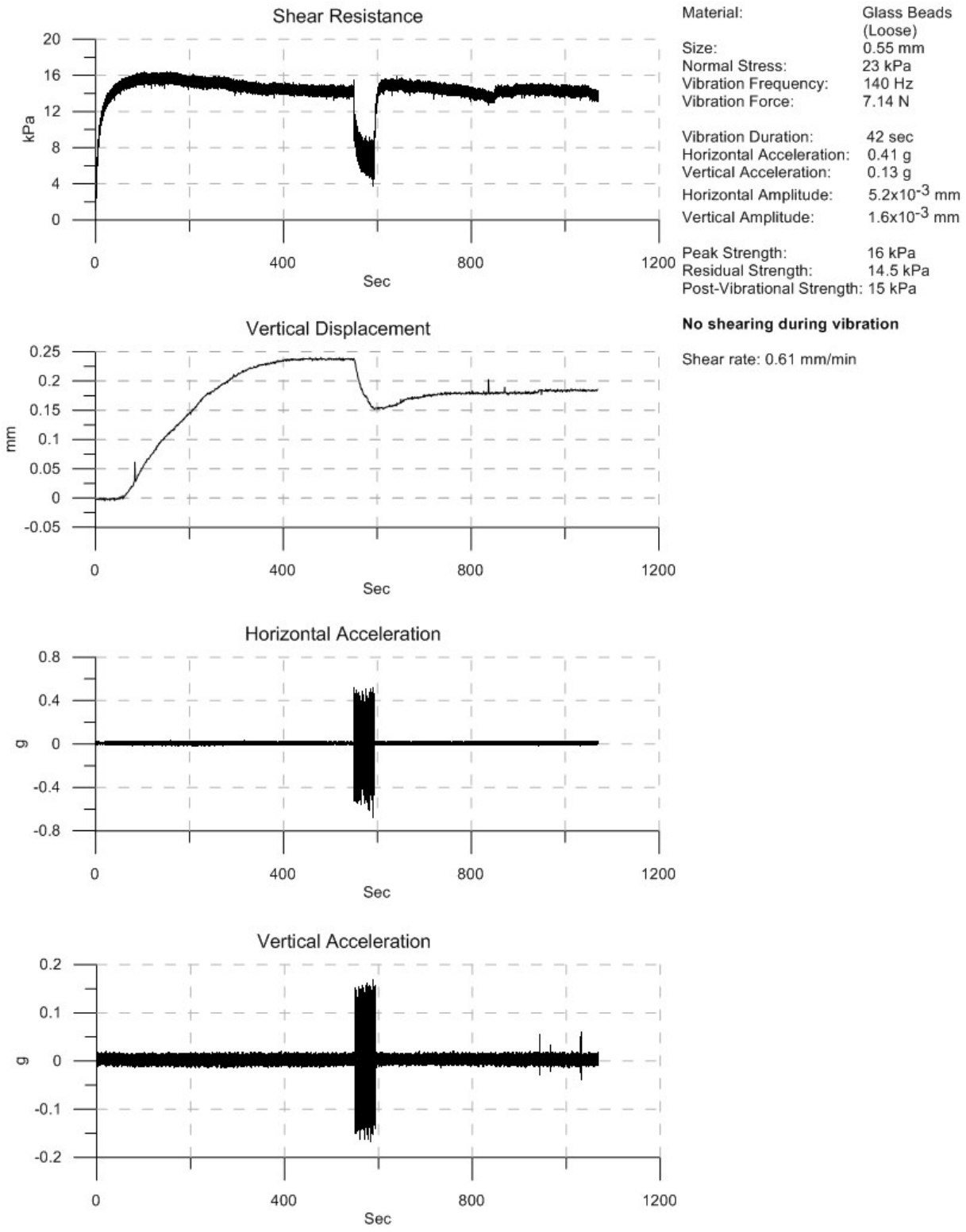

Figure 6.10 Test results of loose 0.55 mm glass beads tested at σ = 23 kPa.

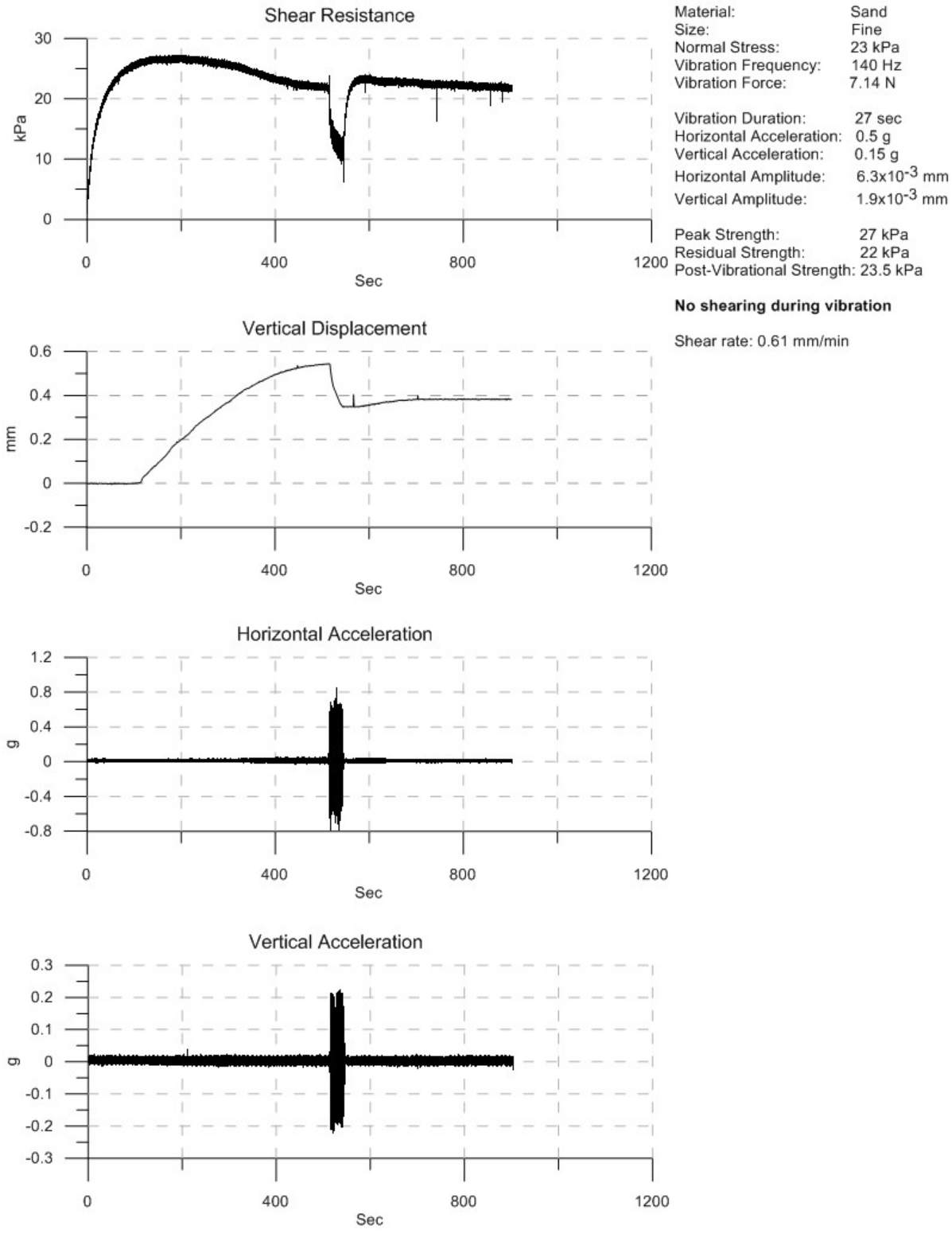

Figure 6.11 Test results of dense fine sand tested at σ = 23 kPa.

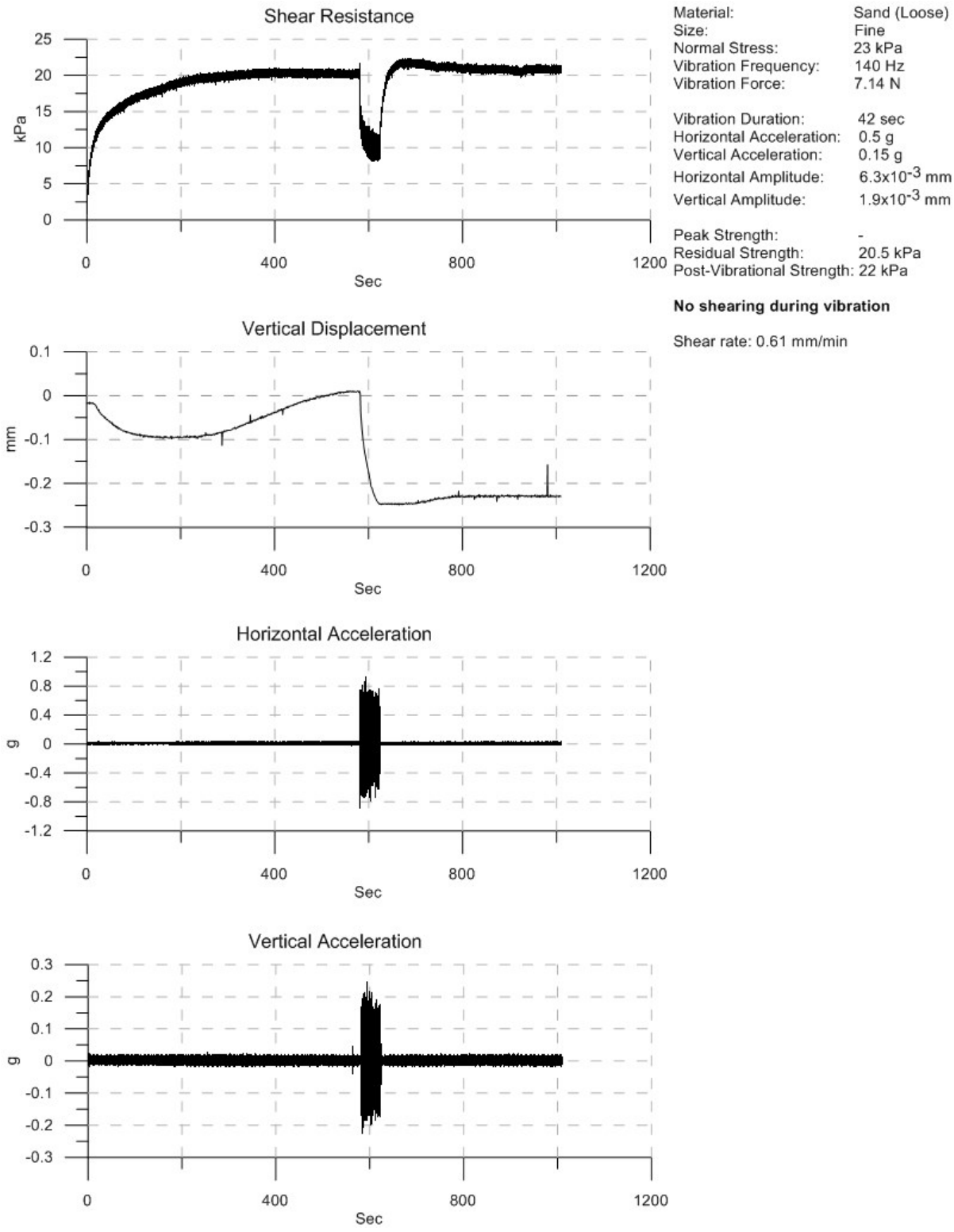

Figure 6.12 Test results of loose fine sand tested at σ = 23 kPa.

The test results of the loose fine sand and 0.55 mm glass beads show that there is similar behavior after vibration termination: samples tested at low normal stresses dilated to a certain degree with the associated changes in shear resistance.

As mentioned in the previous section, the samples of dense fine sand and 0.55 mm glass beads neither compressed nor dilated at the pre-peak vibration application, except for one fine sand sample tested at a normal stress of 23 kPa. This means that the vibration, with the mentioned characteristics, cannot cause any volumetric changes in the tested granular materials at their initial void ratio (or density). Since the same materials (with the same initial density) were tested with the same vibration characteristics, then all the volumetric changes are due to the dilation of the shear zone (due to shearing) and compression (due to vibration). Therefore, the post-vibration dilation of the samples observed can only be attributed to the void ratio increase of the shear zone due to the post-vibration shear of the material. As can be seen in Figs. 6.9 – 6.12, the magnitude of the post-vibration dilation is less than that of the compression caused by the vibration. Therefore, it can be inferred that the post-vibration dilation is due to the actual shear zone *C* (see Fig. 6.8). This proves the previous assumption that the shear zone in a granular material consists of two zones: *B* and *C,* as shown in Fig. 6.8.

The absence of the post-vibration dilation of the granular materials at higher normal stress values implies that the dilation of shear zone *C* at higher normal stresses takes place by means of a reduction in the void ratio of shear zone *B* (see Fig. 6.8).

In addition to the above described experiments, four more dense samples of the 0.55 mm glass beads and four samples of the fine sand were sheared over a smooth glass surface in order to provide additional support to the assumption zones A, B and C exist as outlined in Fig. 6.8.

The samples were tested at normal stresses of 23, 50, 118 and 200 kPa. Vibration was applied to the samples for 30 sec at their residual strength state.

The test results of the eight samples are summarized in Table 6.3 and Figs. 6.13a and 6.13b. Two examples of the fine sand and glass beads tested at a normal stress of 50 kPa are given in Figs. 6.14 and 6.15, respectively.

Table 6.3 Test results of 0.55 mm glass beads and sand sheared over smooth glass surface.

Material	**Normal Stress** σ **kPa**	**Peak Strength** τ_p **kPa**	**Residual Strength** τ_r **kPa**	**Vib.-Res. Strength** τ_{vr} **kPa**	**Residual Strength Loss** $\Delta\tau$ **kPa**	**Horizontal Acceleration** Γ_h	**Vertical Acceleration** Γ_v
0.55 mm Glass Beads	23	-	3	1.5	1.5	0.33	0.17
	50	6	5	3.5	1.5	0.32	0.22
	118	12	9	7.5	1.5	0.3	0.15
	200	21.5	16	14.5	1.5	0.3	0.14
Fine Sand	23	-	3	1.5	1.5	0.33	0.16
	50	6	5.5	4	1.5	0.32	0.18
	118	14.5	12.5	11	1.5	0.32	0.13
	200	25.5	22	20.5	1.5	0.33	0.19

As expected, the residual friction angles of the materials tested over the smooth glass surface are much less than those of the materials themselves, which are 4.1^o for the glass beads and 6.2^o for the fine sand. Both materials have no peak strength at σ = 23 kPa (see Table 6.3), which implies that dense granular materials do not generate peak strength when sheared over a smooth surface at low normal stress values. The peak friction angles of the glass beads and fine sand are 5.9^o and 7.3^o, respectively.

As can be seen from Table 6.3 and Figs. 6.13a and 6.13b, vibration lowers the residual strength of both materials by the same magnitude, $\Delta\tau$=1.5 kPa, at all normal stresses. Therefore, in this case, there are no changes in the residual friction angles of the tested materials.

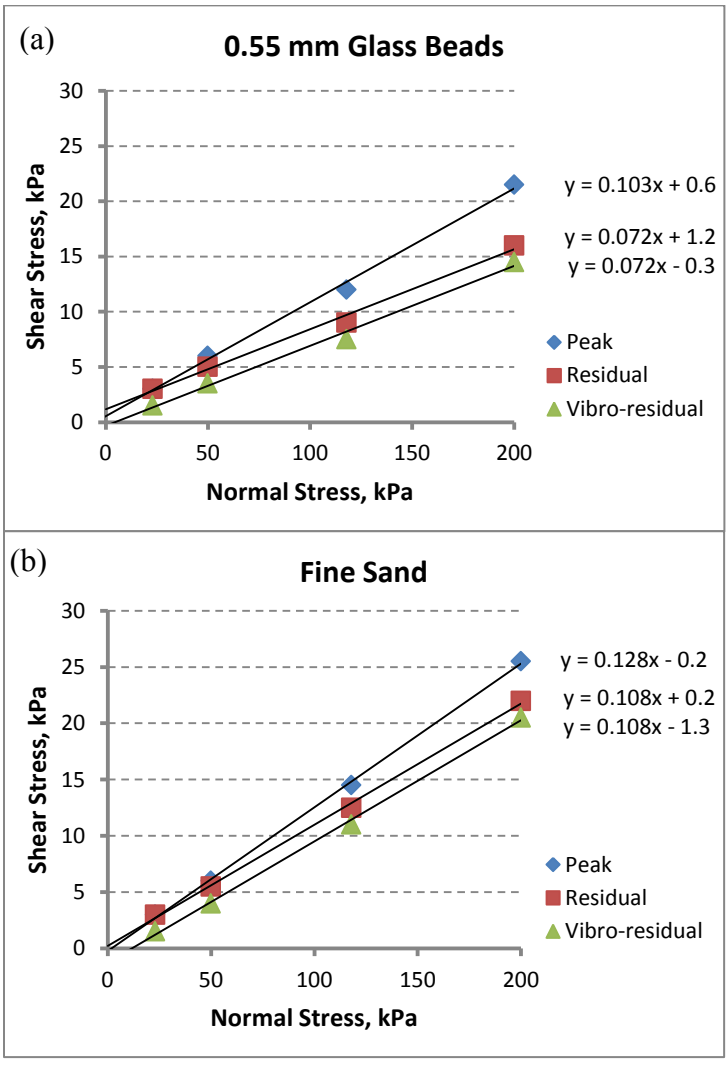

Figure 6.13 Shear strength diagrams of 0.55 mm glass beads (a) and fine sand (b).

The examples presented in Figs. 6.14 and 6.15 show that vibration does not generate any compressive deformations of the samples. In fact, it caused a negligible dilation that took place instantly with no further changes in vertical deformation. A similar behavior of vertical deformation can be observed in the case of the glass beads tested at normal stresses of 23 and 50 kPa, as well as fine sand samples tested at σ = 23, 50 and 118 kPa. The rest of the samples did not experience any vertical deformations upon the application of vibration.

It should also be mentioned that vibration did not cause any post-vibrational changes in the shear resistance of all eight samples. Apparently, the densities of the dense granular materials were not affected by the vibration, and neither were their post-vibrational residual strengths. Therefore, it can be concluded that when a granular material is sheared over a smooth glass surface, the void ratio of the material at the shear surface/zone remains unchanged during and after the application of vibration. This implies that in this case, the entire material of each of the tested samples can be classified as Zone *A* as described earlier in the text and presented in Fig. 6.8.

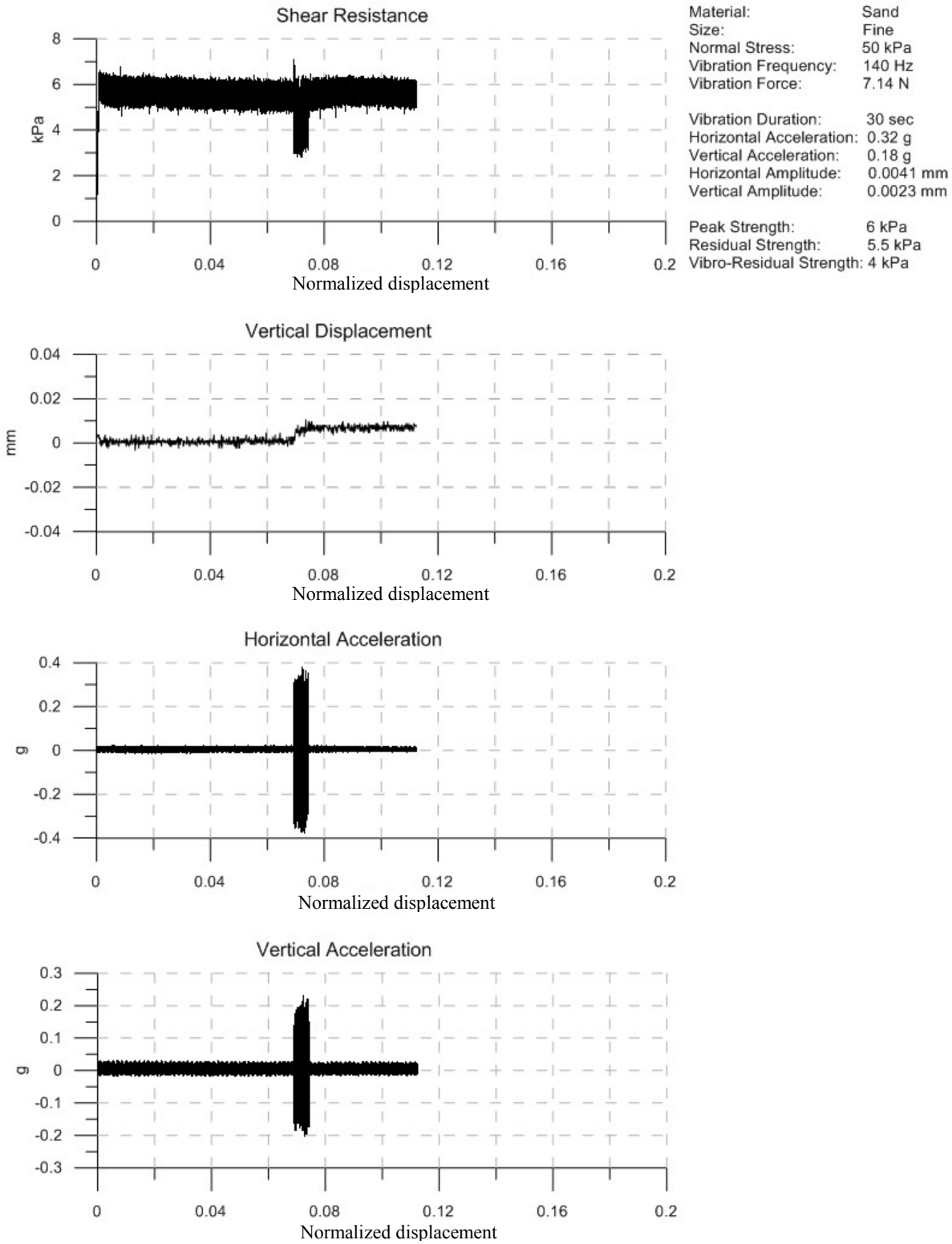

Figure 6.14 An example of test results of fine sand sheared over smooth glass surface.

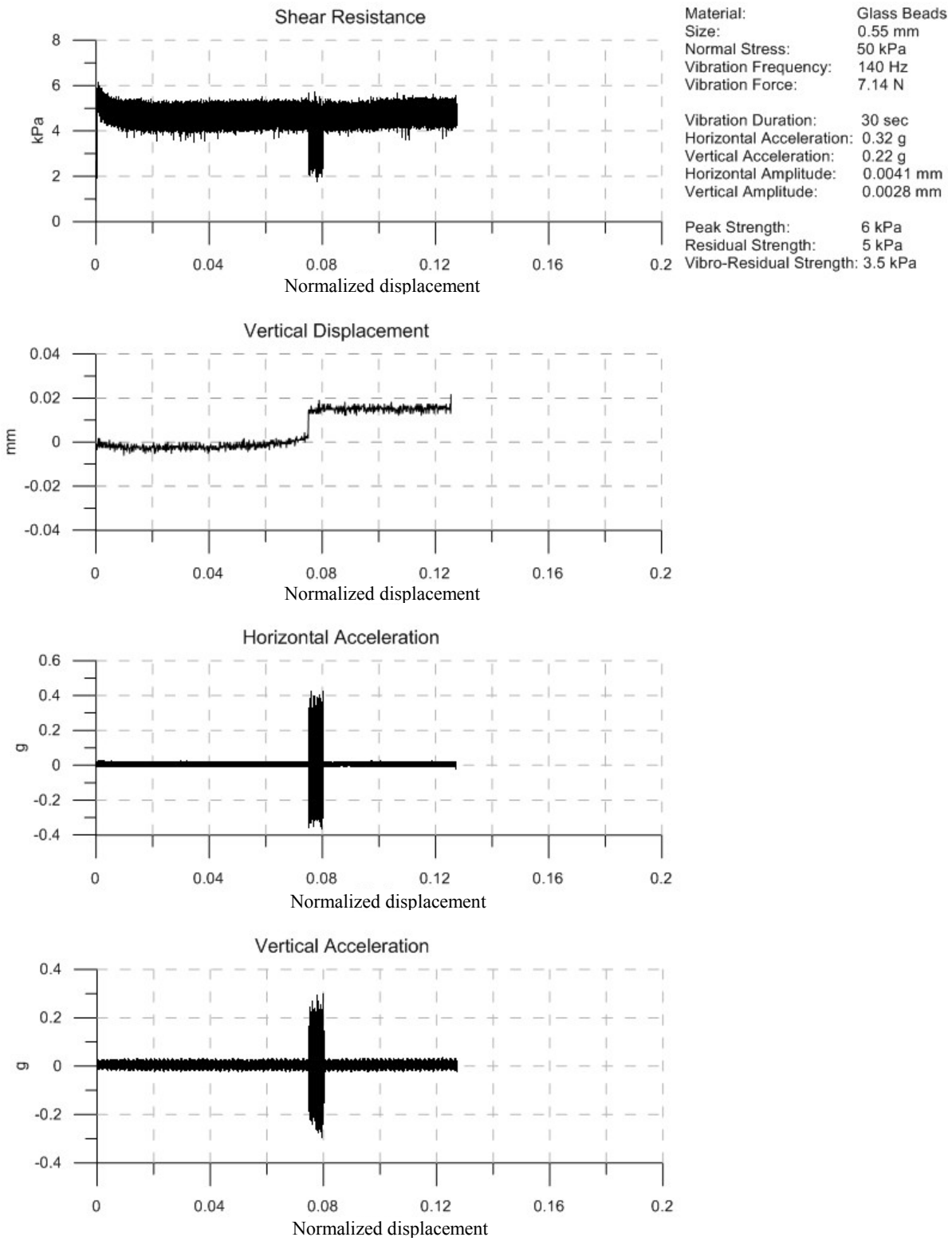

Figure 6.15 Example of test results of 0.55 mm glass beads sheared over smooth glass surface.

6.6 Conclusions

- Vibration of sufficiently strong intensity reduces the residual friction angles of the granular materials in this study.
- All of the tested samples (both types of materials) demonstrate compressive deformation upon application of vibration at the residual strength state.
- Vibration of a given intensity applied at the pre-peak strength state of the granular materials does not affect their peak strengths.
- The magnitude of the pre-peak strength loss of the granular materials caused by vibration is generally the same at all normal stresses, and smaller (especially at higher normal stresses) than the strength loss at the residual strength state.
- It is assumed that vibration of a greater intensity, capable of causing compaction of the granular materials, would densify the samples, which would in turn, result in an increase in their peak strength.
- All of the tested samples do not experience any volumetric changes due to vibration at their pre-peak strength state, except for one sample of fine sand tested at a normal stress of 23 kPa which showed some compression.
- Dense granular material dilates when sheared, thus developing a shear zone. The thickness of this shear zone reaches a certain maximum value, which is greater than the actual thickness of the shear zone required for the sample to remain at the critical state.
- Three zones are identified in a sheared granular material: *A* – zone unaffected by shear of the granular medium, *B* – shear zone portion that has been developed due to the shear of

the material, but does not contribute to the critical state of shear zone *C*, at which the actual shear takes place.

- The concept of the *A*, *B* and *C* zones correlates well with the finite element analysis results obtained by Potts et al. (1987).
- As expected, the residual friction angles of the materials tested over a smooth glass surface are much less than those of the materials themselves.
- Dense granular materials do not generate peak strength when sheared over a smooth surface at low normal stress values.
- The strength loss of the granular materials caused by vibration has the same magnitude at all normal stresses, which means that vibration does not reduce the residual friction angles of the materials sheared over a smooth glass surface.
- When a granular material is sheared over a smooth glass surface, the void ratio of the material at the shear surface/zone remains unchanged during and after the application of vibration.

6.7 References

Abriak, N. E. and Caron J.-F. (2006). "Experimental study of shear in granular media". Advanced Powder Technol., Vol. 17, No. 3, pp. 297–318.

Aidanpaa, J. O., Shen, H. H. and Gupta, R. B. (1996). "Experimental and Numerical Studies of Shear Layers in Granular Shear Cell". J. Eng. Mech., 122, pp. 187-196.

Alshibli, K. A. and Alramahi, B. A. (2006). "Microscopic Evaluation of Strain Distribution in Granular Materials during Shear". J. Geotech. Geoenviron. Eng.132, pp. 80-91.

ASTM D5311. "Standard Test Method for Load Controlled Cyclic Triaxial Strength of Soil".

Bagherzadeh-Khalkhali, A. and Mirghasemi, A. A. (2009). "Numerical and experimental direct shear tests for coarse-grained soils". Particuology, 7, pp. 83–91.

Bardet, J. P., and Proubet, J. (1992). "Shear-Band Analysis in Idealized Granular Material". J. Eng. Mech., 118, pp. 397-415.

Bora, P. K. (1984). "Shear Failure in Granular Media". J. Eng. Mech. 110, pp. 582-598.

Borja, R. I. (2003). "Deformation bands in granular media". Geomechanics: Testing, Modeling, and Simulation. pp. 394-399.

Cox, M. R. and Budhu, M. (2010). "Grain Shape Quantifications and their Relationship to Dilatancy". GeoFlorida 2010: Advances in Analysis, Modeling & Design, pp. 540-549.

Frost, J. D., DeJong, J. T. and Recalde, M. (2002). "Shear failure behavior of granular–continuum interfaces". Engineering Fracture Mechanics, 69, pp. 2029–2048.

Frost, D., Hebeler, G. L., Evans, T. M. and DeJong, J. T. (2004). "Interface behaviour of granular soils". Earth and Space, pp. 65-72.

Härtl, J. and Ooi, J. Y. (2011). "Numerical investigation of particle shape and particle friction on limiting bulk friction in direct shear tests and comparison with experiments". Powder Technology, 212, pp. 231–239.

Kang, D. H., Choo, J. and Yun, T. S. (2012). "Evolution of pore characteristics in the 3D numerical direct shear test". Computers and Geotechnics, 49, pp. 53–61.

Youd, L. T. (1968) Reduction of critical void ratio during steady-state vibration. International symposium on wave propagation and dynamic properties of earth materials, Albuquerque, N. Mex., 1967, Proc.

Li, Y. R. and Aydin, A. (2010). "Behavior of rounded granular materials in direct shear: Mechanisms and quantification of fluctuations". Engineering Geology, 115, pp. 96–104.

Liu, S. H., Sun, D., Matsuoka, H. (2005). "On the interface friction in direct shear test". Computers and Geotechnics, 32, pp. 317–325.

Liu, S. (2010). "Failure Mechanism of Granular Soil Slopes". Earth and Space 2010: Engineering, Science, Construction, and Operations in Challenging Environments, ASCE, pp. 3724-3752.

Mesarovic, S. Dj., Padbidri, J. M. and Muhunthan, B. (2013). "Micromechanics of dilatancy, critical state and shear bands in dense granular matter". Poromechanics V, ASCE, pp. 1067-1074.

Muhlhaus, H. B., and Vardoulakis, I. (1987). "The thickness of shear bands in granular materials." Geotechnique, 37, pp. 271-283.

Nam, S., Gutierrez, M., Diplas, P. and Petrie, J. (2011). "Determination of the shear strength of unsaturated soils using the multistage direct shear test". Engineering Geology, 122, pp. 272–280.

National Instruments website: http://www.ni.com/labview/ (accessed in September, 2013)

Potts, D. M., Dounias, G. T., and Vaughan, P. R. (1987). "Finite element analysis of the direct shear box test". Geotechnique, 37(1), pp. 11-23.

Rechenmacher, A. L. (2005). "Grain scale processes associated with shear banding in sands". Geomechanics II, pp. 342-355.

Roscoe, K. H. (1970). "Tenth Rankine lecture: The influence of strains in soil mechanics", Geotechnique, 20, pp. 129-170.

Sadrekarimi, A. (2008). "Shearing Behavior of Sands in Terms of Compressibility Mechanisms". GeoCongress 2008: Characterization, Monitoring and Modeling of GeoSystems. pp. 197-204.

Widulinski, L., Kozicki, J. and Tejchman, J. (2010). "Comparative Modeling of Shear Localization in Granular Bodies with FEM and DEM". GeoShanghai 2010 International Conference, Soil Behavior and Geo-Micromechanics, pp. 198-203.

7. Chapter 7: Summary, Conclusions and Recommendations

7.1 Summary

The focus of the accomplished research project is the influence of vibration on the strength properties of dry granular media. The granular materials used in the experimental program are dry and free of cementation so as to better explore the mechanism of vibration impacts on the shear strength and deformation characteristics of the tested materials from the standpoint of vibrational fluidization.

In this research work, a new vibrating direct shear apparatus has been designed and built to evaluate the strength and deformation characteristics of soils under a wide range of vibrational accelerations. The apparatus is used throughout the research project to investigate the behavior of dry granular materials at their residual strength states under the influence of vibration with different intensities. The impact of vibration on the normal (overburden) stress and the peak strength of granular materials is evaluated. Experiments have also been conducted to study the post-vibrational behavior of granular materials, as well as the particle shape effect on the strength loss and deformation of the granular media during vibration. Finally, the behavior of the shear zone in the granular materials before, during and after the application of vibration at the pre-peak and residual strength states is investigated.

Chapters 3, 4, 5 and 6 are summaries of the experimental results of about 200 tested samples with different granular materials where the new vibrating direct shear apparatus is used with different testing modes, procedures, normal stresses and vibration intensities. A number of plots have been presented that show the behavior of the granular materials under the impact of

vibration in different testing conditions. The Mohr-Coulomb equation for granular materials has been modified to account for the effect of vibrational fluidization. A new pattern of the shear zone in granular media has been provided which outlines the deformation and shear resistance before, during and after the application of vibration. Finally, some valuable conclusions have been made and will be presented in the next section.

7.2 Conclusions

The following conclusions have been made based on the results of the conducted research project.

1. The new vibrating direct shear apparatus can be successfully used to determine the strength and deformation characteristics of fine and granular soils (up to the size of coarse sand) under different accelerations and frequencies of vibration.
2. Upon application of a sufficiently strong vibration at the critical strength state of a granular material, an immediate strength loss takes place from the residual to the vibro-residual strengths. An increase in vibration intensity results in a larger residual strength loss at a given normal stress.
3. Sufficiently strong vibration reduces the residual friction angle of granular materials. An increase in vibration intensity results in lower vibro-residual friction angles.
4. Initially dense or loose granular material compresses when vibration is applied at its critical strength state. An increase in horizontal vibration acceleration results in greater compression deformation.

5. Although normal stress reduction caused by vibration contributes to the residual strength loss in granular materials, the strength loss is mainly due to the material fluidization.
6. At low vibrational accelerations, the relationship between the residual strength loss and horizontal acceleration is nonlinear for the granular materials that have irregularly shaped particles. The nonlinearity increases with an increase in confining (normal) stress. On the other hand, the relationship between strength loss and horizontal acceleration is linear for glass beads with spherical shaped particles.
7. Besides reducing the friction angles of granular materials, vibration causes the intersection of the shear strength envelop with the normal stress axis at a certain vibro-fluidizational limit value, σ_f, which increases with an increase in vibration intensity. This implies that at a given vibration acceleration, a granular material can fluidize at normal stresses up to the σ_f value, and above this σ_f value, it remains in a solid state. Thus, the Coulomb's equation for dry granular material, $\tau = \sigma \tan \varphi$, can be written as: $\tau = (\sigma + \sigma_f) \tan \varphi_{vr}$, where φ_{vr} is the vibro-residual friction angle of the material.
8. In a wide range of horizontal vibration acceleration values ($0 < \Gamma_h < 4.5$), the reduction of the residual friction angles of the tested granular materials with an increase in vibration intensity is practically linear. The only noticeable deviation from the linear pattern of the relationship between φ and Γ_h is observed at Γ_h values less than 1. Thus, the φ vs. Γ_h plots can be used for the approximation of the changes in residual friction angle of sand sized dry granular materials (with residual friction angles between 21^o to 32^o) when subjected to vibration in the given range of horizontal acceleration values.
9. The plots of the relationship between σ_f and Γ_h for all of the tested materials are linear. At a given vibration intensity, the glass beads have a greater magnitude of σ_f than the sands with

well rounded and angular particle shapes, the plots of which practically coincide. It can be assumed that there is a certain level of roundness, above which, the σ_f vs. Γ_h plot will shift from that of the sands to the one for glass beads.

10. The largest amount of compressive deformation of the granular materials induced by vibration is observed at the lowest normal stress. An increase in normal stress leads to a compression reduction. This phenomenon is also apparent from the magnitude of the post-vibration peak of the shear resistance plots. Higher normal stresses mean lower post-vibration peaks.
11. When vibration is applied at the pre-peak strength state of a dense granular material, it does not lower the peak strength of the material. The vibration may increase the peak strength if its intensity is strong enough to densify the material.
12. It appears that the essence of acoustic fluidization which attempts to explain the large runout distance of big rock avalanches (Melosh, 1979), and vibrational fluidization observed in the above mentioned experiments is the same: the resistance of granular media at the shear interface is affected by the vibration generated by collision of the grains.
13. When a dense granular material is sheared, it dilates, thus developing a shear zone. The thickness of this shear zone reaches a certain maximum value, which is greater than the actual thickness of the shear zone required for the sample to remain at the critical state. Thus, three zones are identified in a sheared granular material: *A* – the zone unaffected by the shear of the granular medium, *B* – the shear zone portion that has been developed due to the shear of the material, but does not contribute to the critical state of shear zone *C,* at which the actual shear takes place. The concept of the *A*, *B* and *C* zones correlates well with the finite element analysis results obtained by Potts et al. (1987).

7.3 Recommendations

Recommendations for future work are as follows.

- The effect of vibration frequency on the strength and deformation characteristics of granular media should be experimentally investigated. It is recommended that experiments be conducted on granular materials by subjecting them to different frequency vibrations at their critical strength states. Depending on the technical characteristics of the vibrational actuator, which is used as part of the vibrating direct shear apparatus, vibration should be applied in the widest possible range of frequency (approximately 5 to 250 Hz) by keeping the vibration amplitude constant, such that the magnitude of the vibrational accelerations is controlled by the frequency of vibration.
- Granular materials can be tested at different moisture contents to investigate the effect of moisture content on the strength and deformation characteristics of the granular media under the influence of vibration.
- Numerical simulations should be carried out by using 3D DEM software to investigate the effect of vibration on the critical void ratio and shear strength of granular materials, and relate the results to the critical state theory of granular materials.
    - The numerical model can be calibrated by using the experimental results of the 0.55 mm glass beads in this work (see Chapters 4 and 5).
    - Numerical simulations can be implemented with a wide range of vibrational accelerations, amplitudes and frequencies.
    - Numerical simulations can be carried out to quantify and visualize the *A*, *B* and *C* shear zones (see Chapter 6) in granular media.

- Numerical simulations can be implemented to evaluate the effect of particle size and shape on the behavior of granular materials during vibration, by creating particles from combined and different sized spheres.

References

Abriak, N. E. and Caron, J. F. (2006). "Experimental study of shear in granular media." Advanced Powder Technol., Vol. 17, No. 3, pp. 297–318.

Aidanpaa, J. O., Shen, H. H. and Gupta, R. B. (1996). "Experimental and Numerical Studies of Shear Layers in Granular Shear Cell." J. Eng. Mech., 122, pp. 187-196.

Alexeev, A., Royzen, V., Dudko, A., Goldshtein, A. and Shapiro, M. (2000). "Mixing and Segregation in Vertically Vibrated Granular Layers." Solid Mechanics and Its Applications, Volume 81, 2000, pp 129-139

Alshibli, K. A. and Alramahi, B. A. (2006). "Microscopic Evaluation of Strain Distribution in Granular Materials during Shear." J. Geotech. Geoenviron. Eng.132, pp. 80-91.

Arango, I. and Seed, H. B. (1974). "Seismic stability and deformation of clay slopes." J. Geotech. Engrg. Div., 100(2), pp. 139–156.

ASTM D5311. "Standard Test Method for Load Controlled Cyclic Triaxial Strength of Soil."

Ayer, J. E. and Soppet, F. E. (1965/1966). "Vibratory Compaction, Part I: Compaction of Spherical Shapes and Part II: Compaction of Angular Shapes." J. Am. Ceramic Soc. 48, 180-183 and 49, 207-210.

Bagherzadeh-Khalkhali, A. and Mirghasemi, A. A. (2009). "Numerical and experimental direct shear tests for coarse-grained soils." Particuology, 7, pp. 83–91.

Bagnold, R. A. (1954). "Experiments on the Gravity-Free Dispersion of Large Solid Spheres in a Newtonian Fluid Under Shear." Proc. Royal Soc. London 225. pp. 49–63.

Bardet, J. P., and Proubet, J. (1992). "Shear-Band Analysis in Idealized Granular Material." J. Eng. Mech., 118, pp. 397-415.

Barkan, D. D. (1962). "Dynamics of Basis and Foundations." Translated from Russian by L. Drashevska, New York, McGraw-Hill, 434 p.

Bjerrum, L., Kringstad, S. and Kummeneje, O. (1961). "The Shear Strength of a Fine Sand." Proc. 5th Int. Conf. Soil Mech. and Found. Eng. pp 29–37.

Bora, P. K. (1984). "Shear Failure in Granular Media." J. Eng. Mech. 110, pp. 582-598.

Borja, R. I. (2003). "Deformation bands in granular media." Geomechanics: Testing, Modeling, and Simulation. pp. 394-399.

Bougie, J. L. (2004). "Continuum Simulations of Fluidized Granular Materials." The University of Texas, Austin.

Bourzutschky, M. and Miller, J. (1995). "Granular Convection in a Vibrated Fluid." Phys. Rev. Lett. 74, 2216-2219.

Brone, D. and Muzzio, F. J. (1997). "Size segregation in vibrated granular systems: A reversible process." Phys. Rev. E. 56[1], pp. 1059-1063.

Clement, E., Vanel, L., Rajchenbach, J. and Duran, J. (1996). "Pattern formation in a vibrated granular layer." Phys. Rev. E, 53, 2972-2975.

Cooke, W., Warr, S., Huntley, J. M. and Ball, R. C. (1996). "Particle size segregation in a two-dimensional bed undergoing vertical vibration," Phys. Rev. E, 53, 2812.

Cox, M. R. and Budhu, M. (2010). "Grain Shape Quantifications and their Relationship to Dilatancy." GeoFlorida 2010: Advances in Analysis, Modeling & Design, pp. 540-549.

Das, B. M. (2011). "Principles of Soil Dynamics," Second Edition. Cengage Learning, 563.

Davies, T. R. H. (1982). "Spreading of Rock Avalanche Debris by Mechanical Fluidization." Rock Mechanics 15; Springer-Verlag, pp. 9-24.

Doudy, S., Fauve, S. and Laroshe, C. (1989). "Subharmonic instabilities and defects in a granular layer under vertical vibrations." Europhys. Lett., 8[7], 621

Evesque, P. and Rajchenbach, J. (1989). "Instability in a sand heap," Phys. Rev. Lett., 62, 44.

Falcon, E., Wunenburger, R., Evesque, P., Fauve, S., Chabot, C., Garrabos, Y. and Beysens, D. (1999). "Cluster formation in a granular medium fluidized by vibrations in low gravity." *Phys. Rev. Lett.*, 83:440.

Fauve, S., Douady, S. and Laroche, C. (1989). "Collective behaviours of granular masses under vertical vibrations." J. Physique C3, 187-191.

Frost, J. D., DeJong, J. T. and Recalde, M. (2002). "Shear failure behavior of granular–continuum interfaces." Engineering Fracture Mechanics, 69, pp. 2029–2048.

Frost, D., Hebeler, G. L., Evans, T. M. and DeJong, J. T. (2004). "Interface behaviour of granular soils." Earth and Space, pp. 65-72.

Gallas, J. A. C., Herrman, H. J. and Sokolowski, S. (1992). "Convection Cells in Vibrating Granular Media." Phys. Rev. Lett. 69, 1371-1374.

Goldshtein, A., Shapiro, M., Moldavsky, L. and Fichman, M. (1995). "Mechanics of collisional motion of granular materials. 2. Wave propagation through vibrofluidized granular layers." J. Fluid Mech., 287, p. 349

Gotzendorfer, A., Tai, C., Kruelle, C. A., Rehberg, I. and Hsiau, S. S. (2006). "Fluidization of a vertically vibrated two-dimensional hard sphere packing: A granular meltdown." Phys. Rev. E 74, 011304.

Härtl, J. and Ooi, J. Y. (2011). "Numerical investigation of particle shape and particle friction on limiting bulk friction in direct shear tests and comparison with experiments." Powder Technology, 212, pp. 231–239.

Housner, G. W. (1954). "Geotechnical problems of destructive earthquakes." Géotechnique, Volume 4, Issue 4, 01 December 1954, pages 153 –162.

Housner, G. W. (1959). "Behavior of structures during earthquakes." Journal of the Engineering Mechanics Division, ASCE, 85, No. EM-4.

Huan, C. (2008). "NMR Experiments on Vibrofluidized and Gas Fluidized Granular Systems." PhD Thesis, University of Massachusetts Amherst.

Hungr, O. (1981). "Dynamics of Rock Avalanches and Other Types of Slope Movements." PhD Thesis, University of Alberta, 506 p.

Idriss, I. M. and Boulanger, R. W. (2008). "Soil liquefaction during earthquakes." Earthquake Engineering Research Institute, Oakland, California.

Ingale, R. A. (2008). "Dynamics of vibrated granular matter." PhD Thesis, The City University of New York.

Jaeger, H. M., Nagel, S. R. and Behringer, R. P. (1996). "Granular solids, liquids, and gases." Rev. Mod. Phys. 68, 1259

Kang, D. H., Choo, J. and Yun, T. S. (2012). "Evolution of pore characteristics in the 3D numerical direct shear test." Computers and Geotechnics, 49, pp. 53–61.

Knight, J. B., Jaeger, H. M. and Nagel, S. R. (1993). "Vibration-induced size separation in granular media: the convection connection." Phys. Rev. Lett., 70, 3728.

Kutergin, V. N. (1989). "The property change patterns of clayey soils under vibration." (in Russian) Moscow: Nauka, 143 p.

Lan, Y. and Rosato, A. D. (1995). "Macroscopic behavior of vibrating beds of smooth inelastic spheres." Phys. Fluids, Vol. 7, No. 8, pp. 1818-1831.

Laroche, C., Douady, S. and Fauve, S. (1989). "Convective Flow of Granular Masses under Vertical Vibration." J. Physique 50, 699-706.

Li, Y. R. and Aydin, A. (2010). "Behavior of rounded granular materials in direct shear: Mechanisms and quantification of fluctuations." Engineering Geology, 115, pp. 96–104.

Liffman, K., Metcalfe, G. and Cleary, P. (1997). "Convection due to horizontal shaking." in: (Behringer and Jenkins (1997)). 405-408.

Liu, S. H., Sun, D., Matsuoka, H. (2005). "On the interface friction in direct shear test." Computers and Geotechnics, 32, pp. 317–325.

Liu, S. (2010). "Failure Mechanism of Granular Soil Slopes." Earth and Space 2010: Engineering, Science, Construction, and Operations in Challenging Environments, ASCE, pp. 3724-3752.

Luding, S. (1995). "Granular materials under vibration: simulations of rotating spheres." *Phys. Rev. E*, 52:4442.

Maslov, N. N. (1959). "Stability Conditions of Saturated Sands." (Russian: Usloviya Ustoychivosti Vodonasishennikh Peskov). M. – L. Gosenergoizdat. 328 p.

Meehan, C. L., Boulanger, R. W. and Duncan, J. M. (2008). "Dynamic Centrifuge Testing of Slickensided Shear Surfaces," Journal of the Geotechnical Engineering Division, American Society of Civil Engineers (month), Vol. 134, No. 8, pp. 1086-1096

Melhus, M. F. (2011). "Effects of Noise and Vibration on the Solid to Liquid Fluidization Transition in Small Dense Granular Systems under Shear." PhD Thesis. Northwestern University, Evanston, Illinois.

Melo, F., Umbanhowar, P. and Swinney, H. L. (1993). "Transition to parametric wave patterns in a vertically oscillated granular layer." Phys. Rev. Letts., 72, 172.

Melo, F., Umbanhowar, P. and Swinney, H. L. (1995). "Hexagons, kinks, and disorder in oscillated granular layers." Phys. Rev. letts., 75, 3838.

Melosh, H. J. (1979). "Acoustic Fluidization: A New Geologic Process?" Journal of Geophysical Research, v. 84: pp. 7513-7520.

Melosh, H. J. and Girdner, K. K. (1995), "Rheology of vibrated granular materials: Application to long-runout landslides." EOS, 76.

Melosh, H. J., (1996). "Dynamical weakening of faults by acoustic fluidization." Nature, 379, pp. 601-606.

Mesarovic, S. Dj., Padbidri, J. M. and Muhunthan, B. (2013). "Micromechanics of dilatancy, critical state and shear bands in dense granular matter." Poromechanics V, ASCE, pp. 1067-1074.

Meschyan, S. R. (1978). "Short-term and long-term strength of clayey soils." (in Russian) Moscow, Nedra, 207 p.

Meschyan, S. R. (1992). "Rheological processes in clayey soils." (in Russian) Yerevan, "Hayastan", 395 p.

Metcalfe, C., Tennakoon, S. G. K., Kondic, L., Schaeffer, D. G. and Behringer, R. P. (2002). "Granular Friction, Coulomb Failure, and the Fluid-Solid Transition for Horizontally Shaken Granular Materials." Physical Review E - Statistical, Nonlinear, and Soft Matter Physics.

Moon, S. J., Swift, J. B., and Swinney, H. L. (2004). "Role of friction in pattern formation in oscillated granular layers." *Phys. Rev. E*, 69(031301):1.

Mujica, N. and Melo, F. (1998). "Solid-liquid transition and hydrodynamic surface waves in vibrated granular layers." *Phys. Rev. Lett.*, 80:5121.

Muhlhaus, H. B., and Vardoulakis, I. (1987). "The thickness of shear bands in granular materials." Geotechnique, 37, pp. 271-283.

Nam, S., Gutierrez, M., Diplas, P. and Petrie, J. (2011). "Determination of the shear strength of unsaturated soils using the multistage direct shear test." Engineering Geology, 122, pp. 272–280.

National Instruments website: http://www.ni.com/labview/ (accessed in September, 2013)

Pak, H. K. and Behringer, R. P. (1993). "Surface waves in vertically vibrated granular materials." Phys. Rev. Lett. 71, 1832

Pak, H. K., Van Doorn, E. and Behringer, R. P. (1995). "Effects of ambient gases on granular materials under vertical vibration." Phys. Rev. Lett., 74, 4643.

Pokrovsky, G. I., Ehrlich, A. A., Laletin, N. V. and Lush, F. A. (1934). "New Methods of Investigation of the Compressibility and Internal Friction in Soils." Vestnik Voyenno-Inzhenernoy Akademii RKKA, no. 6.

Poschel, T. and Rosenkranz, D. E. (1998). "Experimental study of horizontally shaken granular matter – the swelling effect." Lecture Notes in Physics, Volume 503, 1998, pp 96-109

Potts, D. M., Dounias, G. T., and Vaughan, P. R. (1987). "Finite element analysis of the direct shear box test." Geotechnique, 37(1), pp. 11-23.

Pyke, R., Seed, H. B. and Chan, C. K. (1975). "Settlement of sands under multidirectional shaking." Journal of Geotechnical Engineering Division, ASCE, 101, GT-4, pp.379-398.

Rechenmacher, A. L. (2005). "Grain scale processes associated with shear banding in sands." Geomechanics II, pp. 342-355.

Richards, R., Jr., Elms, D. and Budhu, M. (1990). "Dynamic Fluidization of Soils." Journal of Geotechnical Engineering, 116(5), pp. 740–759

Richart, F. E. (1970). "Vibrations of Soils and Foundations." Prentice-Hall, 414 p.

Ristow, G. H., Strasburger, G. and Rehberg, I. (1997). "Phase diagram and scaling of granular materials under horizontal vibrations." *Phys. Rev. Lett.*, 79(5):833.

Robertson, P. K. and Campanella, R. G. (1985). "Liquefaction potential of sands using the CPT." Research Report R69-15, Dept. of Civil Engineering, Massachusetts Institute of Technology, Cambridge, Mass.

Robertson, P. K. and Campanella, R. G. (1986). "Estimating liquefaction potential of sands using the flat plate dilatometer." Geotechnical Testing Journal, 9, No. 1, pp. 38-40.

Roscoe, K. H. (1970). "Tenth Rankine lecture: The influence of strains in soil mechanics." Geotechnique, 20, pp. 129-170.

Sadrekarimi, A. (2008). "Shearing Behavior of Sands in Terms of Compressibility Mechanisms." GeoCongress 2008: Characterization, Monitoring and Modeling of GeoSystems. pp. 197-204.

Sangroya, *R. and Choudhury*, *D.* (2013). "Stability Analysis of Soil Slope Subjected to Blast Induced Vibrations Using FLAC3D." Geo-Congress 2013, pp. 472-481

Savage, S. B. (1988). "Streaming motions in a bed of vibrationaly fluidized dry granular material." J. Fluid Mech., 194:457.

Savchenko, I. A. (1958). "Effect of Vibrations on Internal Friction in Sand." Symposium, Soil Dynamics, Moscow, Gosstroiizdat, No. 2.

Seed, H. B. (1966). "A method for earthquake resistant design of earth dams." Journal of the Soil Mechanics and Foundation Division, ASCE, 92, No. SM-1, pp. 13-41.

Seed, H. B. and Idriss, I. M. (1982). "Ground motions and soil liquefaction during earthquakes." Monograph series, Earthquake Engineering Research Institute, Berkeley, California.

Seed, H. B. and Idriss, I. M. (1983). "Evaluation of liquefaction potential using field performance data." Journal of Geotechnical Engineering, ASCE, 109, No. 3, pp. 458-482.

Shibata, T. and Yukitomo, H. (1969). "Liquefaction Process of Sand during Cyclic Loading." Soils and Foundations, Vol. 3, pp. 54-69.

Shibata, T. and Yukitomo, H. (1970). "Shear strength of sand under a vibrating load." Bulletin of the Disaster Prevention Research Institute, 19(3): pp. 27-37.

Sornette, D. and Sornette, A. (2000). "Acoustic Fluidization for Earthquakes?" Bulletin of the Seismological Society of America, 90, 3, pp. 781-785.

Sunthar, P. and Kumaran, V. (2001). "Characterization of the stationary states of a dilute vibrofluidized granular bed." *Phys. Rev. E*, 64:041303.

Tennakoon, S. G. K. and Behringer, R. P. (1998). "Vertical and horizontal vibration of granular materials: Coulomb friction and a novel switching state." *Phys. Rev. Lett.*, 81(4):794–797.

Toyota, H., Towhata, I., Imamura, S. and Kudo, K. (2004). "Shaking Table Tests on Flow Dynamics in Liquefied Slope." Soils and Foundations, Vol. 44, No. 5, pp. 67 – 84.

Tsimring, L. and Aranson, I. (1997). "Localized and cellular patterns in a vibrated granular layer." Phys. Rev. Lett., 79(2): 213–216.

Umbanhowar, P. B., Melo, F. & Swinney, H. L. (1996). "Localized excitations in a vertically vibrated granular layer." Nature (London) 382, 793

Warr, S., Huntley, J. M. and Jacques, G. T. H. (1995). "Fluidization of a two-dimensional granular system: Experimental study and scaling behavior." Phys. Rev. E, 52, 5583-5595.

Wartman, J., Seed, R. B. and Bray, J. D. (2005). "Shaking table modeling of seismically induced deformations in slopes." J. Geotech. Geoenviron. Eng., 131(5), pp. 610–622.

Wassgren, C. R. (1997). "Vibration of granular materials." PhD Thesis, California Institute of Technology, Pasadena, California.

Widulinski, L., Kozicki, J. and Tejchman, J. (2010). "Comparative Modeling of Shear Localization in Granular Bodies with FEM and DEM." GeoShanghai 2010 International Conference, Soil Behavior and Geo-Micromechanics, pp. 198-203.

Youd, L. T. (1968). "Reduction of critical void ratio during steady-state vibration." International symposium on wave propagation and dynamic properties of earth materials, Albuquerque, N. Mex., 1967, Proc.

Youd, L. T. (1970). "Densification and Shear of Sand during Vibration." ASCE, Journal of the Soil Mechanics and Foundations Division, Vol. 96, No. 3, May/June 1970, pp. 863-880.

Zik, O., Stevans, J. and Rabin, Y. (1992). "Mobility of a sphere in vibrated granular media." Europhys. Lett., Vol. 17, No. 4, pp. 315-319.

APPENDIX

Part 1

The plots provided in this section were used in Chapter 3. Following are the test results of 8 samples of fine sand tested in strain-controlled mode at 8.4 kPa, 23.2 kPa, 36.3 kPa, 50 kPa, 77.3 kPa, 118.2 kPa and 200 kPa normal stresses, as well as 5 samples of fine sand tested in stress-controlled mode at 5 different shear loads, 50 kPa normal stress, 140 Hz vibration frequency and constant vibration intensity.

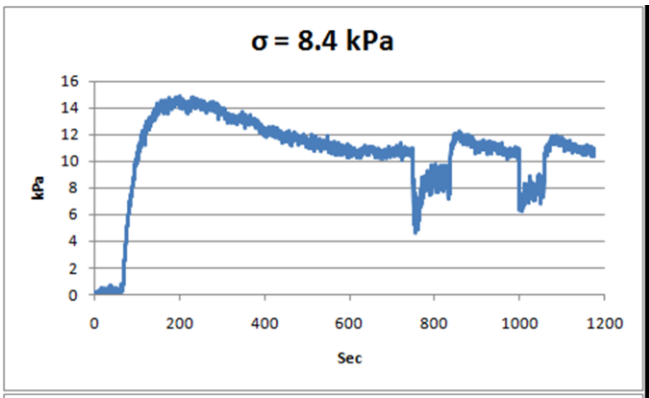
σ = 8.4 kPa
kPa
Sec

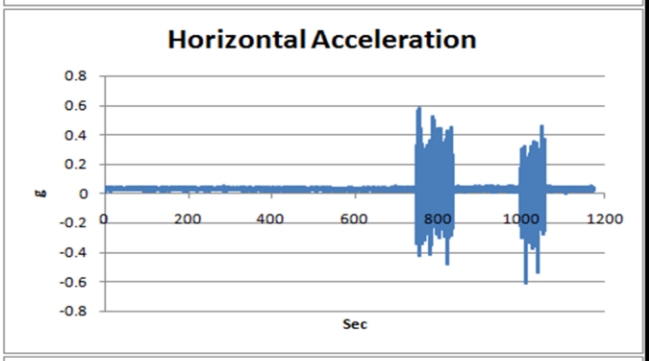
Horizontal Acceleration
g
Sec

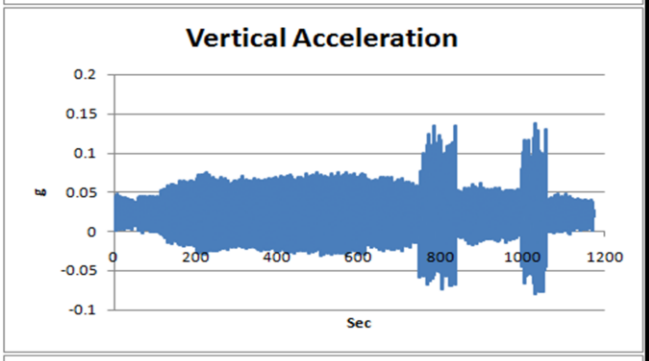
Vertical Acceleration
g
Sec

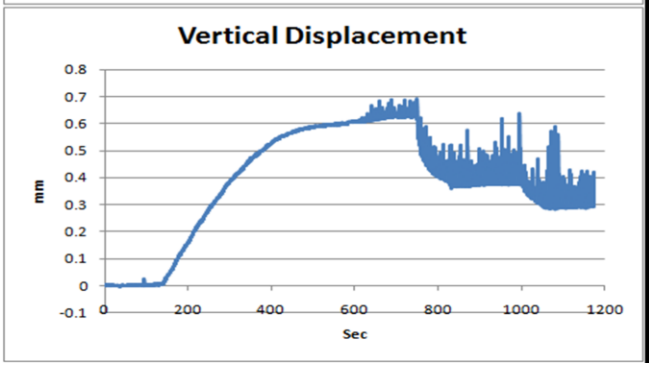
Vertical Displacement
mm
Sec

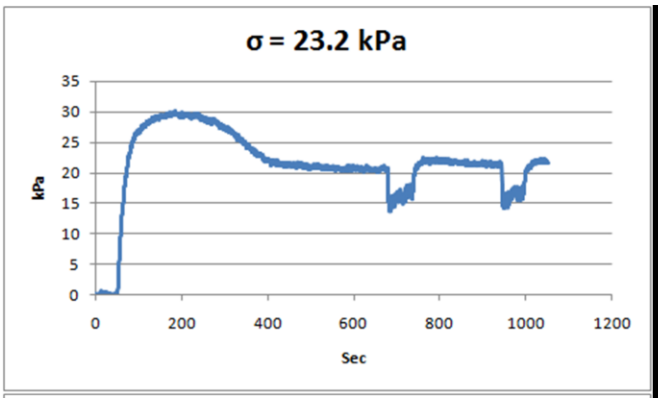
σ = 23.2 kPa
kPa
Sec

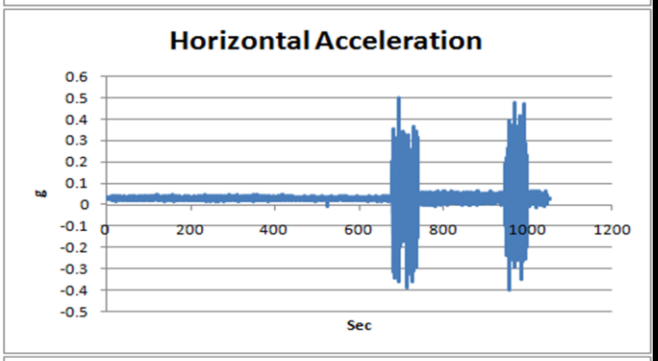
Horizontal Acceleration
g
Sec

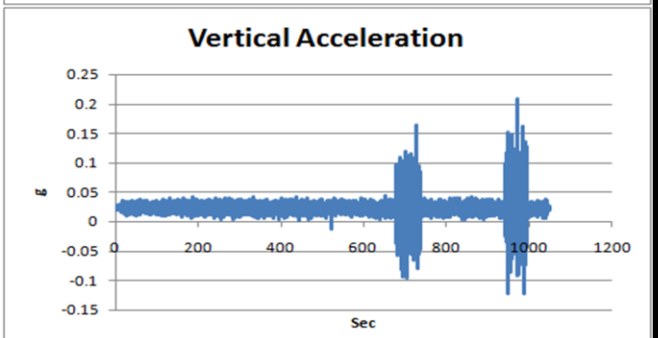
Vertical Acceleration
g
Sec

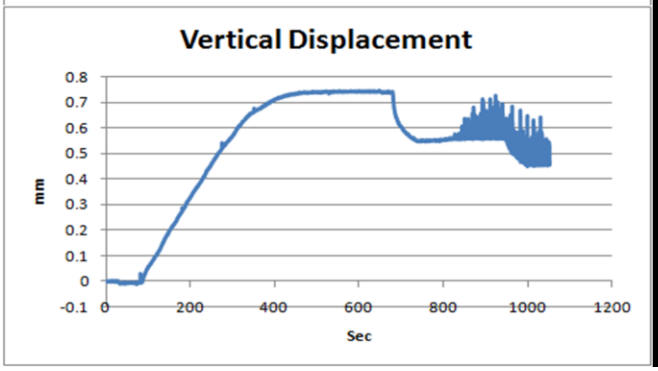
Vertical Displacement
mm
Sec

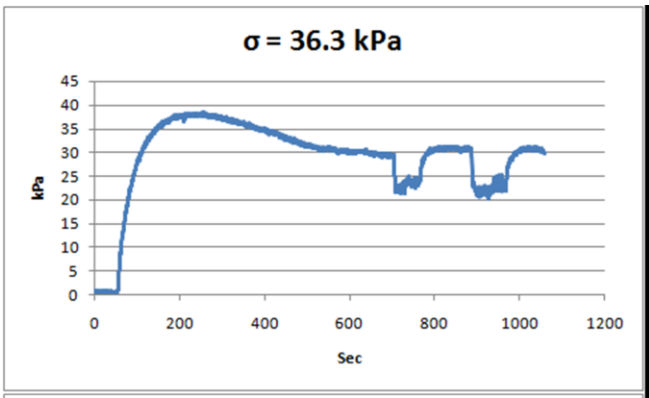
σ = 36.3 kPa
kPa
Sec

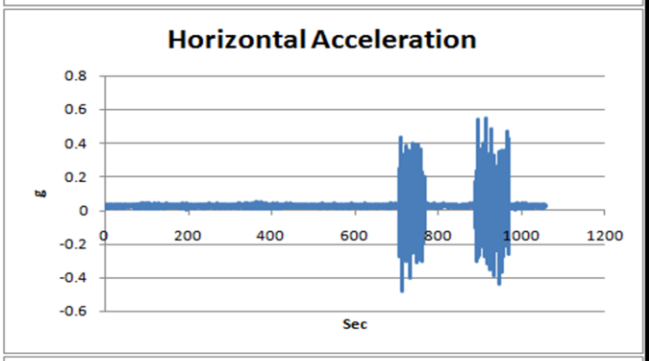
Horizontal Acceleration
g
Sec

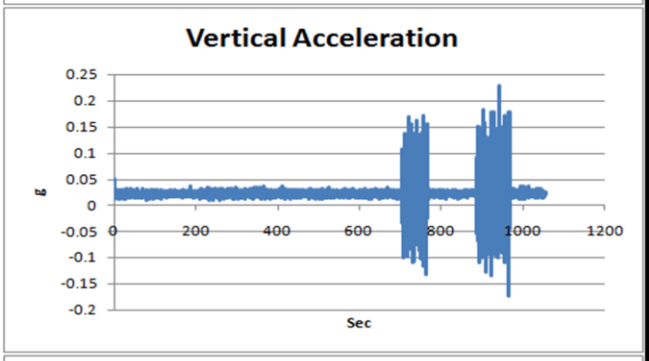
Vertical Acceleration
g
Sec

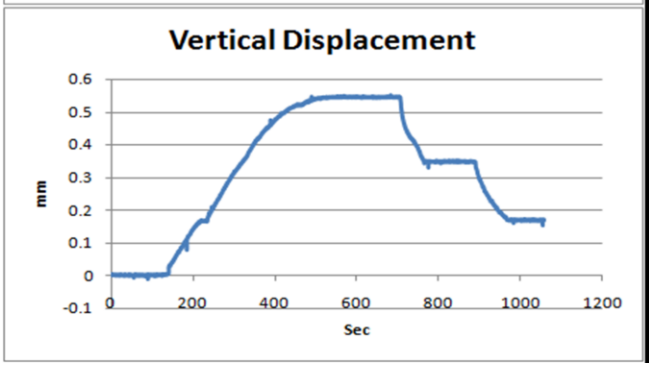
Vertical Displacement
mm
Sec

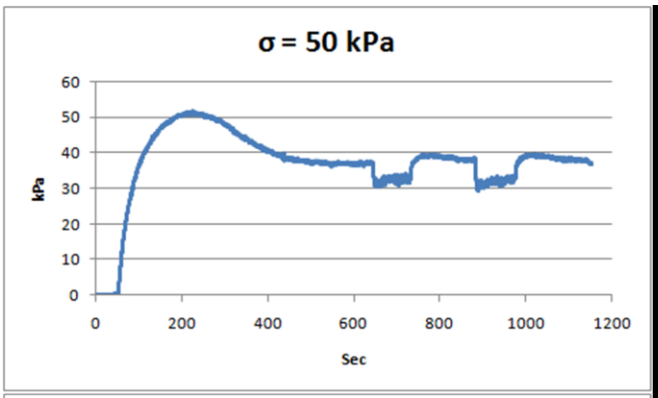
σ = 50 kPa
kPa
Sec

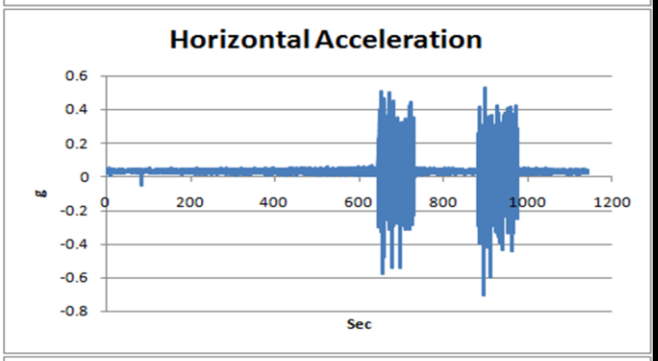
Horizontal Acceleration
g
Sec

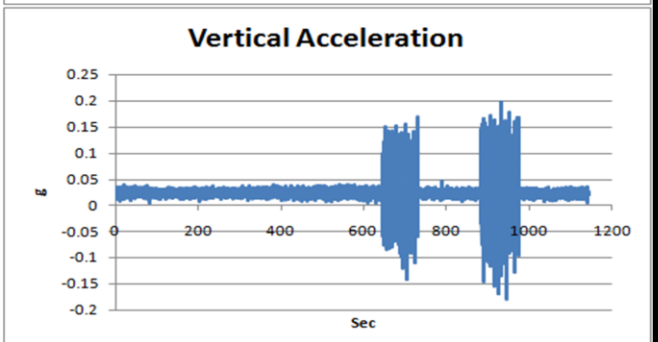
Vertical Acceleration
g
Sec

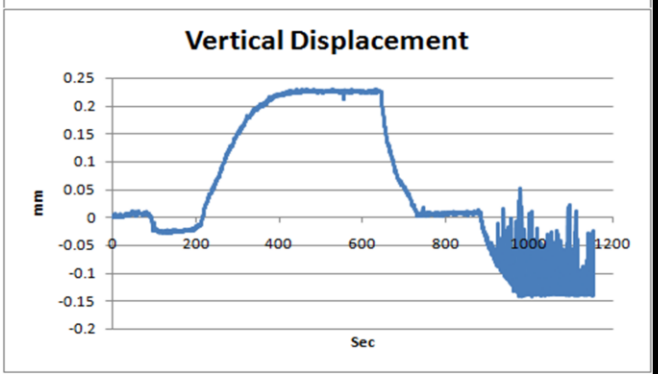
Vertical Displacement
mm
Sec

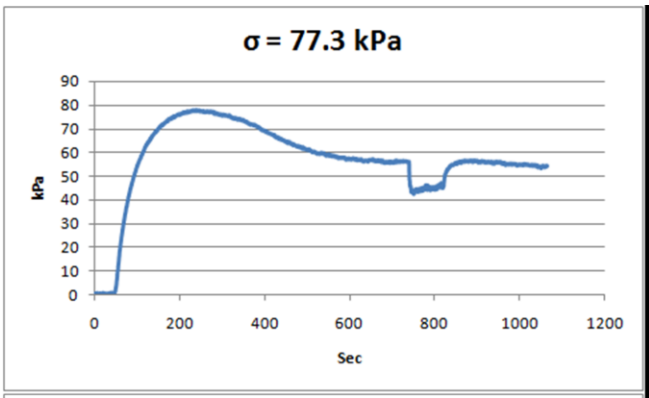
σ = 77.3 kPa
kPa
Sec

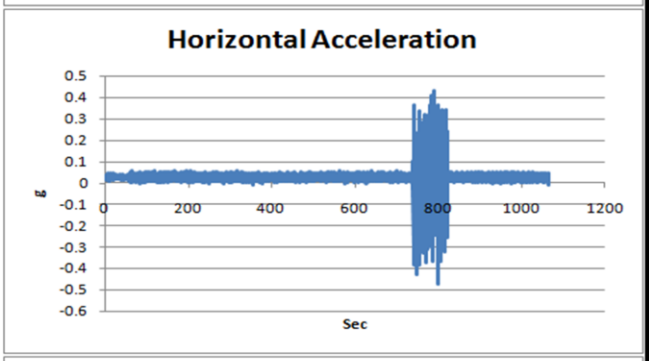
Horizontal Acceleration
g
Sec

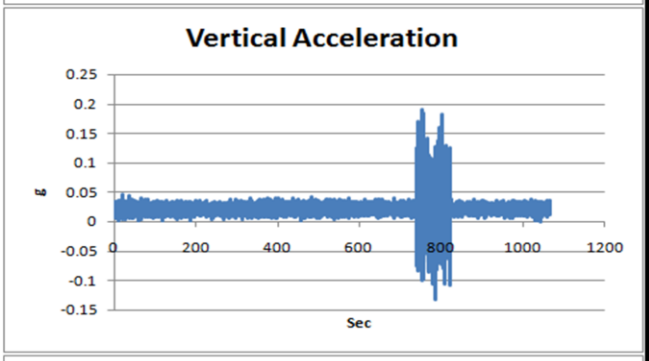
Vertical Acceleration
g
Sec

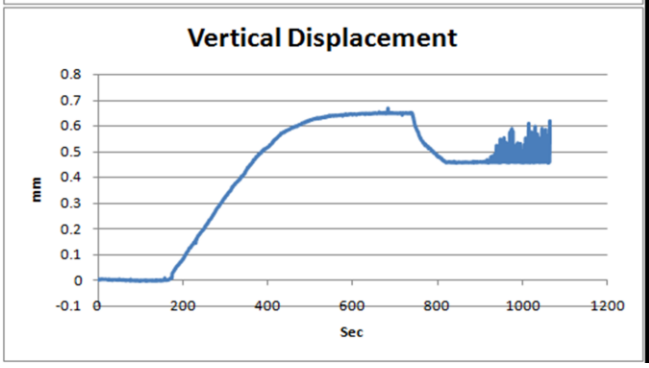
Vertical Displacement
mm
Sec

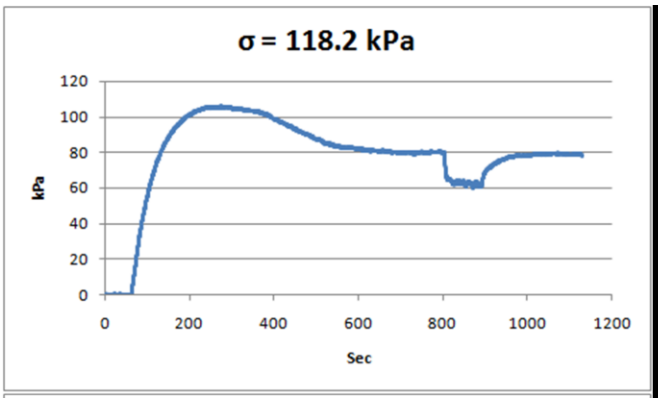
σ = 118.2 kPa
kPa
Sec

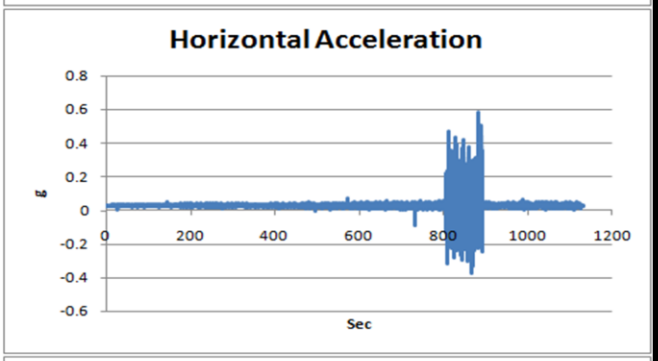
Horizontal Acceleration
g
Sec

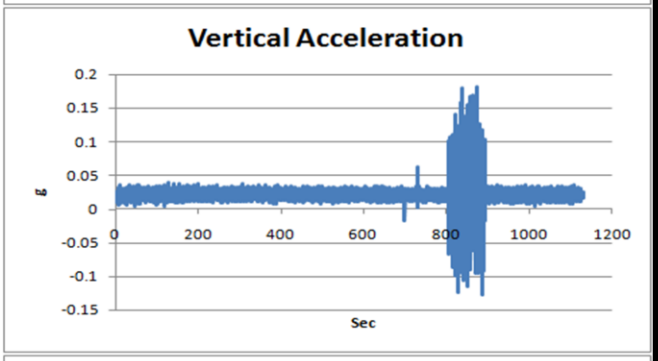
Vertical Acceleration
g
Sec

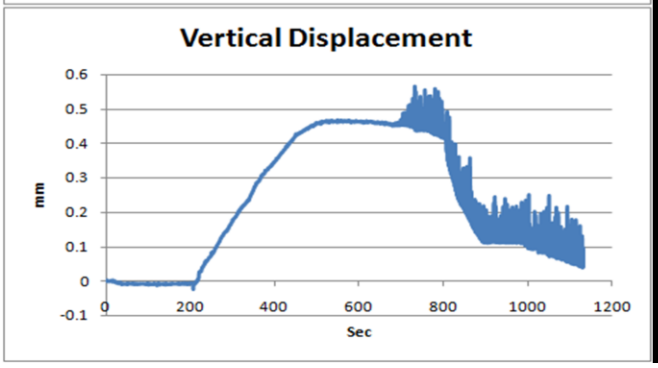
Vertical Displacement
mm
Sec

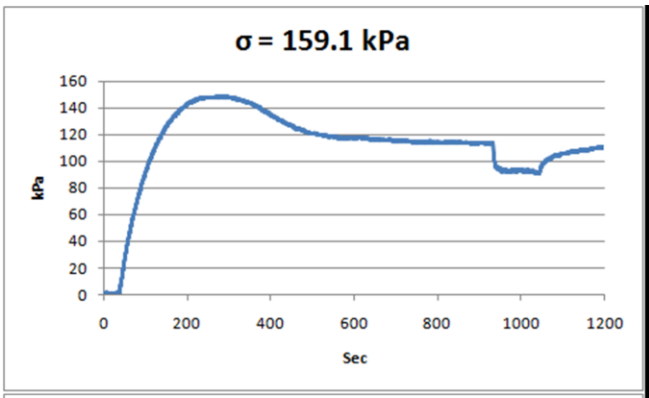
σ = 159.1 kPa
kPa
Sec

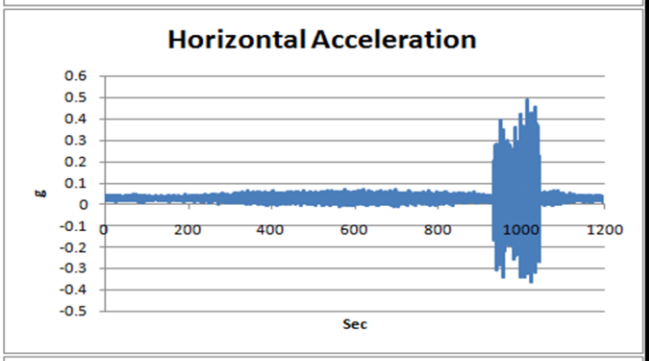
Horizontal Acceleration
g
Sec

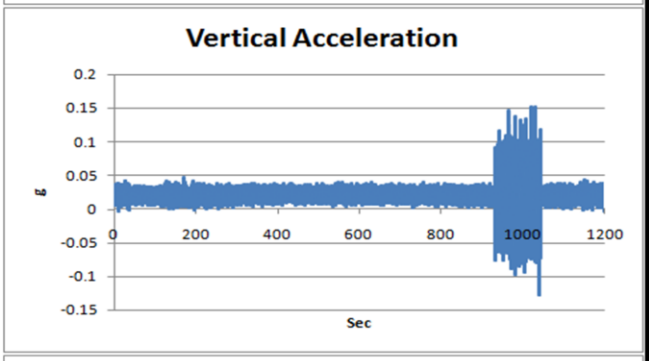
Vertical Acceleration
g
Sec

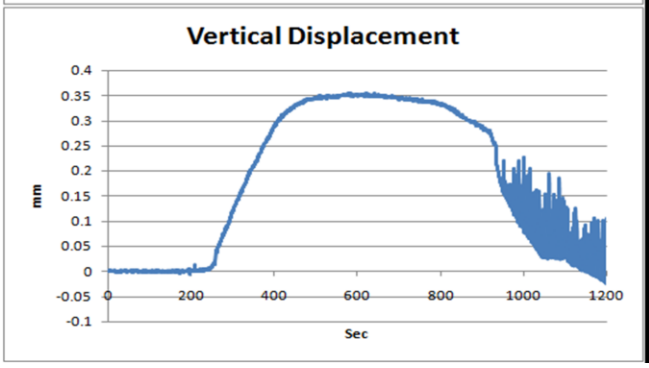
Vertical Displacement
mm
Sec

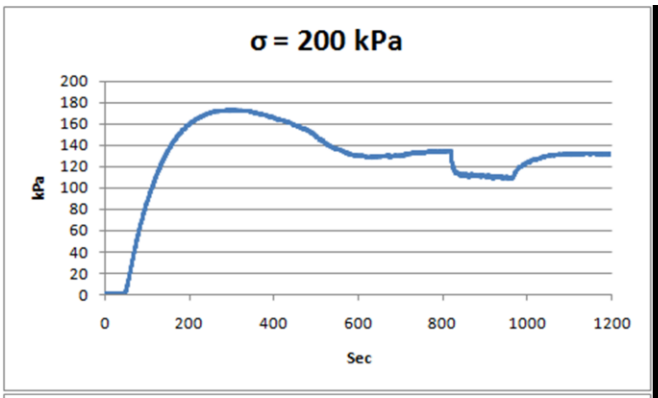
σ = 200 kPa
kPa
Sec

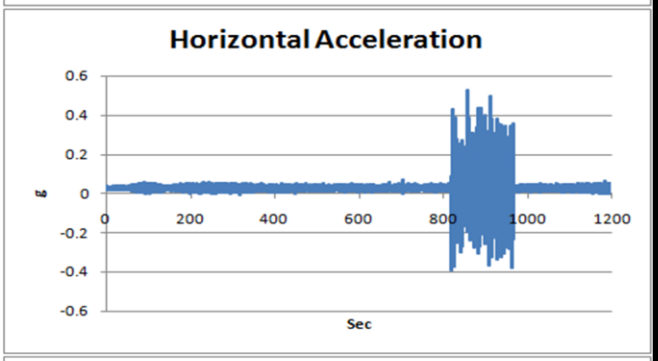
Horizontal Acceleration
g
Sec

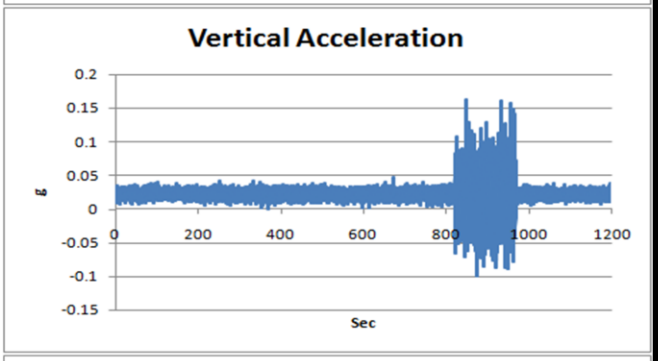
Vertical Acceleration
g
Sec

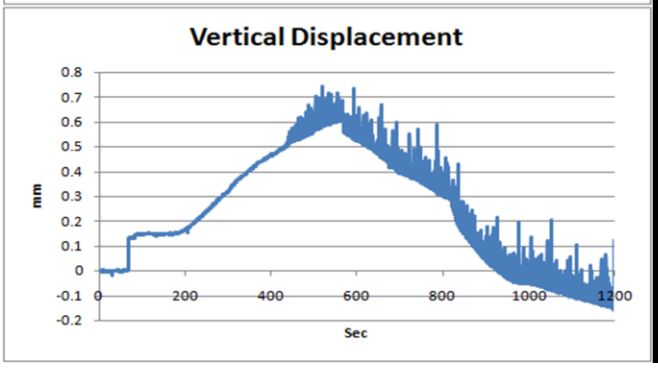
Vertical Displacement
mm
Sec

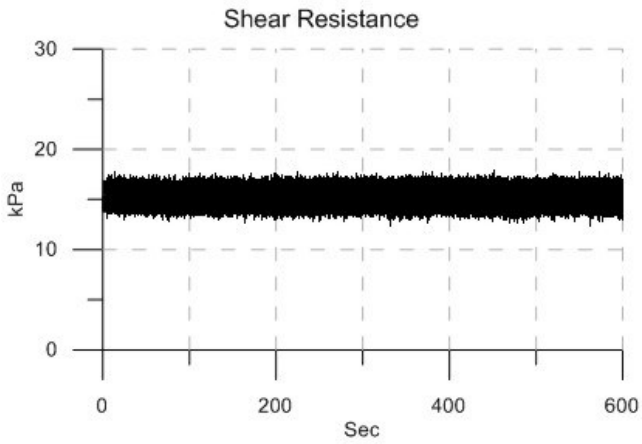

Material:	Fine
Size:	Sand
Normal Stress:	50 kPa
Shear Stress:	0.5τ
Vibration Frequency:	140 Hz
Vibration Force:	7.14 N

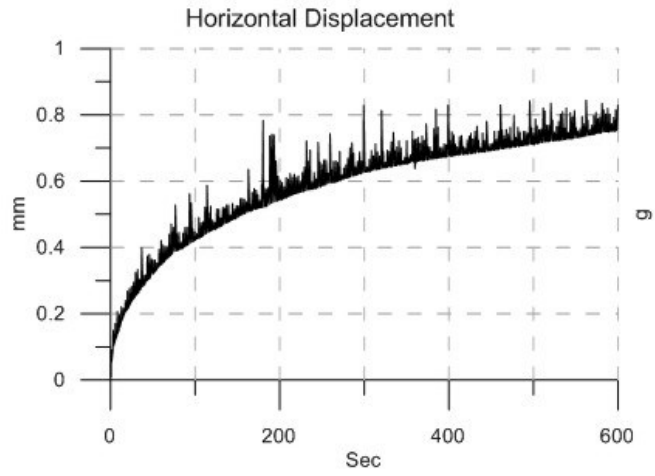

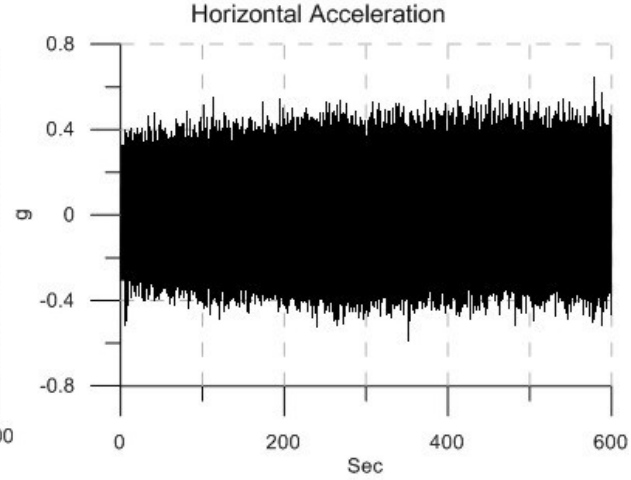

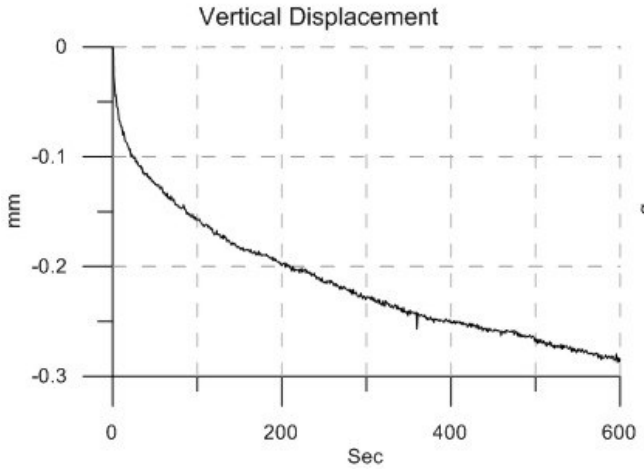

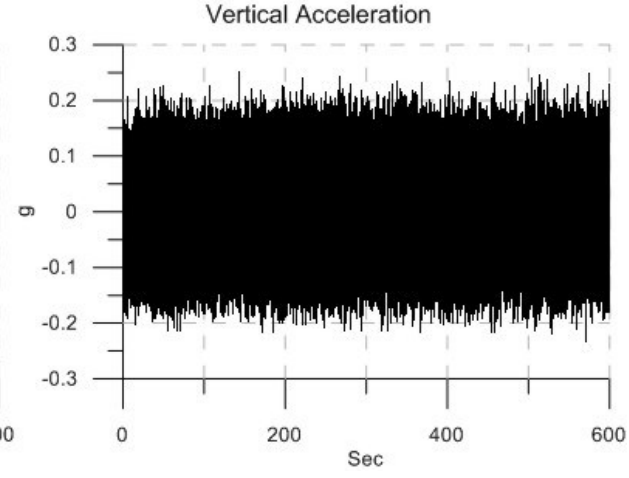

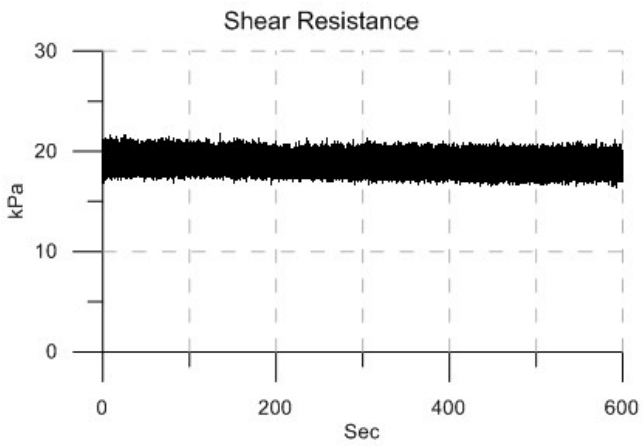

Material:	Fine
Size:	Sand
Normal Stress:	50 kPa
Shear Stress:	0.6τ
Vibration Frequency:	140 Hz
Vibration Force:	7.14 N

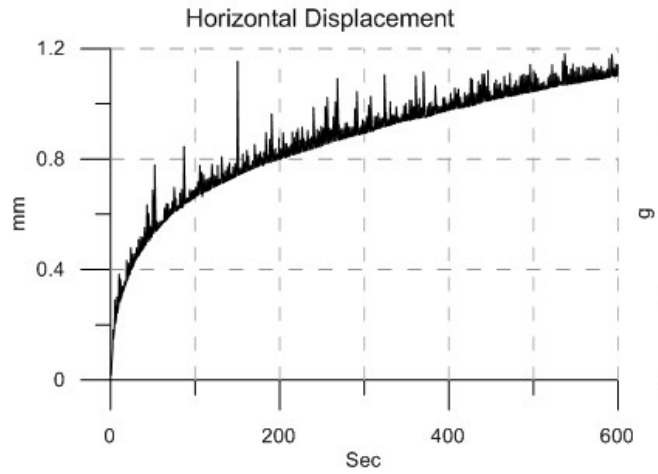

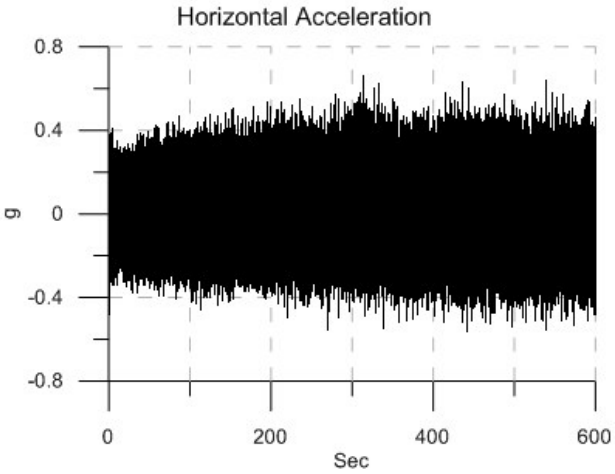

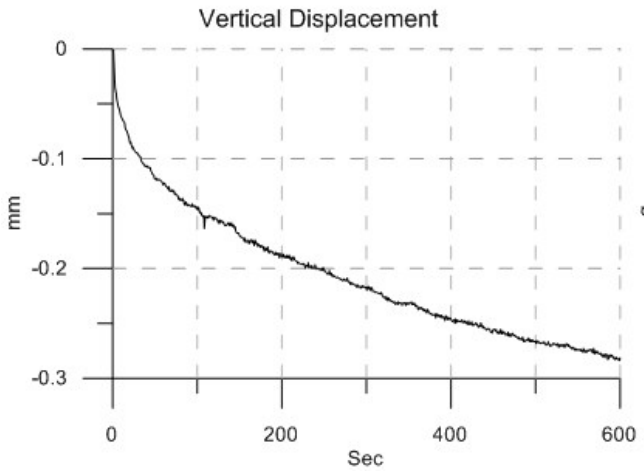

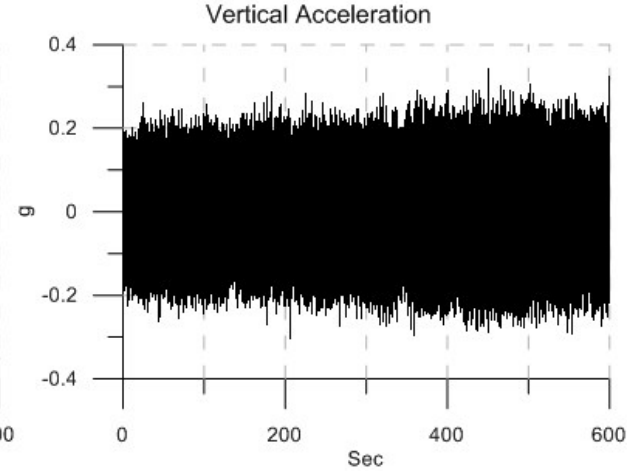

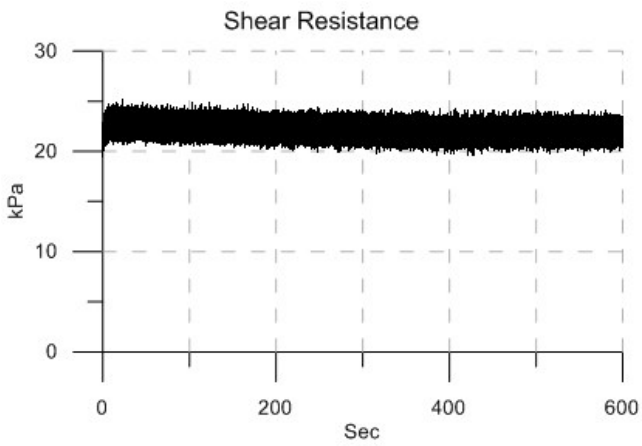

Material:	Fine
Size:	Sand
Normal Stress:	50 kPa
Shear Stress:	0.7τ
Vibration Frequency:	140 Hz
Vibration Force:	7.14 N

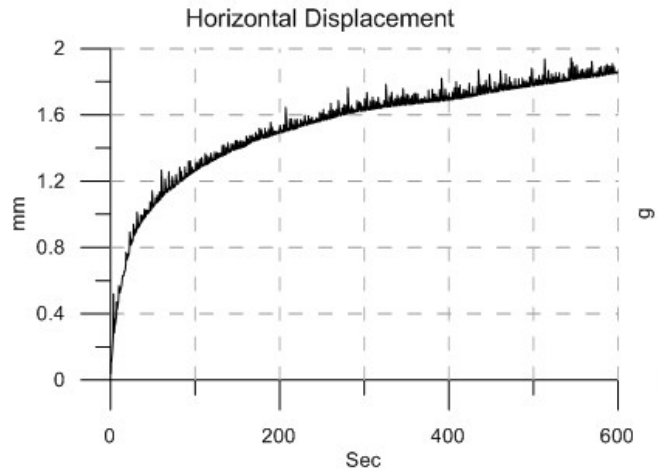

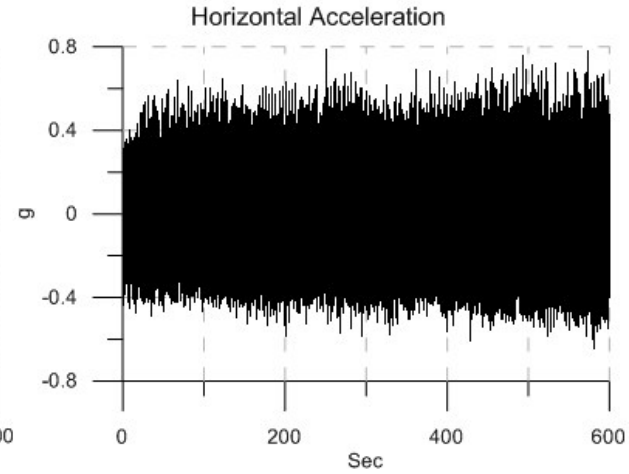

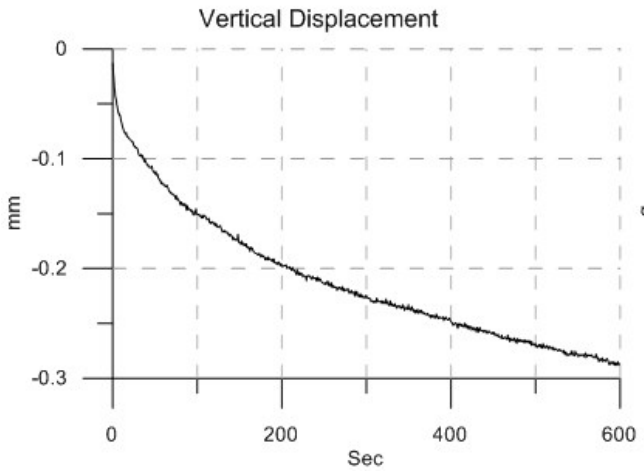

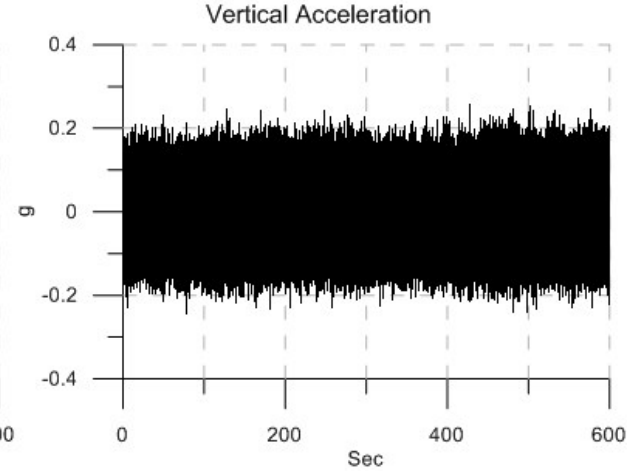

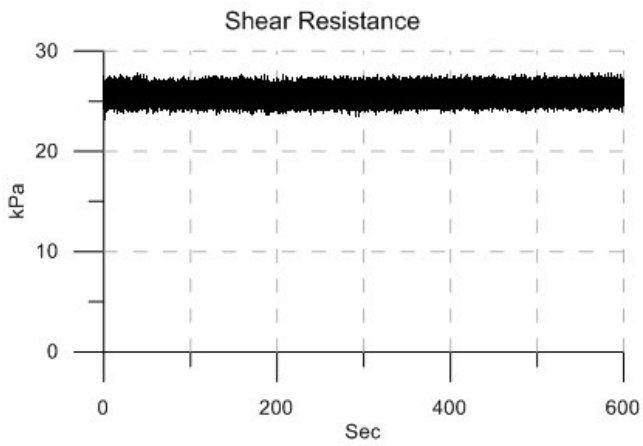

Material:	Fine
Size:	Sand
Normal Stress:	50 kPa
Shear Stress:	0.8τ
Vibration Frequency:	140 Hz
Vibration Force:	7.14 N

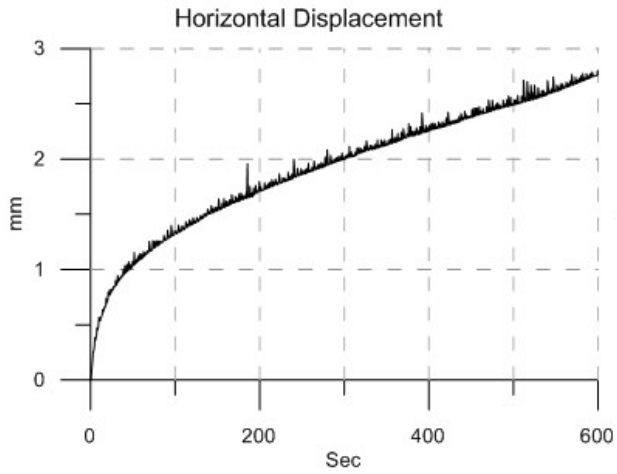

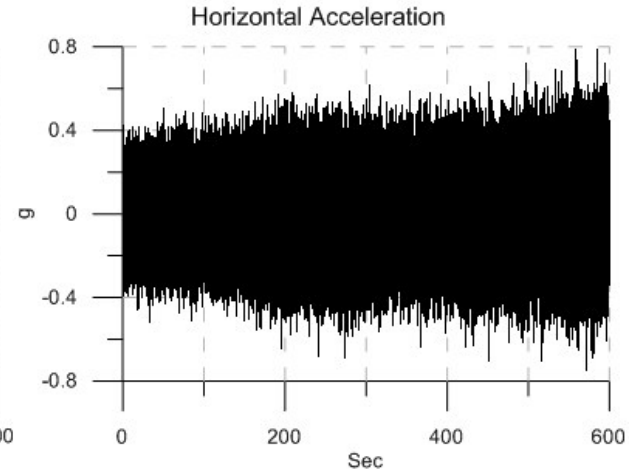

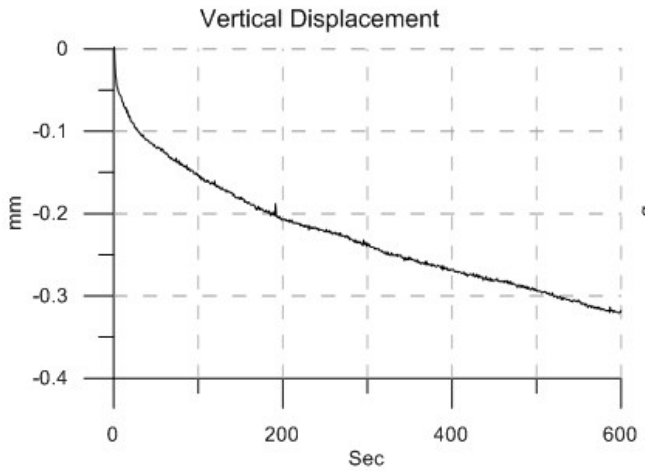

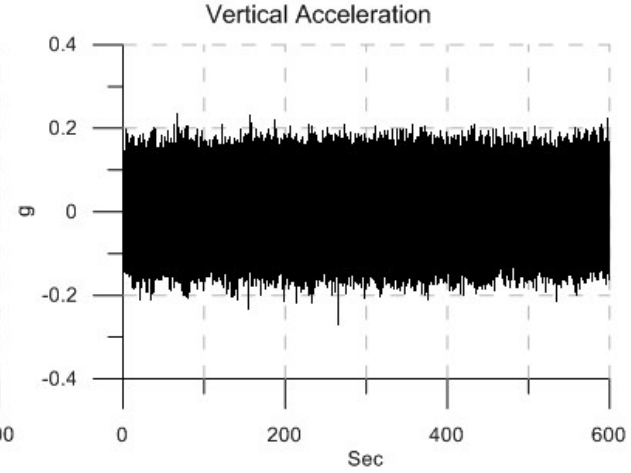

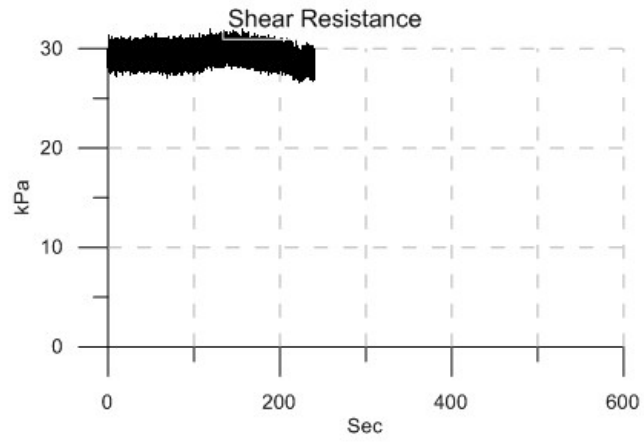

Material:	Fine
Size:	Sand
Normal Stress:	50 kPa
Shear Stress:	0.9τ
Vibration Frequency:	140 Hz
Vibration Force:	7.14 N

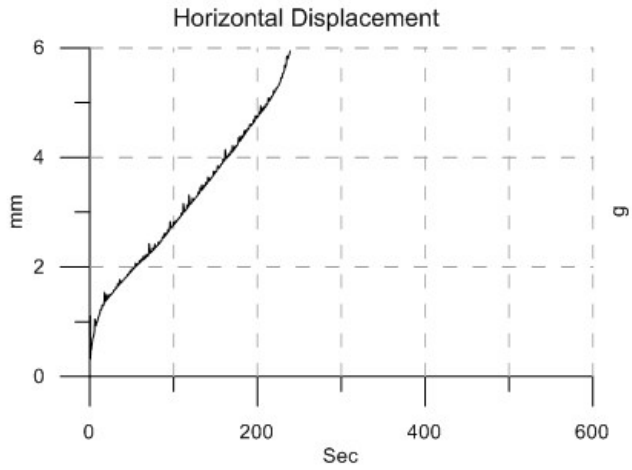

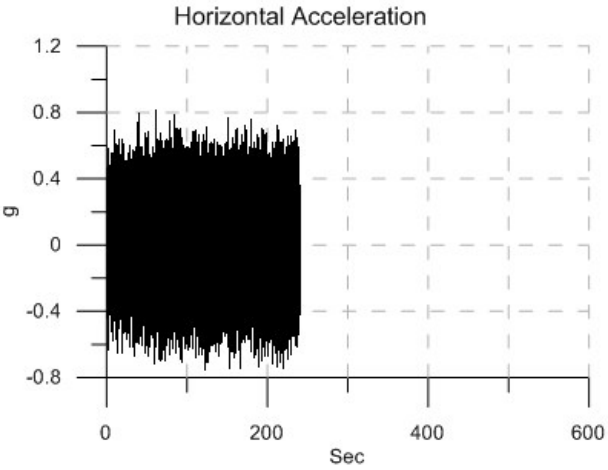

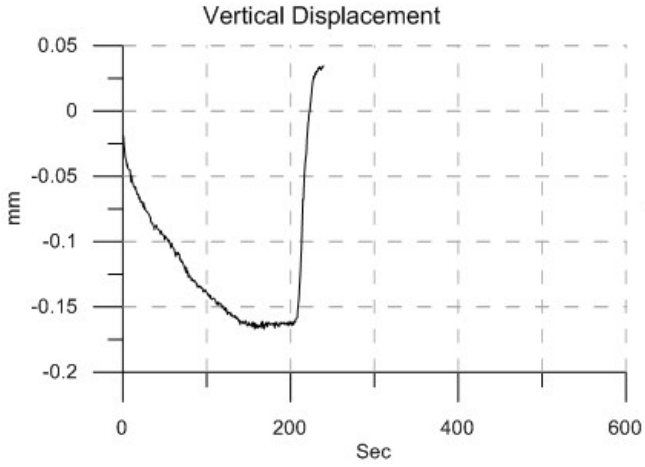

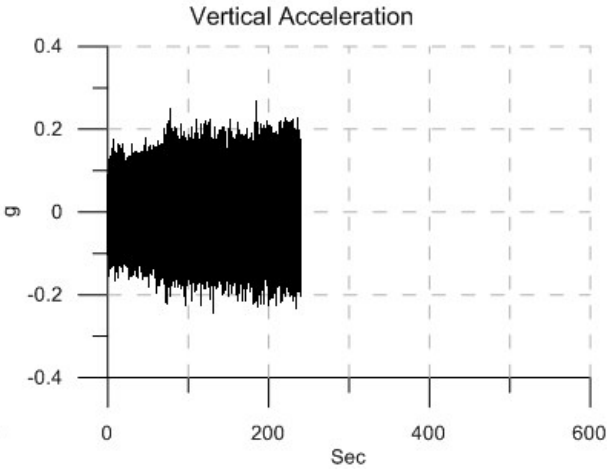

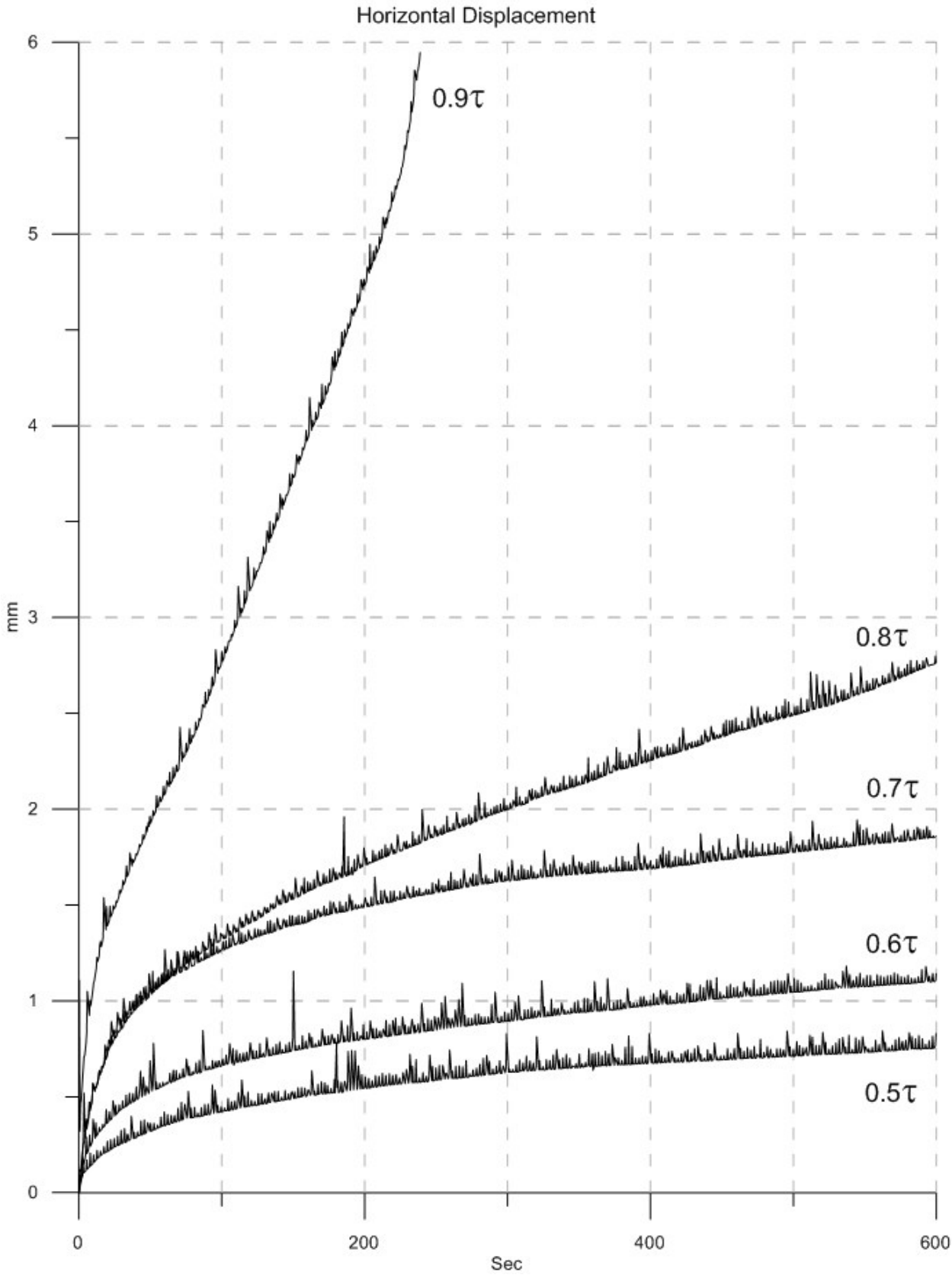
Horizontal Displacement
0.9τ
0.8τ
0.7τ
0.6τ
0.5τ
mm
Sec
0
1
2
3
4
5
6
0
200
400
600

Part 2

The plots provided in this section were used in Chapter 4. Following are the test results of 20 samples of fine sand, 20 samples of coarse sand, 20 samples of 0.1 mm glass beads and 20 samples of 0.55 mm glass beads tested in strain-controlled mode at 23 kPa, 50 kPa, 118 kPa and 200 kPa normal stresses, 5 different vibration intensities and 140 Hz vibration frequency.

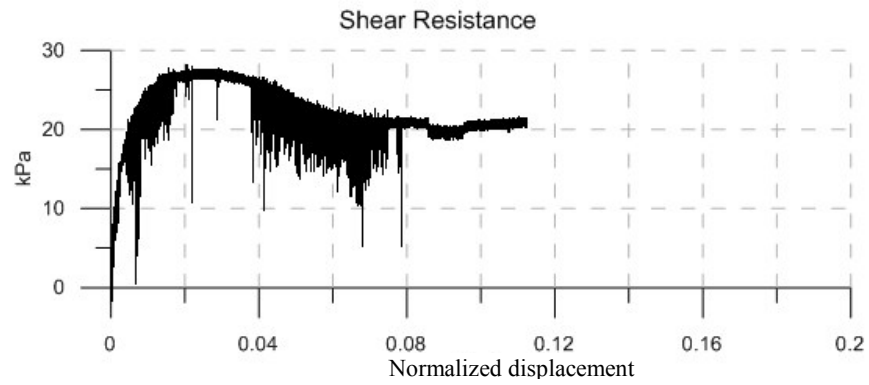

Material:	Sand
Size:	Fine
Normal Stress:	23 kPa
Vibration Frequency:	140 Hz
Vibration Force:	1.61 N
Vibration Duration:	56 sec
Horizontal Acceleration:	0.15 g
Vertical Acceleration:	0.045 g
Horizontal Amplitude:	1.9×10^{-3} mm
Vertical Amplitude:	0.6×10^{-3} mm
Peak Strength:	27 kPa
Residual Strength:	21 kPa
Vibro-Residual Strength:	19.5 kPa

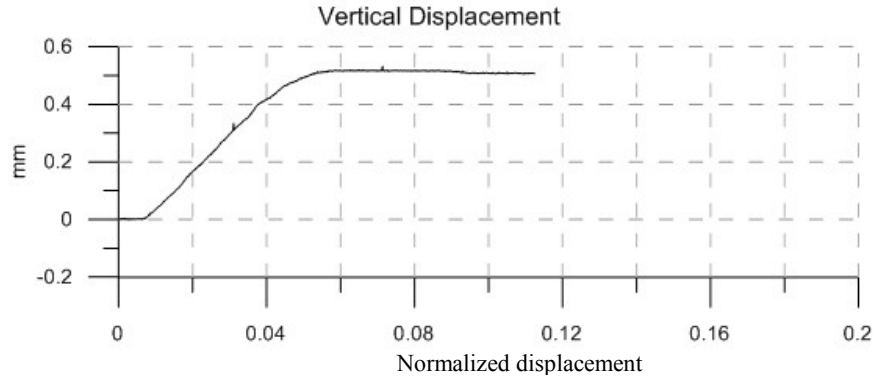

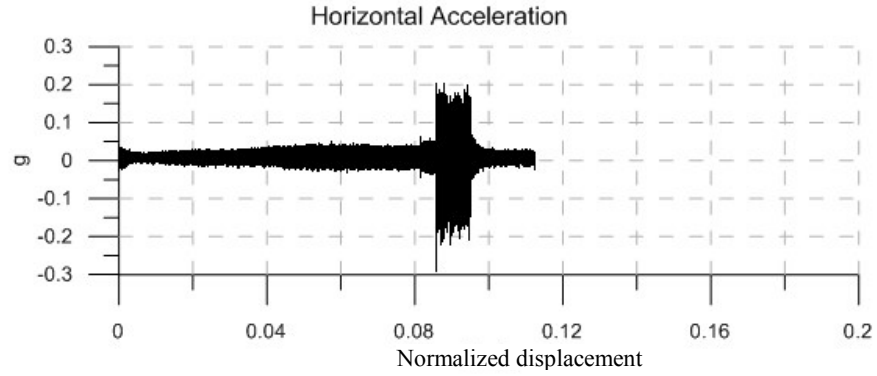

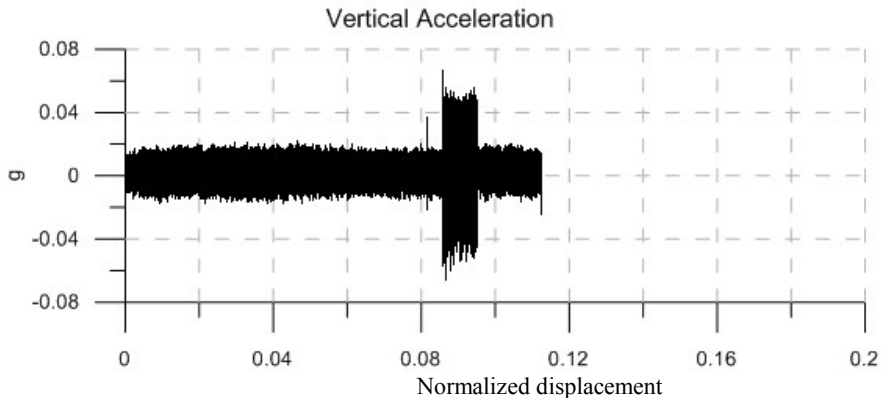

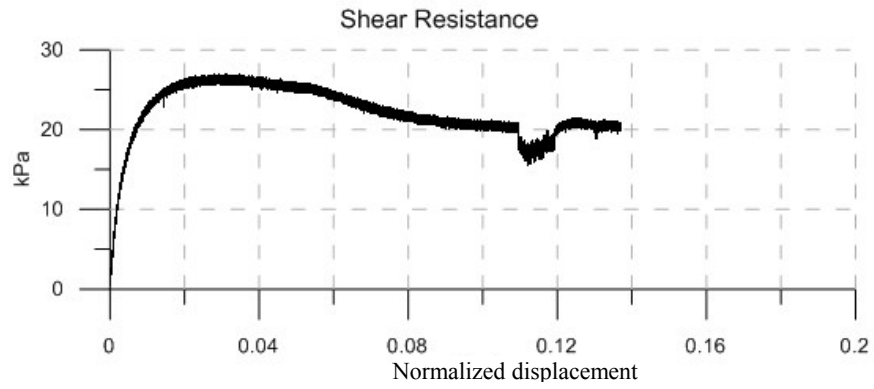

Material:	Sand
Size:	Fine
Normal Stress:	23 kPa
Vibration Frequency:	140 Hz
Vibration Force:	3.22 N
Vibration Duration:	51 sec
Horizontal Acceleration:	0.26 g
Vertical Acceleration:	0.1 g
Horizontal Amplitude:	3.3×10^{-3} mm
Vertical Amplitude:	1.3×10^{-3} mm
Peak Strength:	26.5 kPa
Residual Strength:	20.5 kPa
Vibro-Residual Strength:	17.5 kPa

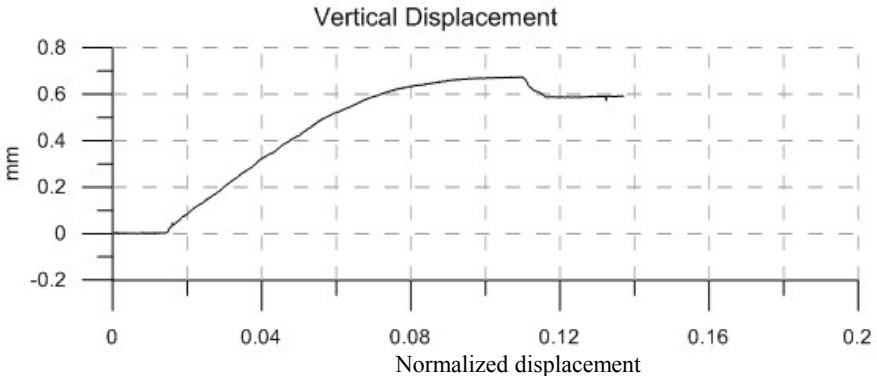

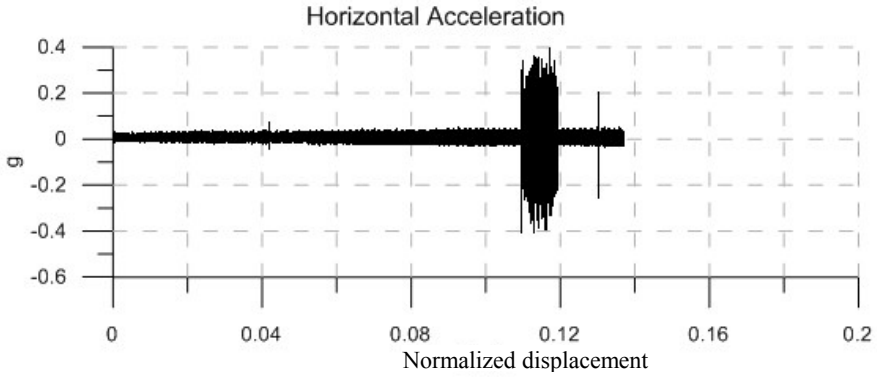

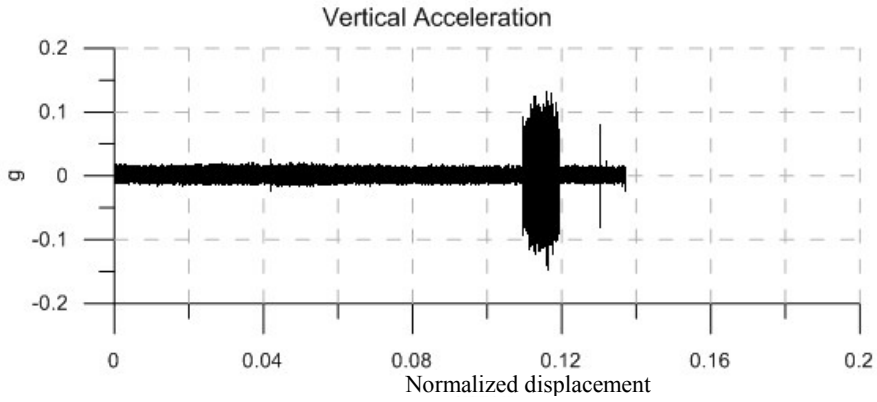

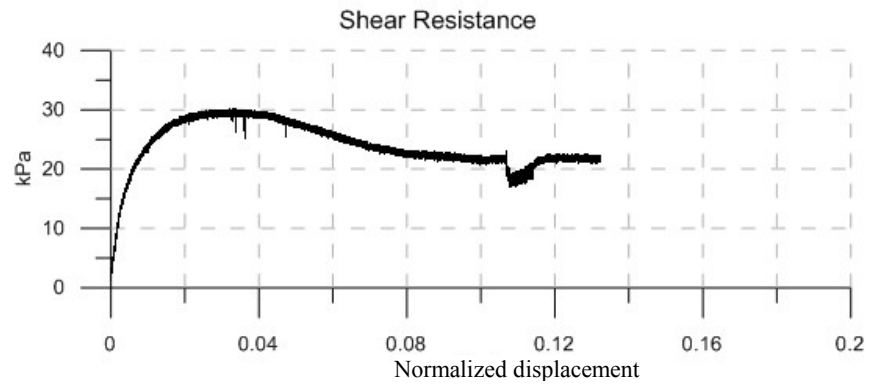

Material:	Sand
Size:	Fine
Normal Stress:	23 kPa
Vibration Frequency:	140 Hz
Vibration Force:	3.71 N
Vibration Duration:	41 sec
Horizontal Acceleration:	0.25 g
Vertical Acceleration:	0.09 g
Horizontal Amplitude:	3.2×10^{-3} mm
Vertical Amplitude:	1.1×10^{-3} mm
Peak Strength:	30 kPa
Residual Strength:	22 kPa
Vibro-Residual Strength:	18.5 kPa

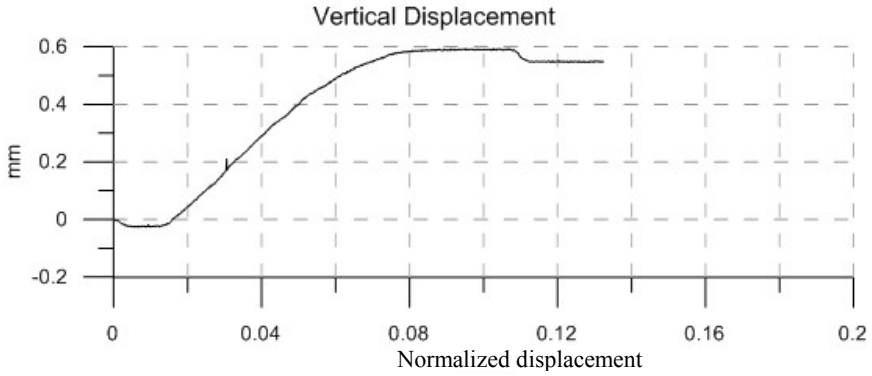

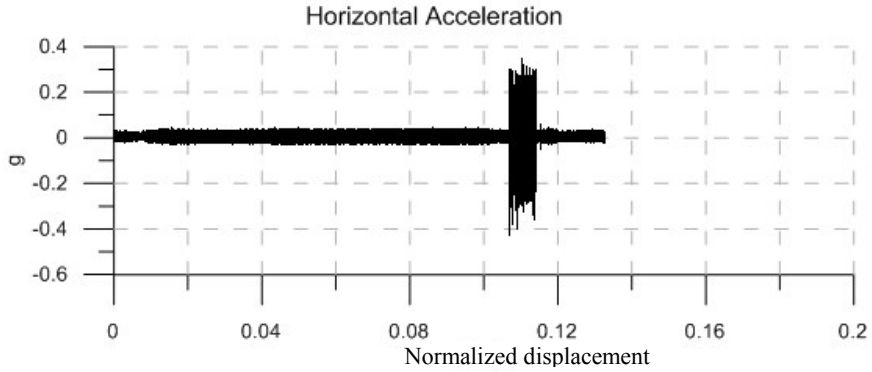

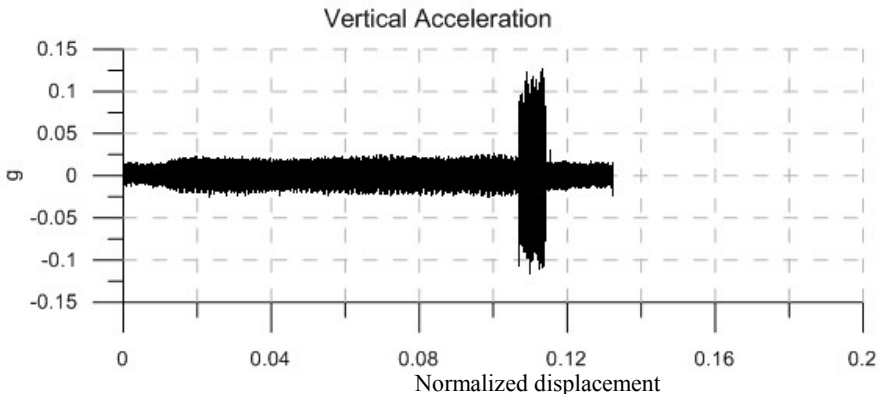

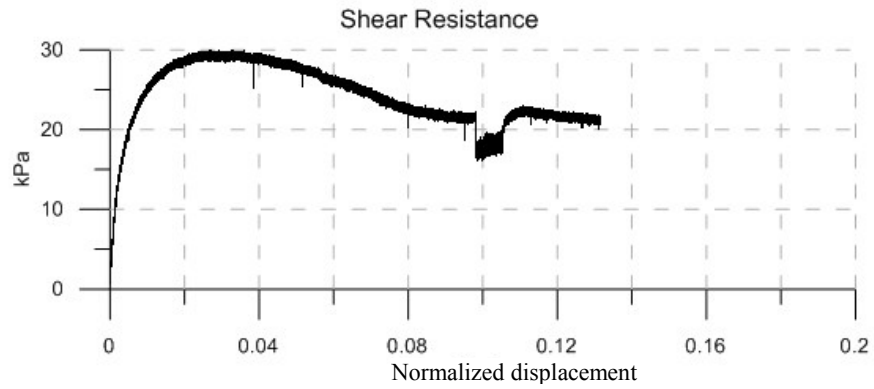

Material:	Sand
Size:	Fine
Normal Stress:	23 kPa
Vibration Frequency:	140 Hz
Vibration Force:	5.18 N
Vibration Duration:	43 sec
Horizontal Acceleration:	0.37 g
Vertical Acceleration:	0.1 g
Horizontal Amplitude:	4.7×10^{-3} mm
Vertical Amplitude:	1.3×10^{-3} mm
Peak Strength:	29.5 kPa
Residual Strength:	22 kPa
Vibro-Residual Strength:	17.5 kPa

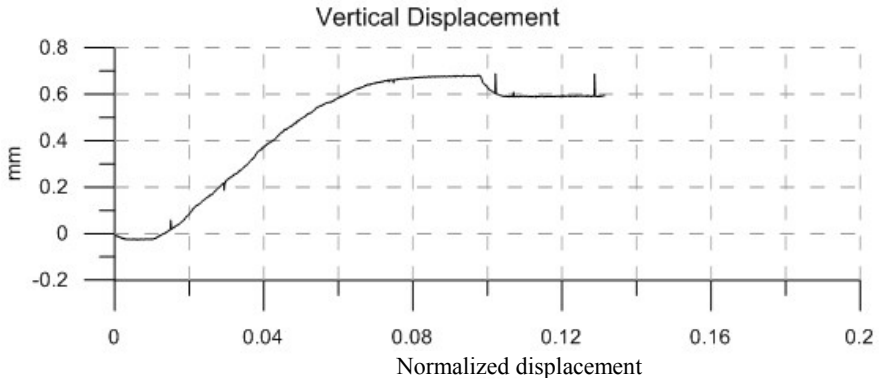

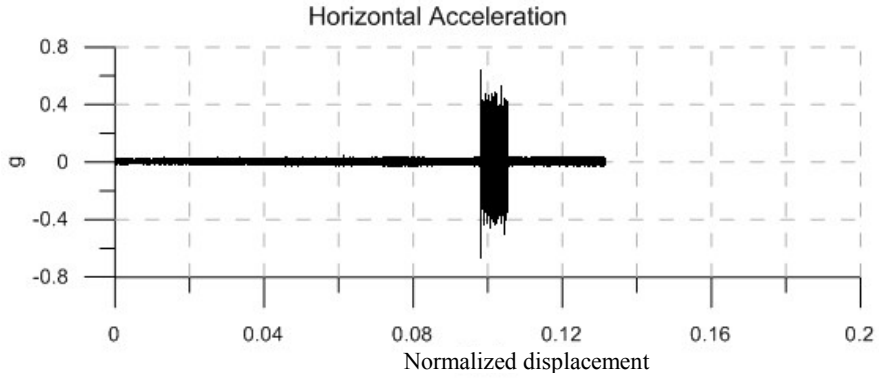

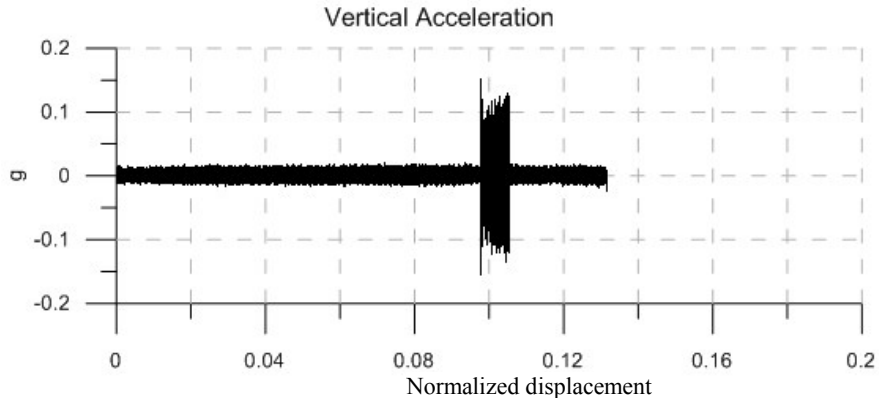

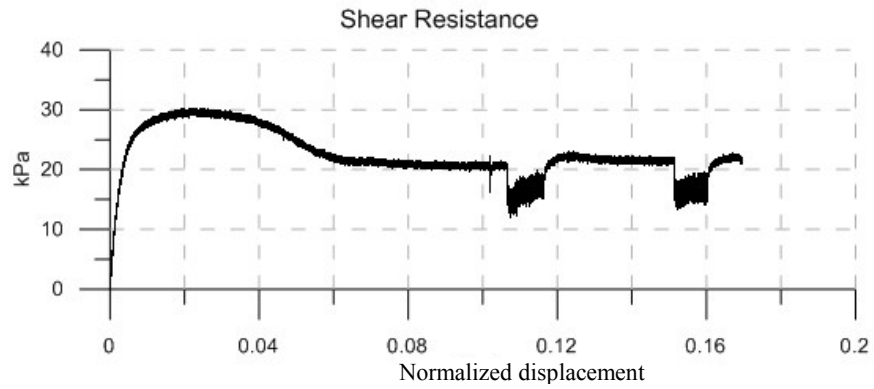

Material:	Sand
Size:	Fine
Normal Stress:	23 kPa
Vibration Frequency:	140 Hz
Vibration Force:	7.14 N
Vibration Duration:	59 sec
Horizontal Acceleration:	0.5 g
Vertical Acceleration:	0.17 g
Horizontal Amplitude:	6.3×10^{-3} mm
Vertical Amplitude:	2.2×10^{-3} mm
Peak Strength:	30 kPa
Residual Strength:	21 kPa
Vibro-Residual Strength:	14.5 kPa

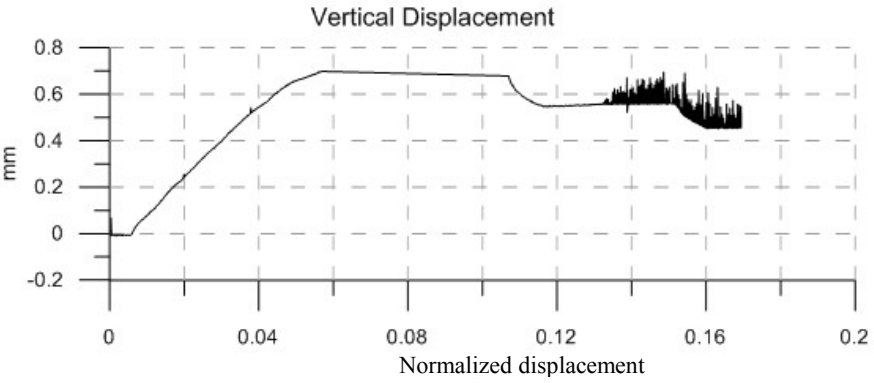

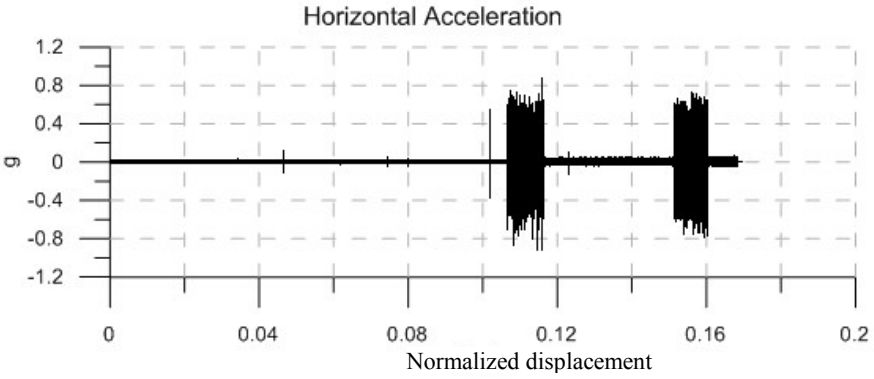

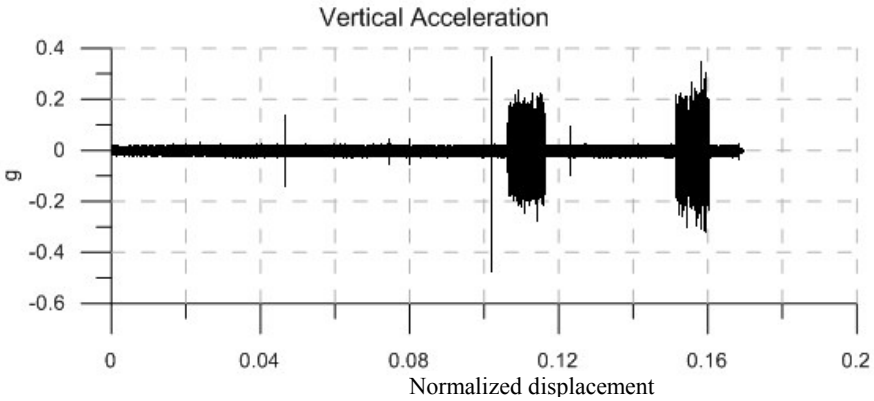

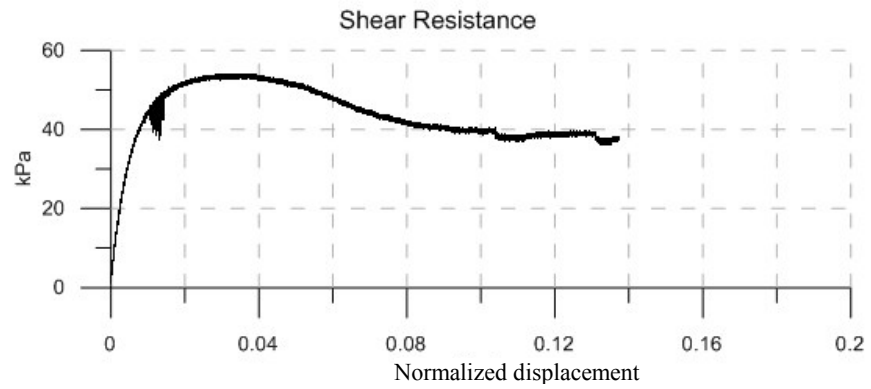

Material:	Sand
Size:	Fine
Normal Stress:	50 kPa
Vibration Frequency:	140 Hz
Vibration Force:	1.61 N
Vibration Duration:	46 sec
Horizontal Acceleration:	0.12 g
Vertical Acceleration:	0.045 g
Horizontal Amplitude:	1.5×10^{-3} mm
Vertical Amplitude:	0.6×10^{-3} mm
Peak Strength:	53.5 kPa
Residual Strength:	40 kPa
Vibro-Residual Strength:	38 kPa

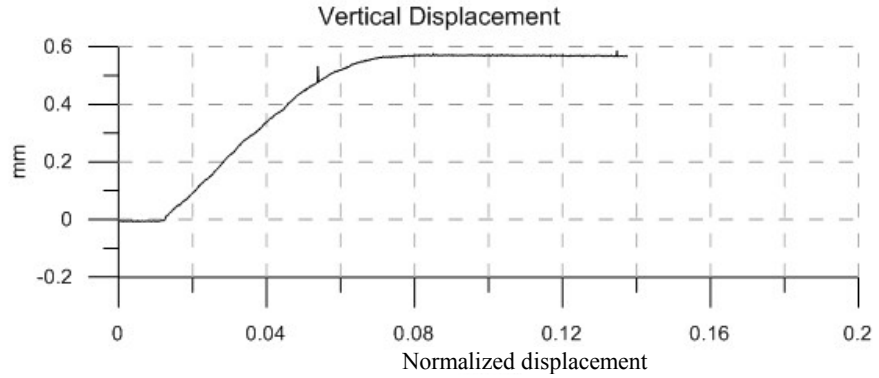

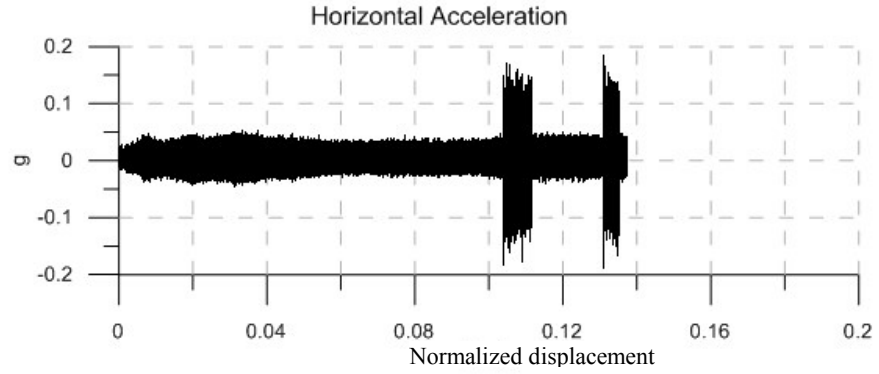

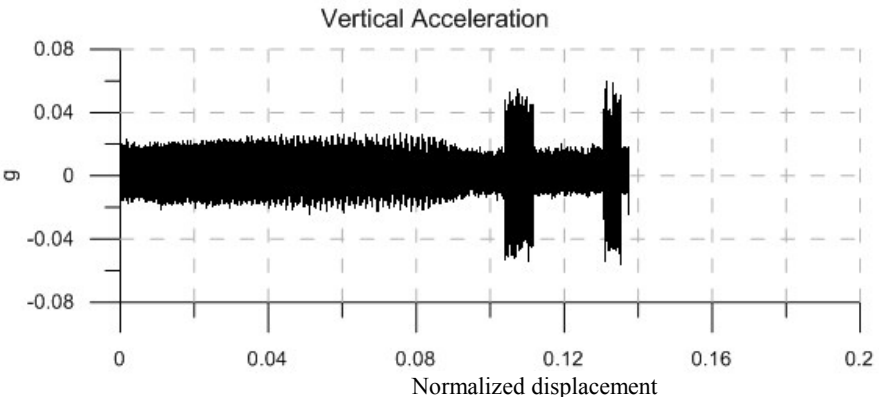

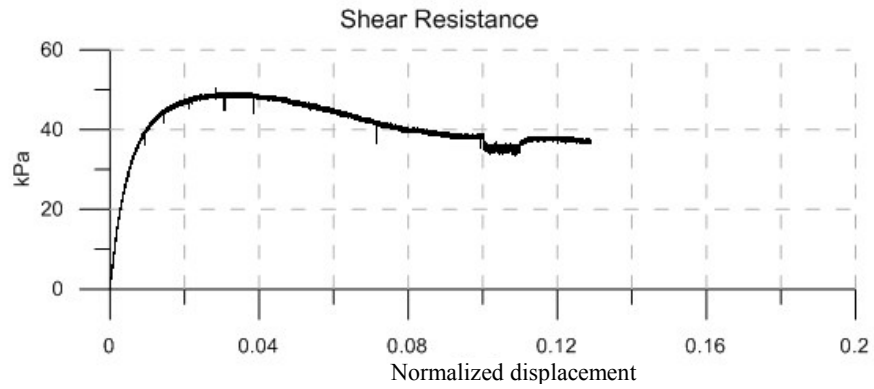

Material:	Sand
Size:	Fine
Normal Stress:	50 kPa
Vibration Frequency:	140 Hz
Vibration Force:	3.22 N
Vibration Duration:	57 sec
Horizontal Acceleration:	0.27 g
Vertical Acceleration:	0.1 g
Horizontal Amplitude:	3.4×10^{-3} mm
Vertical Amplitude:	1.3×10^{-3} mm
Peak Strength:	49 kPa
Residual Strength:	38.5 kPa
Vibro-Residual Strength:	35 kPa

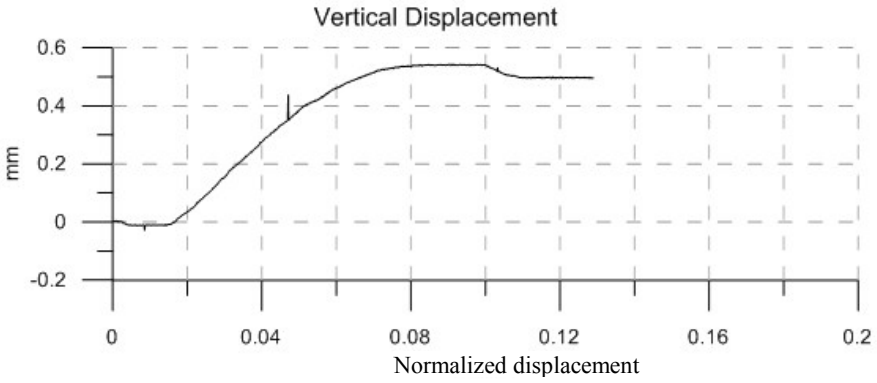

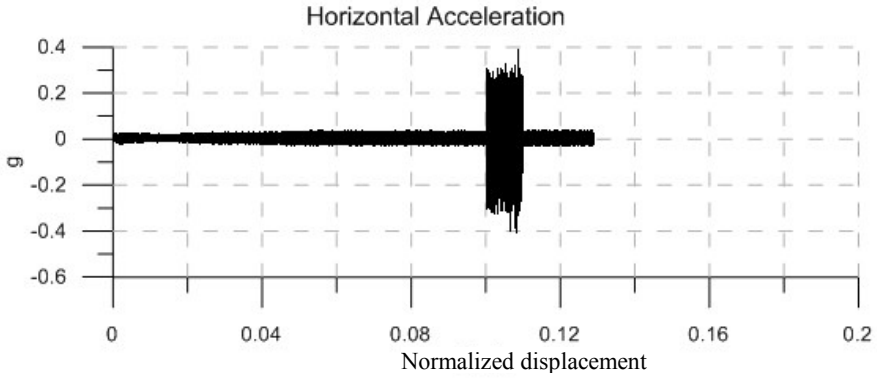

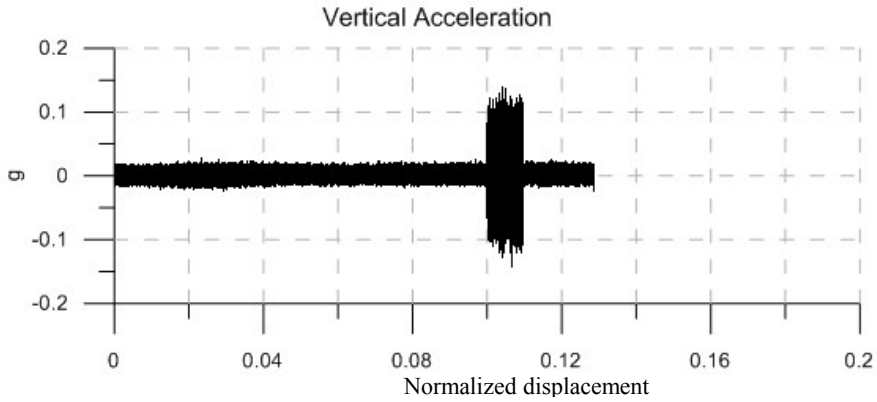

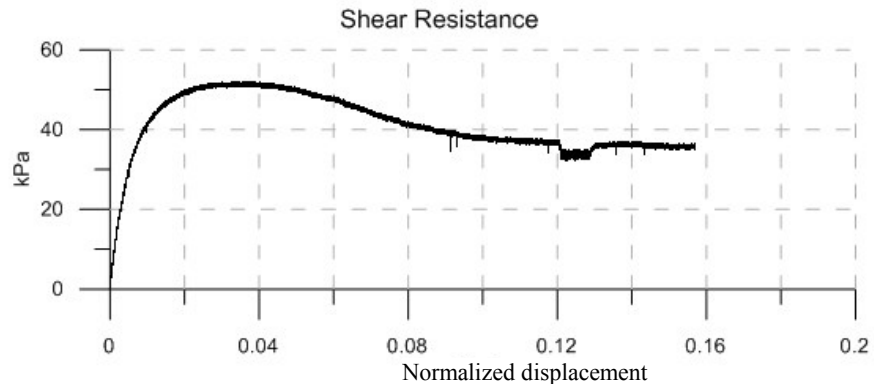

Material:	Sand
Size:	Fine
Normal Stress:	50 kPa
Vibration Frequency:	140 Hz
Vibration Force:	3.71 N
Vibration Duration:	48 sec
Horizontal Acceleration:	0.27 g
Vertical Acceleration:	0.1 g
Horizontal Amplitude:	3.4×10^{-3} mm
Vertical Amplitude:	1.3×10^{-3} mm
Peak Strength:	51.5 kPa
Residual Strength:	37 kPa
Vibro-Residual Strength:	33.5 kPa

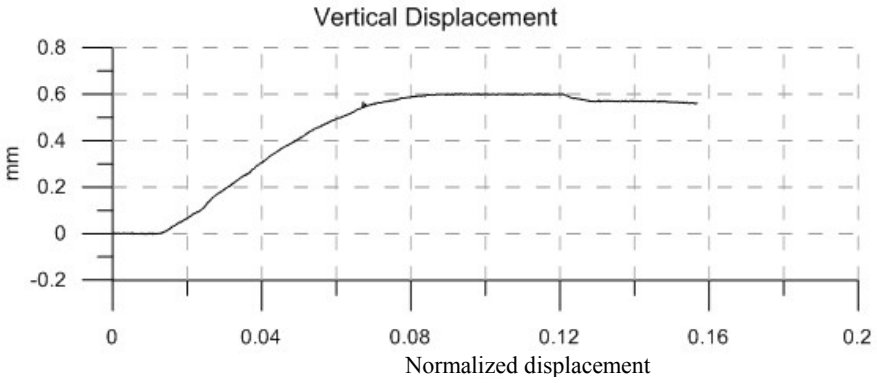

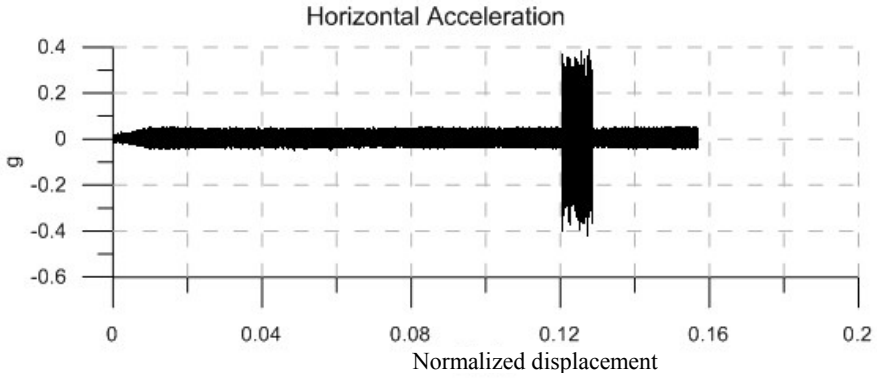

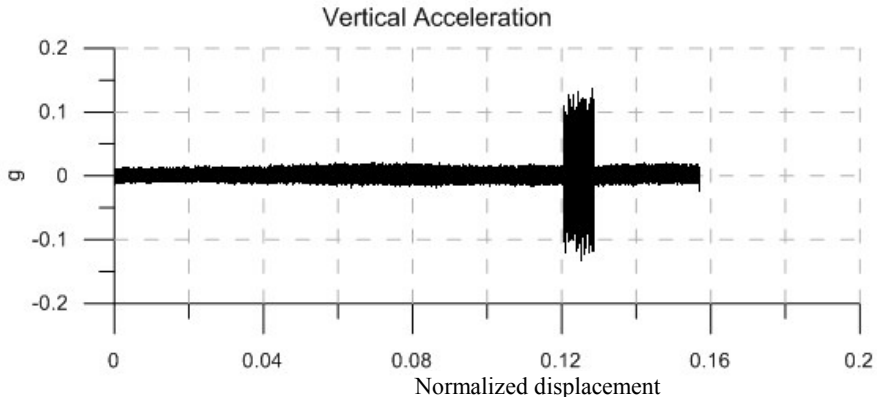

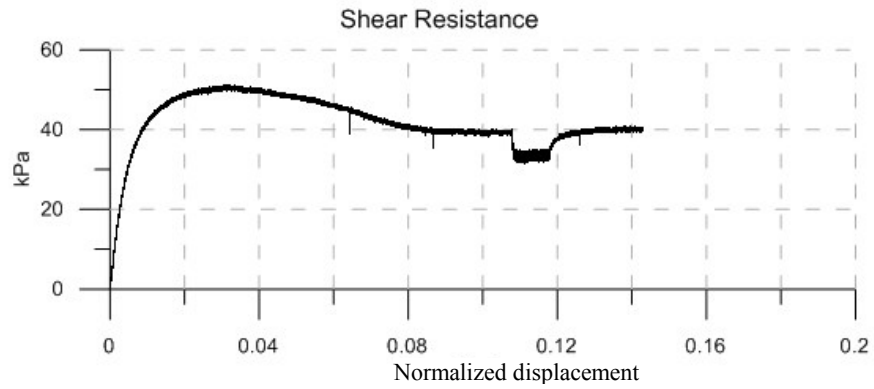

Material:	Sand
Size:	Fine
Normal Stress:	50 kPa
Vibration Frequency:	140 Hz
Vibration Force:	5.18 N
Vibration Duration:	59 sec
Horizontal Acceleration:	0.38 g
Vertical Acceleration:	0.115 g
Horizontal Amplitude:	4.8×10^{-3} mm
Vertical Amplitude:	1.5×10^{-3} mm
Peak Strength:	51 kPa
Residual Strength:	39.5 kPa
Vibro-Residual Strength:	33.5 kPa

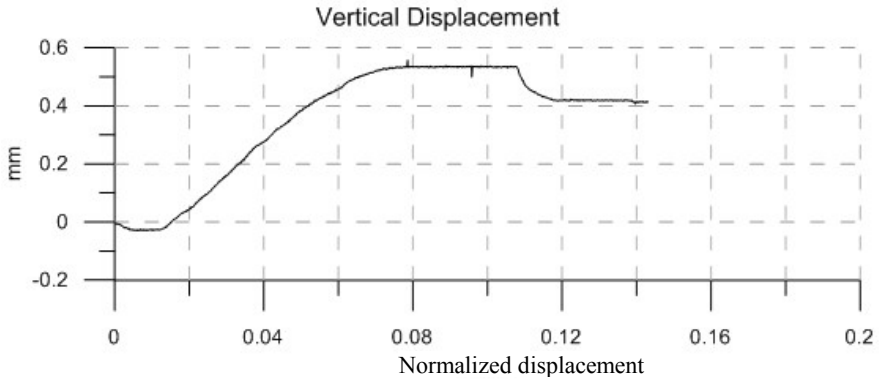

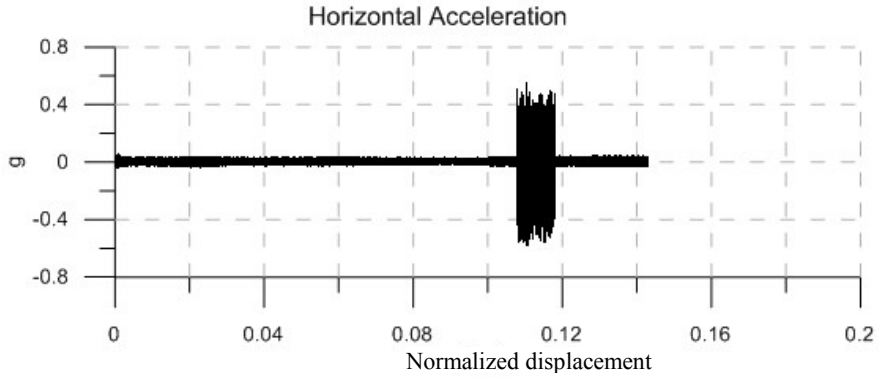

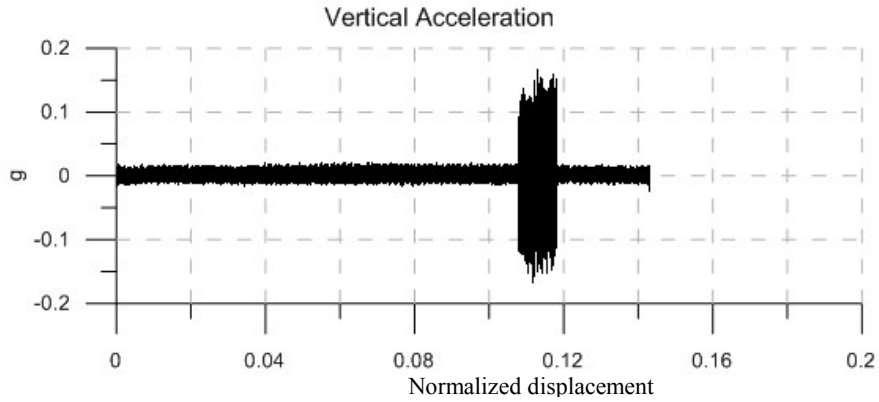

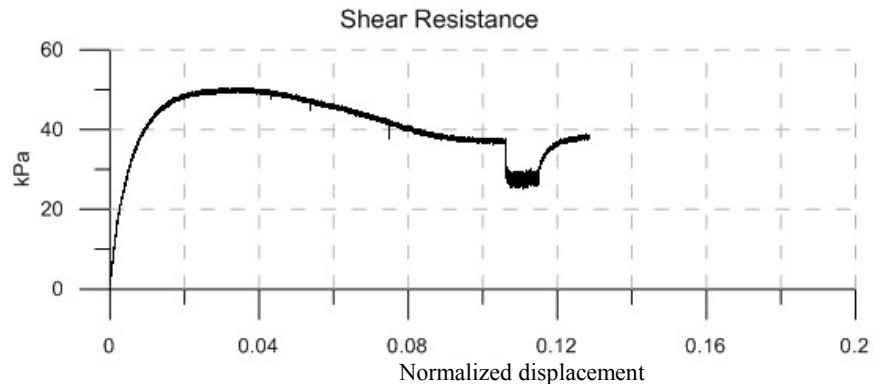

Material:	Sand
Size:	Fine
Normal Stress:	50 kPa
Vibration Frequency:	140 Hz
Vibration Force:	7.14 N
Vibration Duration:	53 sec
Horizontal Acceleration:	0.49 g
Vertical Acceleration:	0.155 g
Horizontal Amplitude:	6.2×10^{-3} mm
Vertical Amplitude:	2.0×10^{-3} mm
Peak Strength:	50.5 kPa
Residual Strength:	37.5 kPa
Vibro-Residual Strength:	27.5 kPa

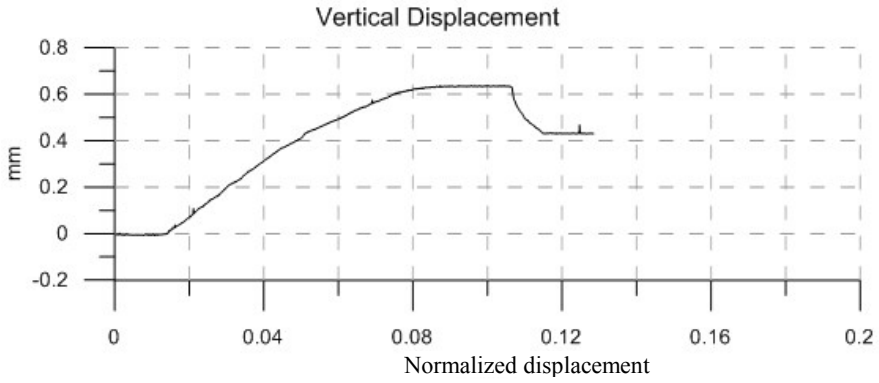

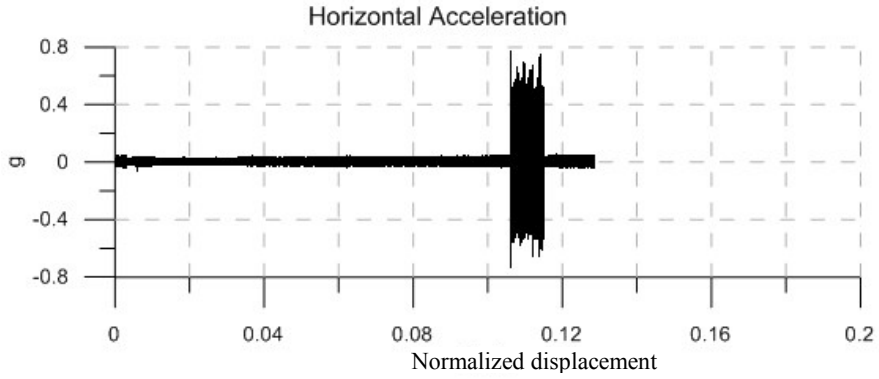

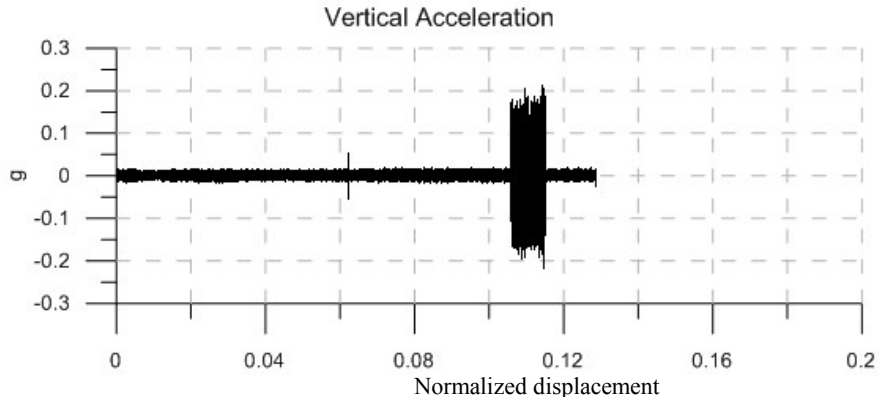

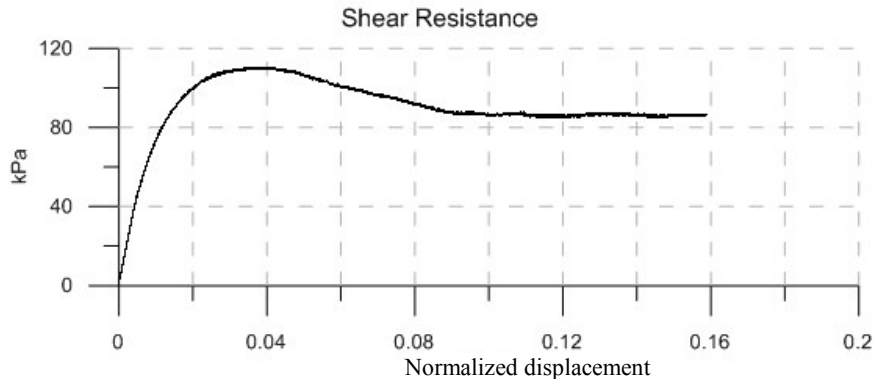

Material:	Sand
Size:	Fine
Normal Stress:	118 kPa
Vibration Frequency:	140 Hz
Vibration Force:	1.61 N
Vibration Duration:	90 sec
Horizontal Acceleration:	0.12 g
Vertical Acceleration:	0.05 g
Horizontal Amplitude:	1.5×10^{-3} mm
Vertical Amplitude:	0.6×10^{-3} mm
Peak Strength:	110 kPa
Residual Strength:	87.5 kPa
Vibro-Residual Strength:	85.5 kPa

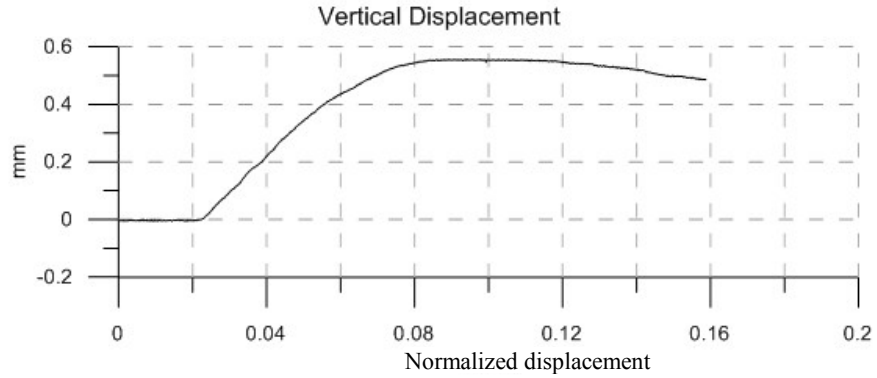

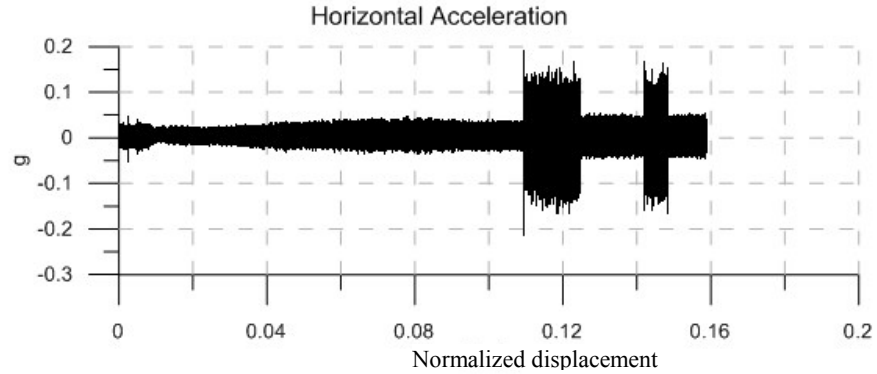

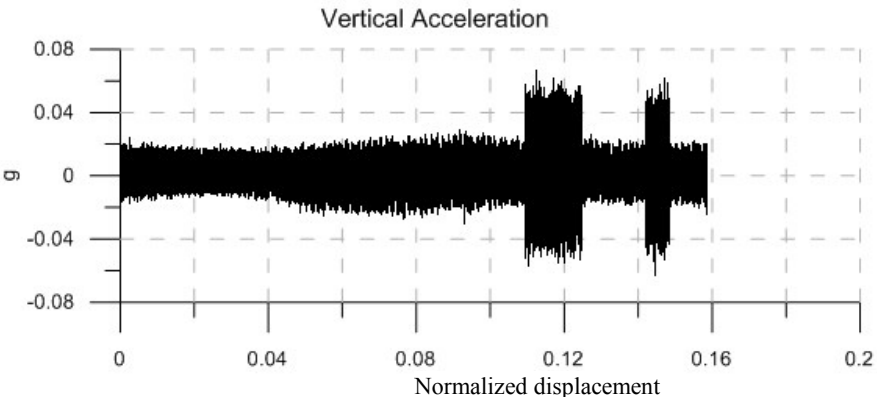

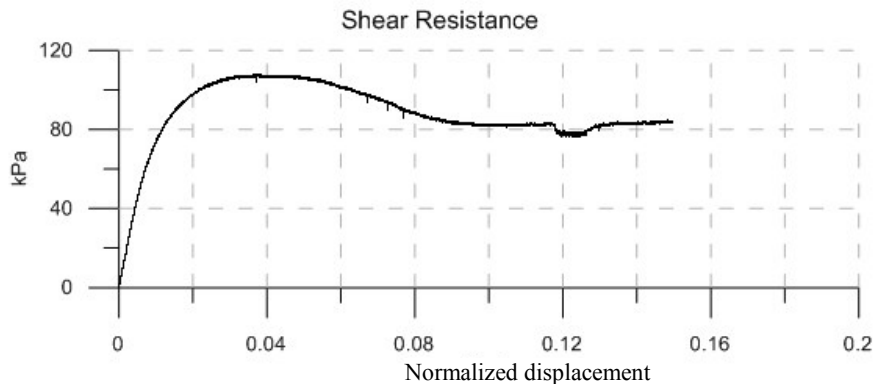

Material:	Sand
Size:	Fine
Normal Stress:	118 kPa
Vibration Frequency:	140 Hz
Vibration Force:	3.22 N
Vibration Duration:	50 sec
Horizontal Acceleration:	0.27 g
Vertical Acceleration:	0.09 g
Horizontal Amplitude:	3.4×10^{-3} mm
Vertical Amplitude:	1.1×10^{-3} mm
Peak Strength:	107.5 kPa
Residual Strength:	83 kPa
Vibro-Residual Strength:	77. kPa

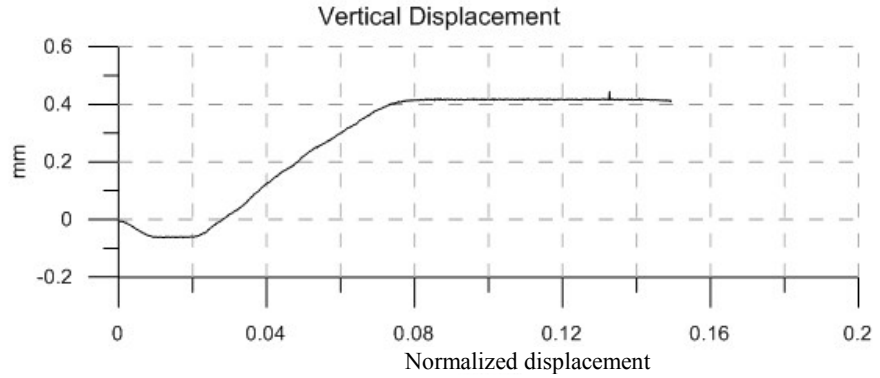

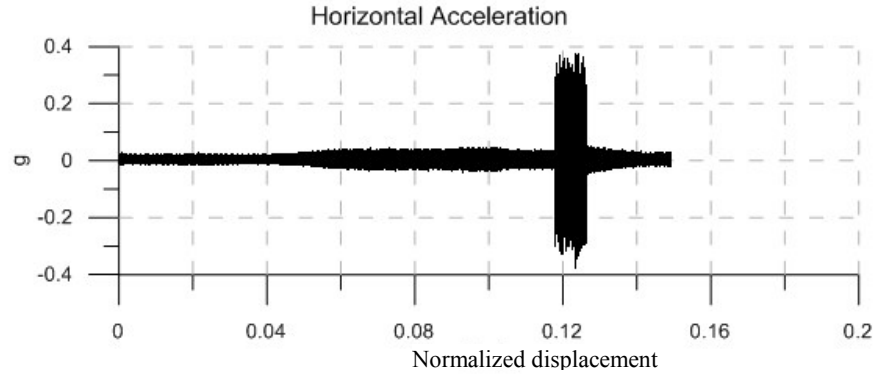

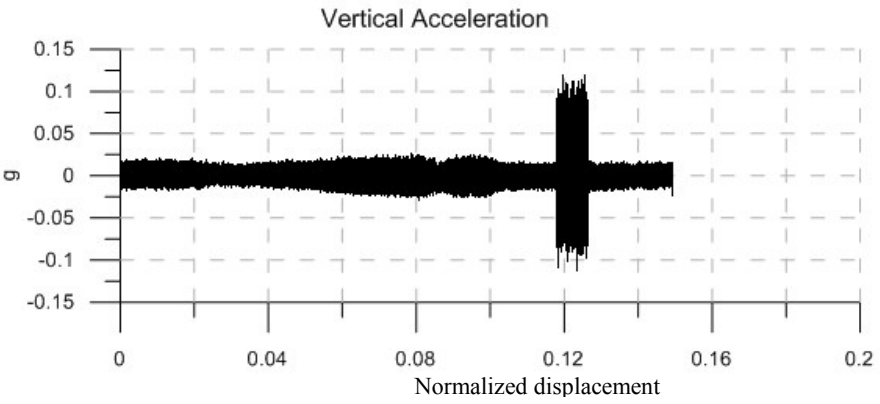

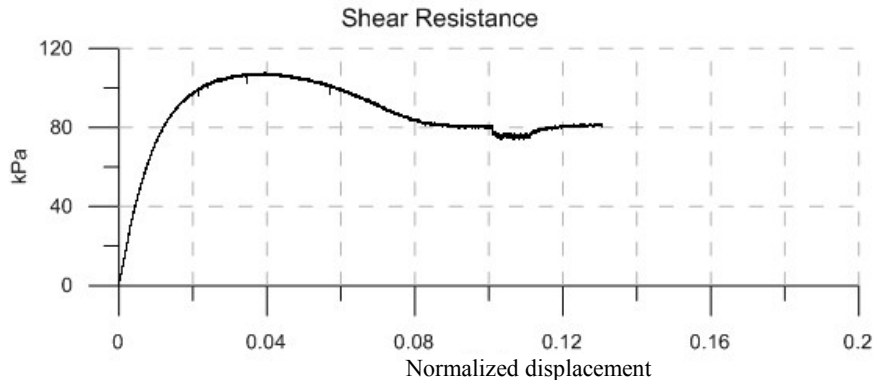

Material:	Sand
Size:	Fine
Normal Stress:	118 kPa
Vibration Frequency:	140 Hz
Vibration Force:	3.71 N
Vibration Duration:	61 sec
Horizontal Acceleration:	0.27 g
Vertical Acceleration:	0.09 g
Horizontal Amplitude:	3.4×10^{-3} mm
Vertical Amplitude:	1.1×10^{-3} mm
Peak Strength:	107.5 kPa
Residual Strength:	81 kPa
Vibro-Residual Strength:	75 kPa

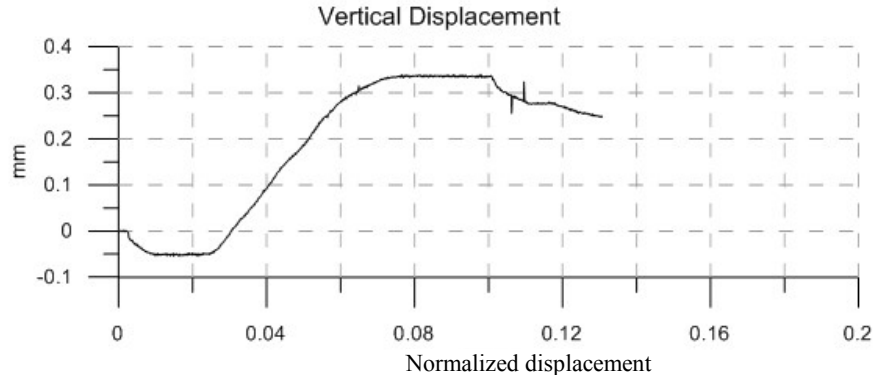

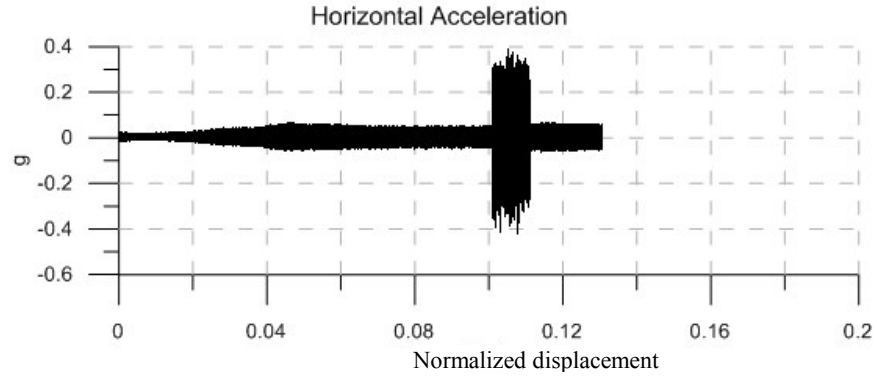

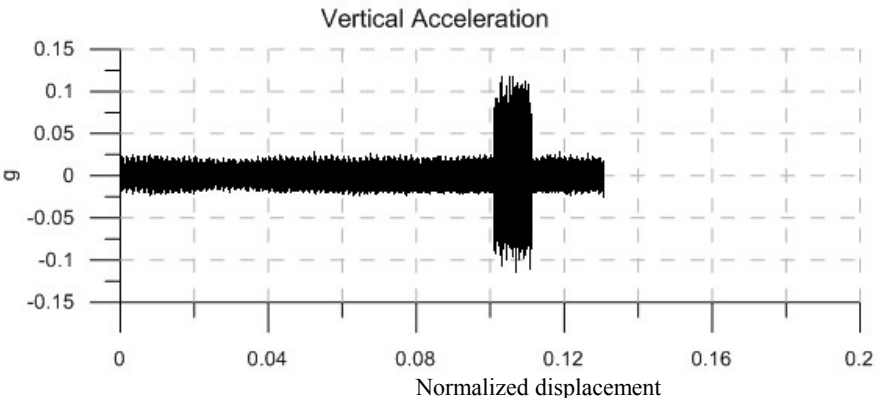

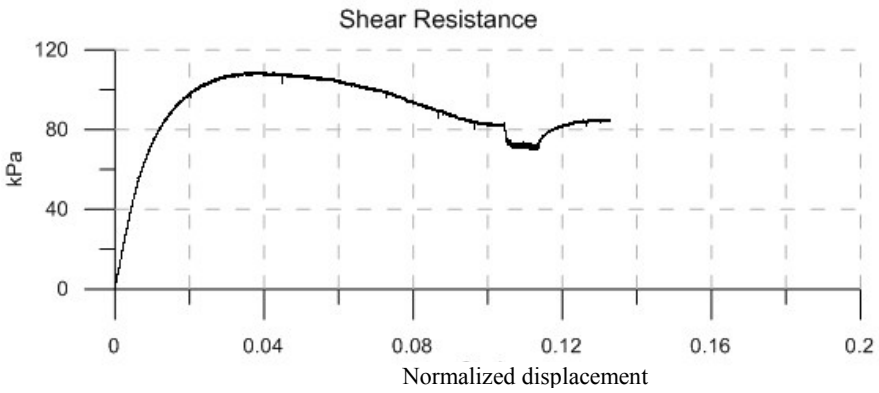

Material:	Sand
Size:	Fine
Normal Stress:	118 kPa
Vibration Frequency:	140 Hz
Vibration Force:	5.18 N
Vibration Duration:	53 sec
Horizontal Acceleration:	0.37 g
Vertical Acceleration:	0.105 g
Horizontal Amplitude:	4.7×10^{-3} mm
Vertical Amplitude:	1.3×10^{-3} mm
Peak Strength:	108.5 kPa
Residual Strength:	82.5 kPa
Vibro-Residual Strength:	71.5 kPa

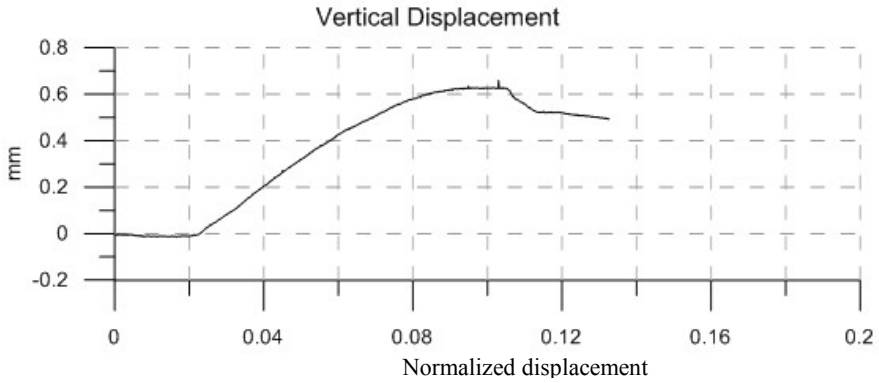

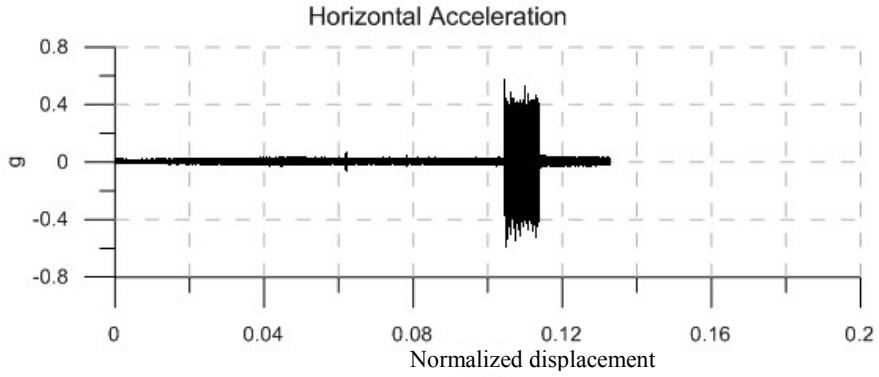

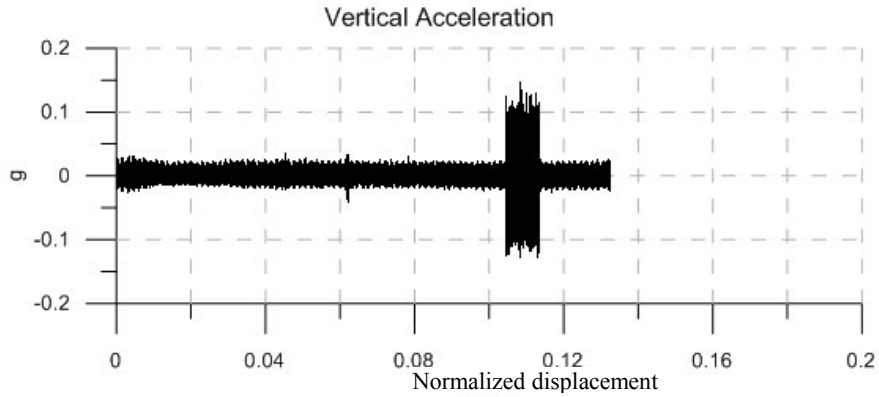

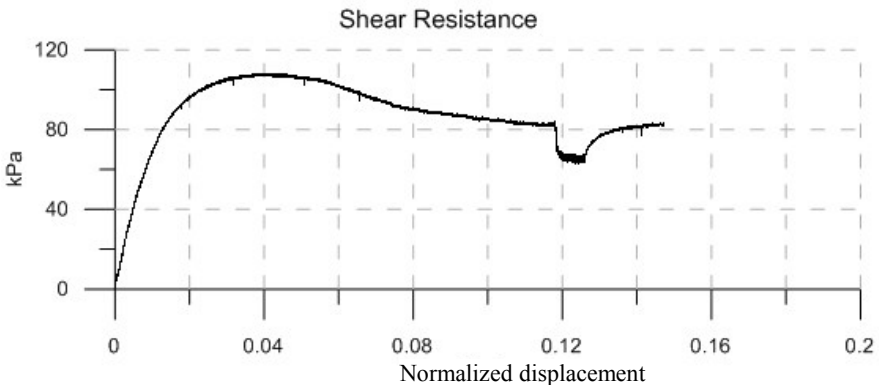

Material:	Sand
Size:	Fine
Normal Stress:	118 kPa
Vibration Frequency:	140 Hz
Vibration Force:	7.14 N
Vibration Duration:	46 sec
Horizontal Acceleration:	0.47 g
Vertical Acceleration:	0.145 g
Horizontal Amplitude:	6.0×10^{-3} mm
Vertical Amplitude:	1.8×10^{-3} mm
Peak Strength:	108 kPa
Residual Strength:	83 kPa
Vibro-Residual Strength:	65 kPa

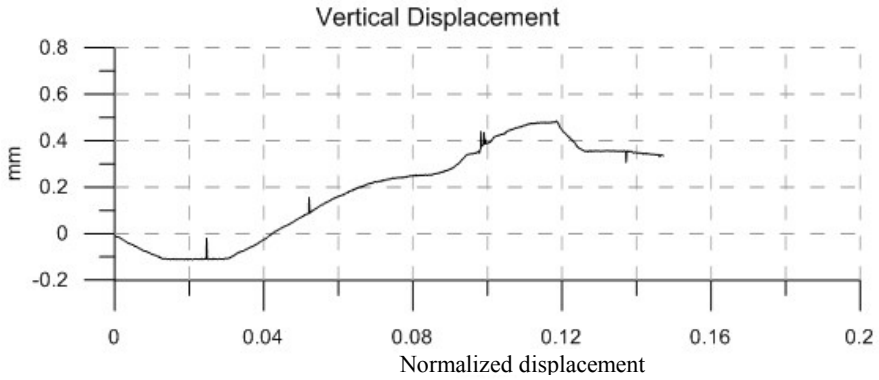

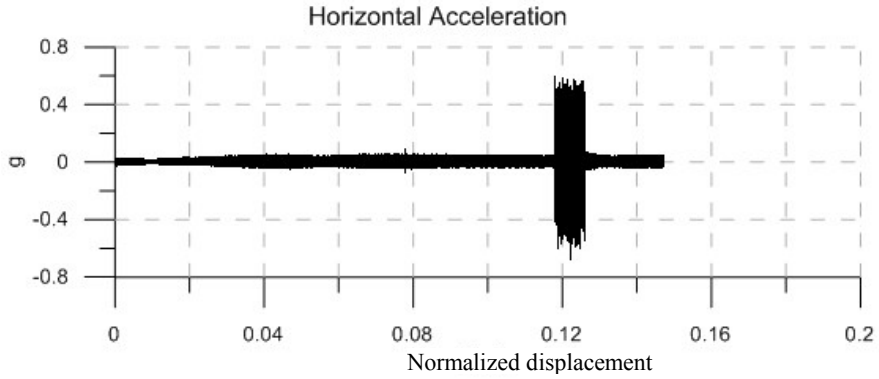

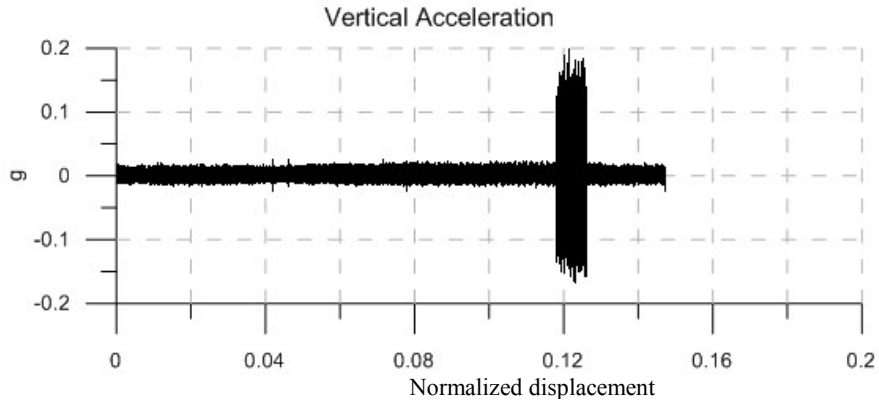

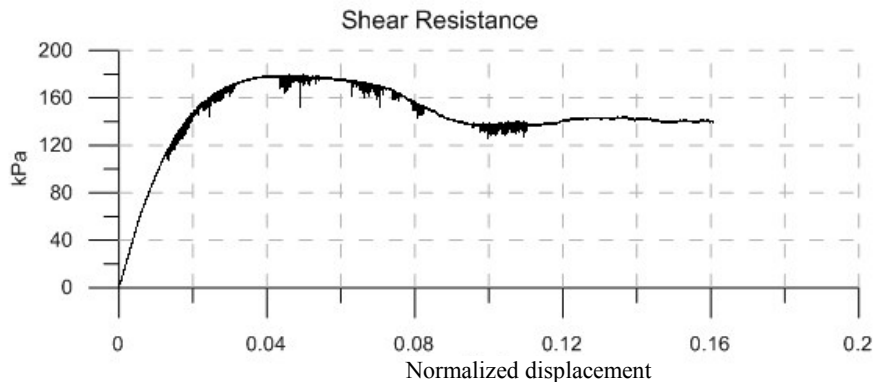

Material:	Sand
Size:	Fine
Normal Stress:	200 kPa
Vibration Frequency:	140 Hz
Vibration Force:	1.61 N
Vibration Duration:	57 sec
Horizontal Acceleration:	0.11 g
Vertical Acceleration:	0.045 g
Horizontal Amplitude:	1.4×10^{-3} mm
Vertical Amplitude:	0.6×10^{-3} mm
Peak Strength:	178.5 kPa
Residual Strength:	139 kPa
Vibro-Residual Strength:	137 kPa

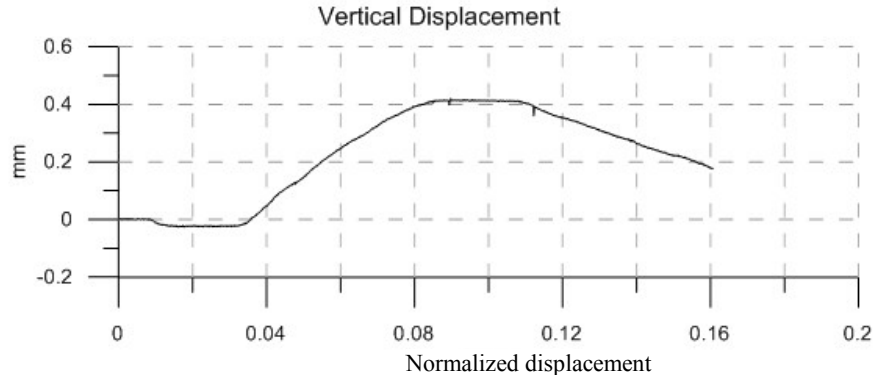

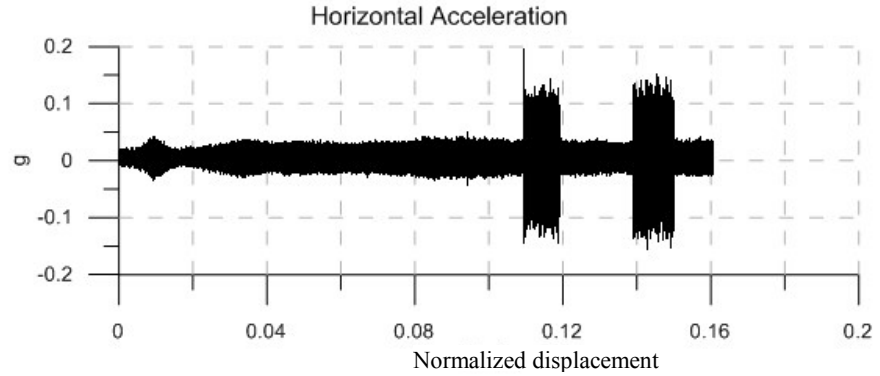

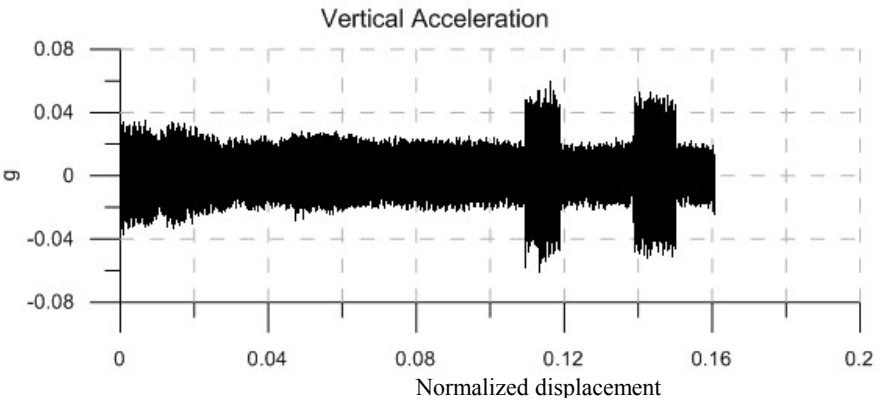

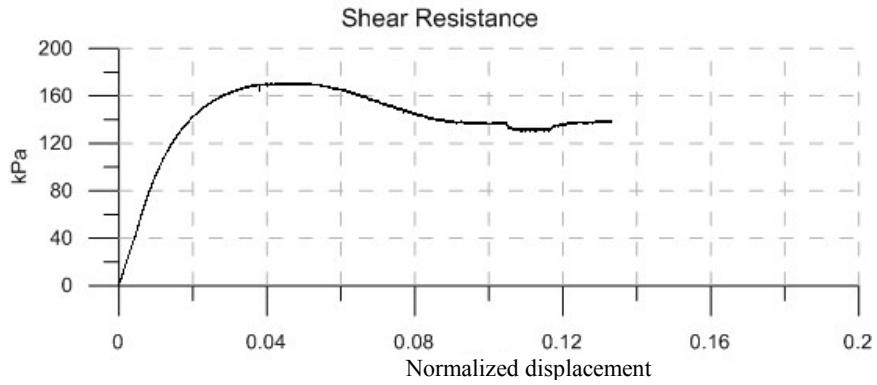

Material:	Sand
Size:	Fine
Normal Stress:	200 kPa
Vibration Frequency:	140 Hz
Vibration Force:	3.22 N
Vibration Duration:	69 sec
Horizontal Acceleration:	0.23 g
Vertical Acceleration:	0.07 g
Horizontal Amplitude:	2.9×10^{-3} mm
Vertical Amplitude:	0.9×10^{-3} mm
Peak Strength:	170.5 kPa
Residual Strength:	137.5 kPa
Vibro-Residual Strength:	131 kPa

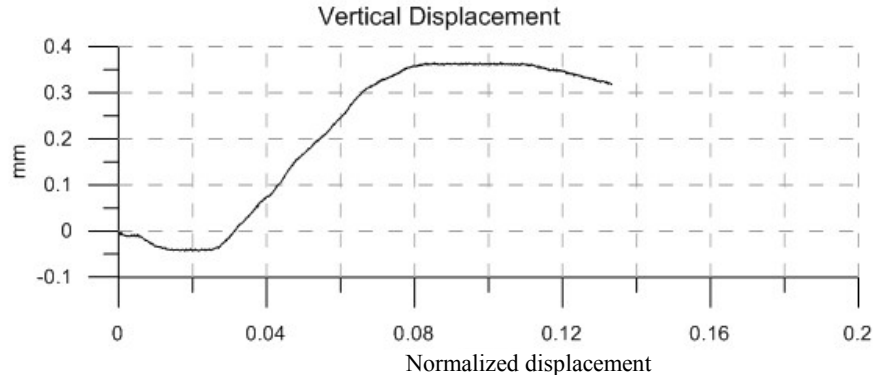

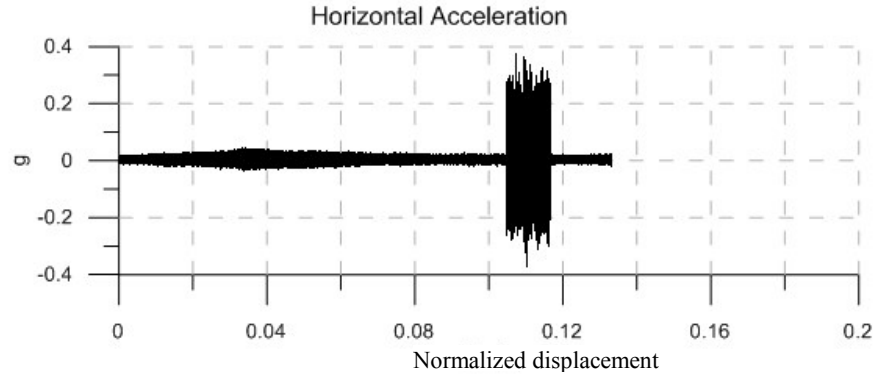

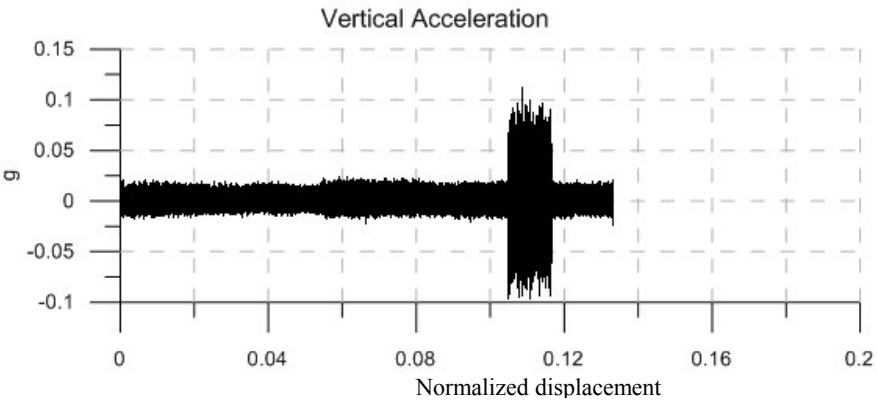

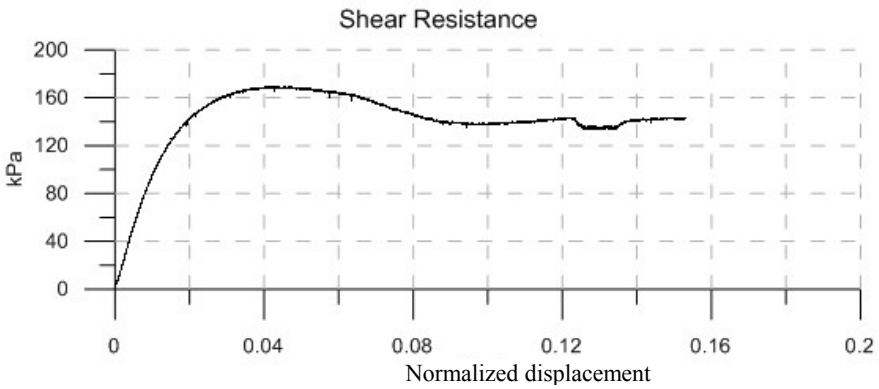

Material:	Sand
Size:	Fine
Normal Stress:	200 kPa
Vibration Frequency:	140 Hz
Vibration Force:	3.71 N
Vibration Duration:	66 sec
Horizontal Acceleration:	0.25 g
Vertical Acceleration:	0.08 g
Horizontal Amplitude:	3.2×10^{-3} mm
Vertical Amplitude:	1.0×10^{-3} mm
Peak Strength:	169 kPa
Residual Strength:	143 kPa
Vibro-Residual Strength:	134.5 kPa

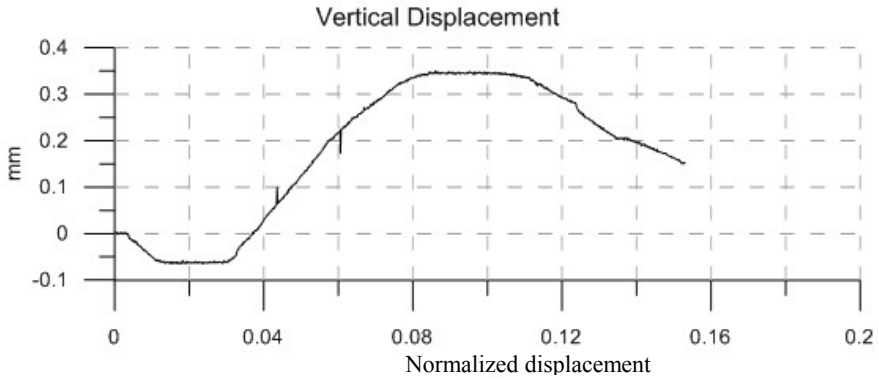

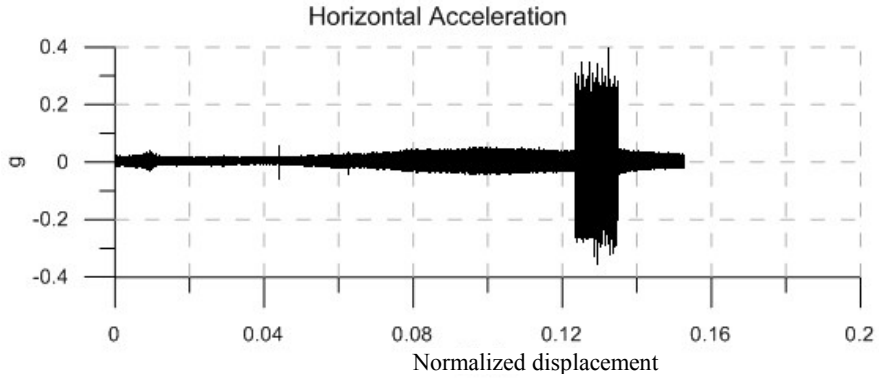

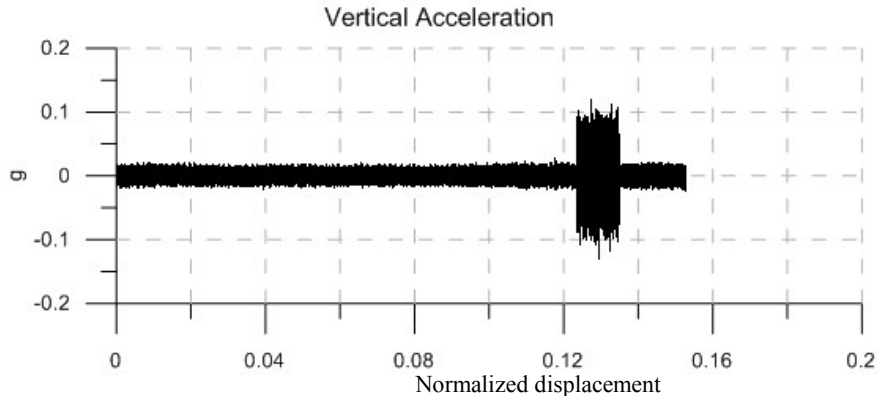

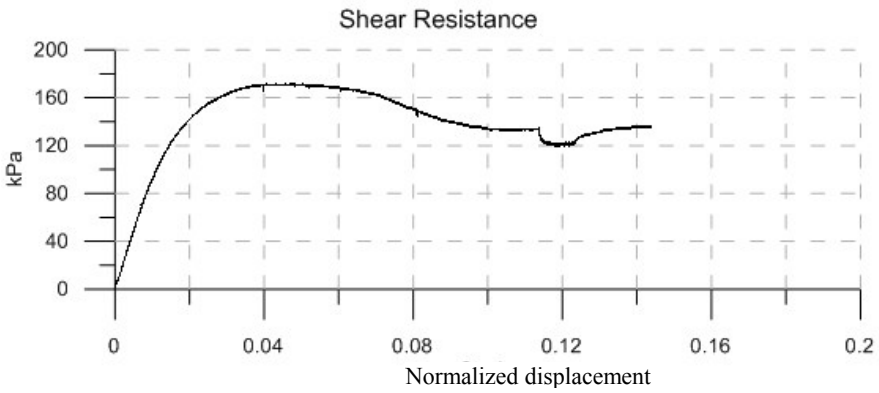

Material:	Sand
Size:	Fine
Normal Stress:	200 kPa
Vibration Frequency:	140 Hz
Vibration Force:	5.18 N
Vibration Duration:	27 sec
Horizontal Acceleration:	0.32 g
Vertical Acceleration:	0.1 g
Horizontal Amplitude:	4.1×10^{-3} mm
Vertical Amplitude:	1.3×10^{-3} mm
Peak Strength:	171 kPa
Residual Strength:	134 kPa
Vibro-Residual Strength:	121 kPa

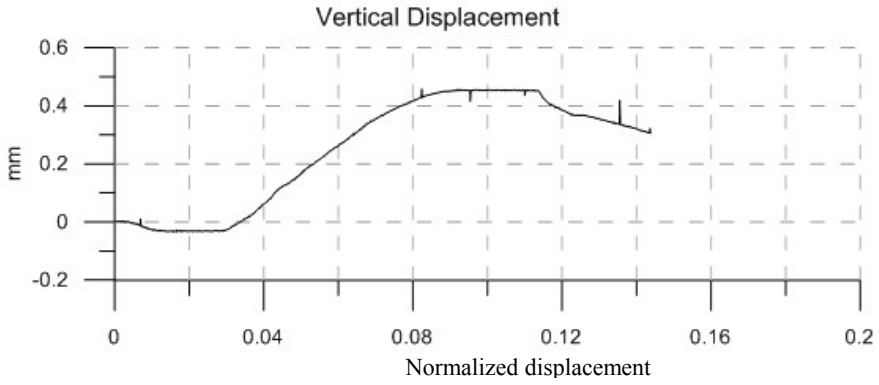

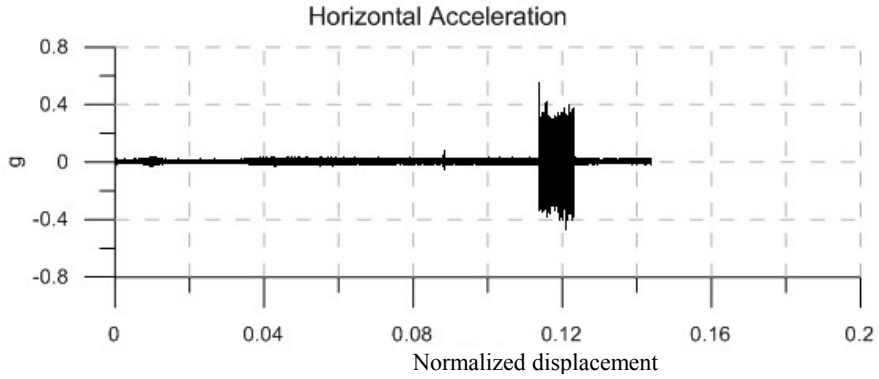

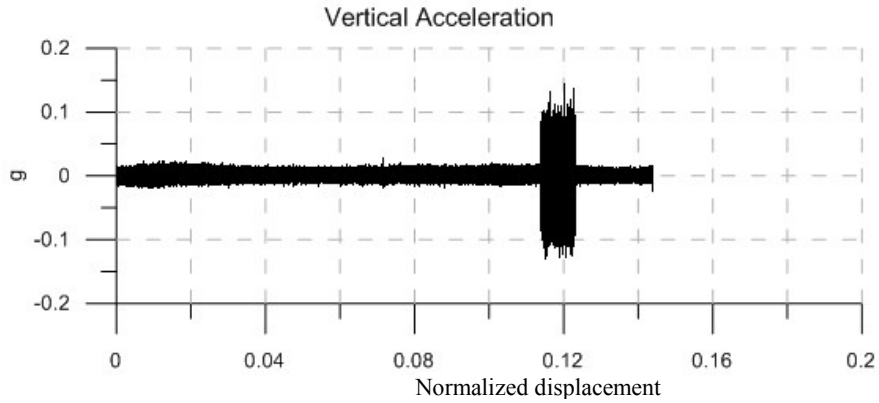

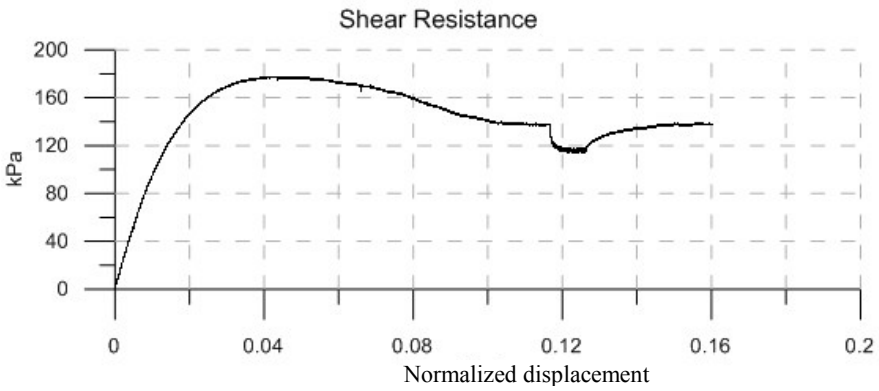

Material:	Sand
Size:	Fine
Normal Stress:	200 kPa
Vibration Frequency:	140 Hz
Vibration Force:	7.14 N
Vibration Duration:	56 sec
Horizontal Acceleration:	0.45 g
Vertical Acceleration:	0.145 g
Horizontal Amplitude:	5.7×10^{-3} mm
Vertical Amplitude:	1.8×10^{-3} mm
Peak Strength:	177 kPa
Residual Strength:	138 kPa
Vibro-Residual Strength:	116 kPa

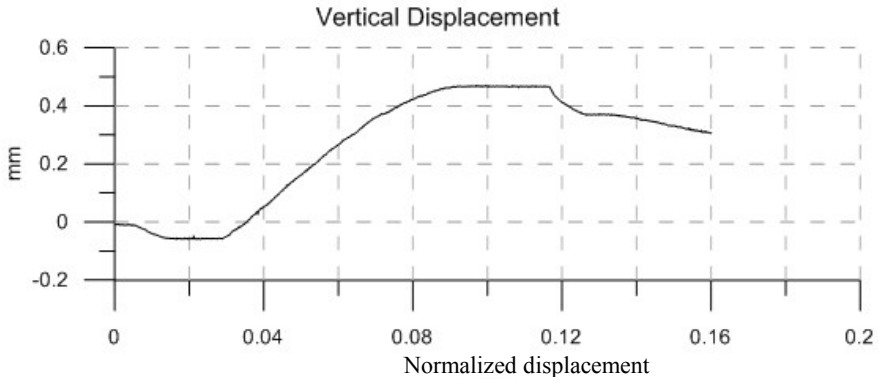

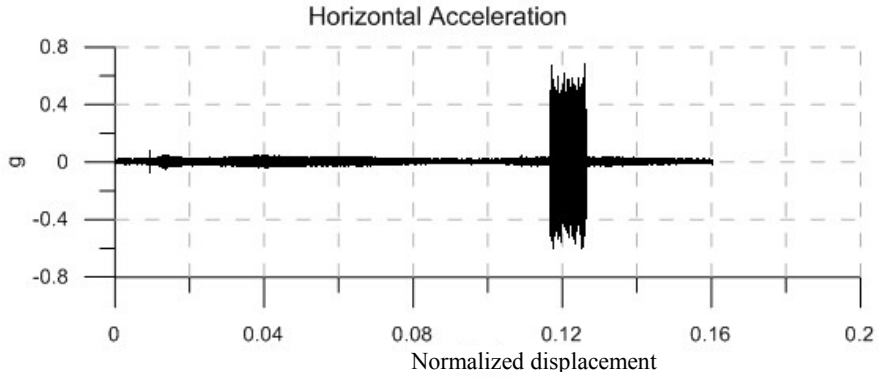

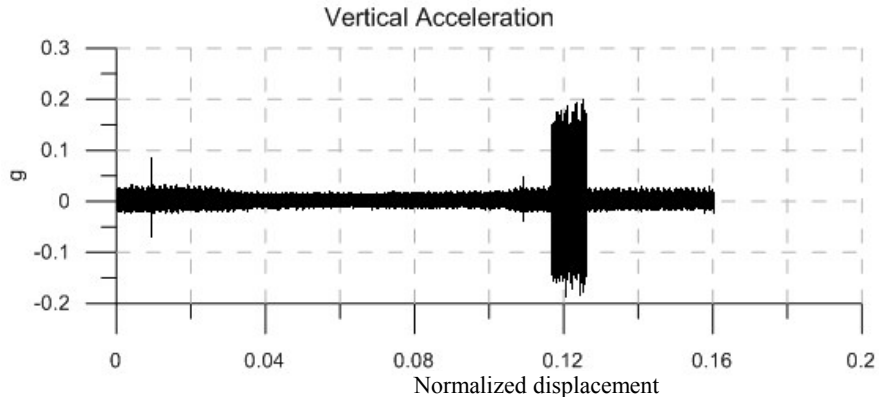

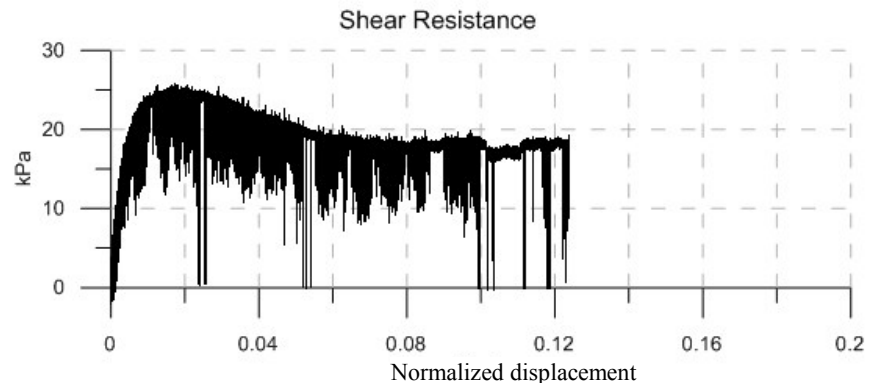

Material:	Sand
Size:	Coarse
Normal Stress:	23 kPa
Vibration Frequency:	140 Hz
Vibration Force:	1.61 N
Vibration Duration:	55 sec
Horizontal Acceleration:	0.12 g
Vertical Acceleration:	0.045 g
Horizontal Amplitude:	1.5×10^{-3} mm
Vertical Amplitude:	0.6×10^{-3} mm
Peak Strength:	25 kPa
Residual Strength:	18.5 kPa
Vibro-Residual Strength:	17 kPa

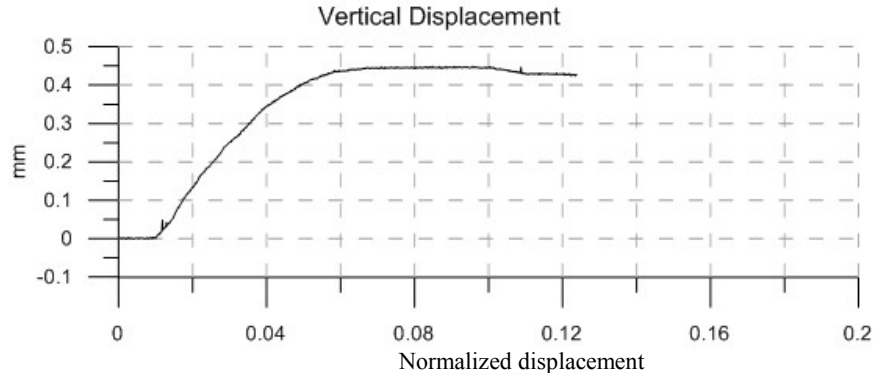

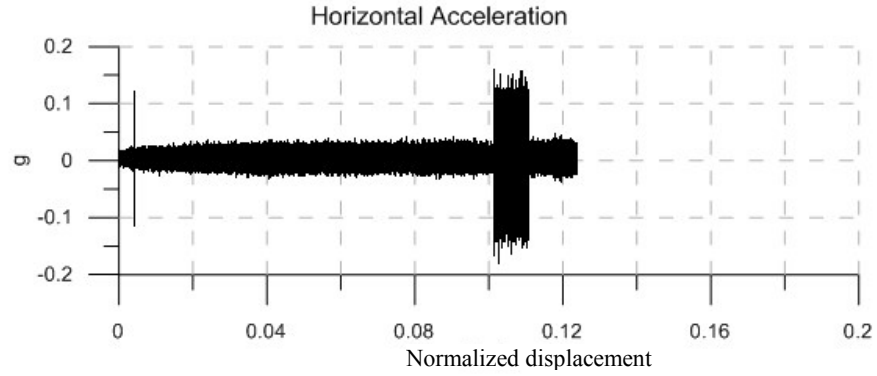

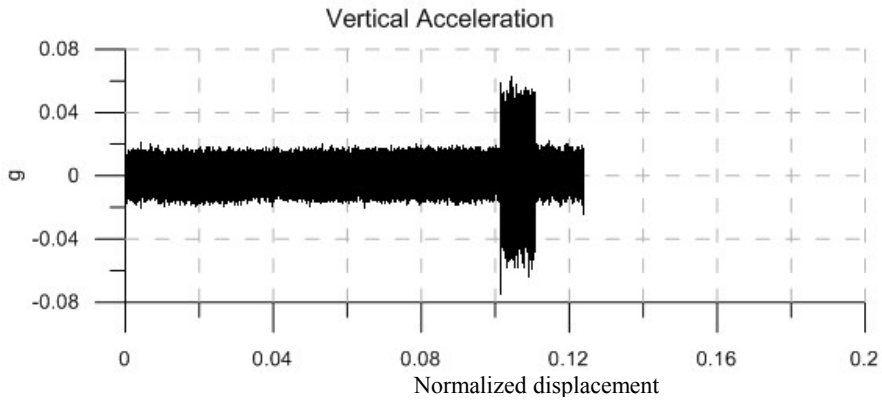

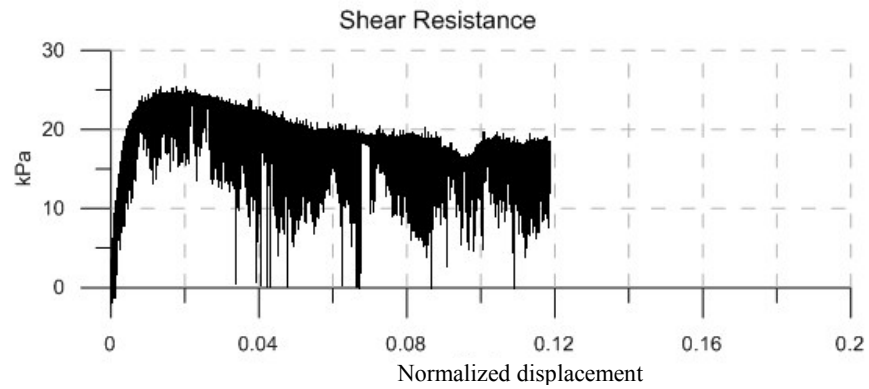

Material:	Sand
Size:	Coarse
Normal Stress:	23 kPa
Vibration Frequency:	140 Hz
Vibration Force:	3.22 N
Vibration Duration:	54 sec
Horizontal Acceleration:	0.2 g
Vertical Acceleration:	0.075 g
Horizontal Amplitude:	2.5×10^{-3} mm
Vertical Amplitude:	1.0×10^{-3} mm
Peak Strength:	24.5 kPa
Residual Strength:	18.5 kPa
Vibro-Residual Strength:	16.5 kPa

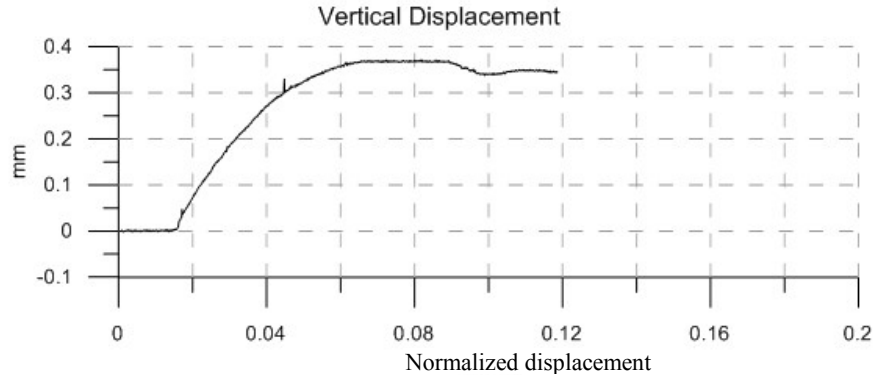

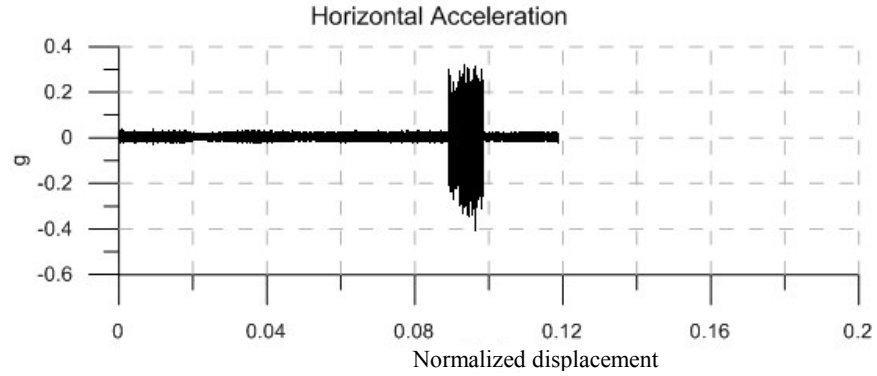

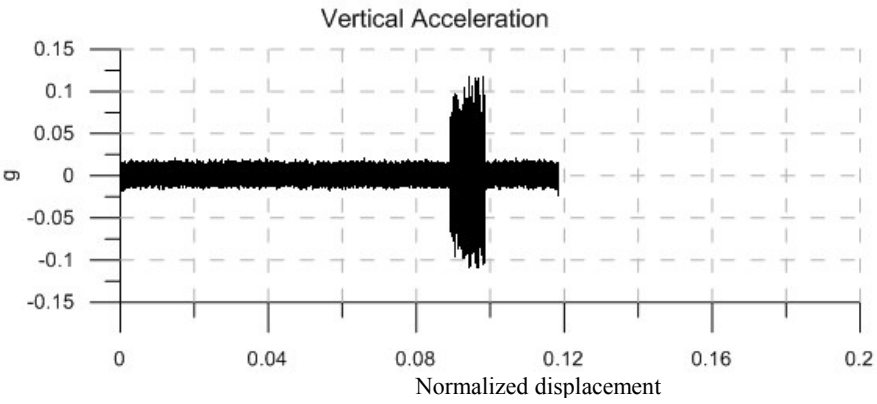

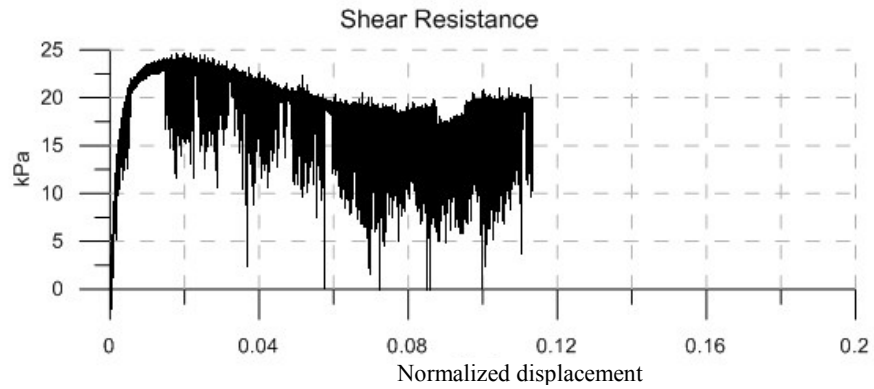

Material:	Sand
Size:	Coarse
Normal Stress:	23 kPa
Vibration Frequency:	140 Hz
Vibration Force:	3.71 N
Vibration Duration:	45 sec
Horizontal Acceleration:	0.23 g
Vertical Acceleration:	0.085 g
Horizontal Amplitude:	2.9×10^{-3} mm
Vertical Amplitude:	1.1×10^{-3} mm
Peak Strength:	24 kPa
Residual Strength:	18.5 kPa
Vibro-Residual Strength:	16 kPa

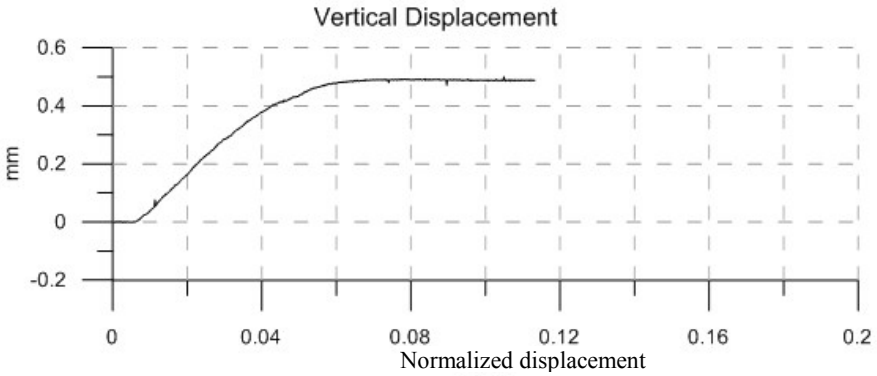

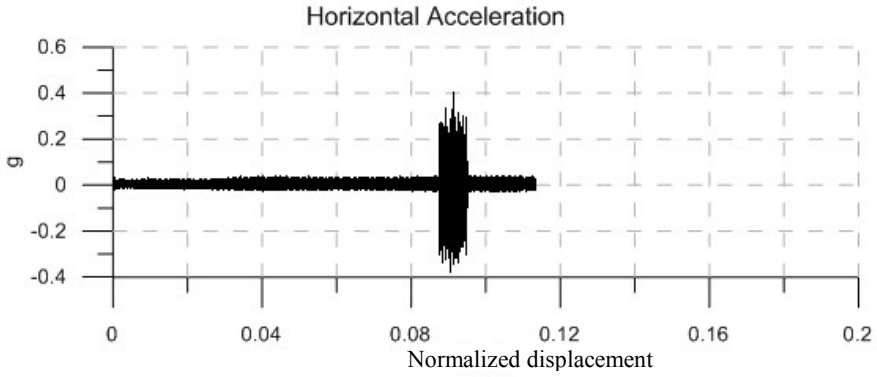

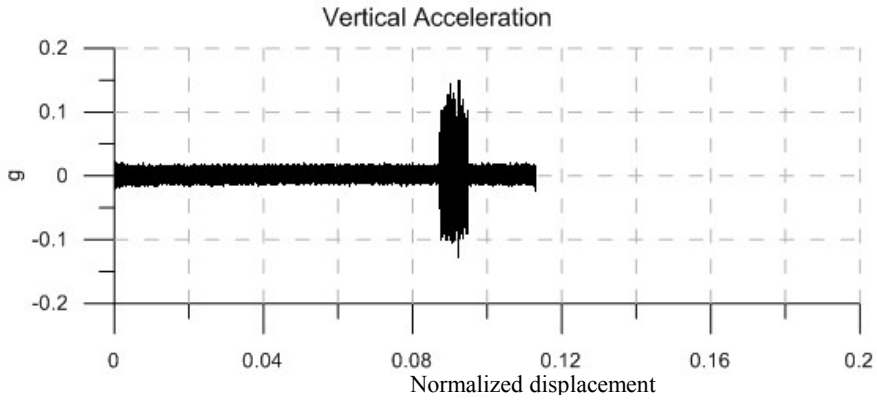

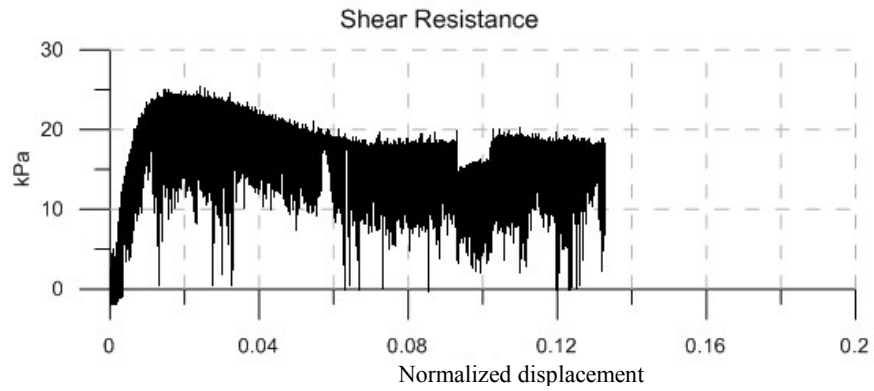

Material:	Sand
Size:	Coarse
Normal Stress:	23 kPa
Vibration Frequency:	140 Hz
Vibration Force:	5.18 N
Vibration Duration:	53 sec
Horizontal Acceleration:	0.35 g
Vertical Acceleration:	0.12 g
Horizontal Amplitude:	4.4×10^{-3} mm
Vertical Amplitude:	1.5×10^{-3} mm
Peak Strength:	24 kPa
Residual Strength:	18 kPa
Vibro-Residual Strength:	14.5 kPa

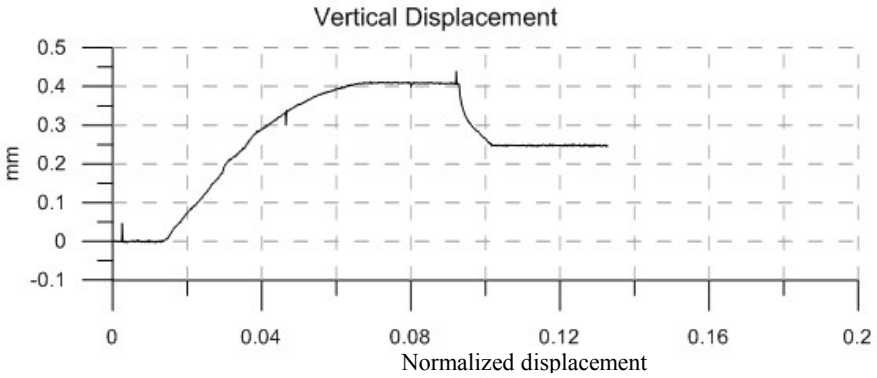

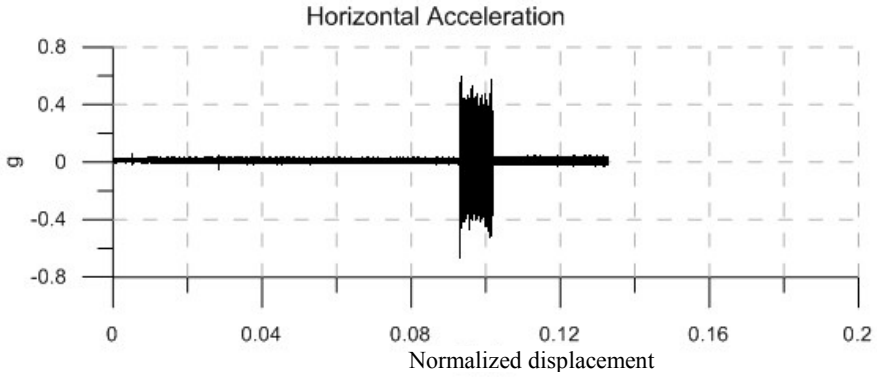

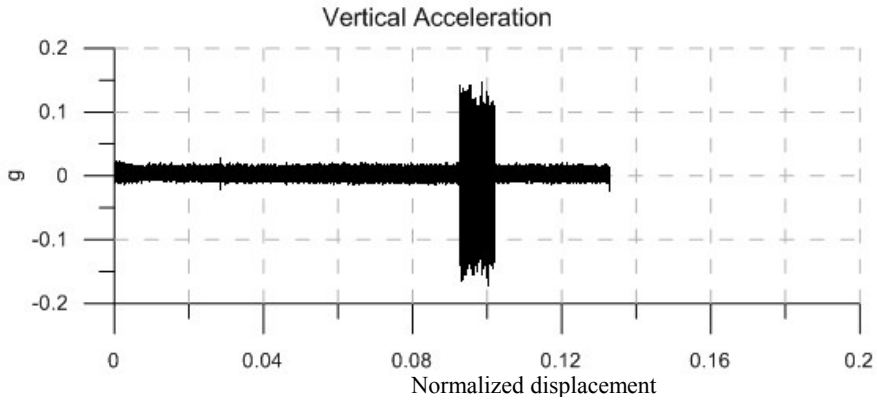

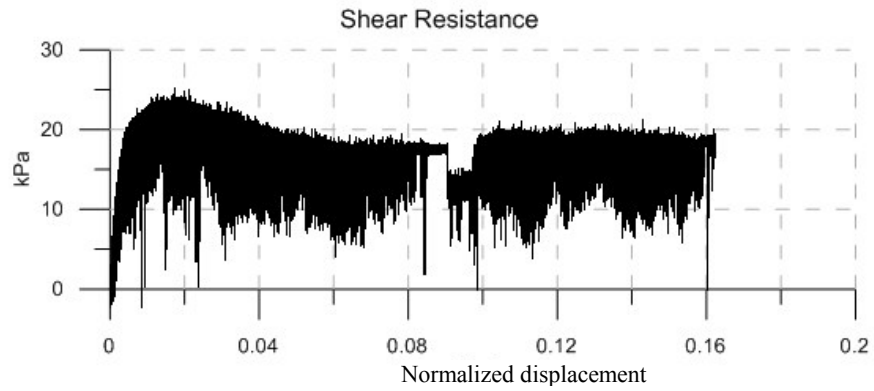

Material:	Sand
Size:	Coarse
Normal Stress:	23 kPa
Vibration Frequency:	140 Hz
Vibration Force:	7.14 N
Vibration Duration:	39 sec
Horizontal Acceleration:	0.59 g
Vertical Acceleration:	0.2 g
Horizontal Amplitude:	7.5×10^{-3} mm
Vertical Amplitude:	2.5×10^{-3} mm
Peak Strength:	23.5 kPa
Residual Strength:	18 kPa
Vibro-Residual Strength:	12 kPa

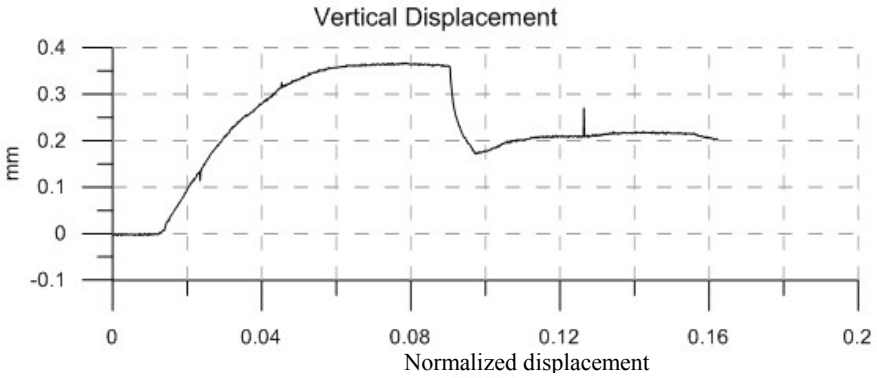

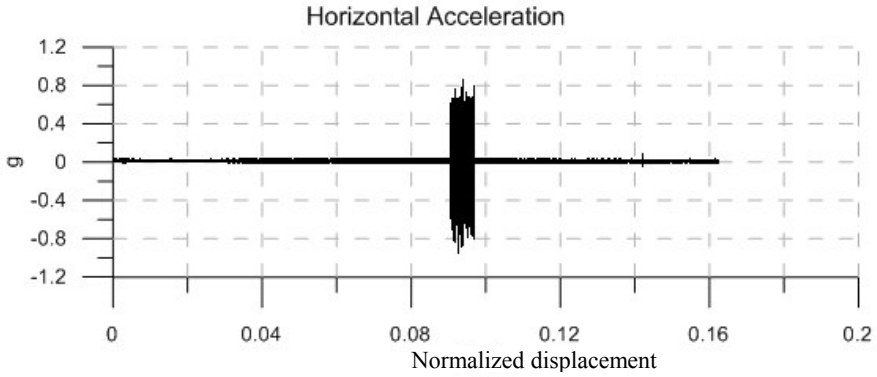

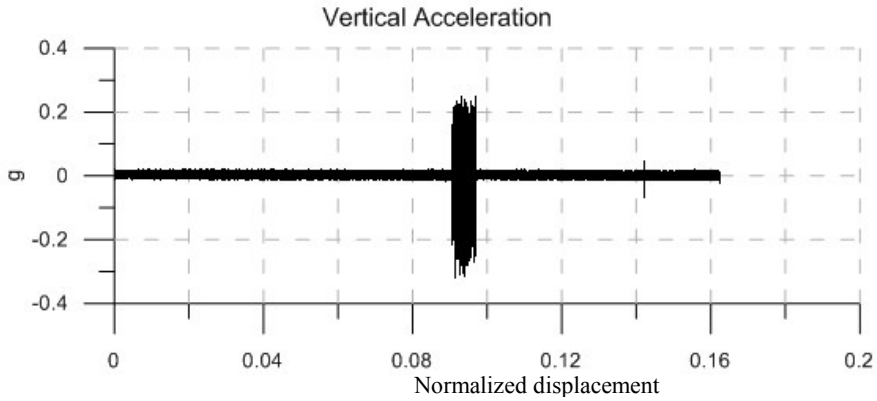

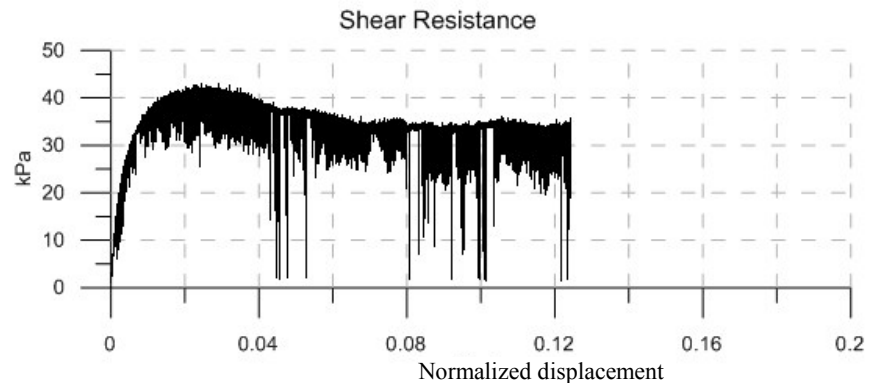

Material:	Sand
Size:	Coarse
Normal Stress:	50 kPa
Vibration Frequency:	140 Hz
Vibration Force:	1.61 N
Vibration Duration:	68 sec
Horizontal Acceleration:	0.12 g
Vertical Acceleration:	0.04 g
Horizontal Amplitude:	1.5×10^{-3} mm
Vertical Amplitude:	0.5×10^{-3} mm
Peak Strength:	42 kPa
Residual Strength:	34.5 kPa
Vibro-Residual Strength:	33 kPa

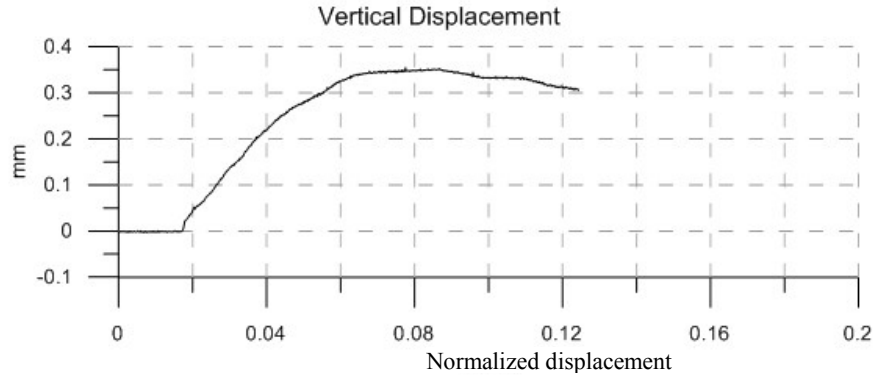

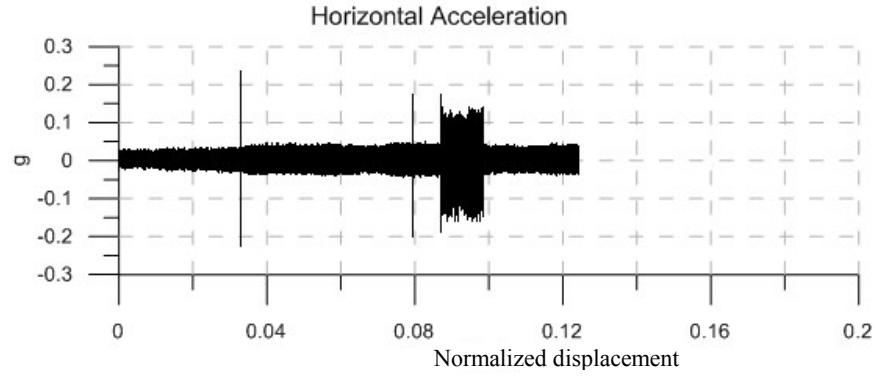

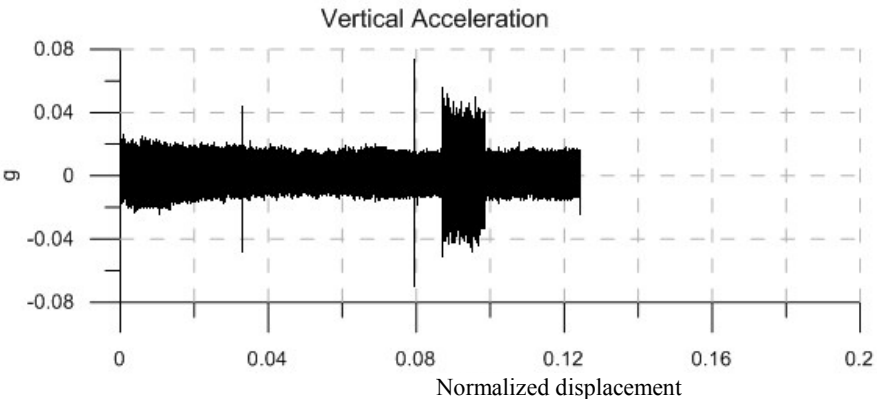

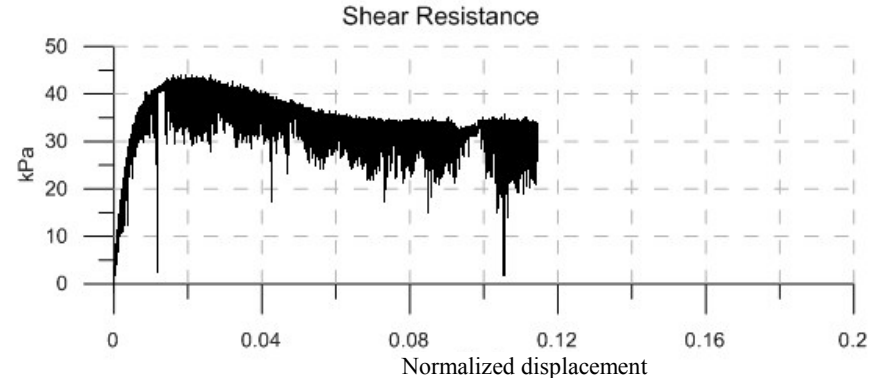

Material:	Sand
Size:	Coarse
Normal Stress:	50 kPa
Vibration Frequency:	140 Hz
Vibration Force:	3.22 N
Vibration Duration:	37 sec
Horizontal Acceleration:	0.2 g
Vertical Acceleration:	0.065 g
Horizontal Amplitude:	2.5×10^{-3} mm
Vertical Amplitude:	0.8×10^{-3} mm
Peak Strength:	43 kPa
Residual Strength:	34 kPa
Vibro-Residual Strength:	31.5 kPa

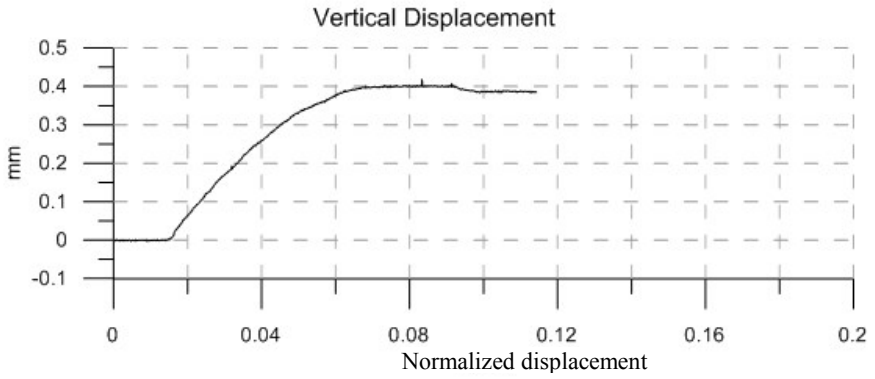

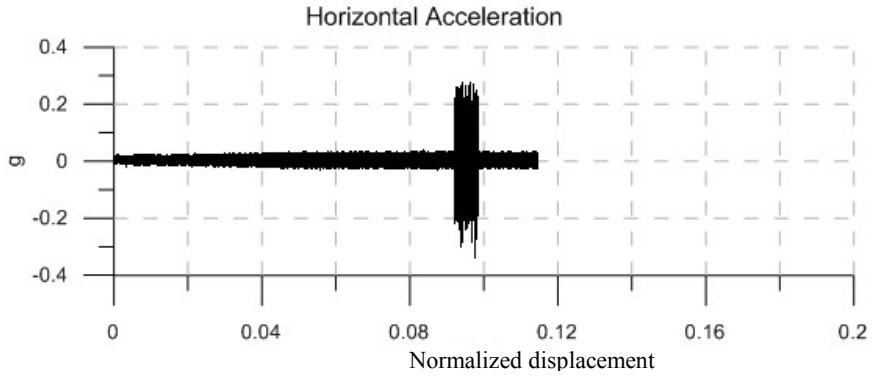

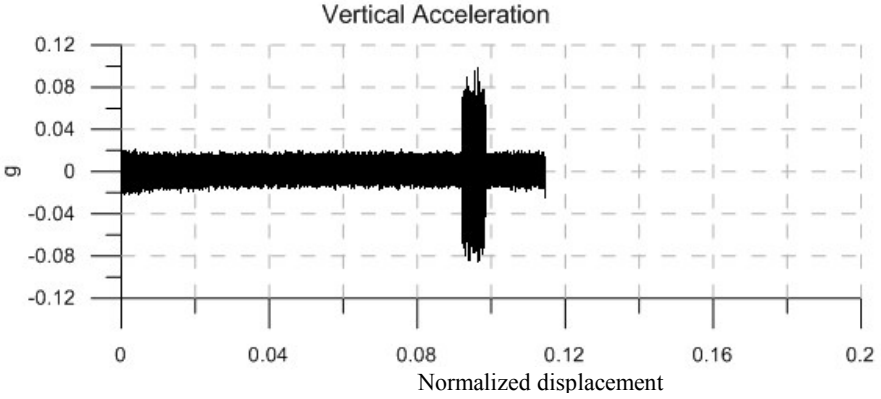

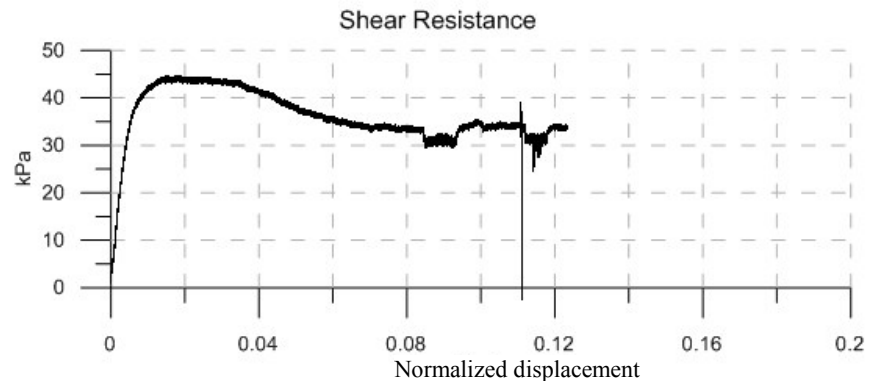

Material:	Sand
Size:	Coarse
Normal Stress:	50 kPa
Vibration Frequency:	140 Hz
Vibration Force:	3.71 N
Vibration Duration:	51 sec
Horizontal Acceleration:	0.22 g
Vertical Acceleration:	0.075 g
Horizontal Amplitude:	2.8×10^{-3} mm
Vertical Amplitude:	1.0×10^{-3} mm
Peak Strength:	44.5 kPa
Residual Strength:	33.5 kPa
Vibro-Residual Strength:	30.5 kPa

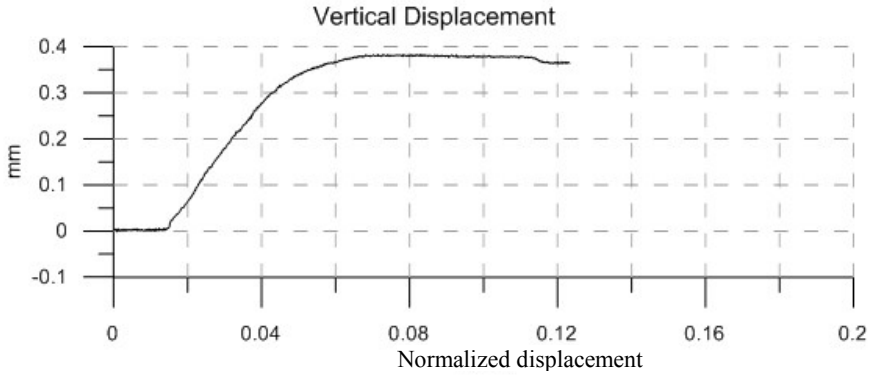

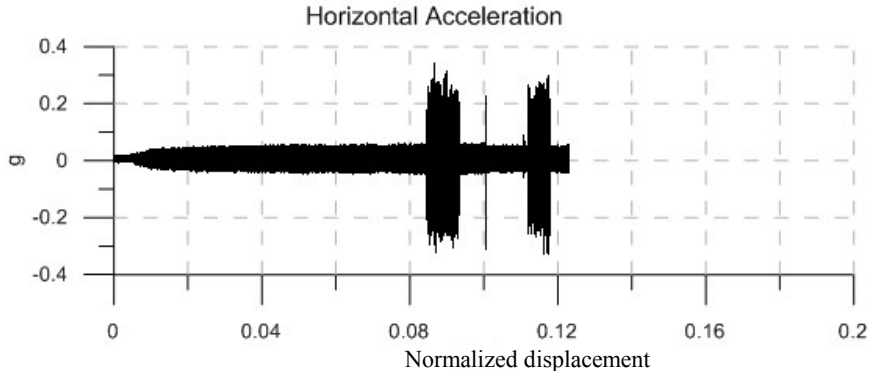

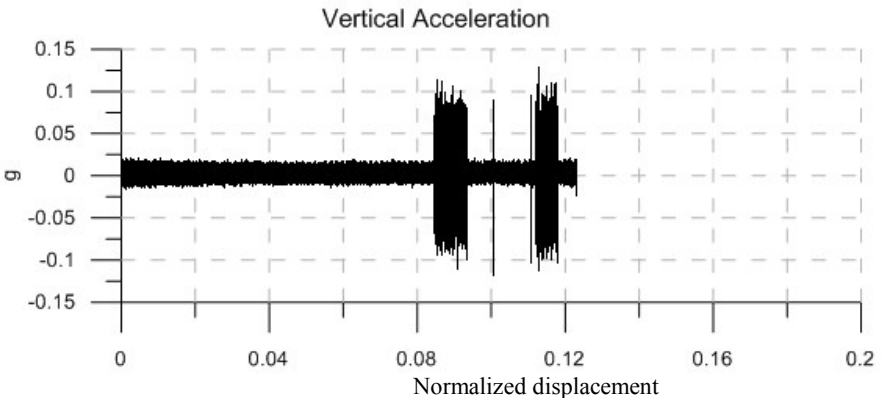

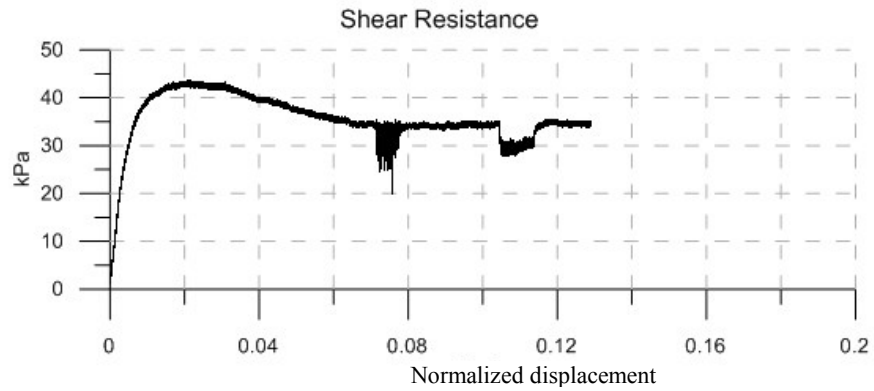

Material:	Sand
Size:	Coarse
Normal Stress:	50 kPa
Vibration Frequency:	140 Hz
Vibration Force:	5.18 N
Vibration Duration:	54 sec
Horizontal Acceleration:	0.33 g
Vertical Acceleration:	0.09 g
Horizontal Amplitude:	4.4×10^{-3} mm
Vertical Amplitude:	1.5×10^{-3} mm
Peak Strength:	43 kPa
Residual Strength:	34.5 kPa
Vibro-Residual Strength:	29.5 kPa

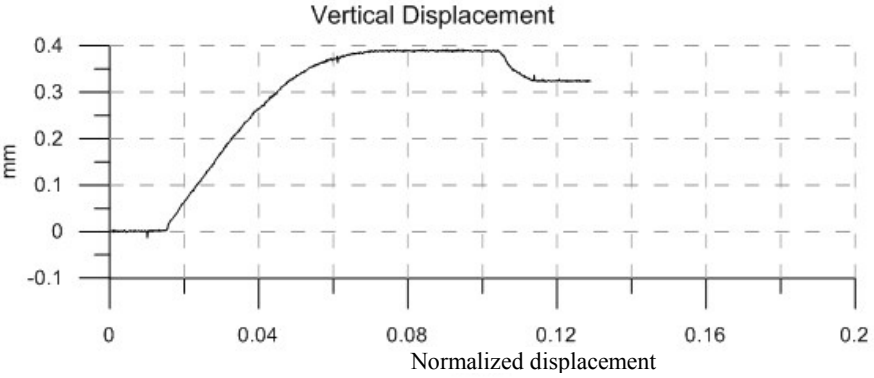

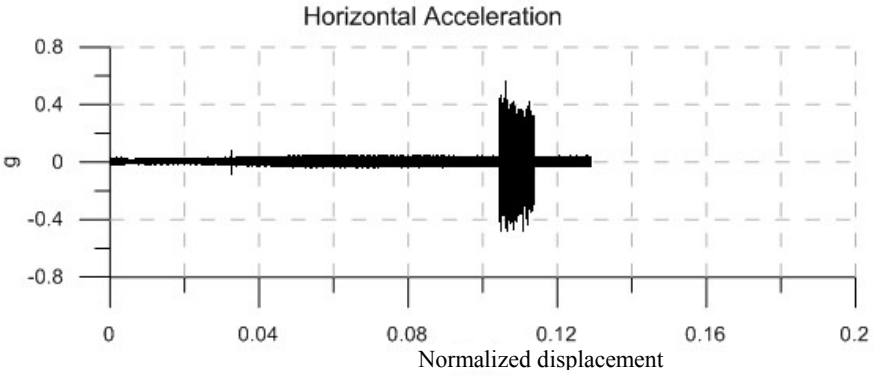

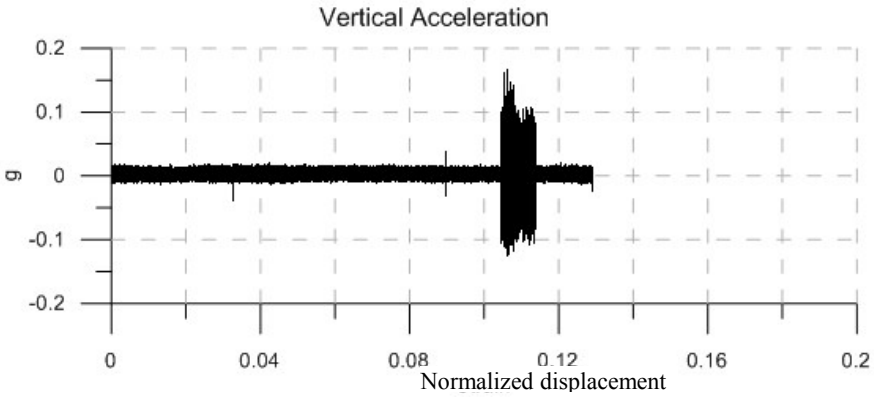

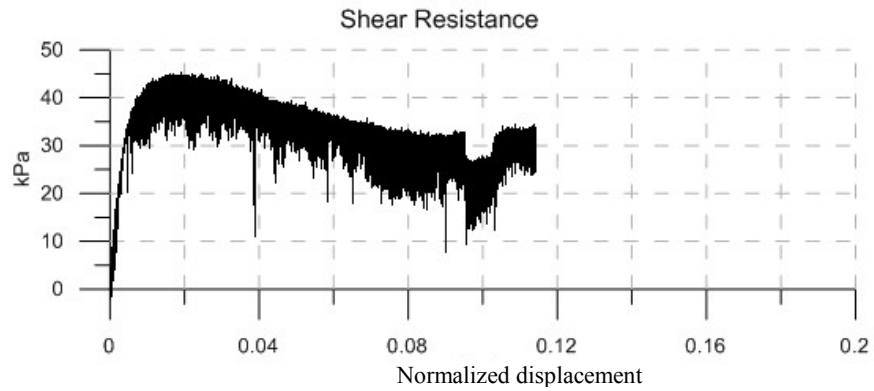

Material:	Sand
Size:	Coarse
Normal Stress:	50 kPa
Vibration Frequency:	140 Hz
Vibration Force:	7.14 N
Vibration Duration:	43 sec
Horizontal Acceleration:	0.4 g
Vertical Acceleration:	0.145 g
Horizontal Amplitude:	5.1×10^{-3} mm
Vertical Amplitude:	1.8×10^{-3} mm
Peak Strength:	44.5 kPa
Residual Strength:	32 kPa
Vibro-Residual Strength:	25.5 kPa

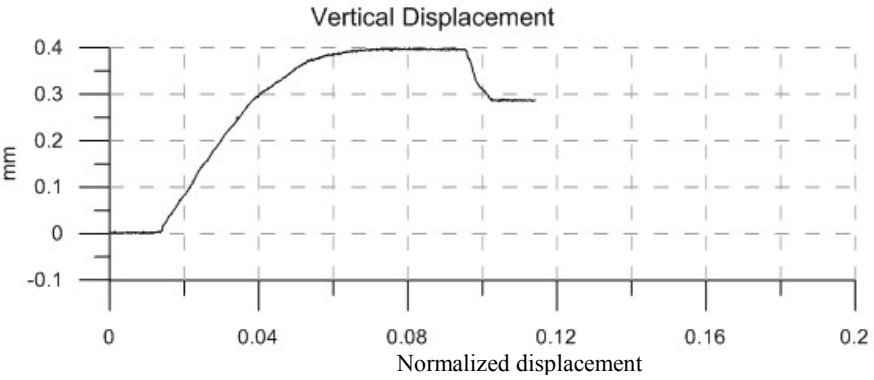

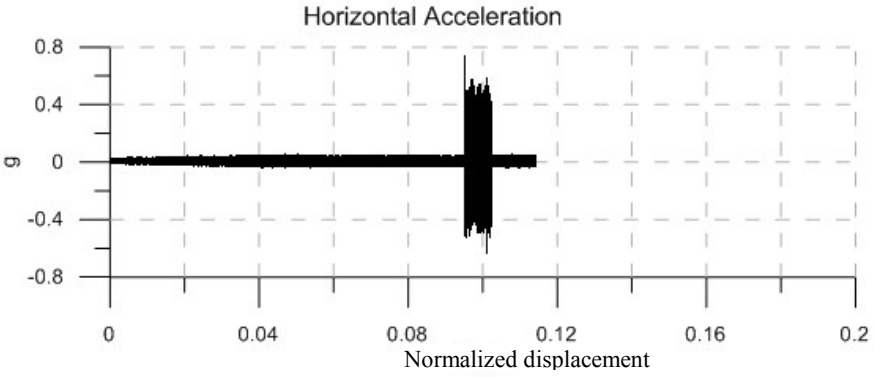

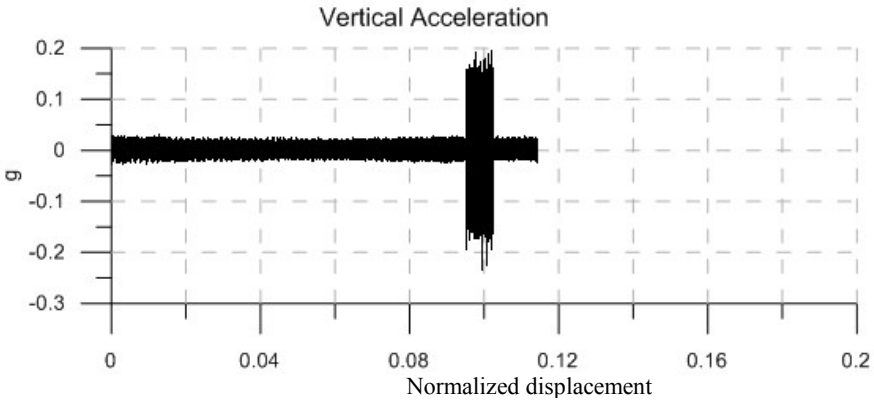

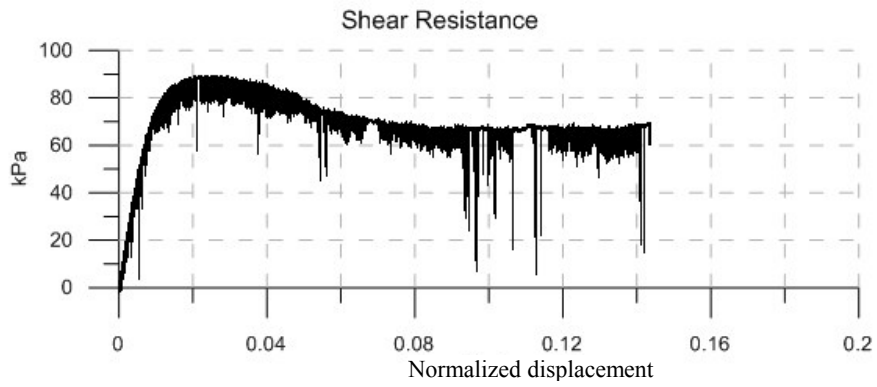

Material:	Sand
Size:	Coarse
Normal Stress:	118 kPa
Vibration Frequency:	140 Hz
Vibration Force:	1.61 N
Vibration Duration:	53 sec
Horizontal Acceleration:	0.1 g
Vertical Acceleration:	0.045 g
Horizontal Amplitude:	1.3×10^{-3} mm
Vertical Amplitude:	0.6×10^{-3} mm
Peak Strength:	88.5 kPa
Residual Strength:	67.5 kPa
Vibro-Residual Strength:	66 kPa

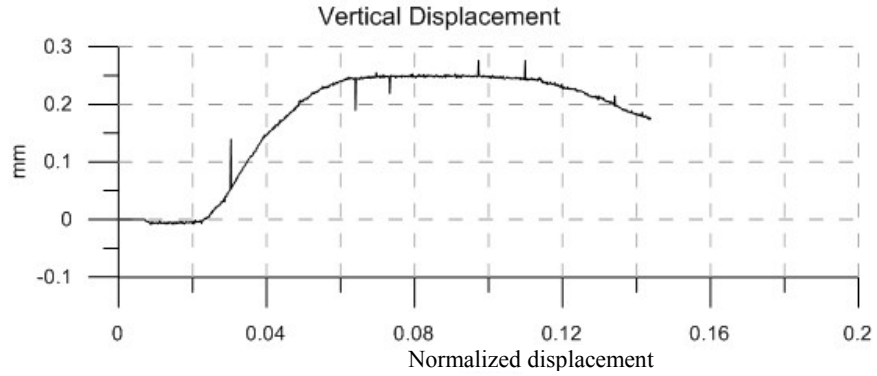

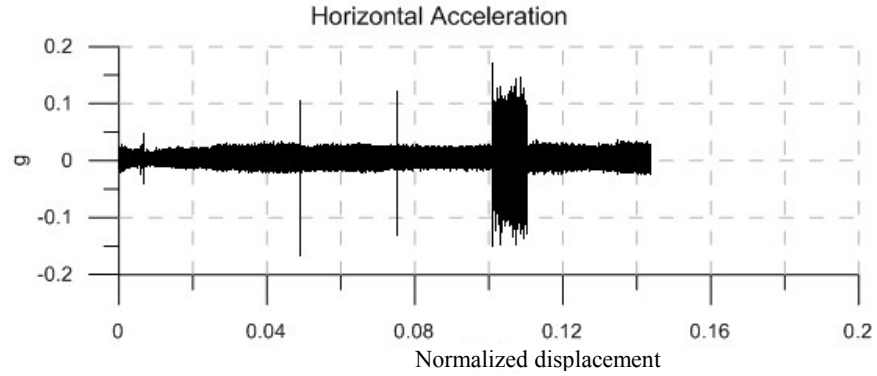

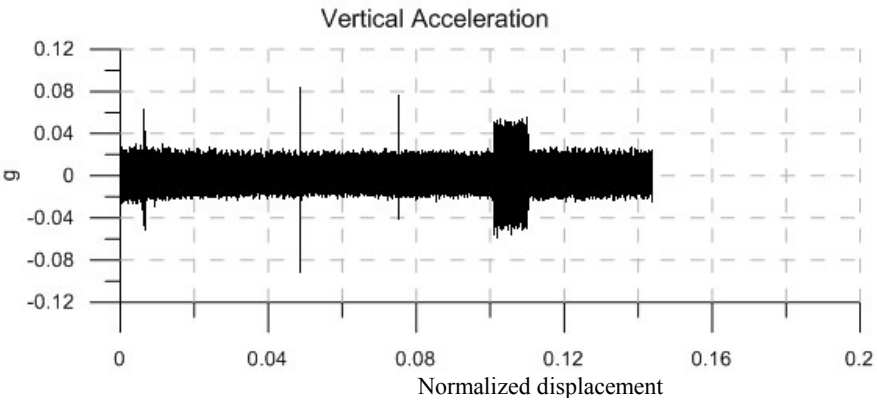

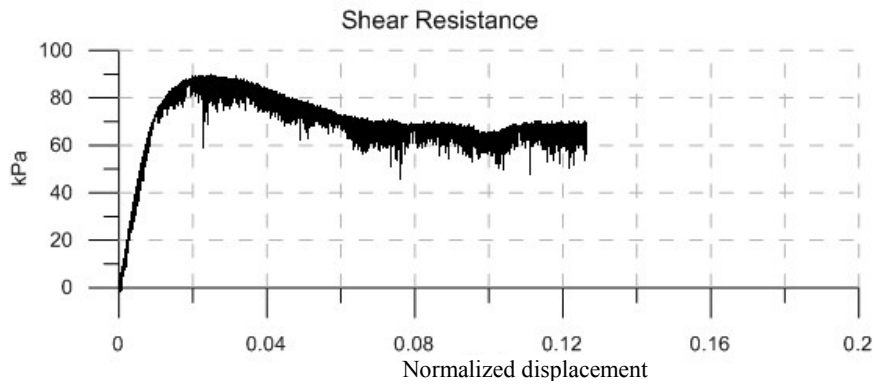

Material:	Sand
Size:	Coarse
Normal Stress:	118 kPa
Vibration Frequency:	140 Hz
Vibration Force:	3.22 N
Vibration Duration:	42 sec
Horizontal Acceleration:	0.19 g
Vertical Acceleration:	0.07 g
Horizontal Amplitude:	2.4×10^{-3} mm
Vertical Amplitude:	0.9×10^{-3} mm
Peak Strength:	89 kPa
Residual Strength:	67.5 kPa
Vibro-Residual Strength:	64.5 kPa

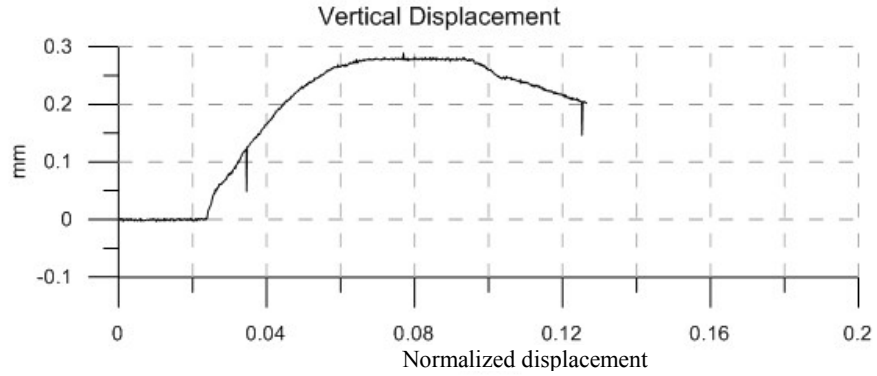

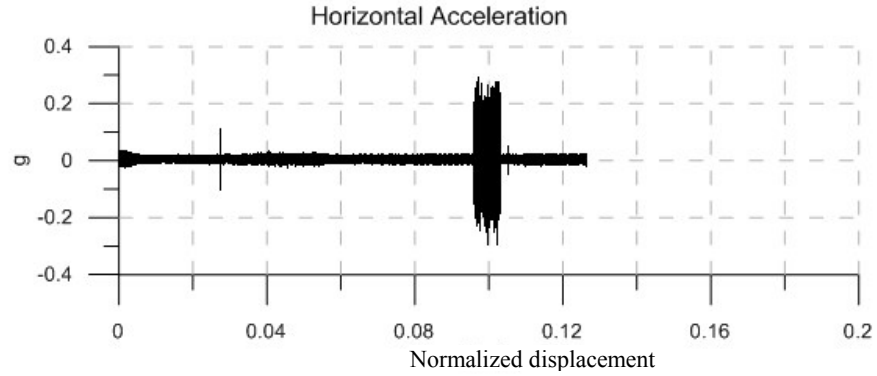

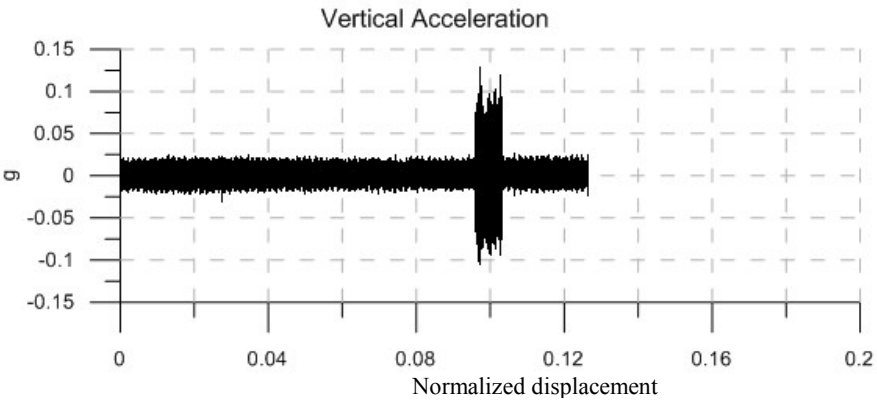

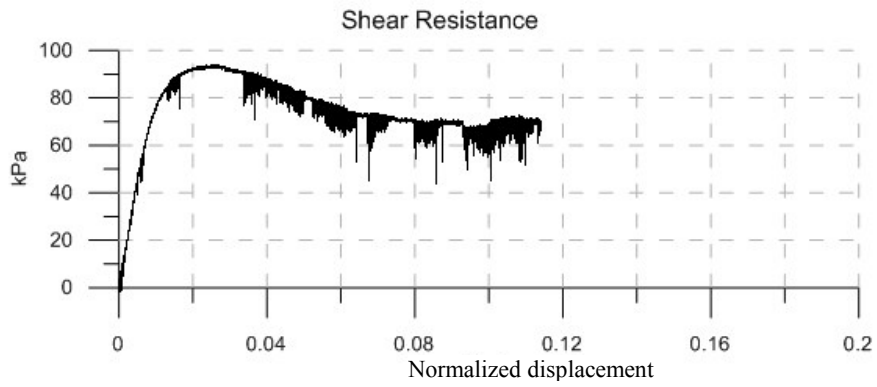

Material:	Sand
Size:	Coarse
Normal Stress:	118 kPa
Vibration Frequency:	140 Hz
Vibration Force:	3.71 N
Vibration Duration:	41 sec
Horizontal Acceleration:	0.21 g
Vertical Acceleration:	0.075 g
Horizontal Amplitude:	2.7×10^{-3} mm
Vertical Amplitude:	1.0×10^{-3} mm
Peak Strength:	93.5 kPa
Residual Strength:	70.5 kPa
Vibro-Residual Strength:	66.5 kPa

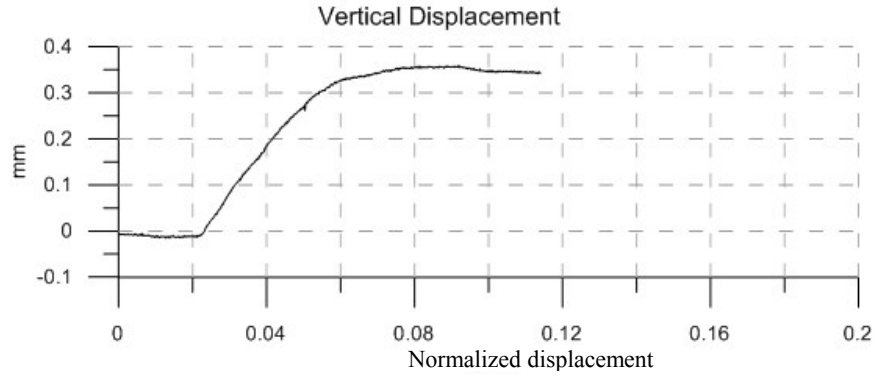

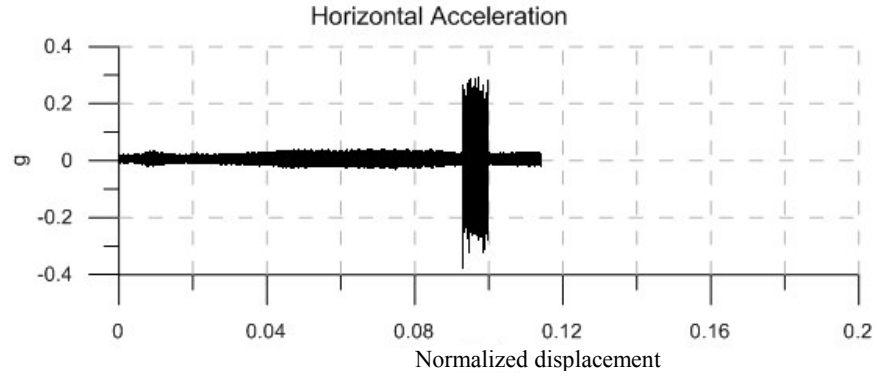

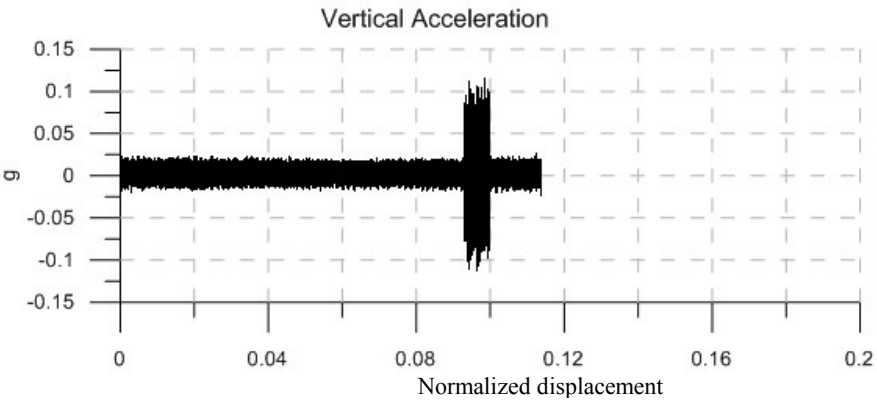

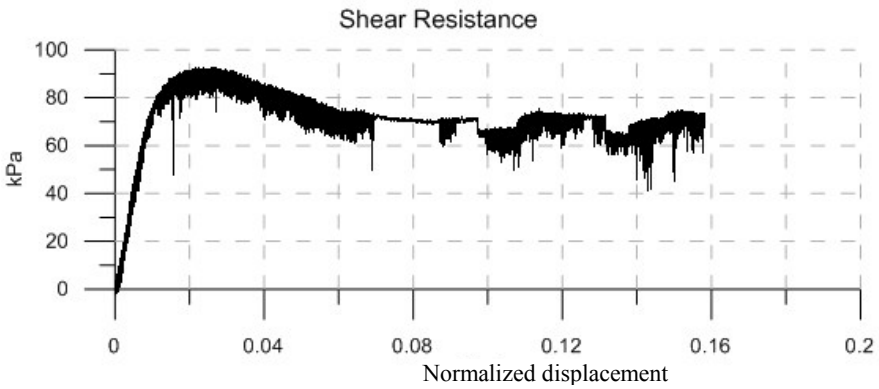

Material:	Sand
Size:	Coarse
Normal Stress:	118 kPa
Vibration Frequency:	140 Hz
Vibration Force:	5.18 N
Vibration Duration:	61 sec
Horizontal Acceleration:	0.28 g
Vertical Acceleration:	0.1 g
Horizontal Amplitude:	3.5×10^{-3} mm
Vertical Amplitude:	1.3×10^{-3} mm
Peak Strength:	91.5 kPa
Residual Strength:	71 kPa
Vibro-Residual Strength:	65.5 kPa

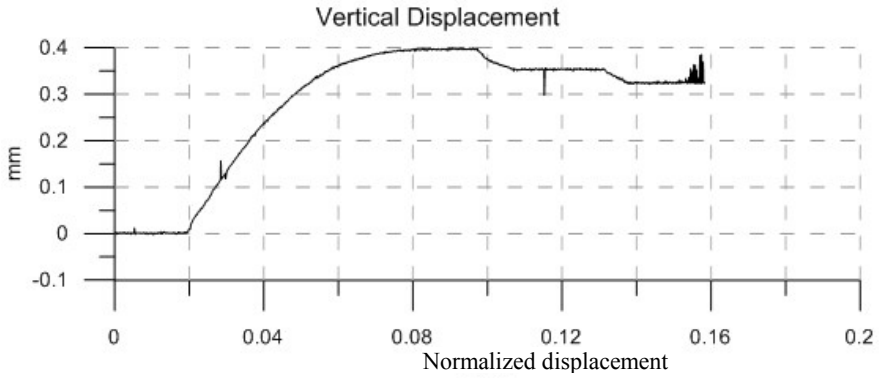

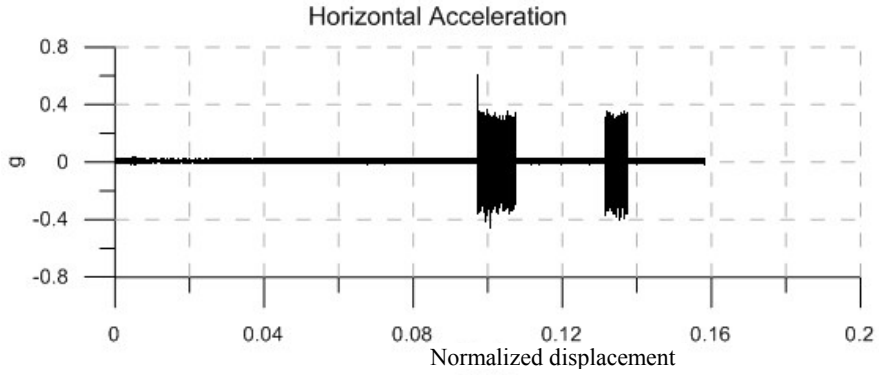

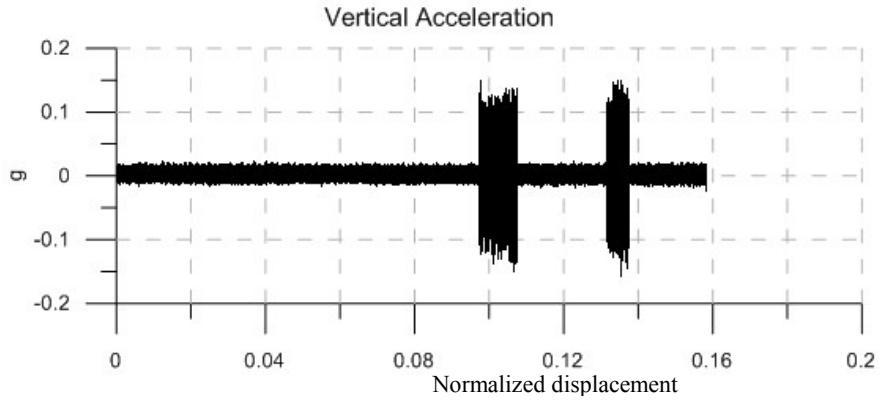

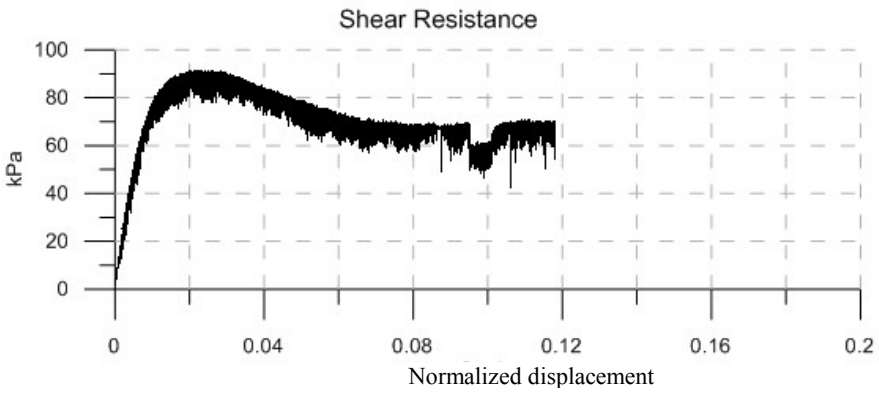

Material:	Sand
Size:	Coarse
Normal Stress:	118 kPa
Vibration Frequency:	140 Hz
Vibration Force:	7.14 N
Vibration Duration:	35 sec
Horizontal Acceleration:	0.39 g
Vertical Acceleration:	0.135 g
Horizontal Amplitude:	4.9×10^{-3} mm
Vertical Amplitude:	1.7×10^{-3} mm
Peak Strength:	91 kPa
Residual Strength:	68.5 kPa
Vibro-Residual Strength:	59 kPa

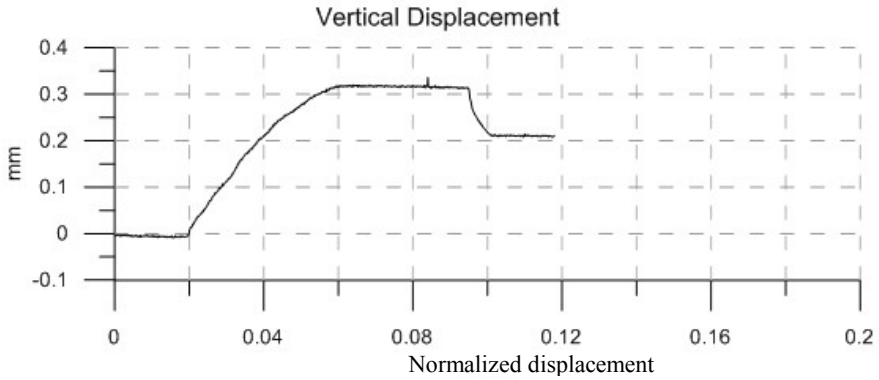

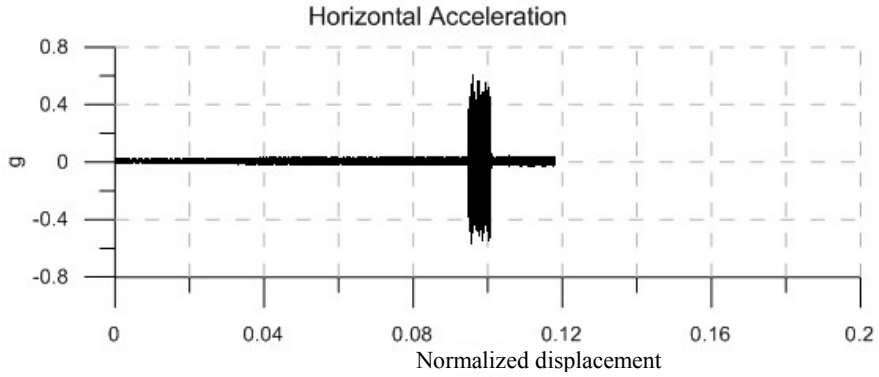

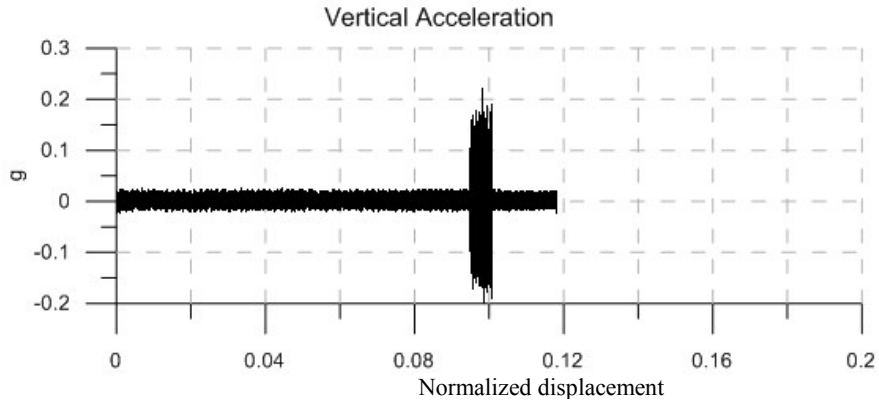

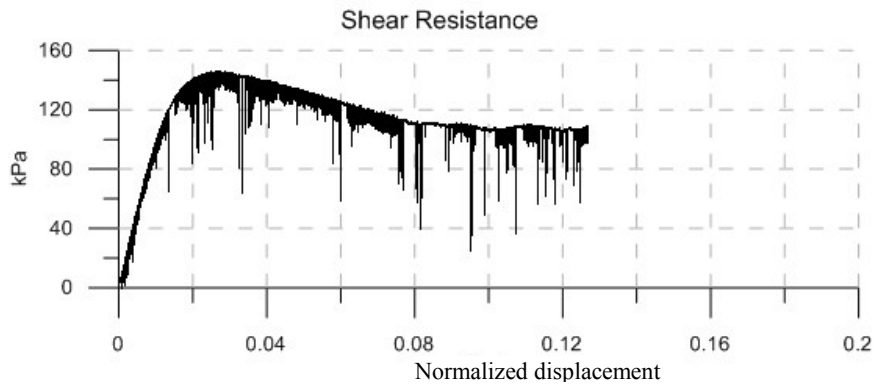

Material:	Sand
Size:	Coarse
Normal Stress:	200 kPa
Vibration Frequency:	140 Hz
Vibration Force:	1.61 N
Vibration Duration:	36 sec
Horizontal Acceleration:	0.1 g
Vertical Acceleration:	0.04 g
Horizontal Amplitude:	1.3×10^{-3} mm
Vertical Amplitude:	0.5×10^{-3} mm
Peak Strength:	145 kPa
Residual Strength:	108.5 kPa
Vibro-Residual Strength:	106.5 kPa

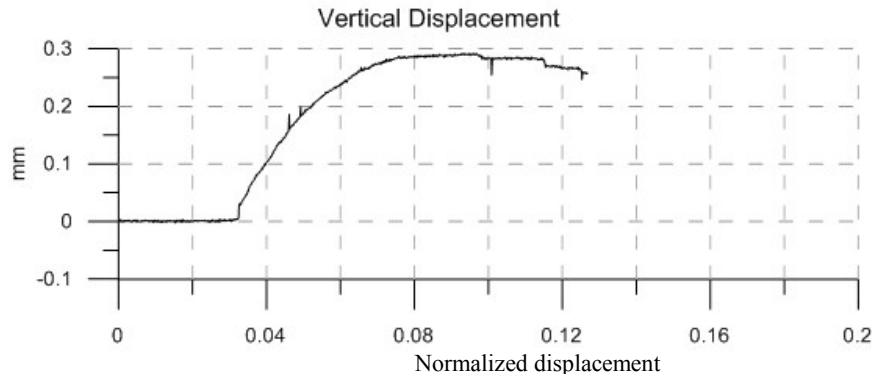

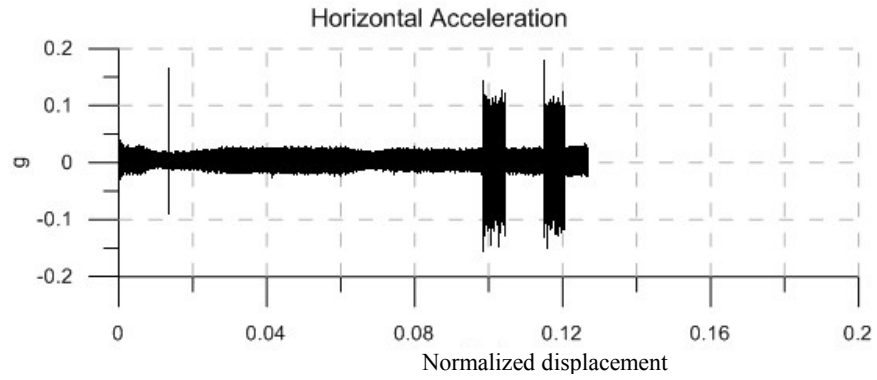

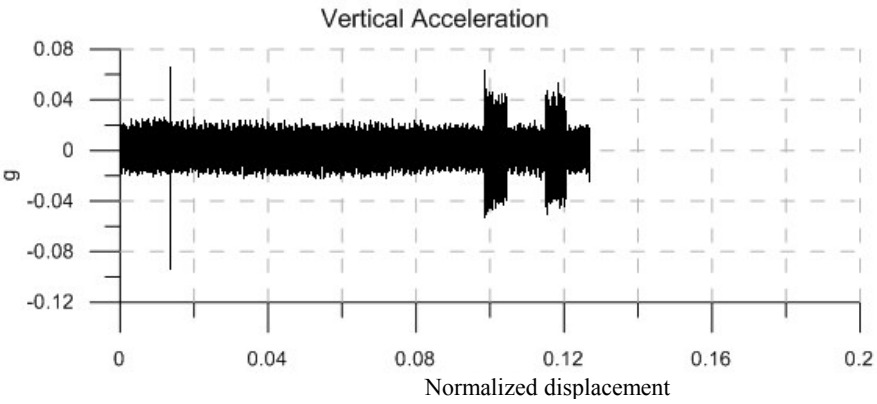

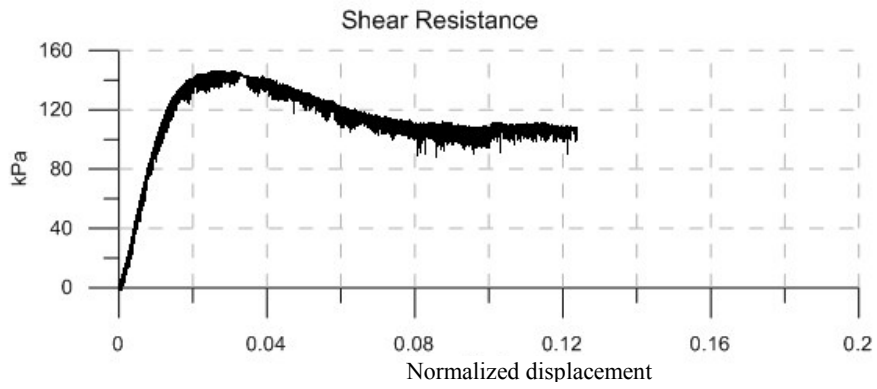

Material:	Sand
Size:	Coarse
Normal Stress:	200 kPa
Vibration Frequency:	140 Hz
Vibration Force:	3.22 N
Vibration Duration:	62 sec
Horizontal Acceleration:	0.18 g
Vertical Acceleration:	0.07 g
Horizontal Amplitude:	2.3×10^{-3} mm
Vertical Amplitude:	0.9×10^{-3} mm
Peak Strength:	145.5 kPa
Residual Strength:	111 kPa
Vibro-Residual Strength:	107 kPa

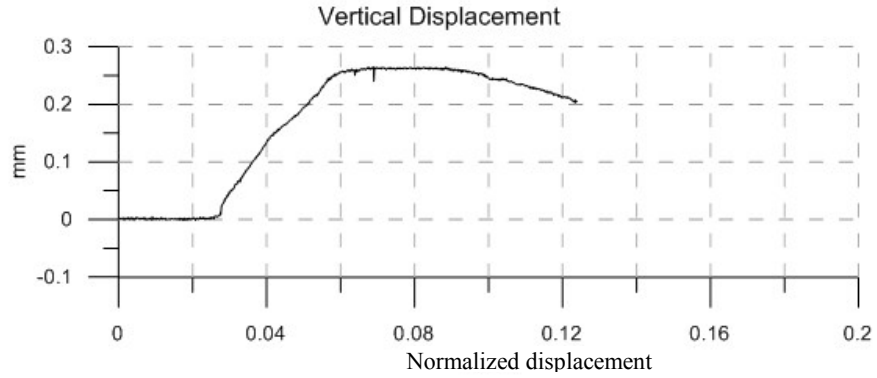

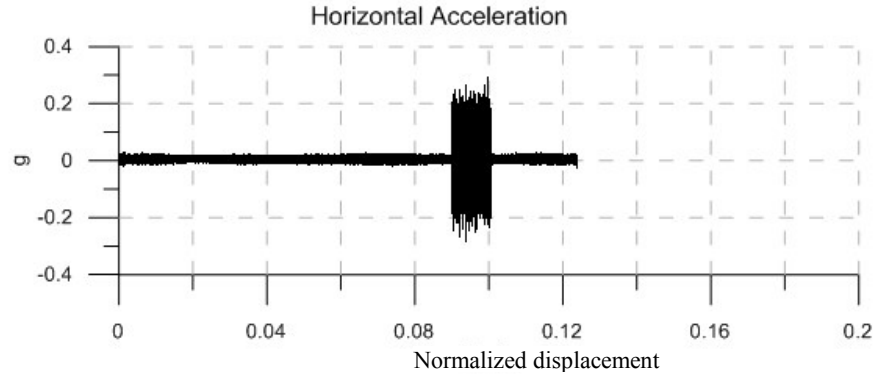

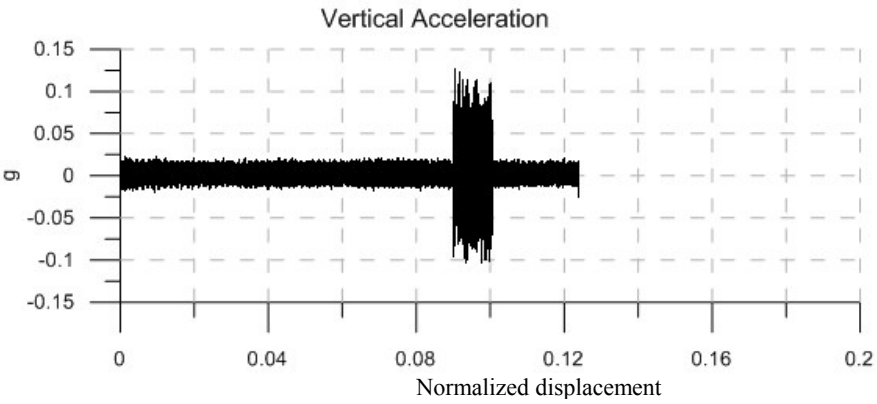

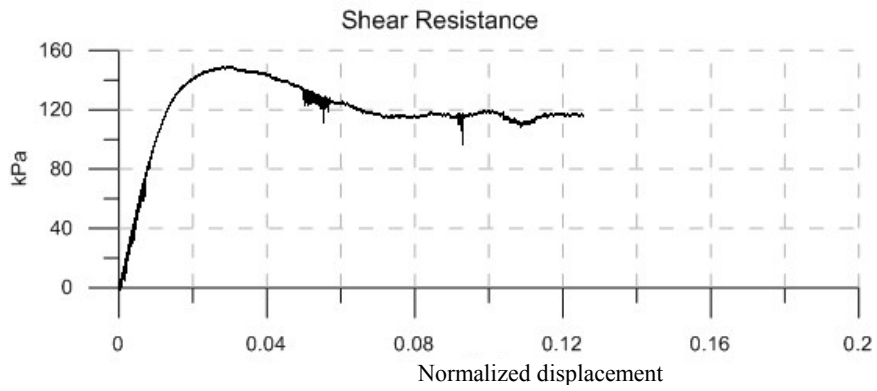

Material:	Sand
Size:	Coarse
Normal Stress:	200 kPa
Vibration Frequency:	140 Hz
Vibration Force:	3.71 N
Vibration Duration:	50 sec
Horizontal Acceleration:	0.2 g
Vertical Acceleration:	0.075 g
Horizontal Amplitude:	2.5×10^{-3} mm
Vertical Amplitude:	1.0×10^{-3} mm
Peak Strength:	148.5 kPa
Residual Strength:	116 kPa
Vibro-Residual Strength:	111 kPa

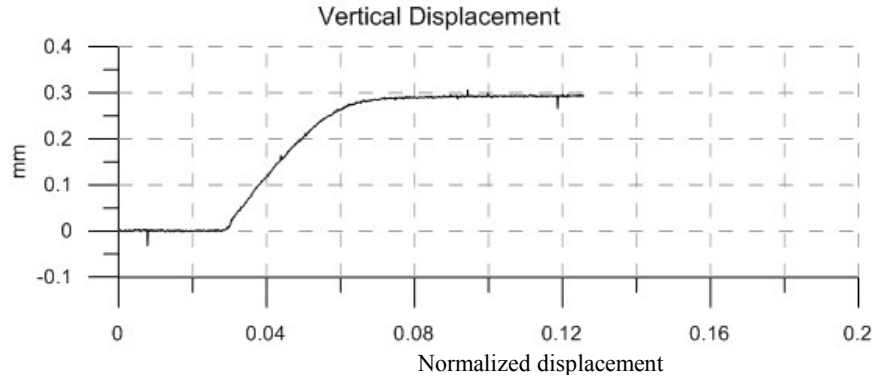

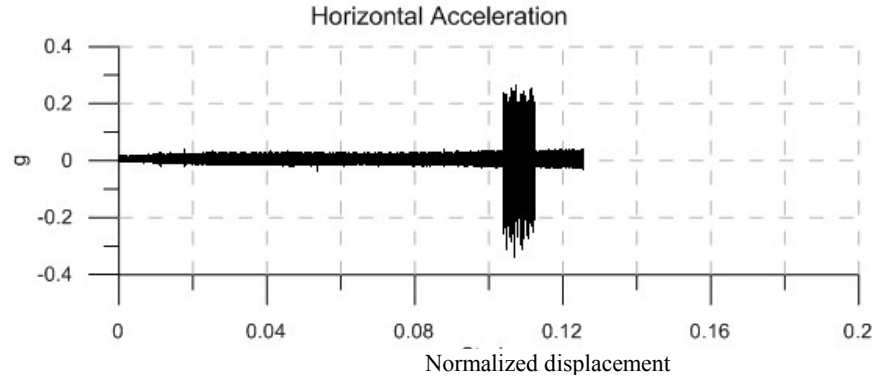

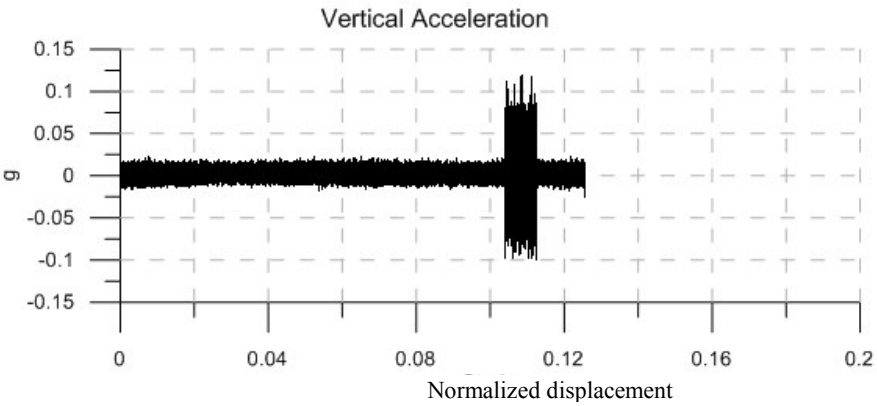

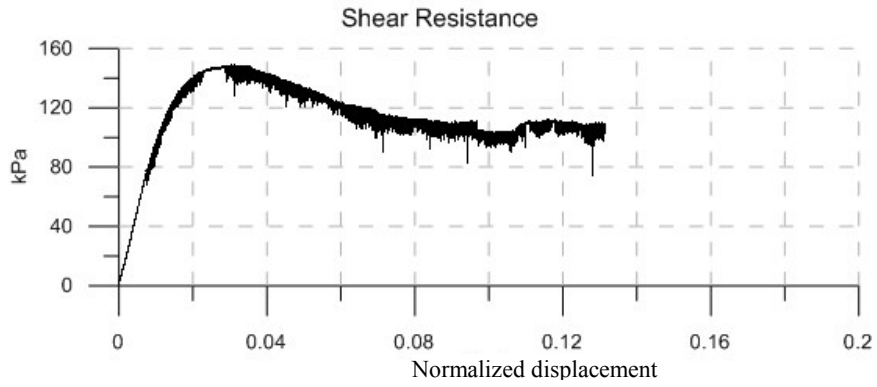

Material:	Sand
Size:	Coarse
Normal Stress:	200 kPa
Vibration Frequency:	140 Hz
Vibration Force:	5.18 N
Vibration Duration:	62 sec
Horizontal Acceleration:	0.28 g
Vertical Acceleration:	0.075 g
Horizontal Amplitude:	3.5×10^{-3} mm
Vertical Amplitude:	1.0×10^{-3} mm
Peak Strength:	148 kPa
Residual Strength:	110 kPa
Vibro-Residual Strength:	102 kPa

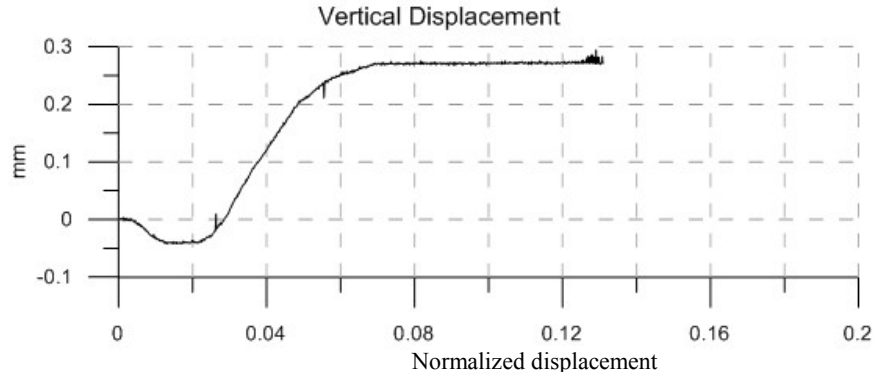

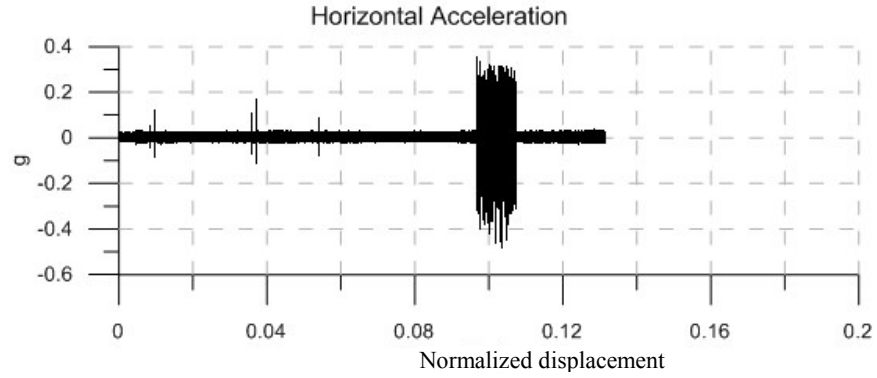

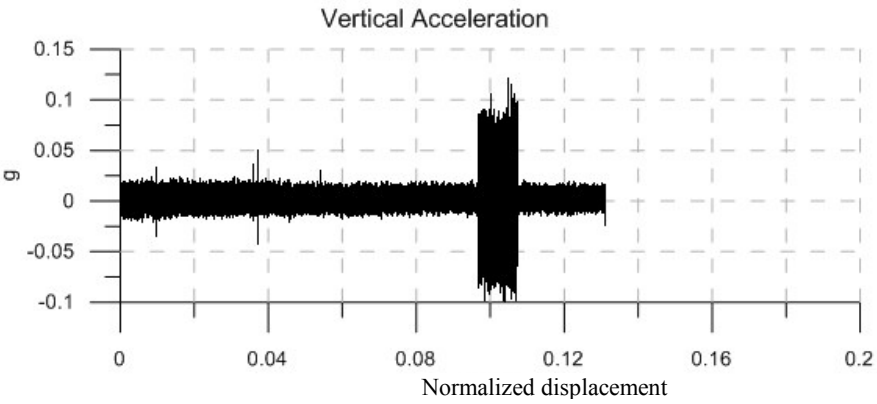

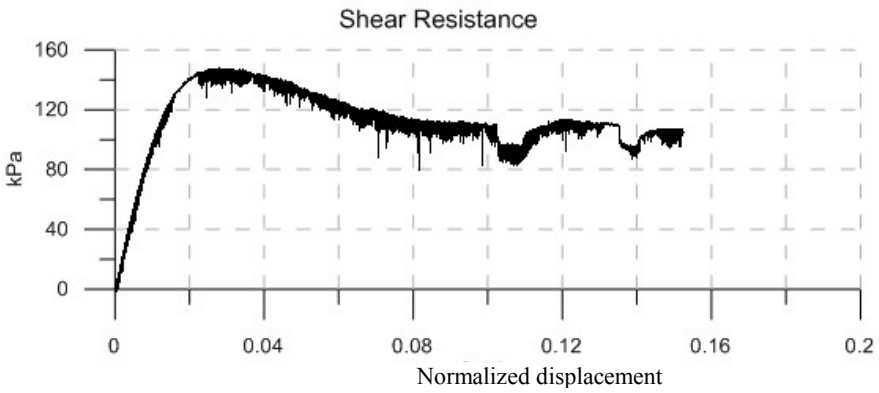

Material:	Sand
Size:	Coarse
Normal Stress:	200 kPa
Vibration Frequency:	140 Hz
Vibration Force:	7.14 N
Vibration Duration:	40 sec
Horizontal Acceleration:	0.39 g
Vertical Acceleration:	0.1 g
Horizontal Amplitude:	4.9×10^{-3} mm
Vertical Amplitude:	1.3×10^{-3} mm
Peak Strength:	147 kPa
Residual Strength:	109 kPa
Vibro-Residual Strength:	95 kPa

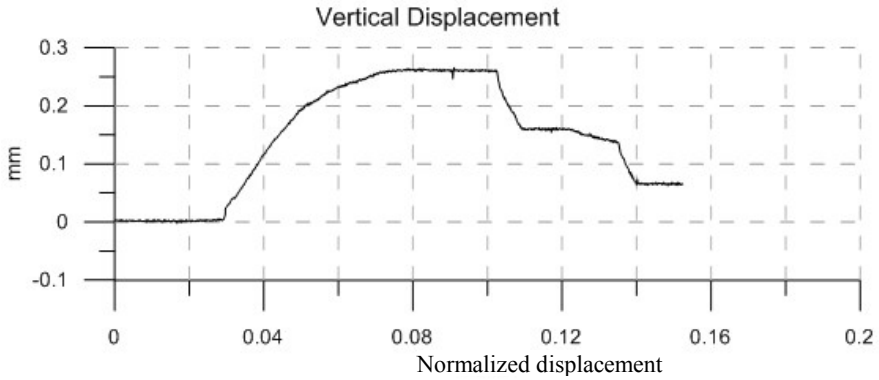

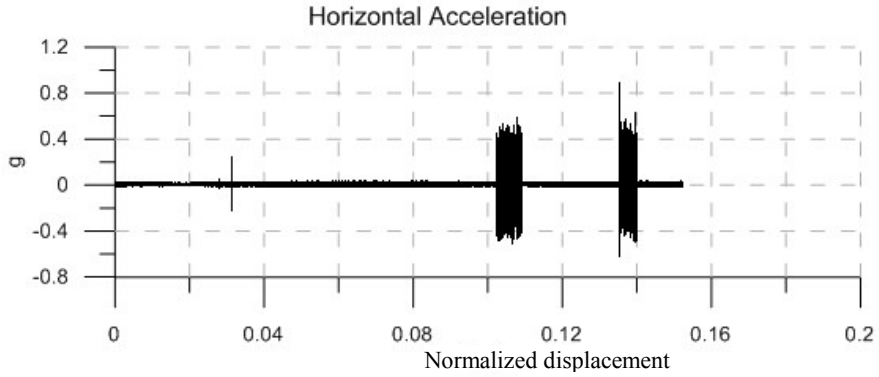

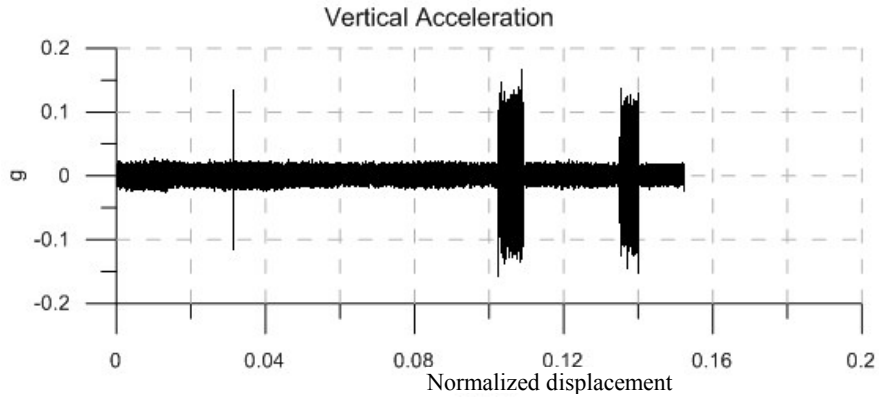

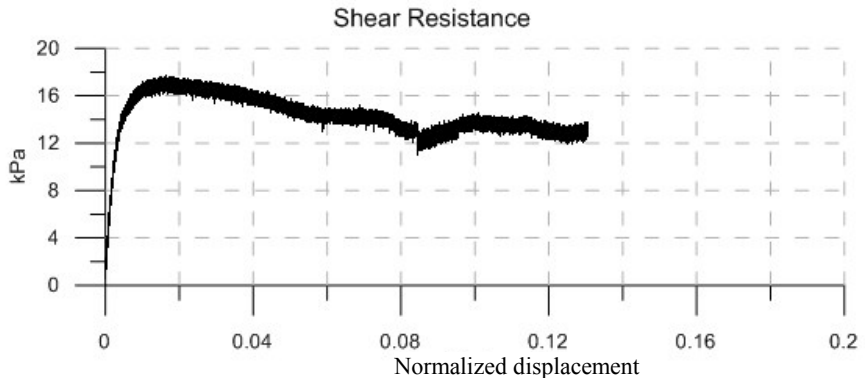

Material:	Glass Beads
Size:	0.55 mm
Normal Stress:	23 kPa
Vibration Frequency:	140 Hz
Vibration Force:	1.61 N
Vibration Duration:	64 sec
Horizontal Acceleration:	0.11 g
Vertical Acceleration:	0.04 g
Horizontal Amplitude:	1.4×10^{-3} mm
Vertical Amplitude:	0.5×10^{-3} mm
Peak Strength:	17.5 kPa
Residual Strength:	13.5 kPa
Vibro-Residual Strength:	12.5 kPa

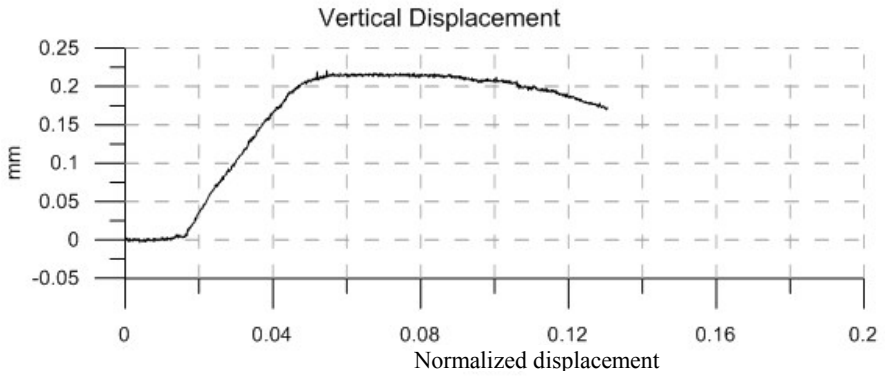

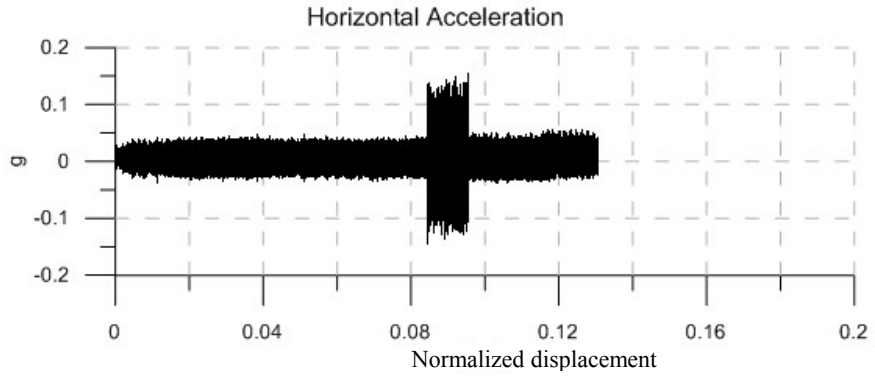

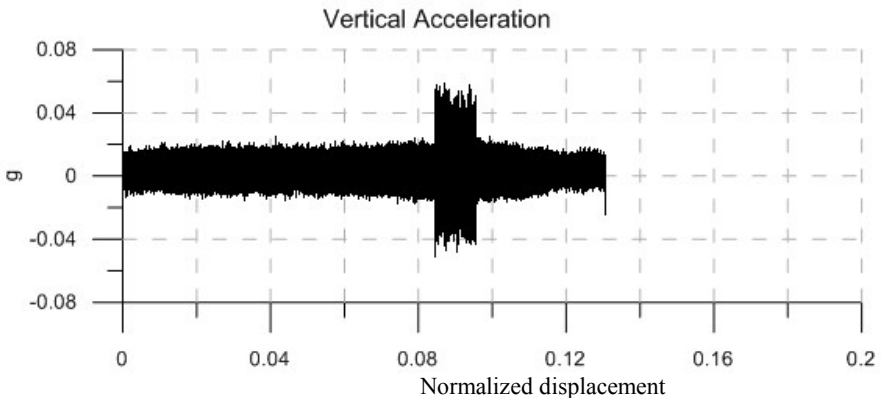

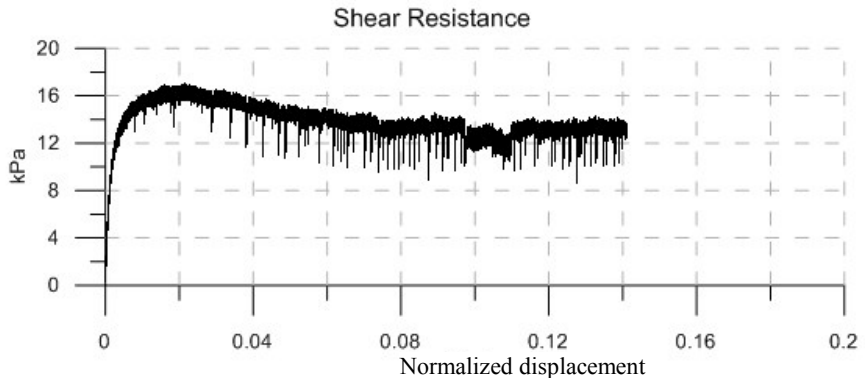

Material:	Glass Beads
Size:	0.55 mm
Normal Stress:	23 kPa
Vibration Frequency:	140 Hz
Vibration Force:	3.22 N
Vibration Duration:	74 sec
Horizontal Acceleration:	0.175 g
Vertical Acceleration:	0.07 g
Horizontal Amplitude:	2.2×10^{-3} mm
Vertical Amplitude:	0.9×10^{-3} mm
Peak Strength:	17 kPa
Residual Strength:	14 kPa
Vibro-Residual Strength:	12.5 kPa

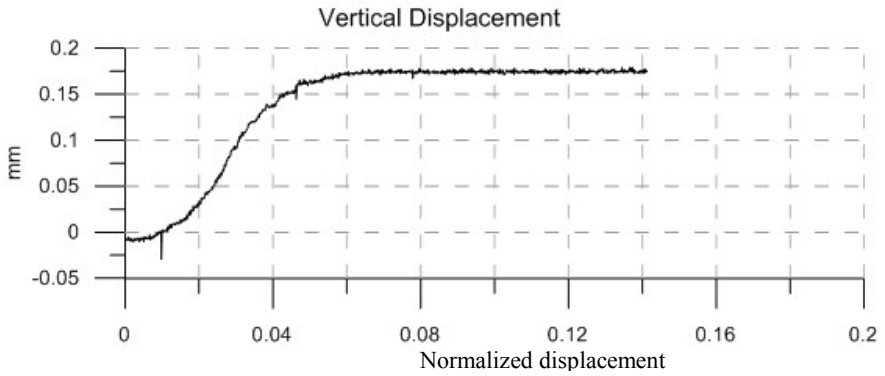

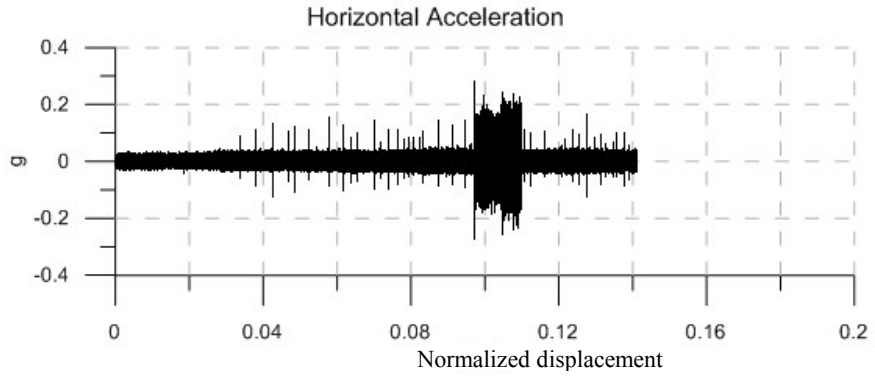

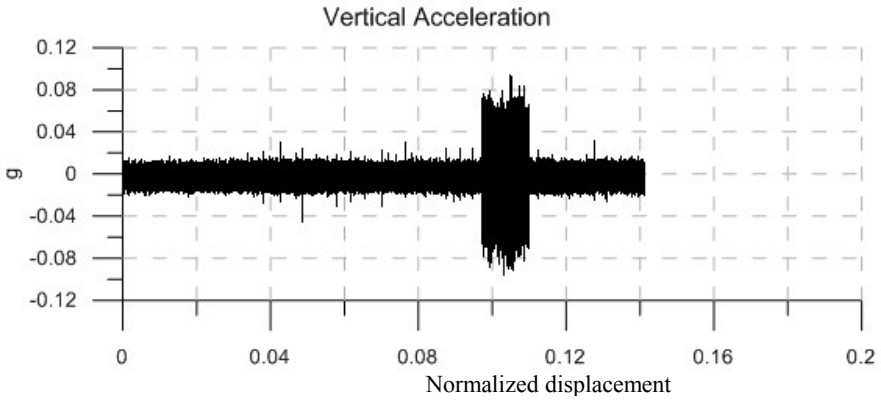

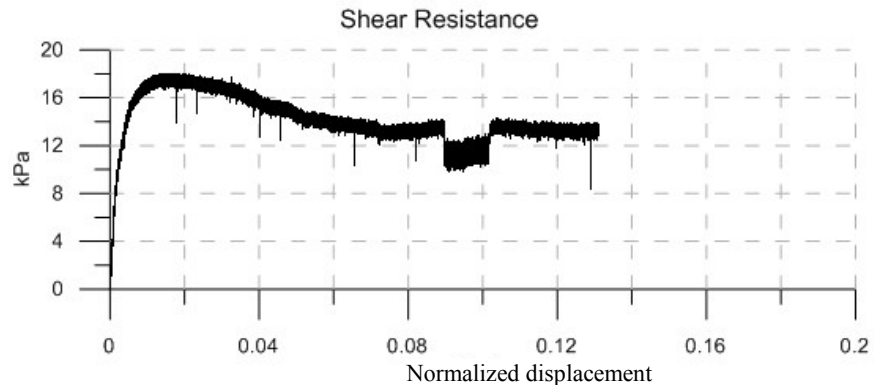

Material:	Glass Beads
Size:	0.55 mm
Normal Stress:	23 kPa
Vibration Frequency:	140 Hz
Vibration Force:	3.71 N
Vibration Duration:	72 sec
Horizontal Acceleration:	0.28 g
Vertical Acceleration:	0.1 g
Horizontal Amplitude:	3.5×10^{-3} mm
Vertical Amplitude:	1.3×10^{-3} mm
Peak Strength:	18 kPa
Residual Strength:	14 kPa
Vibro-Residual Strength:	11.5 kPa

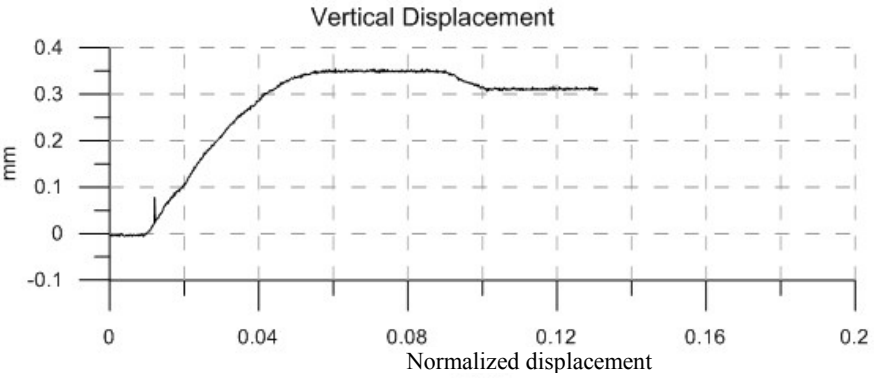

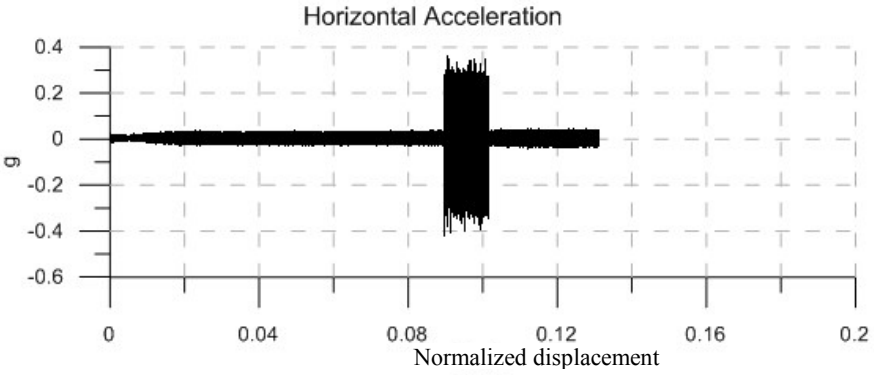

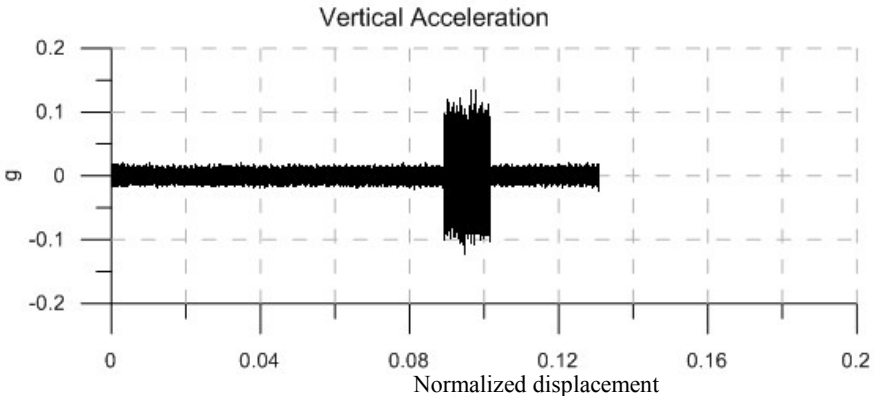

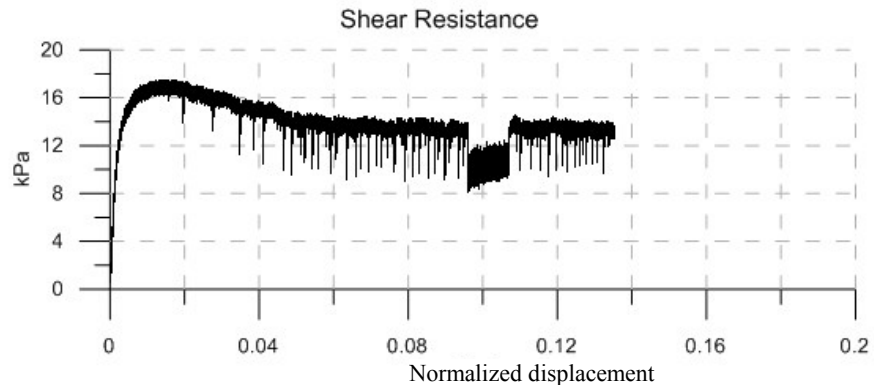

Material:	Glass Beads
Size:	0.55 mm
Normal Stress:	23 kPa
Vibration Frequency:	140 Hz
Vibration Force:	5.18 N
Vibration Duration:	64 sec
Horizontal Acceleration:	0.325 g
Vertical Acceleration:	0.105 g
Horizontal Amplitude:	4.1×10^{-3} mm
Vertical Amplitude:	1.3×10^{-3} mm
Peak Strength:	17 kPa
Residual Strength:	14 kPa
Vibro-Residual Strength:	10.5 kPa

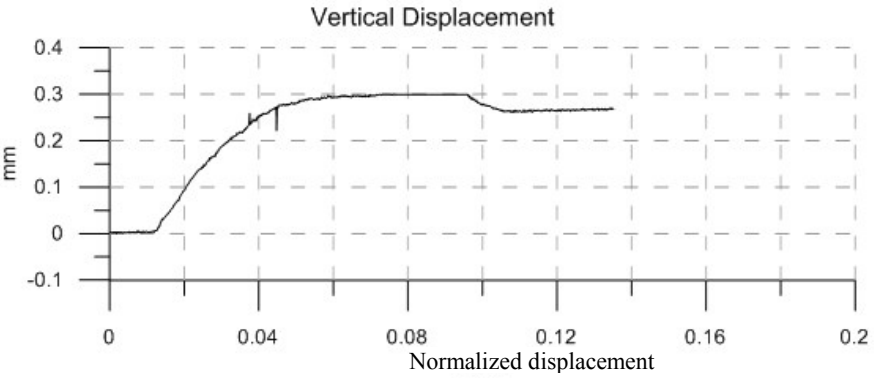

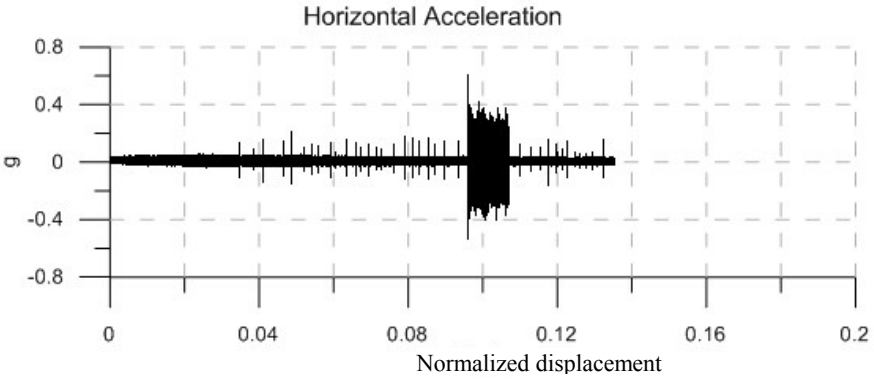

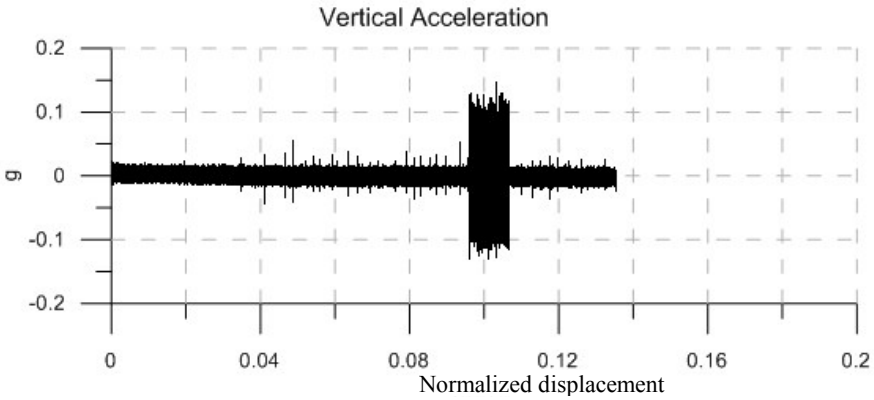

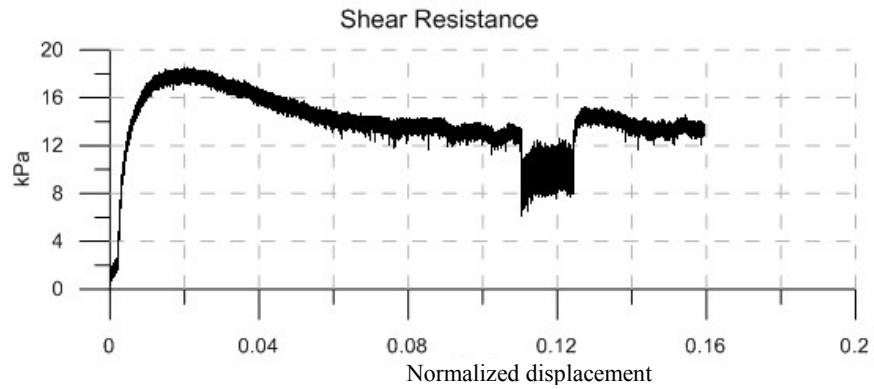

Material:	Glass Beads
Size:	0.55 mm
Normal Stress:	23 kPa
Vibration Frequency:	140 Hz
Vibration Force:	7.14 N
Vibration Duration:	81 sec
Horizontal Acceleration:	0.46 g
Vertical Acceleration:	0.16 g
Horizontal Amplitude:	5.8×10^{-3} mm
Vertical Amplitude:	2.0×10^{-3} mm
Peak Strength:	18 kPa
Residual Strength:	13.5 kPa
Vibro-Residual Strength:	9 kPa

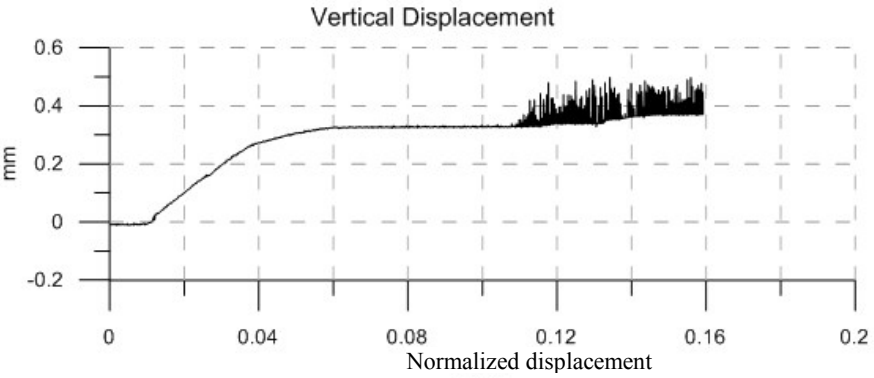

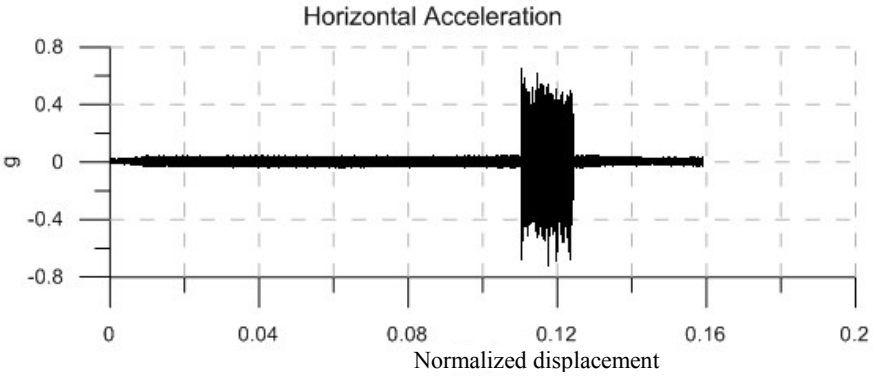

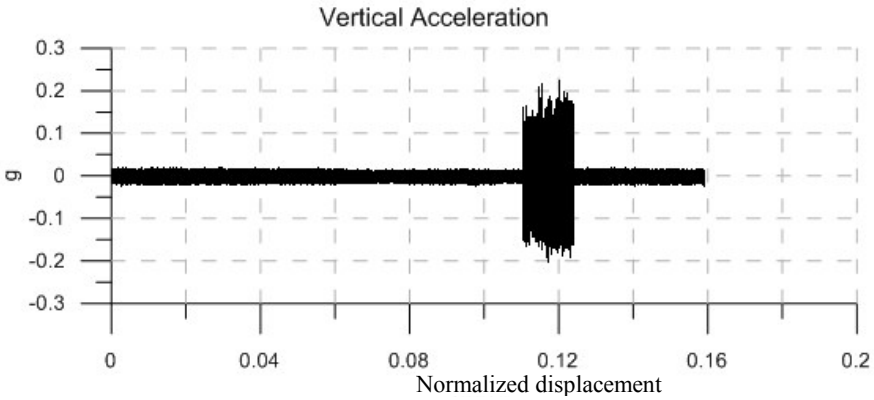

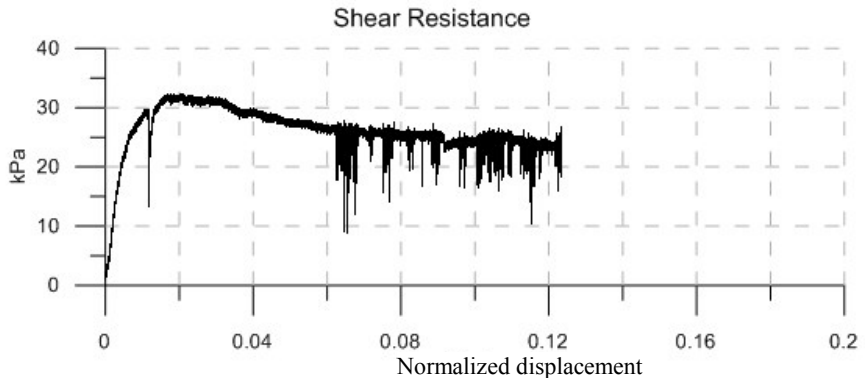

Material:	Glass Beads
Size:	0.55 mm
Normal Stress:	50 kPa
Vibration Frequency:	140 Hz
Vibration Force:	1.61 N
Vibration Duration:	61 sec
Horizontal Acceleration:	0.11 g
Vertical Acceleration:	0.035 g
Horizontal Amplitude:	1.4×10^{-3} mm
Vertical Amplitude:	0.4×10^{-3} mm
Peak Strength:	32 kPa
Residual Strength:	25.5 kPa
Vibro-Residual Strength:	24 kPa

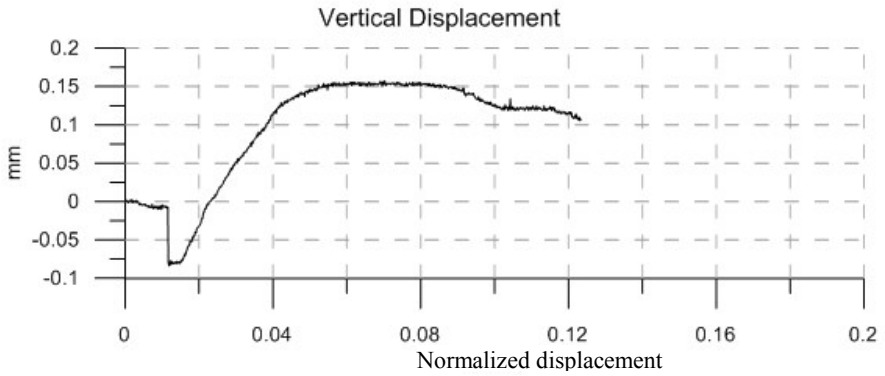

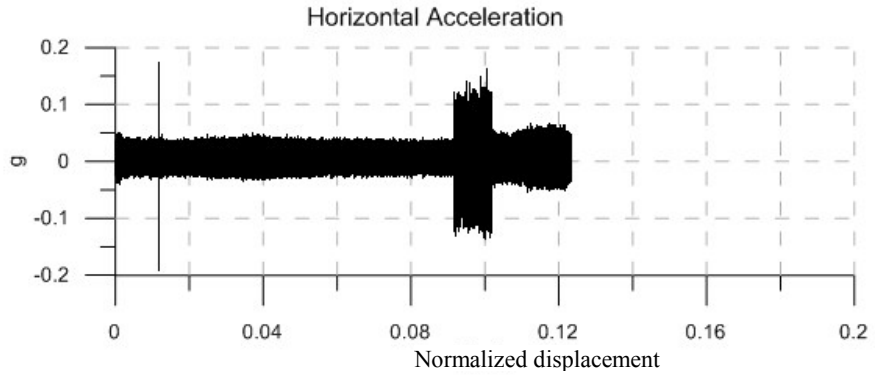

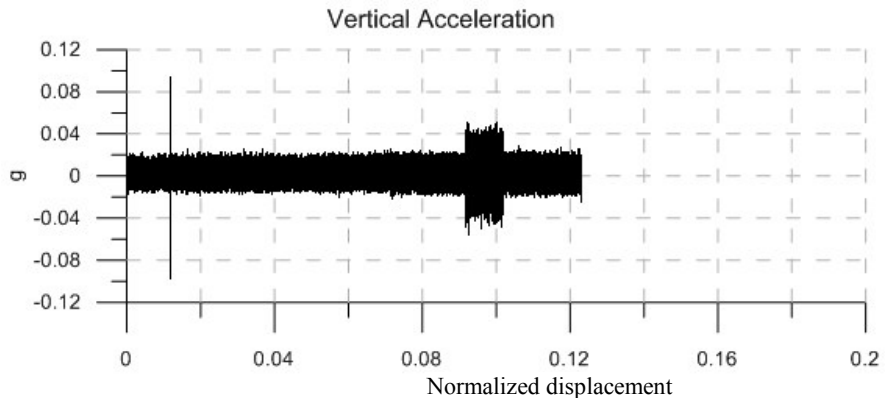

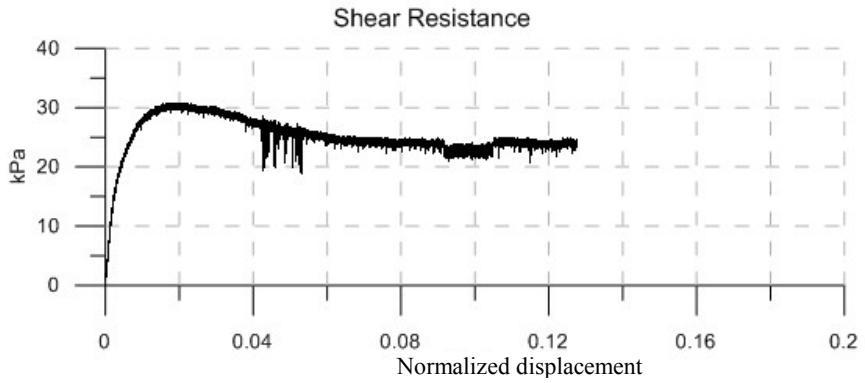

Material:	Glass Beads
Size:	0.55 mm
Normal Stress:	50 kPa
Vibration Frequency:	140 Hz
Vibration Force:	3.22 N
Vibration Duration:	79 sec
Horizontal Acceleration:	0.175 g
Vertical Acceleration:	0.07 g
Horizontal Amplitude:	2.2×10^{-3} mm
Vertical Amplitude:	0.9×10^{-3} mm
Peak Strength:	30.5 kPa
Residual Strength:	24.5 kPa
Vibro-Residual Strength:	22.5 kPa

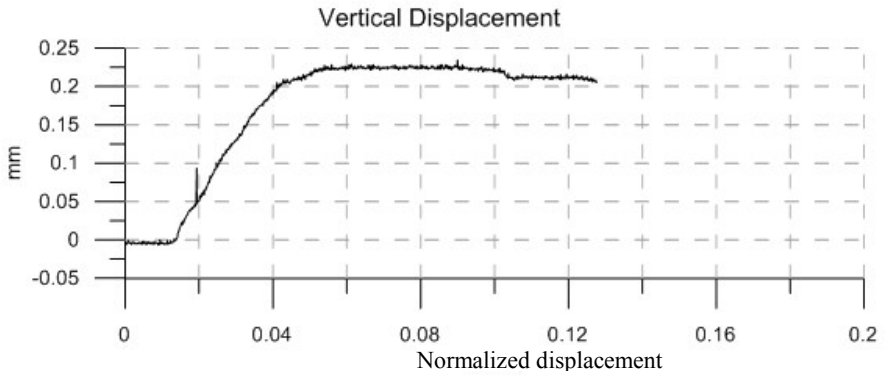

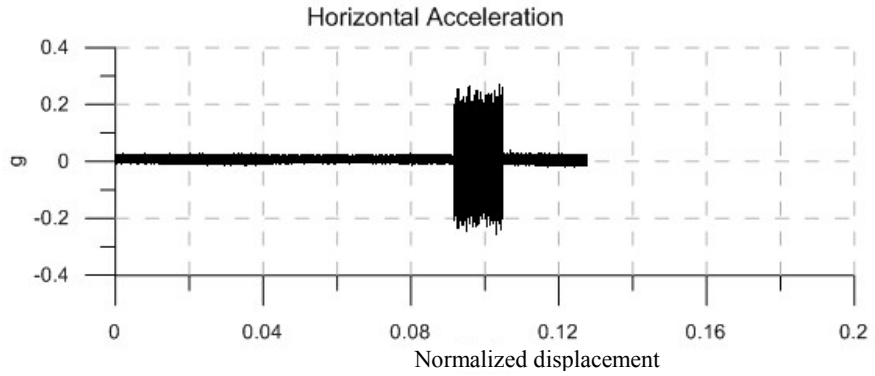

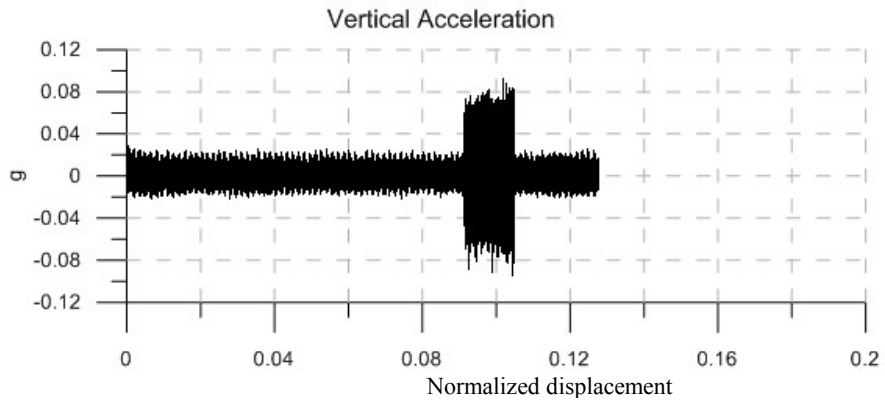

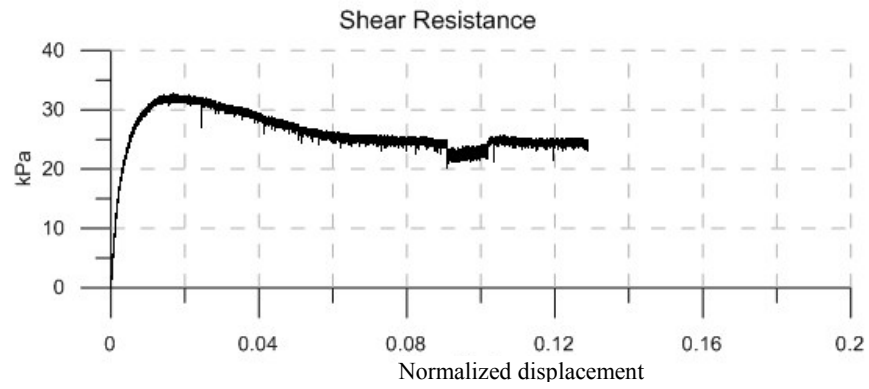

Material:	Glass Beads
Size:	0.55 mm
Normal Stress:	50 kPa
Vibration Frequency:	140 Hz
Vibration Force:	3.71 N
Vibration Duration:	66 sec
Horizontal Acceleration:	0.23 g
Vertical Acceleration:	0.085 g
Horizontal Amplitude:	2.9×10^{-3} mm
Vertical Amplitude:	1.1×10^{-3} mm
Peak Strength:	32 kPa
Residual Strength:	25.5 kPa
Vibro-Residual Strength:	22.5 kPa

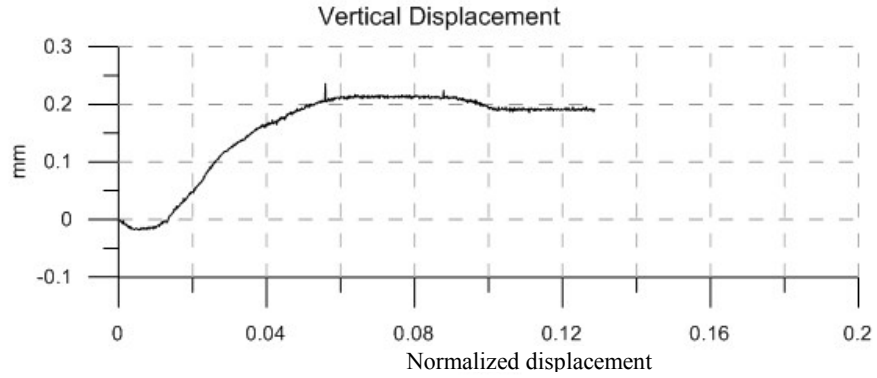

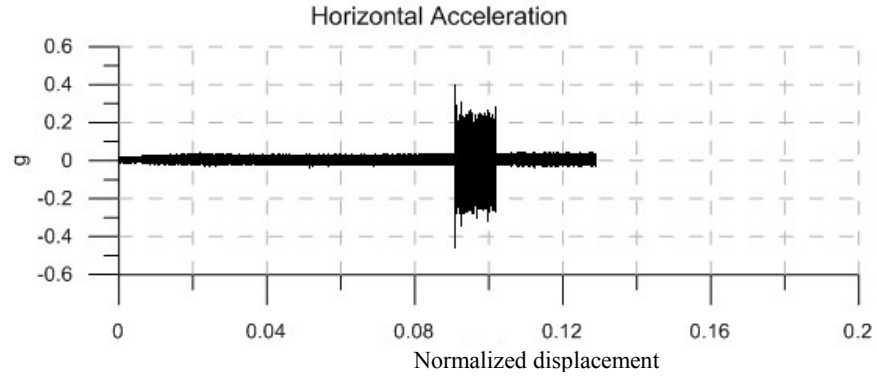

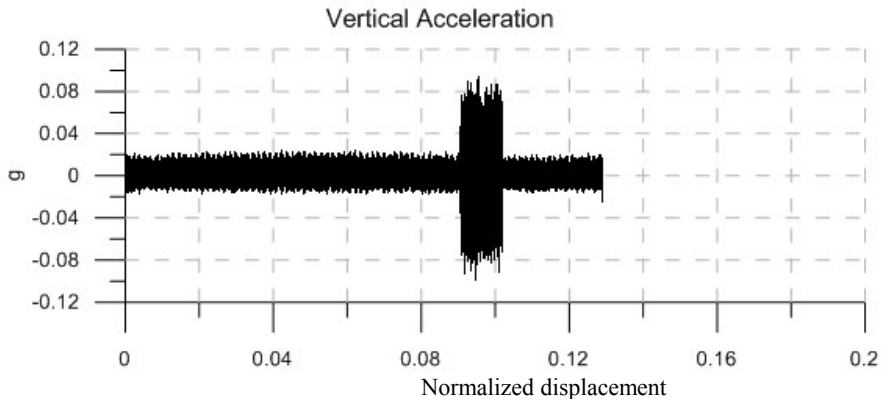

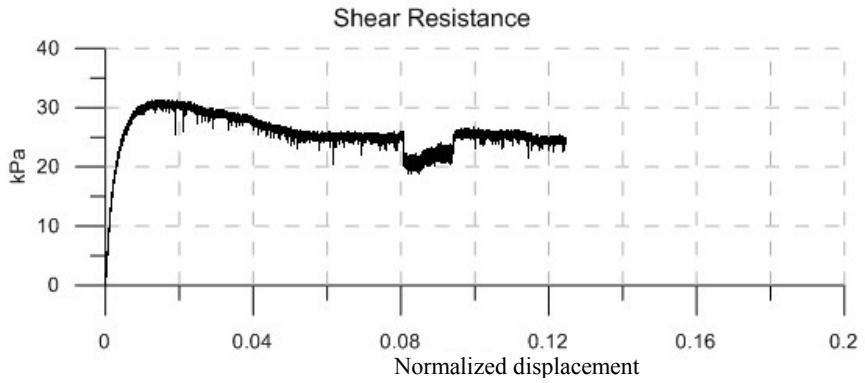

Material:	Glass Beads
Size:	0.55 mm
Normal Stress:	50 kPa
Vibration Frequency:	140 Hz
Vibration Force:	5.18 N
Vibration Duration:	78 sec
Horizontal Acceleration:	0.325 g
Vertical Acceleration:	0.105 g
Horizontal Amplitude:	4.1×10^{-3} mm
Vertical Amplitude:	1.3×10^{-3} mm
Peak Strength:	31 kPa
Residual Strength:	25.5 kPa
Vibro-Residual Strength:	21 kPa

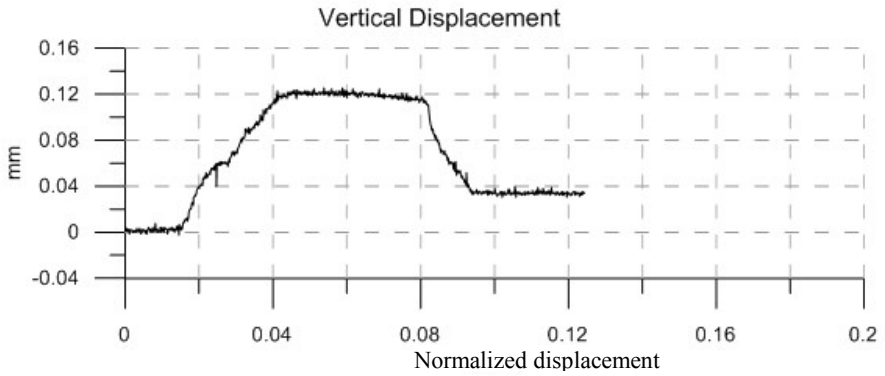

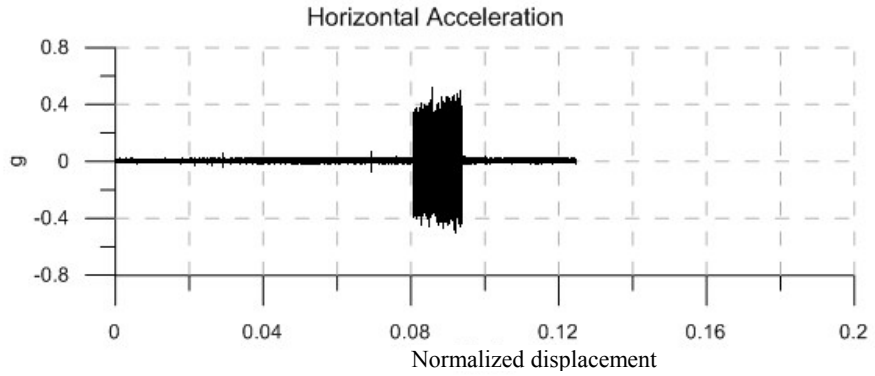

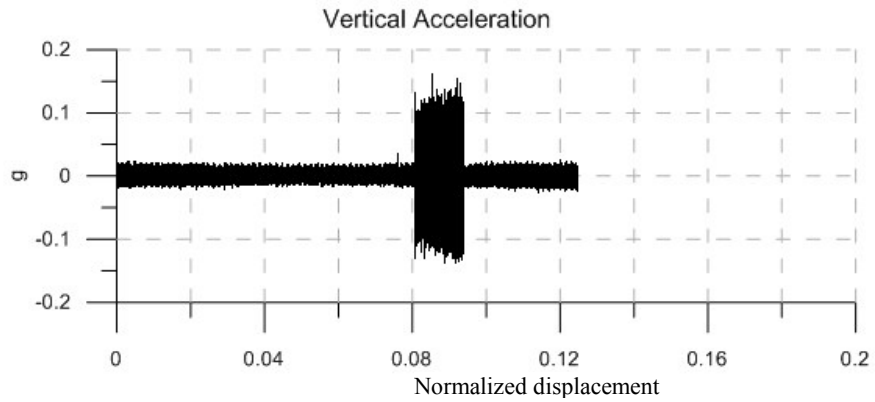

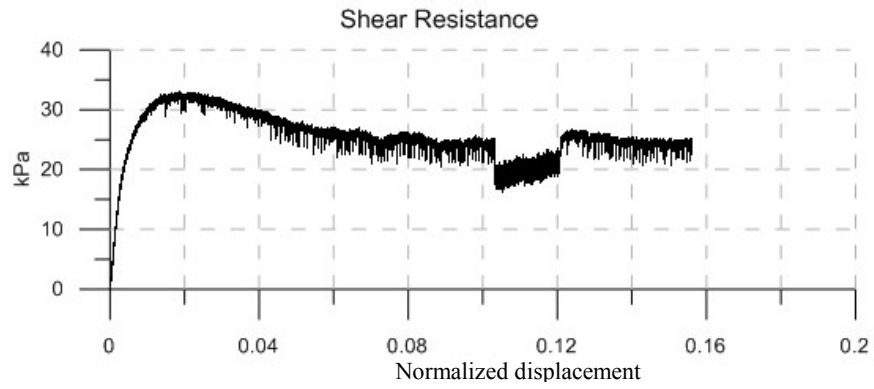

Material:	Glass Beads
Size:	0.55 mm
Normal Stress:	50 kPa
Vibration Frequency:	140 Hz
Vibration Force:	7.14 N
Vibration Duration:	103 sec
Horizontal Acceleration:	0.46 g
Vertical Acceleration:	0.16 g
Horizontal Amplitude:	5.8×10^{-3} mm
Vertical Amplitude:	2.0×10^{-3} mm
Peak Strength:	32.5 kPa
Residual Strength:	25 kPa
Vibro-Residual Strength:	19 kPa

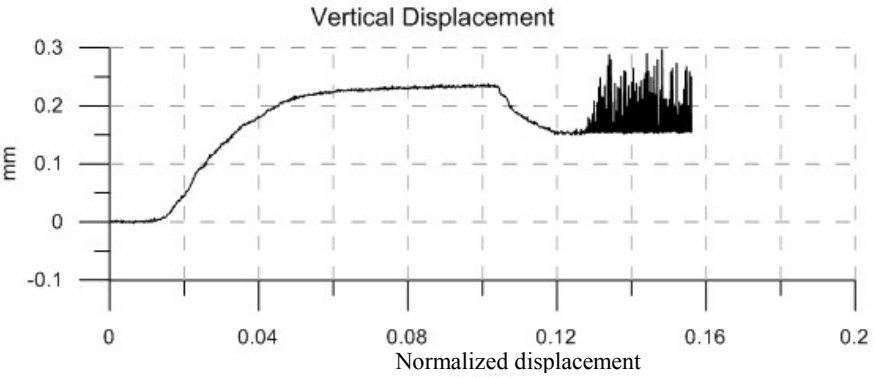

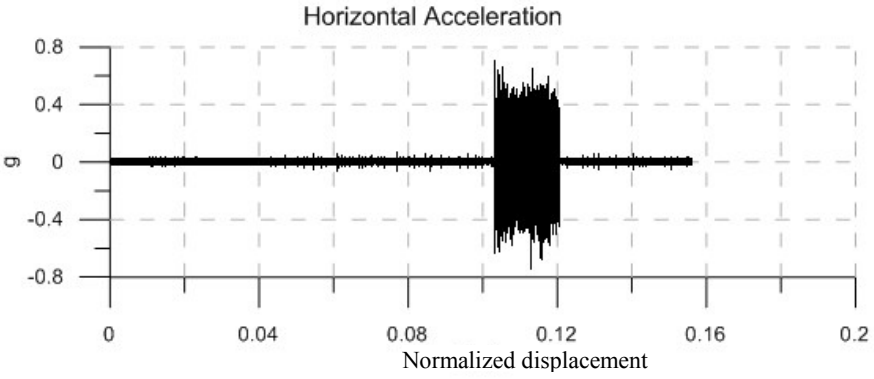

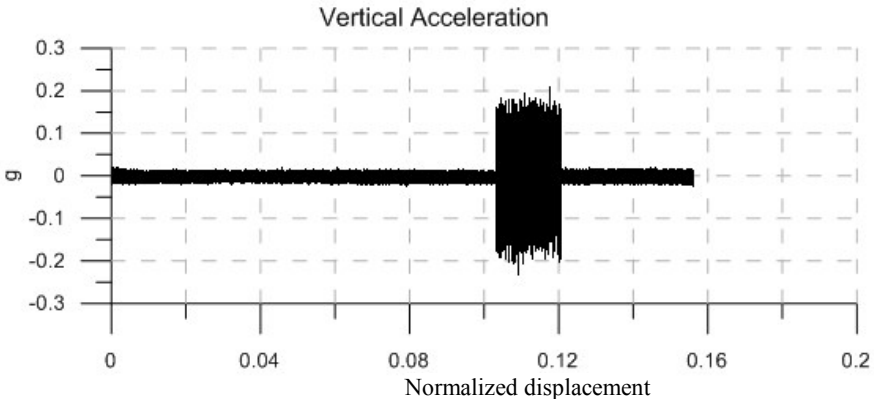

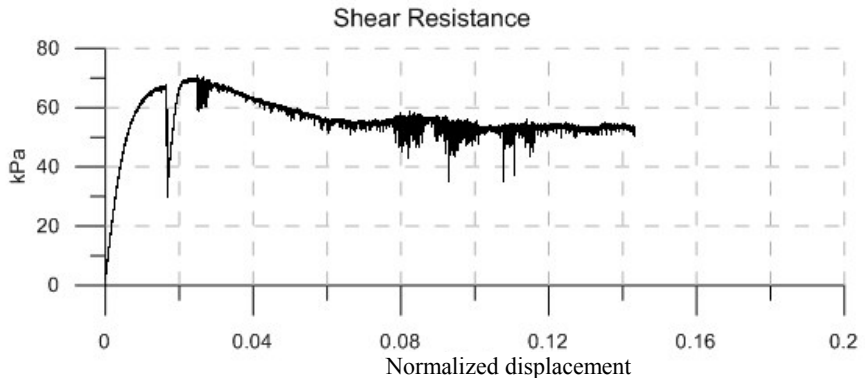

Material:	Glass Beads
Size:	0.55 mm
Normal Stress:	118 kPa
Vibration Frequency:	140 Hz
Vibration Force:	1.61 N
Vibration Duration:	81 sec
Horizontal Acceleration:	0.08 g
Vertical Acceleration:	0.035 g
Horizontal Amplitude:	1.0×10^{-3} mm
Vertical Amplitude:	0.4×10^{-3} mm
Peak Strength:	69 kPa
Residual Strength:	55.5 kPa
Vibro-Residual Strength:	53.5 kPa

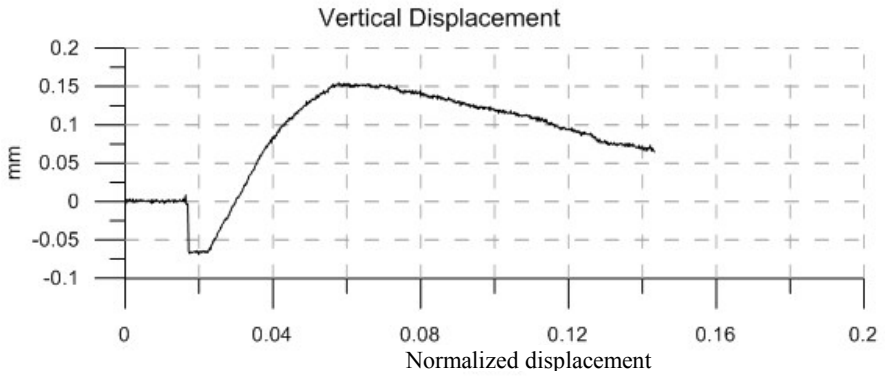

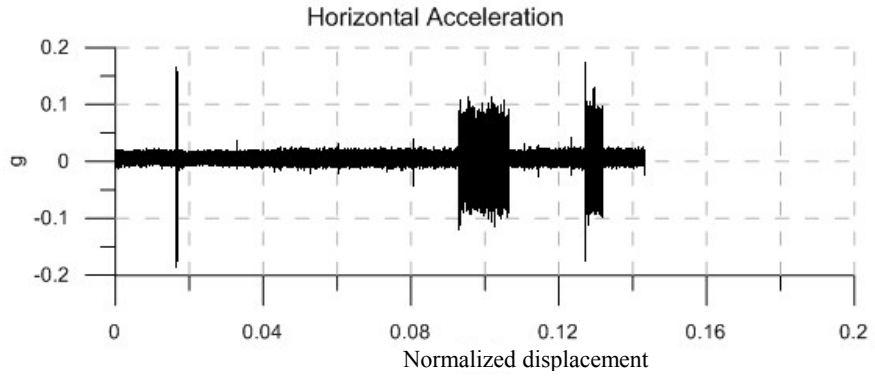

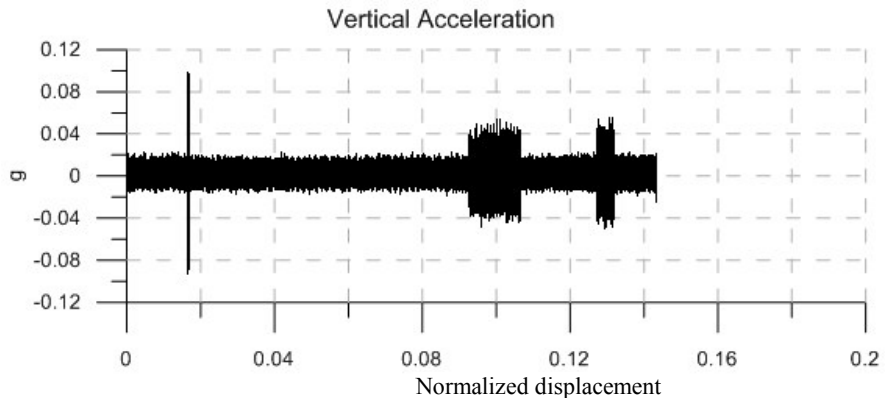

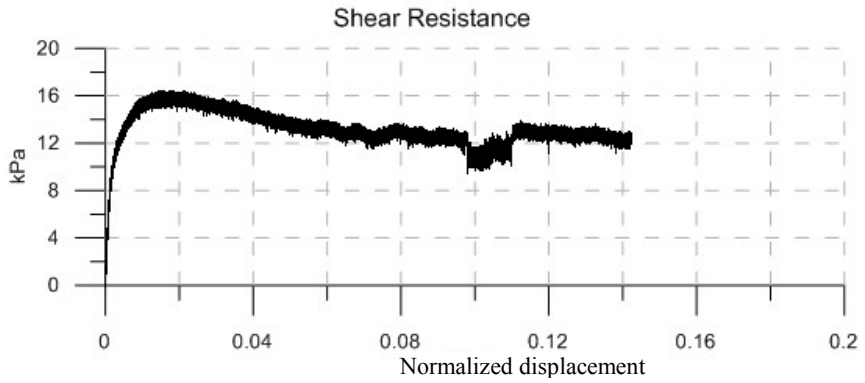

Material:	Glass Beads
Size:	0.55 mm
Normal Stress:	118 kPa
Vibration Frequency:	140 Hz
Vibration Force:	3.22 N
Vibration Duration:	91 sec
Horizontal Acceleration:	0.175 g
Vertical Acceleration:	0.07 g
Horizontal Amplitude:	2.2×10^{-3} mm
Vertical Amplitude:	0.9×10^{-3} mm
Peak Strength:	65 kPa
Residual Strength:	51.5 kPa
Vibro-Residual Strength:	47.5 kPa

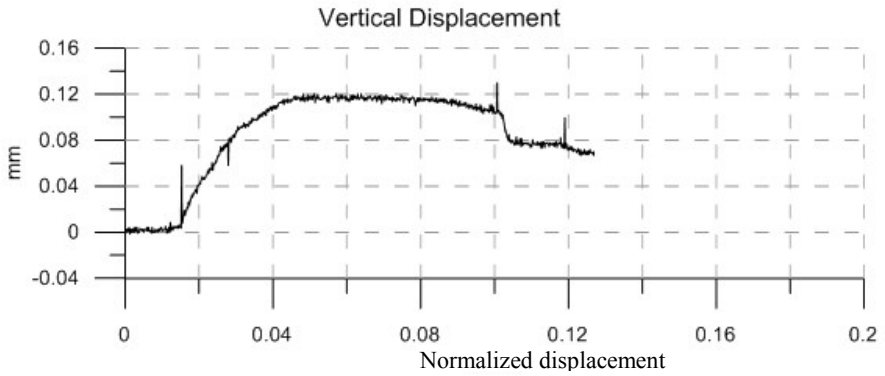

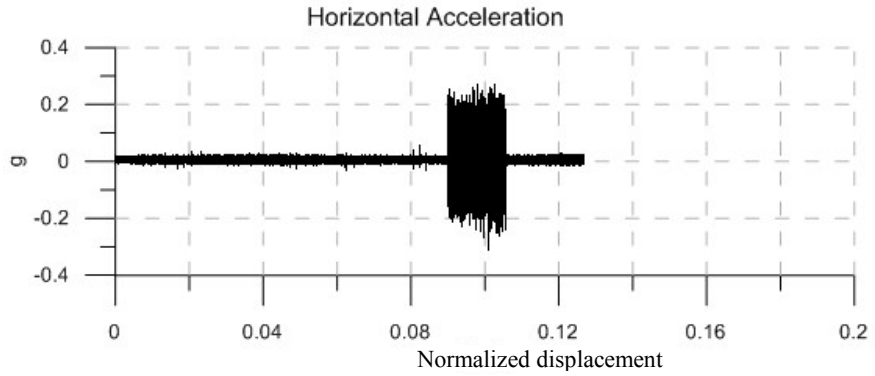

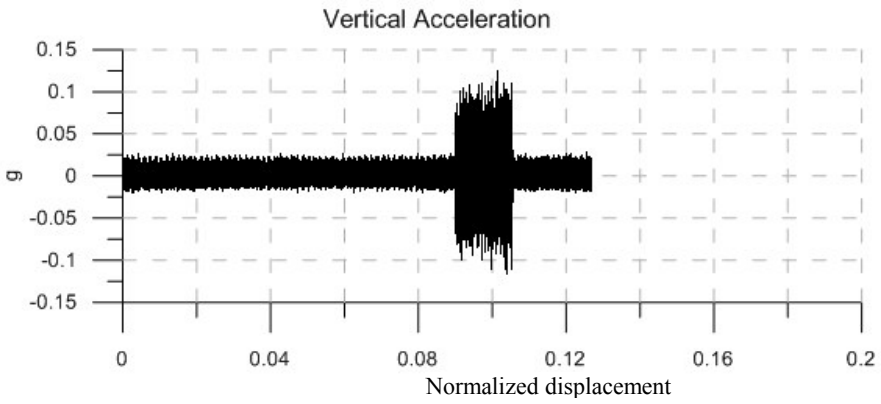

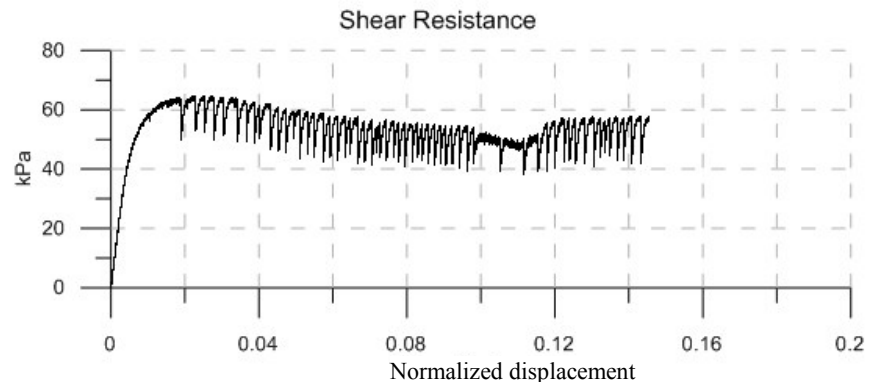

Material:	Glass Beads
Size:	0.55 mm
Normal Stress:	118 kPa
Vibration Frequency:	140 Hz
Vibration Force:	3.71 N
Vibration Duration:	108 sec
Horizontal Acceleration:	0.23 g
Vertical Acceleration:	0.09 g
Horizontal Amplitude:	2.9×10^{-3} mm
Vertical Amplitude:	1.1×10^{-3} mm
Peak Strength:	64 kPa
Residual Strength:	54 kPa
Vibro-Residual Strength:	48.5 kPa

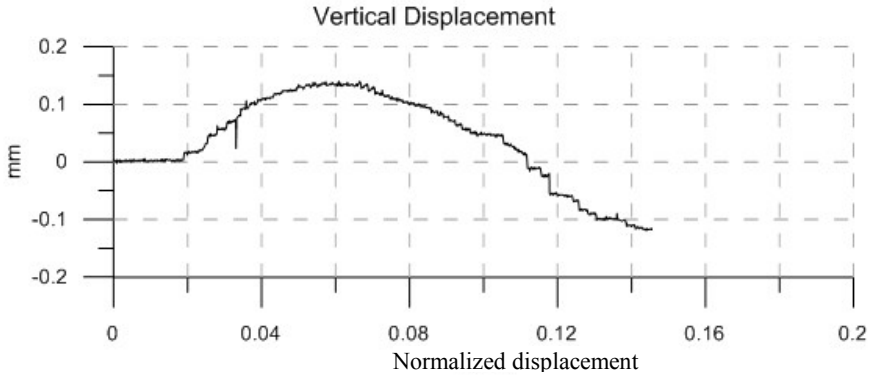

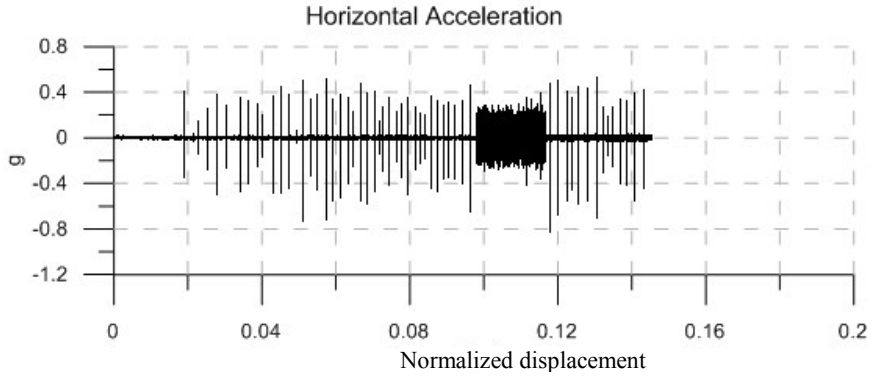

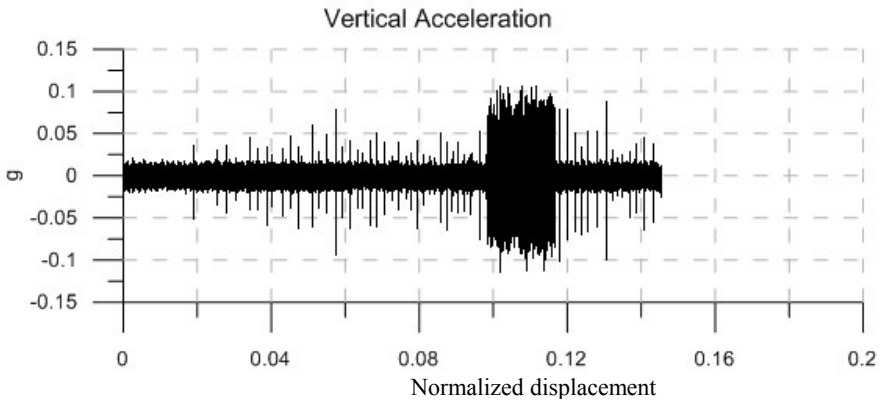

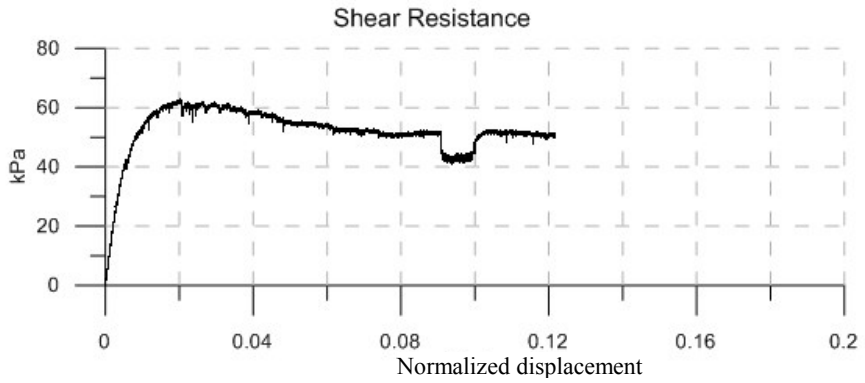

Material:	Glass Beads
Size:	0.55 mm
Normal Stress:	118 kPa
Vibration Frequency:	140 Hz
Vibration Force:	5.18 N
Vibration Duration:	50 sec
Horizontal Acceleration:	0.325 g
Vertical Acceleration:	0.105 g
Horizontal Amplitude:	4.1×10^{-3} mm
Vertical Amplitude:	1.3×10^{-3} mm
Peak Strength:	62.5 kPa
Residual Strength:	51.5 kPa
Vibro-Residual Strength:	43 kPa

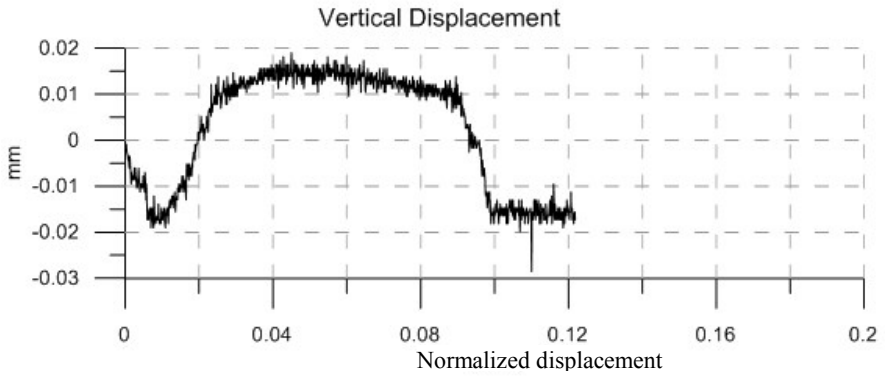

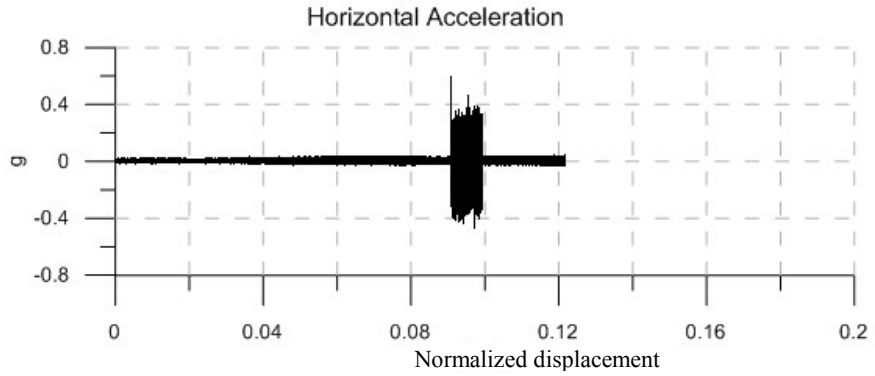

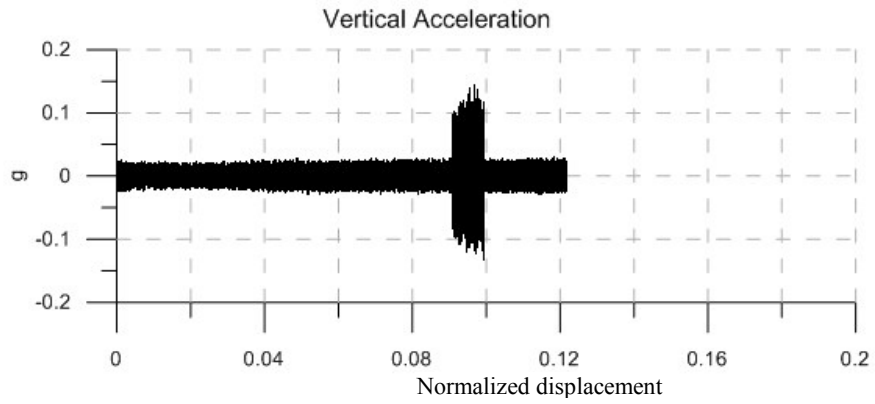

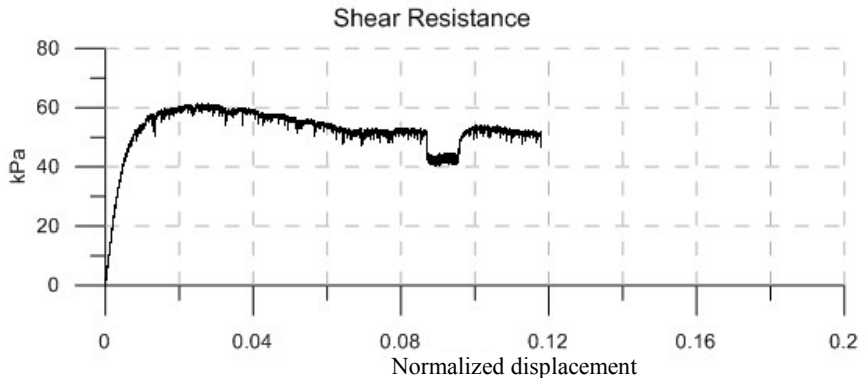

Material:	Glass Beads
Size:	0.55 mm
Normal Stress:	118 kPa
Vibration Frequency:	140 Hz
Vibration Force:	7.14 N
Vibration Duration:	51 sec
Horizontal Acceleration:	0.42 g
Vertical Acceleration:	0.16 g
Horizontal Amplitude:	5.3×10^{-3} mm
Vertical Amplitude:	2.0×10^{-3} mm
Peak Strength:	61.5 kPa
Residual Strength:	53 kPa
Vibro-Residual Strength:	42 kPa

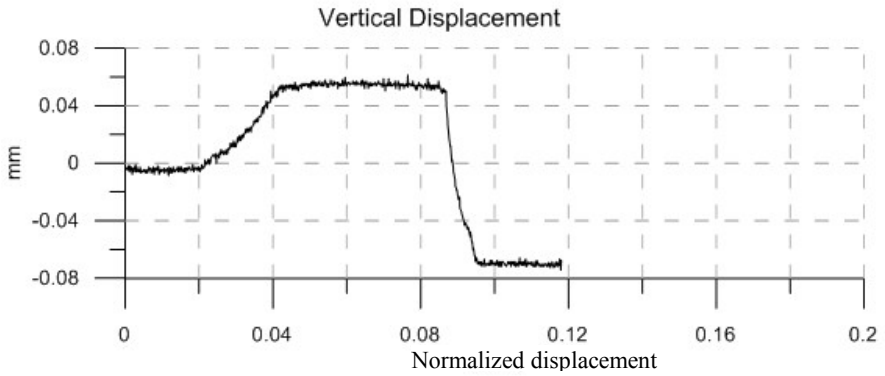

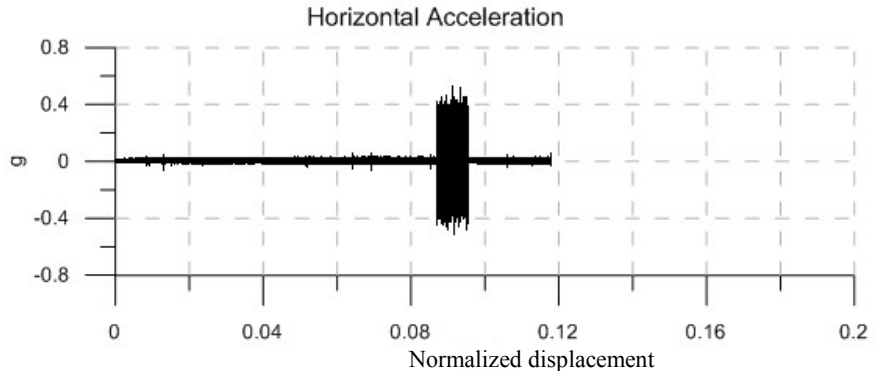

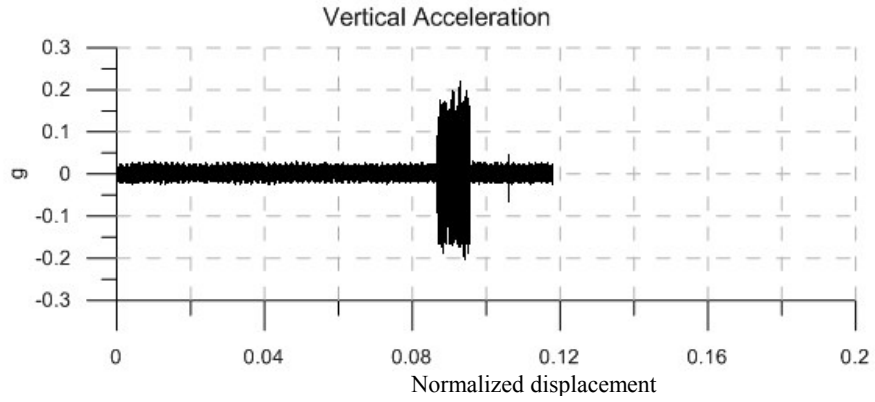

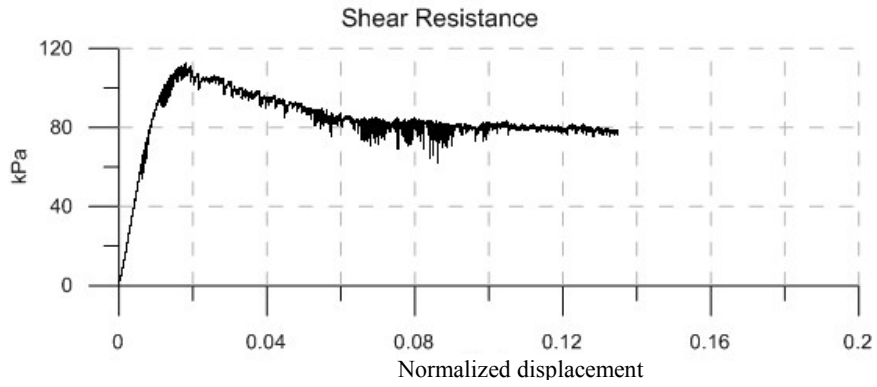

Material:	Glass Beads
Size:	0.55 mm
Normal Stress:	200 kPa
Vibration Frequency:	140 Hz
Vibration Force:	1.61 N
Vibration Duration:	93 sec
Horizontal Acceleration:	0.09 g
Vertical Acceleration:	0.035 g
Horizontal Amplitude:	1.1×10^{-3} mm
Vertical Amplitude:	0.4×10^{-3} mm
Peak Strength:	111 kPa
Residual Strength:	82 kPa
Vibro-Residual Strength:	79 kPa

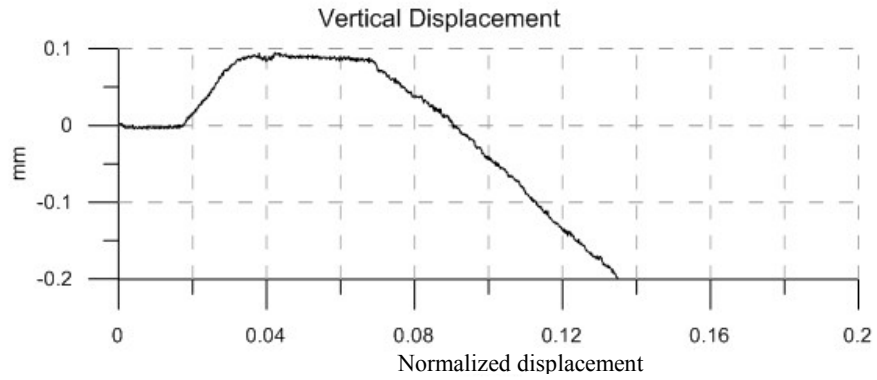

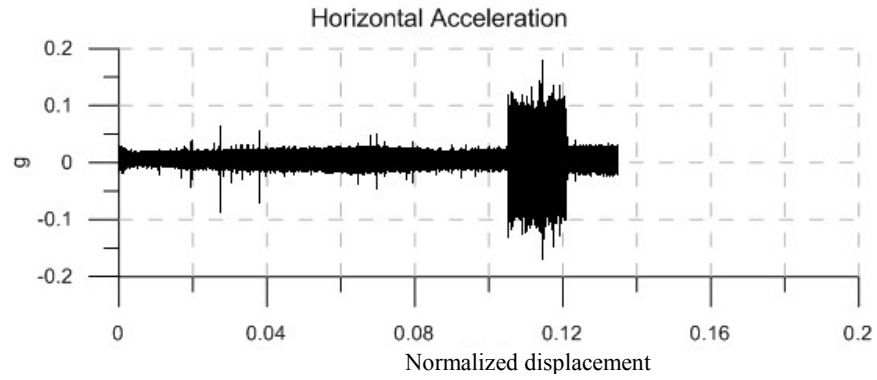

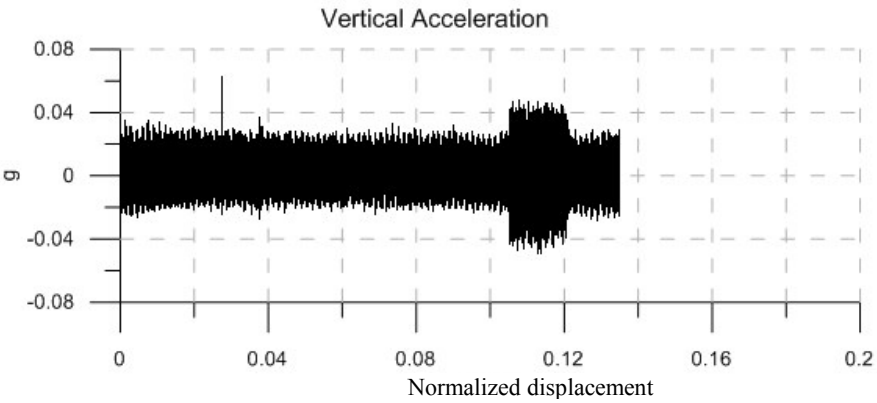

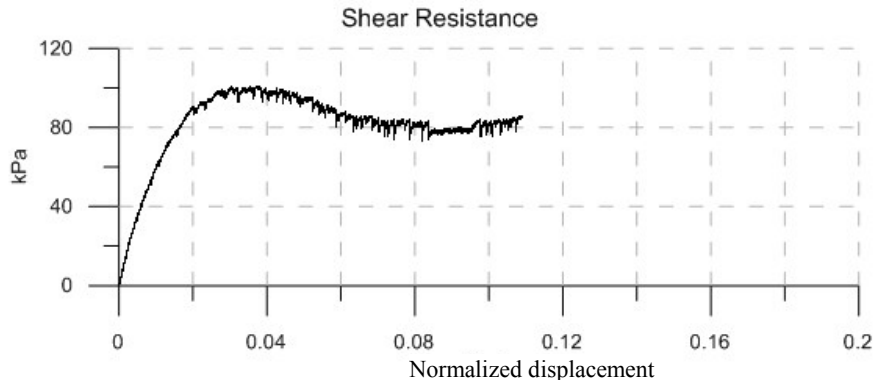

Material:	Glass Beads
Size:	0.55 mm
Normal Stress:	200 kPa
Vibration Frequency:	140 Hz
Vibration Force:	3.22 N
Vibration Duration:	70 sec
Horizontal Acceleration:	0.17 g
Vertical Acceleration:	0.07 g
Horizontal Amplitude:	2.2×10^{-3} mm
Vertical Amplitude:	0.9×10^{-3} mm
Peak Strength:	101 kPa
Residual Strength:	84 kPa
Vibro-Residual Strength:	78 kPa

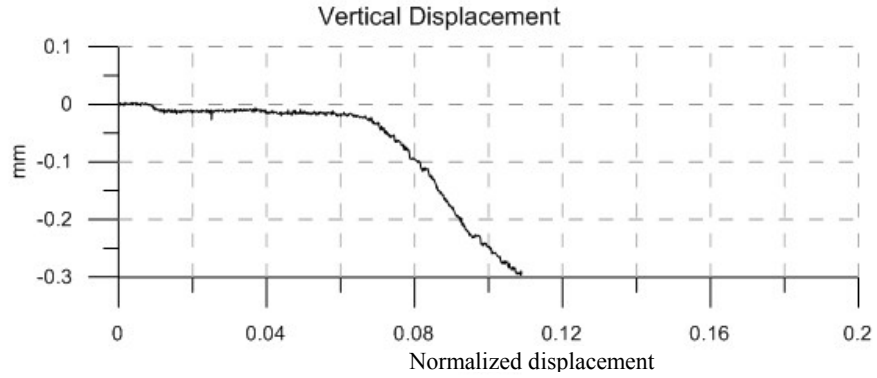

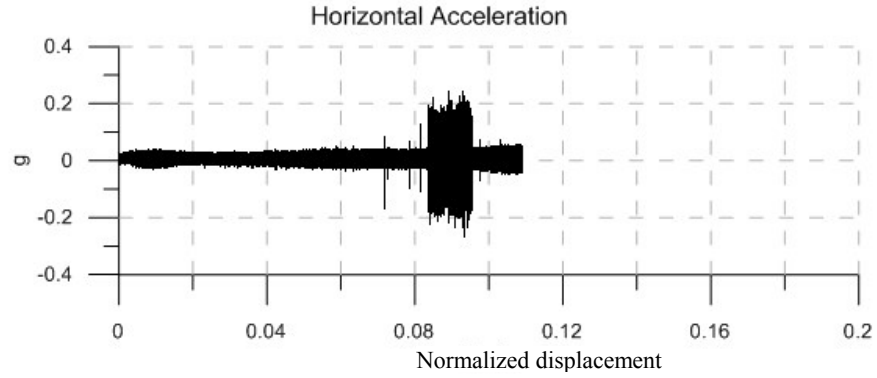

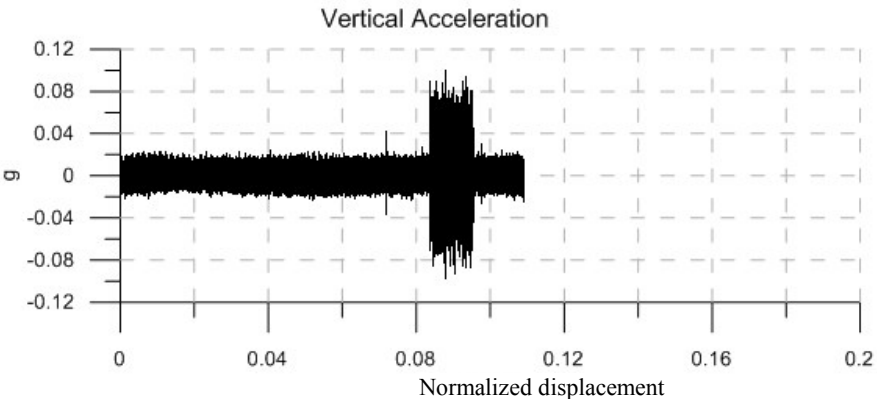

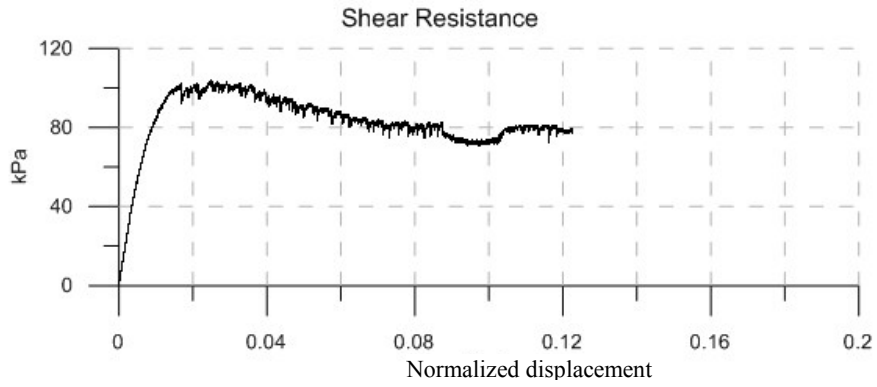

Material:	Glass Beads
Size:	0.55 mm
Normal Stress:	200 kPa
Vibration Frequency:	140 Hz
Vibration Force:	3.71 N
Vibration Duration:	88 sec
Horizontal Acceleration:	0.23 g
Vertical Acceleration:	0.085 g
Horizontal Amplitude:	2.9×10^{-3} mm
Vertical Amplitude:	1.1×10^{-3} mm
Peak Strength:	103 kPa
Residual Strength:	82 kPa
Vibro-Residual Strength:	73 kPa

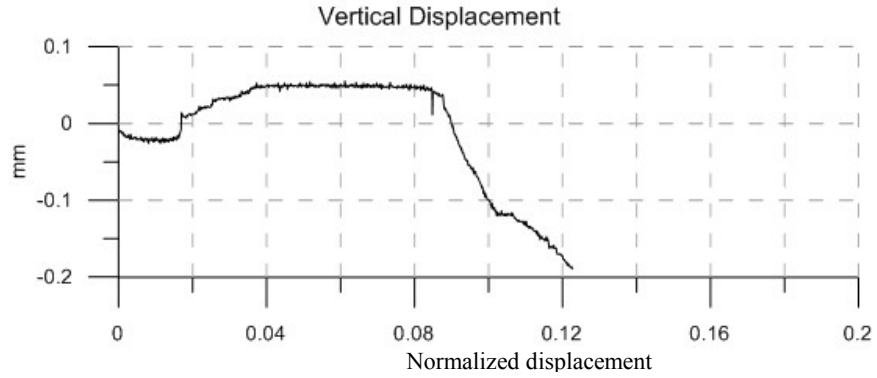

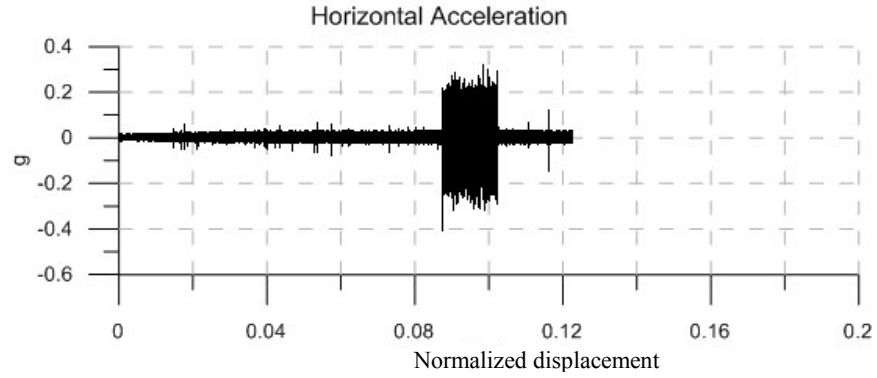

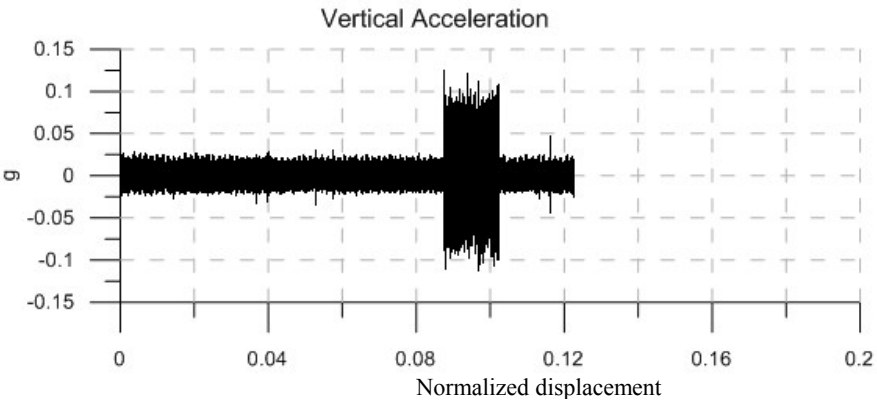

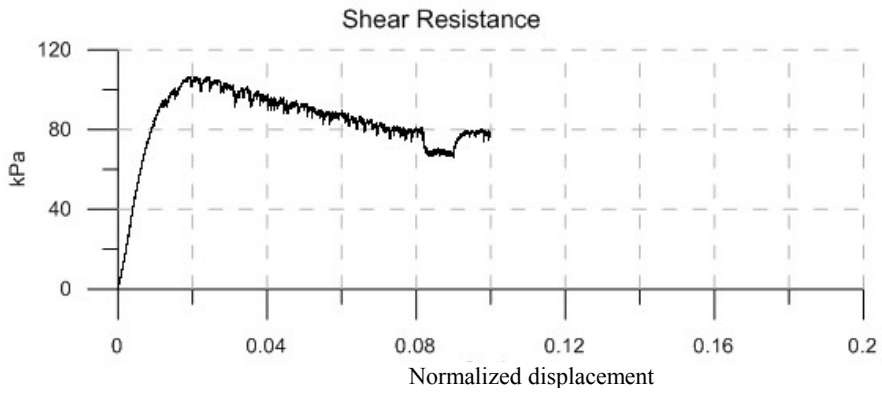

Material:	Glass Beads
Size:	0.55 mm
Normal Stress:	200 kPa
Vibration Frequency:	140 Hz
Vibration Force:	5.18 N
Vibration Duration:	46 sec
Horizontal Acceleration:	0.325 g
Vertical Acceleration:	0.09 g
Horizontal Amplitude:	4.1×10^{-3} mm
Vertical Amplitude:	1.1×10^{-3} mm
Peak Strength:	106 kPa
Residual Strength:	81 kPa
Vibro-Residual Strength:	68 kPa

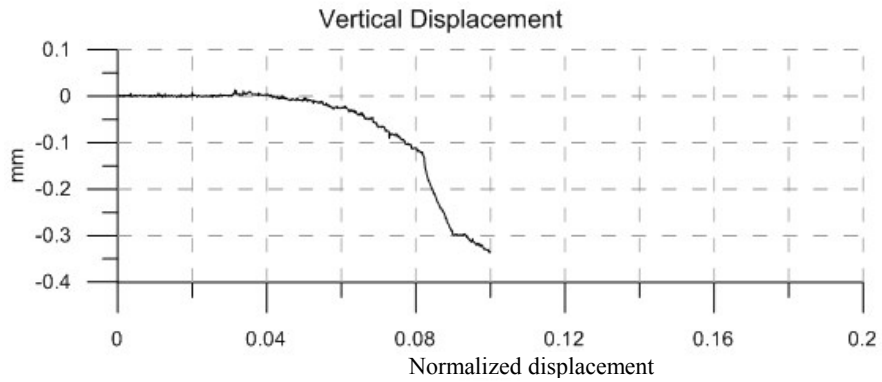

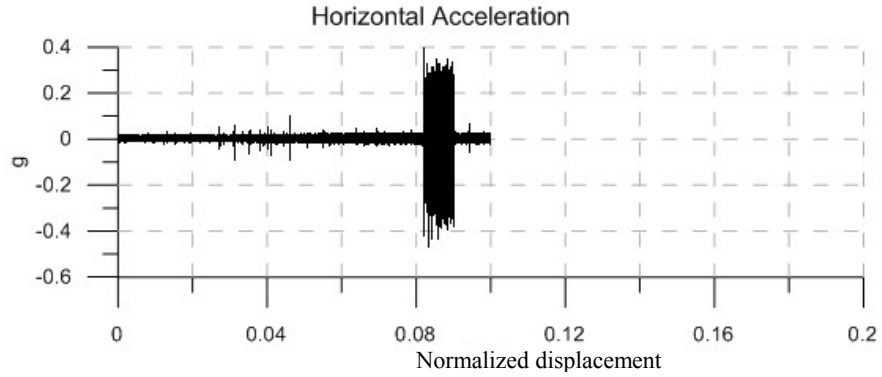

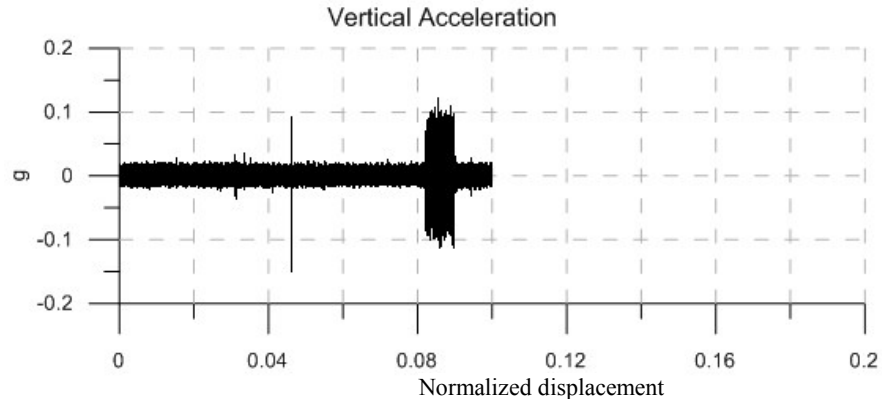

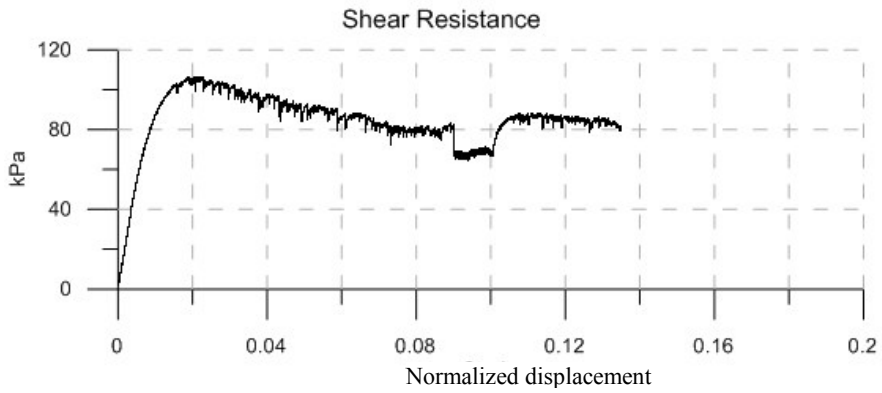

Material:	Glass Beads
Size:	0.55 mm
Normal Stress:	200 kPa
Vibration Frequency:	140 Hz
Vibration Force:	7.14 N
Vibration Duration:	63 sec
Horizontal Acceleration:	0.43 g
Vertical Acceleration:	0.14 g
Horizontal Amplitude:	5.5×10^{-3} mm
Vertical Amplitude:	1.7×10^{-3} mm
Peak Strength:	106 kPa
Residual Strength:	83 kPa
Vibro-Residual Strength:	66.5 kPa

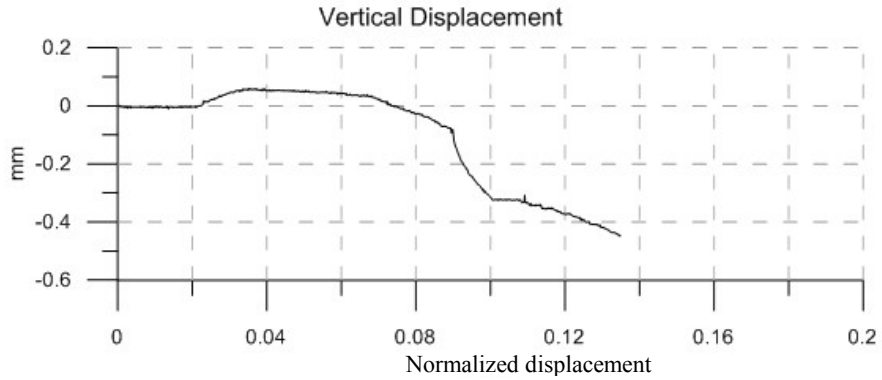

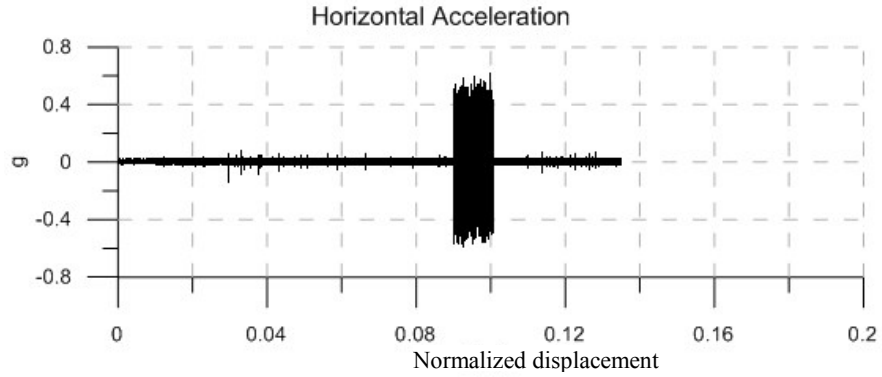

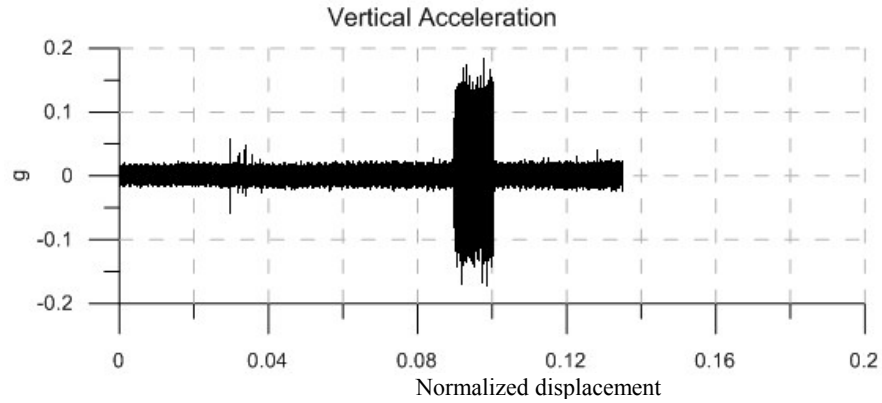

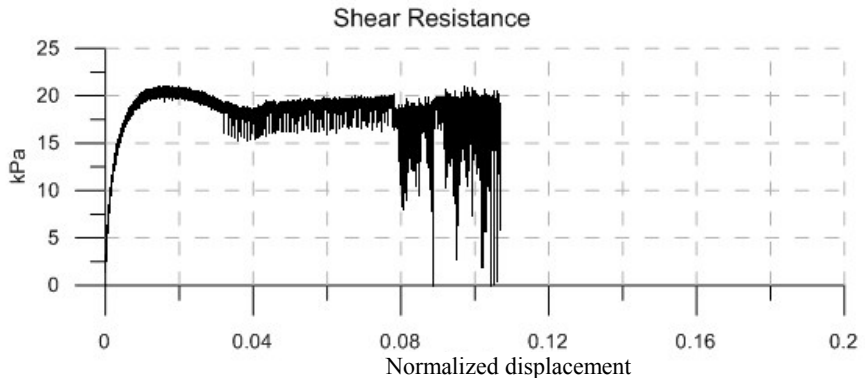

Material:	Glass Beads
Size:	0.1 mm
Normal Stress:	23 kPa
Vibration Frequency:	140 Hz
Vibration Force:	1.61 N
Vibration Duration:	58 sec
Horizontal Acceleration:	0.1 g
Vertical Acceleration:	0.03 g
Horizontal Amplitude:	1.3×10^{-3} mm
Vertical Amplitude:	0.4×10^{-3} mm
Peak Strength:	21 kPa
Residual Strength:	19.5 kPa
Vibro-Residual Strength:	18 kPa

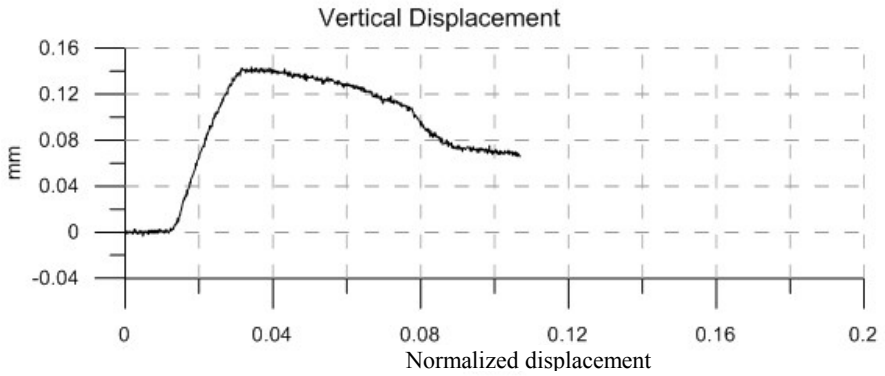

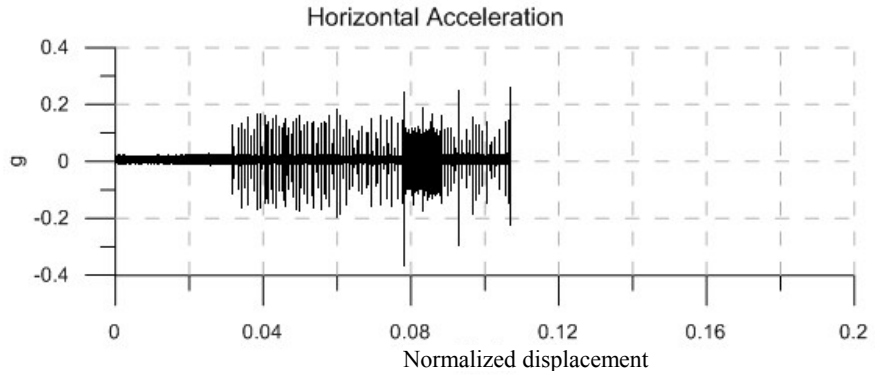

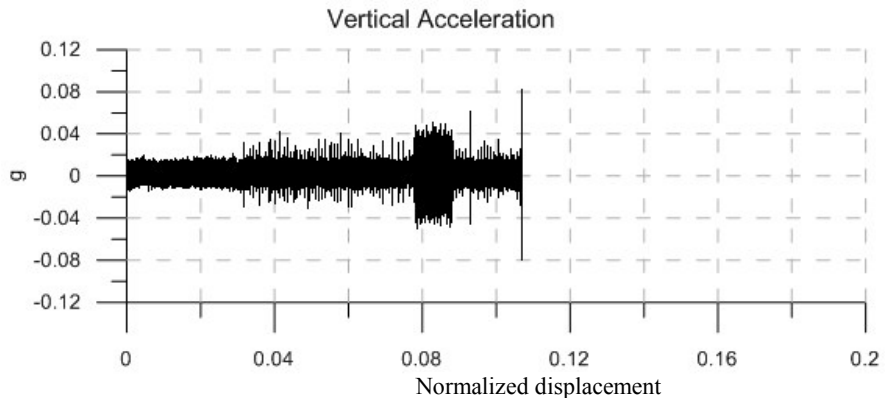

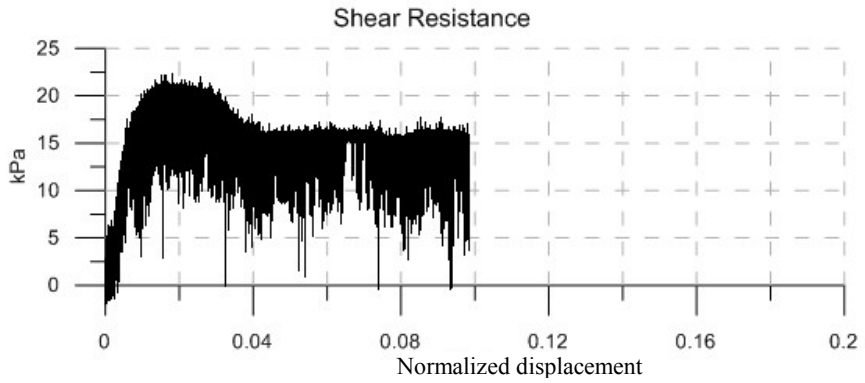

Material:	Glass Beads
Size:	0.1 mm
Normal Stress:	23 kPa
Vibration Frequency:	140 Hz
Vibration Force:	3.22 N
Vibration Duration:	49 sec
Horizontal Acceleration:	0.22 g
Vertical Acceleration:	0.09 g
Horizontal Amplitude:	2.8×10^{-3} mm
Vertical Amplitude:	1.1×10^{-3} mm
Peak Strength:	21 kPa
Residual Strength:	16.5 kPa
Vibro-Residual Strength:	15 kPa

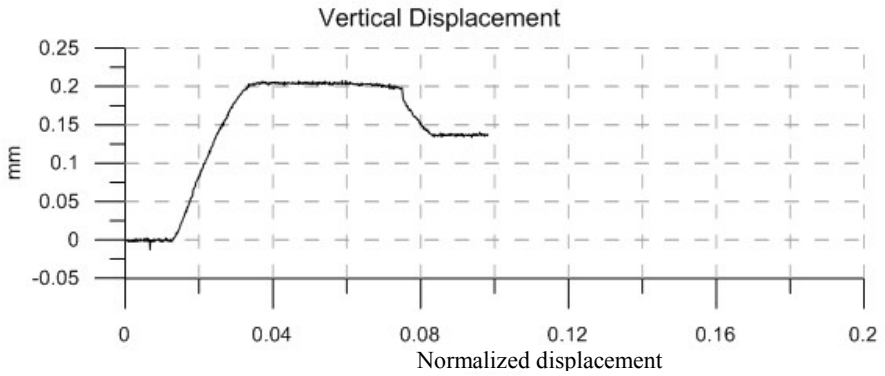

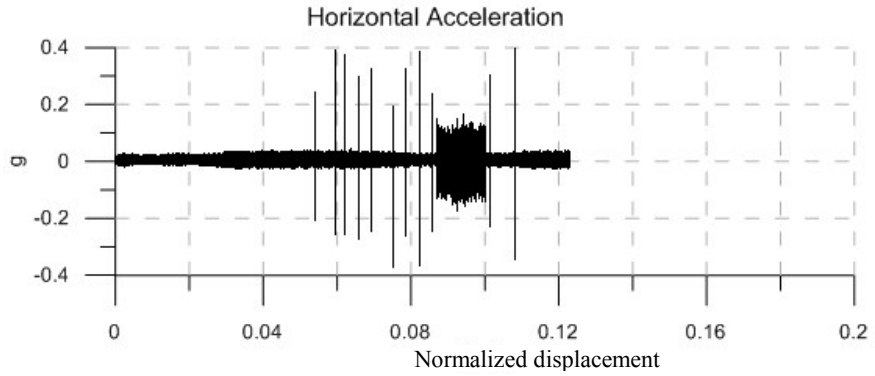

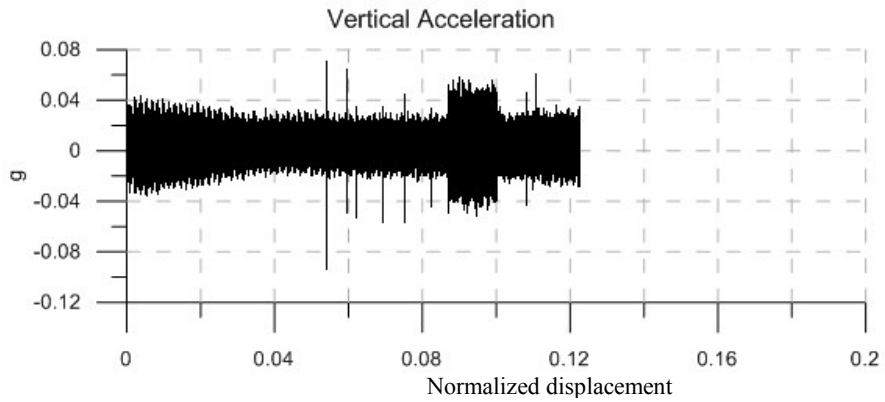

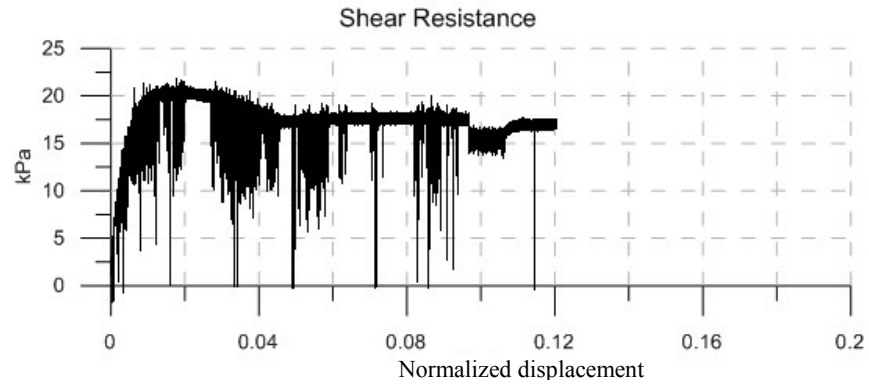

Material:	Glass Beads
Size:	0.1 mm
Normal Stress:	23 kPa
Vibration Frequency:	140 Hz
Vibration Force:	3.71 N
Vibration Duration:	57 sec
Horizontal Acceleration:	0.25 g
Vertical Acceleration:	0.075 g
Horizontal Amplitude:	3.2×10^{-3} mm
Vertical Amplitude:	1.0×10^{-3} mm
Peak Strength:	21 kPa
Residual Strength:	18 kPa
Vibro-Residual Strength:	15.5 kPa

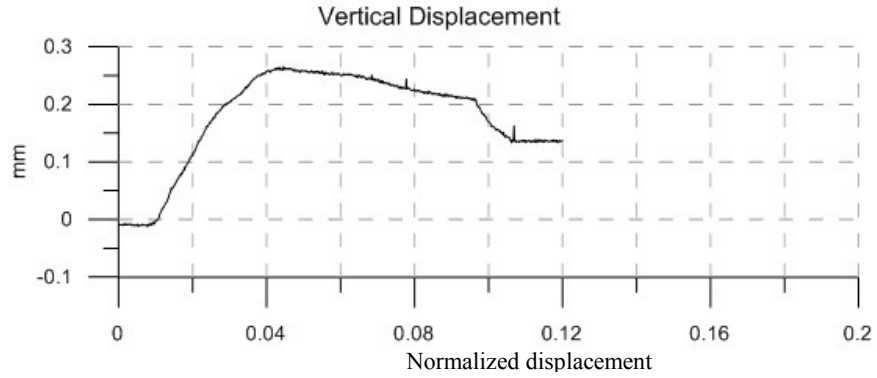

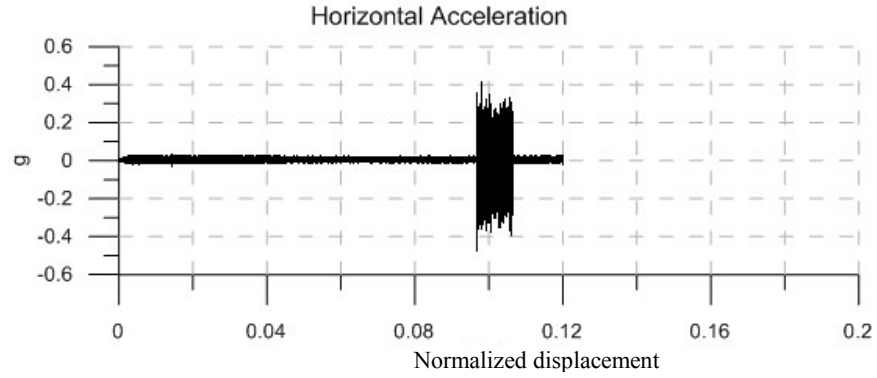

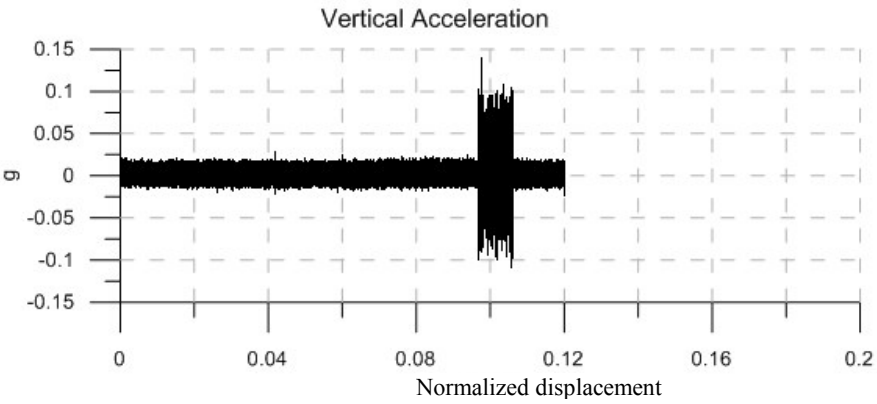

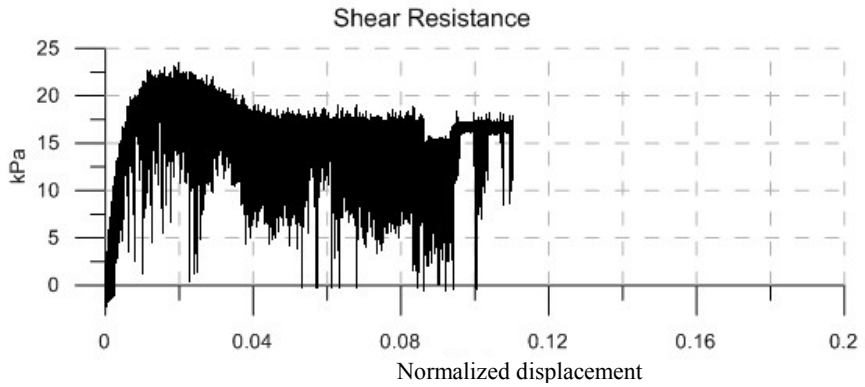

Material:	Glass Beads
Size:	0.1 mm
Normal Stress:	23 kPa
Vibration Frequency:	140 Hz
Vibration Force:	5.18 N
Vibration Duration:	43 sec
Horizontal Acceleration:	0.42 g
Vertical Acceleration:	0.11 g
Horizontal Amplitude:	5.3×10^{-3} mm
Vertical Amplitude:	1.4×10^{-3} mm
Peak Strength:	21.5 kPa
Residual Strength:	17 kPa
Vibro-Residual Strength:	14 kPa

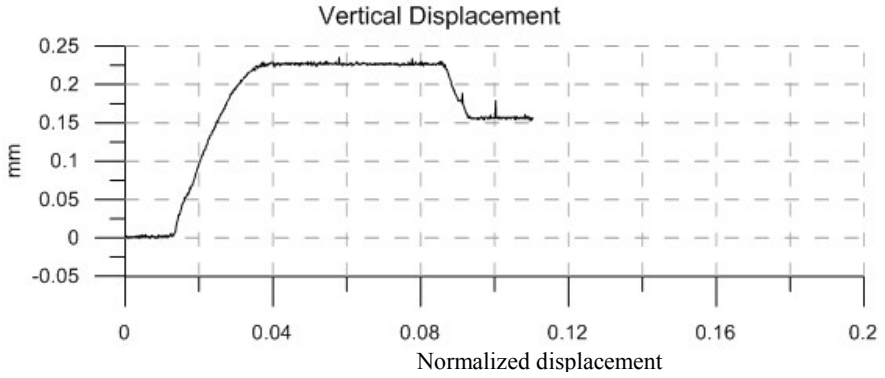

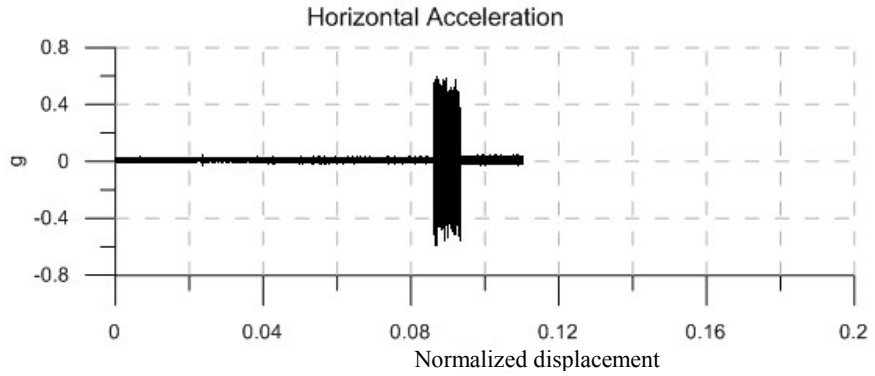

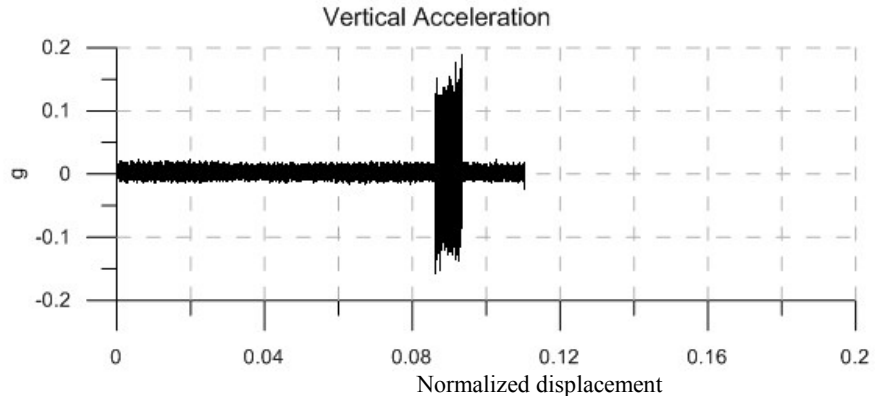

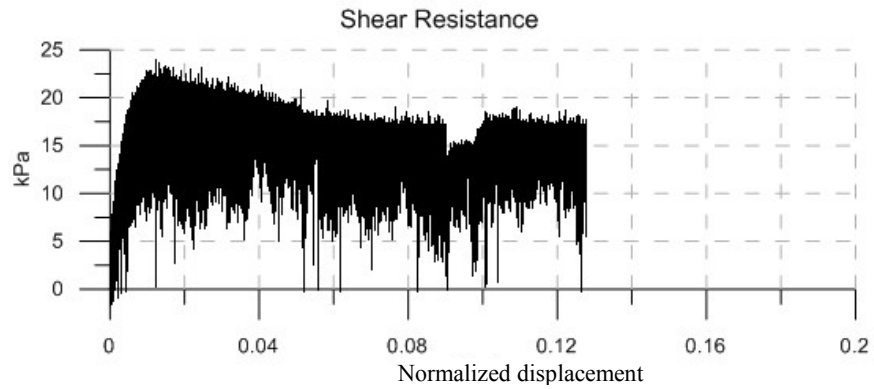

Material:	Glass Beads
Size:	0.1 mm
Normal Stress:	23 kPa
Vibration Frequency:	140 Hz
Vibration Force:	7.14 N
Vibration Duration:	50 sec
Horizontal Acceleration:	0.5 g
Vertical Acceleration:	0.14 g
Horizontal Amplitude:	6.3×10^{-3} mm
Vertical Amplitude:	1.8×10^{-3} mm
Peak Strength:	22 kPa
Residual Strength:	17 kPa
Vibro-Residual Strength:	13 kPa

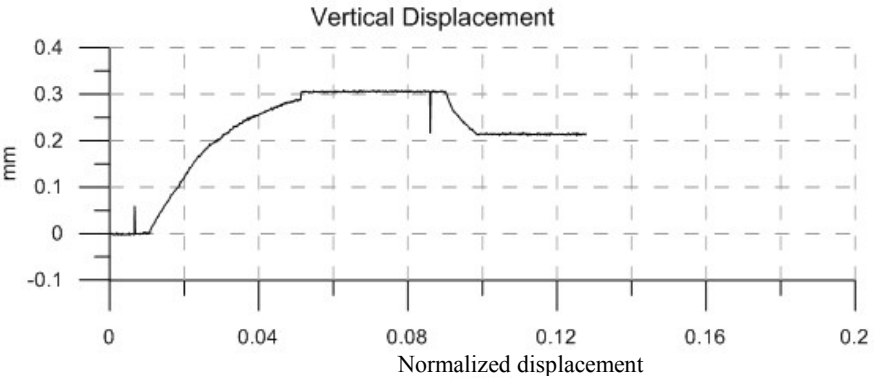

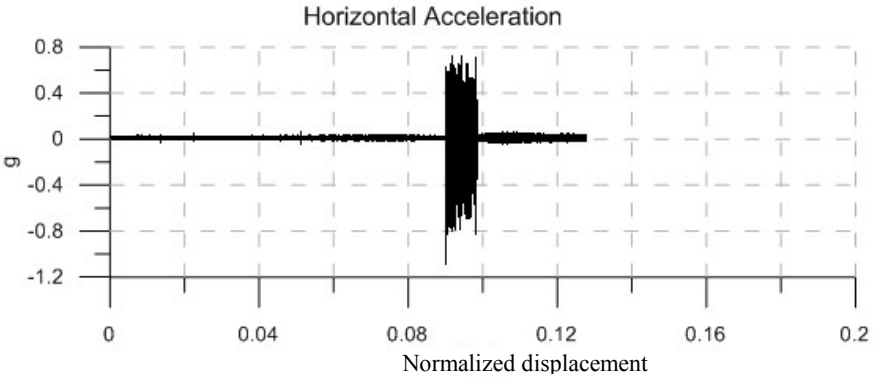

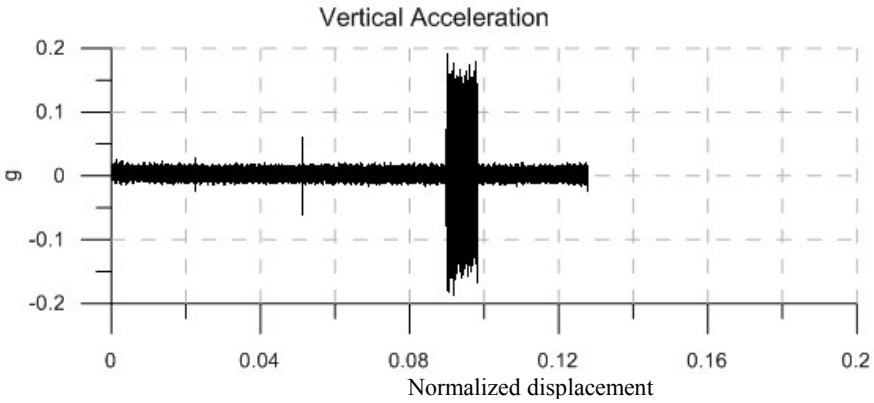

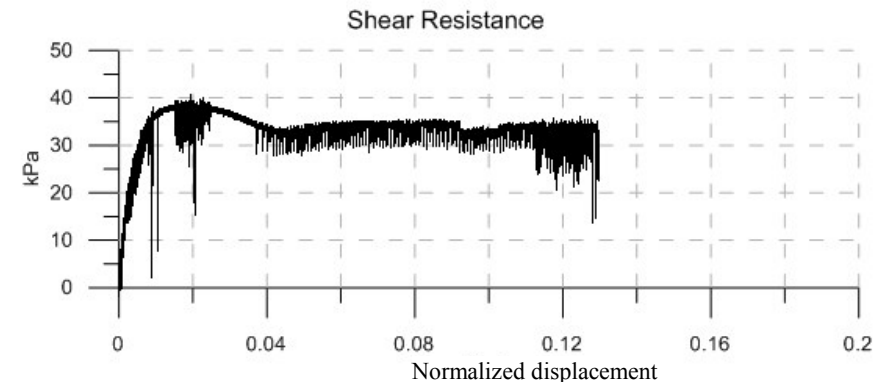

Material:	Glass Beads
Size:	0.1 mm
Normal Stress:	50 kPa
Vibration Frequency:	140 Hz
Vibration Force:	1.61 N
Vibration Duration:	59 sec
Horizontal Acceleration:	0.11 g
Vertical Acceleration:	0.03 g
Horizontal Amplitude:	1.4×10^{-3} mm
Vertical Amplitude:	0.4×10^{-3} mm
Peak Strength:	38.5 kPa
Residual Strength:	35 kPa
Vibro-Residual Strength:	33 kPa

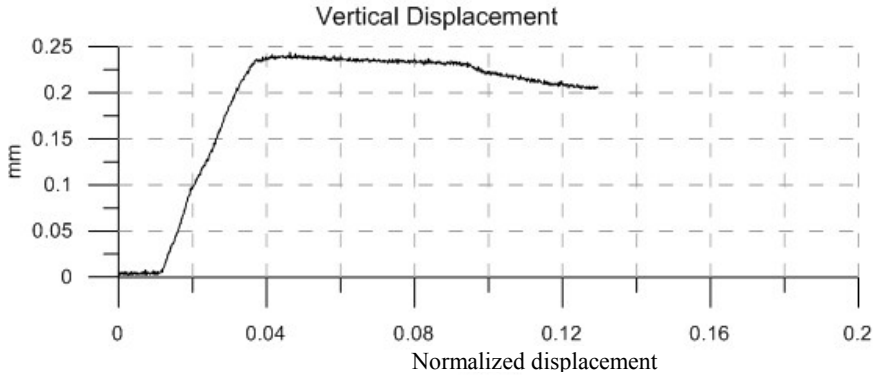

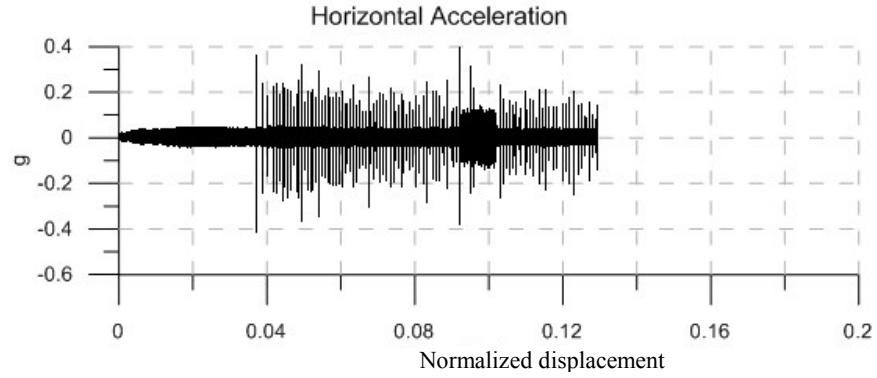

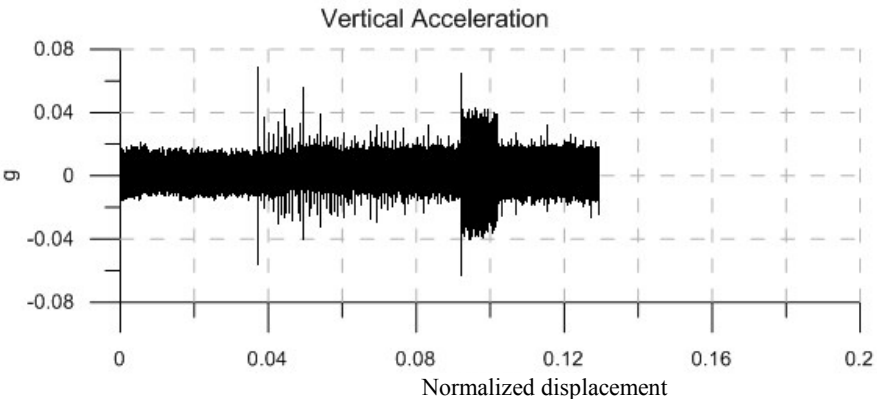

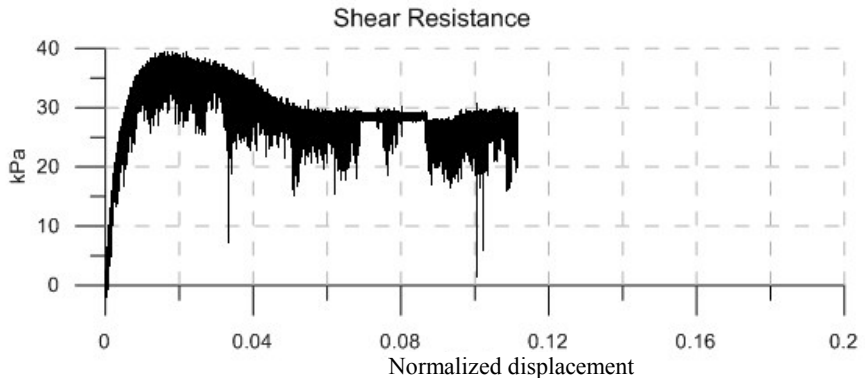

Material:	Glass Beads
Size:	0.1 mm
Normal Stress:	50 kPa
Vibration Frequency:	140 Hz
Vibration Force:	3.22 N
Vibration Duration:	42 sec
Horizontal Acceleration:	0.23 g
Vertical Acceleration:	0.08 g
Horizontal Amplitude:	2.9×10^{-3} mm
Vertical Amplitude:	1.0×10^{-3} mm
Peak Strength:	38.5 kPa
Residual Strength:	29 kPa
Vibro-Residual Strength:	26.5 kPa

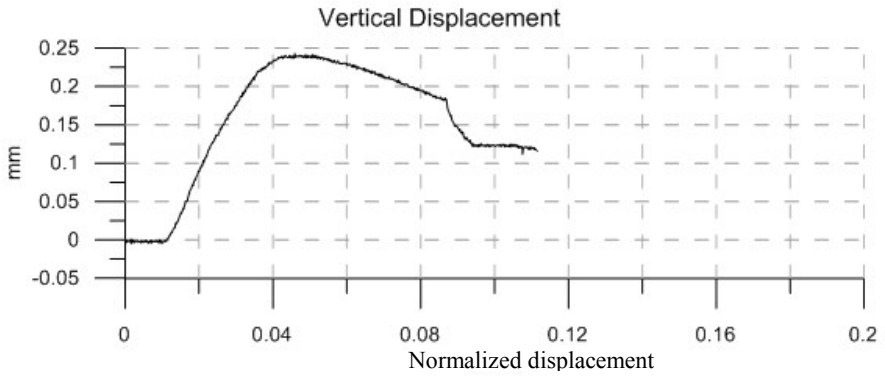

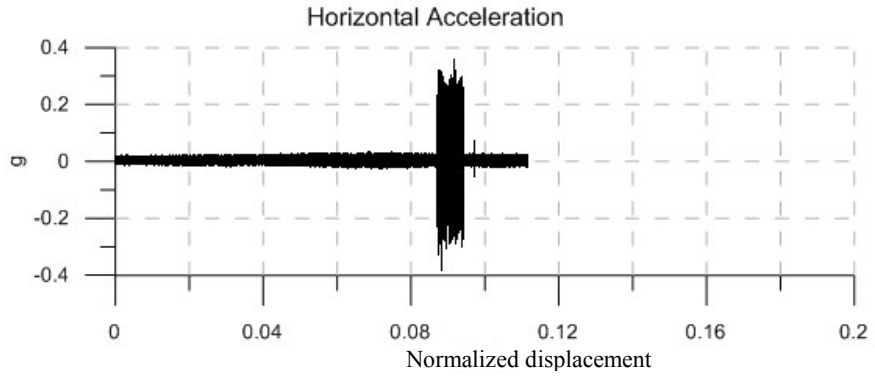

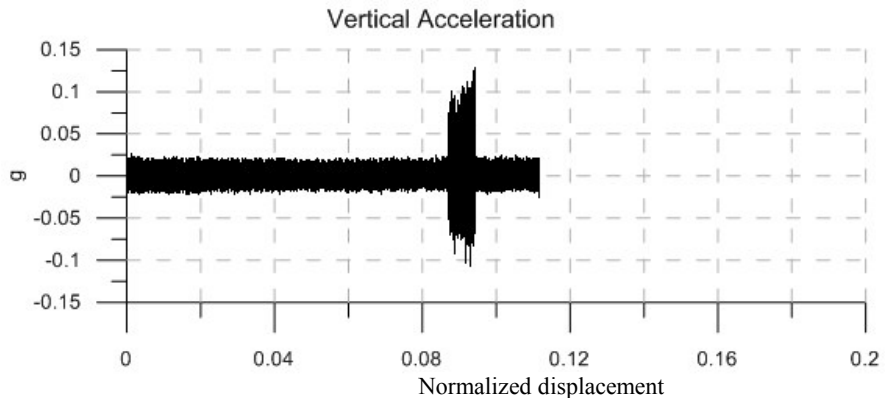

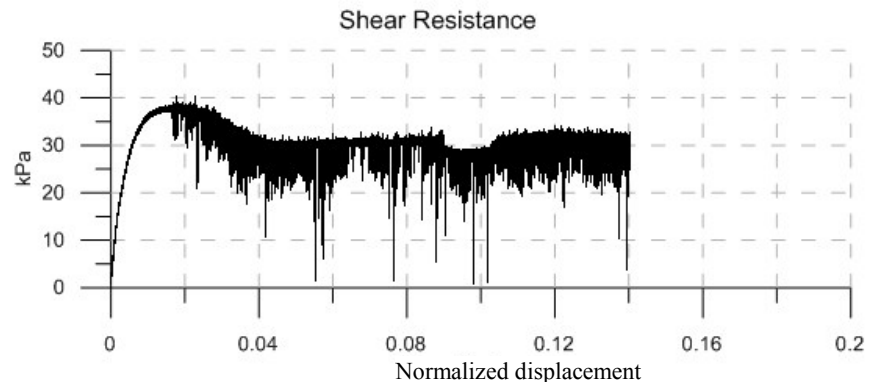

Material:	Glass Beads
Size:	0.1 mm
Normal Stress:	50 kPa
Vibration Frequency:	140 Hz
Vibration Force:	3.71 N
Vibration Duration:	74 sec
Horizontal Acceleration:	0.28 g
Vertical Acceleration:	0.09 g
Horizontal Amplitude:	3.5×10^{-3} mm
Vertical Amplitude:	1.1×10^{-3} mm
Peak Strength:	38 kPa
Residual Strength:	31.5 kPa
Vibro-Residual Strength:	28 kPa

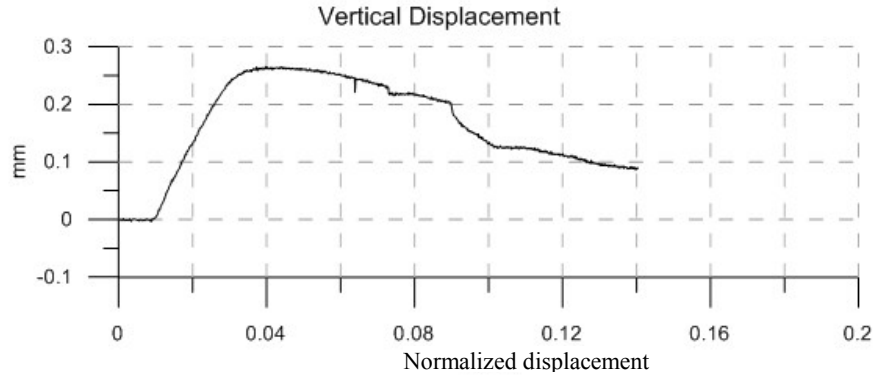

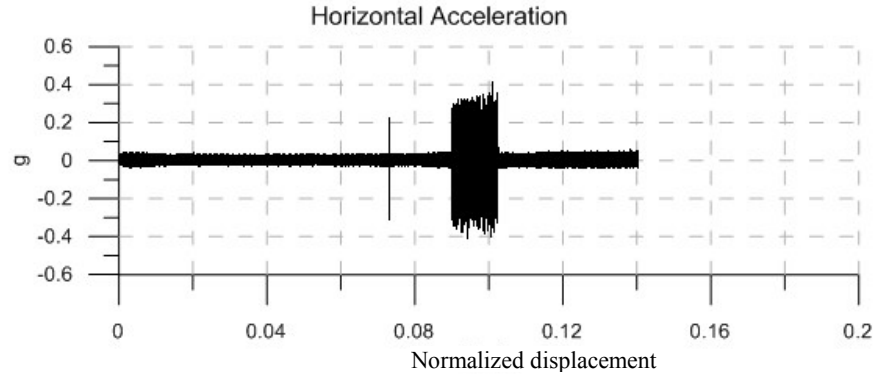

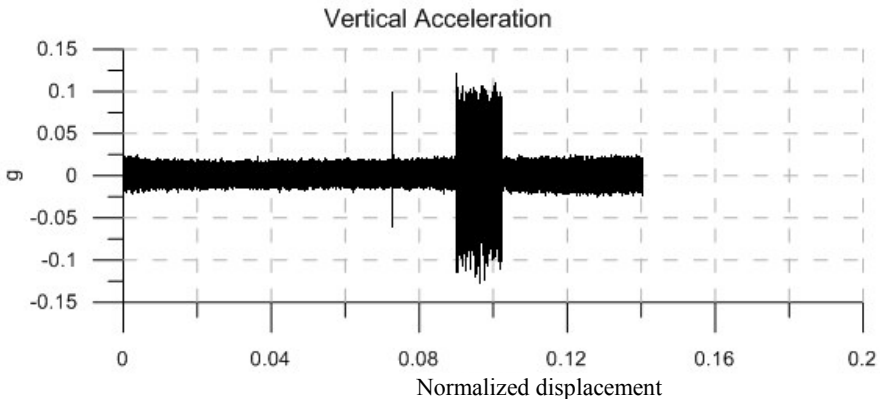

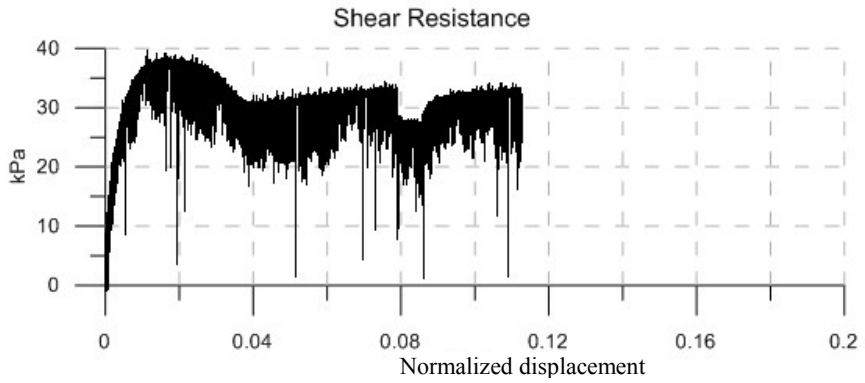

Material:	Glass Beads
Size:	0.1 mm
Normal Stress:	50 kPa
Vibration Frequency:	140 Hz
Vibration Force:	5.18 N
Vibration Duration:	40 sec
Horizontal Acceleration:	0.38 g
Vertical Acceleration:	0.11 g
Horizontal Amplitude:	4.8×10^{-3} mm
Vertical Amplitude:	1.4×10^{-3} mm
Peak Strength:	38 kPa
Residual Strength:	32.5 kPa
Vibro-Residual Strength:	26 kPa

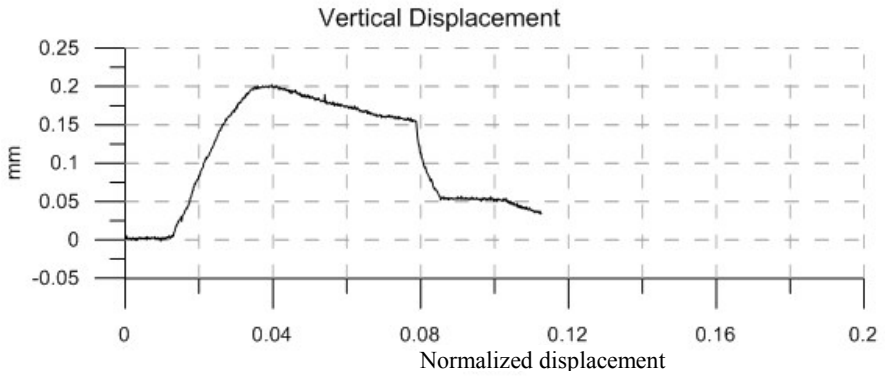

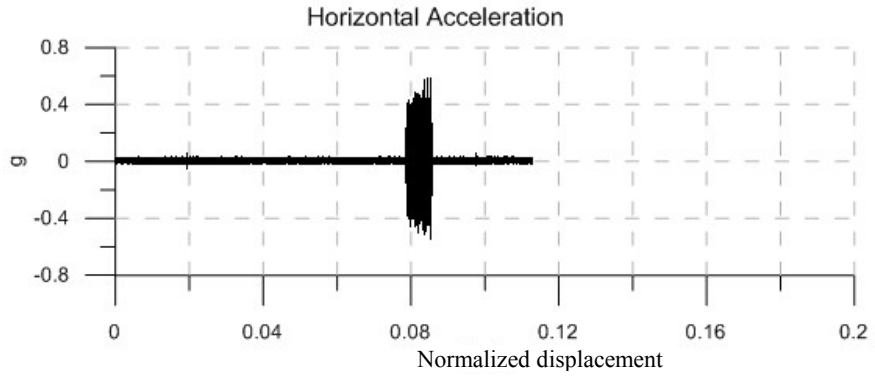

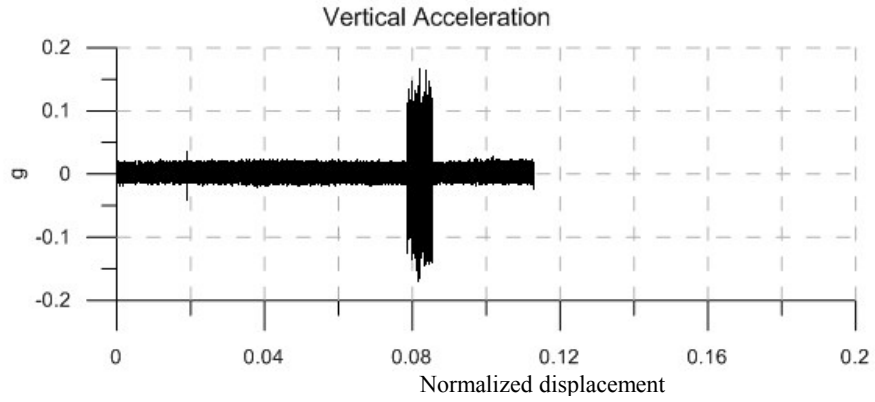

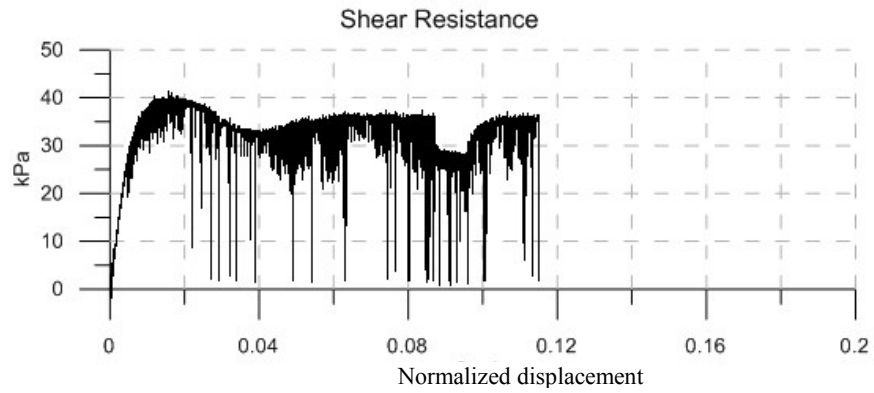

Material:	Glass Beads
Size:	0.1 mm
Normal Stress:	50 kPa
Vibration Frequency:	140 Hz
Vibration Force:	7.14 N
Vibration Duration:	51 sec
Horizontal Acceleration:	0.43 g
Vertical Acceleration:	0.13 g
Horizontal Amplitude:	5.5×10^{-3} mm
Vertical Amplitude:	1.6×10^{-3} mm
Peak Strength:	39.5 kPa
Residual Strength:	36 kPa
Vibro-Residual Strength:	26.5 kPa

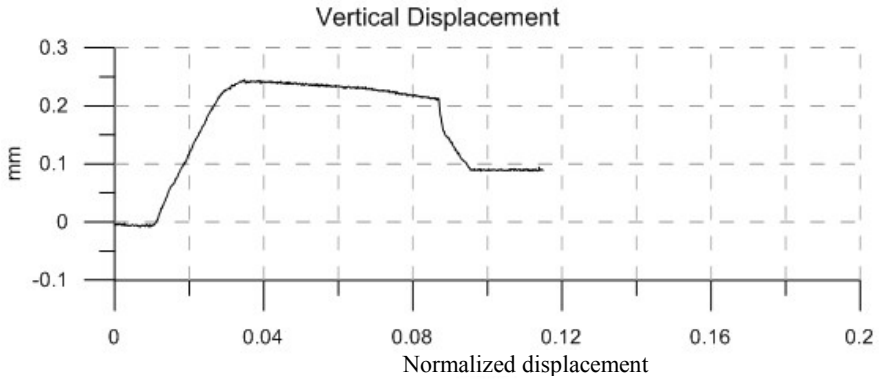

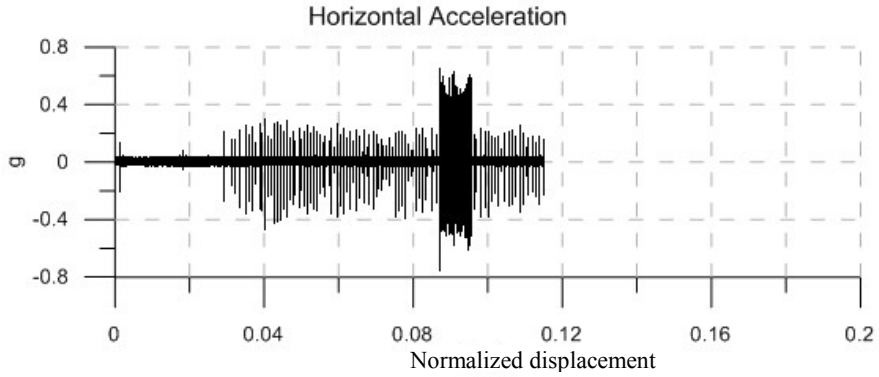

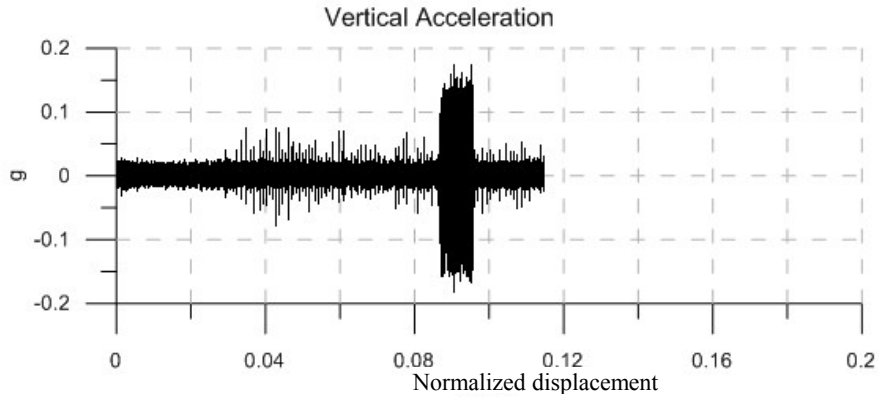

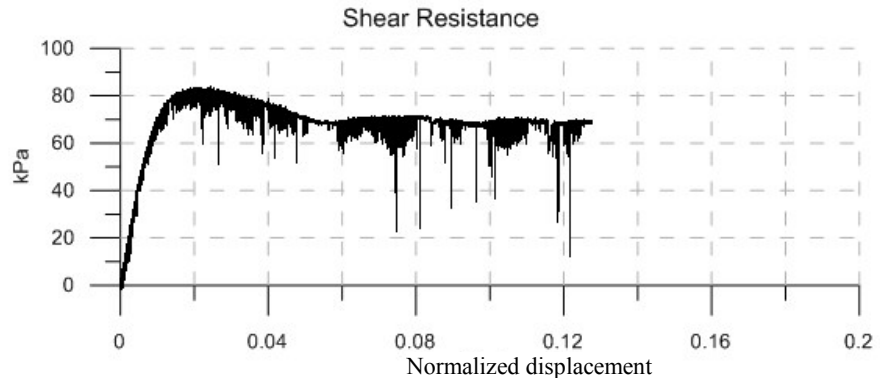

Material:	Glass Beads
Size:	0.1 mm
Normal Stress:	118 kPa
Vibration Frequency:	140 Hz
Vibration Force:	1.61 N
Vibration Duration:	93 sec
Horizontal Acceleration:	0.12 g
Vertical Acceleration:	0.04 g
Horizontal Amplitude:	1.5×10^{-3} mm
Vertical Amplitude:	0.5×10^{-3} mm
Peak Strength:	82.5 kPa
Residual Strength:	71 kPa
Vibro-Residual Strength:	68 kPa

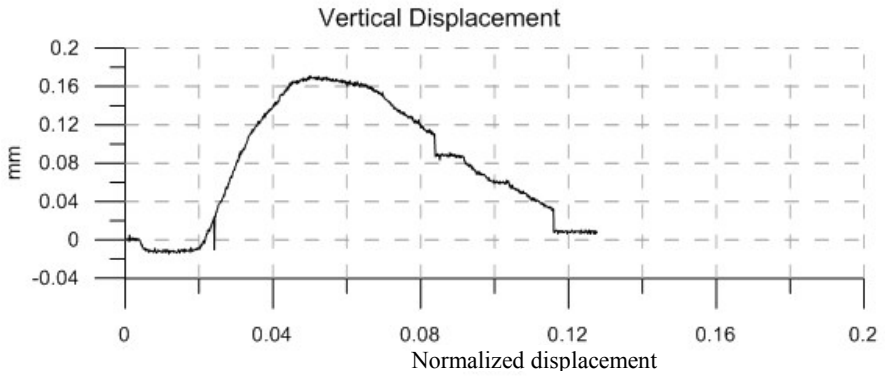

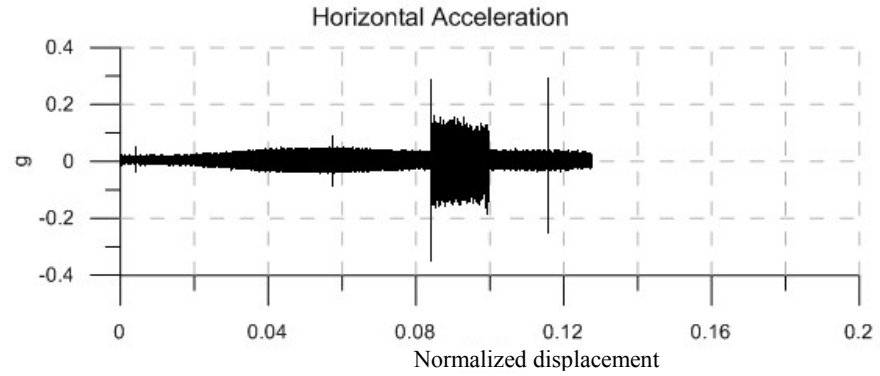

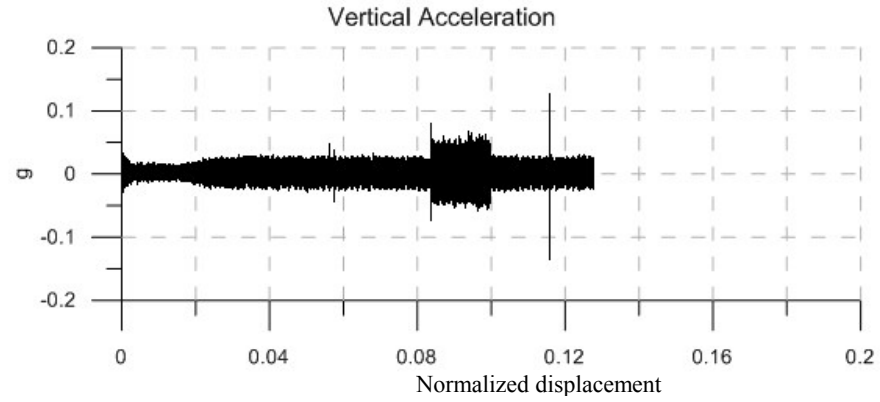

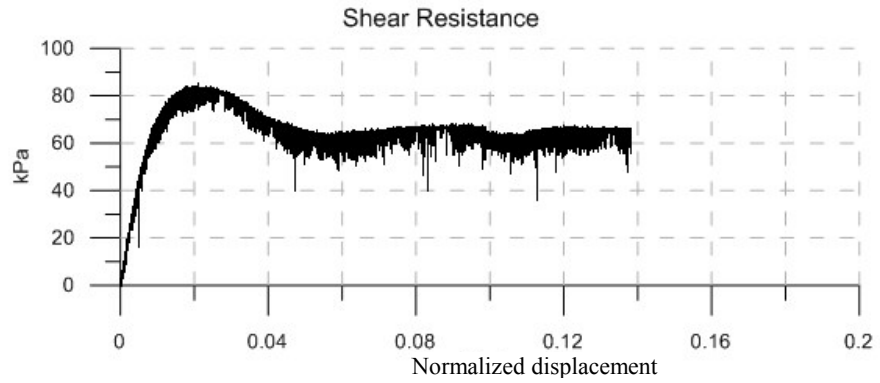

Material:	Glass Beads
Size:	0.1 mm
Normal Stress:	118 kPa
Vibration Frequency:	140 Hz
Vibration Force:	3.22 N
Vibration Duration:	64 sec
Horizontal Acceleration:	0.22 g
Vertical Acceleration:	0.07 g
Horizontal Amplitude:	2.9×10^{-3} mm
Vertical Amplitude:	1.0×10^{-3} mm
Peak Strength:	83.5 kPa
Residual Strength:	67 kPa
Vibro-Residual Strength:	63 kPa

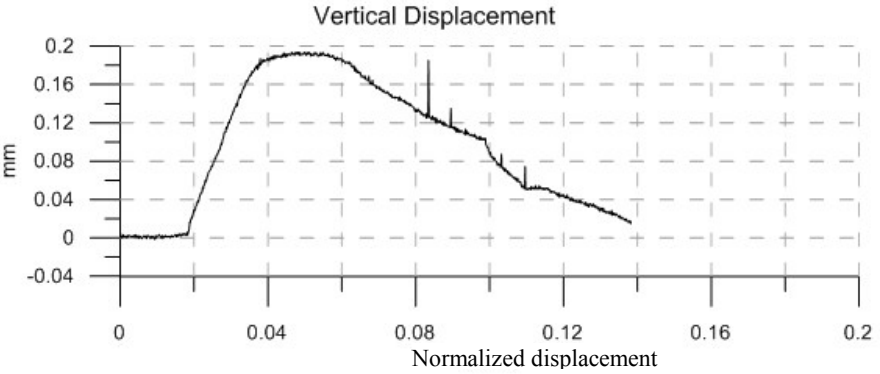

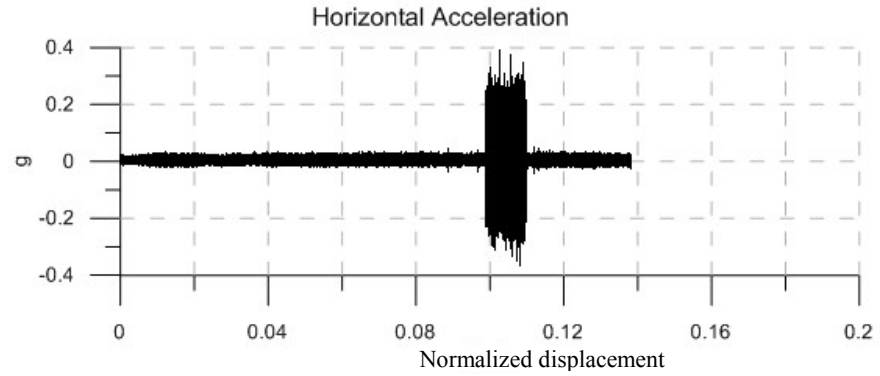

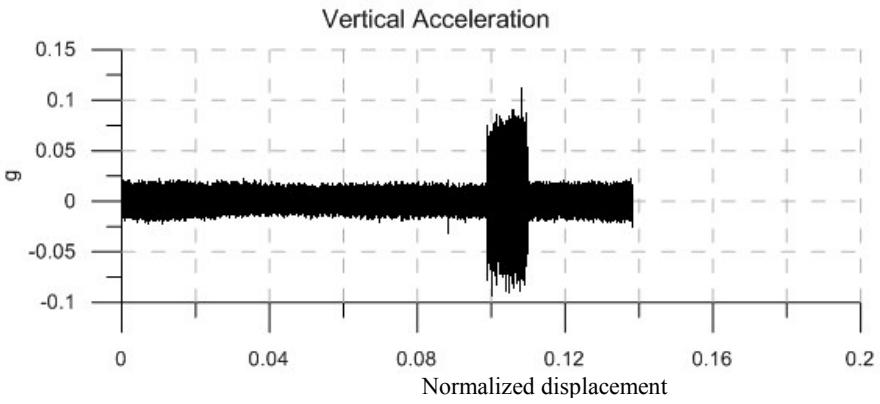

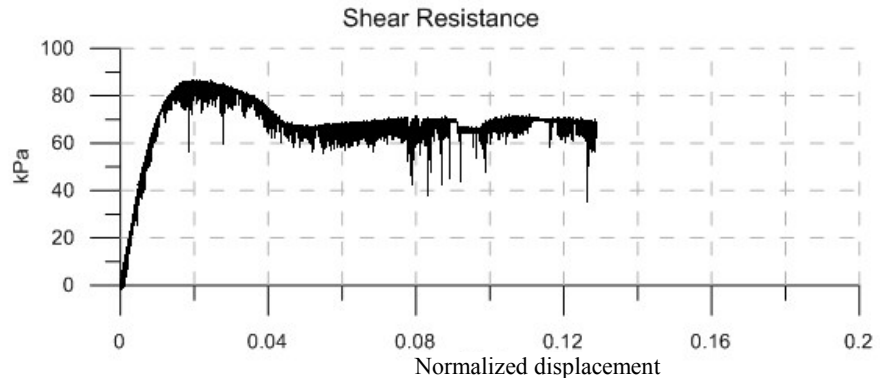

Material:	Glass Beads
Size:	0.1 mm
Normal Stress:	118 kPa
Vibration Frequency:	140 Hz
Vibration Force:	3.71 N
Vibration Duration:	39 sec
Horizontal Acceleration:	0.24 g
Vertical Acceleration:	0.08 g
Horizontal Amplitude:	3.0×10^{-3} mm
Vertical Amplitude:	1.0×10^{-3} mm
Peak Strength:	85.5 kPa
Residual Strength:	70 kPa
Vibro-Residual Strength:	65 kPa

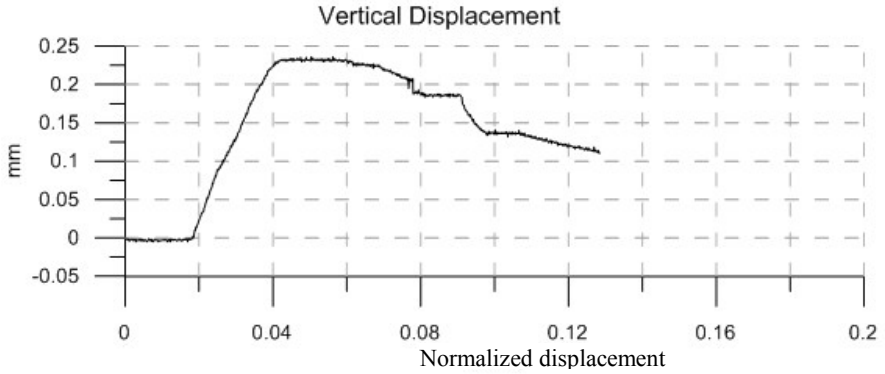

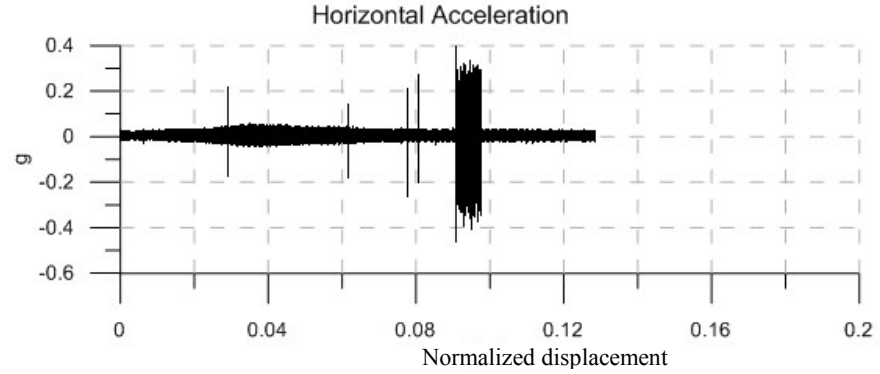

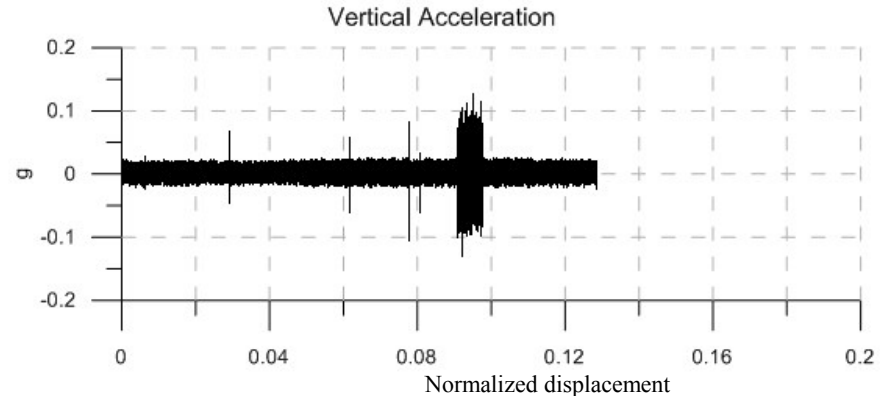

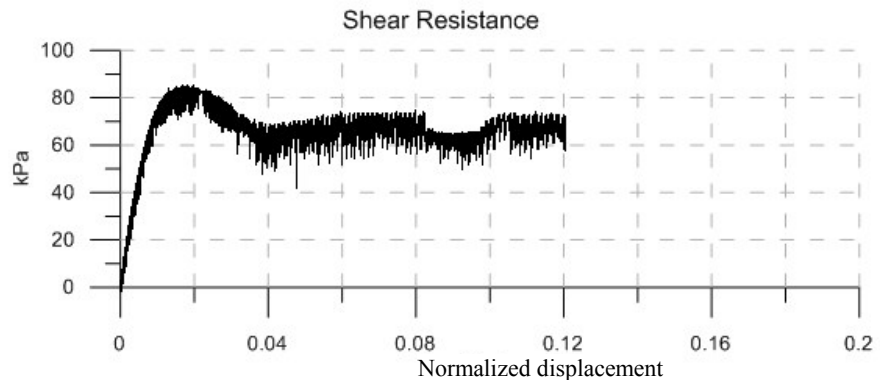

Material:	Glass Beads
Size:	0.1 mm
Normal Stress:	118 kPa
Vibration Frequency:	140 Hz
Vibration Force:	5.18 N
Vibration Duration:	88 sec
Horizontal Acceleration:	0.325 g
Vertical Acceleration:	0.105 g
Horizontal Amplitude:	4.1×10^{-3} mm
Vertical Amplitude:	1.3×10^{-3} mm
Peak Strength:	84 kPa
Residual Strength:	73 kPa
Vibro-Residual Strength:	63 kPa

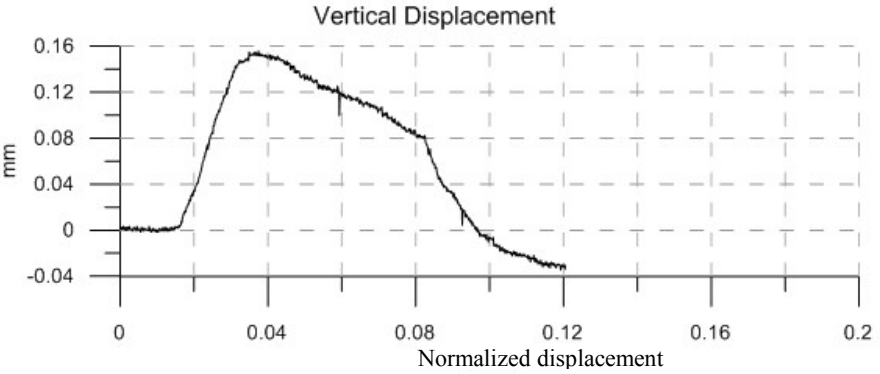

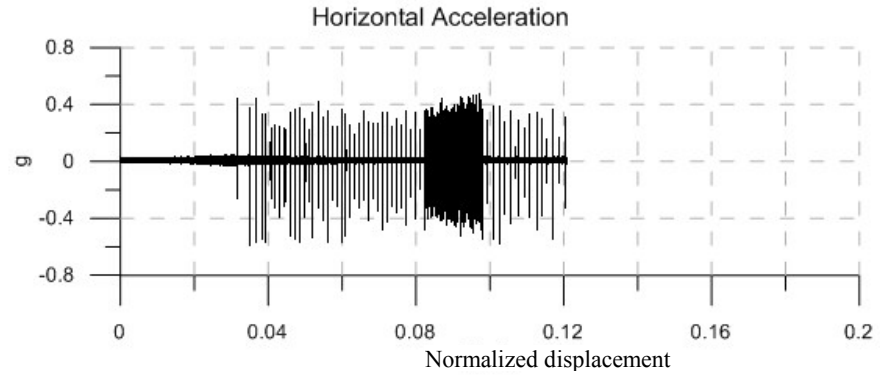

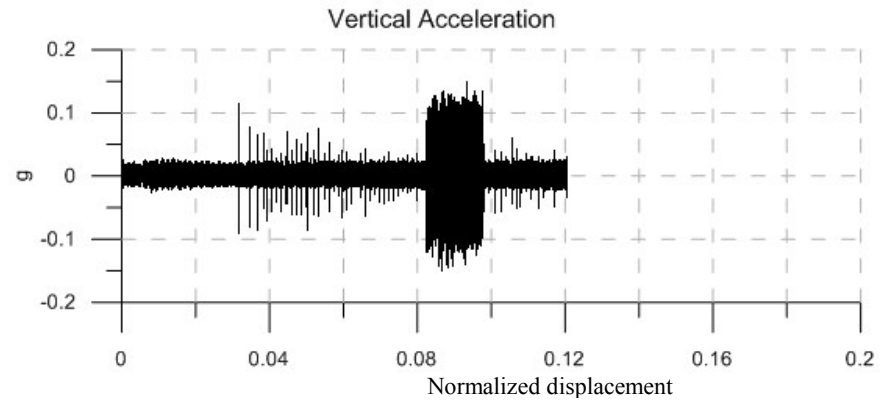

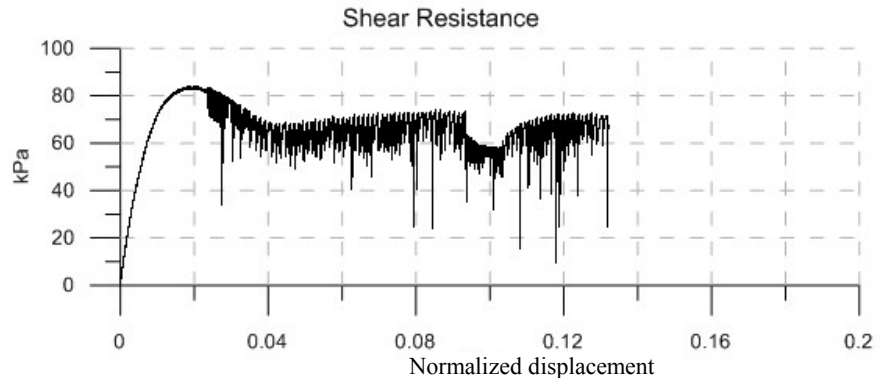

Material:	Glass Beads
Size:	0.1 mm
Normal Stress:	118 kPa
Vibration Frequency:	140 Hz
Vibration Force:	7.14 N
Vibration Duration:	59 sec
Horizontal Acceleration:	0.43 g
Vertical Acceleration:	0.15 g
Horizontal Amplitude:	5.5×10^{-3} mm
Vertical Amplitude:	1.9×10^{-3} mm
Peak Strength:	83.5 kPa
Residual Strength:	73 kPa
Vibro-Residual Strength:	56 kPa

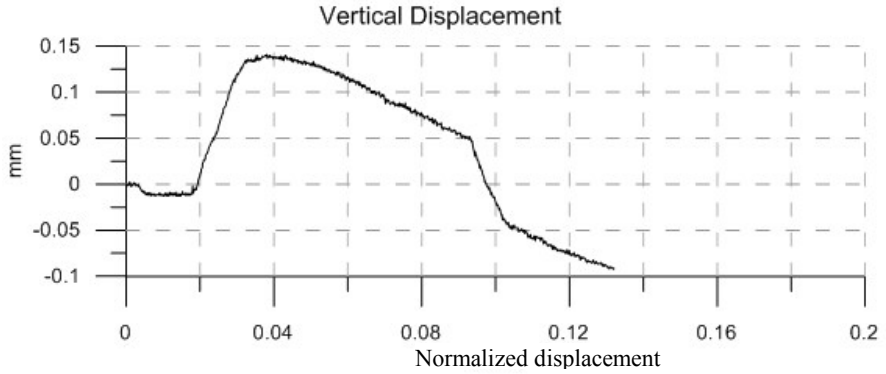

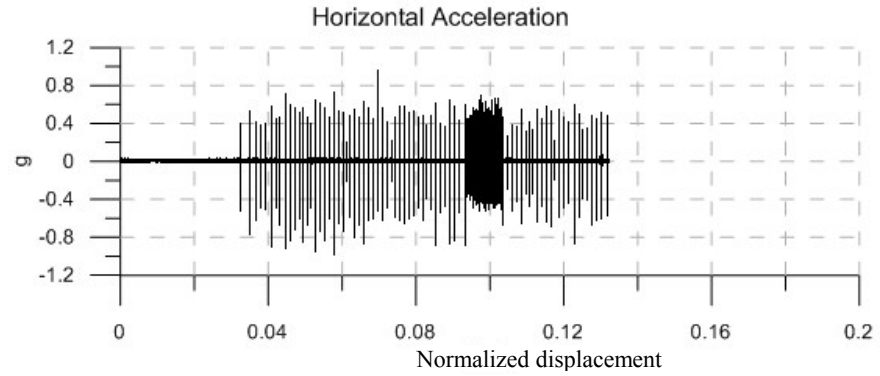

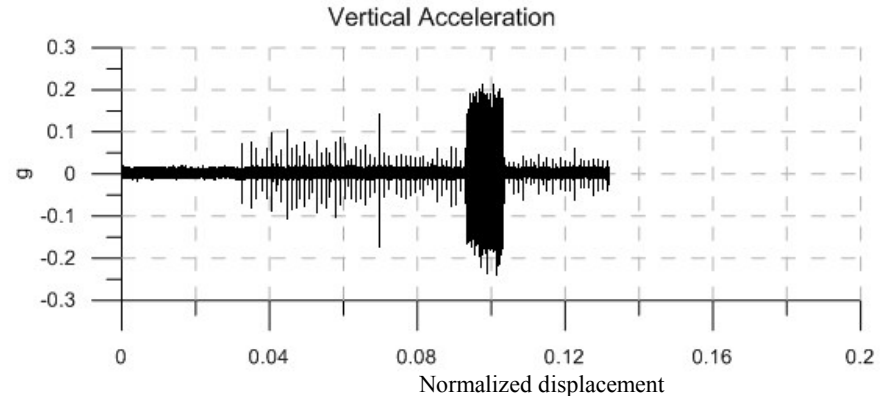

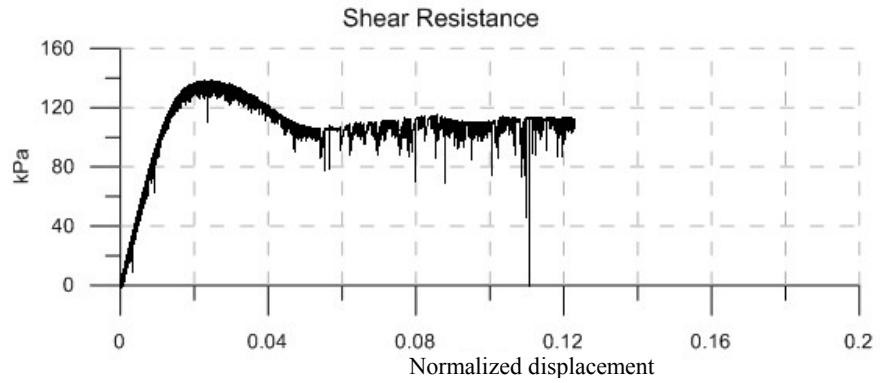

Material:	Glass Beads
Size:	0.1 mm
Normal Stress:	200 kPa
Vibration Frequency:	140 Hz
Vibration Force:	1.61 N
Vibration Duration:	77 sec
Horizontal Acceleration:	0.12 g
Vertical Acceleration:	0.04 g
Horizontal Amplitude:	1.5×10^{-3} mm
Vertical Amplitude:	0.5×10^{-3} mm
Peak Strength:	137.5 kPa
Residual Strength:	113 kPa
Vibro-Residual Strength:	109.5 kPa

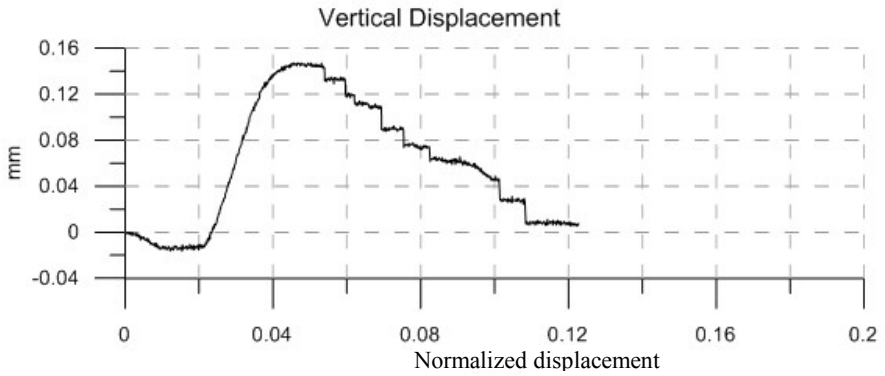

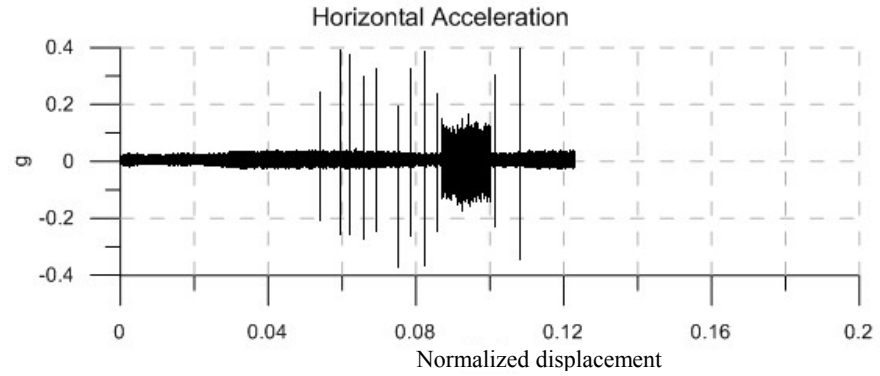

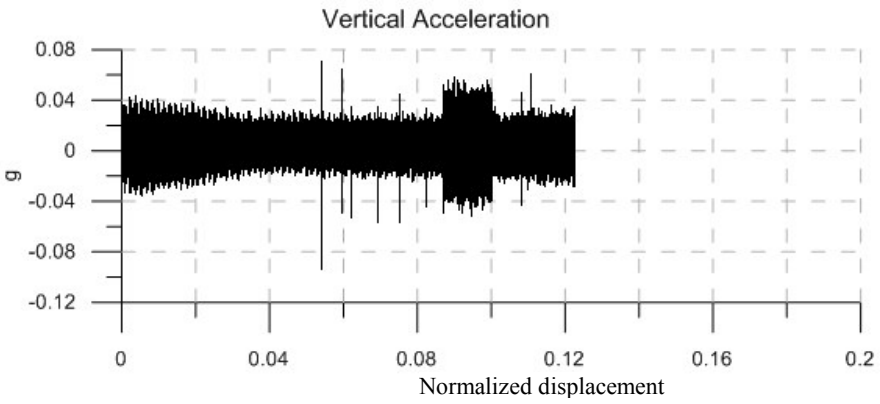

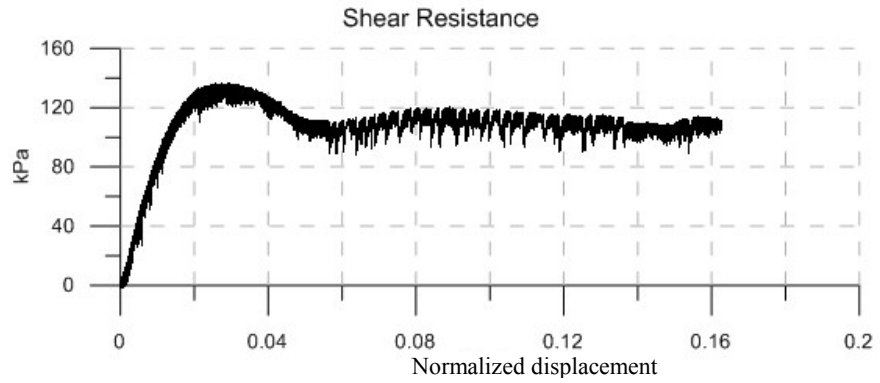

Material:	Glass Beads
Size:	0.1 mm
Normal Stress:	200 kPa
Vibration Frequency:	140 Hz
Vibration Force:	3.22 N
Vibration Duration:	85 sec
Horizontal Acceleration:	0.2 g
Vertical Acceleration:	0.065 g
Horizontal Amplitude:	2.5×10^{-3} mm
Vertical Amplitude:	0.8×10^{-3} mm
Peak Strength:	135.5 kPa
Residual Strength:	114 kPa
Vibro-Residual Strength:	108 kPa

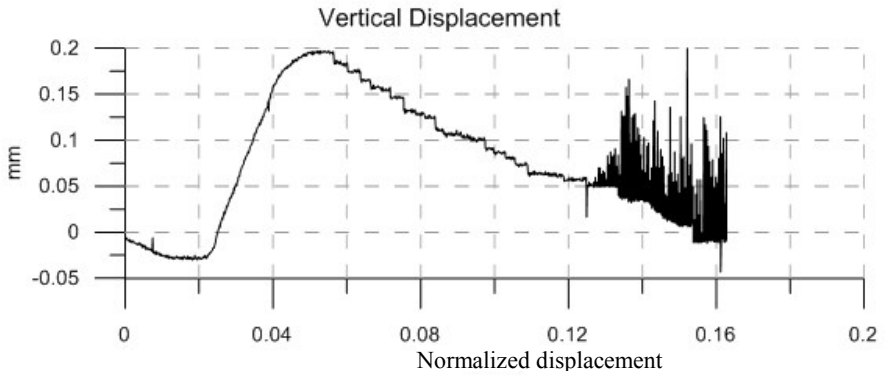

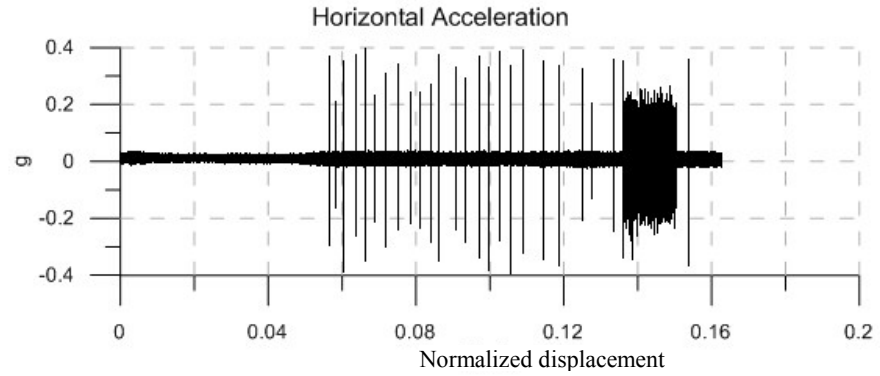

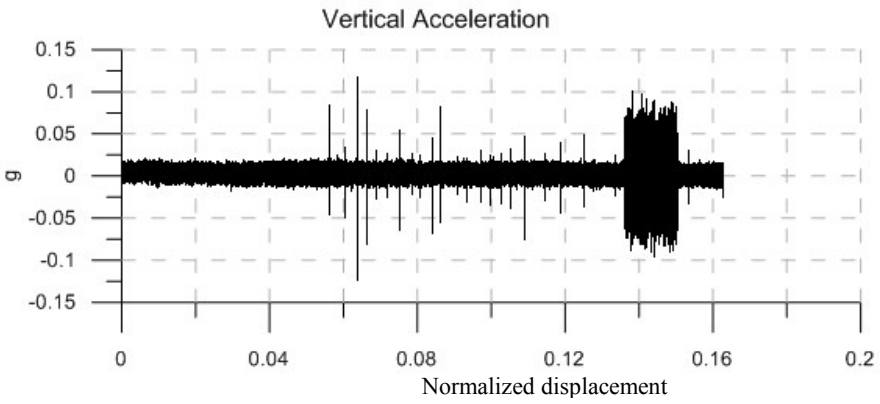

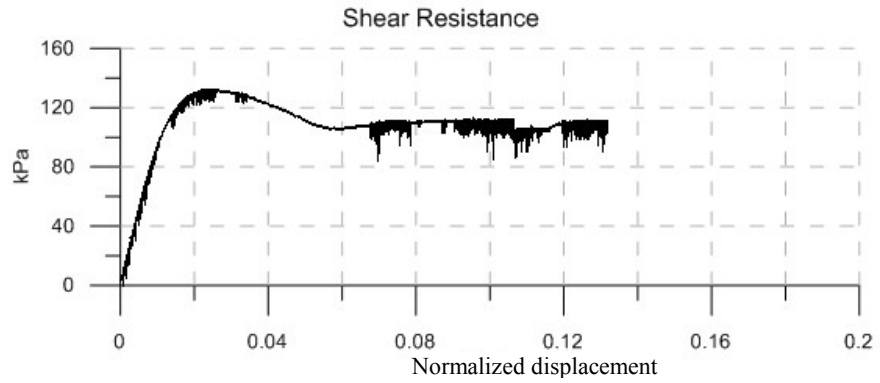

Material:	Glass Beads
Size:	0.1 mm
Normal Stress:	200 kPa
Vibration Frequency:	140 Hz
Vibration Force:	3.71 N
Vibration Duration:	56 sec
Horizontal Acceleration:	0.23 g
Vertical Acceleration:	0.07 g
Horizontal Amplitude:	2.9×10^{-3} mm
Vertical Amplitude:	0.9×10^{-3} mm
Peak Strength:	132 kPa
Residual Strength:	111.5 kPa
Vibro-Residual Strength:	105 kPa

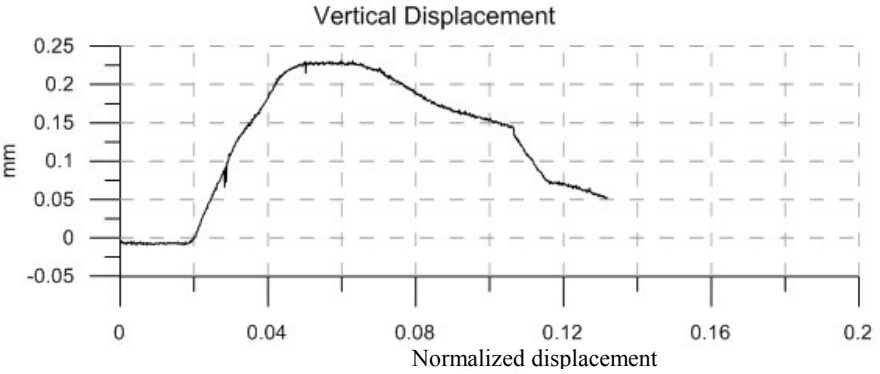

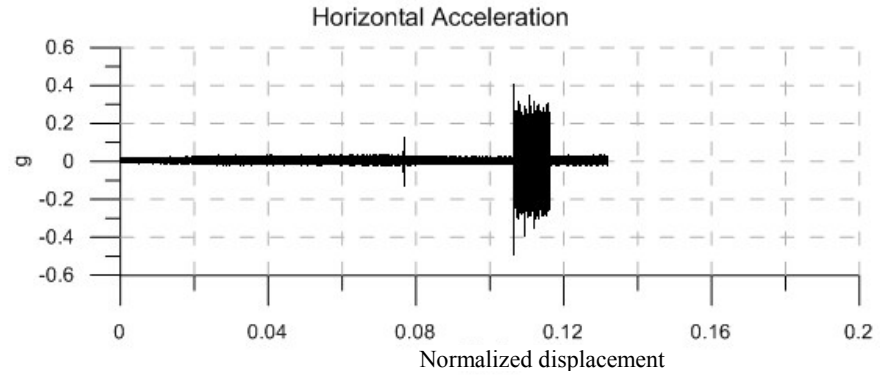

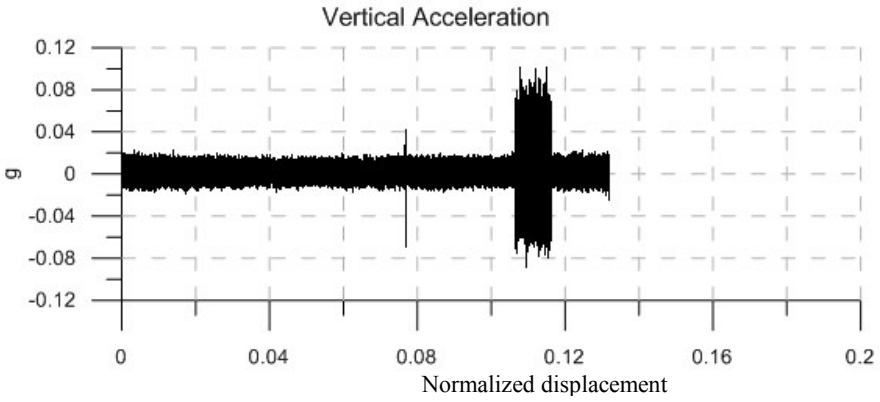

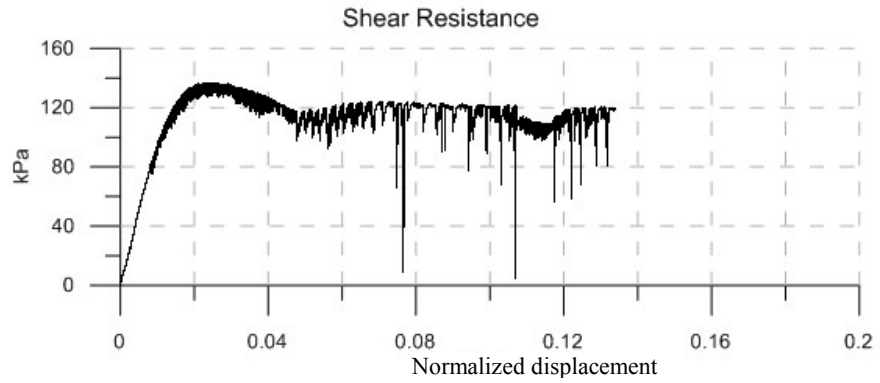

Material:	Glass Beads
Size:	0.1 mm
Normal Stress:	200 kPa
Vibration Frequency:	140 Hz
Vibration Force:	5.18 N
Vibration Duration:	57 sec
Horizontal Acceleration:	0.3 g
Vertical Acceleration:	0.09 g
Horizontal Amplitude:	3.8×10^{-3} mm
Vertical Amplitude:	1.1×10^{-3} mm
Peak Strength:	136 kPa
Residual Strength:	121 kPa
Vibro-Residual Strength:	108 kPa

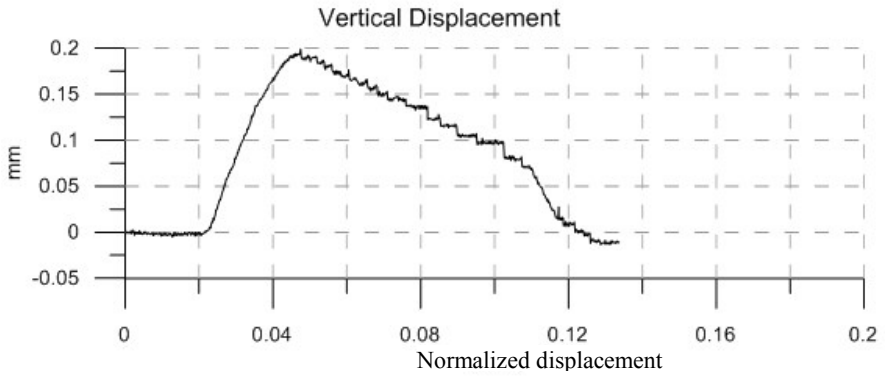

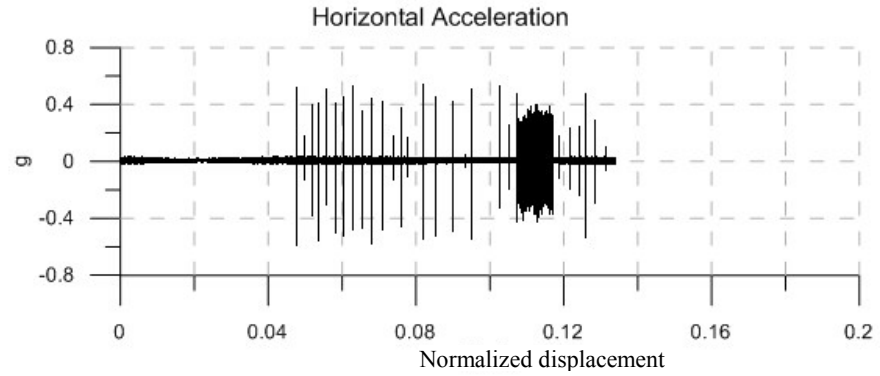

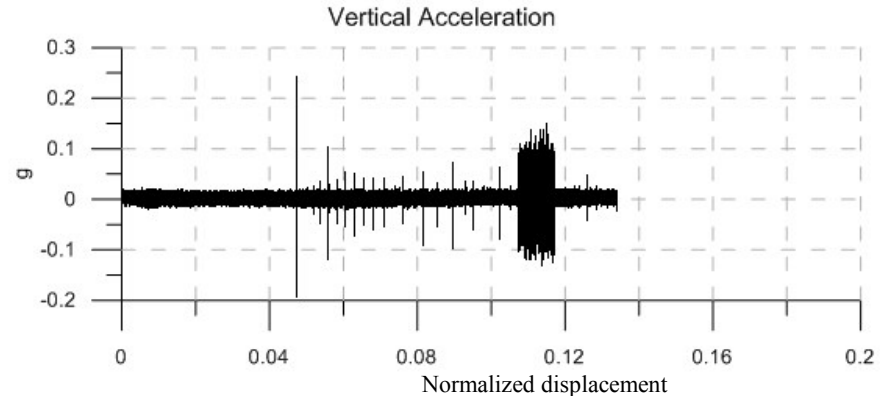

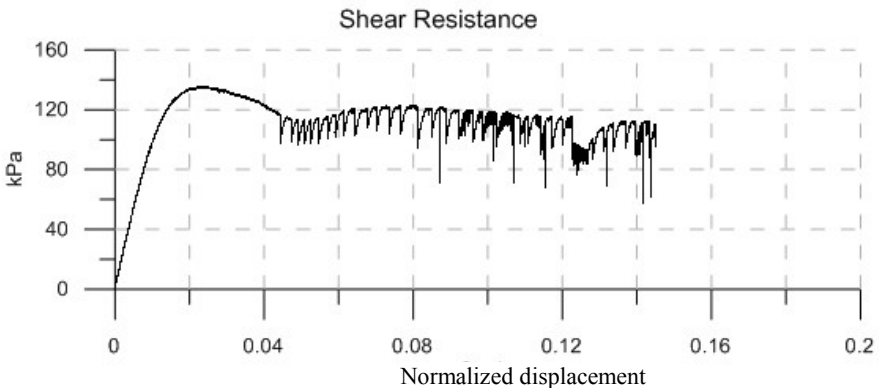

Material:	Glass Beads
Size:	0.1 mm
Normal Stress:	200 kPa
Vibration Frequency:	140 Hz
Vibration Force:	7.14 N
Vibration Duration:	26 sec
Horizontal Acceleration:	0.38 g
Vertical Acceleration:	0.13 g
Horizontal Amplitude:	4.8×10^{-3} mm
Vertical Amplitude:	1.6×10^{-3} mm
Peak Strength:	135 kPa
Residual Strength:	115 kPa
Vibro-Residual Strength:	94 kPa

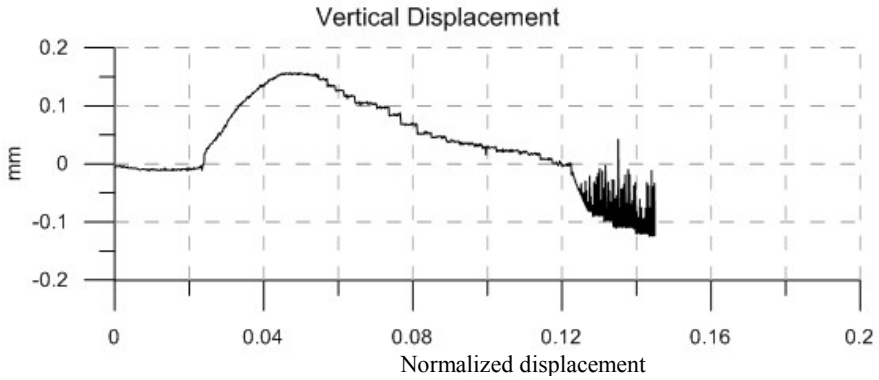

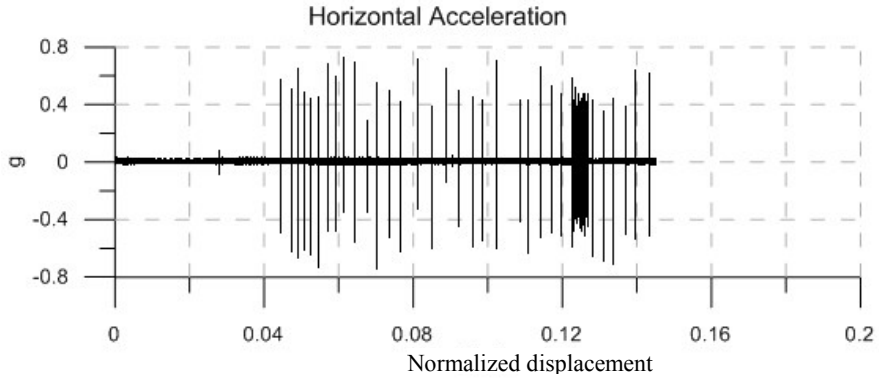

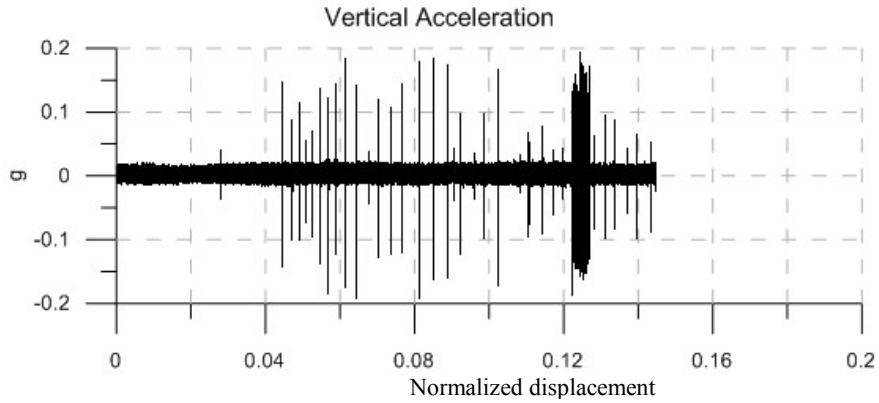

Part 3

The plots provided in this section were used in Chapter 5. Following are the test results of 18 samples of fine sand, 18 samples of coarse sand and 24 samples of 0.55 mm glass beads tested in strain-controlled mode at 8 kPa, 23 kPa, 36 kPa, 50 kPa, 118 kPa and 200 kPa normal stresses, different vibration intensities and 60 Hz vibration frequency.

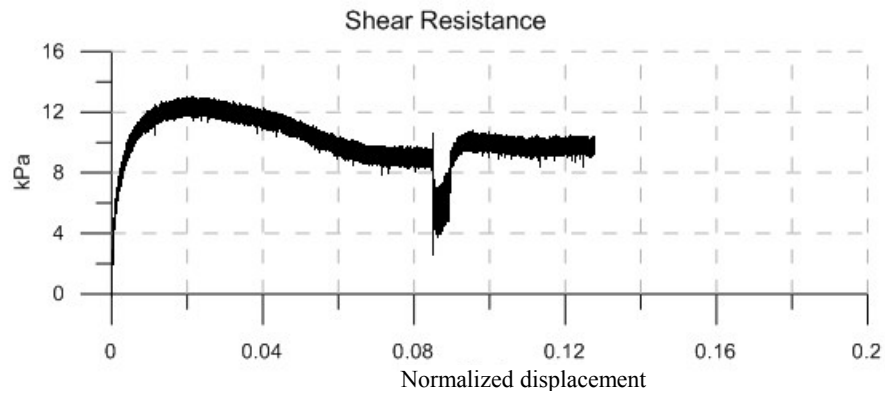

Material:	Sand
Size:	Fine
Normal Stress:	8 kPa
Vibration Frequency:	60 Hz
Vibration Duration:	25 sec
Horizontal Acceleration:	0.43 g
Vertical Acceleration:	0.07 g
Horizontal Amplitude:	0.0297 mm
Vertical Amplitude:	0.0048 mm
Peak Strength:	12.5 kPa
Residual Strength:	9 kPa
Vibro-Residual Strength:	5 kPa

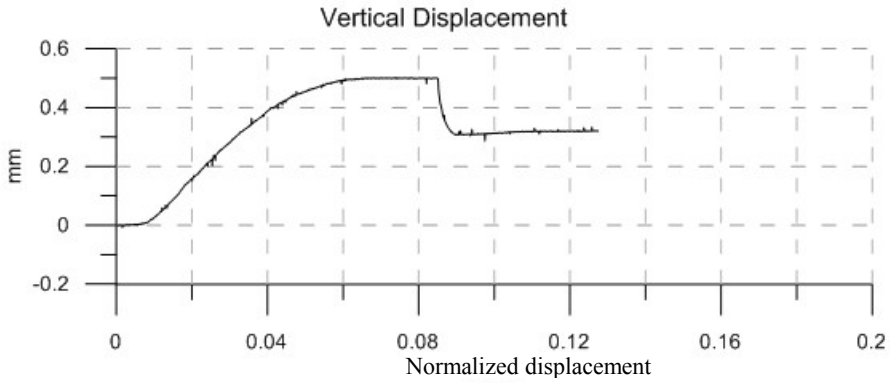

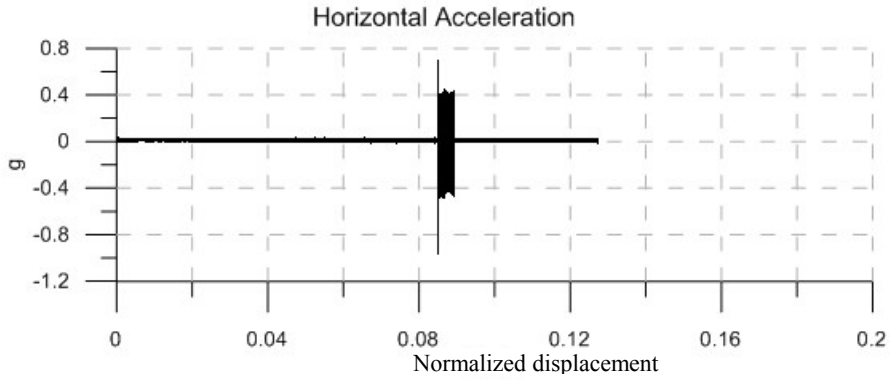

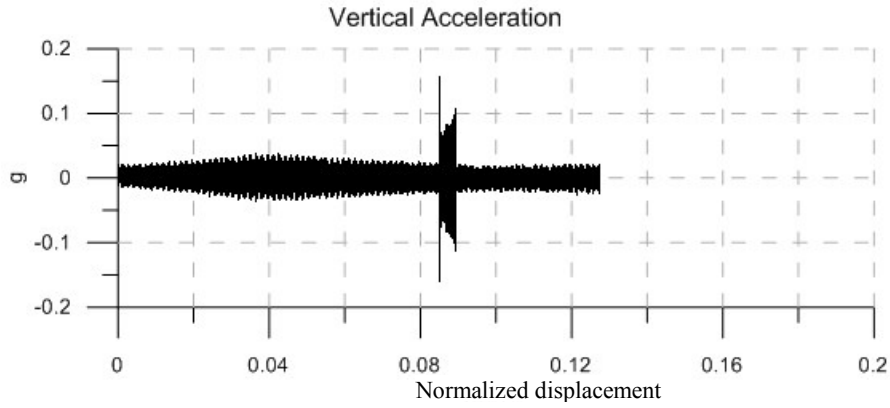

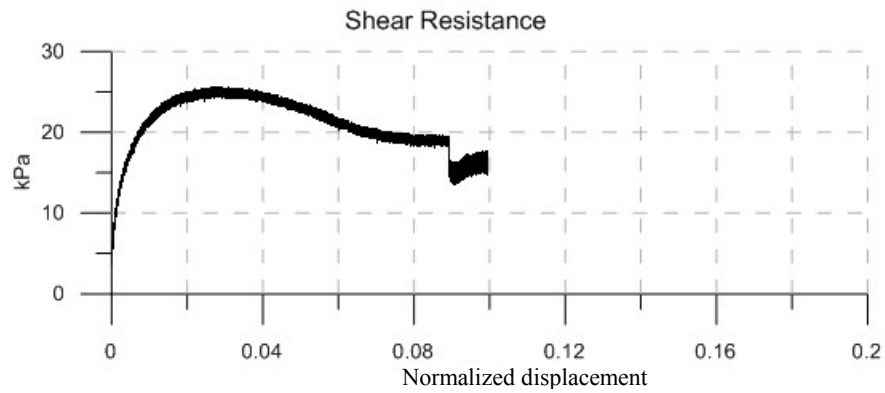

Material:	Sand
Size:	Fine
Normal Stress:	23 kPa
Vibration Frequency:	60 Hz
Vibration Duration:	61 sec
Horizontal Acceleration:	0.43 g
Vertical Acceleration:	0.14 g
Horizontal Amplitude:	0.0297 mm
Vertical Amplitude:	0.0097 mm
Peak Strength:	25 kPa
Residual Strength:	19 kPa
Vibro-Residual Strength:	14.5 kPa

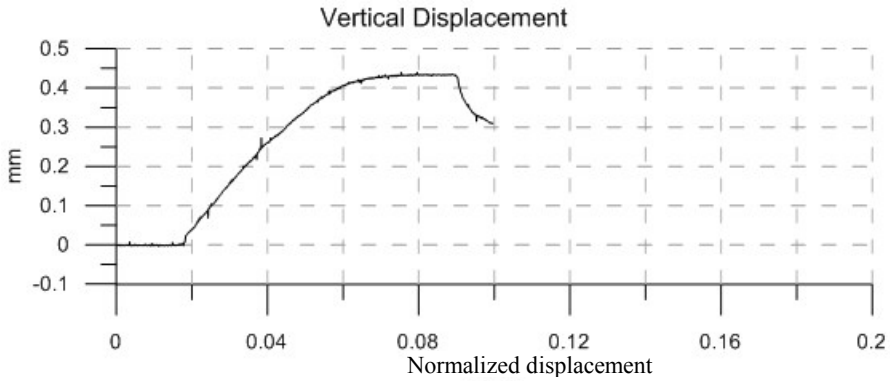

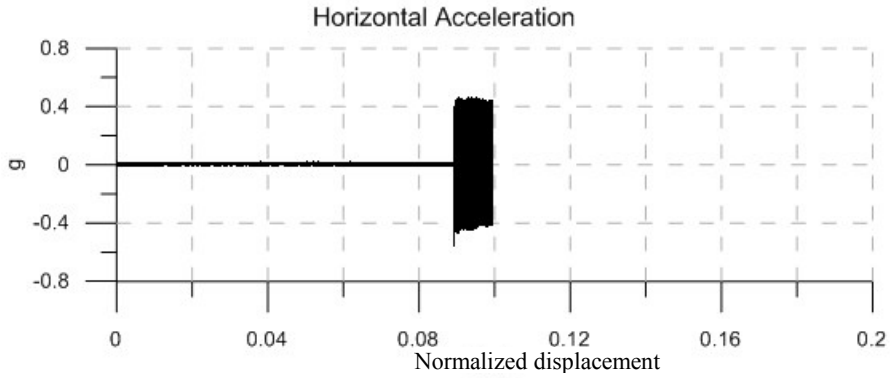

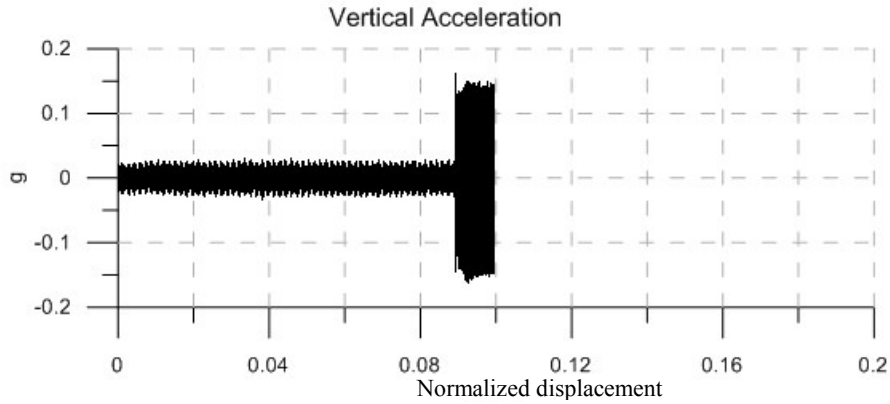

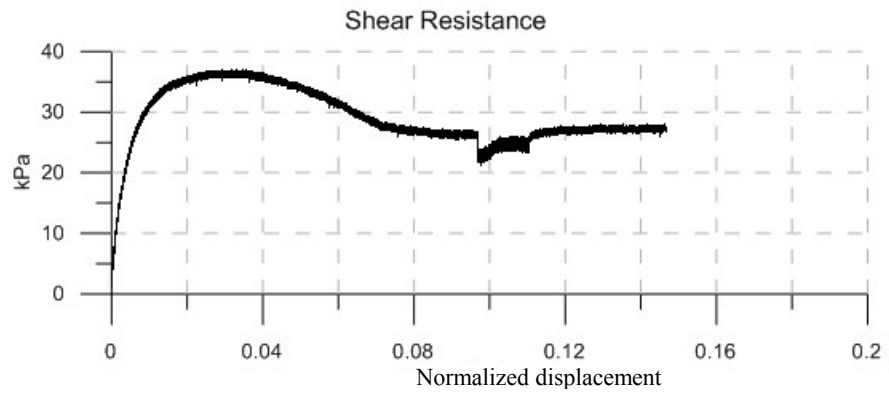

Material:	Sand
Size:	Fine
Normal Stress:	36 kPa
Vibration Frequency:	60 Hz
Vibration Duration:	80 sec
Horizontal Acceleration:	0.4 g
Vertical Acceleration:	0.13 g
Horizontal Amplitude:	0.0276 mm
Vertical Amplitude:	0.0090 mm
Peak Strength:	36.5 kPa
Residual Strength:	26.5 kPa
Vibro-Residual Strength:	22.5 kPa

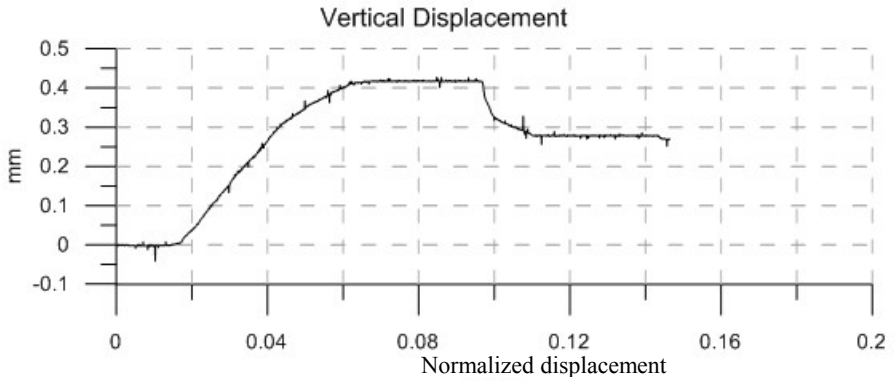

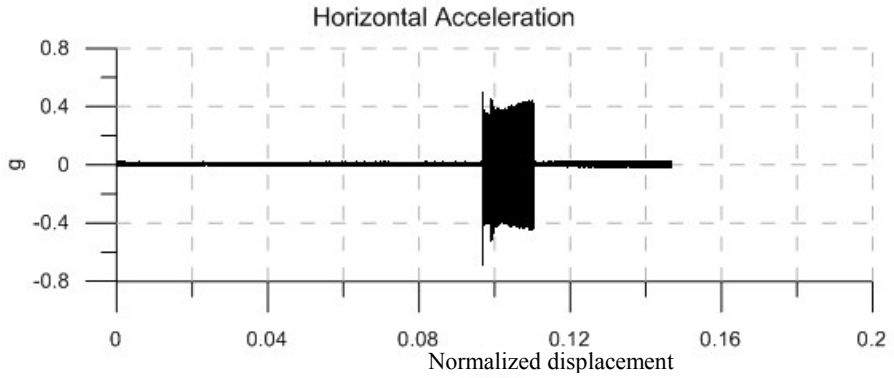

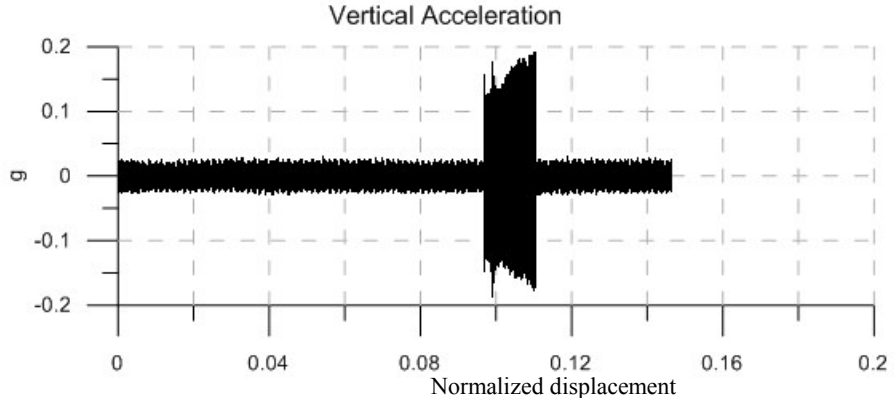

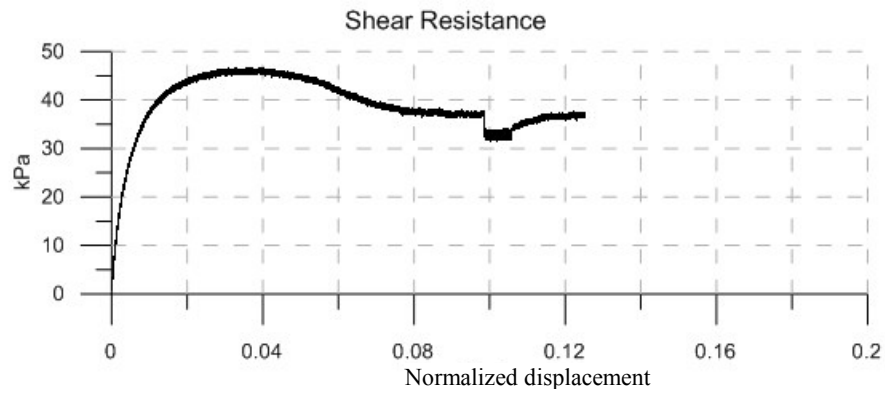

Material:	Sand
Size:	Fine
Normal Stress:	50 kPa
Vibration Frequency:	60 Hz
Vibration Duration:	43 sec
Horizontal Acceleration:	0.41 g
Vertical Acceleration:	0.13 g
Horizontal Amplitude:	0.0283 mm
Vertical Amplitude:	0.0090 mm
Peak Strength:	46 kPa
Residual Strength:	37.5 kPa
Vibro-Residual Strength:	32.5 kPa

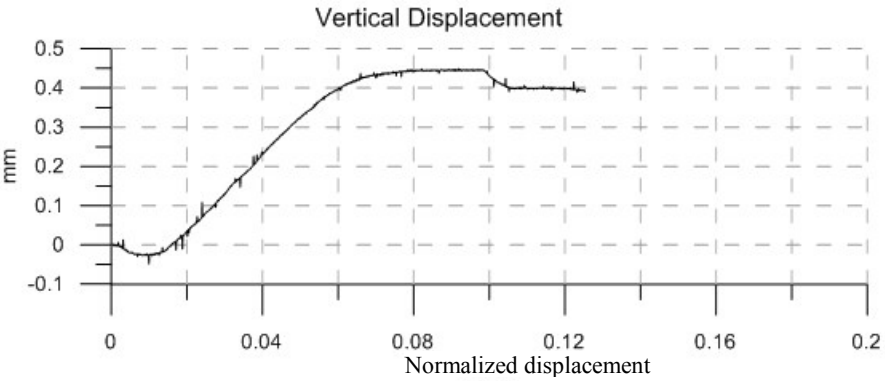

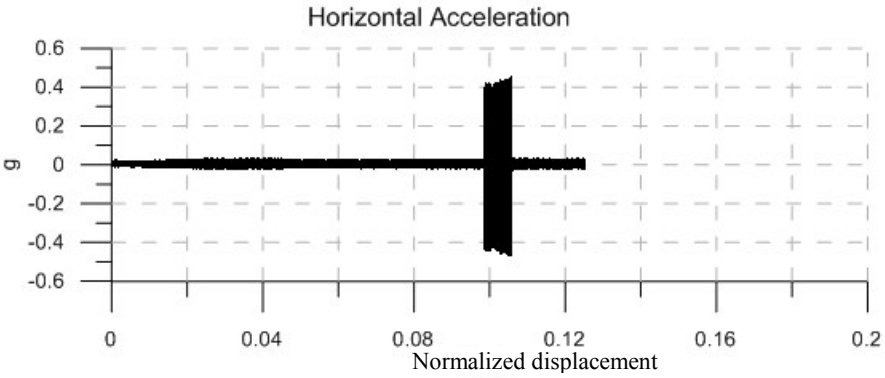

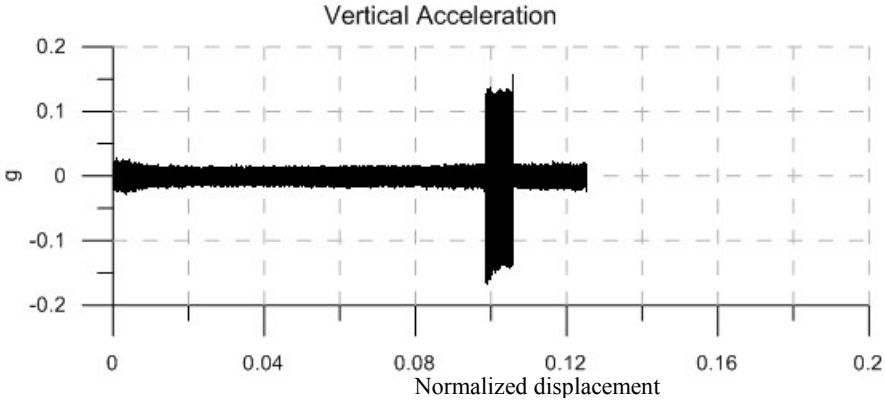

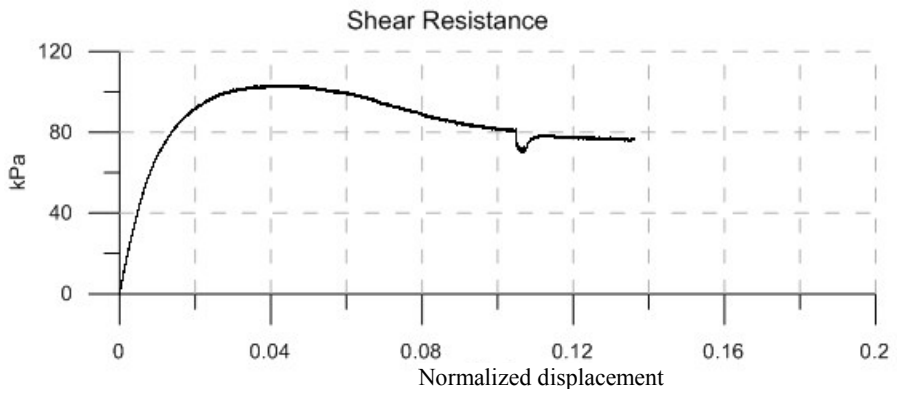

Material:	Sand
Size:	Fine
Normal Stress:	118 kPa
Vibration Frequency:	60 Hz
Vibration Duration:	15 sec
Horizontal Acceleration:	0.43 g
Vertical Acceleration:	0.18 g
Horizontal Amplitude:	0.0297 mm
Vertical Amplitude:	0.0124 mm
Peak Strength:	103 kPa
Residual Strength:	81 kPa
Vibro-Residual Strength:	71.5 kPa

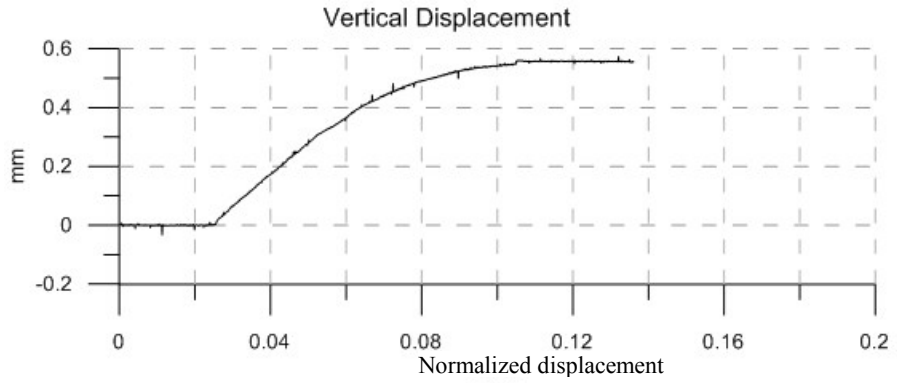

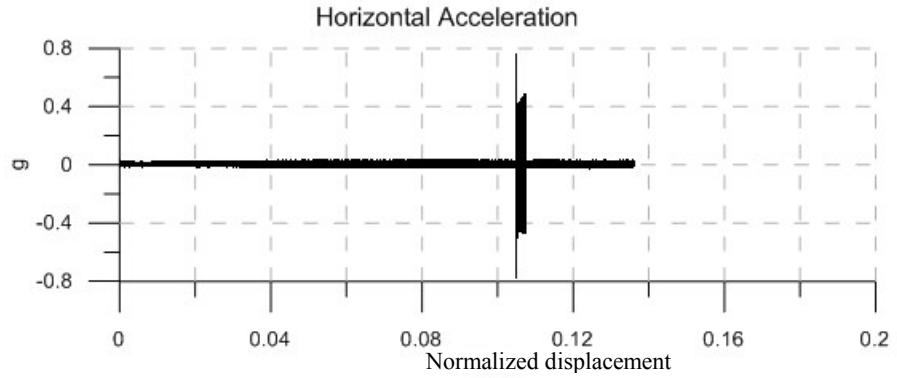

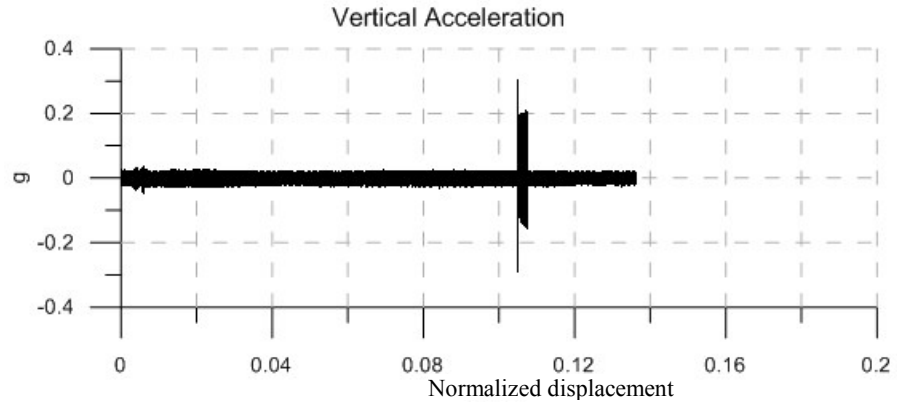

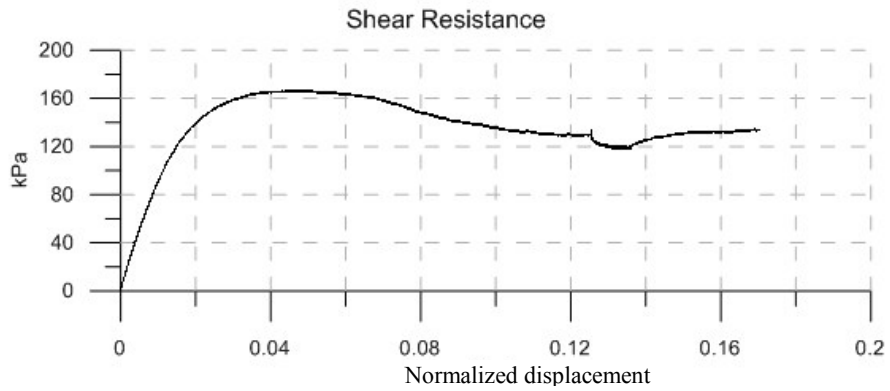

Material:	Sand
Size:	Fine
Normal Stress:	200 kPa
Vibration Frequency:	60 Hz
Vibration Duration:	62 sec
Horizontal Acceleration:	0.40 g
Vertical Acceleration:	0.08 g
Horizontal Amplitude:	0.0276 mm
Vertical Amplitude:	0.0055 mm
Peak Strength:	166 kPa
Residual Strength:	130 kPa
Vibro-Residual Strength:	118.5 kPa

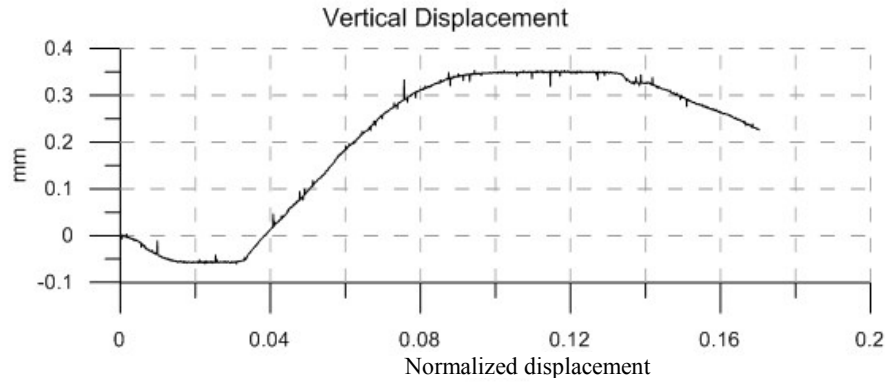

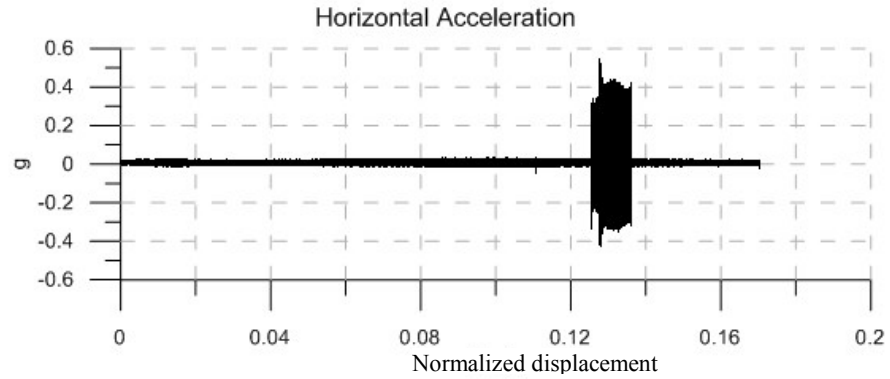

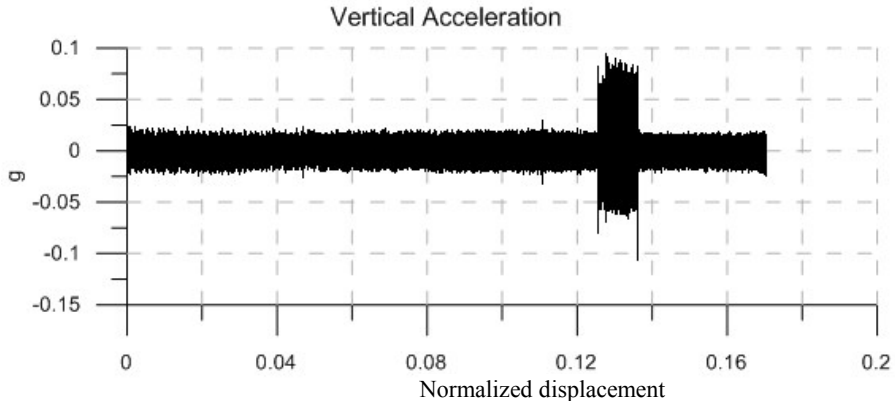

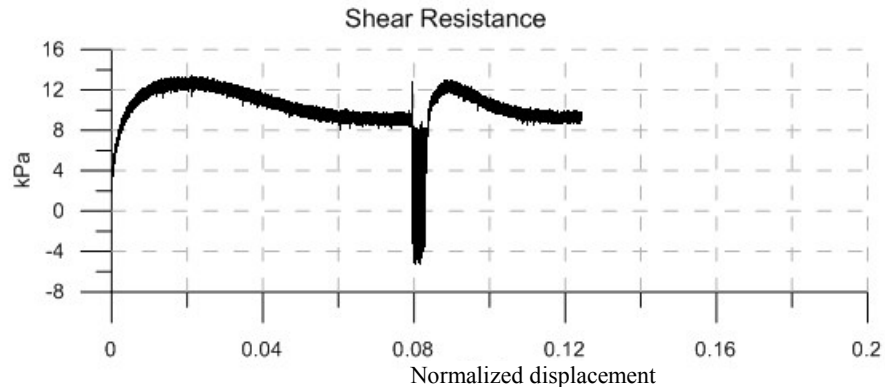

Material:	Sand
Size:	Fine
Normal Stress:	8 kPa
Vibration Frequency:	60 Hz
Vibration Duration:	19 sec
Horizontal Acceleration:	2.50 g
Vertical Acceleration:	0.22 g
Horizontal Amplitude:	0.1726 mm
Vertical Amplitude:	0.0152 mm
Peak Strength:	13 kPa
Residual Strength:	9.5 kPa
Vibro-Residual Strength:	0 kPa

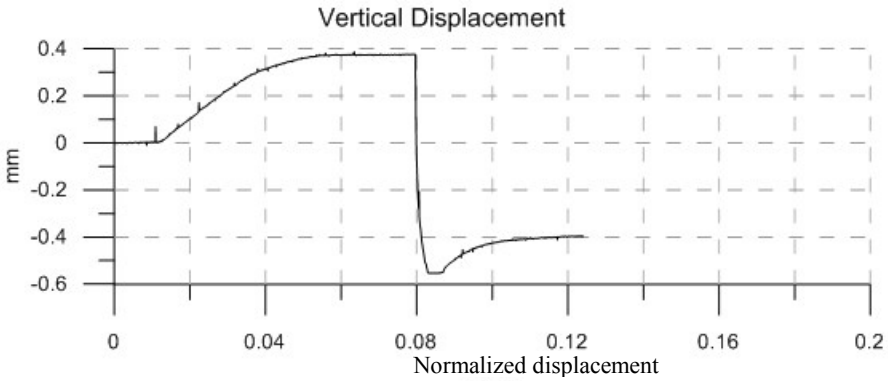

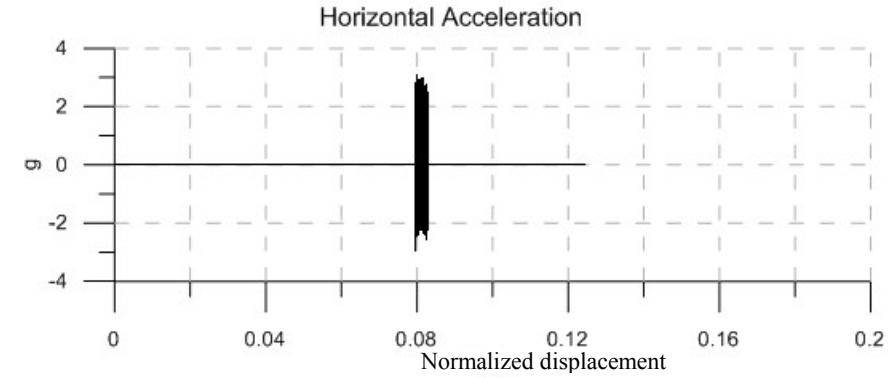

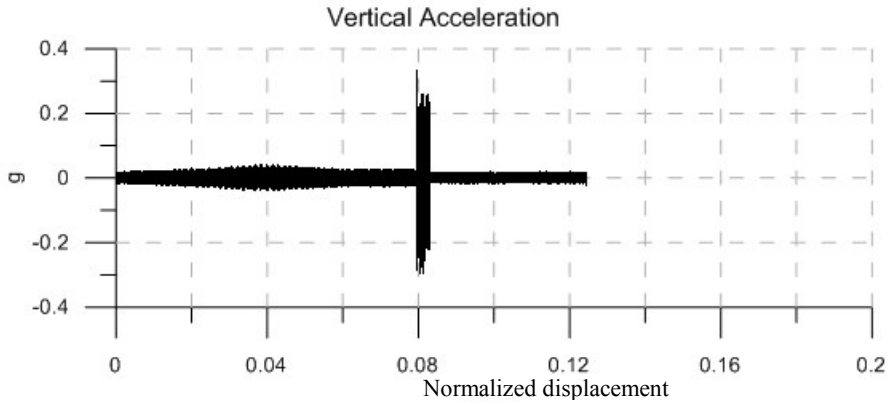

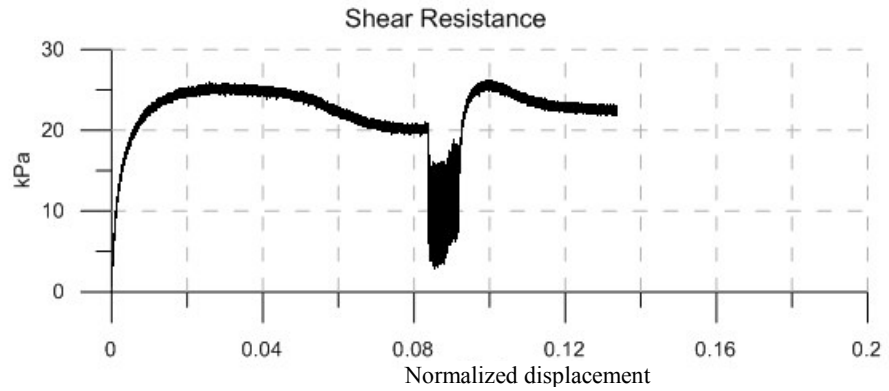

Material:	Sand
Size:	Fine
Normal Stress:	23 kPa
Vibration Frequency:	60 Hz
Vibration Duration:	46 sec
Horizontal Acceleration:	2.50 g
Vertical Acceleration:	0.40 g
Horizontal Amplitude:	0.1726 mm
Vertical Amplitude:	0.0276 mm
Peak Strength:	25 kPa
Residual Strength:	20.5 kPa
Vibro-Residual Strength:	8 kPa

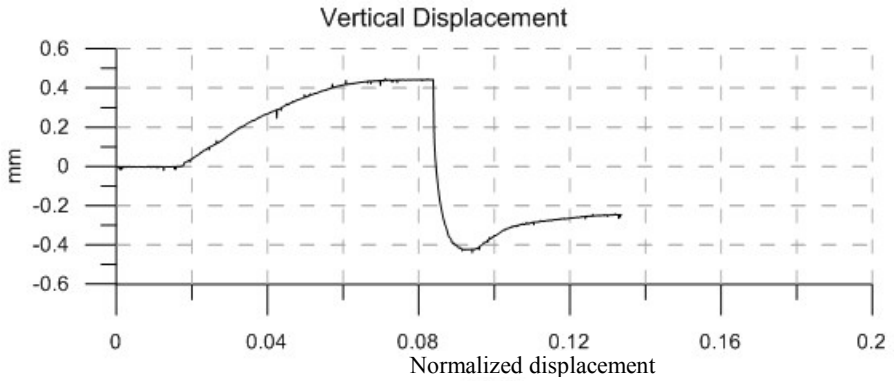

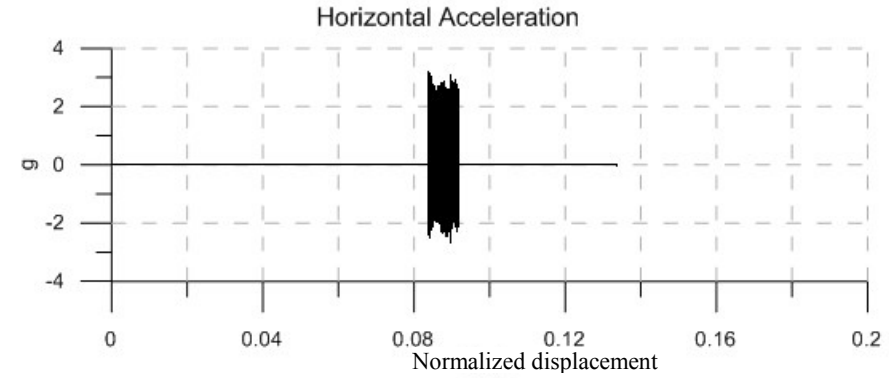

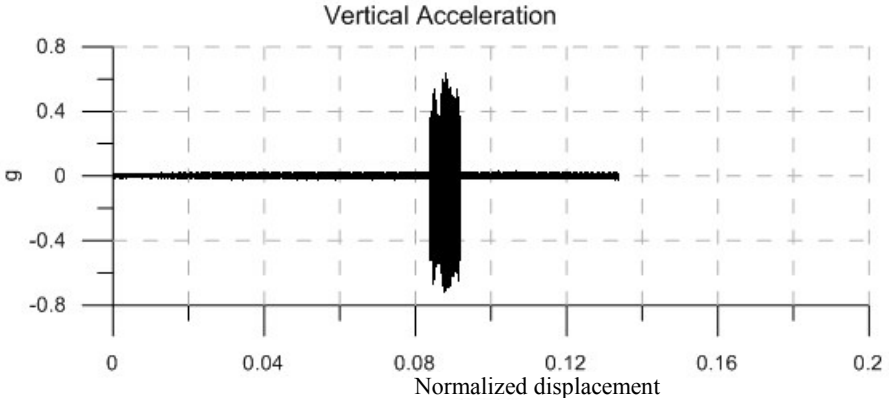

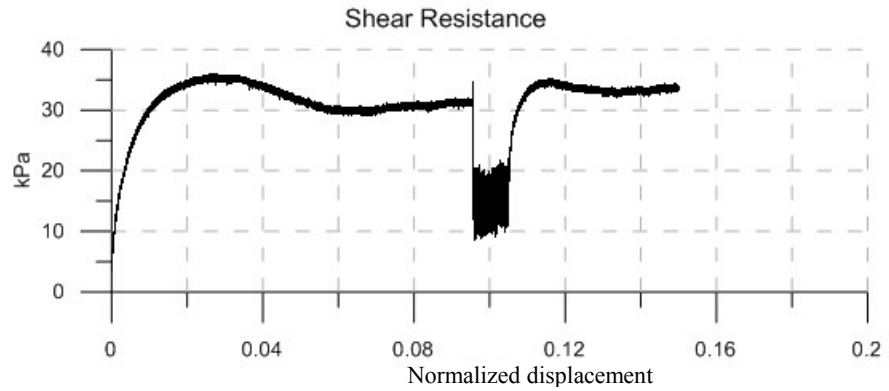

Material:	Sand
Size:	Fine
Normal Stress:	36 kPa
Vibration Frequency:	60 Hz
Vibration Duration:	55 sec
Horizontal Acceleration:	2.60 g
Vertical Acceleration:	0.58 g
Horizontal Amplitude:	0.1795 mm
Vertical Amplitude:	0.0400 mm
Peak Strength:	35.5 kPa
Residual Strength:	31 kPa
Vibro-Residual Strength:	14 kPa

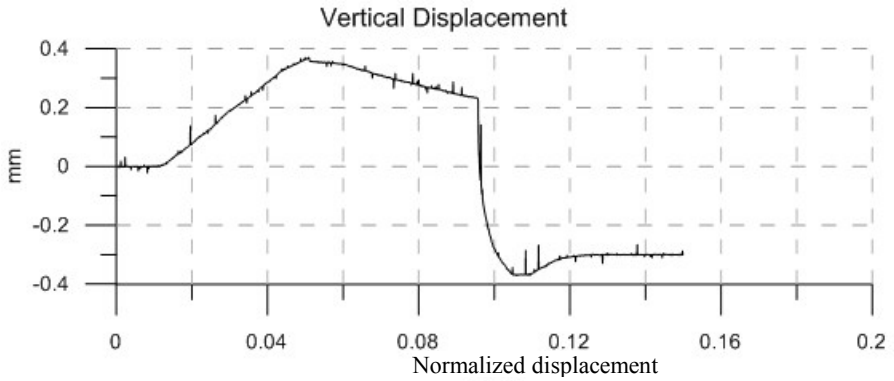

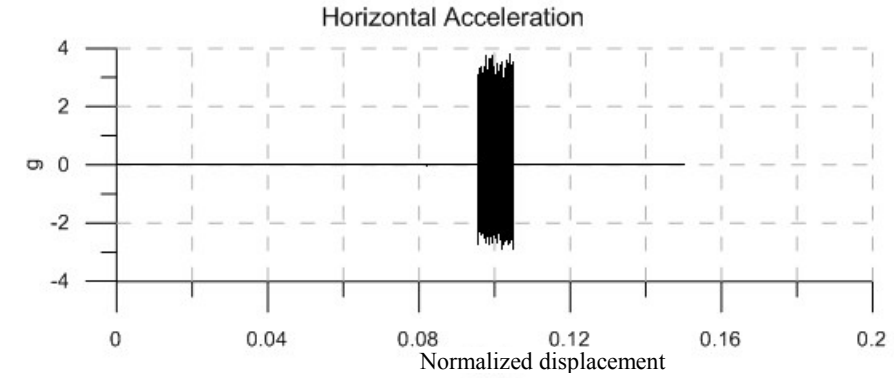

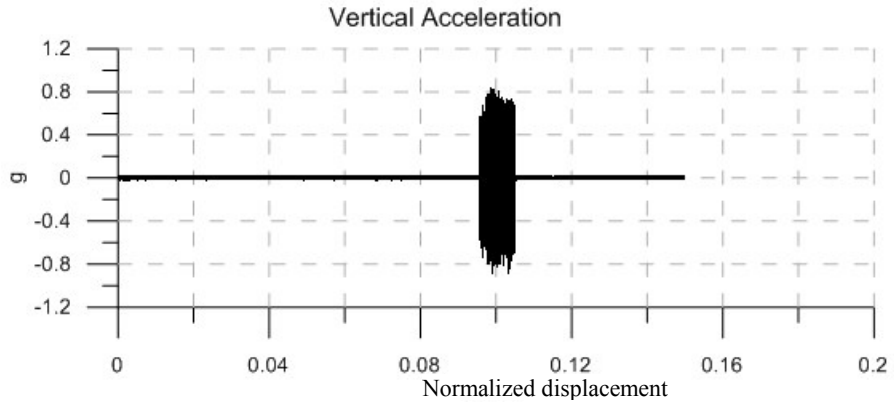

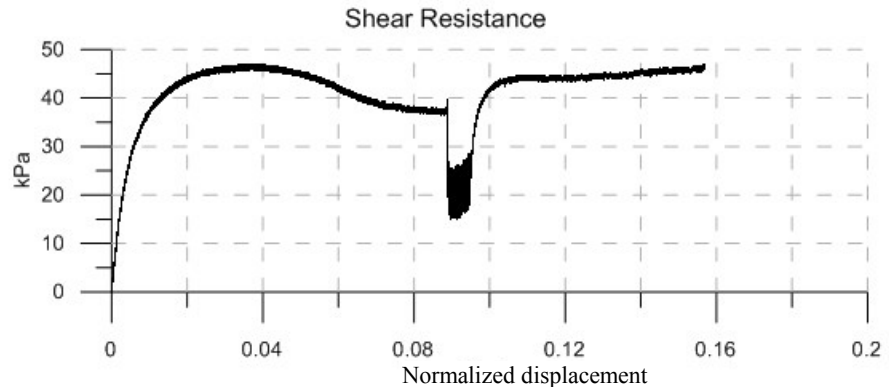

Material:	Sand
Size:	Fine
Normal Stress:	50 kPa
Vibration Frequency:	60 Hz
Vibration Duration:	35 sec
Horizontal Acceleration:	2.30 g
Vertical Acceleration:	0.40 g
Horizontal Amplitude:	0.1588 mm
Vertical Amplitude:	0.0276 mm
Peak Strength:	46.5 kPa
Residual Strength:	37.5 kPa
Vibro-Residual Strength:	19.5 kPa

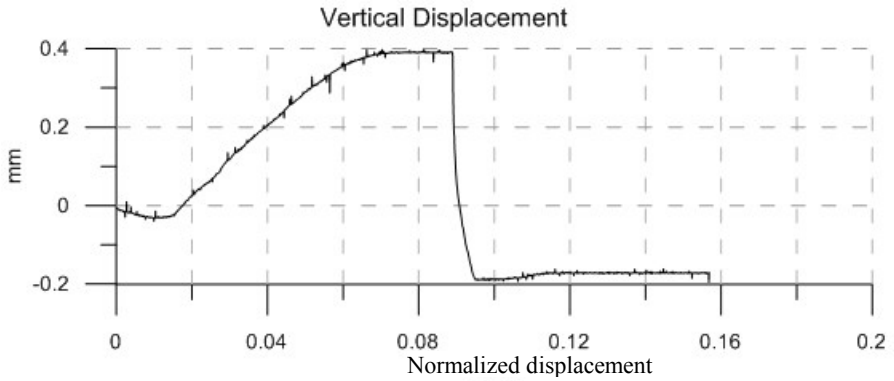

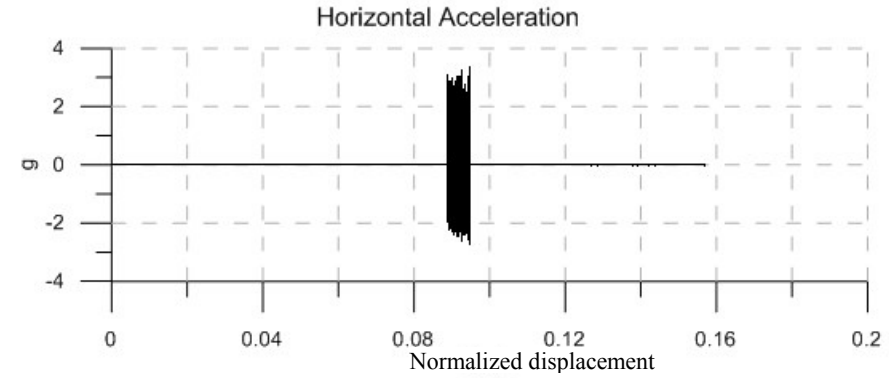

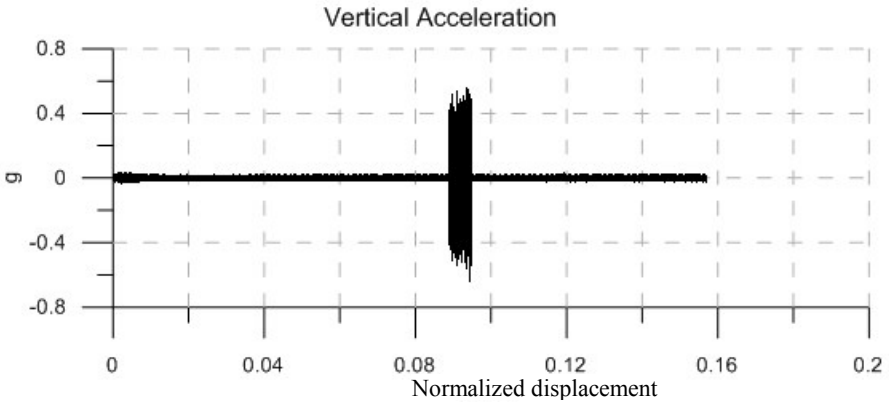

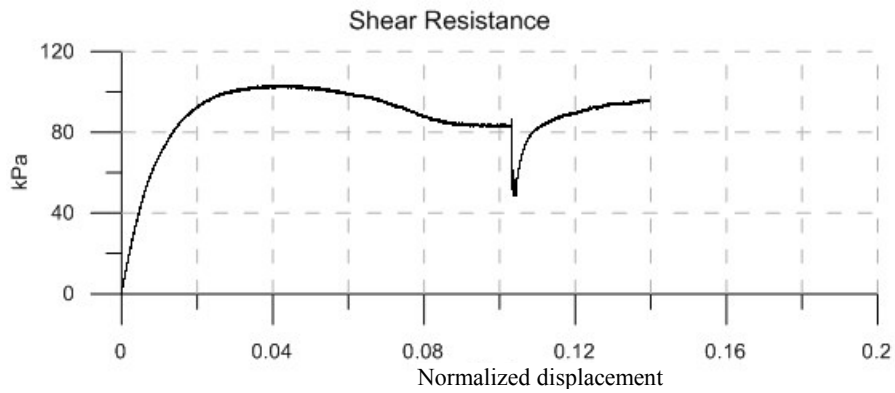

Material:	Sand
Size:	Fine
Normal Stress:	118 kPa
Vibration Frequency:	60 Hz
Vibration Duration:	8 sec
Horizontal Acceleration:	2.30 g
Vertical Acceleration:	0.75 g
Horizontal Amplitude:	0.1588 mm
Vertical Amplitude:	0.0518 mm
Peak Strength:	102.5 kPa
Residual Strength:	83.5 kPa
Vibro-Residual Strength:	51 kPa

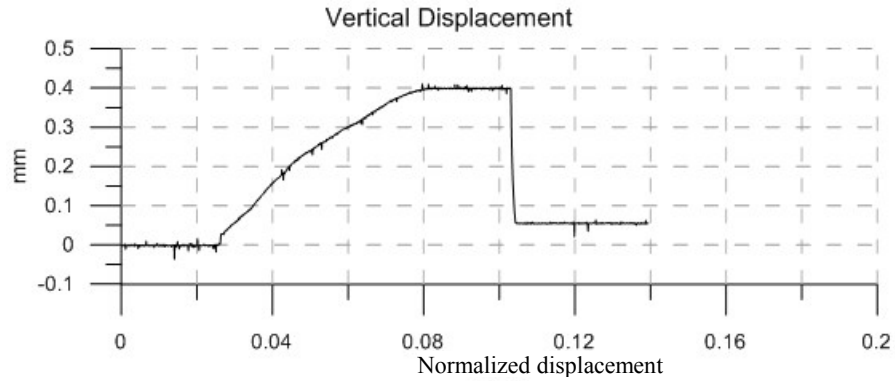

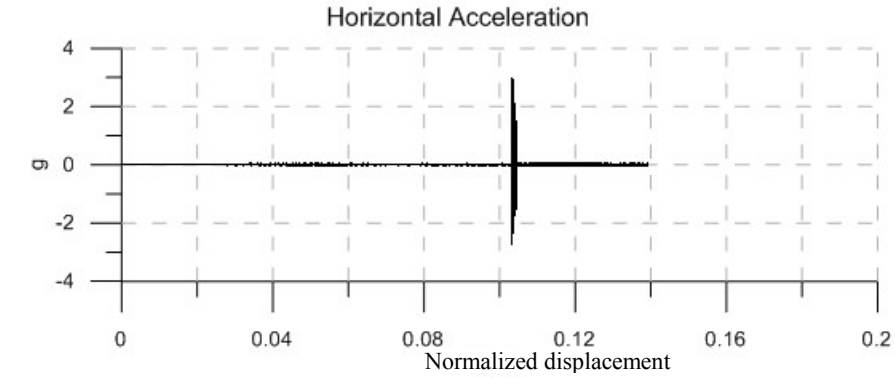

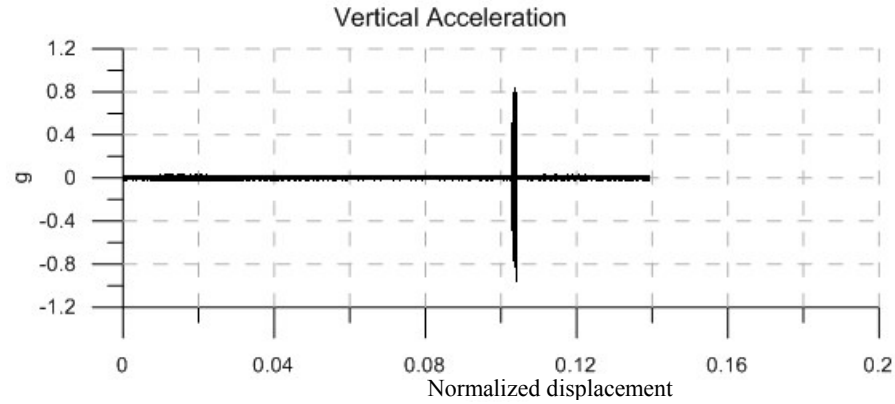

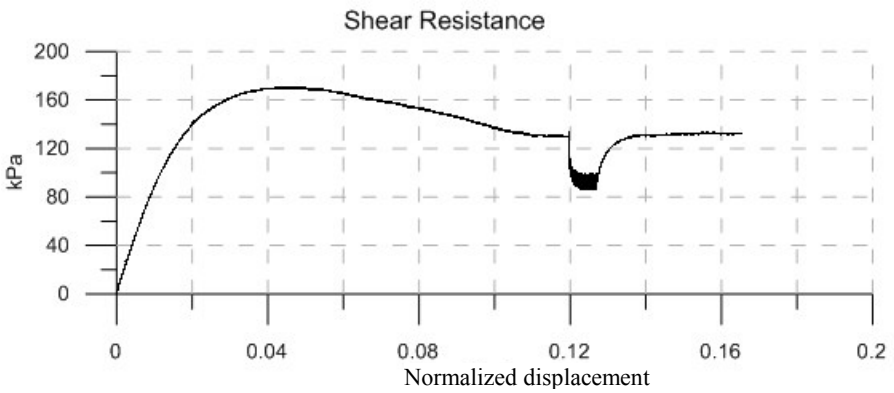

Material:	Sand
Size:	Fine
Normal Stress:	200 kPa
Vibration Frequency:	60 Hz
Vibration Duration:	43 sec
Horizontal Acceleration:	2.30 g
Vertical Acceleration:	0.70 g
Horizontal Amplitude:	0.1588 mm
Vertical Amplitude:	0.0483 mm
Peak Strength:	170.5 kPa
Residual Strength:	130 kPa
Vibro-Residual Strength:	91 kPa

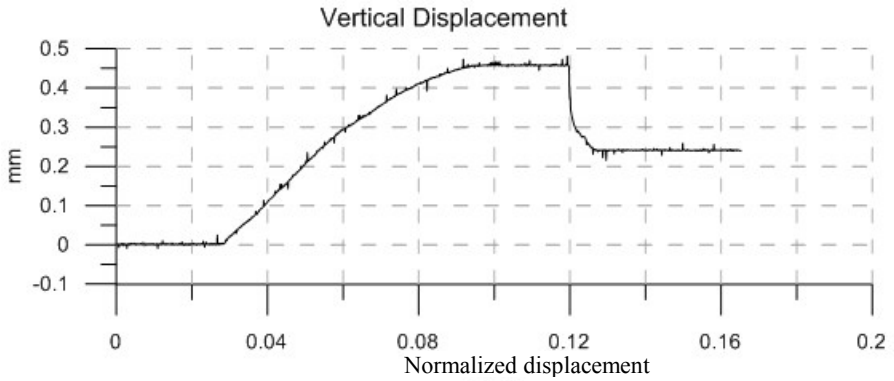

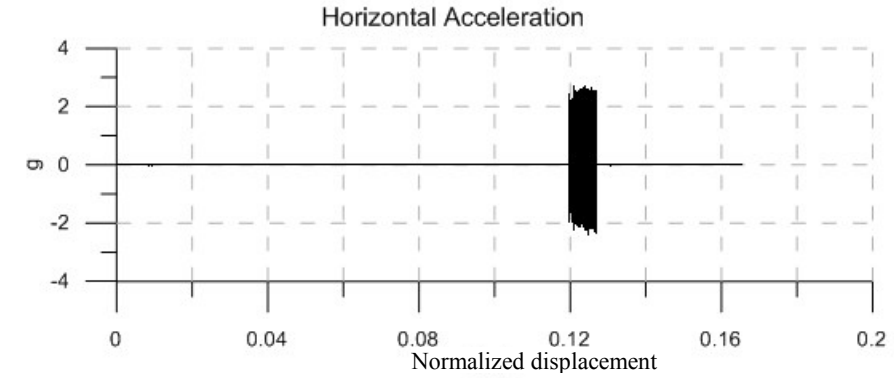

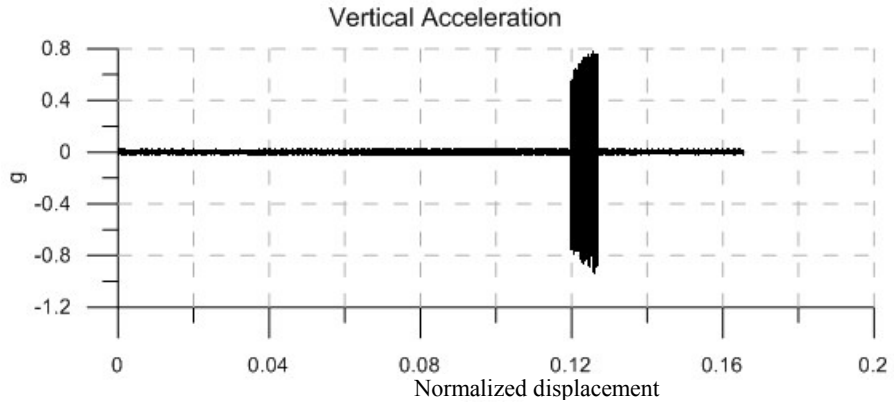

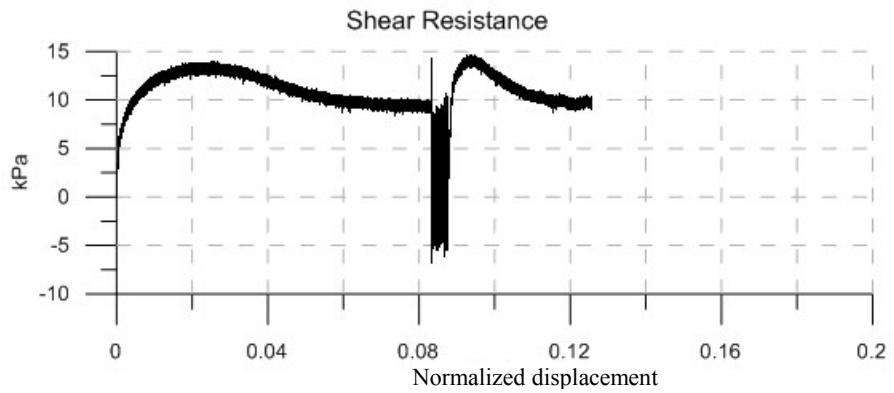

Material:	Sand
Size:	Fine
Normal Stress:	8 kPa
Vibration Frequency:	60 Hz
Vibration Force:	#1
Vibration Duration:	27 sec
Horizontal Acceleration:	3.5 g
Vertical Acceleration:	0.4 g
Horizontal Amplitude:	0.2416 mm
Vertical Amplitude:	0.0276 mm
Peak Strength:	13.5 kPa
Residual Strength:	9.5 kPa
Vibro-Residual Strength:	0 kPa

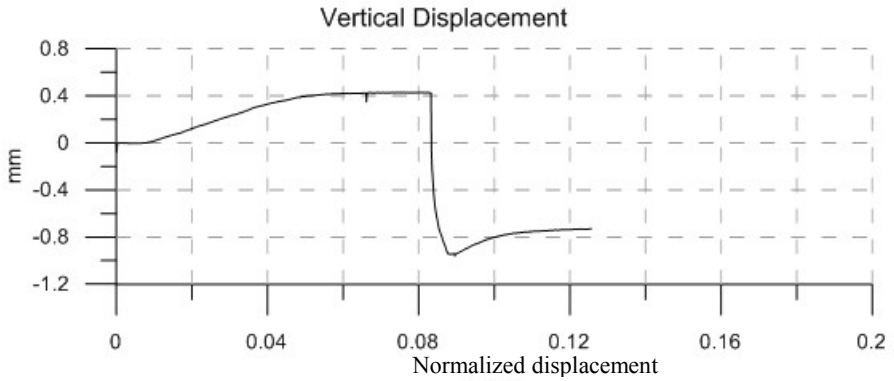

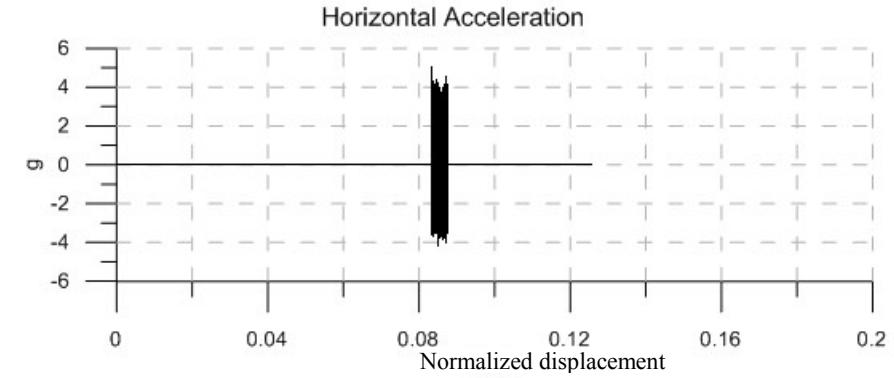

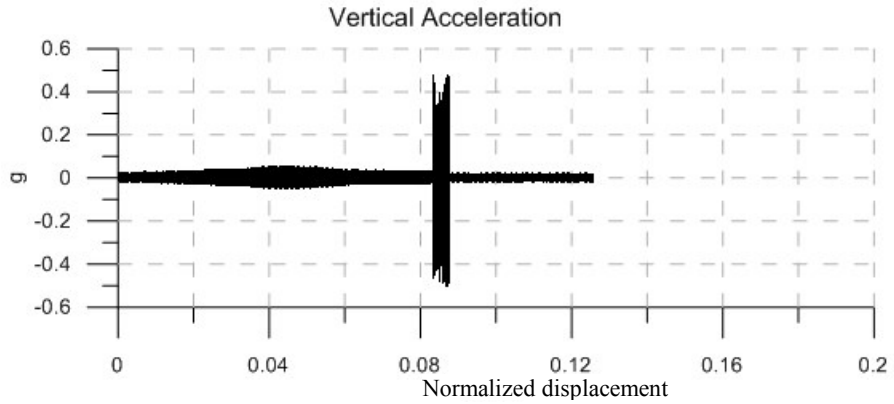

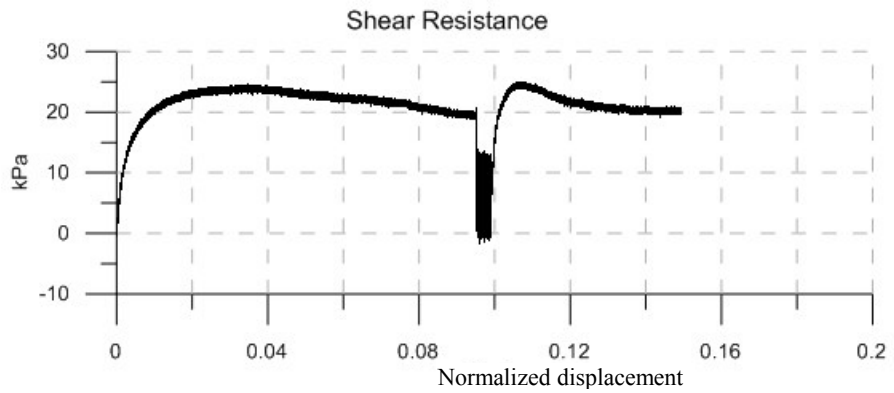

Material:	Sand
Size:	Fine
Normal Stress:	23 kPa
Vibration Frequency:	60 Hz
Vibration Force:	#1
Vibration Duration:	23 sec
Horizontal Acceleration:	3.9 g
Vertical Acceleration:	0.65 g
Horizontal Amplitude:	0.2692 mm
Vertical Amplitude:	0.0449 mm
Peak Strength:	24 kPa
Residual Strength:	20 kPa
Vibro-Residual Strength:	0 kPa

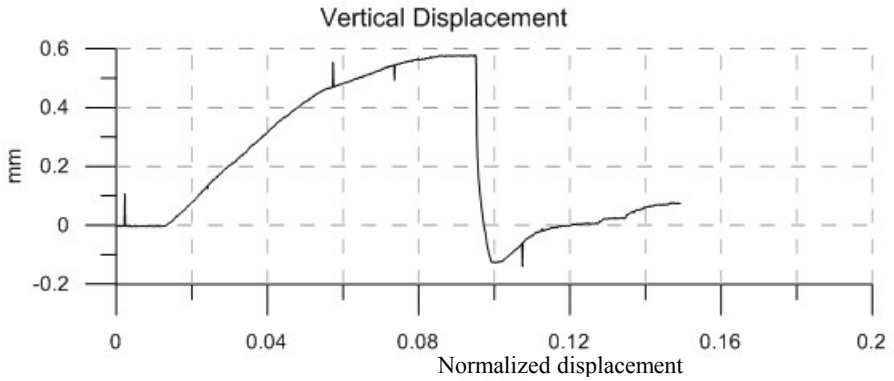

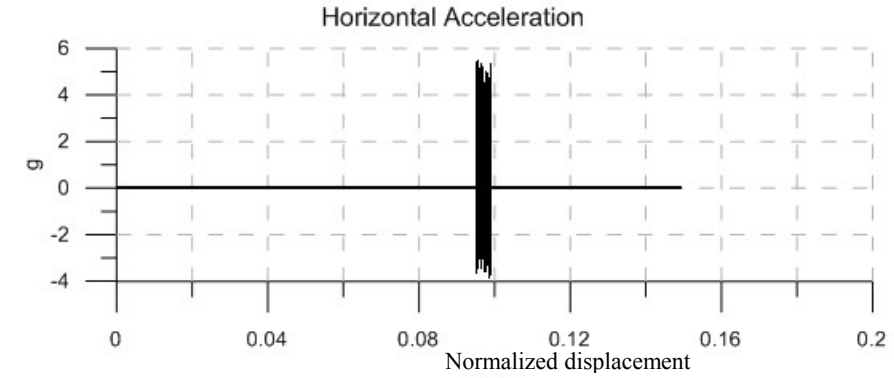

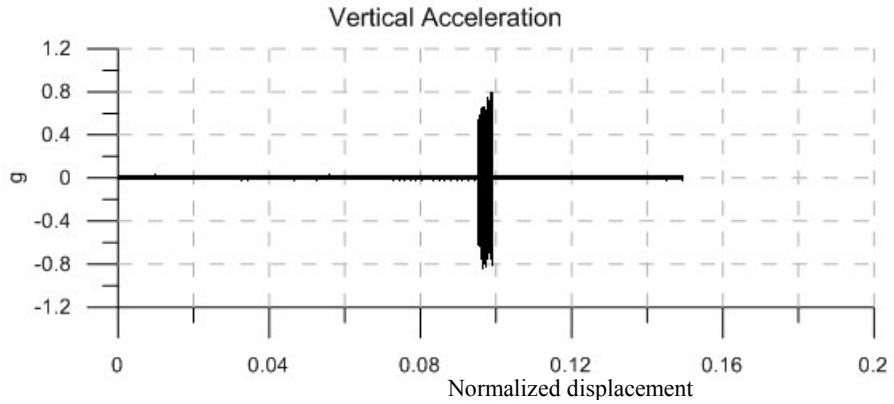

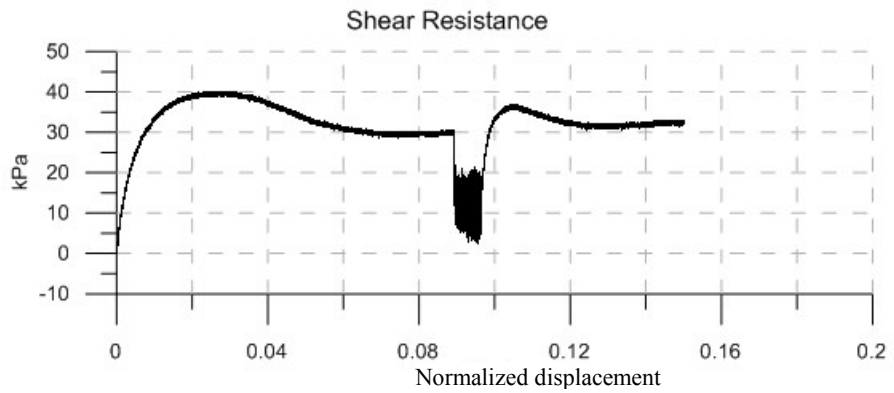

Material:	Sand
Size:	Fine
Normal Stress:	36 kPa
Vibration Frequency:	60 Hz
Vibration Force:	#1
Vibration Duration:	41 sec
Horizontal Acceleration:	4 g
Vertical Acceleration:	0.85 g
Horizontal Amplitude:	0.2761 mm
Vertical Amplitude:	0.0587 mm
Peak Strength:	39.5 kPa
Residual Strength:	30 kPa
Vibro-Residual Strength:	5 kPa

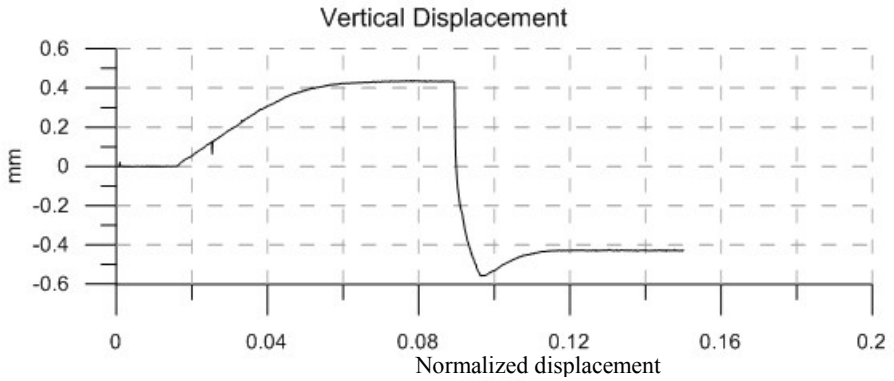

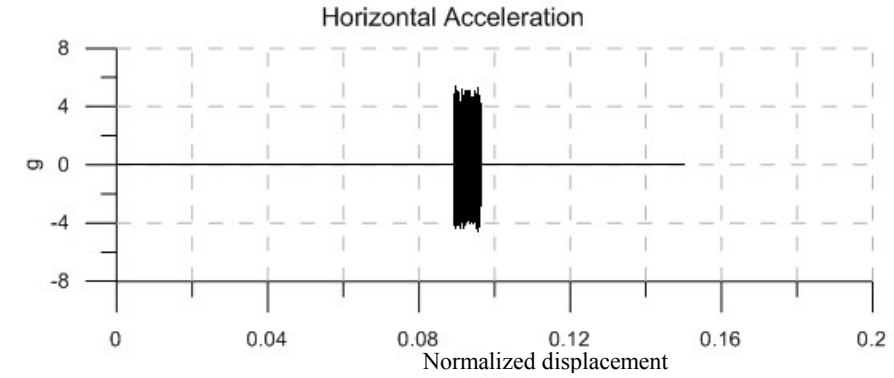

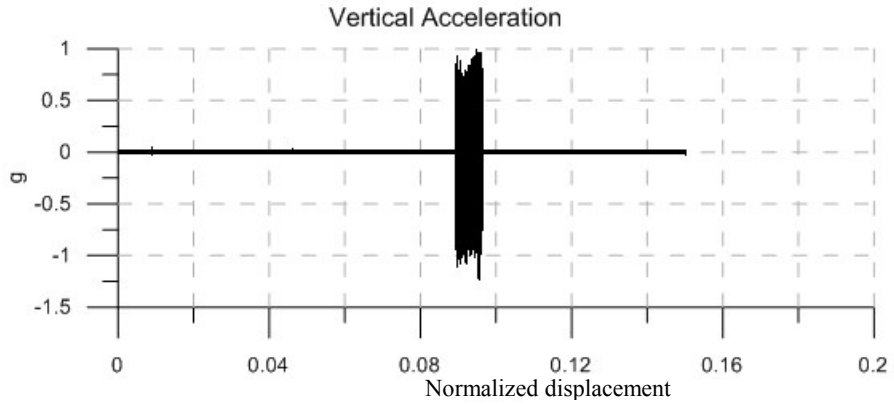

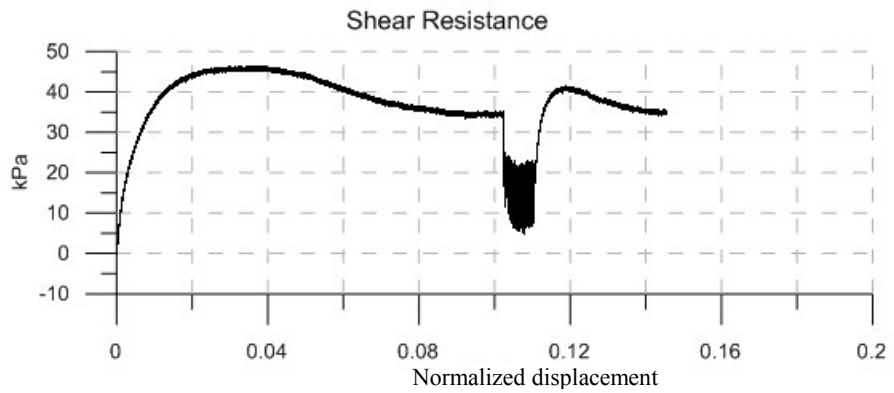

Material:	Sand
Size:	Fine
Normal Stress:	50 kPa
Vibration Frequency:	60 Hz
Vibration Force:	#1
Vibration Duration:	49 sec
Horizontal Acceleration:	4.5 g
Vertical Acceleration:	0.7 g
Horizontal Amplitude:	0.3106 mm
Vertical Amplitude:	0.0483 mm
Peak Strength:	46 kPa
Residual Strength:	34.5 kPa
Vibro-Residual Strength:	8 kPa

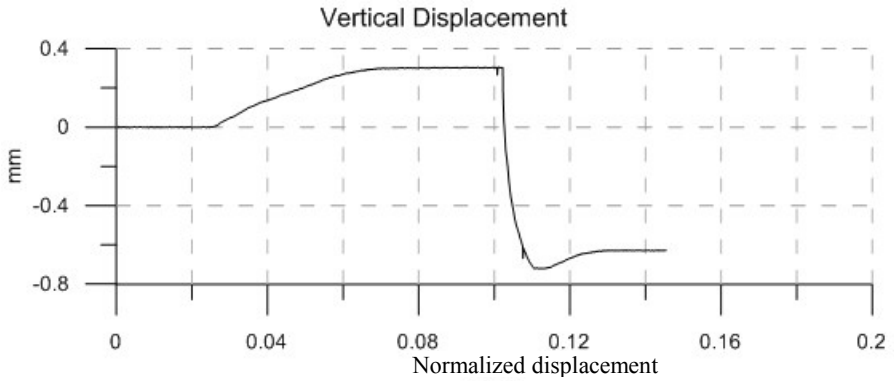

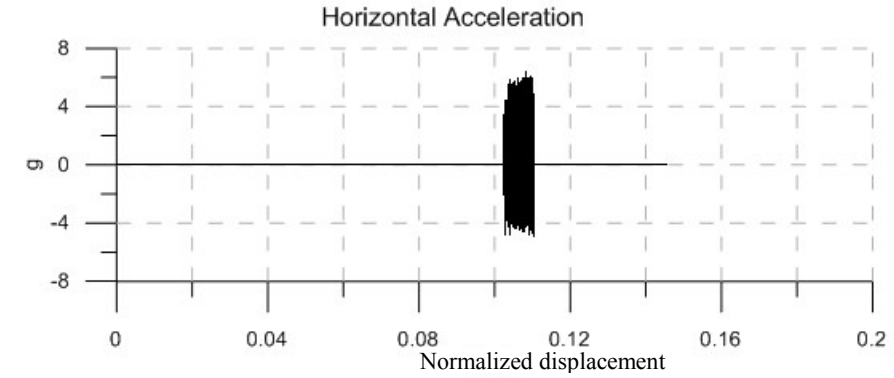

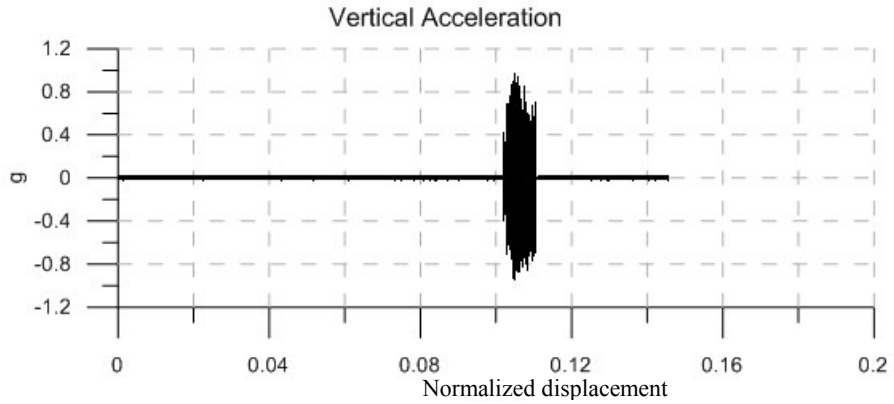

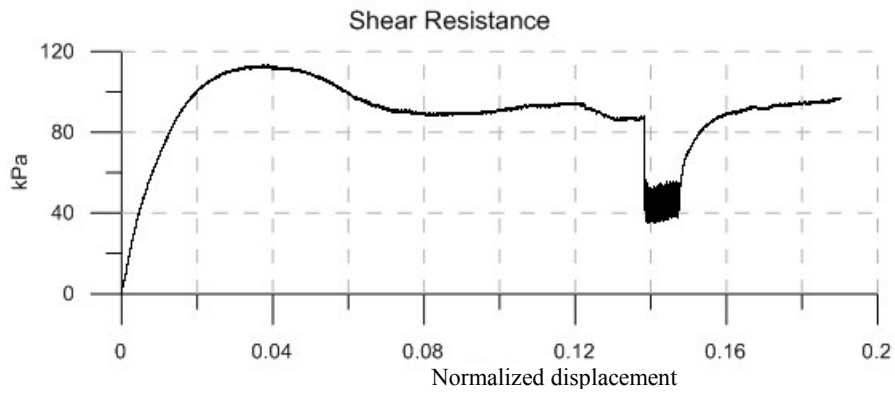

Material:	Sand
Size:	Fine
Normal Stress:	118 kPa
Vibration Frequency:	60 Hz
Vibration Force:	#1
Vibration Duration:	54 sec
Horizontal Acceleration:	4 g
Vertical Acceleration:	0.7 g
Horizontal Amplitude:	0.2761 mm
Vertical Amplitude:	0.0483 mm
Peak Strength:	112.5 kPa
Residual Strength:	87 kPa
Vibro-Residual Strength:	38 kPa

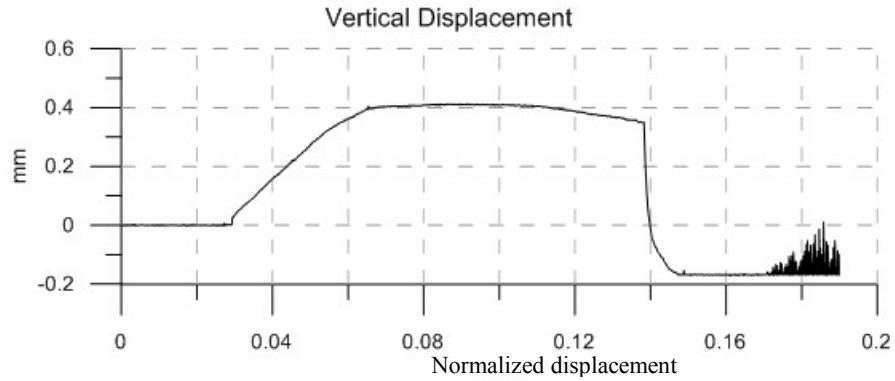

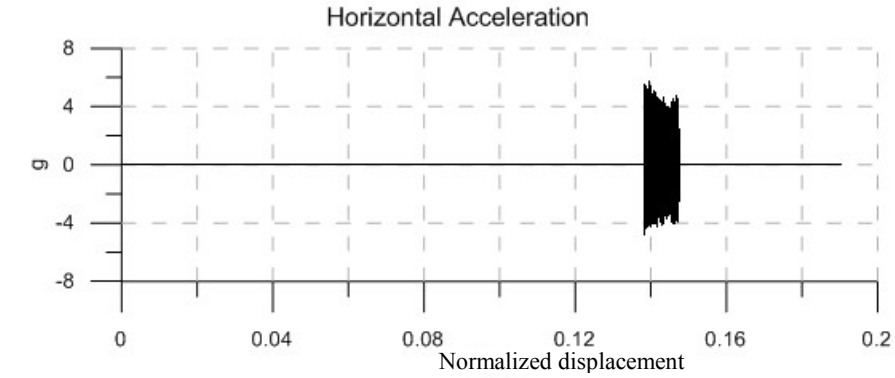

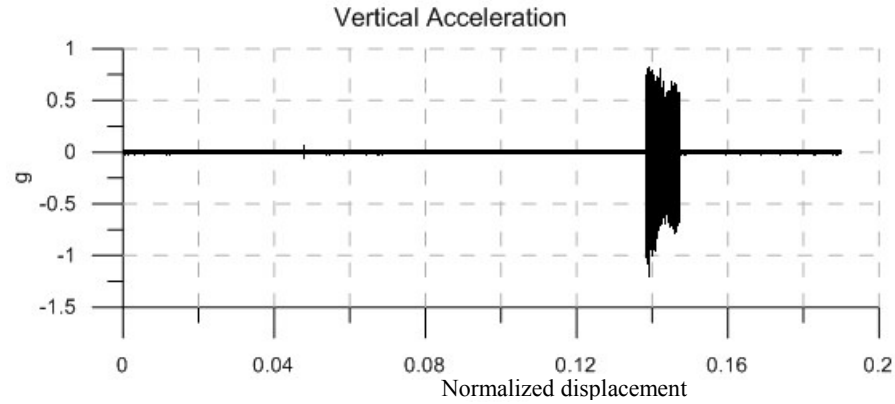

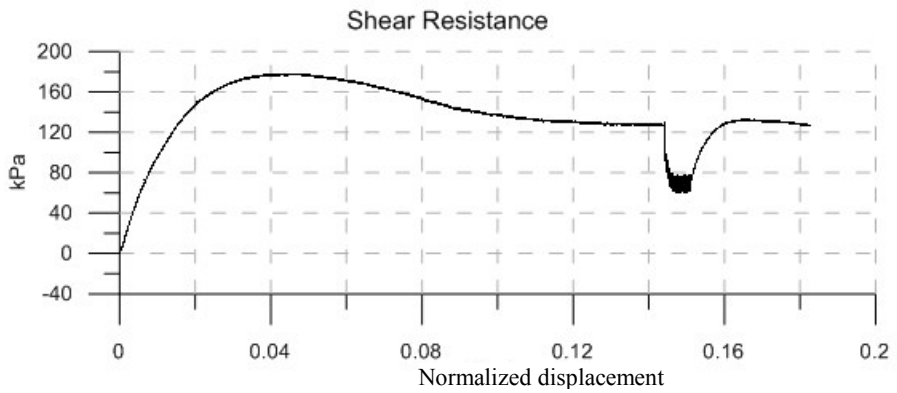

Material:	Sand
Size:	Fine
Normal Stress:	200 kPa
Vibration Frequency:	60 Hz
Vibration Force:	#1
Vibration Duration:	42 sec
Horizontal Acceleration:	4.5 g
Vertical Acceleration:	1.3 g
Horizontal Amplitude:	0.3106 mm
Vertical Amplitude:	0.0897 mm
Peak Strength:	178 kPa
Residual Strength:	128 kPa
Vibro-Residual Strength:	62 kPa

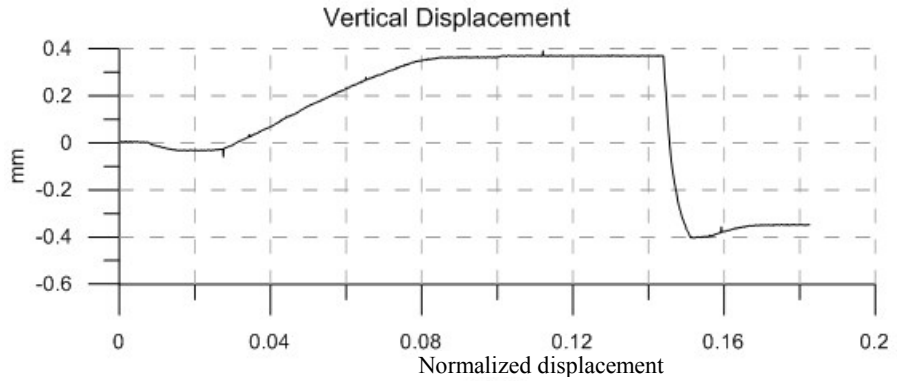

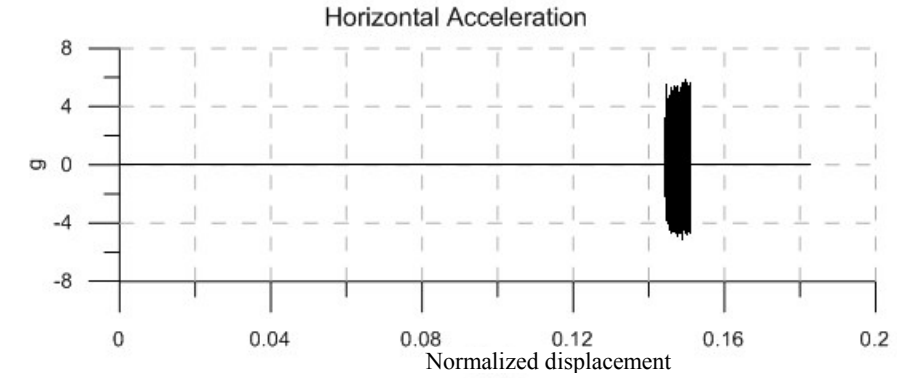

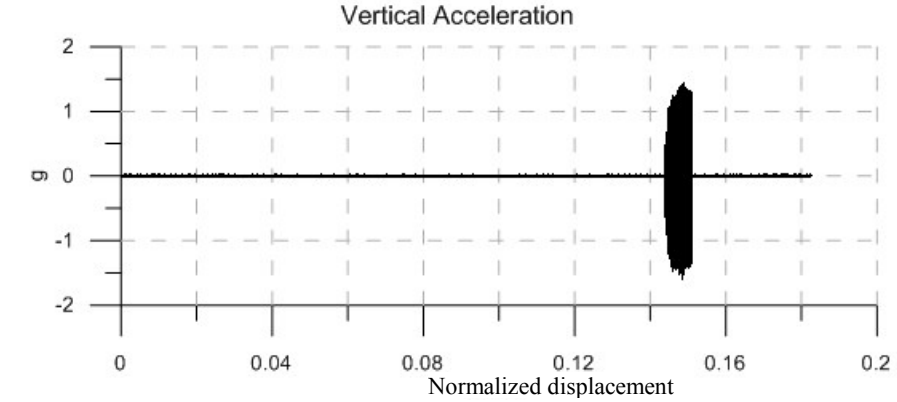

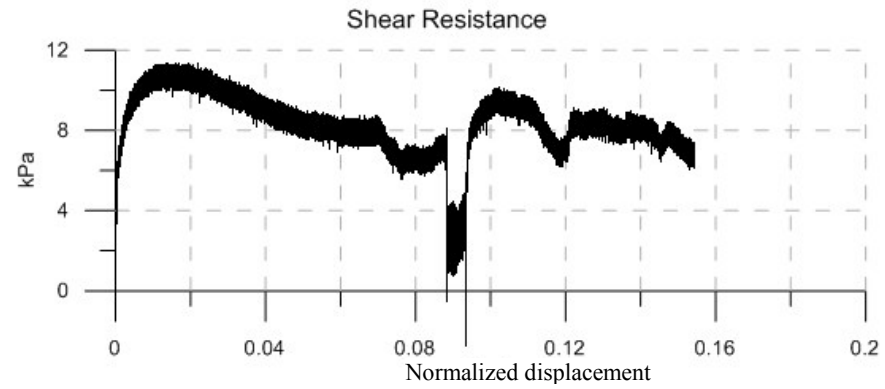

Material:	Sand
Size:	Coarse
Normal Stress:	8 kPa
Vibration Frequency:	60 Hz
Vibration Duration:	30 sec
Horizontal Acceleration:	0.44 g
Vertical Acceleration:	0.04 g
Horizontal Amplitude:	0.0304 mm
Vertical Amplitude:	0.0028 mm
Peak Strength:	11 kPa
Residual Strength:	7.5 kPa
Vibro-Residual Strength:	1.5 kPa

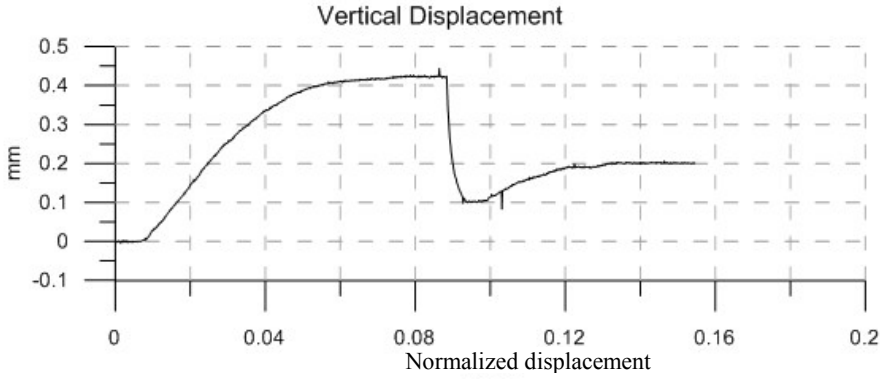

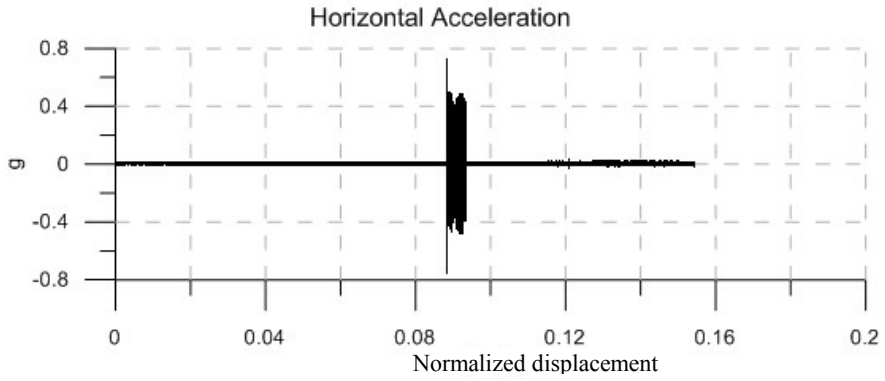

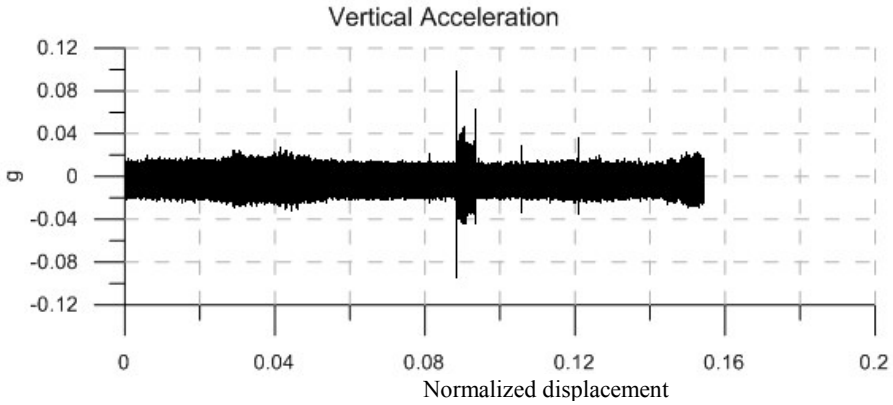

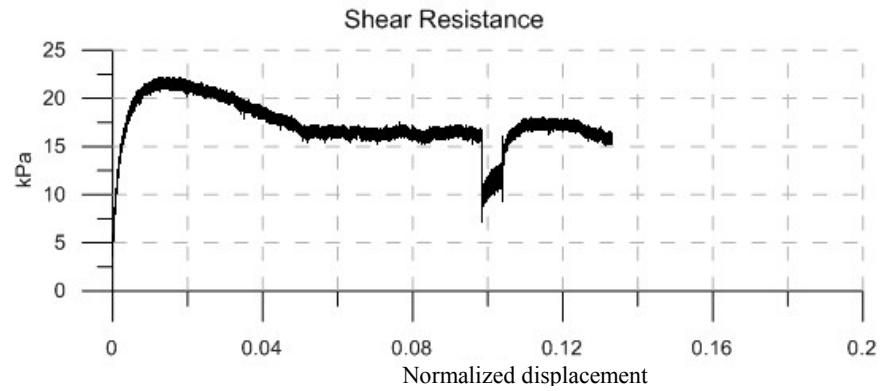

Material:	Sand
Size:	Coarse
Normal Stress:	23 kPa
Vibration Frequency:	60 Hz
Vibration Duration:	33 sec
Horizontal Acceleration:	0.47 g
Vertical Acceleration:	0.08 g
Horizontal Amplitude:	0.0324 mm
Vertical Amplitude:	0.0055 mm
Peak Strength:	21.5 kPa
Residual Strength:	16.5 kPa
Vibro-Residual Strength:	9.5 kPa

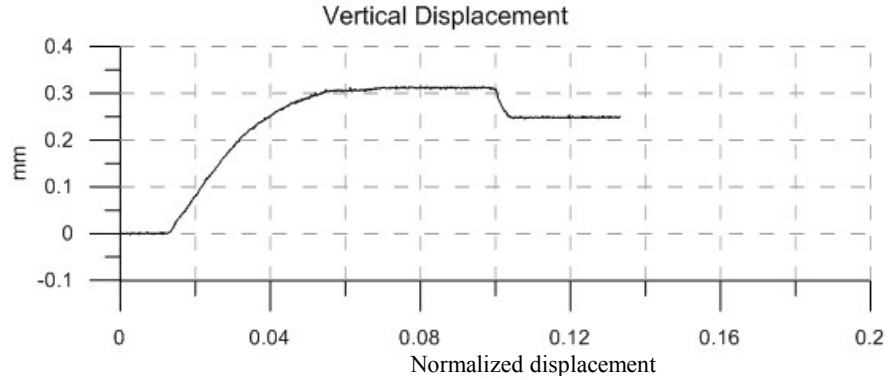

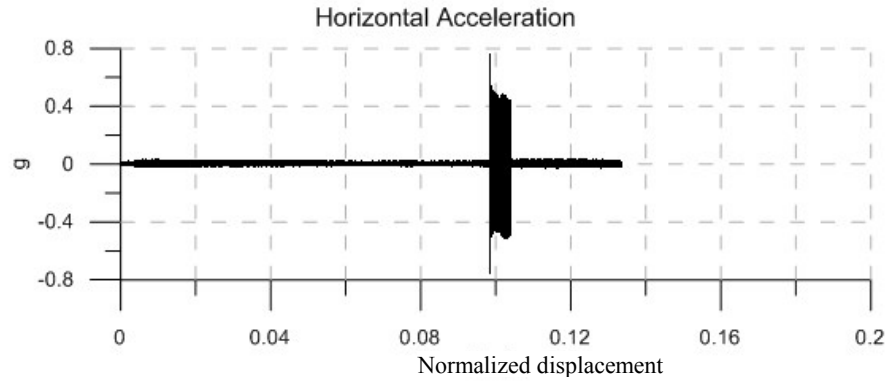

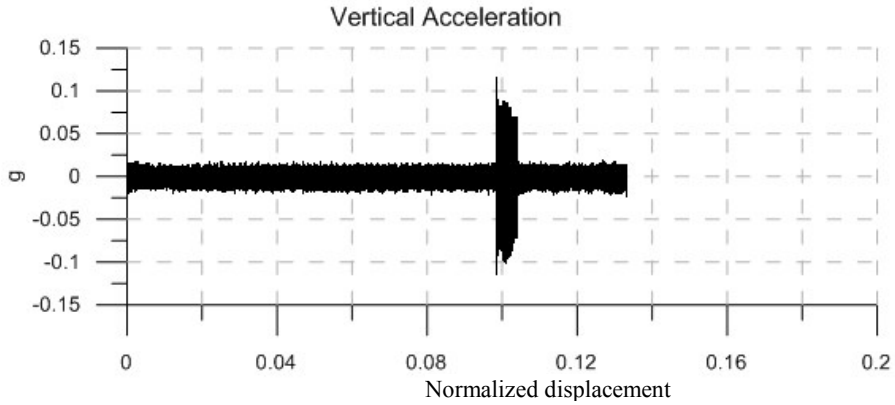

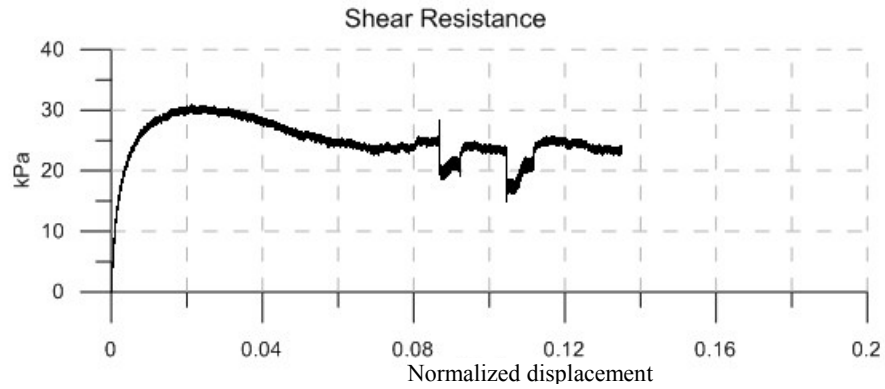

Material:	Sand
Size:	Coarse
Normal Stress:	36 kPa
Vibration Frequency:	60 Hz
Vibration Duration:	33 sec
Horizontal Acceleration:	0.47 g
Vertical Acceleration:	0.1 g
Horizontal Amplitude:	0.0324 mm
Vertical Amplitude:	0.0069 mm
Peak Strength:	30 kPa
Residual Strength:	25 kPa
Vibro-Residual Strength:	19 kPa

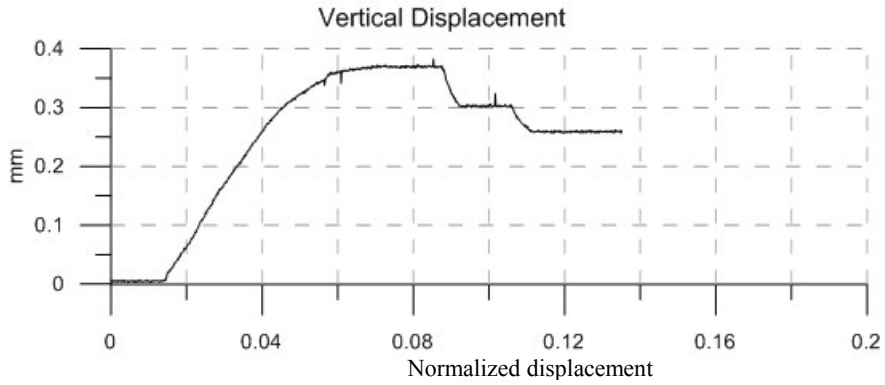

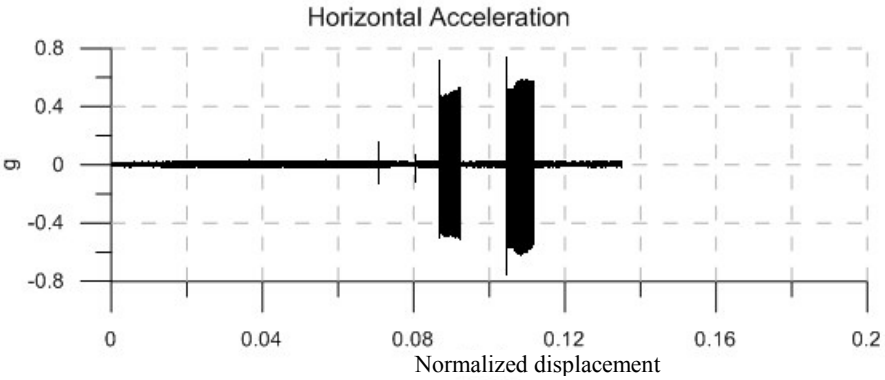

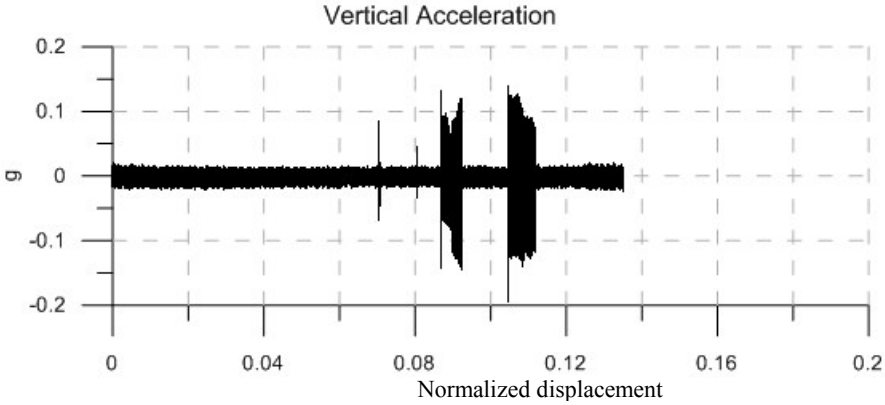

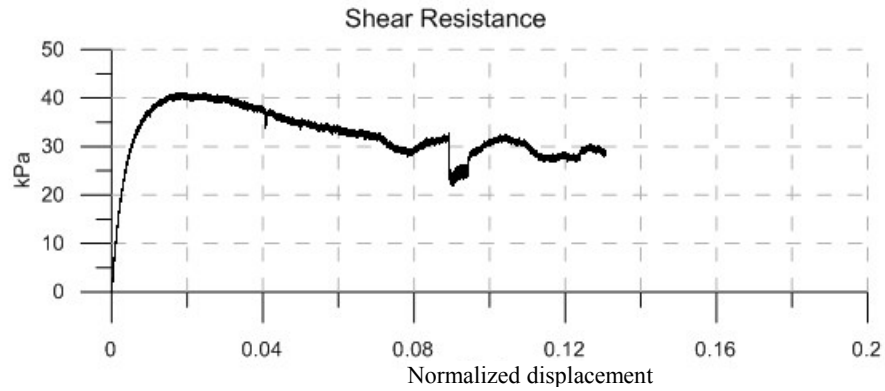

Material:	Sand
Size:	Coarse
Normal Stress:	50 kPa
Vibration Frequency:	60 Hz
Vibration Duration:	30 sec
Horizontal Acceleration:	0.46 g
Vertical Acceleration:	0.15 g
Horizontal Amplitude:	0.0318 mm
Vertical Amplitude:	0.0104 mm
Peak Strength:	40.5 kPa
Residual Strength:	32 kPa
Vibro-Residual Strength:	22.5 kPa

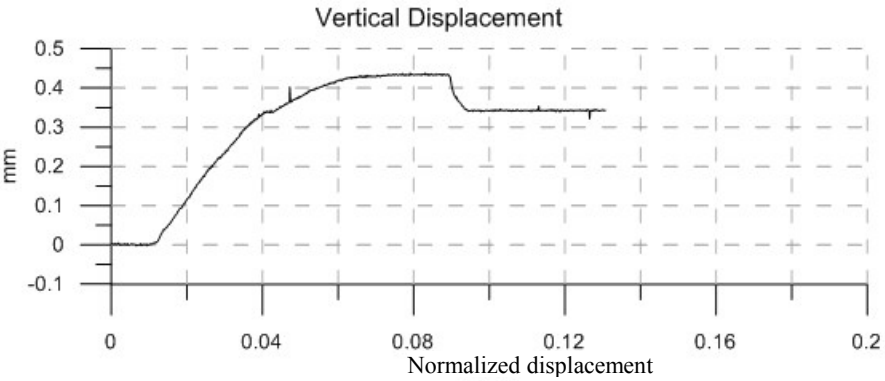

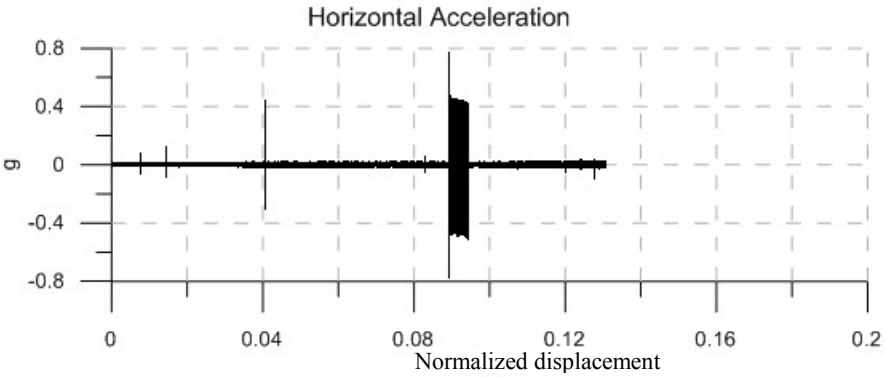

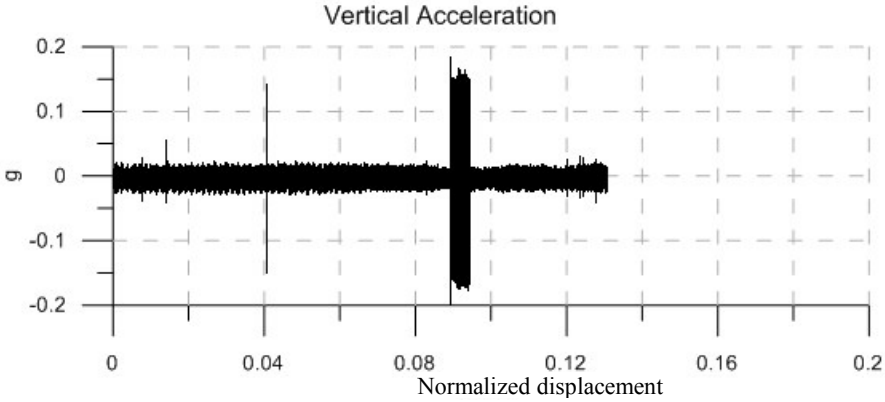

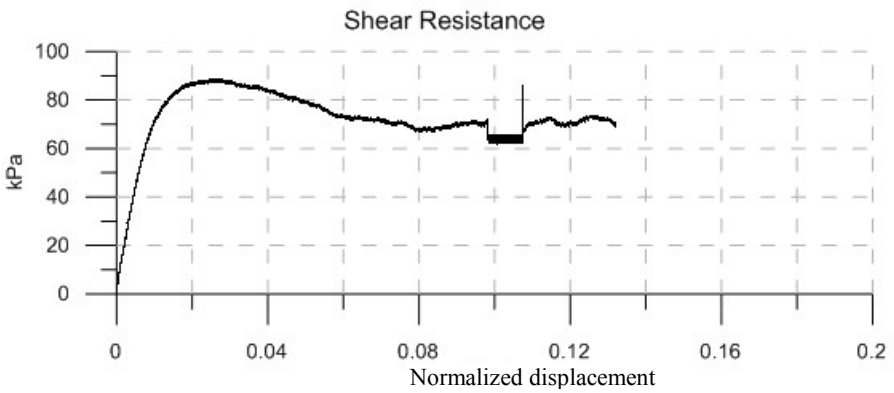

Material:	Sand
Size:	Coarse
Normal Stress:	118 kPa
Vibration Frequency:	60 Hz
Vibration Duration:	54 sec
Horizontal Acceleration:	0.42 g
Vertical Acceleration:	0.15 g
Horizontal Amplitude:	0.0290 mm
Vertical Amplitude:	0.0104 mm
Peak Strength:	88 kPa
Residual Strength:	71 kPa
Vibro-Residual Strength:	62.5 kPa

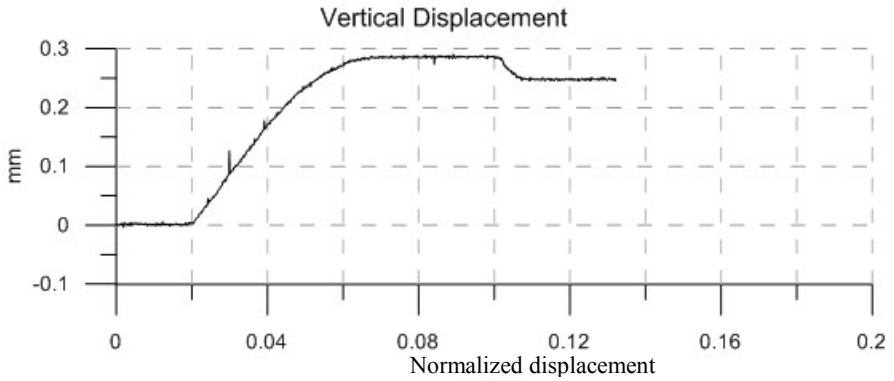

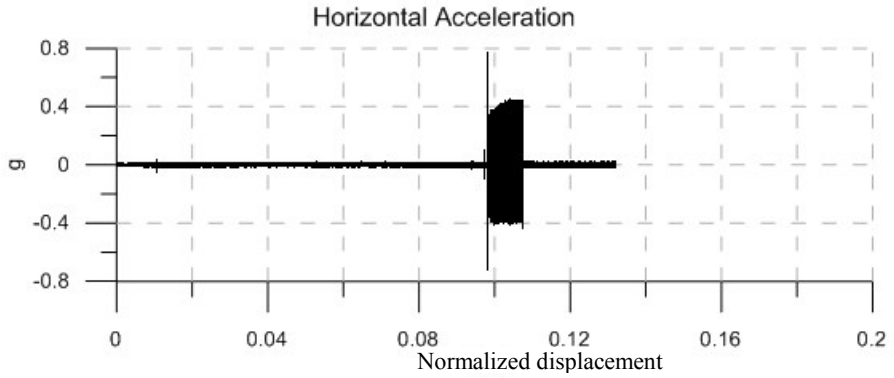

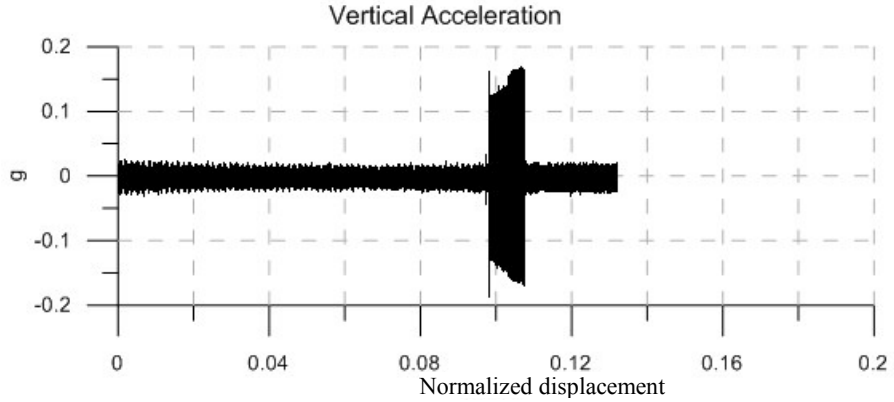

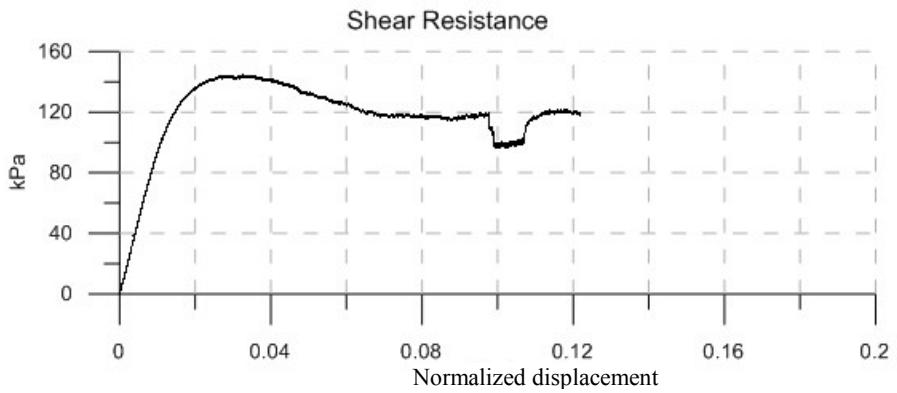

Material:	Sand
Size:	Coarse
Normal Stress:	200 kPa
Vibration Frequency:	60 Hz
Vibration Duration:	54 sec
Horizontal Acceleration:	0.4 g
Vertical Acceleration:	0.21 g
Horizontal Amplitude:	0.0276 mm
Vertical Amplitude:	0.0145 mm
Peak Strength:	144 kPa
Residual Strength:	119 kPa
Vibro-Residual Strength:	97 kPa

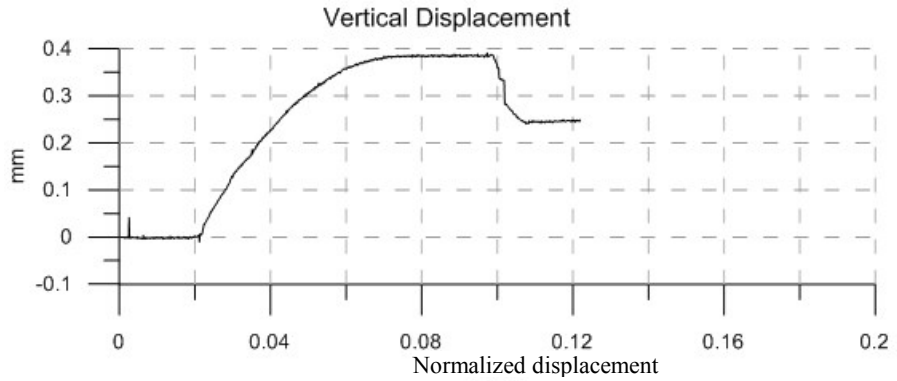

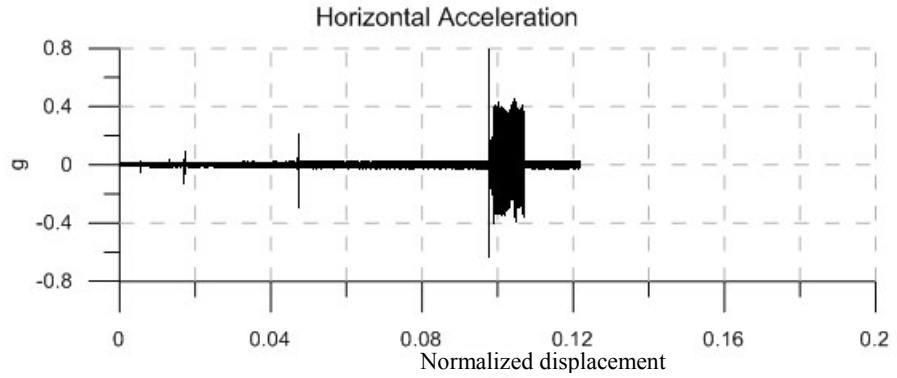

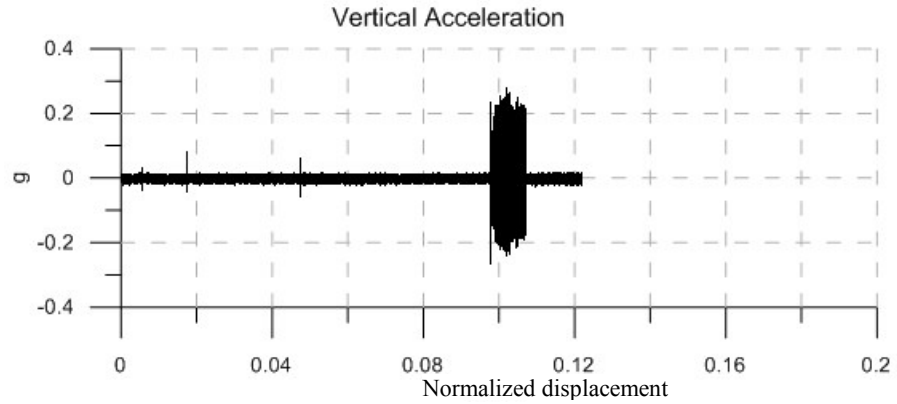

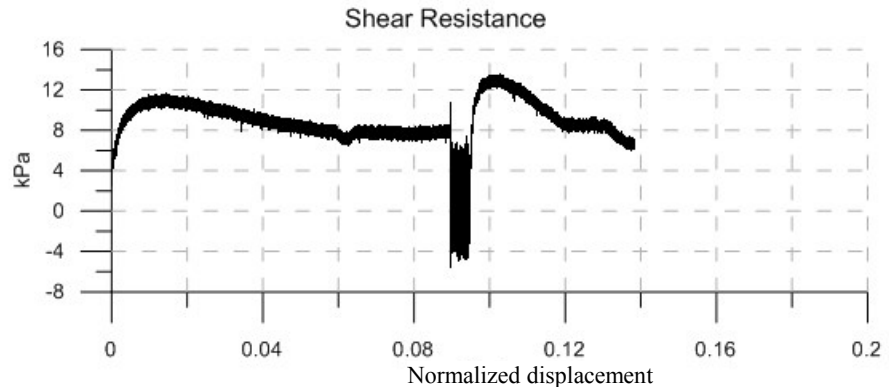

Material:	Sand
Size:	Coarse
Normal Stress:	8 kPa
Vibration Frequency:	60 Hz
Vibration Duration:	30 sec
Horizontal Acceleration:	2.3 g
Vertical Acceleration:	0.52 g
Horizontal Amplitude:	0.1588 mm
Vertical Amplitude:	0.0359 mm
Peak Strength:	11 kPa
Residual Strength:	8 kPa
Vibro-Residual Strength:	0 kPa

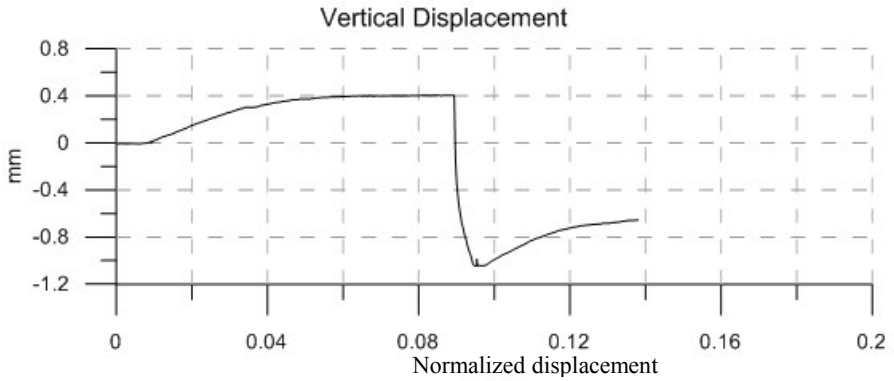

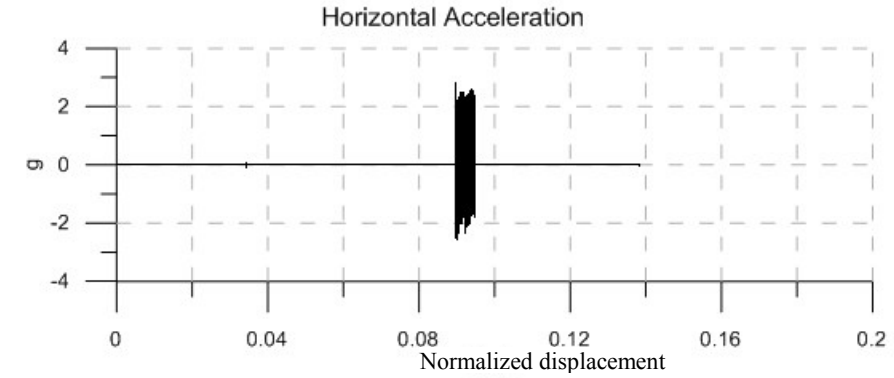

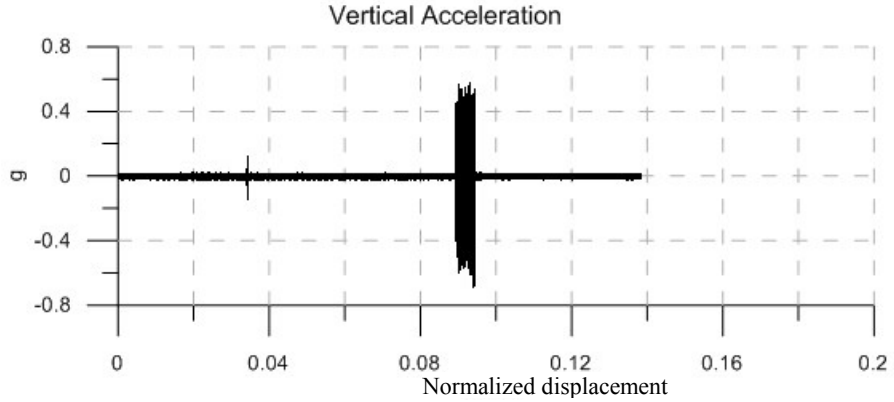

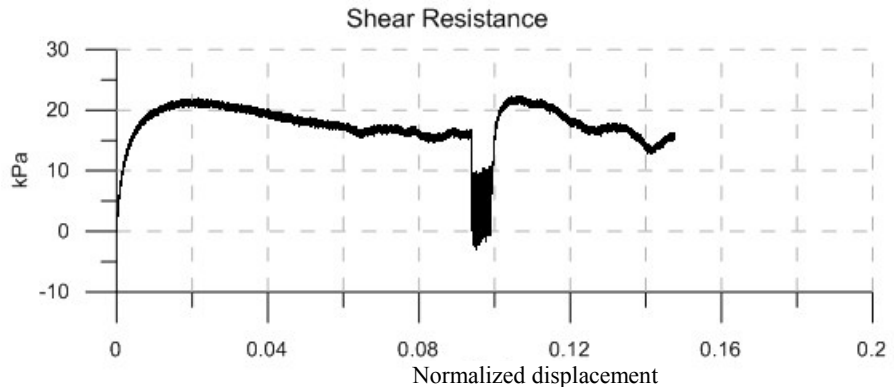

Material:	Sand
Size:	Coarse
Normal Stress:	23 kPa
Vibration Frequency:	60 Hz
Vibration Duration:	30 sec
Horizontal Acceleration:	2.6 g
Vertical Acceleration:	0.52 g
Horizontal Amplitude:	0.1795 mm
Vertical Amplitude:	0.0359 mm
Peak Strength:	21 kPa
Residual Strength:	16 kPa
Vibro-Residual Strength:	0 kPa

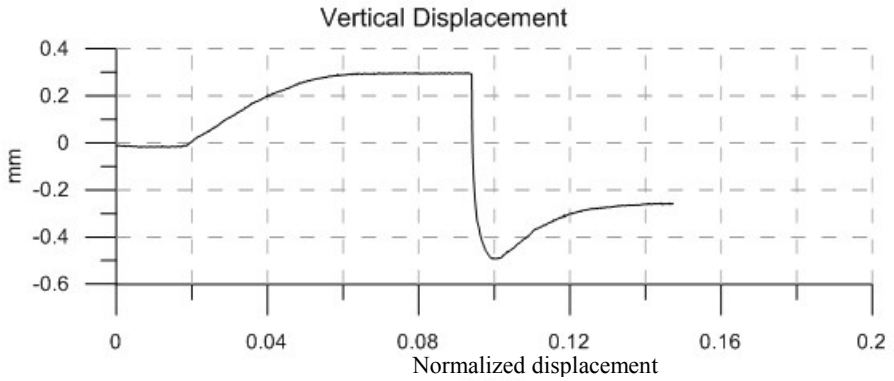

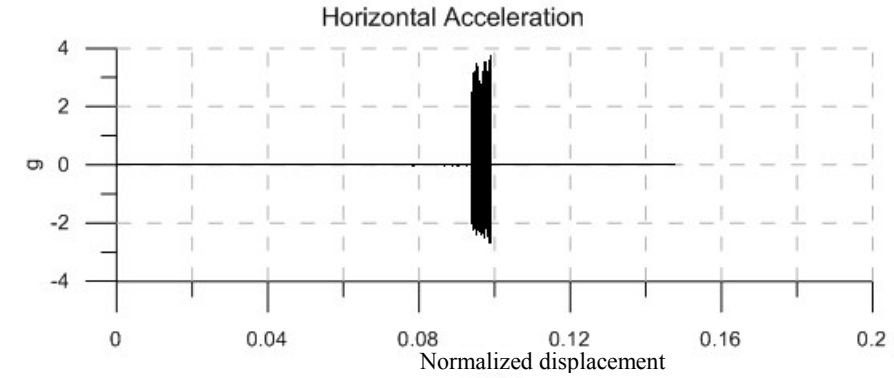

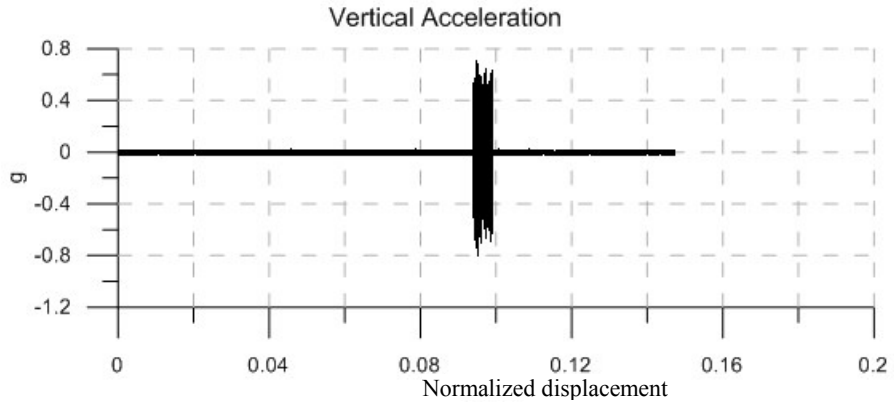

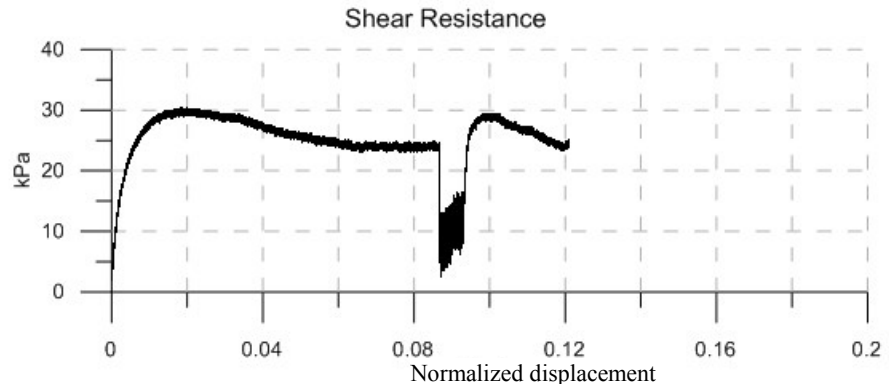

Material:	Sand
Size:	Coarse
Normal Stress:	36 kPa
Vibration Frequency:	60 Hz
Vibration Duration:	30 sec
Horizontal Acceleration:	2.7 g
Vertical Acceleration:	0.49 g
Horizontal Amplitude:	0.1864 mm
Vertical Amplitude:	0.0338 mm
Peak Strength:	29.5 kPa
Residual Strength:	24 kPa
Vibro-Residual Strength:	7 kPa

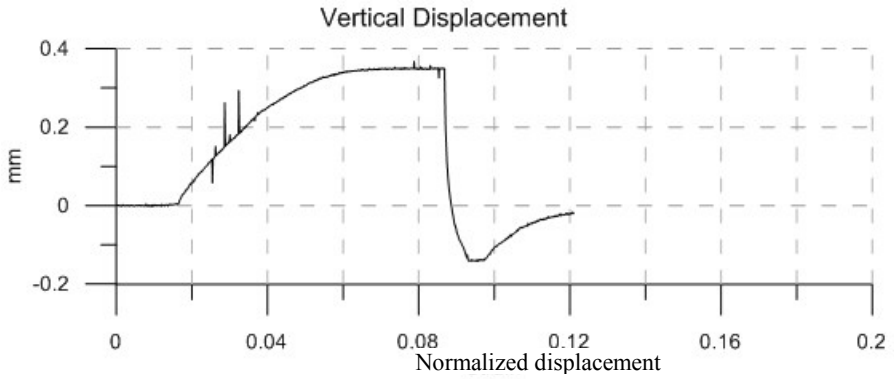

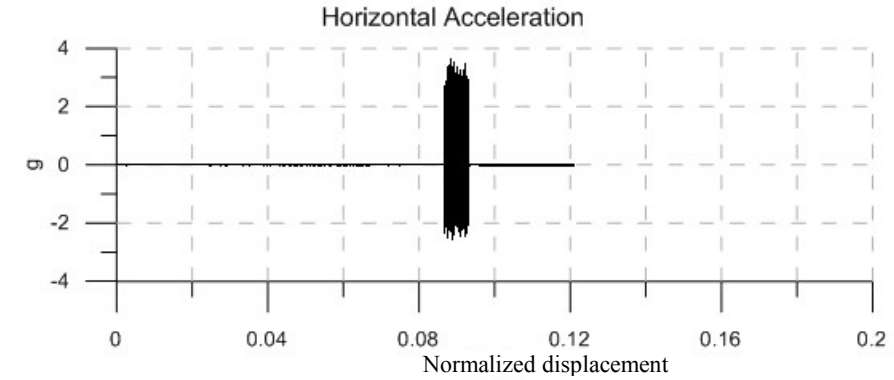

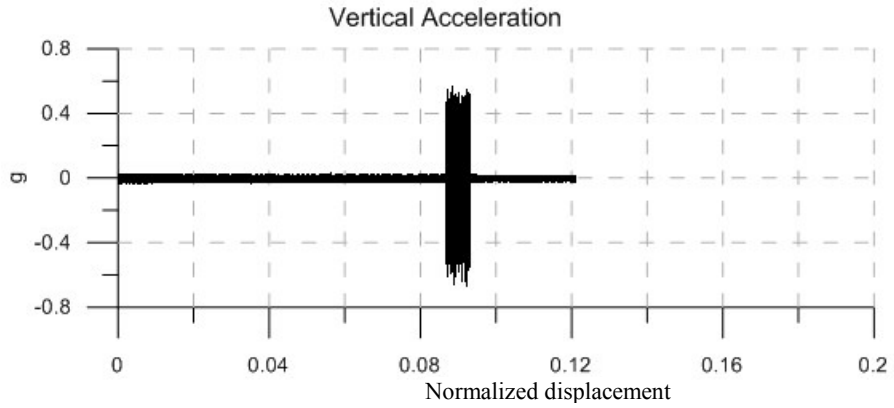

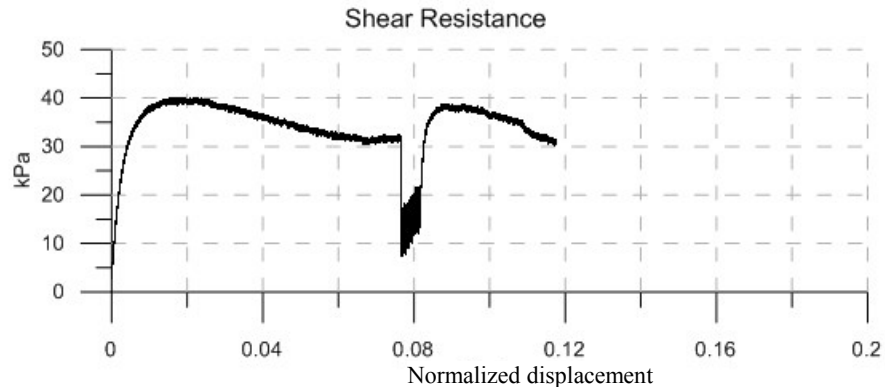

Material:	Sand
Size:	Coarse
Normal Stress:	50 kPa
Vibration Frequency:	60 Hz
Vibration Duration:	30 sec
Horizontal Acceleration:	2.8 g
Vertical Acceleration:	0.49 g
Horizontal Amplitude:	0.1933 mm
Vertical Amplitude:	0.0338 mm
Peak Strength:	39.5 kPa
Residual Strength:	31.5 kPa
Vibro-Residual Strength:	11 kPa

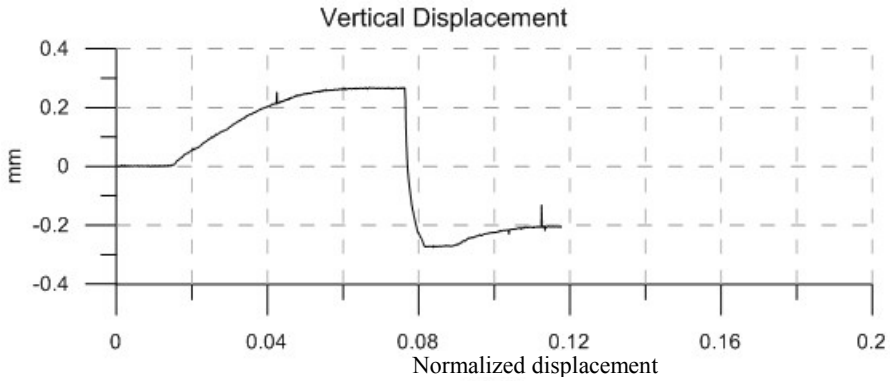

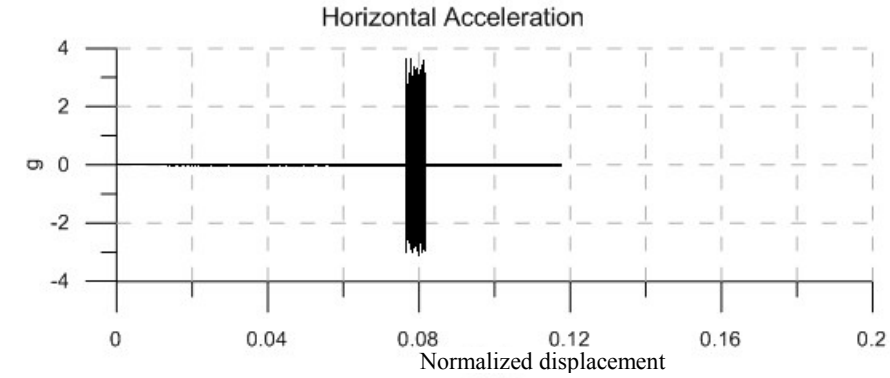

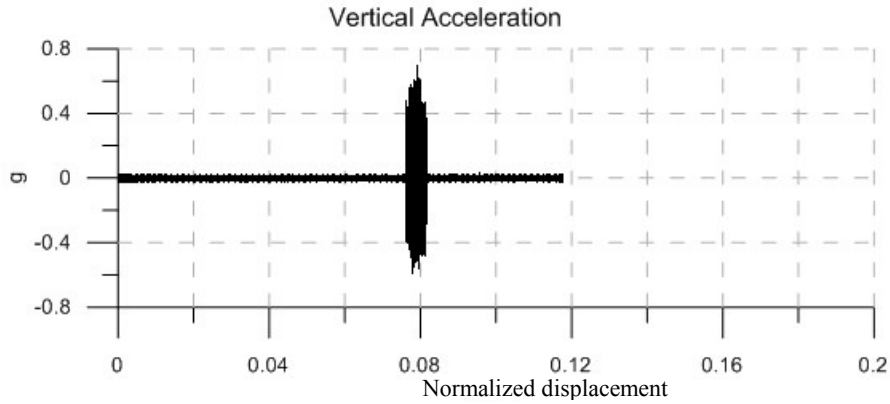

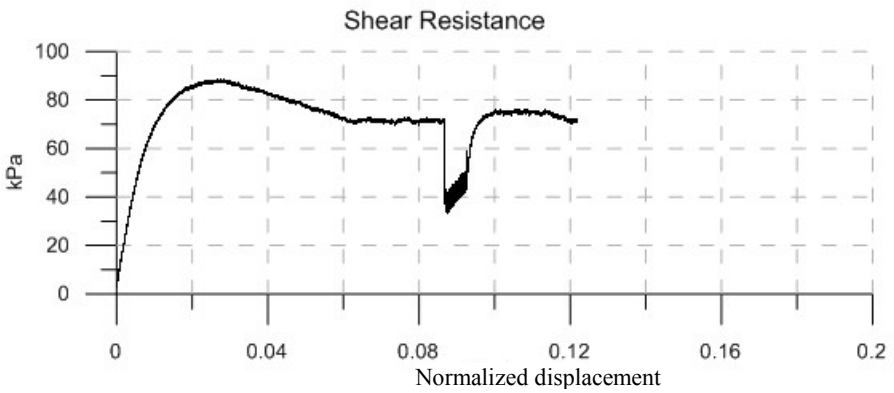

Material:	Sand
Size:	Coarse
Normal Stress:	118 kPa
Vibration Frequency:	60 Hz
Vibration Duration:	35 sec
Horizontal Acceleration:	2.3 g
Vertical Acceleration:	0.52 g
Horizontal Amplitude:	0.1588 mm
Vertical Amplitude:	0.0359 mm
Peak Strength:	88 kPa
Residual Strength:	71.5 kPa
Vibro-Residual Strength:	36 kPa

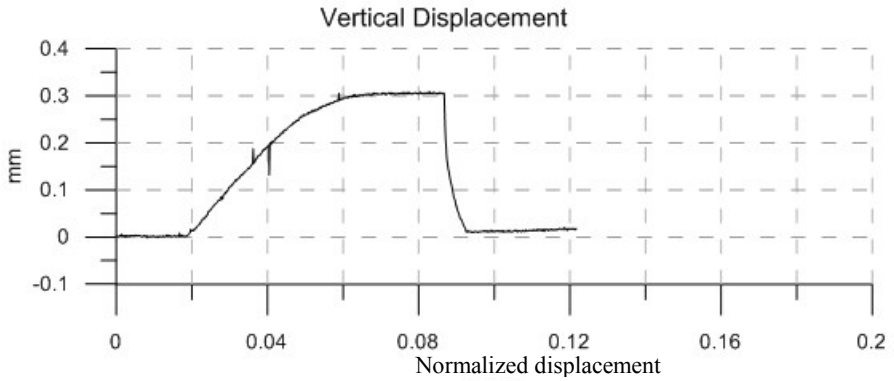

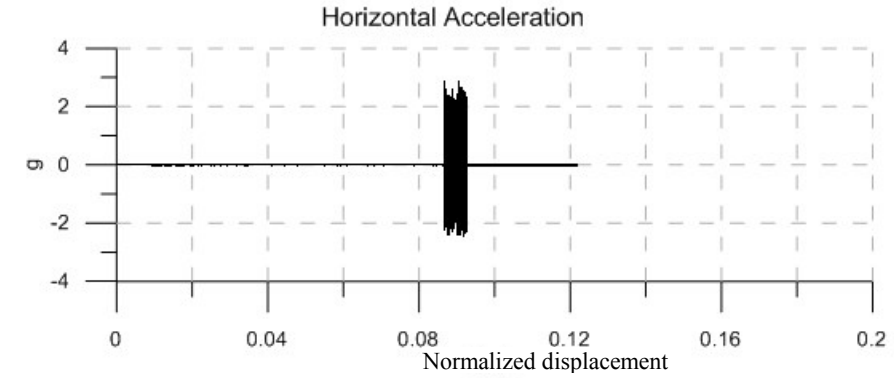

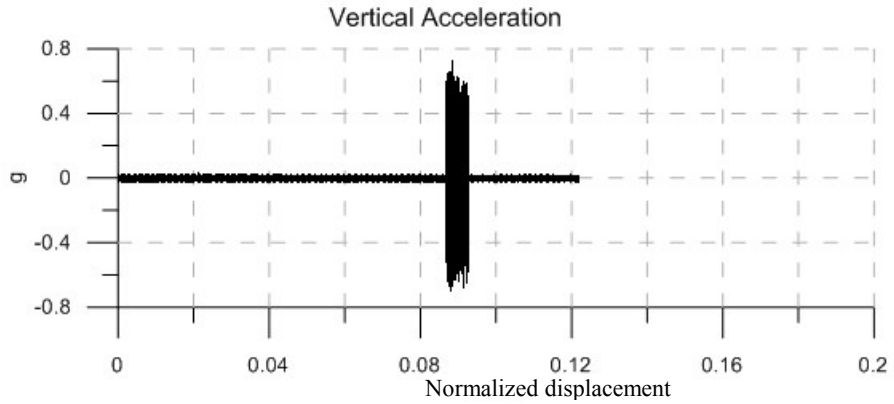

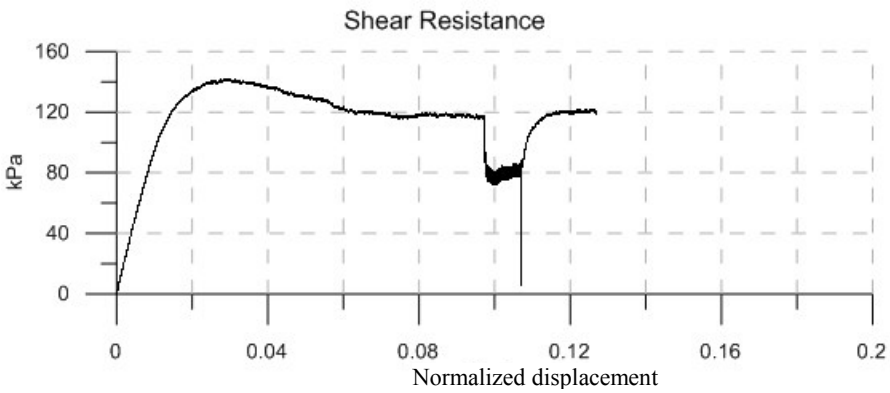

Material:	Sand
Size:	Coarse
Normal Stress:	200 kPa
Vibration Frequency:	60 Hz
Vibration Duration:	58 sec
Horizontal Acceleration:	2.3 g
Vertical Acceleration:	0.75 g
Horizontal Amplitude:	0.1588 mm
Vertical Amplitude:	0.0518 mm
Peak Strength:	141.5 kPa
Residual Strength:	117.5 kPa
Vibro-Residual Strength:	76 kPa

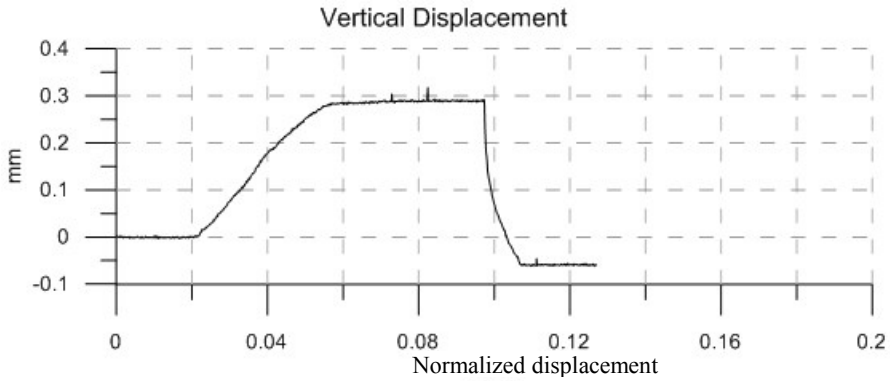

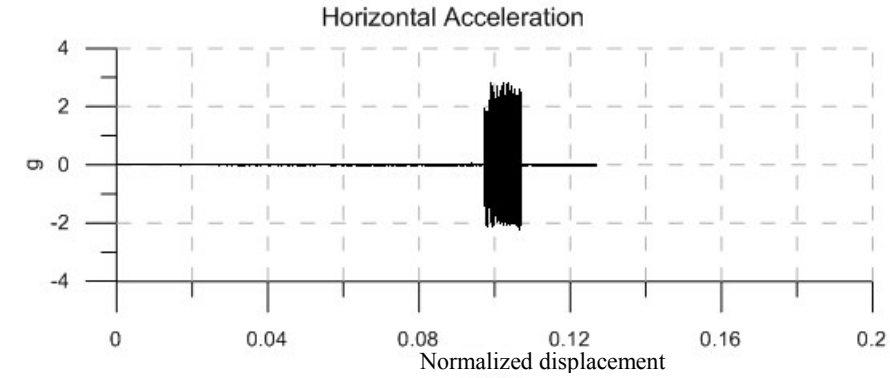

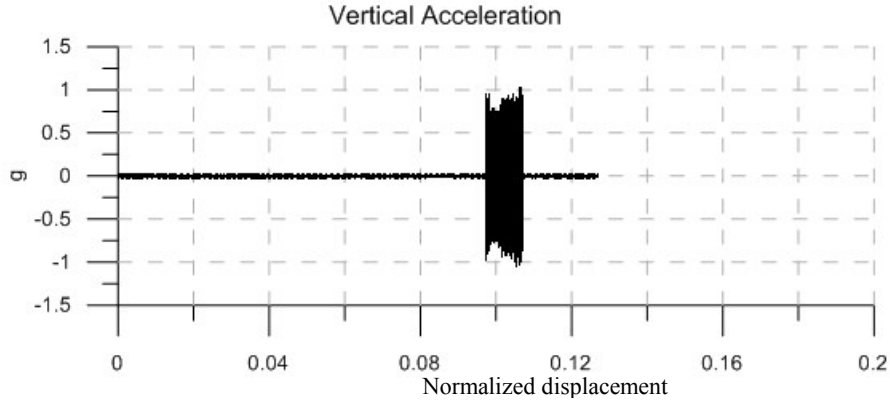

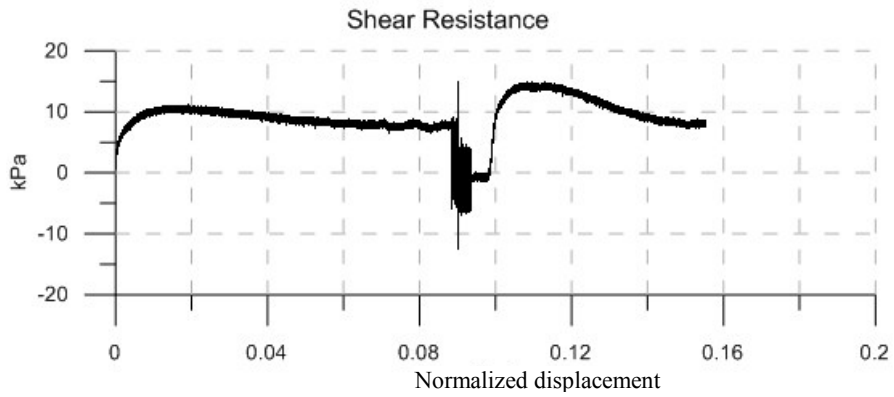

Material:	Sand
Size:	Coarse
Normal Stress:	8 kPa
Vibration Frequency:	60 Hz
Vibration Duration:	30 sec
Horizontal Acceleration:	4.6 g
Vertical Acceleration:	1.1 g
Horizontal Amplitude:	0.3175 mm
Vertical Amplitude:	0.0759 mm
Peak Strength:	10.5 kPa
Residual Strength:	8 kPa
Vibro-Residual Strength:	0 kPa

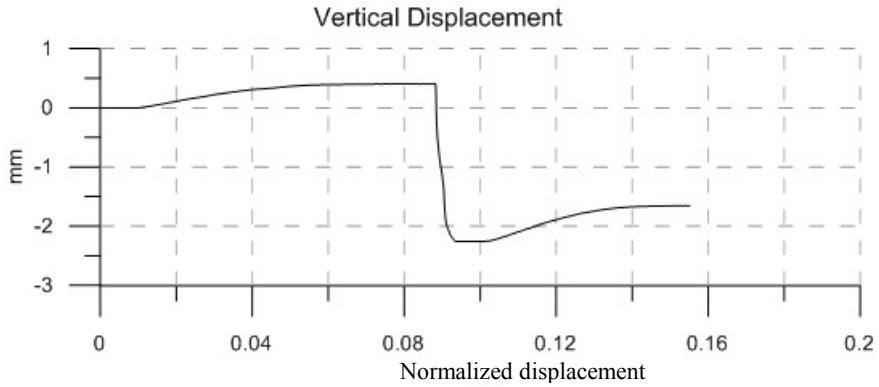

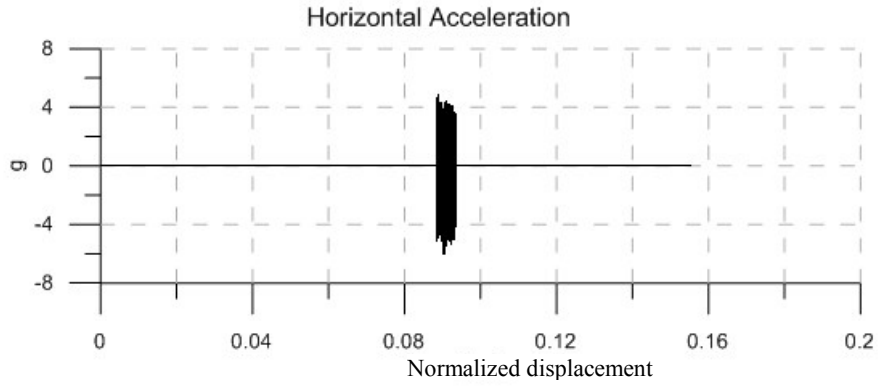

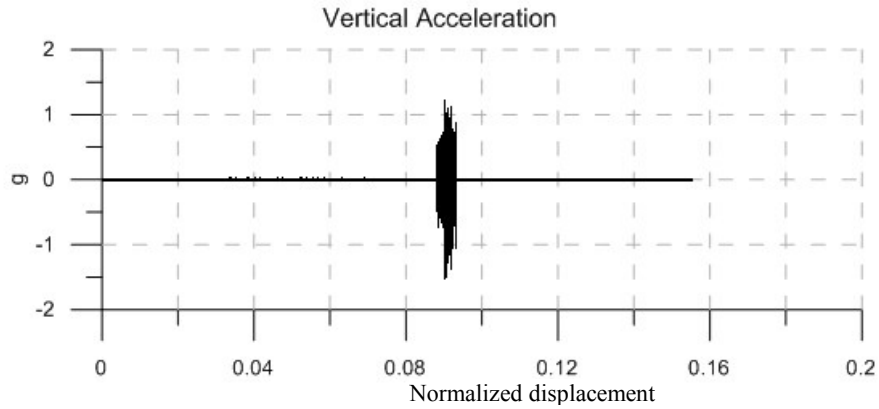

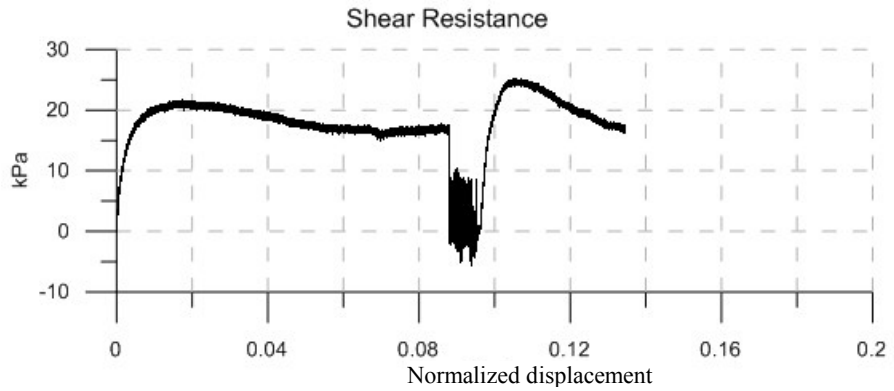

Material:	Sand
Size:	Coarse
Normal Stress:	23 kPa
Vibration Frequency:	60 Hz
Vibration Duration:	42 sec
Horizontal Acceleration:	4.2 g
Vertical Acceleration:	1.1 g
Horizontal Amplitude:	0.2899 mm
Vertical Amplitude:	0.0759 mm
Peak Strength:	21 kPa
Residual Strength:	17 kPa
Vibro-Residual Strength:	0 kPa

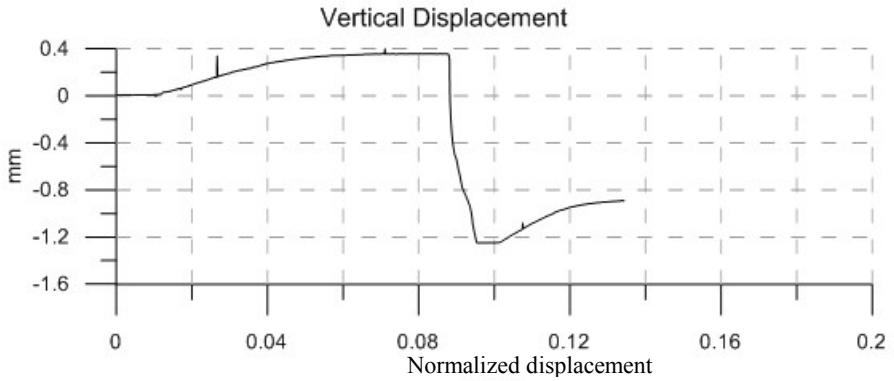

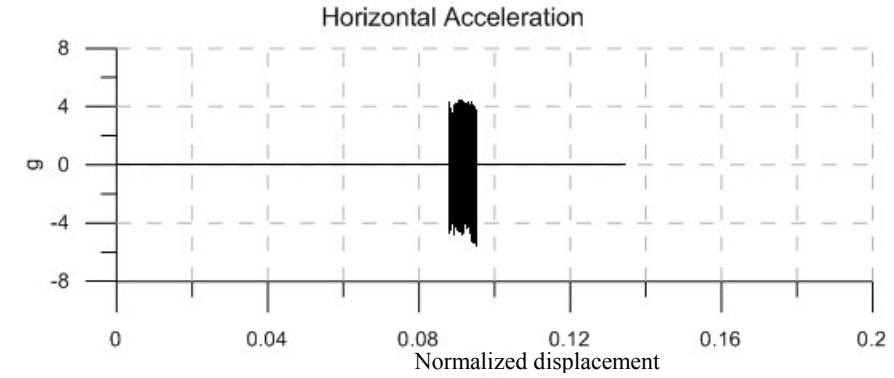

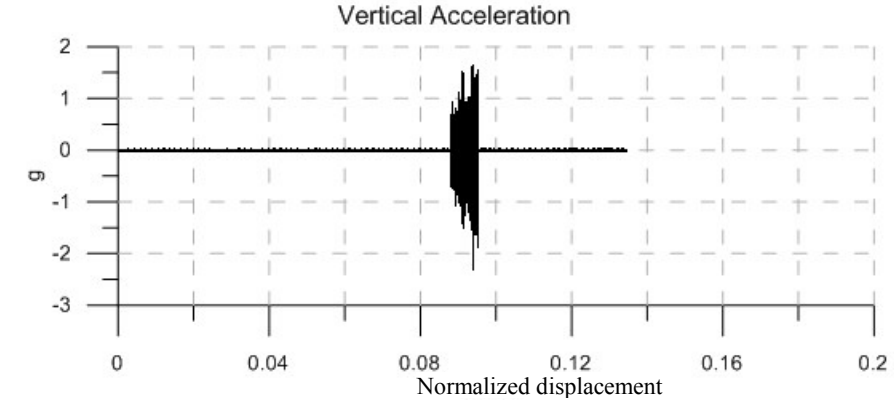

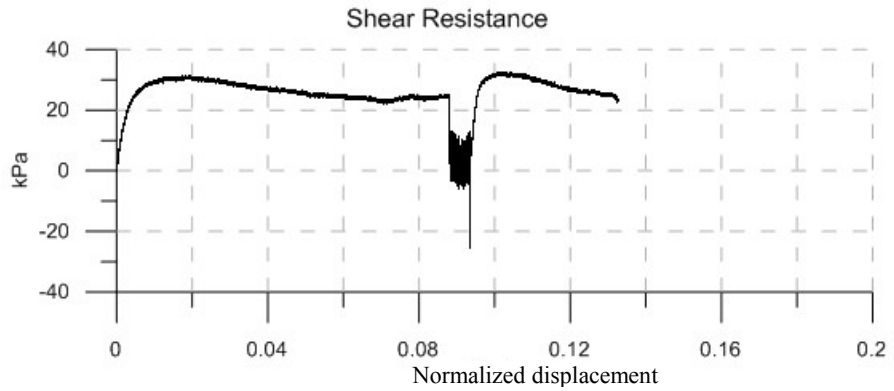

Material:	Sand
Size:	Coarse
Normal Stress:	36 kPa
Vibration Frequency:	60 Hz
Vibration Duration:	33 sec
Horizontal Acceleration:	4.1 g
Vertical Acceleration:	1.2 g
Horizontal Amplitude:	0.2830 mm
Vertical Amplitude:	0.0828 mm
Peak Strength:	31 kPa
Residual Strength:	24.5 kPa
Vibro-Residual Strength:	0 kPa

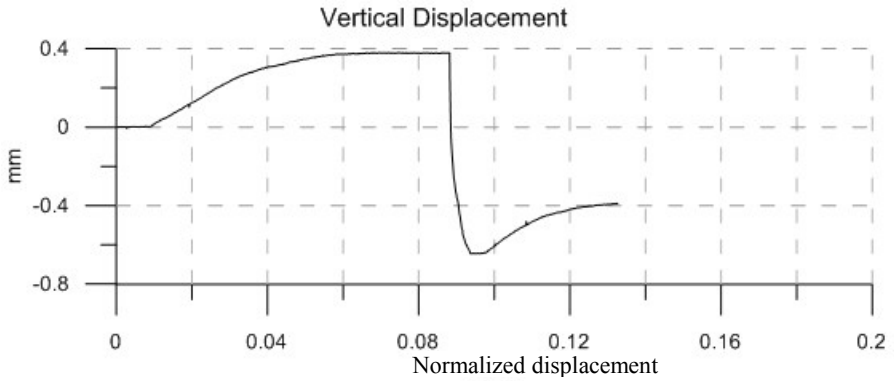

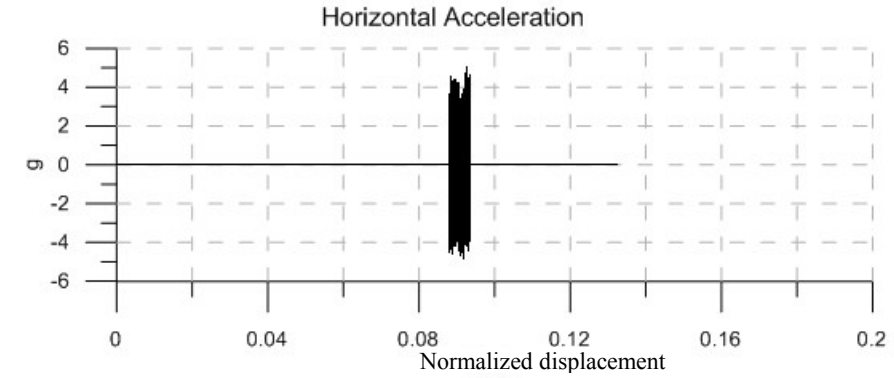

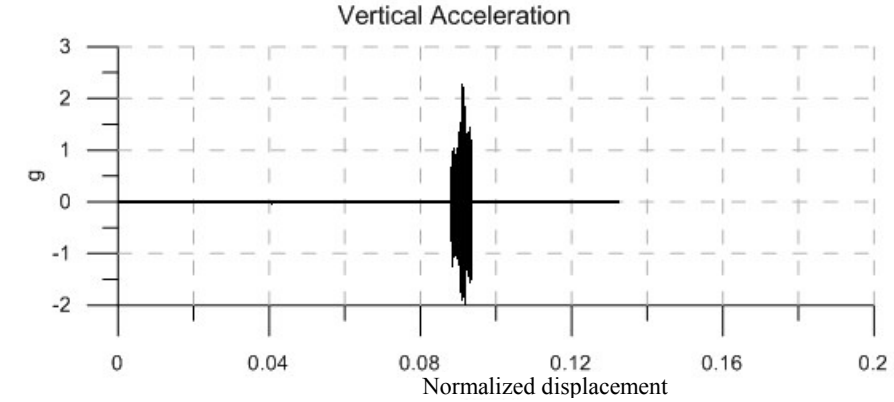

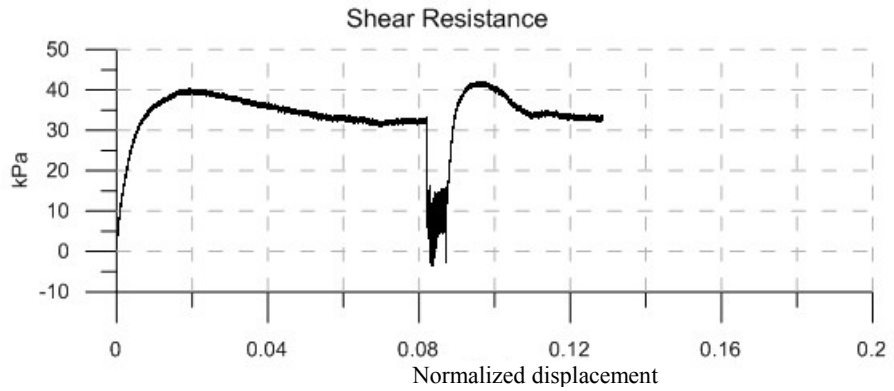

Material:	Sand
Size:	Coarse
Normal Stress:	50 kPa
Vibration Frequency:	60 Hz
Vibration Duration:	30 sec
Horizontal Acceleration:	4.5 g
Vertical Acceleration:	0.8 g
Horizontal Amplitude:	0.3106 mm
Vertical Amplitude:	0.0552 mm
Peak Strength:	40 kPa
Residual Strength:	32.5 kPa
Vibro-Residual Strength:	4 kPa

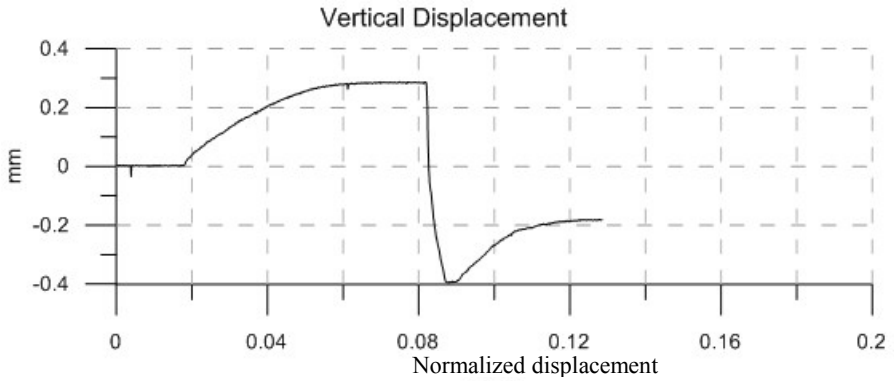

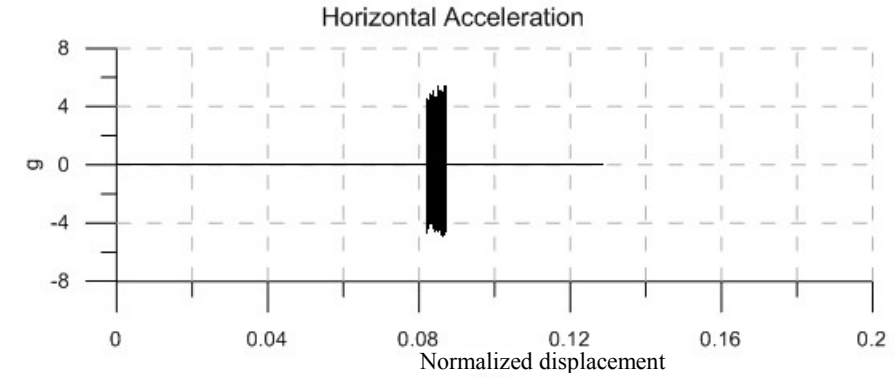

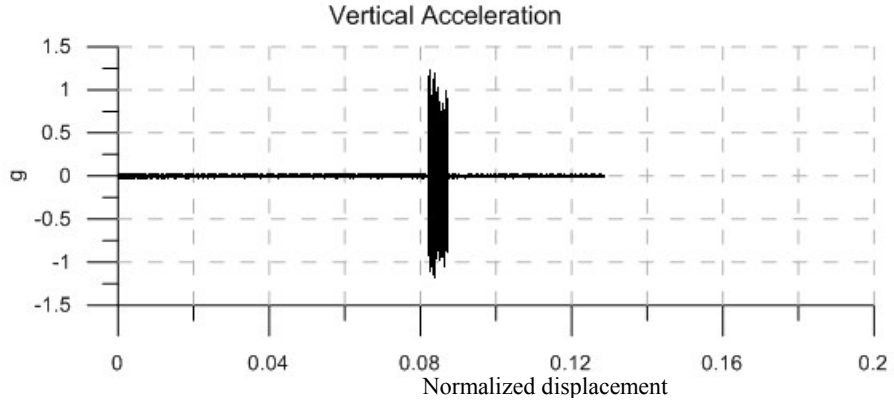

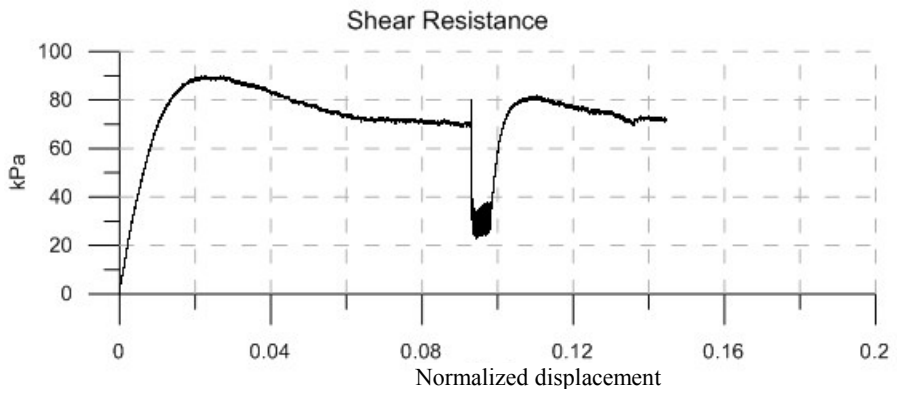

Material:	Sand
Size:	Coarse
Normal Stress:	118 kPa
Vibration Frequency:	60 Hz
Vibration Duration:	30 sec
Horizontal Acceleration:	4.2 g
Vertical Acceleration:	1.0 g
Horizontal Amplitude:	0.2899 mm
Vertical Amplitude:	0.0690 mm
Peak Strength:	89 kPa
Residual Strength:	71 kPa
Vibro-Residual Strength:	27.5 kPa

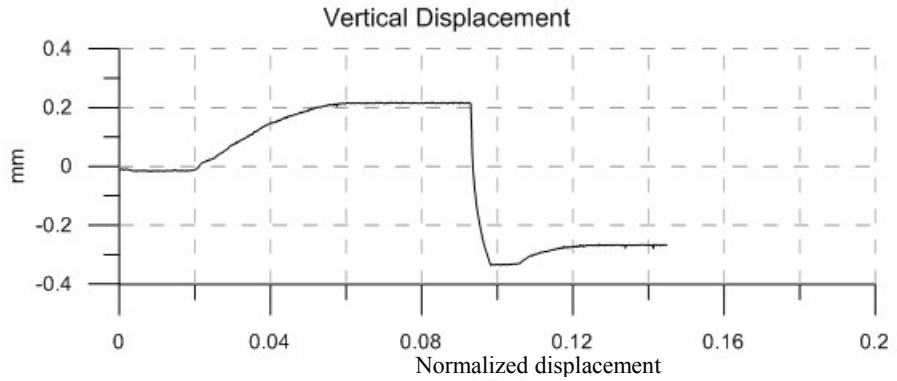

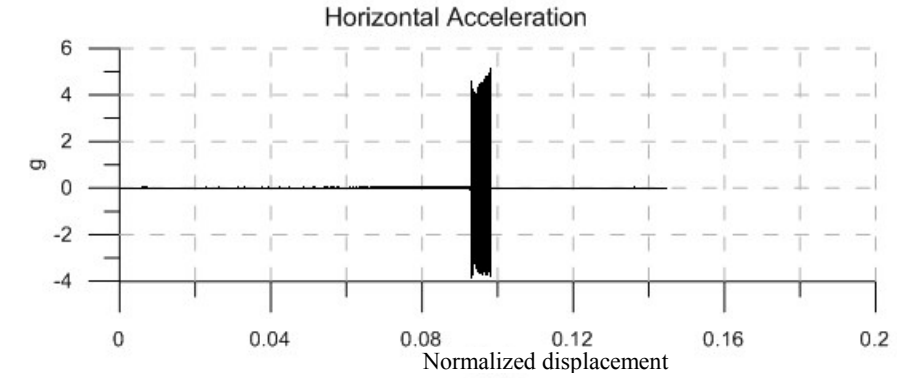

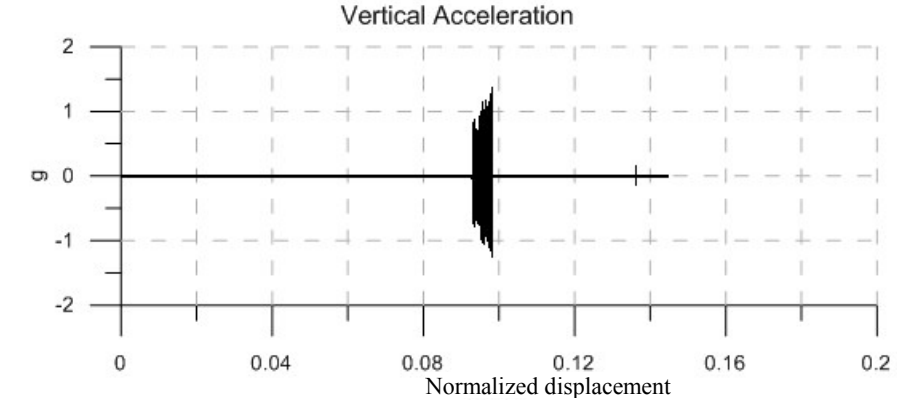

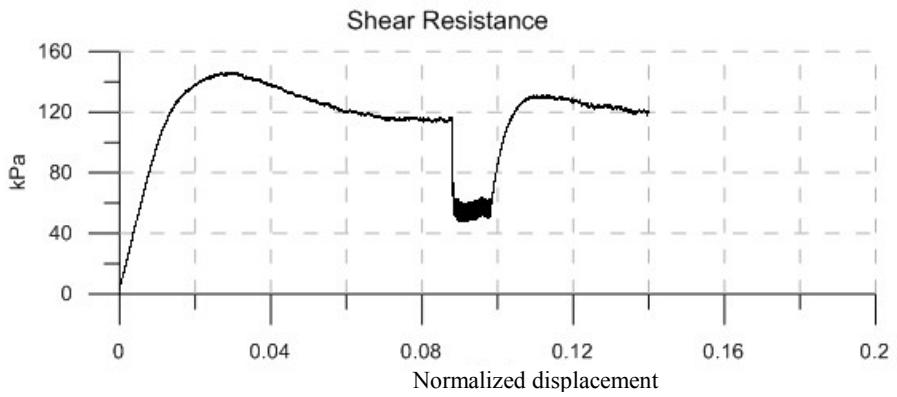

Material:	Sand
Size:	Coarse
Normal Stress:	200 kPa
Vibration Frequency:	60 Hz
Vibration Duration:	60 sec
Horizontal Acceleration:	4.1 g
Vertical Acceleration:	1.4 g
Horizontal Amplitude:	0.2830 mm
Vertical Amplitude:	0.0966 mm
Peak Strength:	145.5 kPa
Residual Strength:	115.5 kPa
Vibro-Residual Strength:	52 kPa

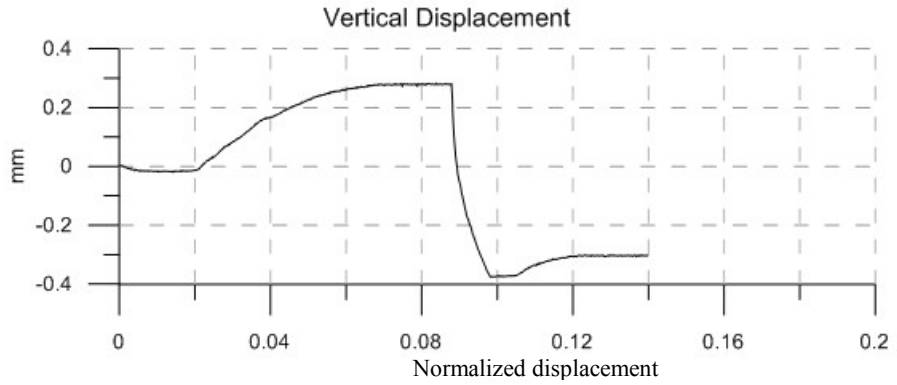

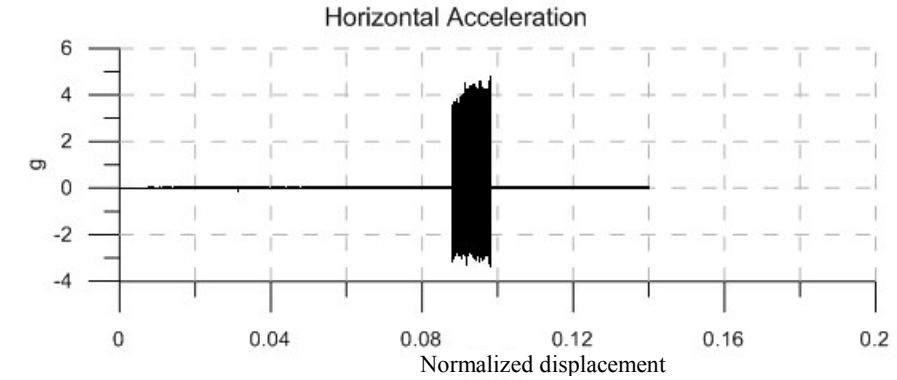

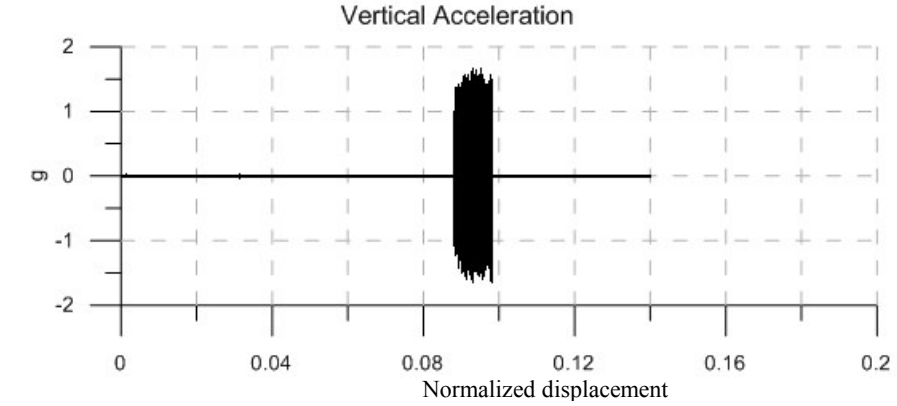

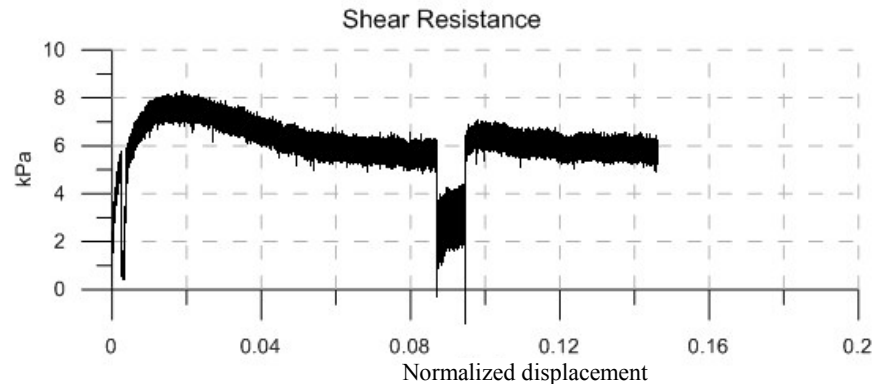

Material:	Glass Beads
Size:	0.55 mm
Normal Stress:	8 kPa
Vibration Frequency:	60 Hz
Vibration Duration:	45 sec
Horizontal Acceleration:	0.4 g
Vertical Acceleration:	0.04 g
Horizontal Amplitude:	0.0276 mm
Vertical Amplitude:	0.0028 mm
Peak Strength:	8 kPa
Residual Strength:	6 kPa
Vibro-Residual Strength:	2 kPa

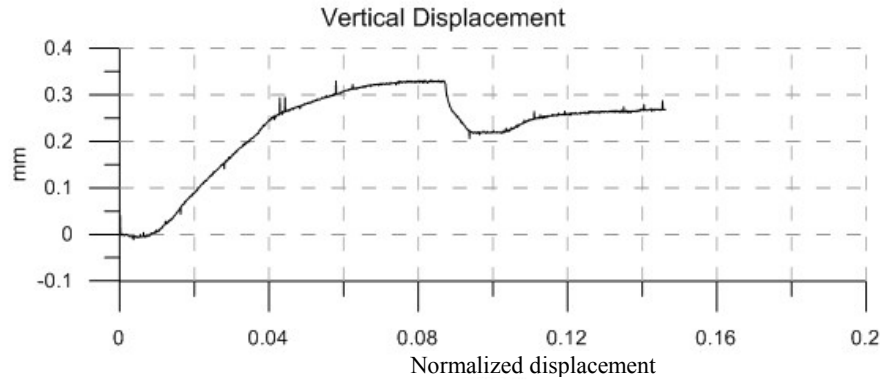

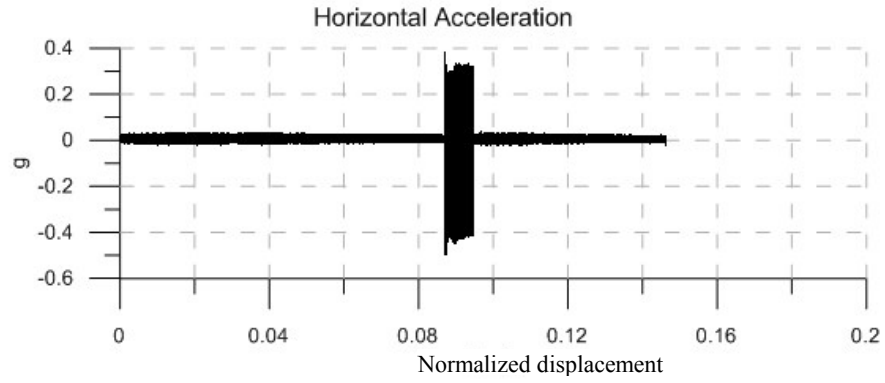

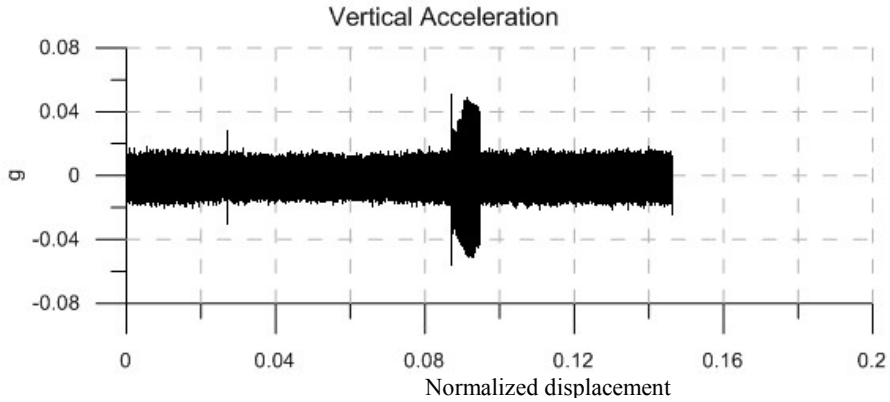

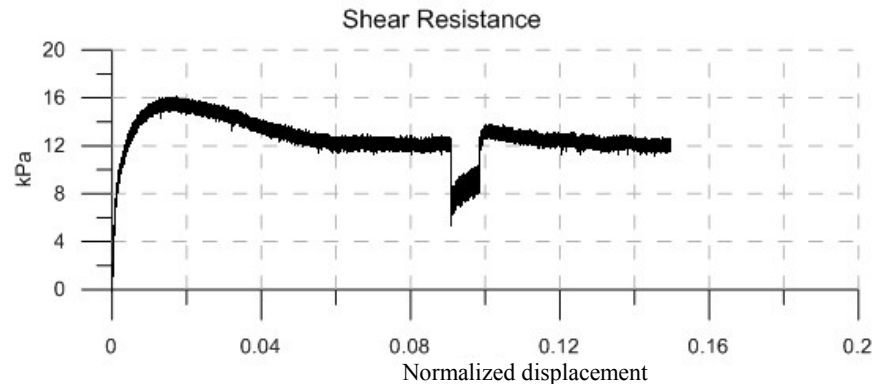

Material:	Glass Beads
Size:	0.55 mm
Normal Stress:	23 kPa
Vibration Frequency:	60 Hz
Vibration Duration:	45 sec
Horizontal Acceleration:	0.55 g
Vertical Acceleration:	0.08 g
Horizontal Amplitude:	0.0380 mm
Vertical Amplitude:	0.0055 mm
Peak Strength:	16 kPa
Residual Strength:	12.5 kPa
Vibro-Residual Strength:	7 kPa

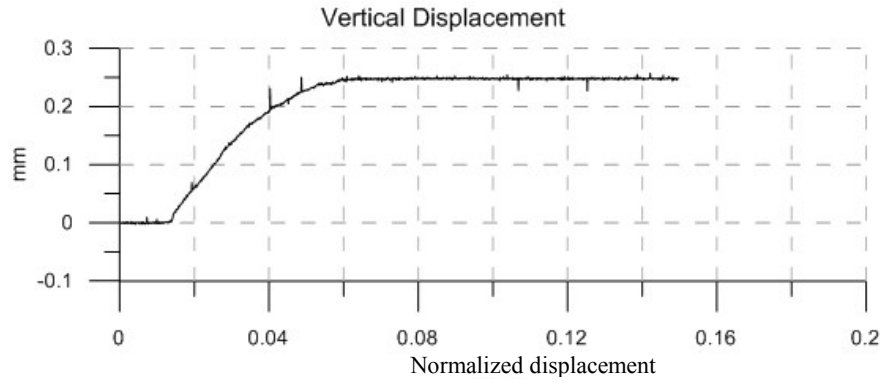

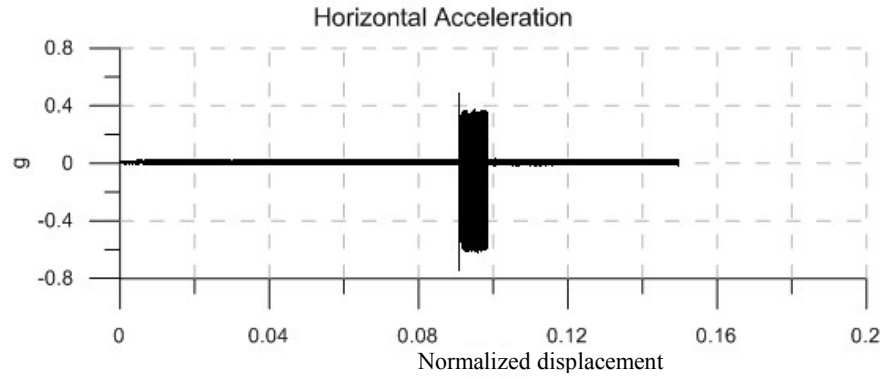

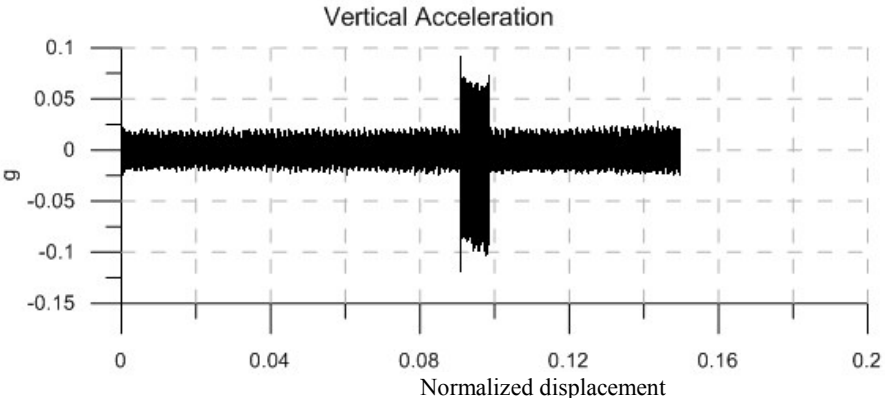

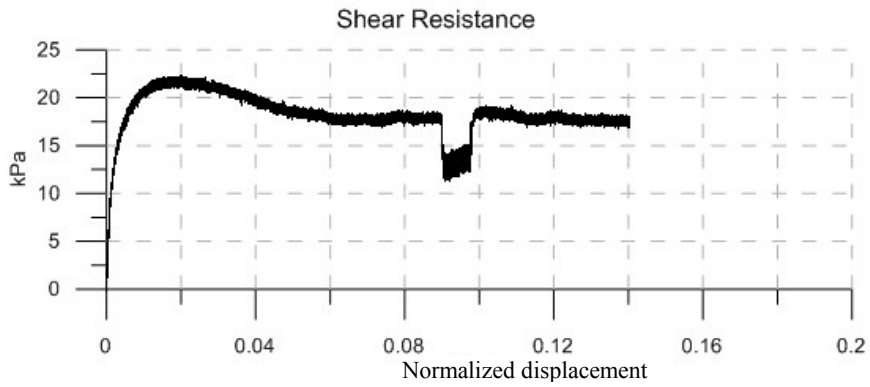

Material:	Glass Beads
Size:	0.55 mm
Normal Stress:	36 kPa
Vibration Frequency:	60 Hz
Vibration Duration:	45 sec
Horizontal Acceleration:	0.35 g
Vertical Acceleration:	0.15 g
Horizontal Amplitude:	0.0242 mm
Vertical Amplitude:	0.0104 mm
Peak Strength:	22 kPa
Residual Strength:	19 kPa
Vibro-Residual Strength:	12.5 kPa

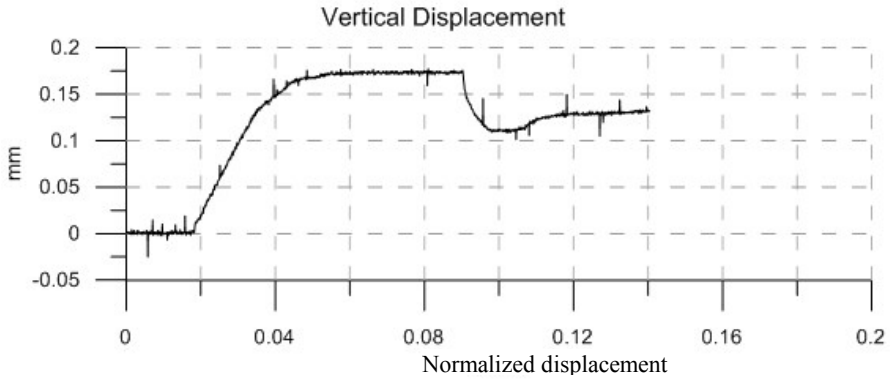

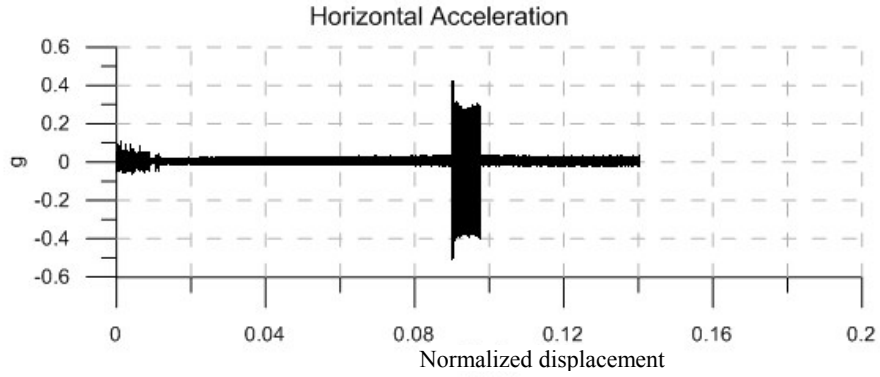

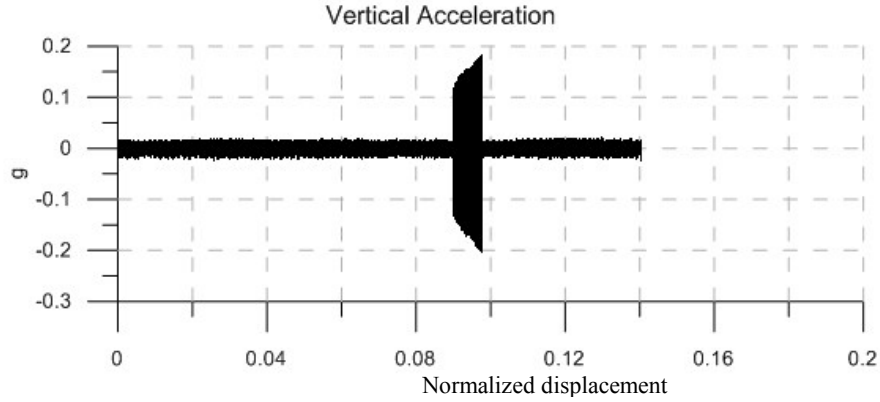

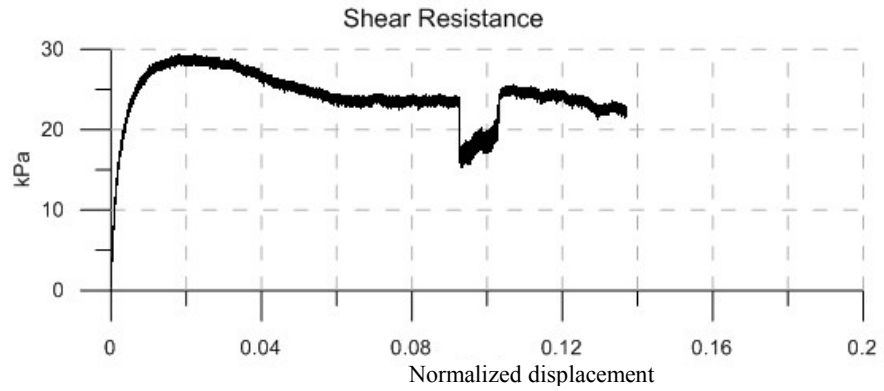

Material:	Glass Beads
Size:	0.55 mm
Normal Stress:	50 kPa
Vibration Frequency:	60 Hz
Vibration Duration:	60 sec
Horizontal Acceleration:	0.5 g
Vertical Acceleration:	0.15 g
Horizontal Amplitude:	0.0345 mm
Vertical Amplitude:	0.0104 mm
Peak Strength:	29 kPa
Residual Strength:	24 kPa
Vibro-Residual Strength:	17 kPa

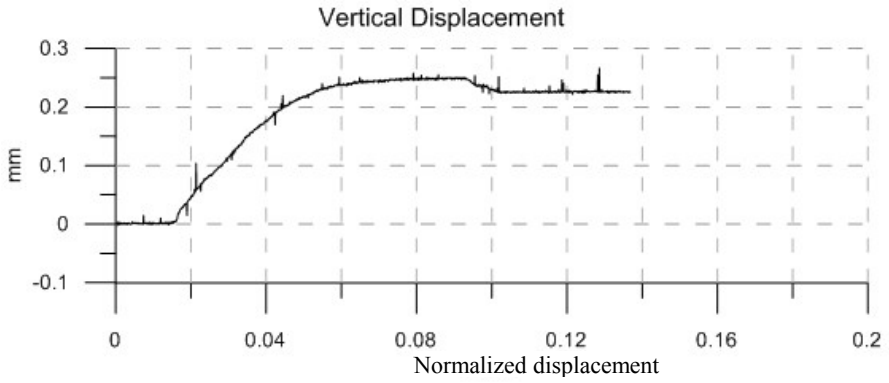

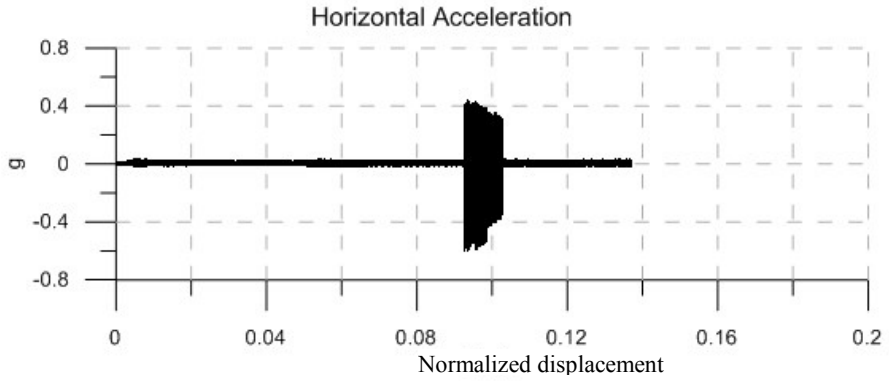

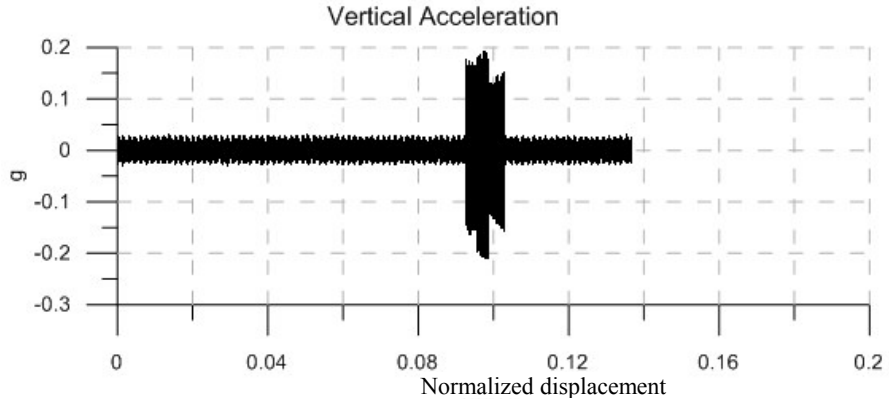

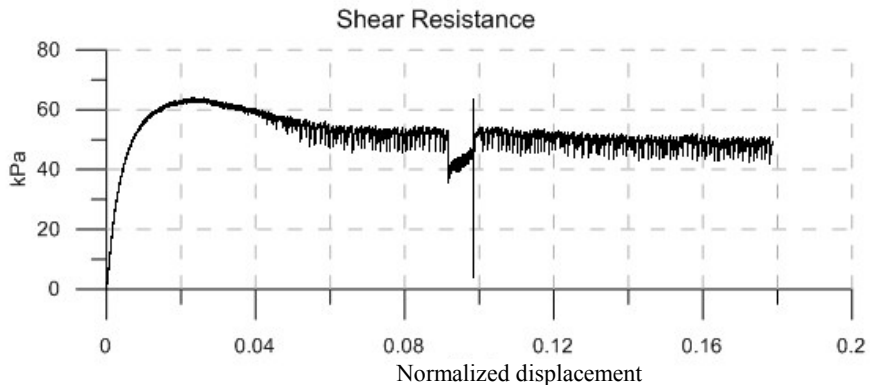

Material:	Glass Beads
Size:	0.55 mm
Normal Stress:	118 kPa
Vibration Frequency:	60 Hz
Vibration Duration:	41 sec
Horizontal Acceleration:	0.44 g
Vertical Acceleration:	0.13 g
Horizontal Amplitude:	0.0304 mm
Vertical Amplitude:	0.0090 mm
Peak Strength:	63.5 kPa
Residual Strength:	53 kPa
Vibro-Residual Strength:	38 kPa

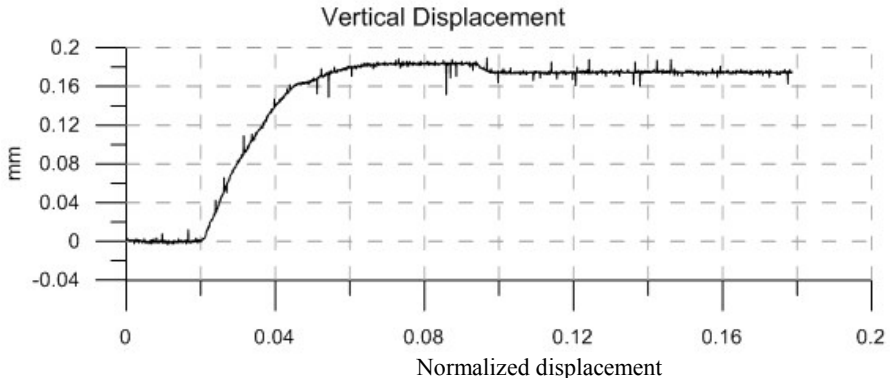

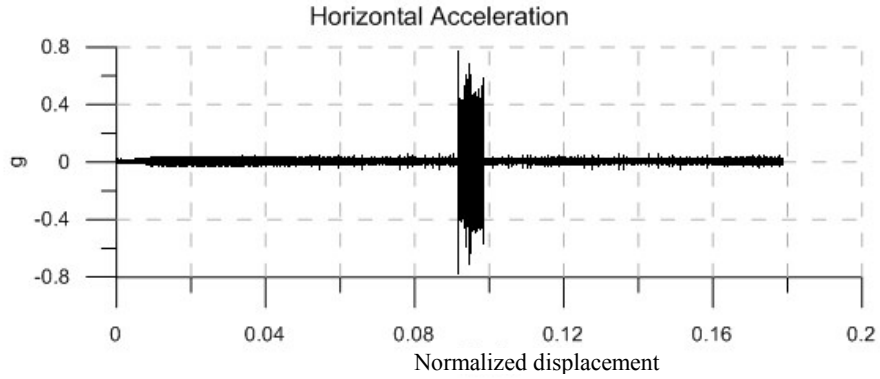

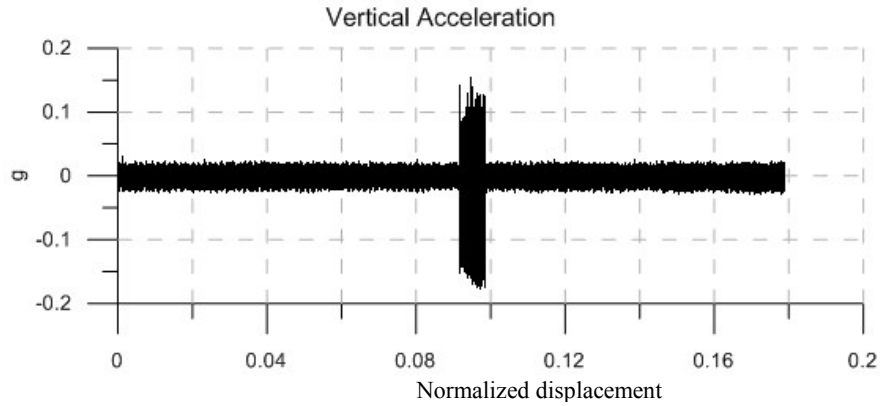

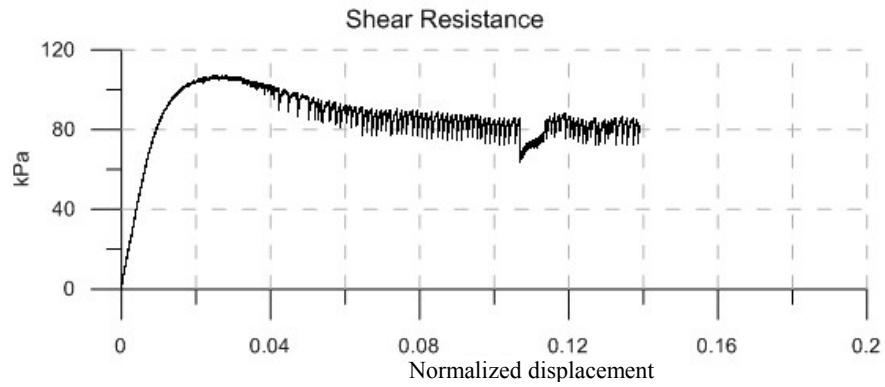

Material:	Glass Beads
Size:	0.55 mm
Normal Stress:	200 kPa
Vibration Frequency:	60 Hz
Vibration Duration:	39 sec
Horizontal Acceleration:	0.4 g
Vertical Acceleration:	0.11 g
Horizontal Amplitude:	0.0276 mm
Vertical Amplitude:	0.0076 mm
Peak Strength:	107 kPa
Residual Strength:	85 kPa
Vibro-Residual Strength:	66 kPa

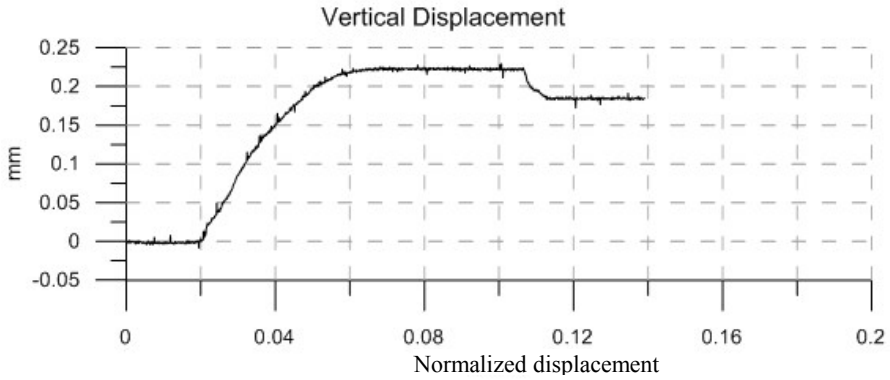

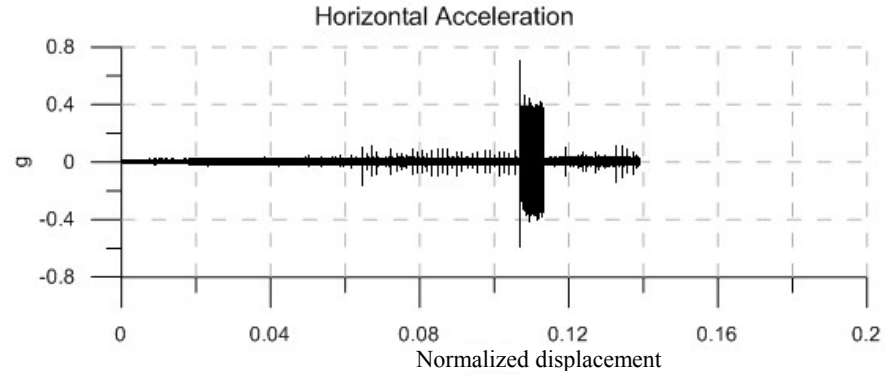

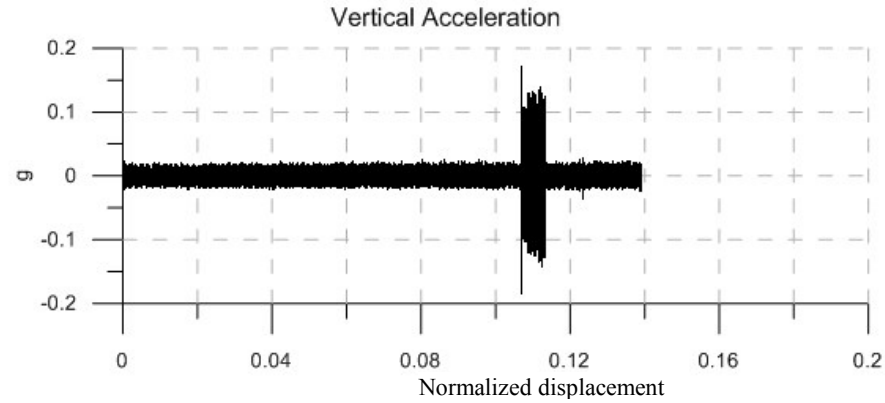

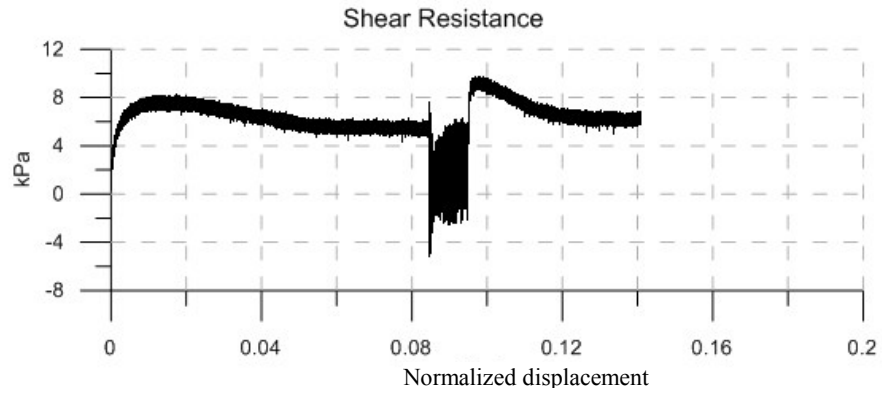

Material:	Glass Beads
Size:	0.55 mm
Normal Stress:	8 kPa
Vibration Frequency:	60 Hz
Vibration Duration:	59 sec
Horizontal Acceleration:	1.55 g
Vertical Acceleration:	0.3 g
Horizontal Amplitude:	0.1070 mm
Vertical Amplitude:	0.0207 mm
Peak Strength:	8 kPa
Residual Strength:	6 kPa
Vibro-Residual Strength:	0 kPa

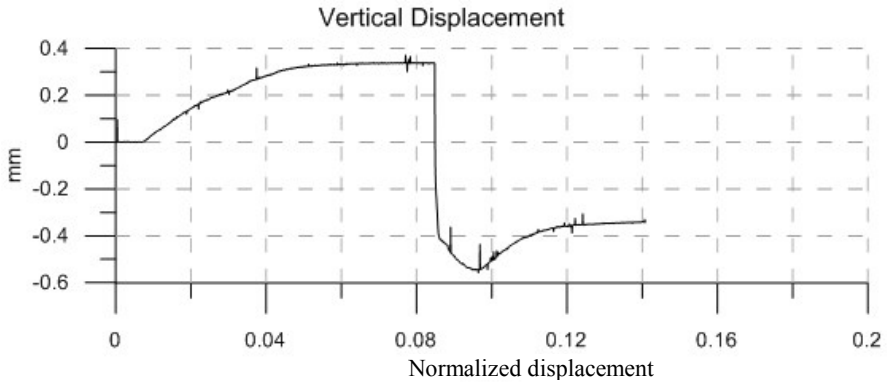

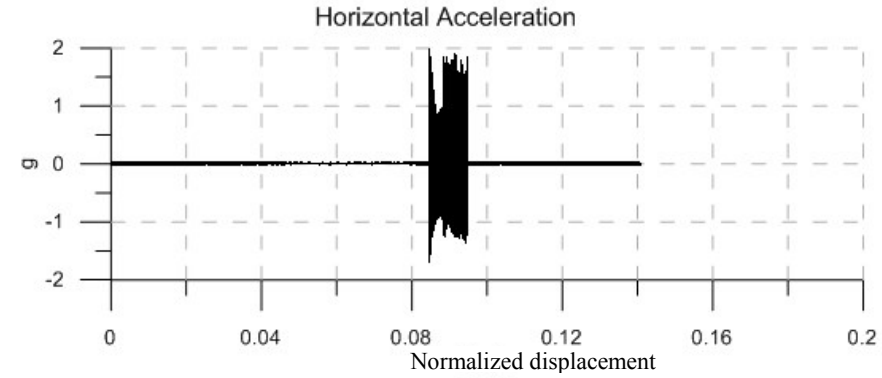

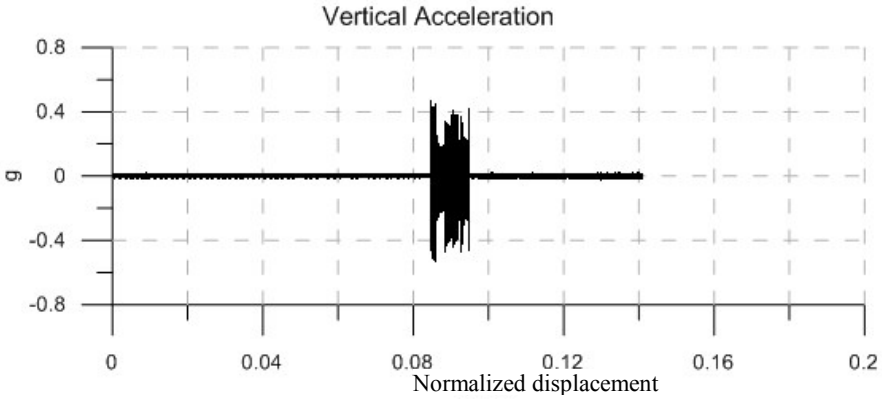

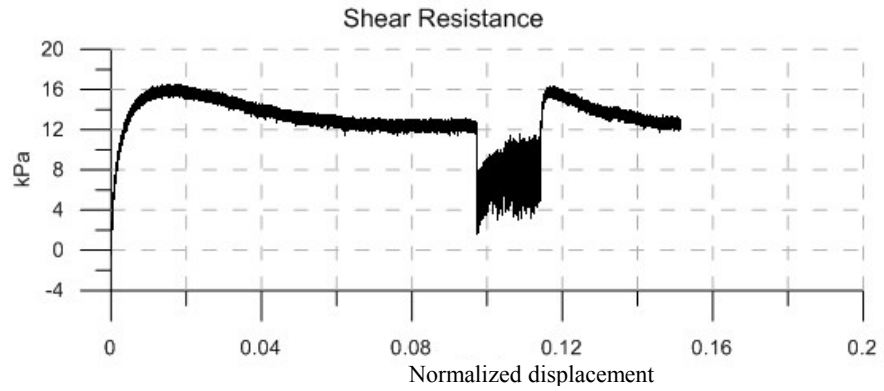

Material:	Glass Beads
Size:	0.55 mm
Normal Stress:	23 kPa
Vibration Frequency:	60 Hz
Vibration Duration:	100 sec
Horizontal Acceleration:	1.4 g
Vertical Acceleration:	0.2 g
Horizontal Amplitude:	0.0966 mm
Vertical Amplitude:	0.0138 mm
Peak Strength:	16 kPa
Residual Strength:	12.5 kPa
Vibro-Residual Strength:	4 kPa

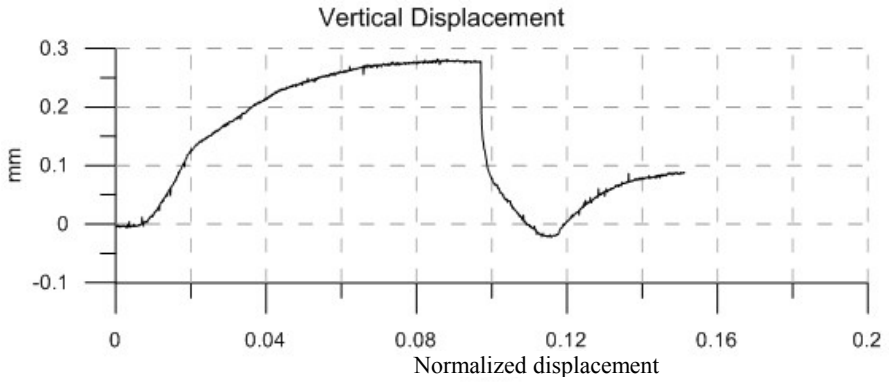

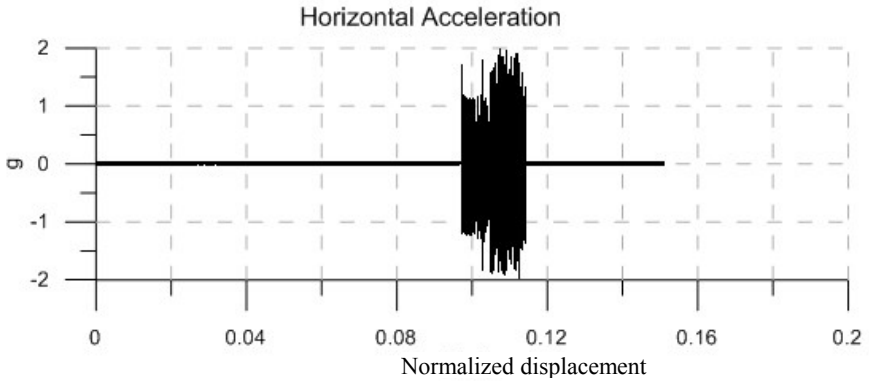

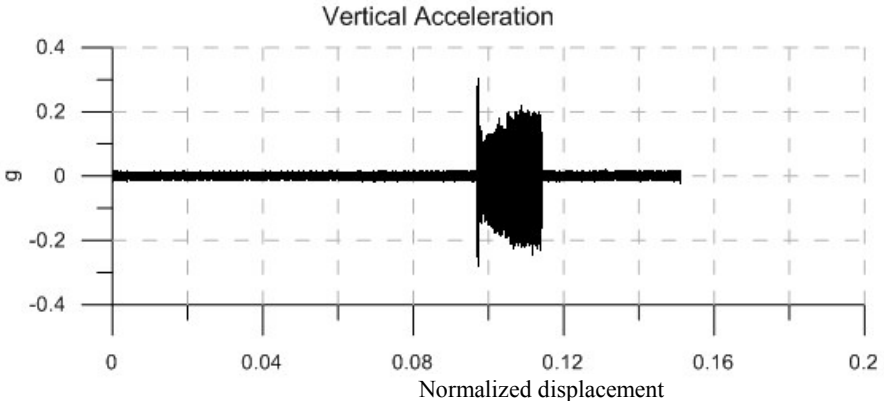

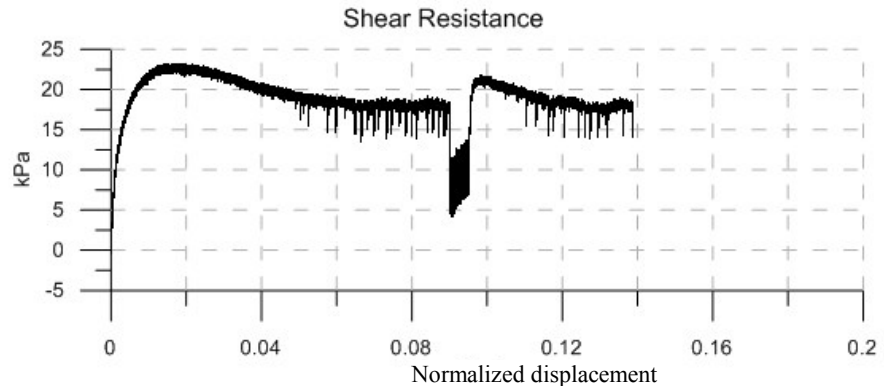

Material:	Glass Beads
Size:	0.55 mm
Normal Stress:	36 kPa
Vibration Frequency:	60 Hz
Vibration Duration:	30 sec
Horizontal Acceleration:	1.55 g
Vertical Acceleration:	0.2 g
Horizontal Amplitude:	0.1070 mm
Vertical Amplitude:	0.0138 mm
Peak Strength:	23 kPa
Residual Strength:	18.5 kPa
Vibro-Residual Strength:	6.5 kPa

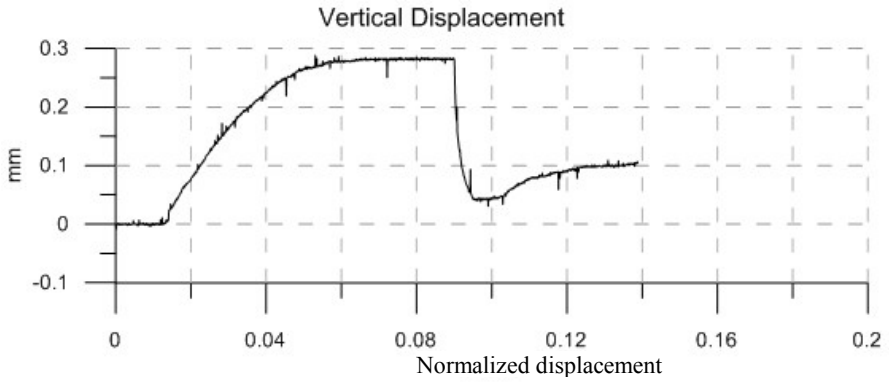

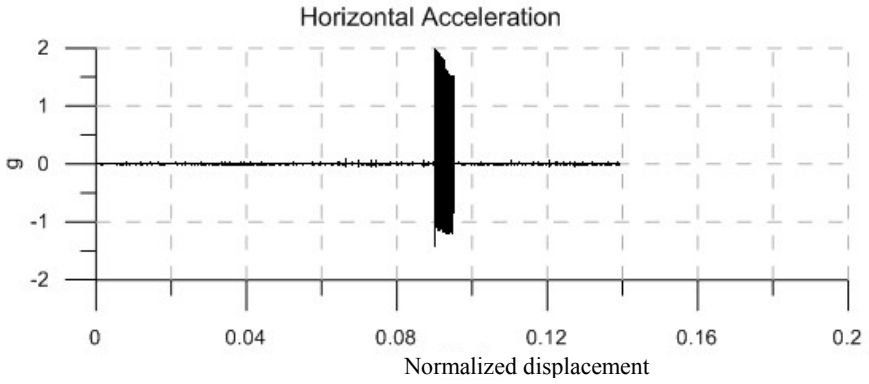

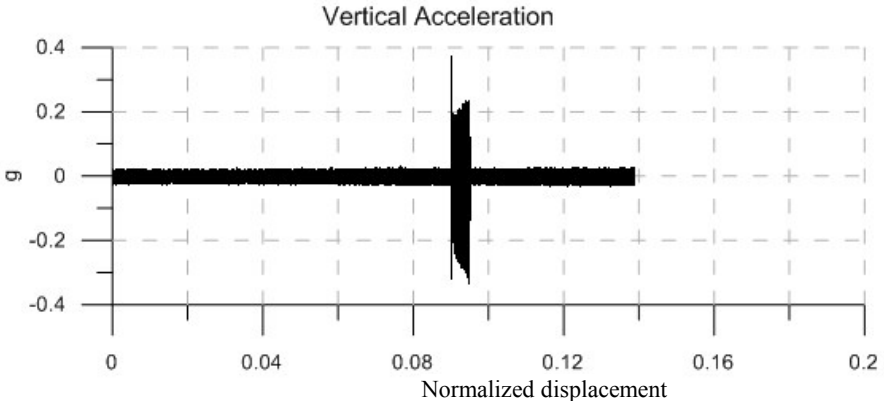

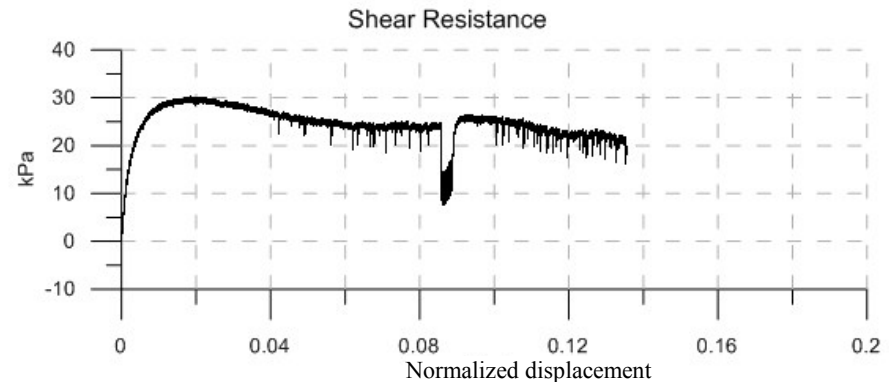

Material:	Glass Beads
Size:	0.55 mm
Normal Stress:	50 kPa
Vibration Frequency:	60 Hz
Vibration Duration:	17 sec
Horizontal Acceleration:	1.4 g
Vertical Acceleration:	0.18 g
Horizontal Amplitude:	0.0966 mm
Vertical Amplitude:	0.0124 mm
Peak Strength:	30 kPa
Residual Strength:	24 kPa
Vibro-Residual Strength:	10 kPa

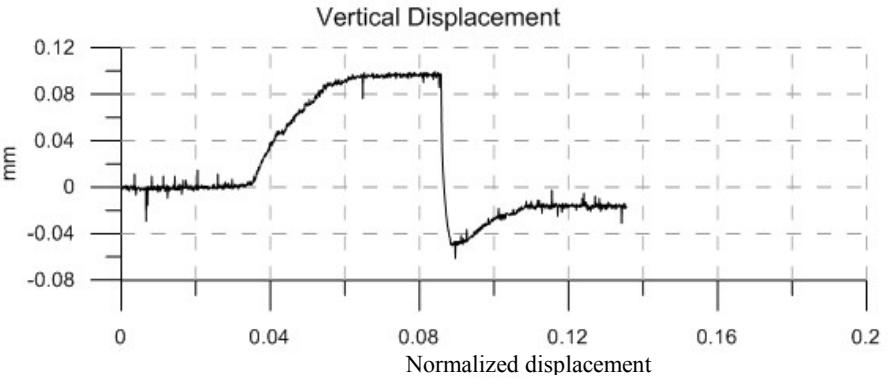

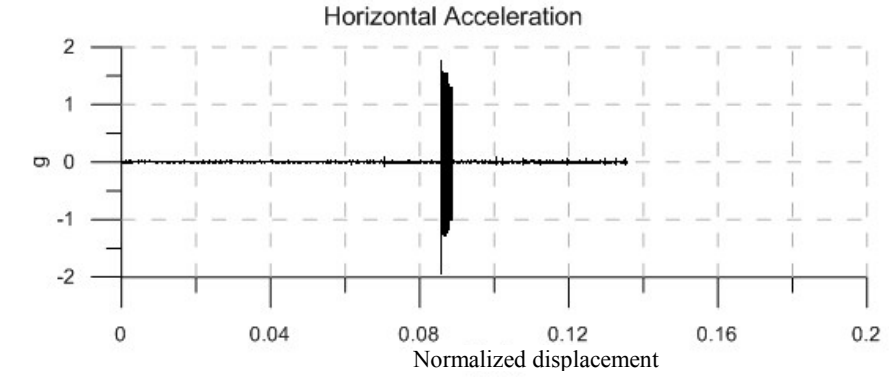

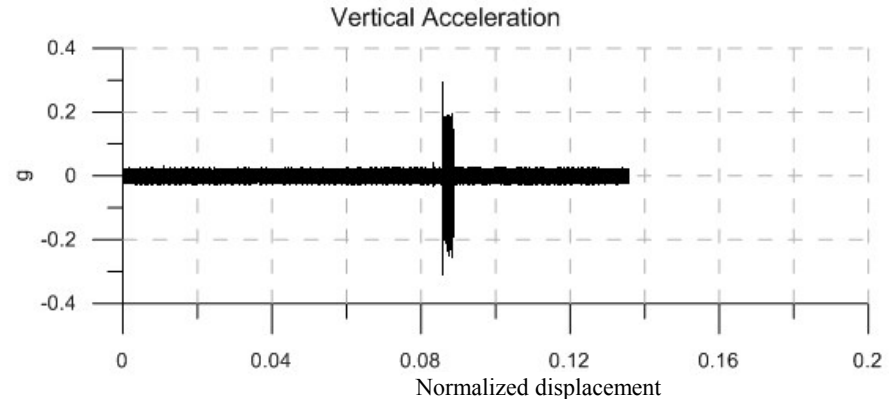

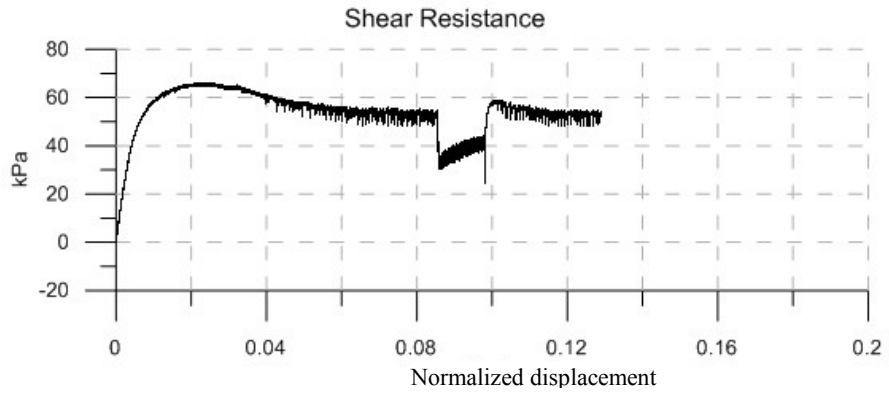

Material:	Glass Beads
Size:	0.55 mm
Normal Stress:	118 kPa
Vibration Frequency:	60 Hz
Vibration Duration:	73 sec
Horizontal Acceleration:	1.2 g
Vertical Acceleration:	0.42 g
Horizontal Amplitude:	0.0828 mm
Vertical Amplitude:	0.0290 mm
Peak Strength:	65.5 kPa
Residual Strength:	54.5 kPa
Vibro-Residual Strength:	32 kPa

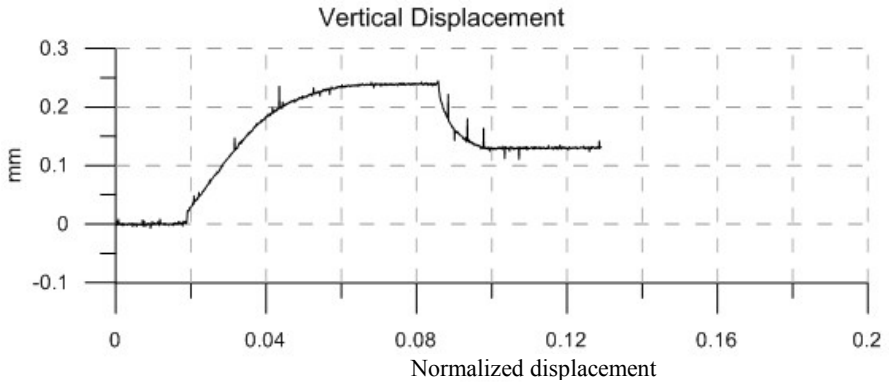

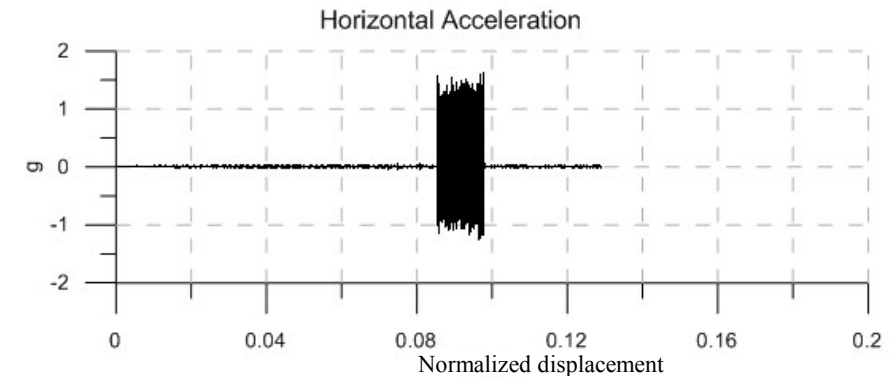

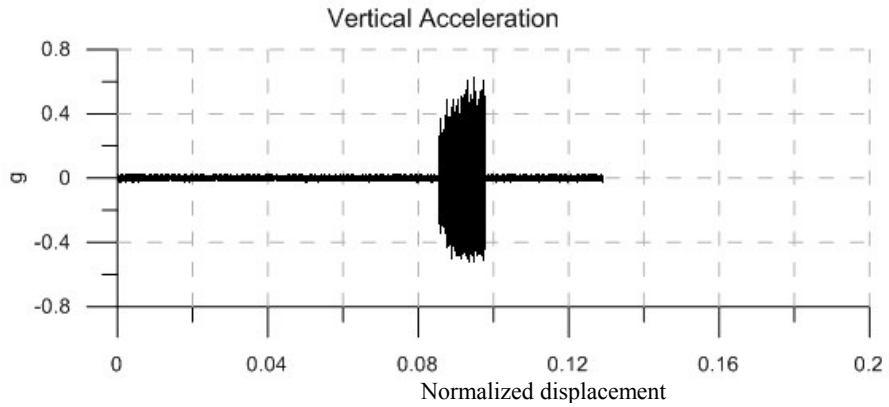

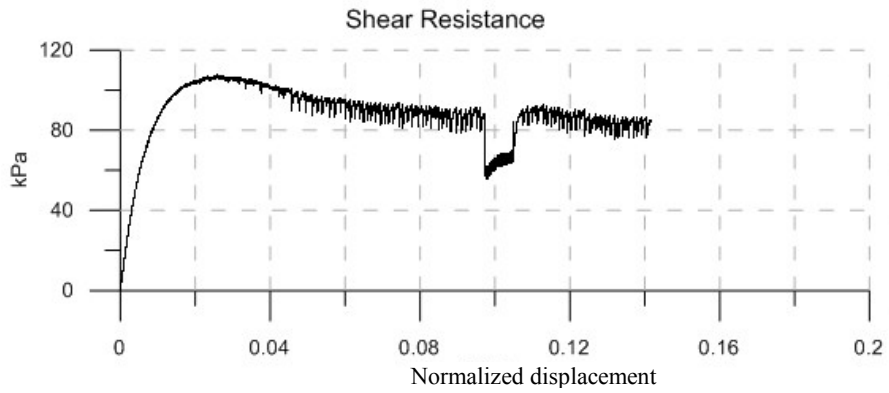

Material:	Glass Beads
Size:	0.55 mm
Normal Stress:	200 kPa
Vibration Frequency:	60 Hz
Vibration Duration:	45 sec
Horizontal Acceleration:	1.2 g
Vertical Acceleration:	0.35 g
Horizontal Amplitude:	0.0828 mm
Vertical Amplitude:	0.0242 mm
Peak Strength:	107 kPa
Residual Strength:	91 kPa
Vibro-Residual Strength:	58 kPa

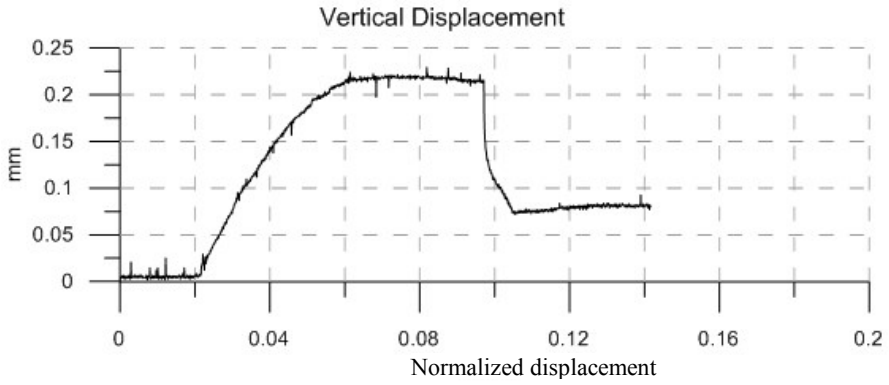

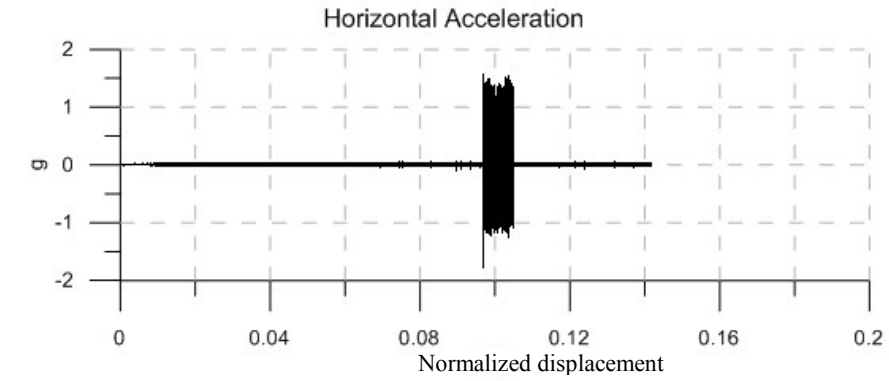

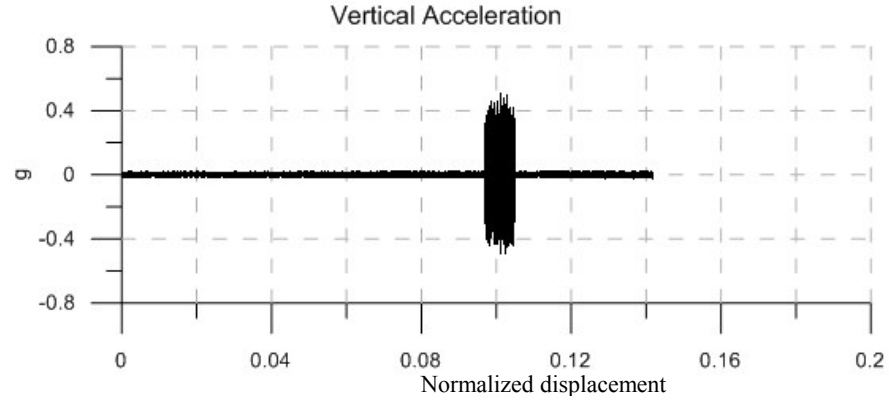

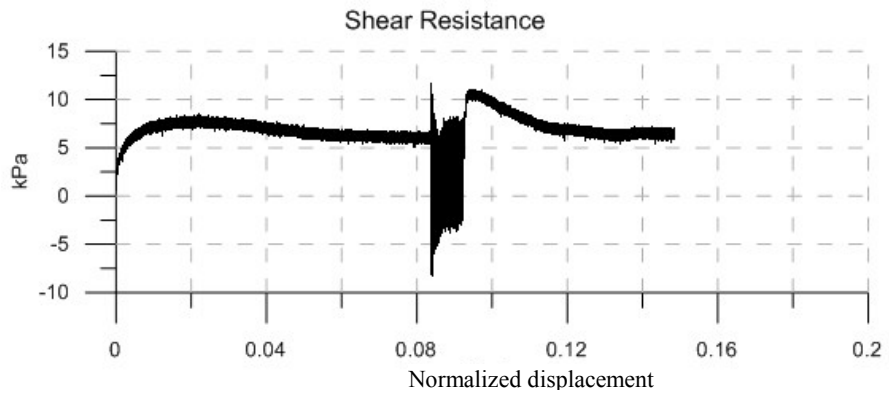

Material:	Glass Beads
Size:	0.55 mm
Normal Stress:	8 kPa
Vibration Frequency:	60 Hz
Vibration Duration:	50 sec
Horizontal Acceleration:	2.2 g
Vertical Acceleration:	0.45 g
Horizontal Amplitude:	0.1519 mm
Vertical Amplitude:	0.0311 mm
Peak Strength:	8 kPa
Residual Strength:	6 kPa
Vibro-Residual Strength:	0 kPa

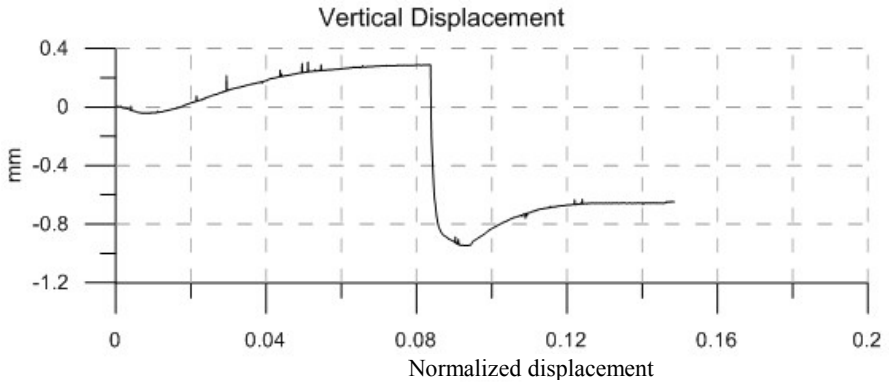

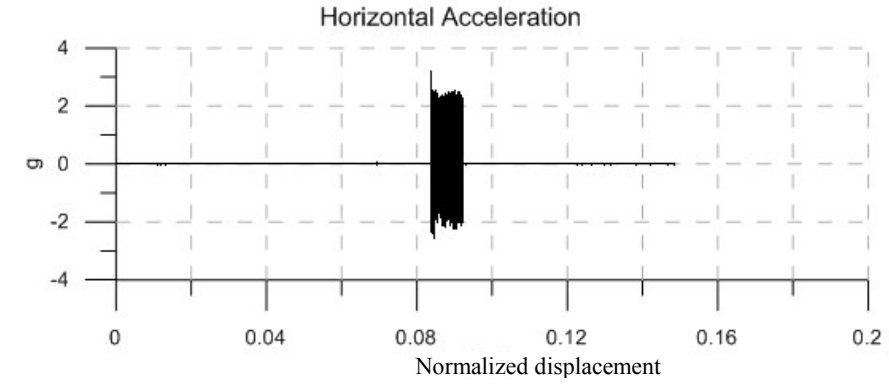

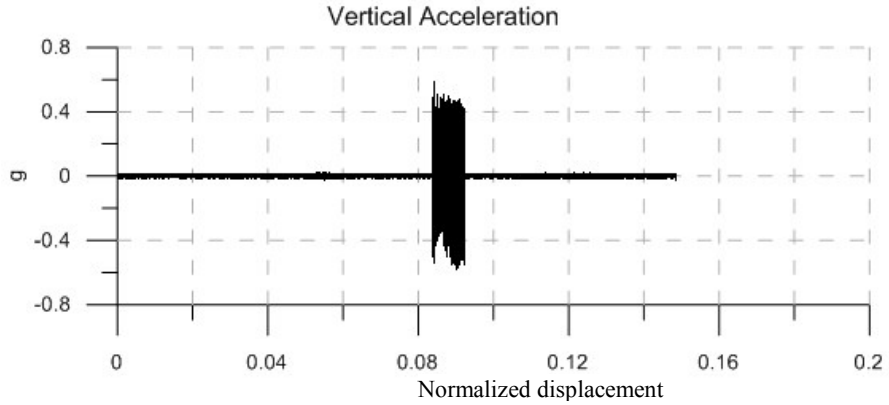

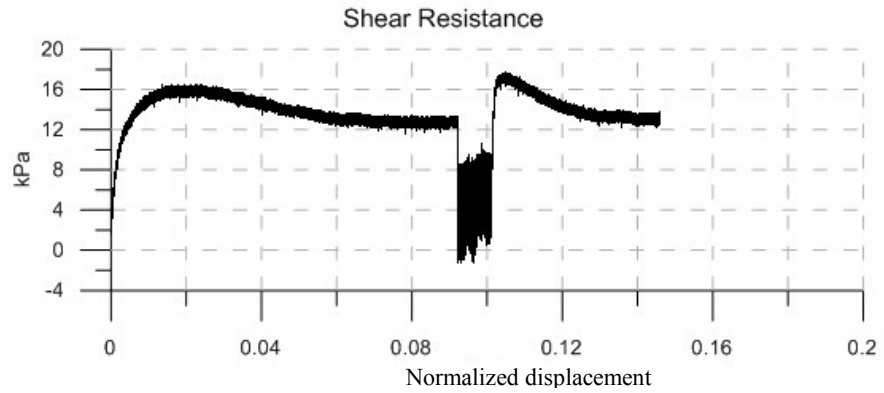

Material:	Glass Beads
Size:	0.55 mm
Normal Stress:	23 kPa
Vibration Frequency:	60 Hz
Vibration Duration:	53 sec
Horizontal Acceleration:	2 g
Vertical Acceleration:	0.32 g
Horizontal Amplitude:	0.1381 mm
Vertical Amplitude:	0.0221 mm
Peak Strength:	16 kPa
Residual Strength:	13 kPa
Vibro-Residual Strength:	1 kPa

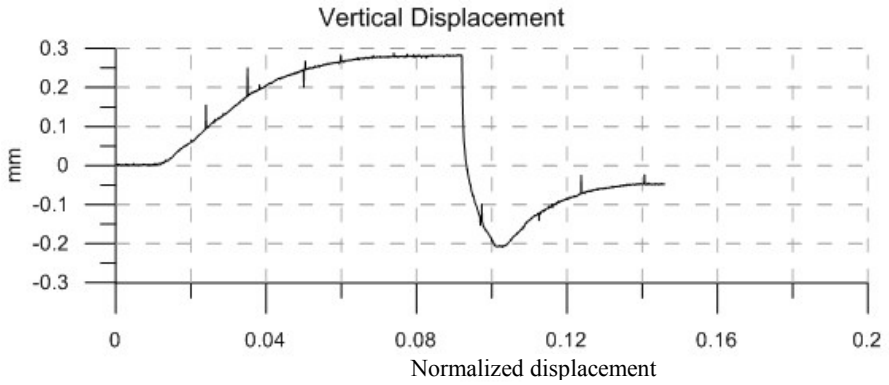

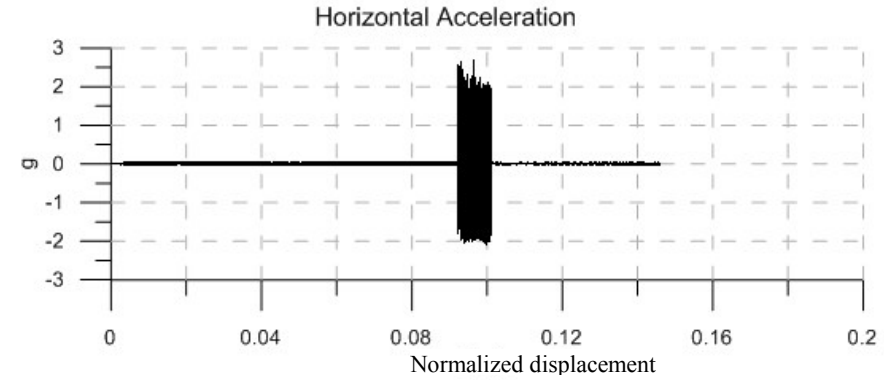

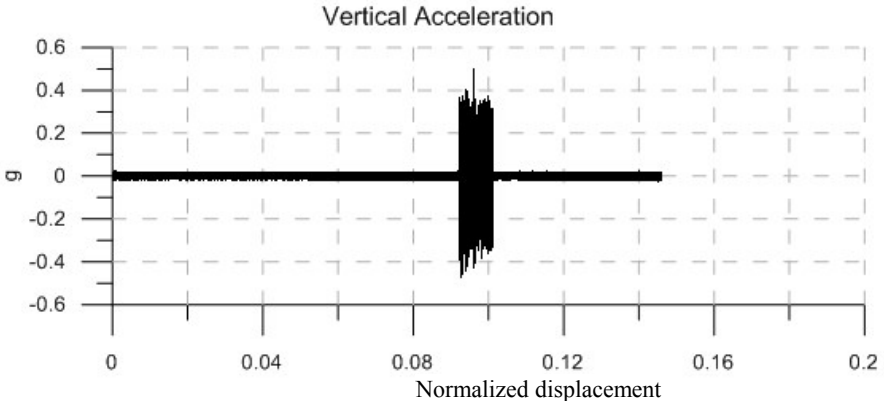

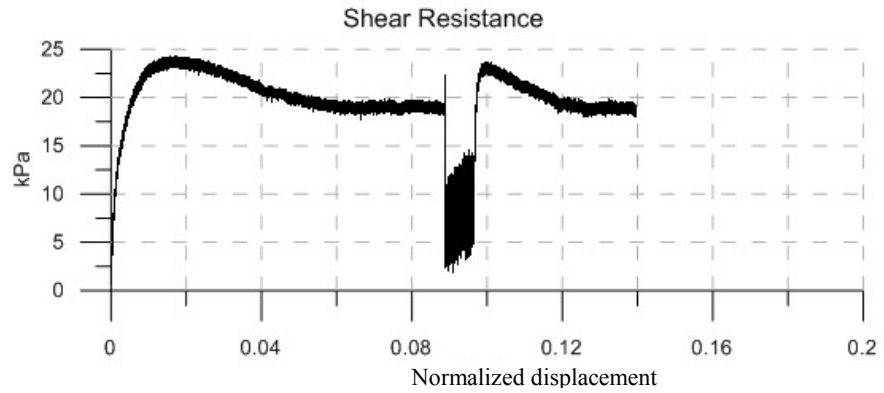

Material:	Glass Beads
Size:	0.55 mm
Normal Stress:	36 kPa
Vibration Frequency:	60 Hz
Vibration Duration:	45 sec
Horizontal Acceleration:	2.2 g
Vertical Acceleration:	0.32 g
Horizontal Amplitude:	0.1519 mm
Vertical Amplitude:	0.0221 mm
Peak Strength:	24 kPa
Residual Strength:	19 kPa
Vibro-Residual Strength:	4.5 kPa

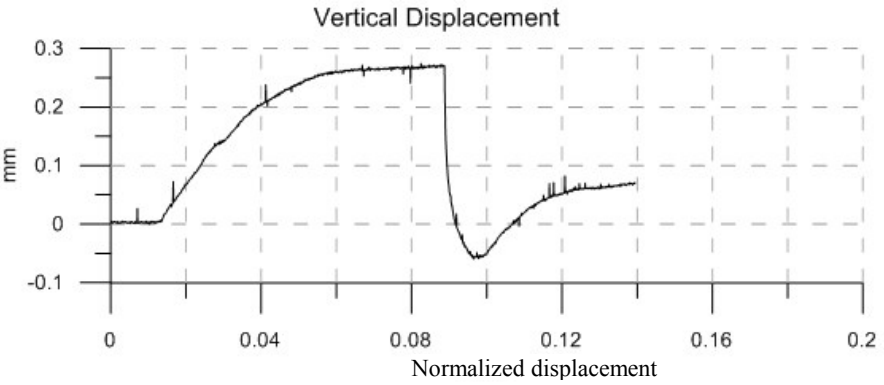

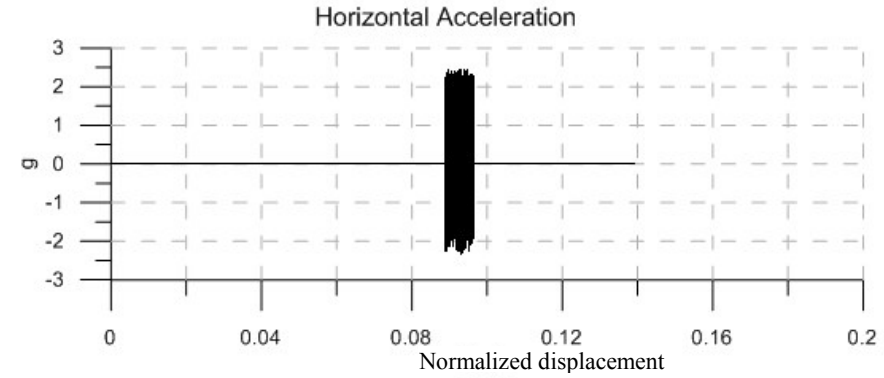

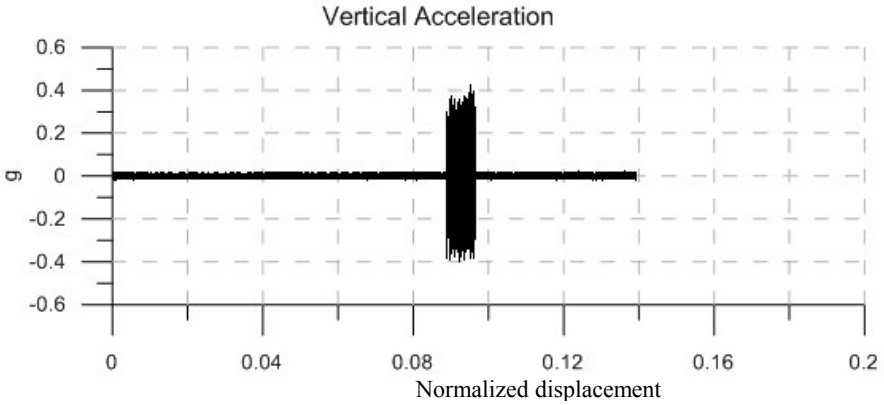

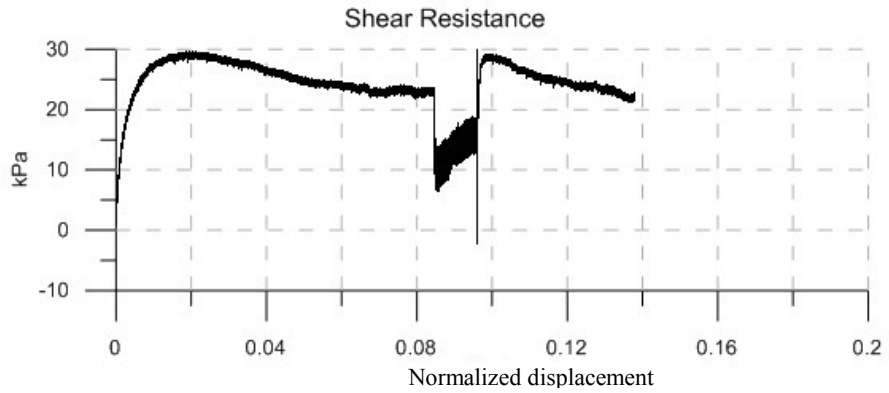

Material:	Glass Beads
Size:	0.55 mm
Normal Stress:	50 kPa
Vibration Frequency:	60 Hz
Vibration Duration:	66 sec
Horizontal Acceleration:	2.1 g
Vertical Acceleration:	0.22 g
Horizontal Amplitude:	0.1450 mm
Vertical Amplitude:	0.0152 mm
Peak Strength:	29.5 kPa
Residual Strength:	23 kPa
Vibro-Residual Strength:	8 kPa

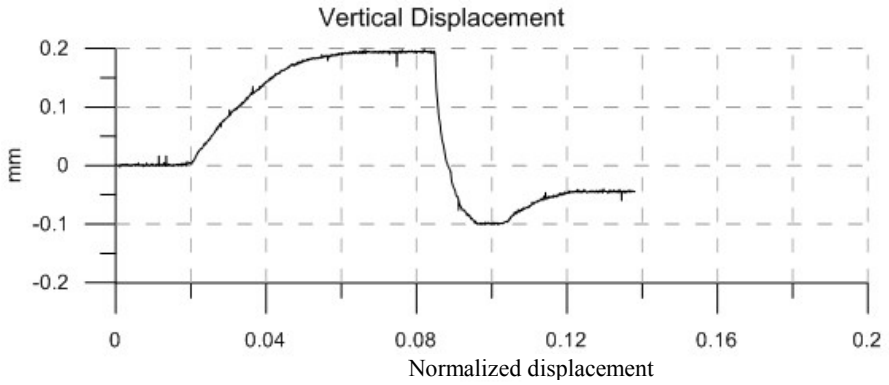

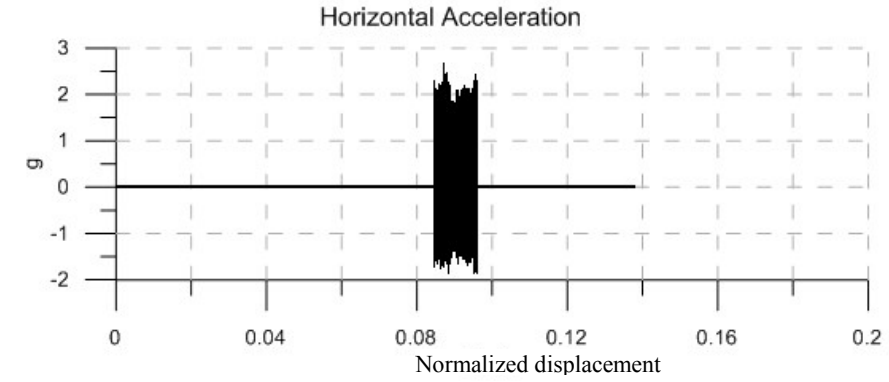

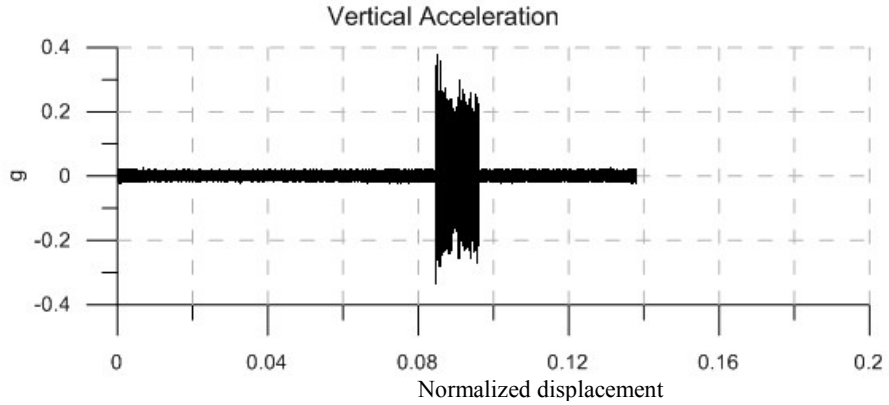

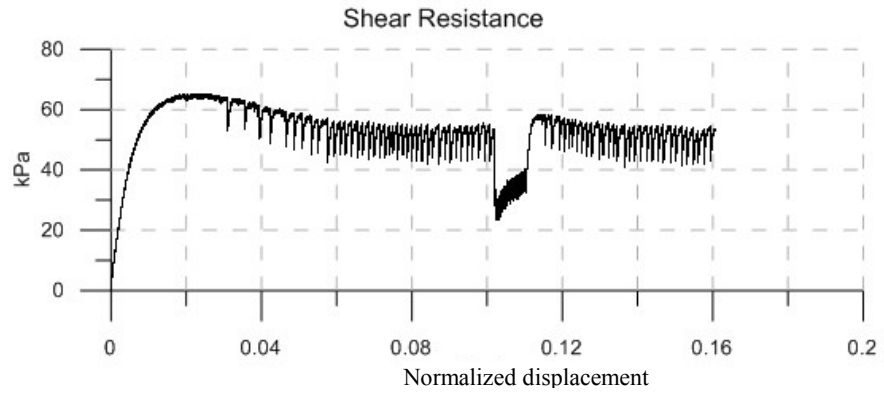

Material:	Glass Beads
Size:	0.55 mm
Normal Stress:	118 kPa
Vibration Frequency:	60 Hz
Vibration Duration:	50 sec
Horizontal Acceleration:	2.2 g
Vertical Acceleration:	0.41 g
Horizontal Amplitude:	0.1519 mm
Vertical Amplitude:	0.0283 mm
Peak Strength:	65 kPa
Residual Strength:	54 kPa
Vibro-Residual Strength:	26 kPa

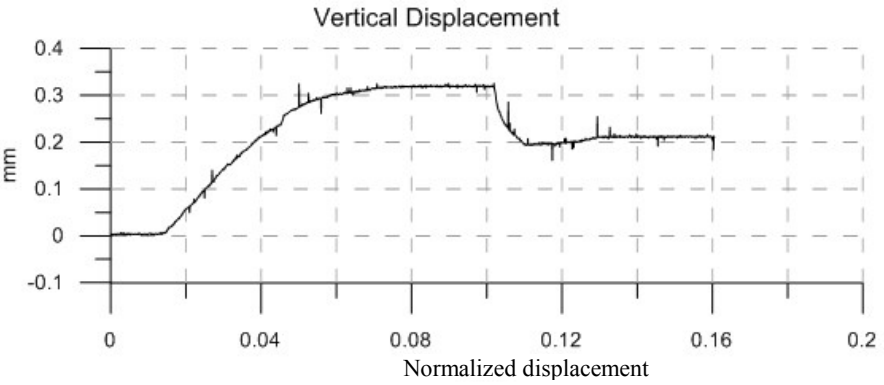

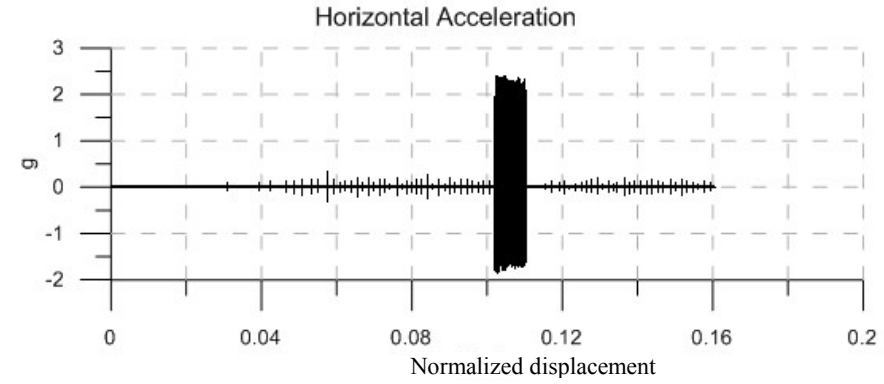

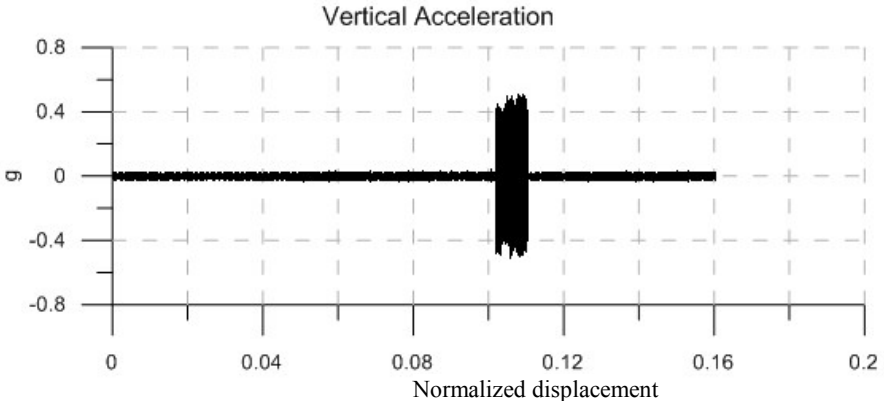

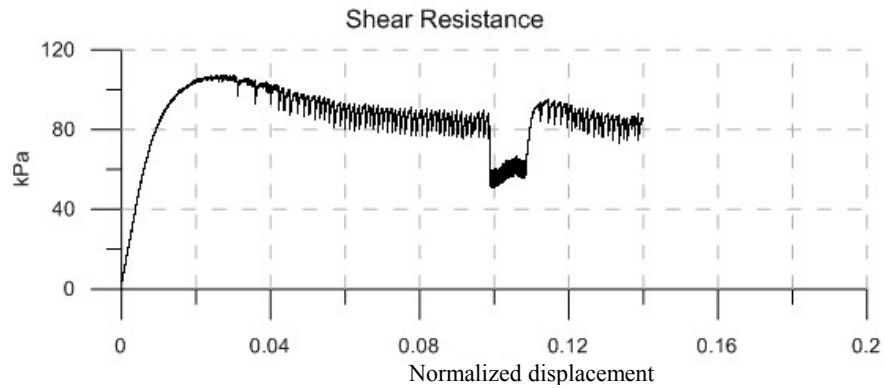

Material:	Glass Beads
Size:	0.55 mm
Normal Stress:	200 kPa
Vibration Frequency:	60 Hz
Vibration Duration:	56 sec
Horizontal Acceleration:	2 g
Vertical Acceleration:	0.41 g
Horizontal Amplitude:	0.1381 mm
Vertical Amplitude:	0.0283 mm
Peak Strength:	107 kPa
Residual Strength:	88 kPa
Vibro-Residual Strength:	53 kPa

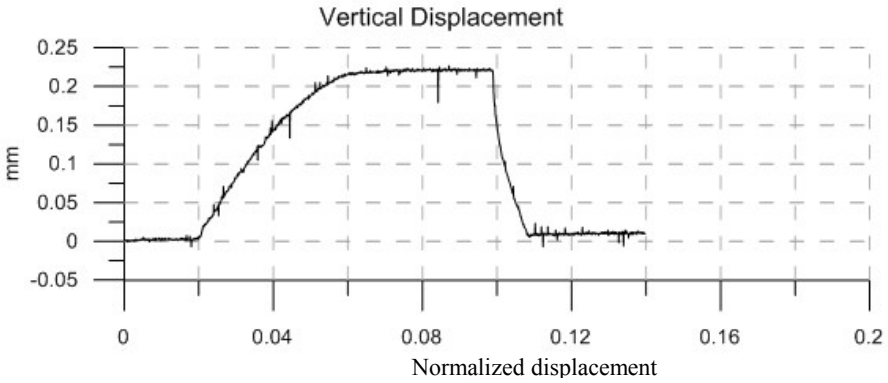

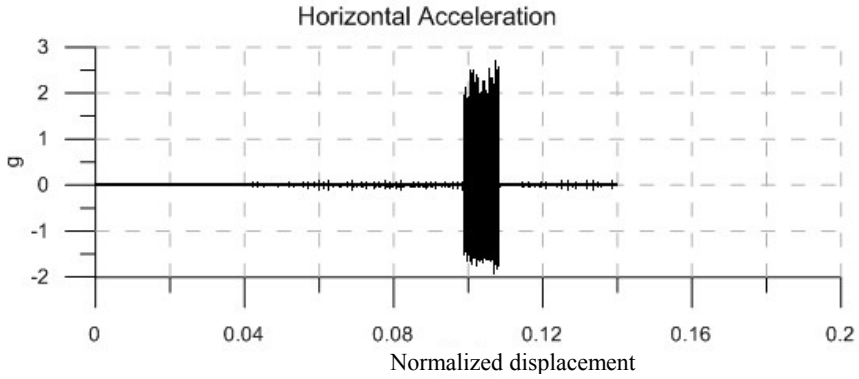

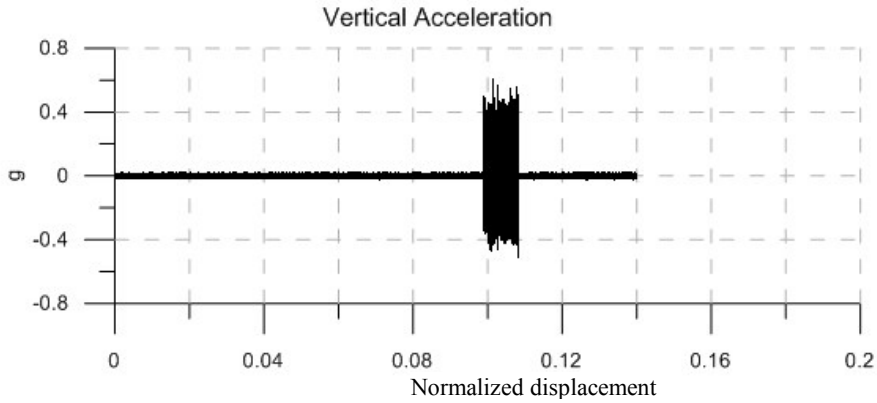

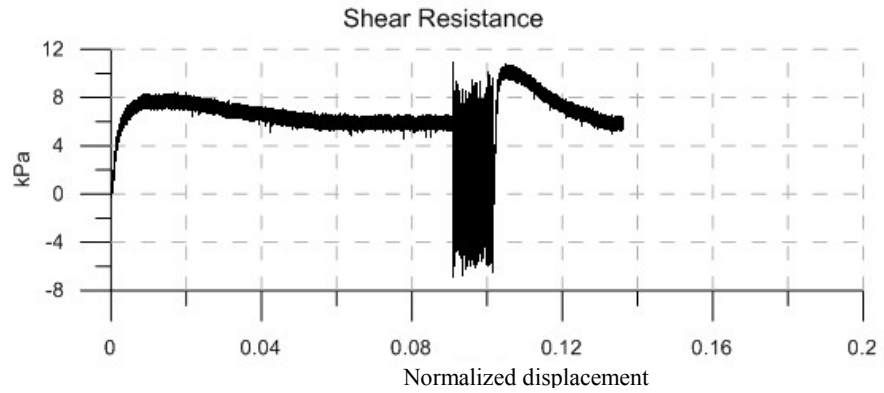

Material:	Glass Beads
Size:	0.55 mm
Normal Stress:	8 kPa
Vibration Frequency:	60 Hz
Vibration Force:	#1
Vibration Duration:	63 sec
Horizontal Acceleration:	3.5 g
Vertical Acceleration:	0.38 g
Horizontal Amplitude:	0.2416 mm
Vertical Amplitude:	0.0262 mm
Peak Strength:	8 kPa
Residual Strength:	6 kPa
Vibro-Residual Strength:	0 kPa

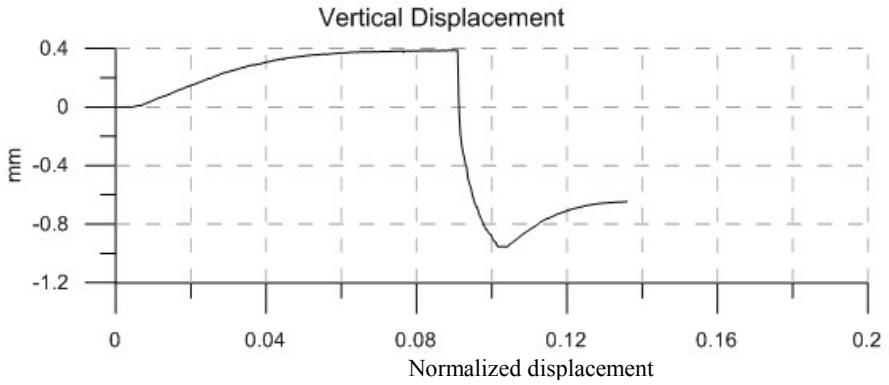

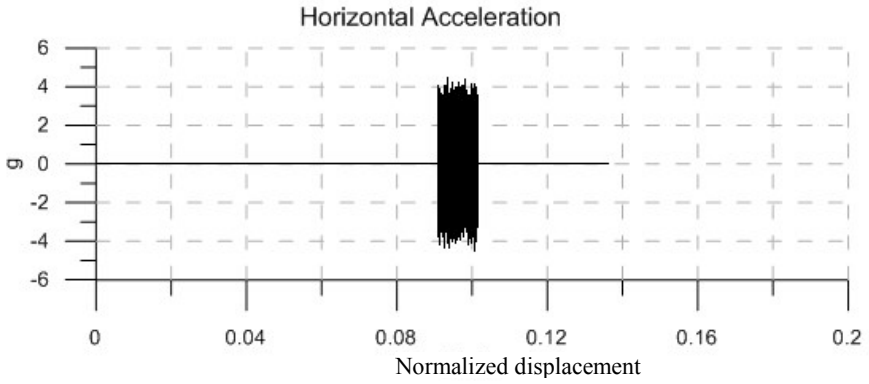

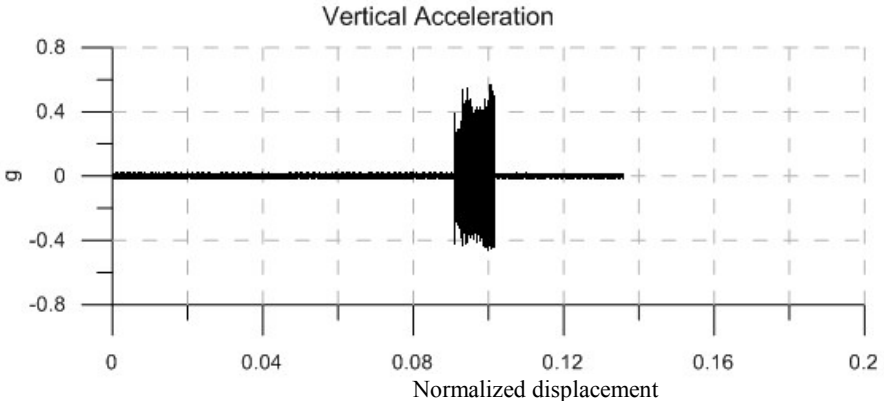

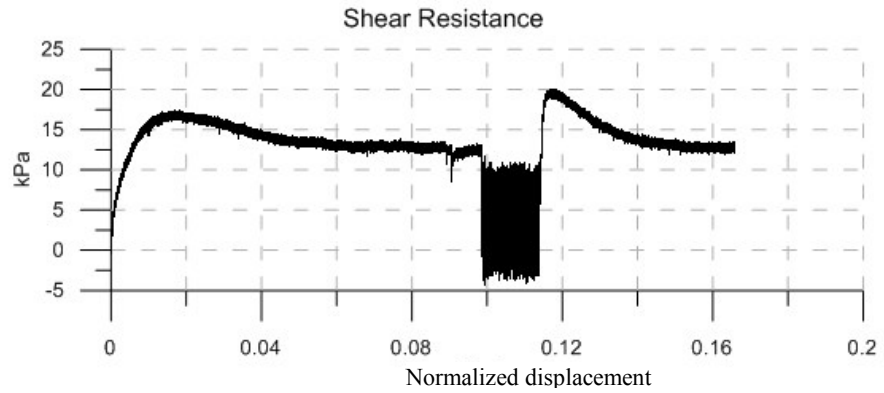

Material:	Glass Beads
Size:	0.55 mm
Normal Stress:	23 kPa
Vibration Frequency:	60 Hz
Vibration Force:	#1
Vibration Duration:	88 sec
Horizontal Acceleration:	3.5 g
Vertical Acceleration:	0.7 g
Horizontal Amplitude:	0.2416 mm
Vertical Amplitude:	0.0483 mm
Peak Strength:	17 kPa
Residual Strength:	13 kPa
Vibro-Residual Strength:	0 kPa

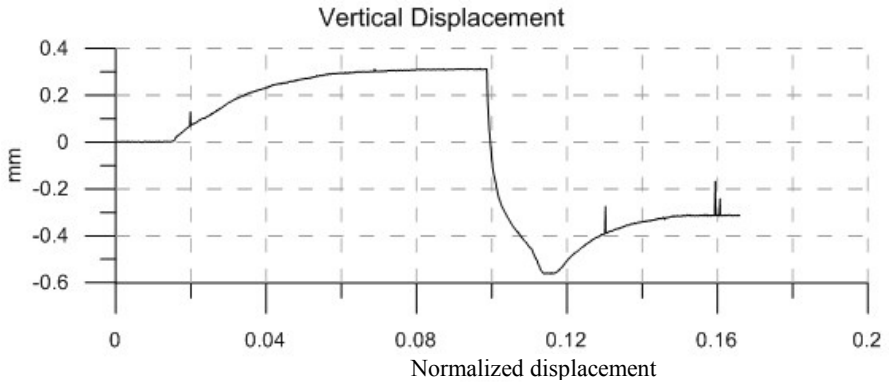

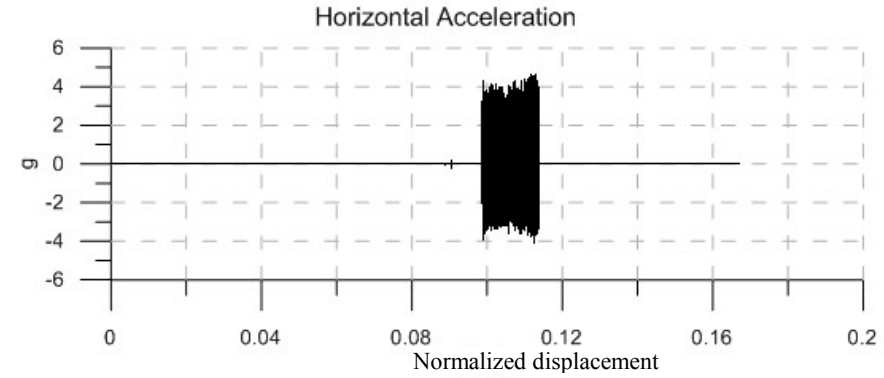

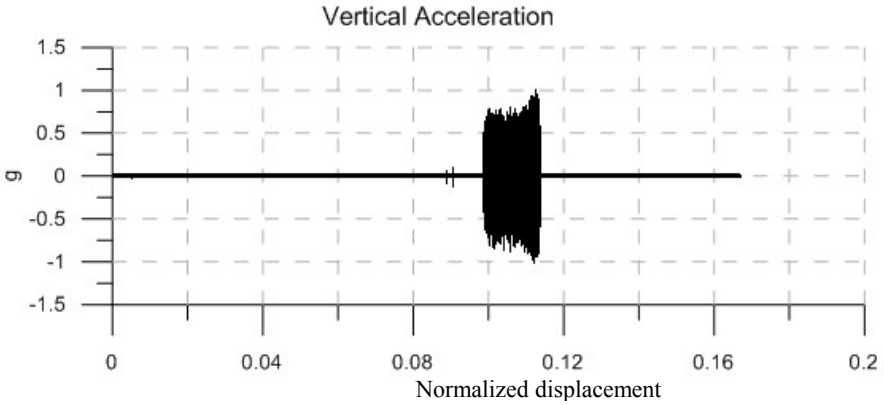

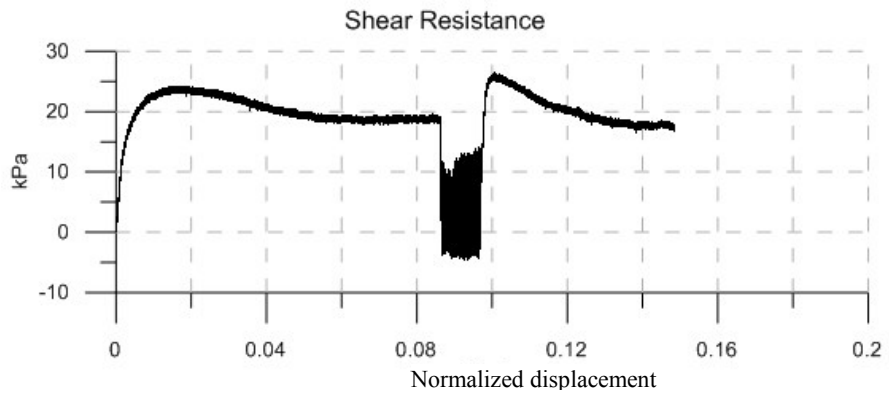

Material:	Glass Beads
Size:	0.55 mm
Normal Stress:	36 kPa
Vibration Frequency:	60 Hz
Vibration Force:	#1
Vibration Duration:	62 sec
Horizontal Acceleration:	3.4 g
Vertical Acceleration:	0.9 g
Horizontal Amplitude:	0.2347 mm
Vertical Amplitude:	0.0621 mm
Peak Strength:	24 kPa
Residual Strength:	19 kPa
Vibro-Residual Strength:	0 kPa

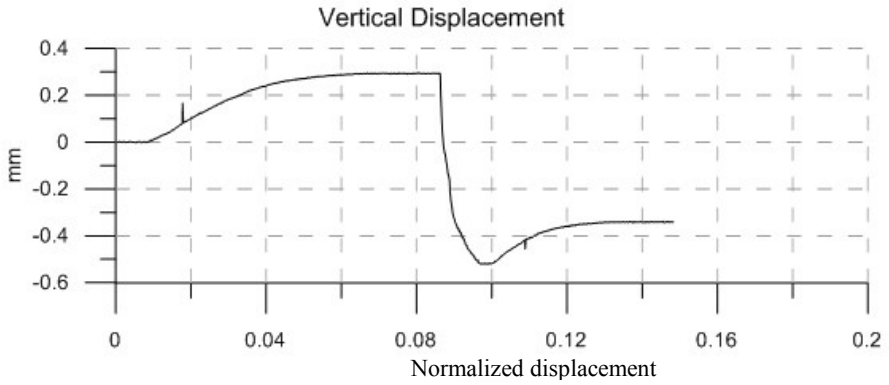

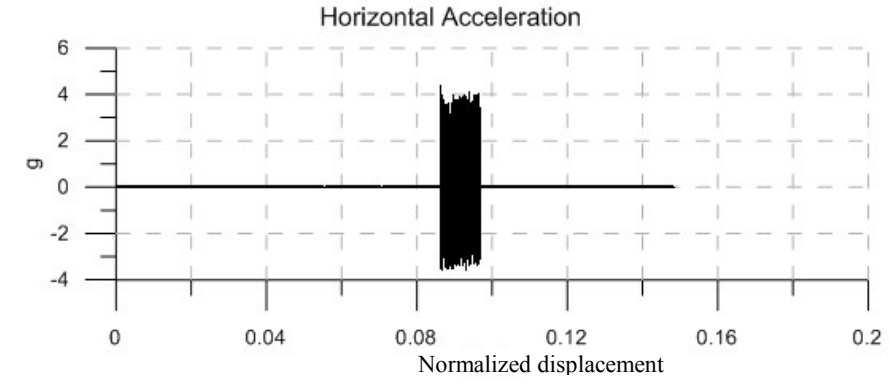

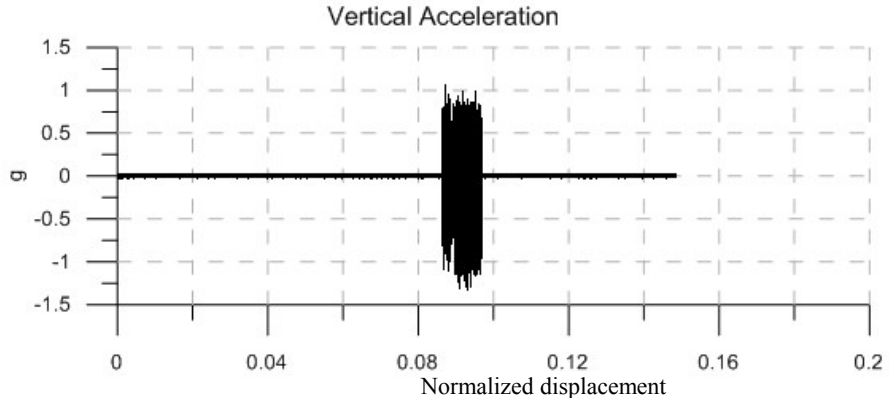

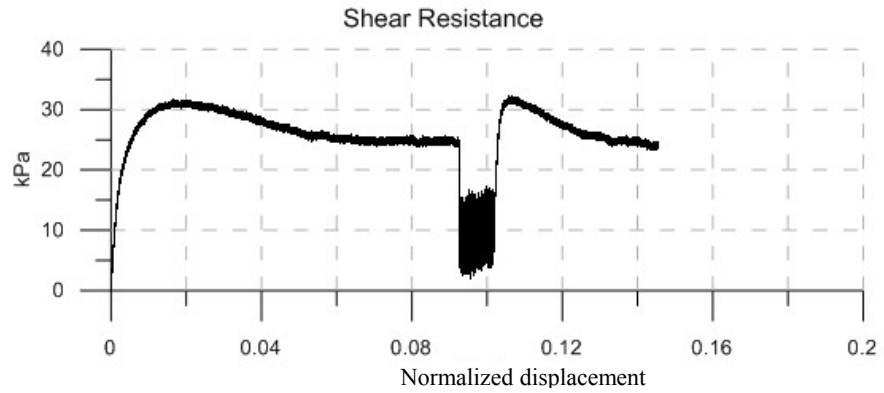

Material:	Glass Beads
Size:	0.55 mm
Normal Stress:	50 kPa
Vibration Frequency:	60 Hz
Vibration Force:	#1
Vibration Duration:	54 sec
Horizontal Acceleration:	3.4 g
Vertical Acceleration:	0.75 g
Horizontal Amplitude:	0.2347 mm
Vertical Amplitude:	0.0518 mm
Peak Strength:	31 kPa
Residual Strength:	25 kPa
Vibro-Residual Strength:	4 kPa

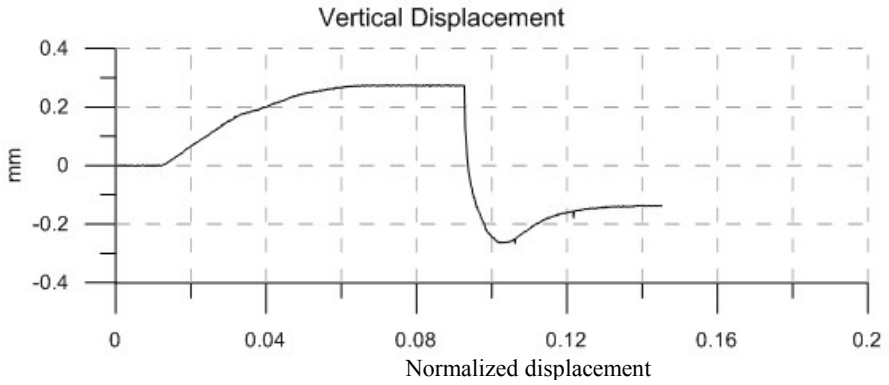

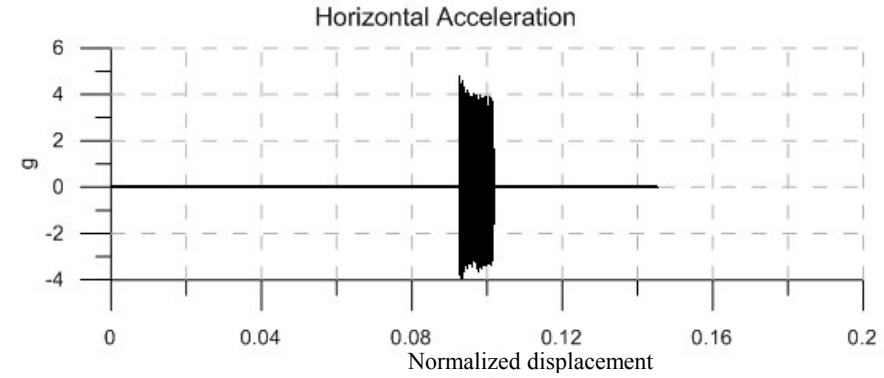

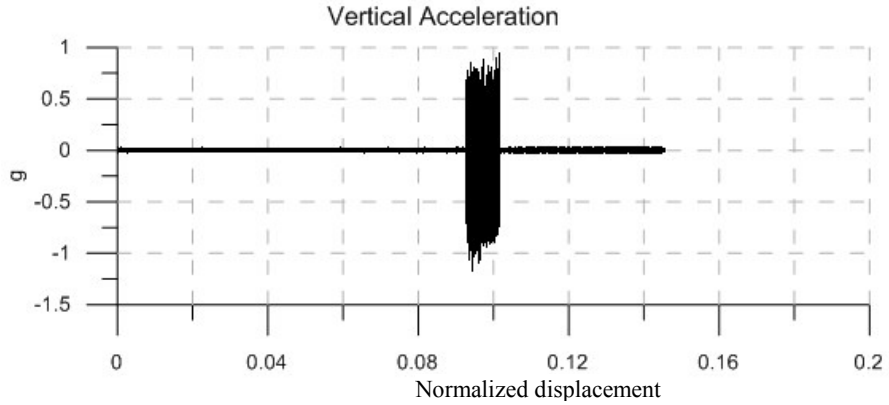

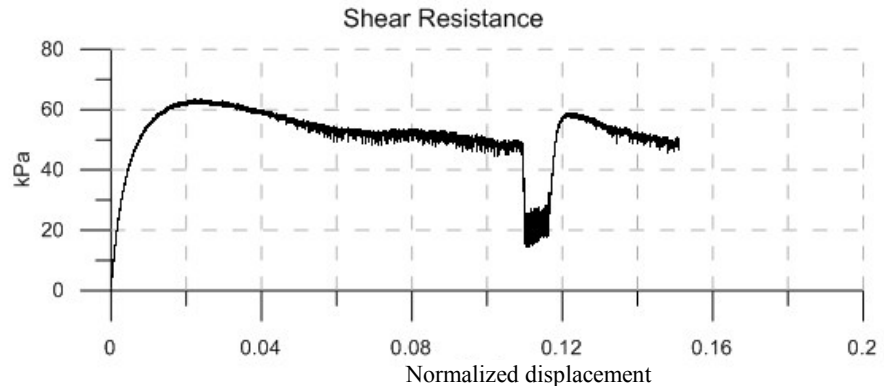

Material:	Glass Beads
Size:	0.55 mm
Normal Stress:	118 kPa
Vibration Frequency:	60 Hz
Vibration Force:	#1
Vibration Duration:	40 sec
Horizontal Acceleration:	3.3 g
Vertical Acceleration:	0.75 g
Horizontal Amplitude:	0.2278 mm
Vertical Amplitude:	0.0518 mm
Peak Strength:	63 kPa
Residual Strength:	50 kPa
Vibro-Residual Strength:	17 kPa

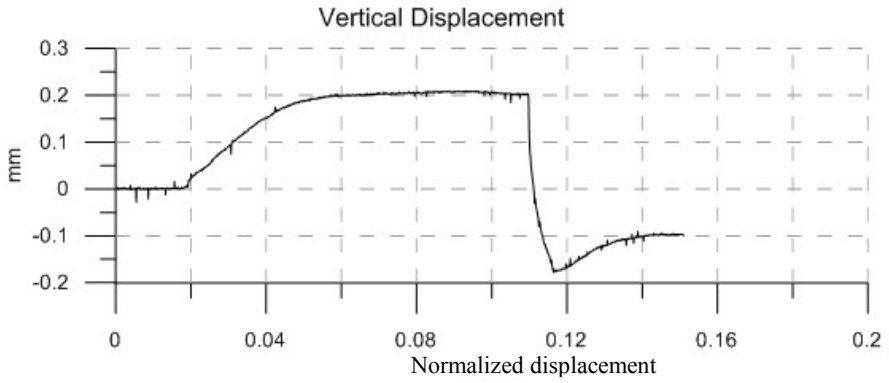

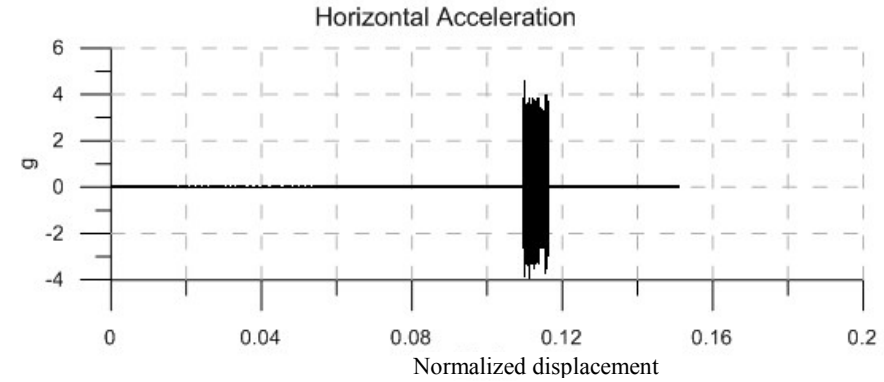

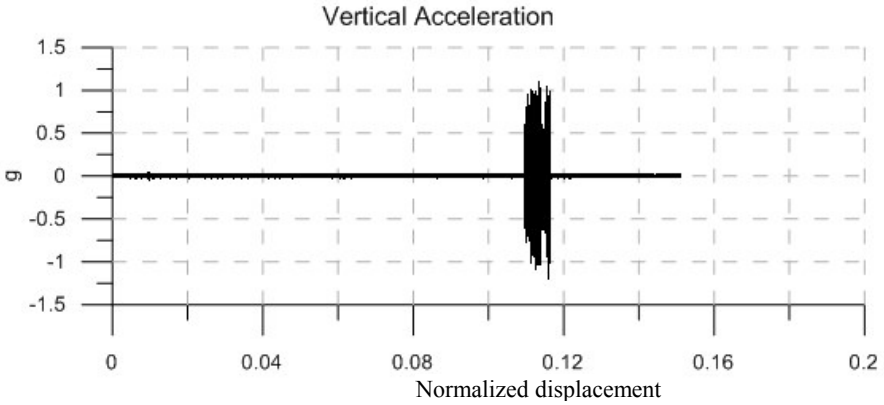

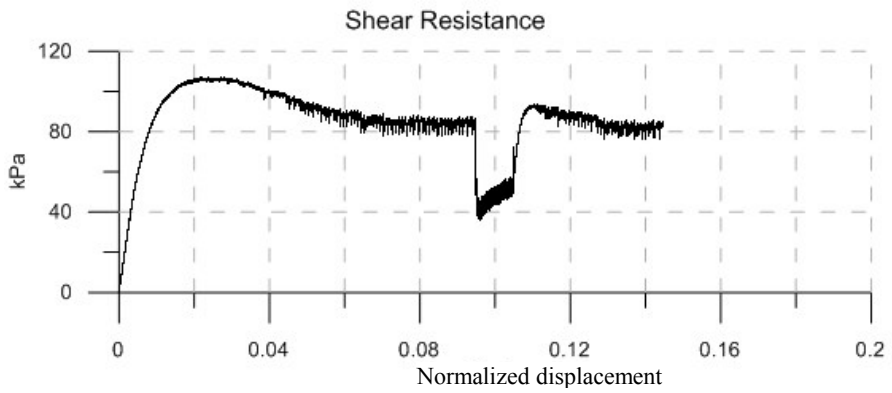

Material:	Glass Beads
Size:	0.55 mm
Normal Stress:	200 kPa
Vibration Frequency:	60 Hz
Vibration Force:	#1
Vibration Duration:	58 sec
Horizontal Acceleration:	3.3 g
Vertical Acceleration:	0.65 g
Horizontal Amplitude:	0.2278 mm
Vertical Amplitude:	0.0449 mm
Peak Strength:	106 kPa
Residual Strength:	86 kPa
Vibro-Residual Strength:	40 kPa

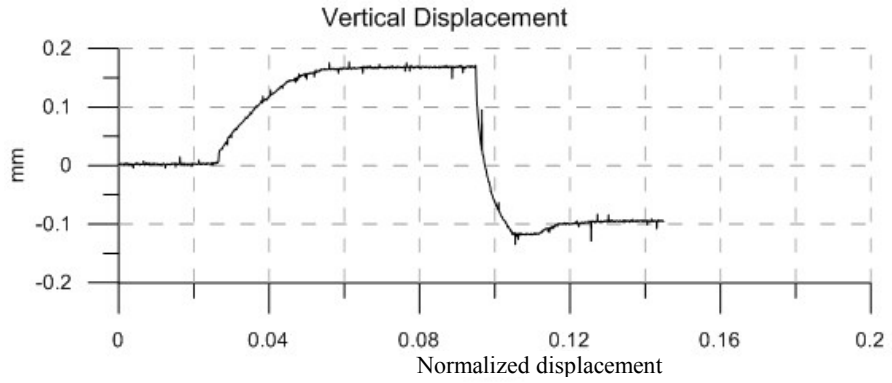

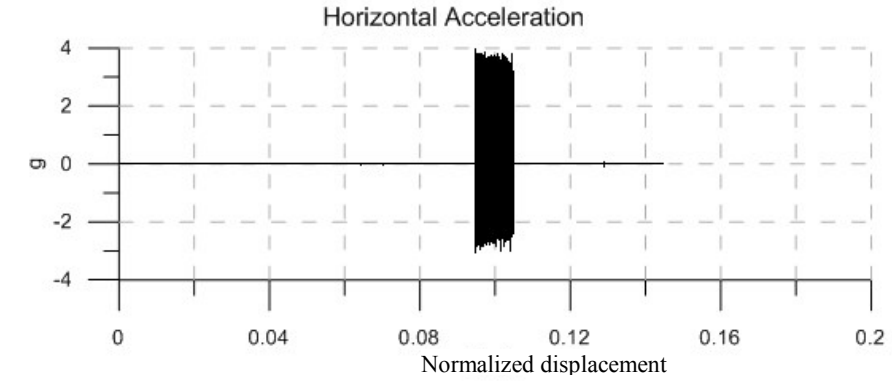

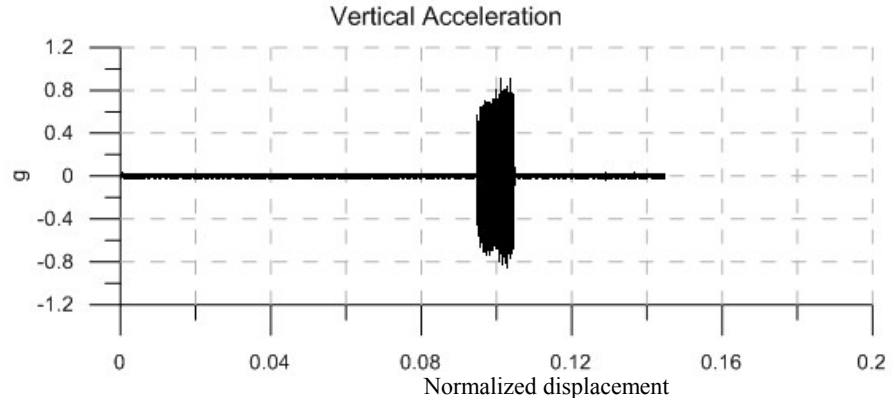

Part 4

The plots provided in this section were used in Chapter 6. Following are the test results of a few sample sets.

Set 1: 4 samples of fine sand and 4 samples of 0.55 mm glass beads tested in strain-controlled mode over a smooth glass surface at 23 kPa, 50 kPa, 118 kPa and 200 kPa normal stresses, constant vibration intensity and 140 Hz vibration frequency.

Set 2: 4 samples of fine sand and 4 samples of 0.55 mm glass beads tested in strain-controlled mode at 23 kPa, 50 kPa, 118 kPa and 200 kPa normal stresses, constant vibration intensity and 140 Hz vibration frequency applied at the pre-peak and residual strength states of the samples.

Set 3: 12 samples of loose and dense fine sand samples, as well as 12 samples of loose and dense 0.55 mm glass beads tested in strain-controlled mode at 23 kPa, 50 kPa, 118 kPa and 200 kPa normal stresses, and no shearing during the application of vibration having constant intensity and 140 Hz frequency.

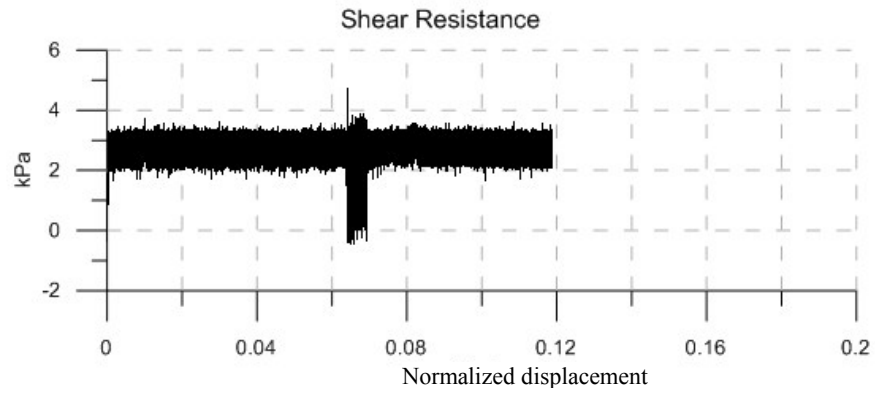

Material:	Sand
Size:	Fine
Normal Stress:	23 kPa
Vibration Frequency:	140 Hz
Vibration Force:	7.14 N
Vibration Duration:	30 sec
Horizontal Acceleration:	0.33 g
Vertical Acceleration:	0.16 g
Horizontal Amplitude:	0.0042 mm
Vertical Amplitude:	0.0020 mm
Peak Strength:	- kPa
Residual Strength:	3 kPa
Vibro-Residual Strength:	1.5 kPa

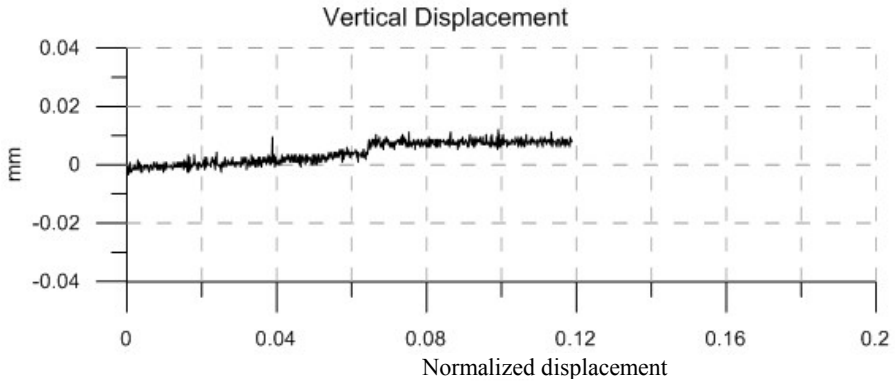

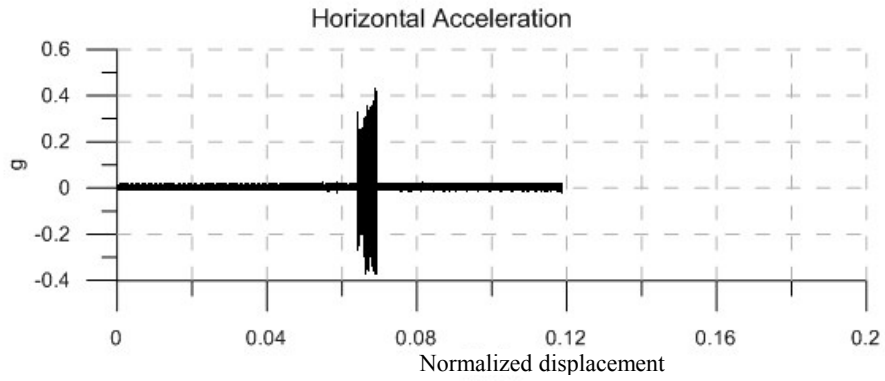

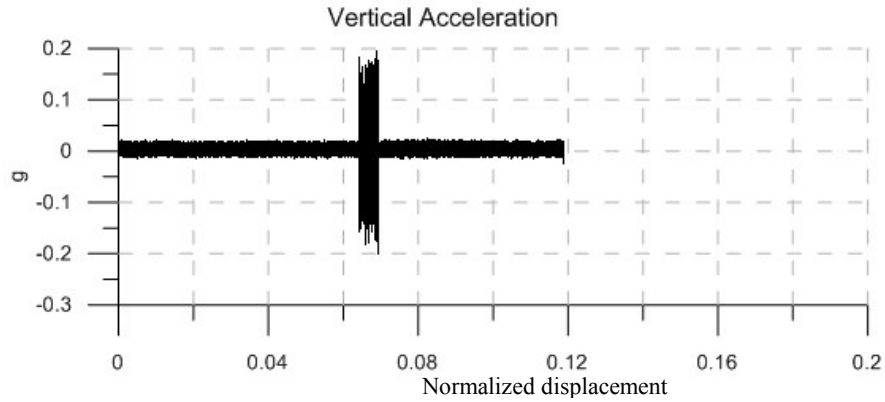

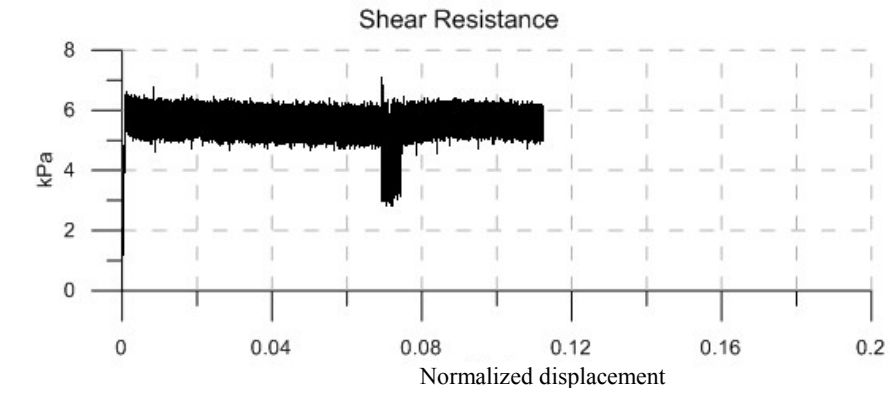

Material:	Sand
Size:	Fine
Normal Stress:	50 kPa
Vibration Frequency:	140 Hz
Vibration Force:	7.14 N
Vibration Duration:	30 sec
Horizontal Acceleration:	0.32 g
Vertical Acceleration:	0.18 g
Horizontal Amplitude:	0.0041 mm
Vertical Amplitude:	0.0023 mm
Peak Strength:	6 kPa
Residual Strength:	5.5 kPa
Vibro-Residual Strength:	4 kPa

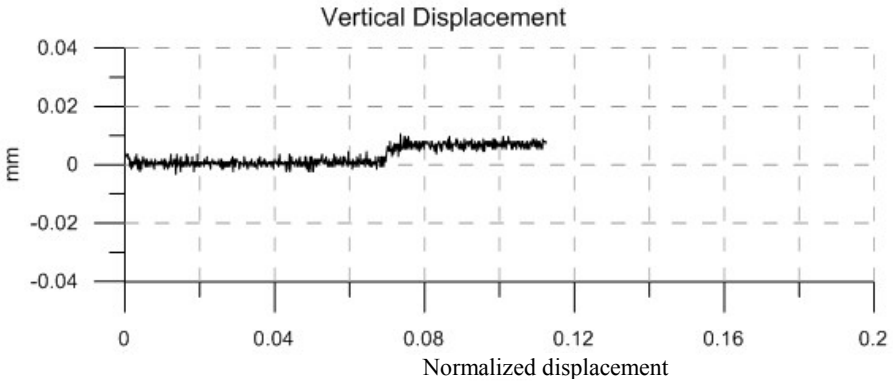

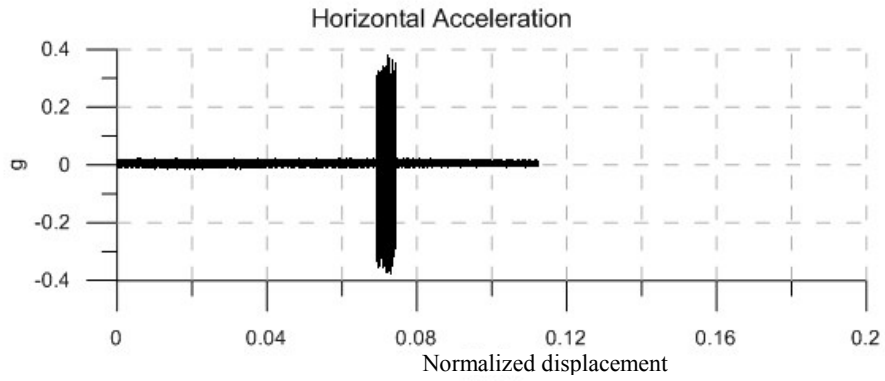

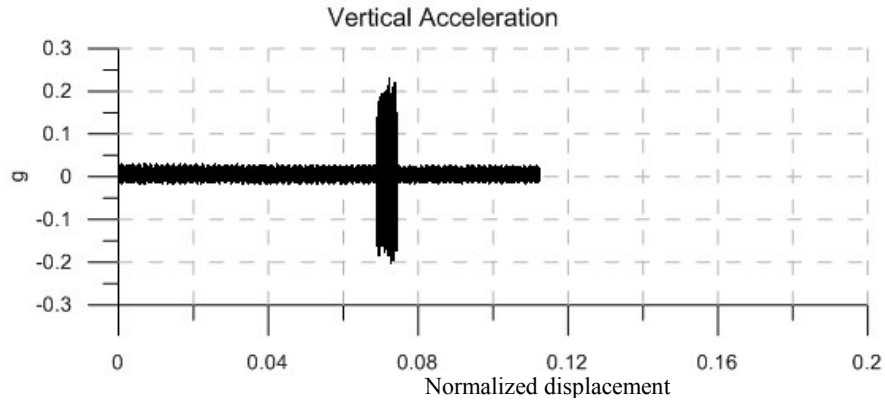

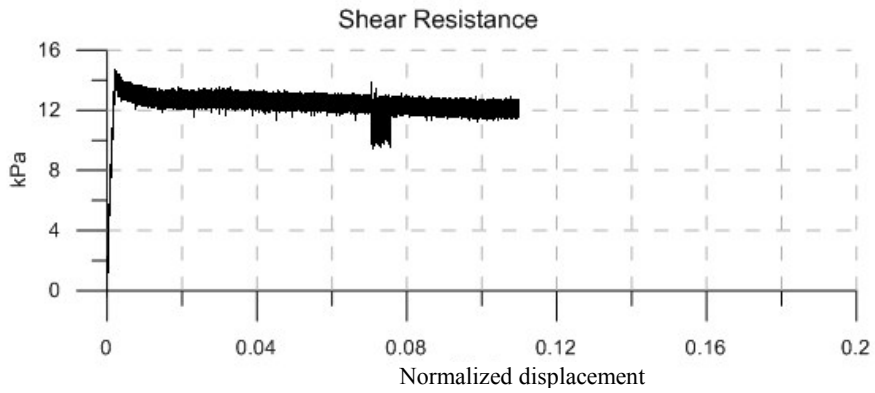

Material:	Sand
Size:	Fine
Normal Stress:	118 kPa
Vibration Frequency:	140 Hz
Vibration Force:	7.14 N
Vibration Duration:	30 sec
Horizontal Acceleration:	0.32 g
Vertical Acceleration:	0.13 g
Horizontal Amplitude:	0.0041 mm
Vertical Amplitude:	0.0016 mm
Peak Strength:	14.5 kPa
Residual Strength:	12.5 kPa
Vibro-Residual Strength:	11 kPa

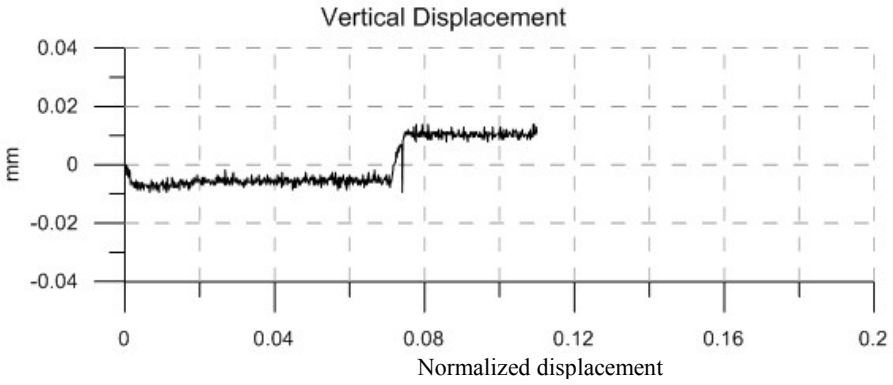

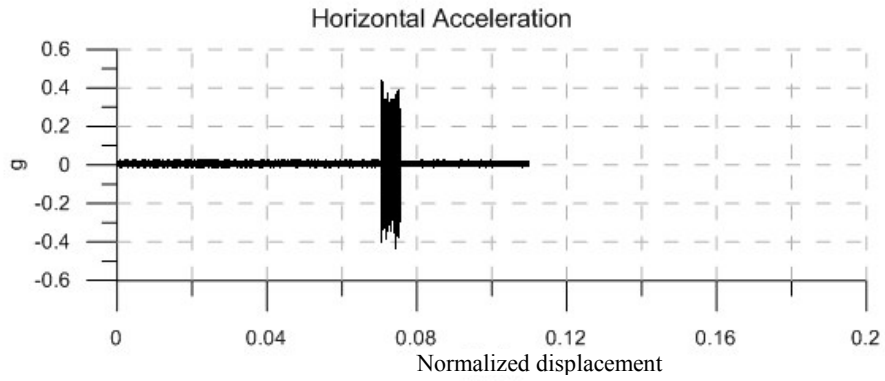

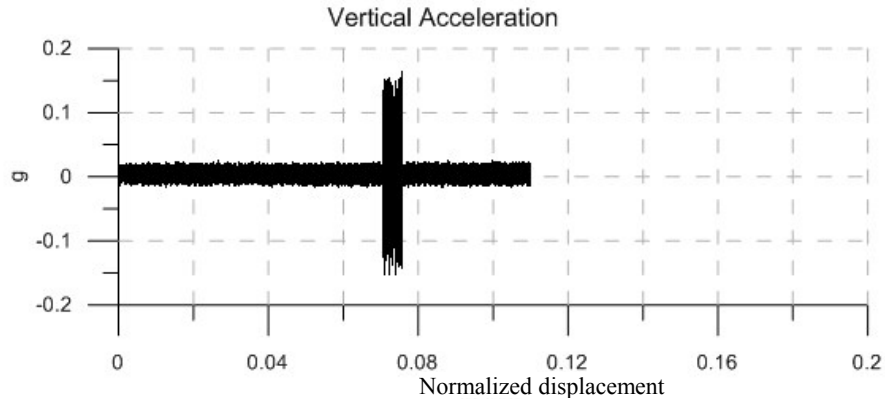

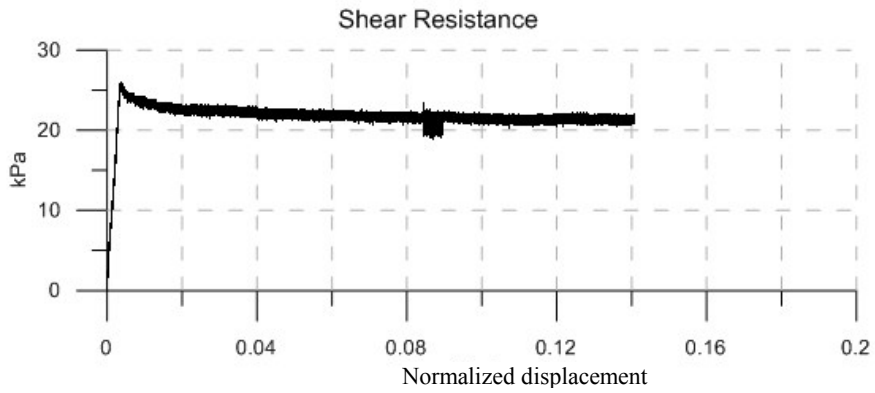

Material:	Sand
Size:	Fine
Normal Stress:	200 kPa
Vibration Frequency:	140 Hz
Vibration Force:	7.14 N
Vibration Duration:	30 sec
Horizontal Acceleration:	0.33 g
Vertical Acceleration:	0.19 g
Horizontal Amplitude:	0.0042 mm
Vertical Amplitude:	0.0024 mm
Peak Strength:	25.5 kPa
Residual Strength:	22 kPa
Vibro-Residual Strength:	20.5 kPa

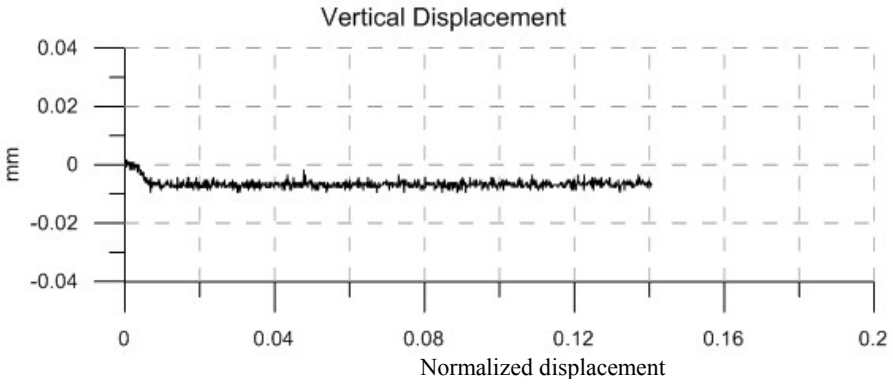

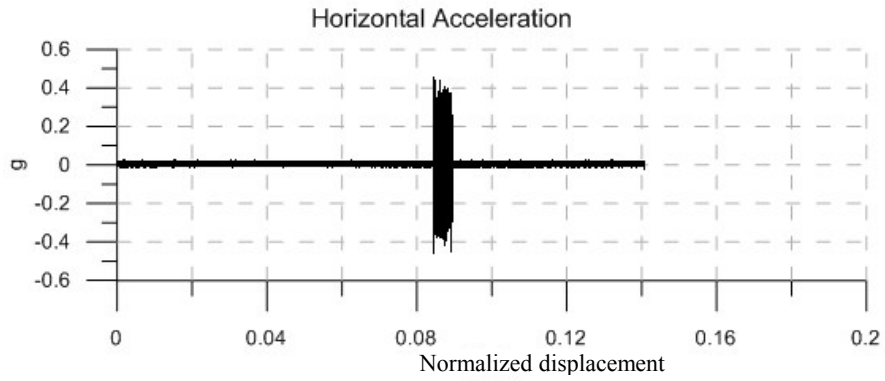

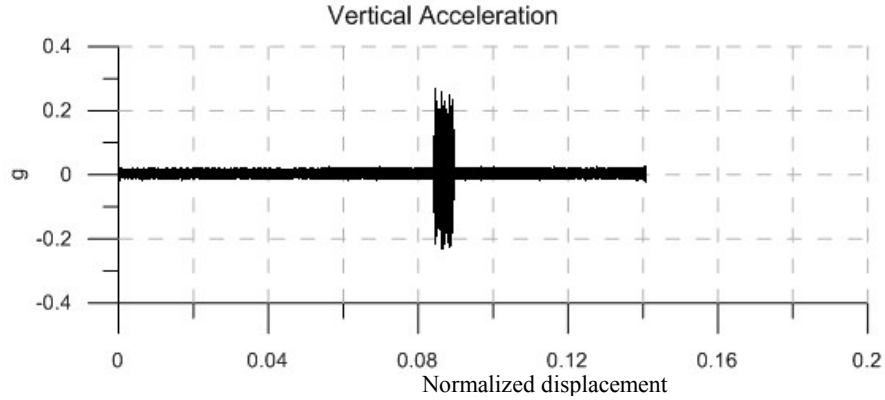

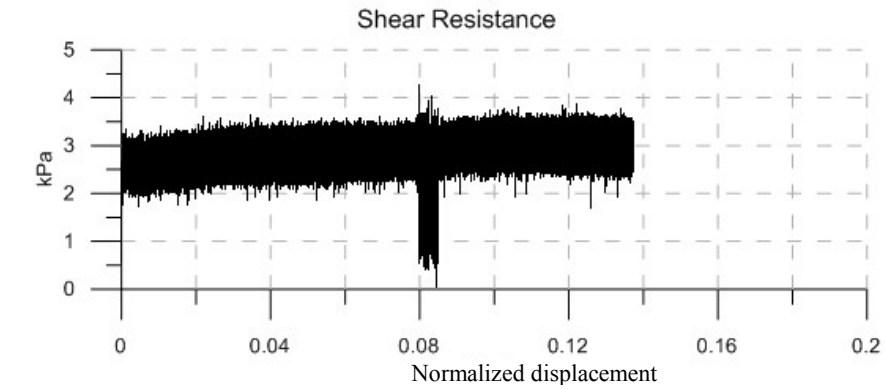

Material:	Glass Beads
Size:	0.55 mm
Normal Stress:	23 kPa
Vibration Frequency:	140 Hz
Vibration Force:	7.14 N
Vibration Duration:	30 sec
Horizontal Acceleration:	0.33 g
Vertical Acceleration:	0.17 g
Horizontal Amplitude:	0.0042 mm
Vertical Amplitude:	0.0022 mm
Peak Strength:	- kPa
Residual Strength:	3 kPa
Vibro-Residual Strength:	1.5 kPa

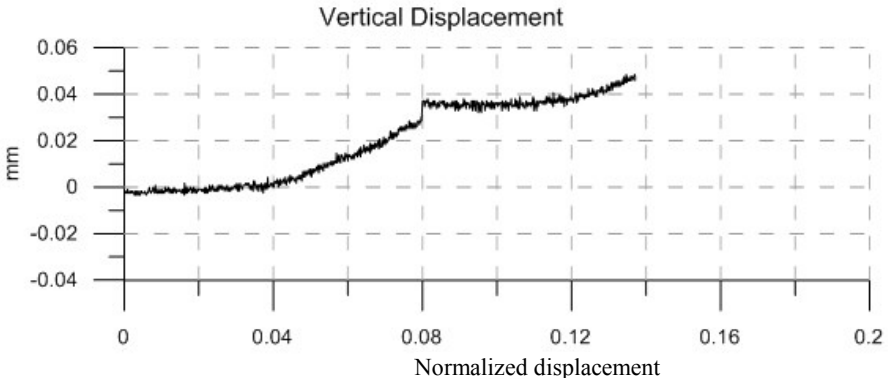

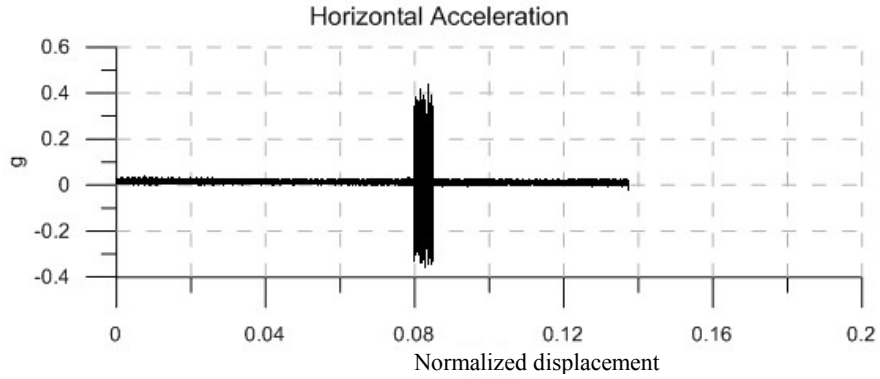

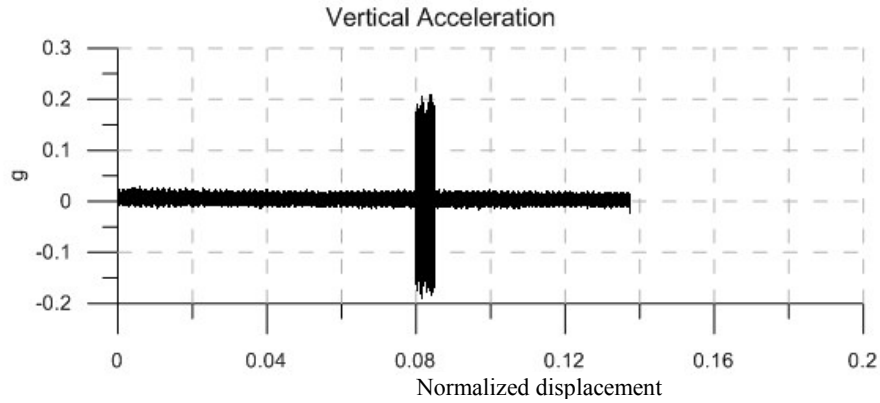

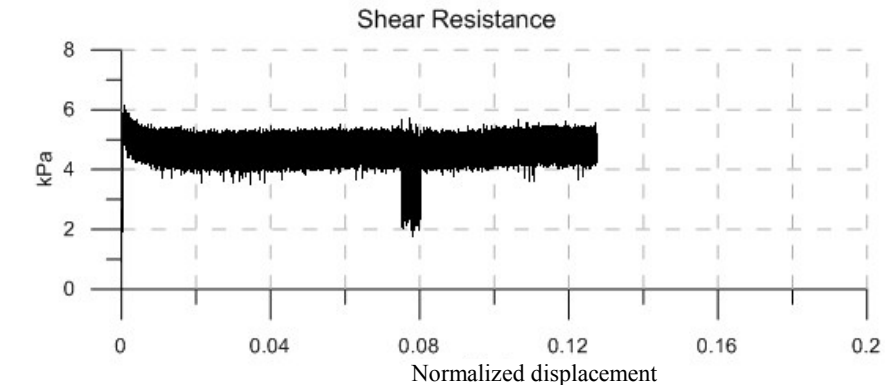

Material:	Glass Beads
Size:	0.55 mm
Normal Stress:	50 kPa
Vibration Frequency:	140 Hz
Vibration Force:	7.14 N
Vibration Duration:	30 sec
Horizontal Acceleration:	0.32 g
Vertical Acceleration:	0.22 g
Horizontal Amplitude:	0.0041 mm
Vertical Amplitude:	0.0028 mm
Peak Strength:	6 kPa
Residual Strength:	5 kPa
Vibro-Residual Strength:	3.5 kPa

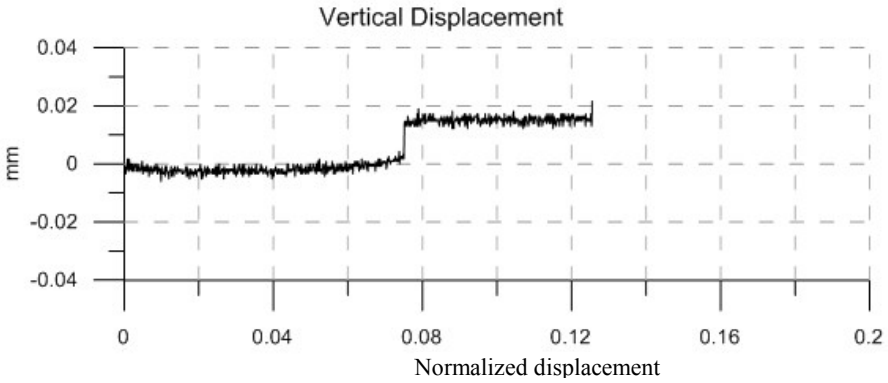

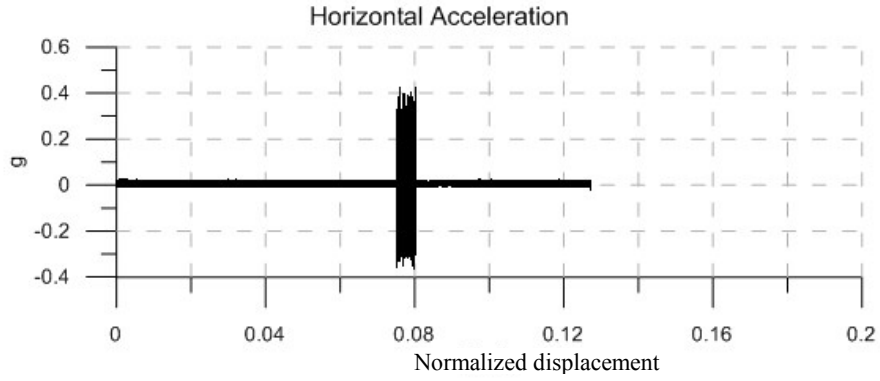

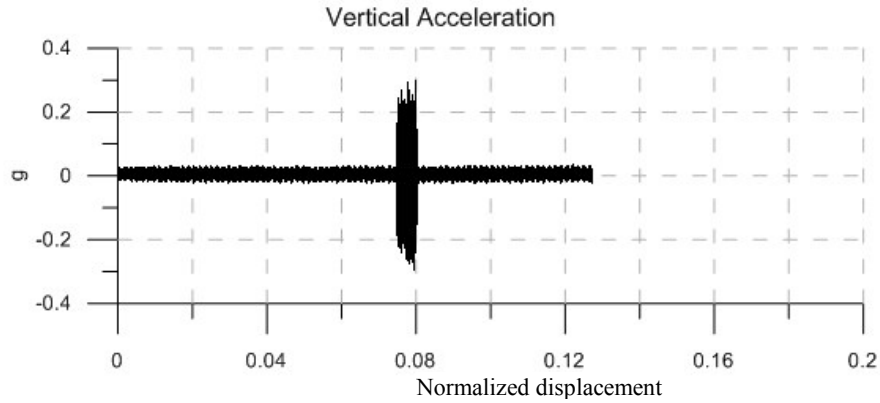

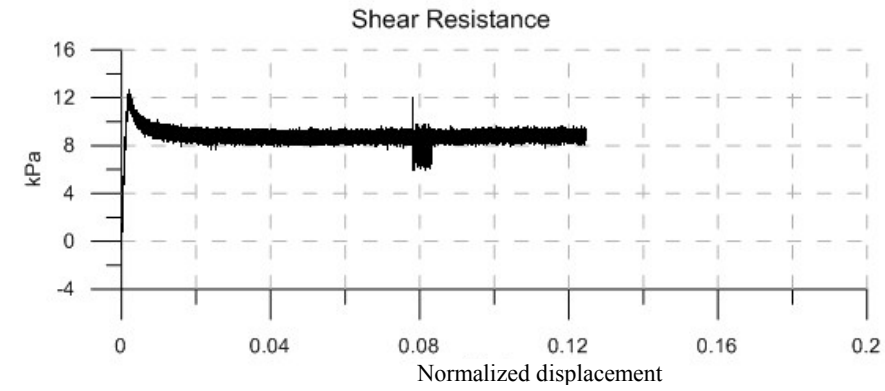

Material:	Glass Beads
Size:	0.55 mm
Normal Stress:	118 kPa
Vibration Frequency:	140 Hz
Vibration Force:	7.14 N
Vibration Duration:	30 sec
Horizontal Acceleration:	0.30 g
Vertical Acceleration:	0.15 g
Horizontal Amplitude:	0.0038 mm
Vertical Amplitude:	0.0019 mm
Peak Strength:	12 kPa
Residual Strength:	9 kPa
Vibro-Residual Strength:	7.5 kPa

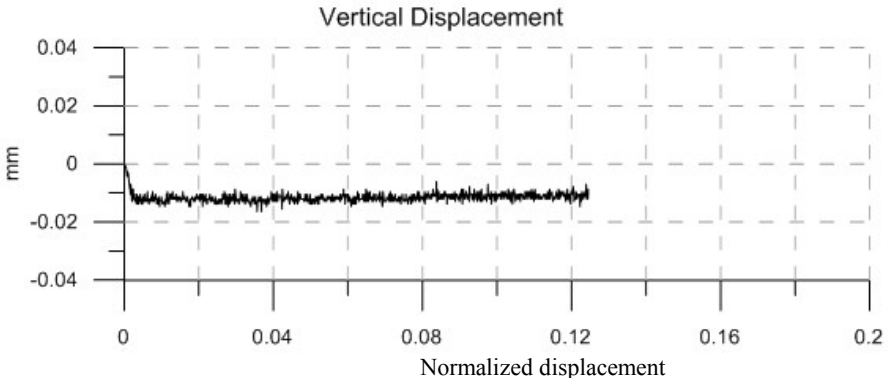

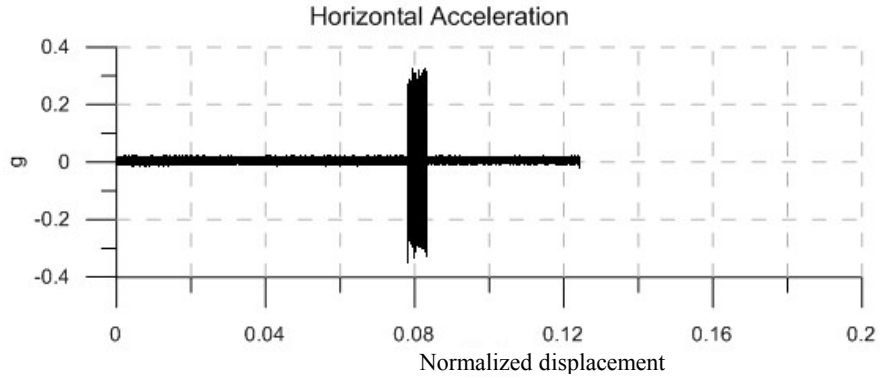

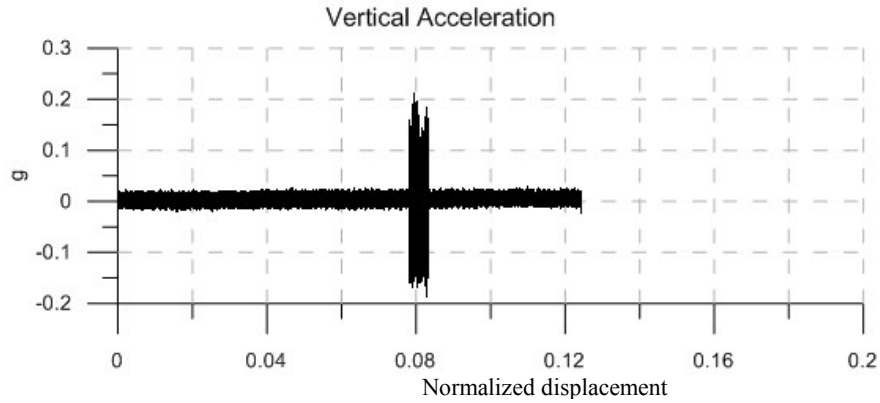

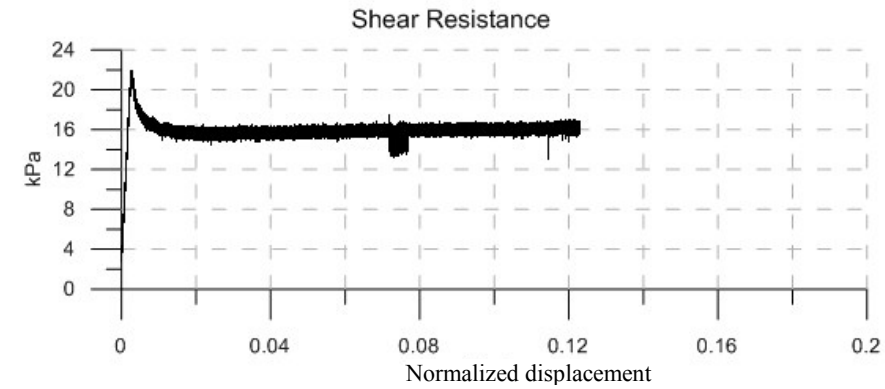

Material:	Glass Beads
Size:	0.55 mm
Normal Stress:	200 kPa
Vibration Frequency:	140 Hz
Vibration Force:	7.14 N
Vibration Duration:	30 sec
Horizontal Acceleration:	0.30 g
Vertical Acceleration:	0.14 g
Horizontal Amplitude:	0.0038 mm
Vertical Amplitude:	0.0018 mm
Peak Strength:	21.5 kPa
Residual Strength:	16 kPa
Vibro-Residual Strength:	14.5 kPa

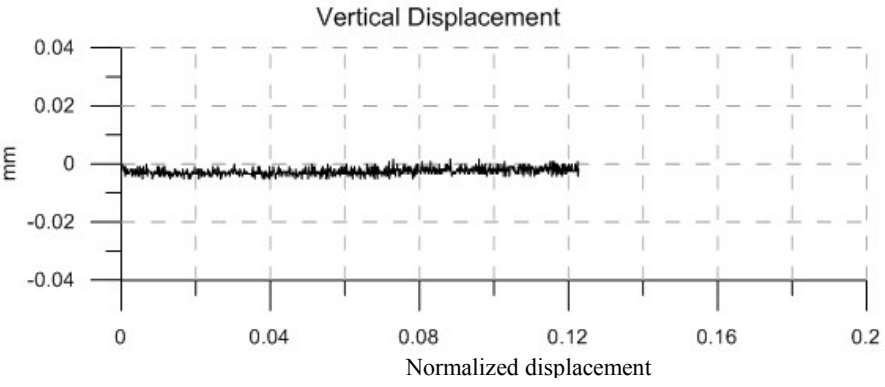

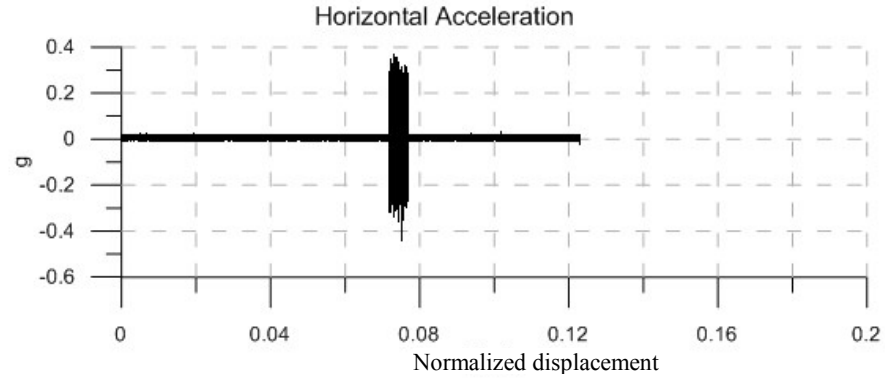

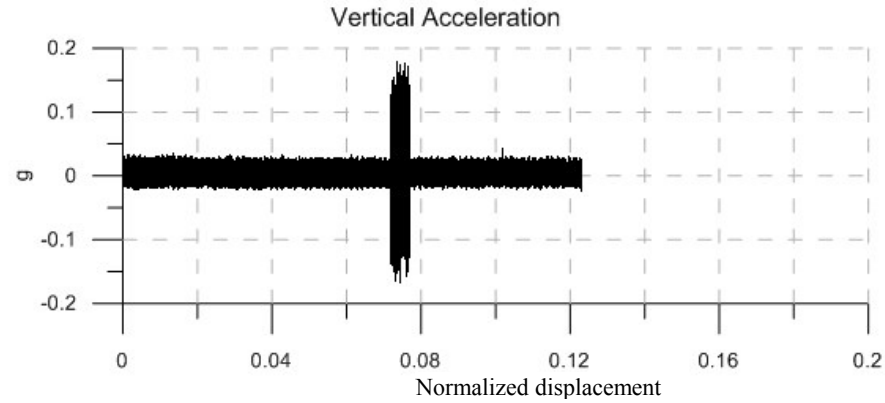

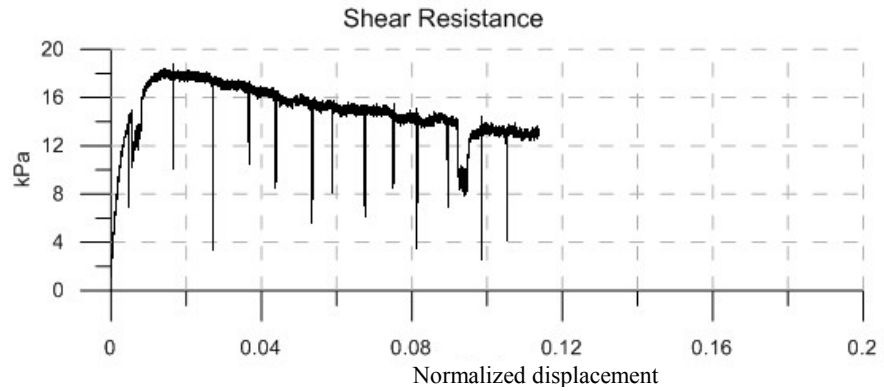

Material:	Glass Beads
Size:	0.55 mm
Normal Stress:	23 kPa
Vibration Frequency:	140 Hz
Vibration Force:	7.14 N
Vibration Duration:	15 sec
Pre-peak strength loss:	4 kPa
Residual strength loss:	5 kPa
Peak Strength:	18 kPa
Residual Strength:	14 kPa
Vibro-Residual Strength:	9 kPa

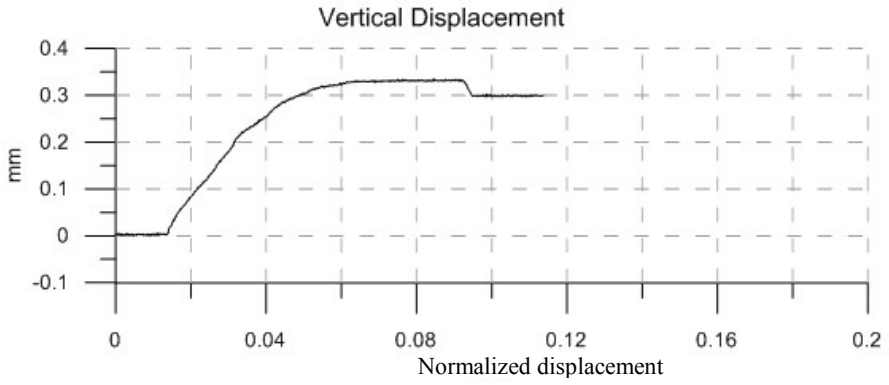

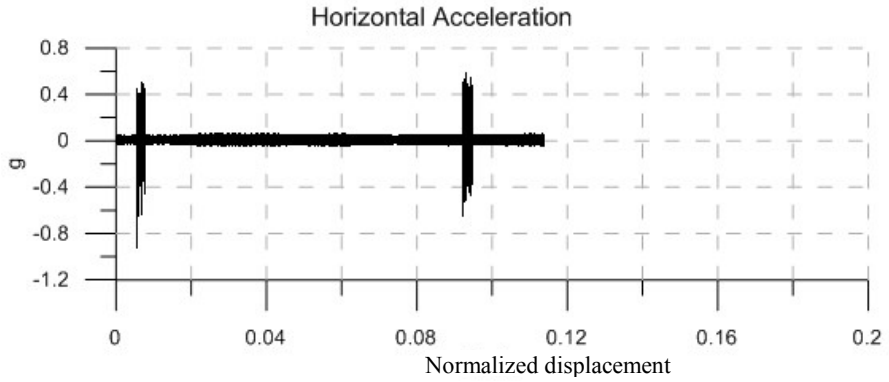

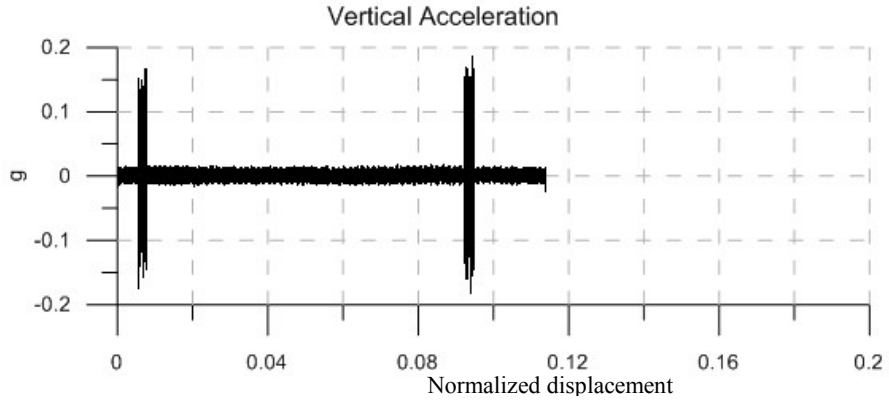

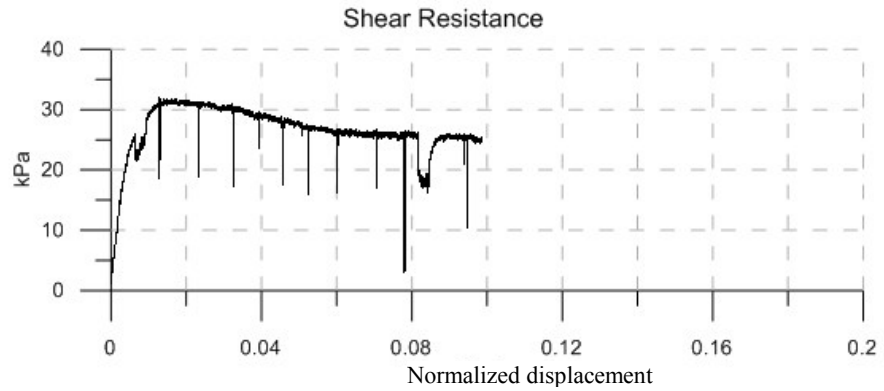

Material:	Glass Beads
Size:	0.55 mm
Normal Stress:	50 kPa
Vibration Frequency:	140 Hz
Vibration Force:	7.14 N
Vibration Duration:	15 sec
Pre-peak strength loss:	4 kPa
Residual strength loss:	8 kPa
Peak Strength:	31.5 kPa
Residual Strength:	26 kPa
Vibro-Residual Strength:	18 kPa

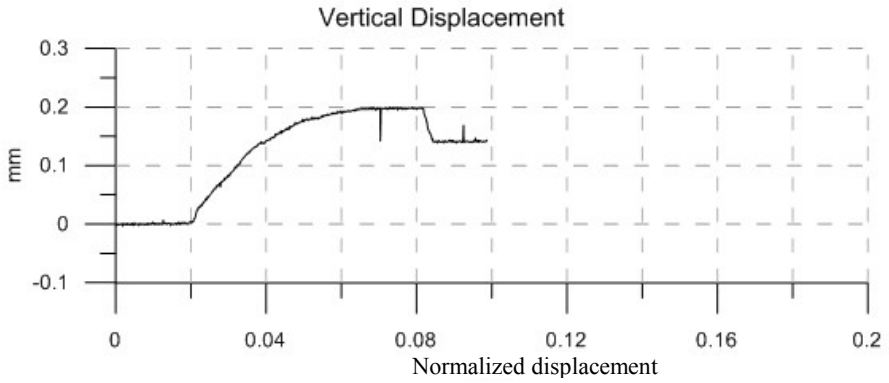

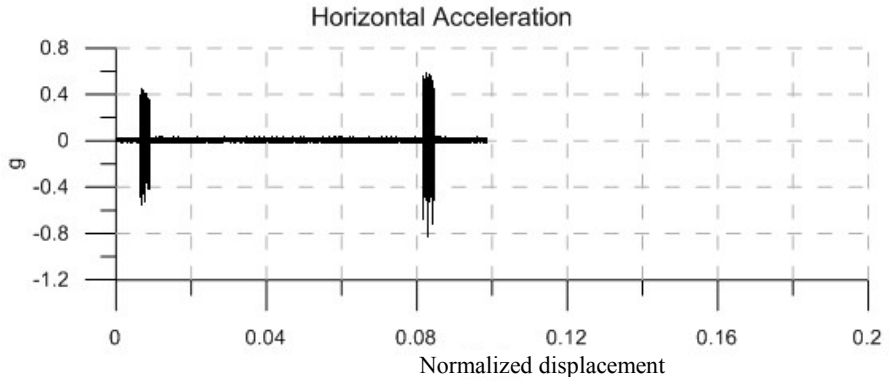

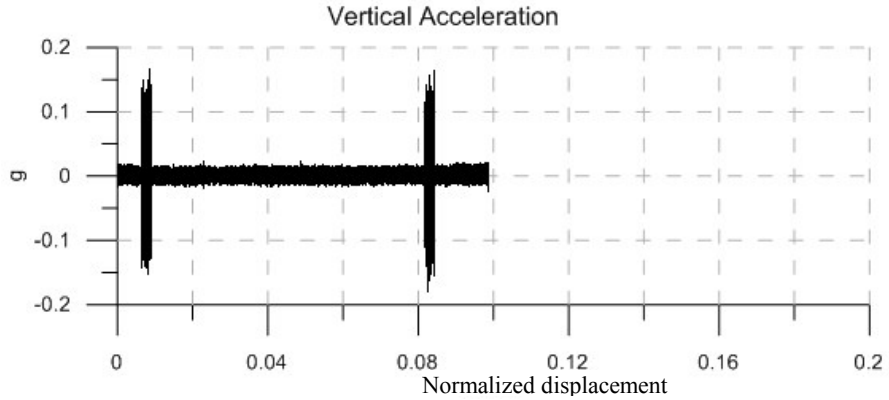

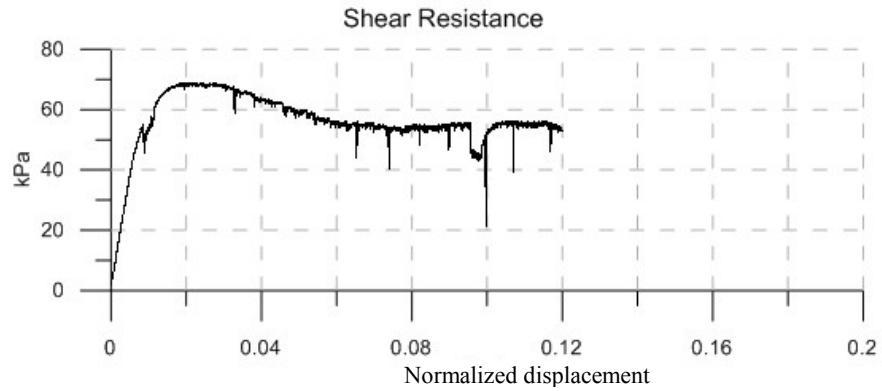

Material:	Glass Beads
Size:	0.55 mm
Normal Stress:	118 kPa
Vibration Frequency:	140 Hz
Vibration Force:	7.14 N
Vibration Duration:	15 sec
Pre-peak strength loss:	4 kPa
Residual strength loss:	11 kPa
Peak Strength:	68.5 kPa
Residual Strength:	55.5 kPa
Vibro-Residual Strength:	44.5 kPa

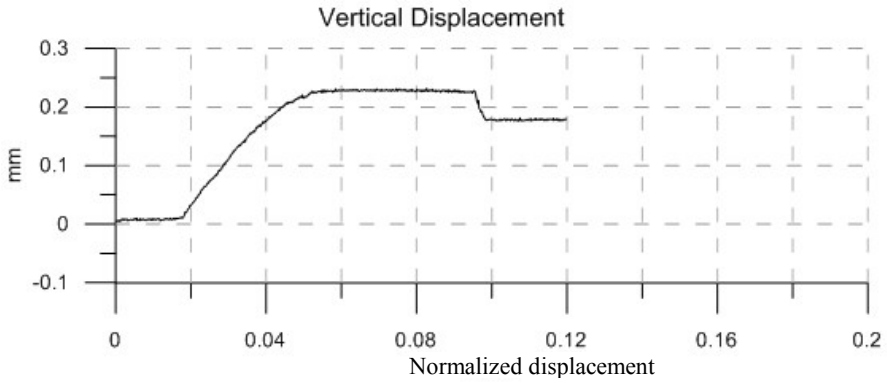

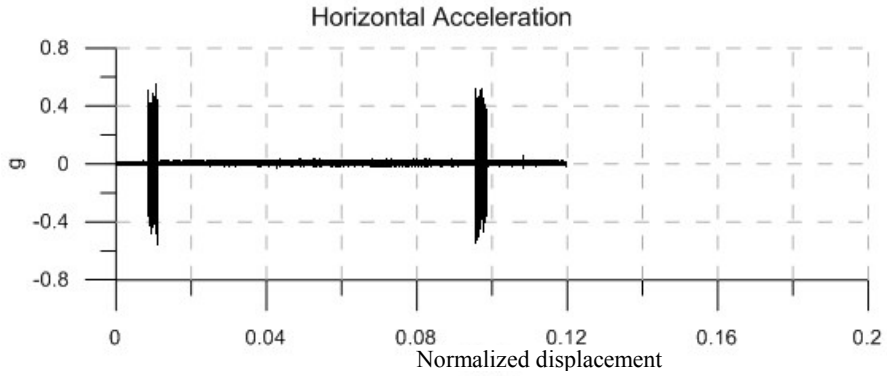

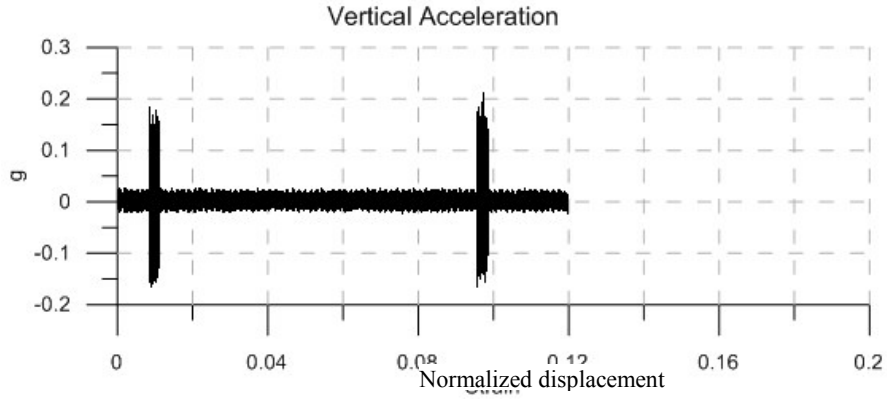

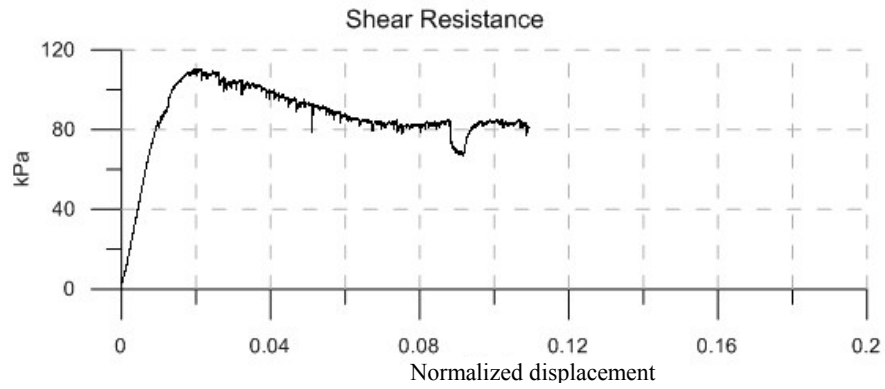

Material:	Glass Beads
Size:	0.55 mm
Normal Stress:	200 kPa
Vibration Frequency:	140 Hz
Vibration Force:	7.14 N
Vibration Duration:	15 sec
Pre-peak strength loss:	3 kPa
Residual strength loss:	16 kPa
Peak Strength:	110.5 kPa
Residual Strength:	85 kPa
Vibro-Residual Strength:	69 kPa

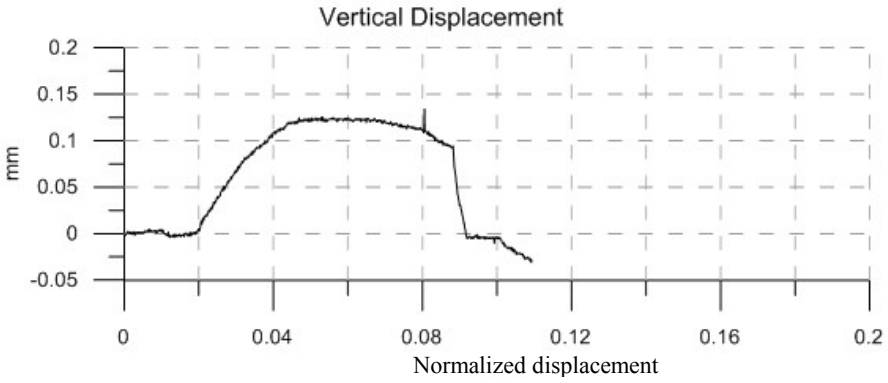

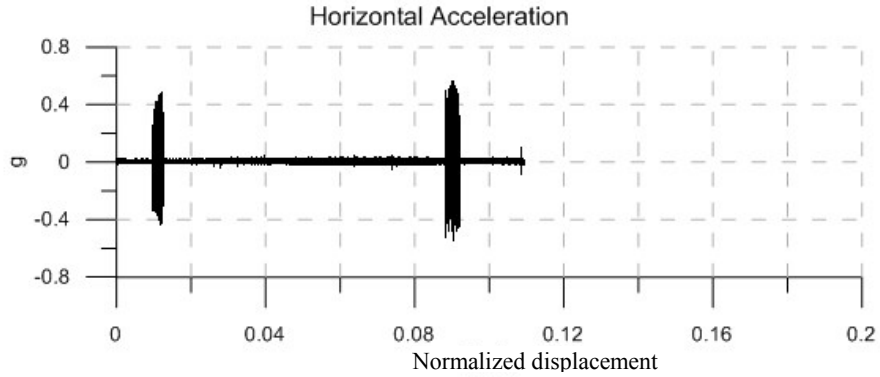

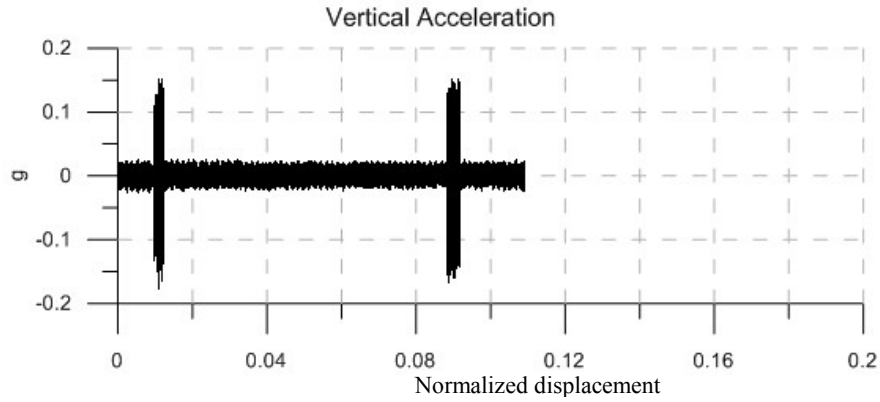

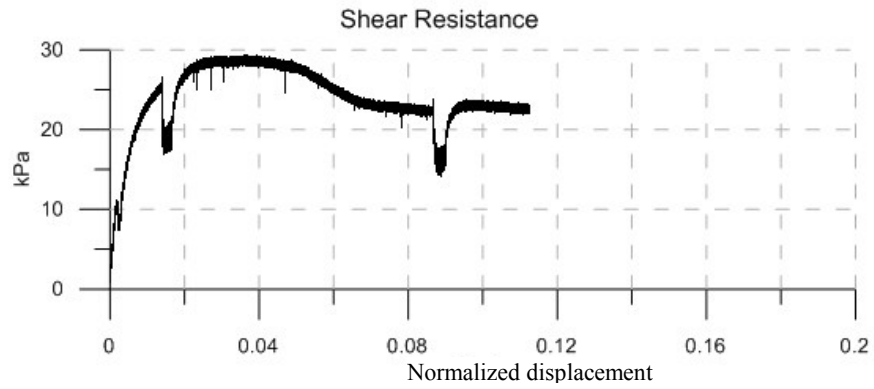

Material:	Sand
Size:	Fine
Normal Stress:	23 kPa
Vibration Frequency:	140 Hz
Vibration Force:	7.14 N
Vibration Duration:	15 sec
Horizontal Acceleration:	0.48 g
Vertical Acceleration:	0.14 g
Horizontal Amplitude:	6.1×10^{-3} mm
Vertical Amplitude:	1.8×10^{-3} mm
Peak Strength:	29 kPa
Residual Strength:	22.5 kPa
Vibro-Residual Strength:	16 kPa

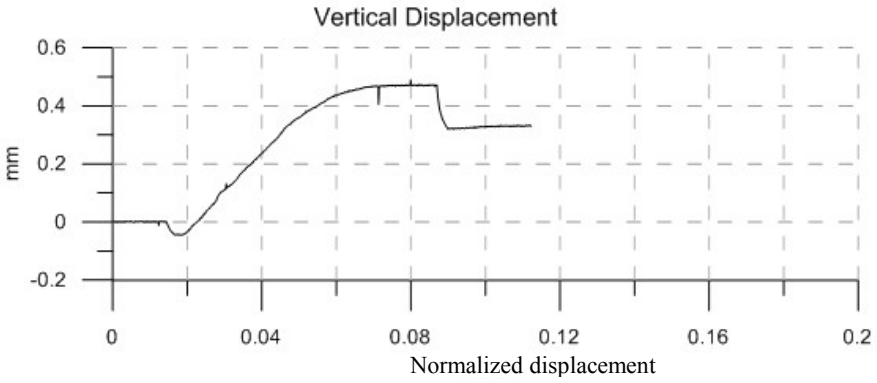

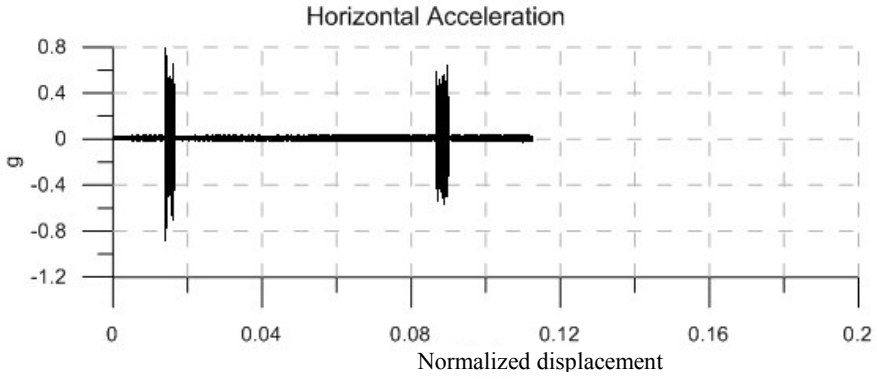

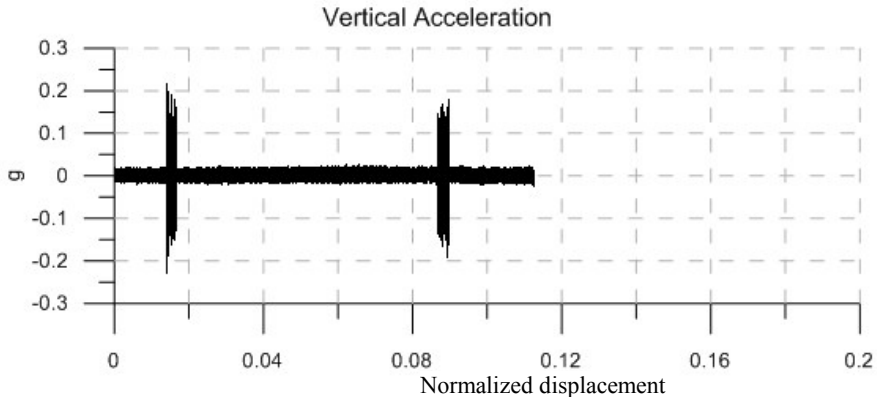

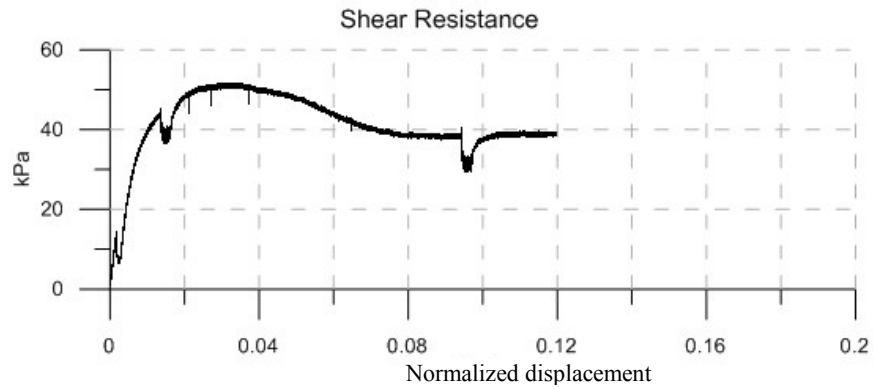

Material:	Sand
Size:	Fine
Normal Stress:	50 kPa
Vibration Frequency:	140 Hz
Vibration Force:	7.14 N
Vibration Duration:	15 sec
Horizontal Acceleration:	0.48 g
Vertical Acceleration:	0.14 g
Horizontal Amplitude:	6.1×10^{-3} mm
Vertical Amplitude:	1.8×10^{-3} mm
Peak Strength:	51 kPa
Residual Strength:	38.5 kPa
Vibro-Residual Strength:	31 kPa

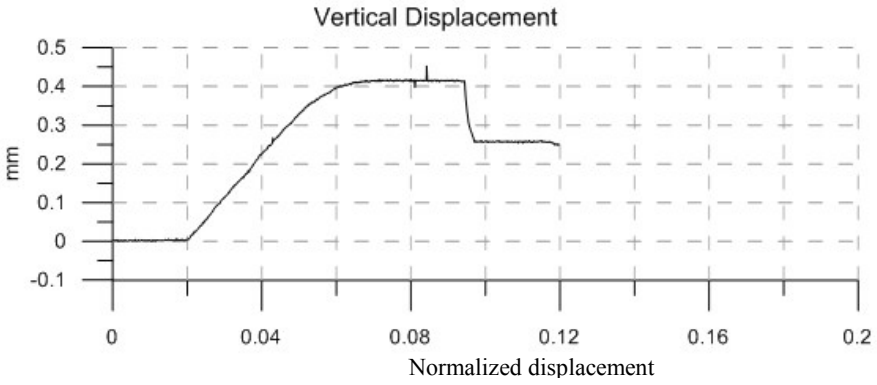

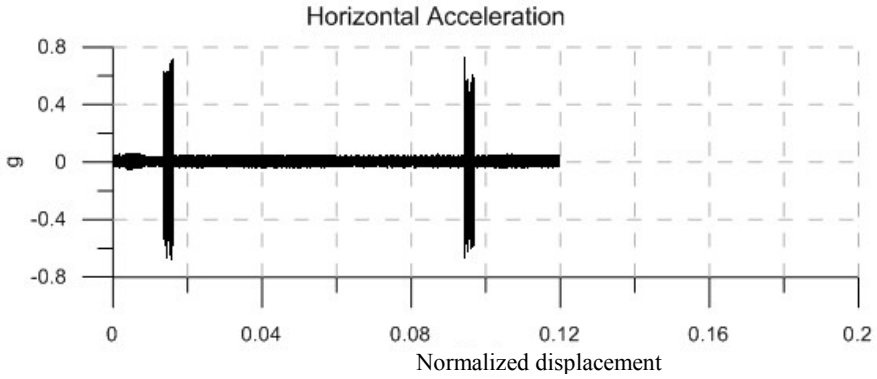

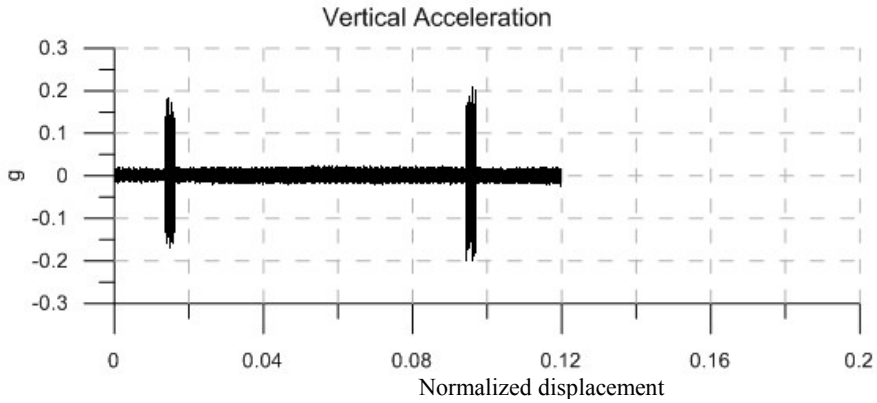

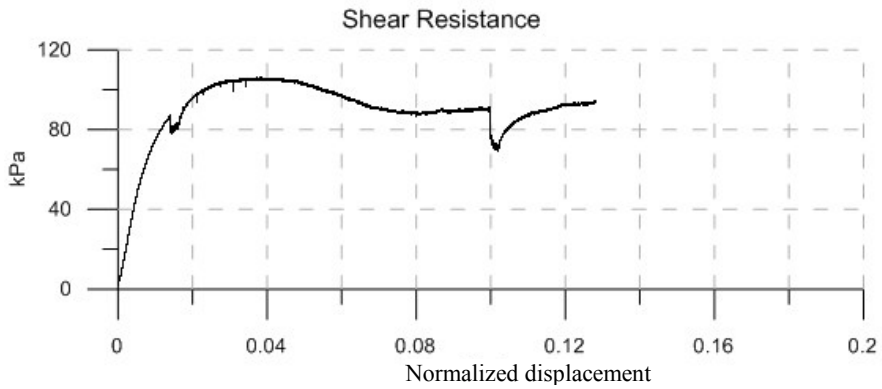

Material:	Sand
Size:	Fine
Normal Stress:	118 kPa
Vibration Frequency:	140 Hz
Vibration Force:	7.14 N
Vibration Duration:	15 sec
Horizontal Acceleration:	0.46 g
Vertical Acceleration:	0.14 g
Horizontal Amplitude:	5.8×10^{-3} mm
Vertical Amplitude:	1.8×10^{-3} mm
Peak Strength:	105.5 kPa
Residual Strength:	90 kPa
Vibro-Residual Strength:	71 kPa

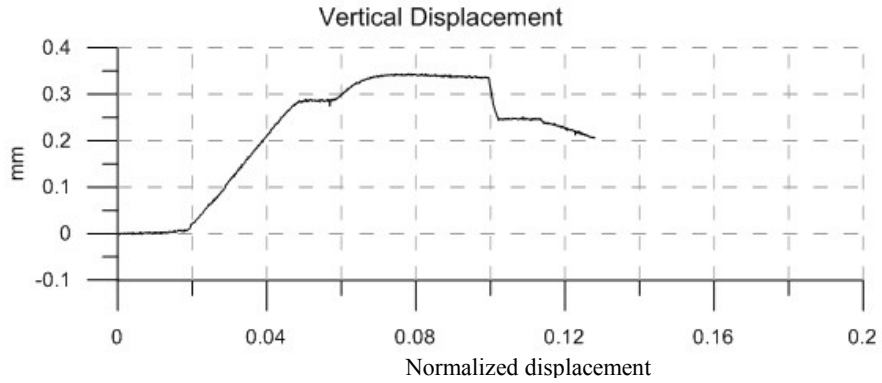

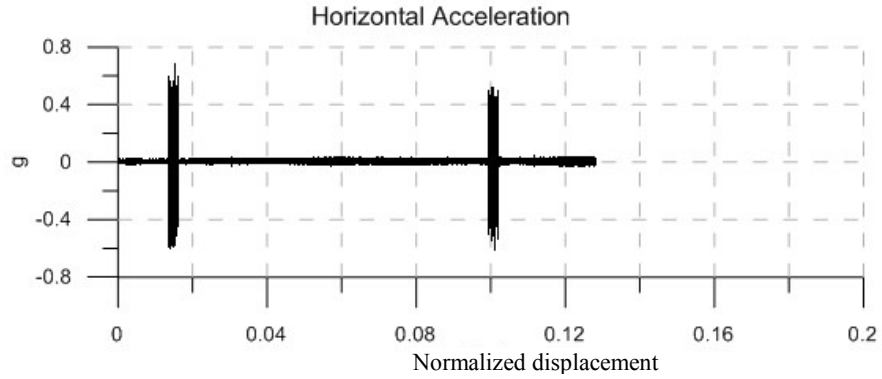

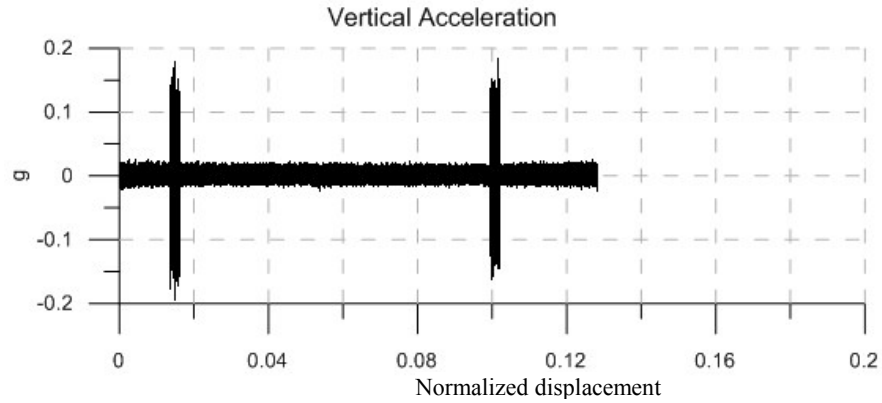

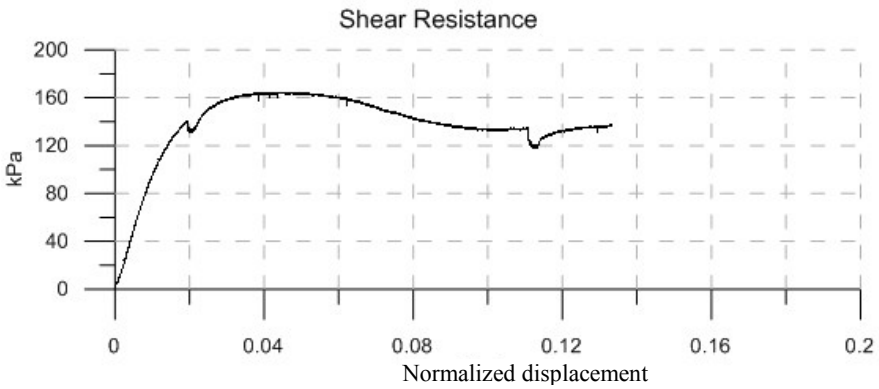

Material:	Sand
Size:	Fine
Normal Stress:	200 kPa
Vibration Frequency:	140 Hz
Vibration Force:	7.14 N
Vibration Duration:	15 sec
Horizontal Acceleration:	0.42 g
Vertical Acceleration:	0.14 g
Horizontal Amplitude:	5.3×10^{-3} mm
Vertical Amplitude:	1.8×10^{-3} mm
Peak Strength:	164 kPa
Residual Strength:	134 kPa
Vibro-Residual Strength:	119 kPa

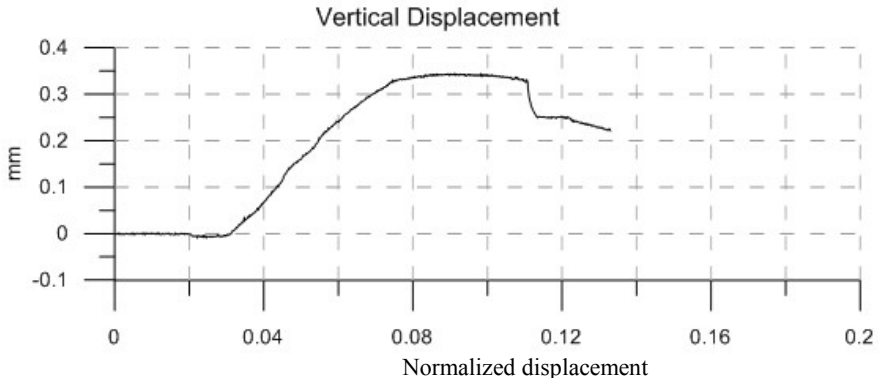

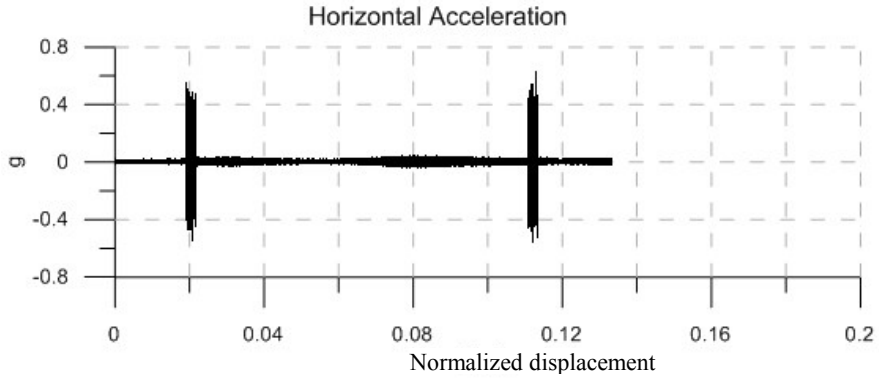

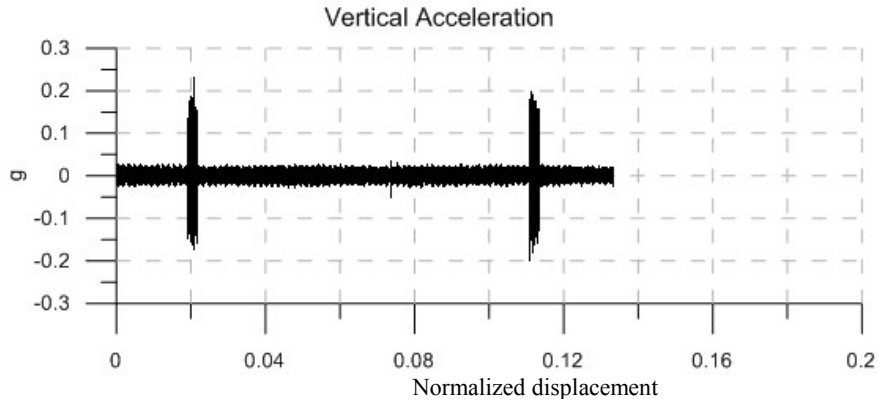

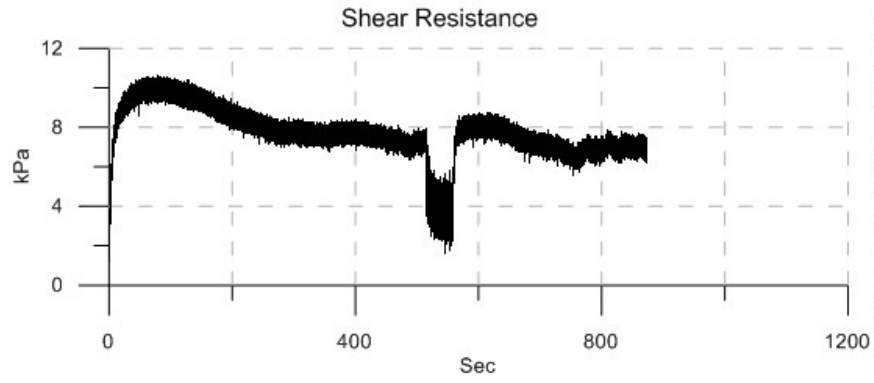

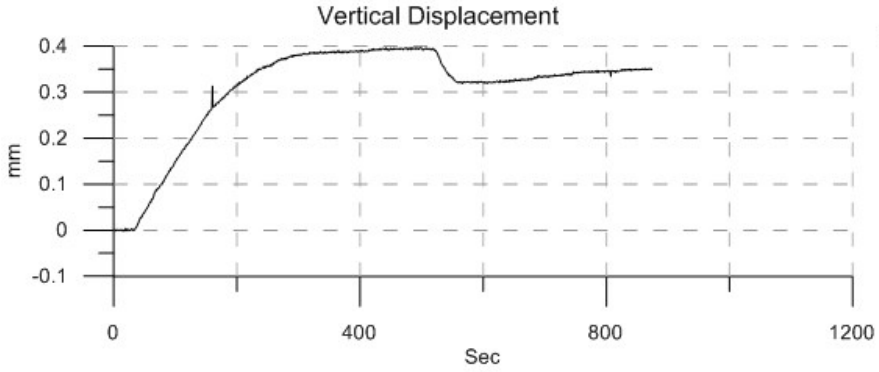

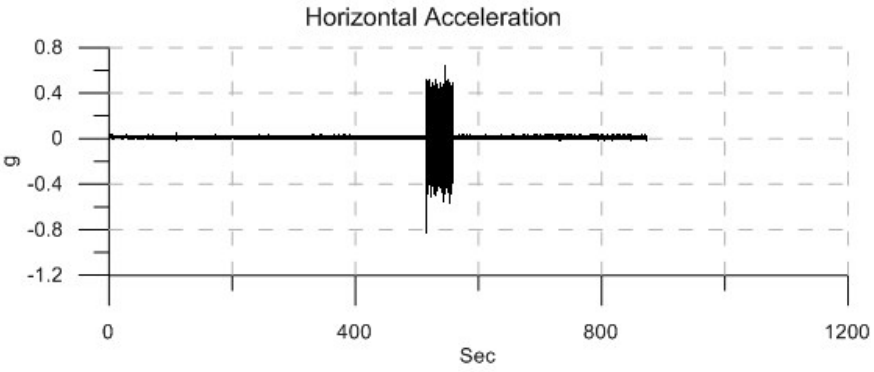

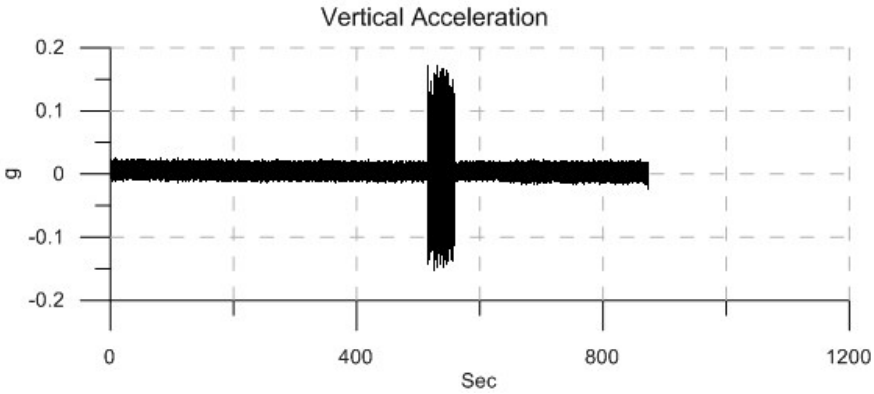

Material:	Glass Beads
Size:	0.55 mm
Normal Stress:	8 kPa
Vibration Frequency:	140 Hz
Vibration Force:	7.14 N
Vibration Duration:	43 sec
Horizontal Acceleration:	0.42 g
Vertical Acceleration:	0.12 g
Horizontal Amplitude:	5.3×10^{-3} mm
Vertical Amplitude:	1.5×10^{-3} mm
Peak Strength:	10 kPa
Residual Strength:	7.5 kPa
Post-Vibrational Strength:	8.5 kPa

No shearing during vibration

Shear rate: 0.61 mm/min

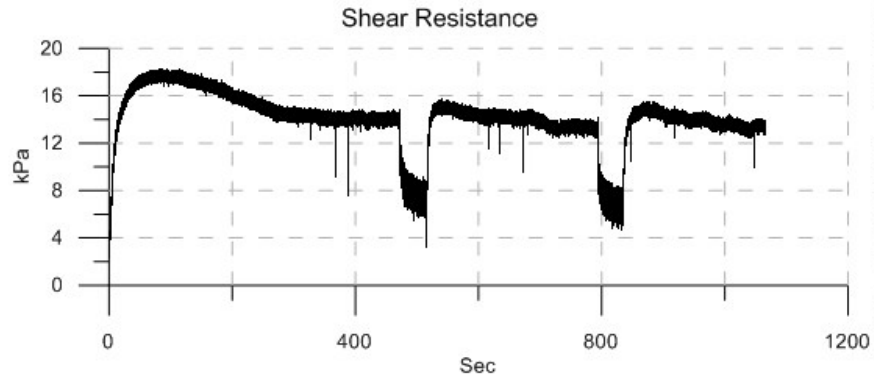

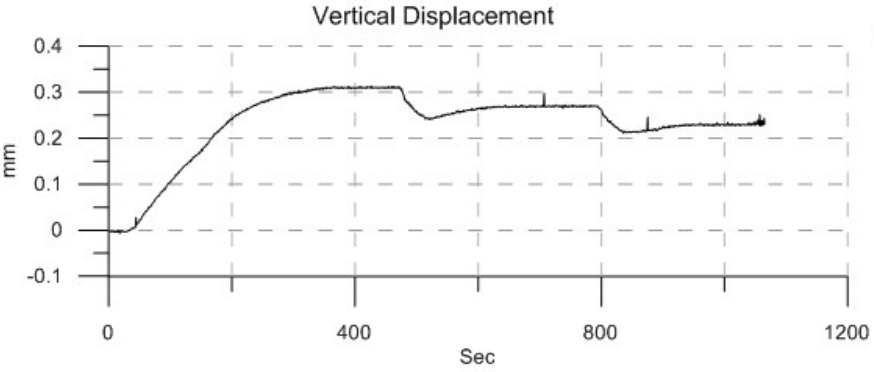

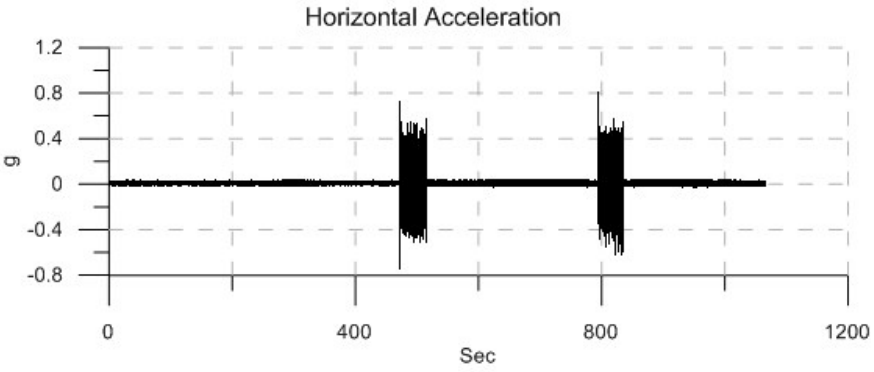

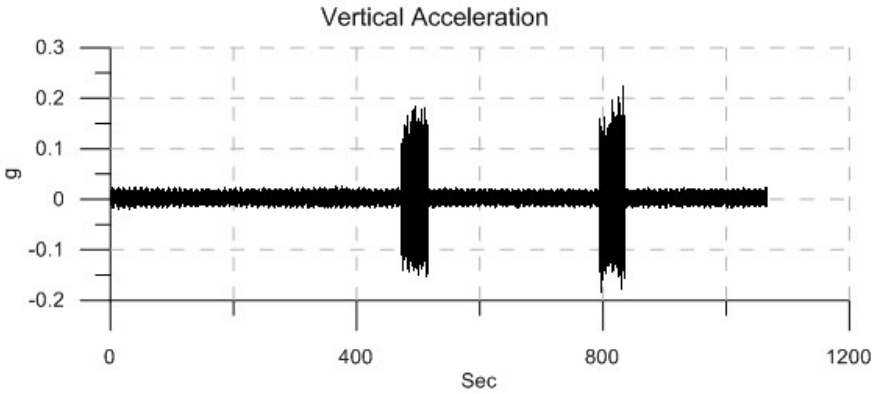

Material:	Glass Beads
Size:	0.55 mm
Normal Stress:	23 kPa
Vibration Frequency:	140 Hz
Vibration Force:	7.14 N
Vibration Duration:	42 sec
Horizontal Acceleration:	0.37 g
Vertical Acceleration:	0.12 g
Horizontal Amplitude:	4.7×10^{-3} mm
Vertical Amplitude:	1.5×10^{-3} mm
Peak Strength:	18 kPa
Residual Strength:	14 kPa
Post-Vibrational Strength:	15 kPa

No shearing during vibration

Shear rate: 0.61 mm/min

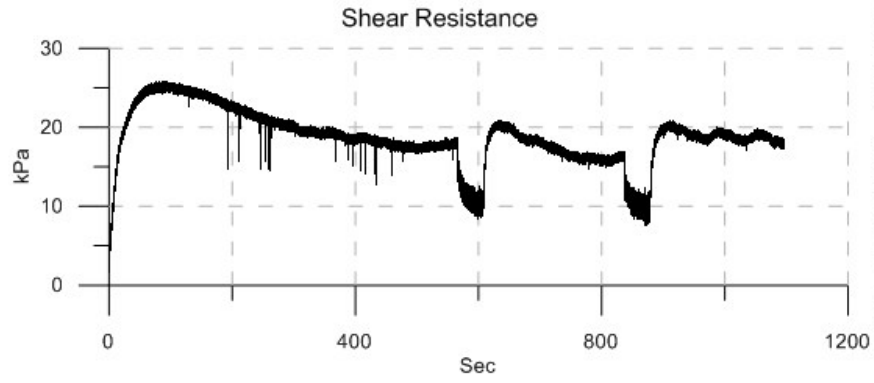

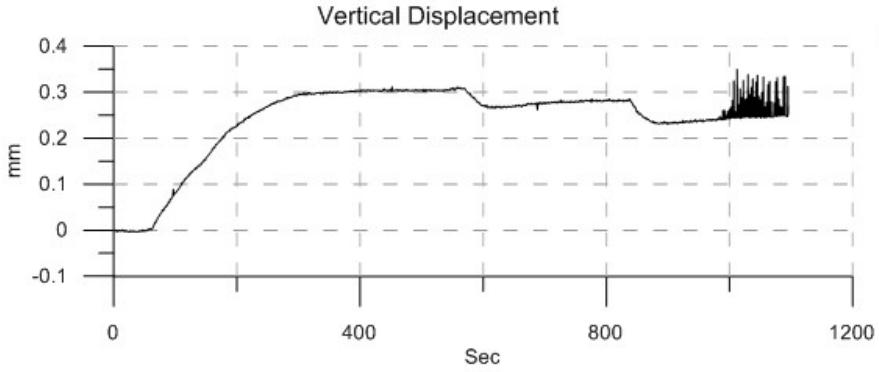

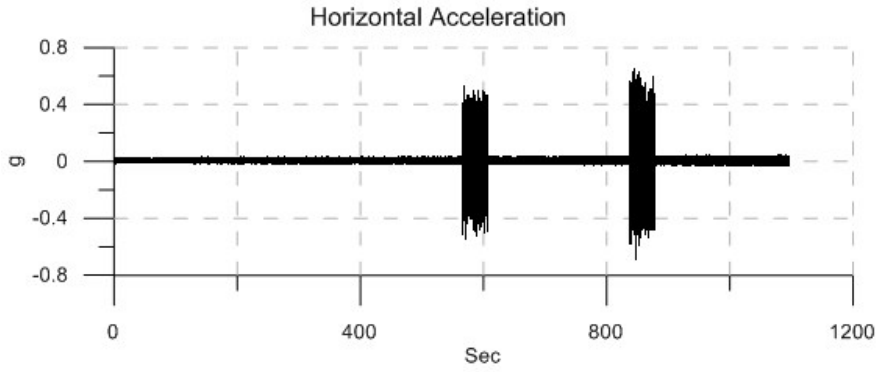

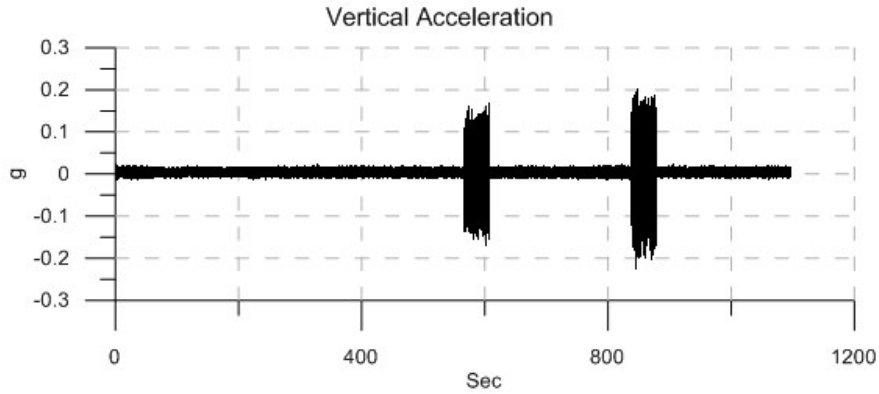

Material:	Glass Beads
Size:	0.55 mm
Normal Stress:	36 kPa
Vibration Frequency:	140 Hz
Vibration Force:	7.14 N
Vibration Duration:	40 sec
Horizontal Acceleration:	0.37 g
Vertical Acceleration:	0.12 g
Horizontal Amplitude:	4.7×10^{-3} mm
Vertical Amplitude:	1.5×10^{-3} mm
Peak Strength:	25.5 kPa
Residual Strength:	18 kPa
Post-Vibrational Strength:	20 kPa

No shearing during vibration

Shear rate: 0.61 mm/min

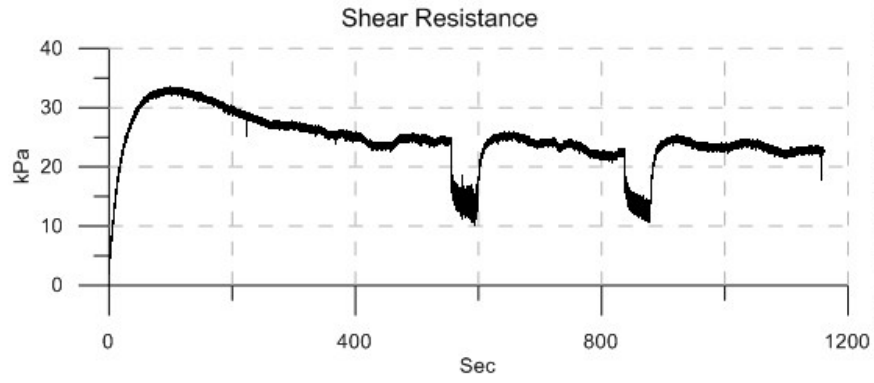

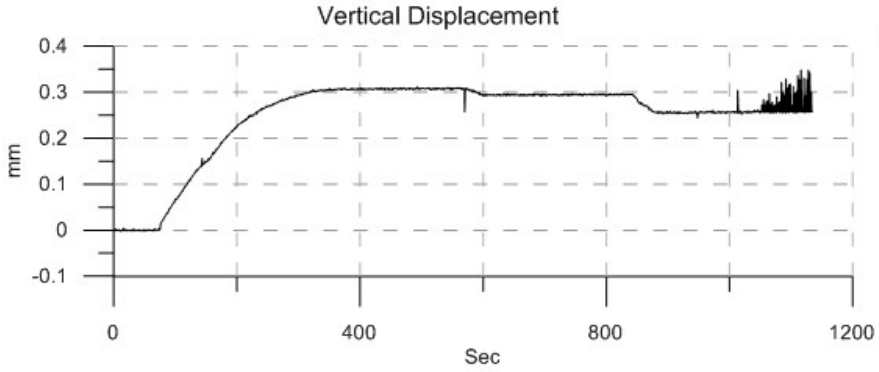

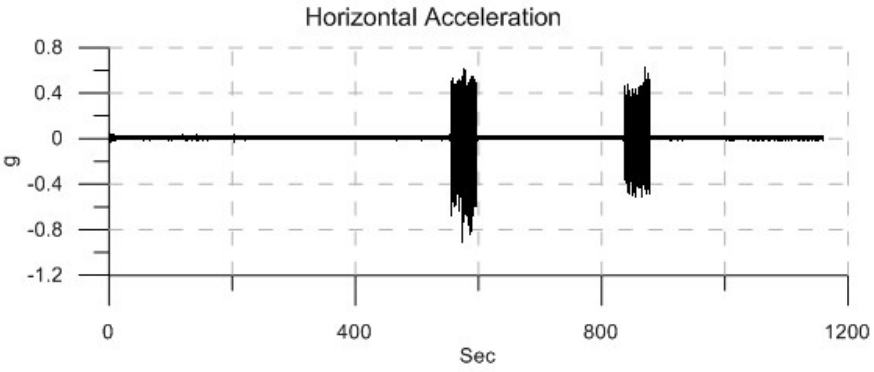

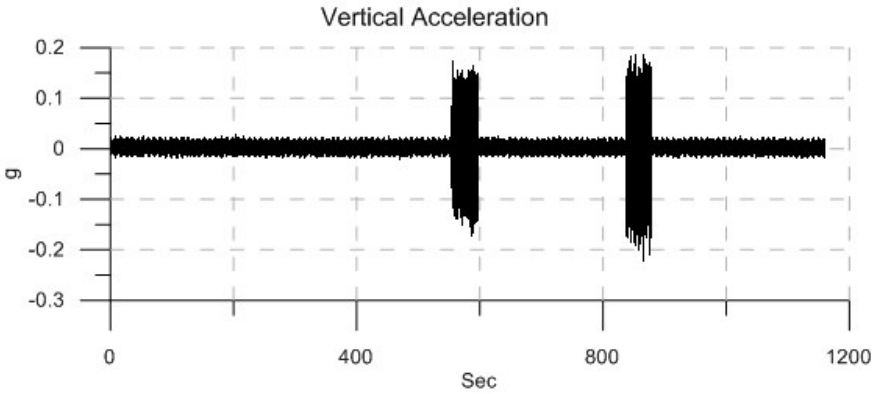

Material:	Glass Beads
Size:	0.55 mm
Normal Stress:	50 kPa
Vibration Frequency:	140 Hz
Vibration Force:	7.14 N
Vibration Duration:	42 sec
Horizontal Acceleration:	0.42 g
Vertical Acceleration:	0.12 g
Horizontal Amplitude:	5.3×10^{-3} mm
Vertical Amplitude:	1.5×10^{-3} mm
Peak Strength:	33 kPa
Residual Strength:	24.5 kPa
Post-Vibrational Strength:	25.5 kPa

No shearing during vibration

Shear rate: 0.61 mm/min

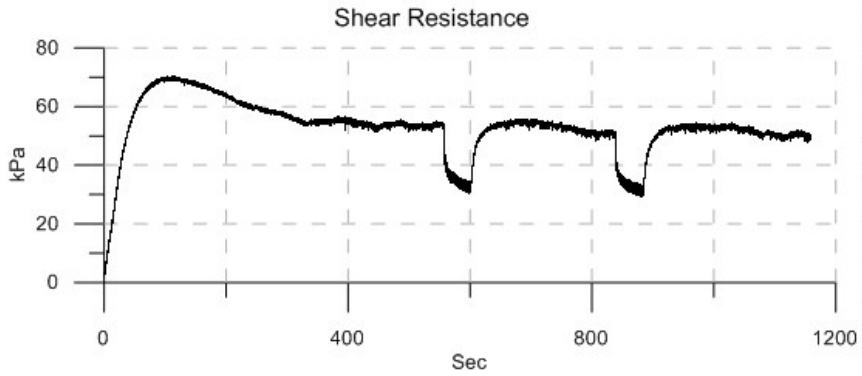

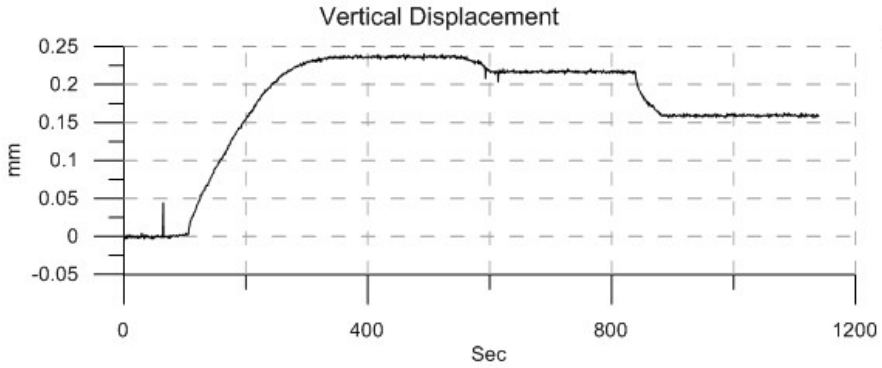

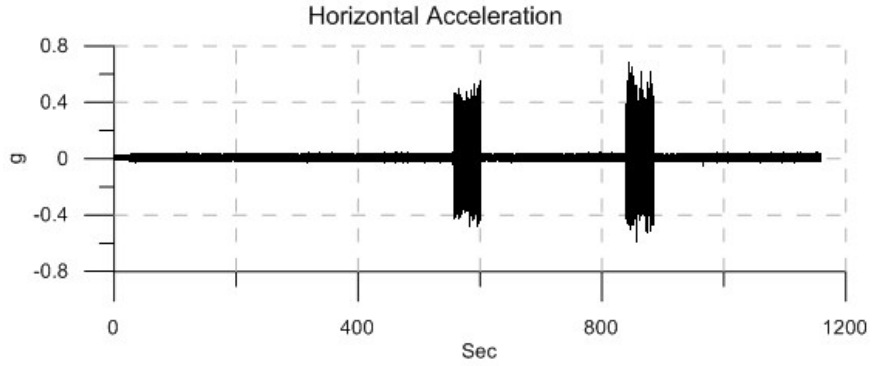

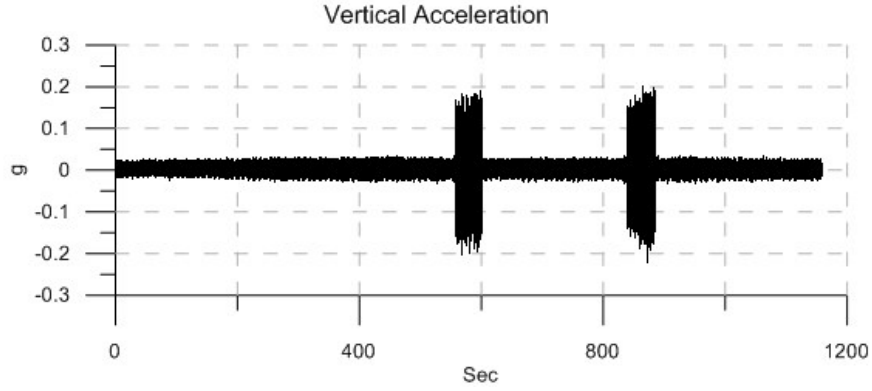

Material:	Glass Beads
Size:	0.55 mm
Normal Stress:	118 kPa
Vibration Frequency:	140 Hz
Vibration Force:	7.14 N
Vibration Duration:	44 sec
Horizontal Acceleration:	0.37 g
Vertical Acceleration:	0.13 g
Horizontal Amplitude:	4.7×10^{-3} mm
Vertical Amplitude:	1.6×10^{-3} mm
Peak Strength:	70 kPa
Residual Strength:	54 kPa
Post-Vibrational Strength:	55 kPa

No shearing during vibration

Shear rate: 0.61 mm/min

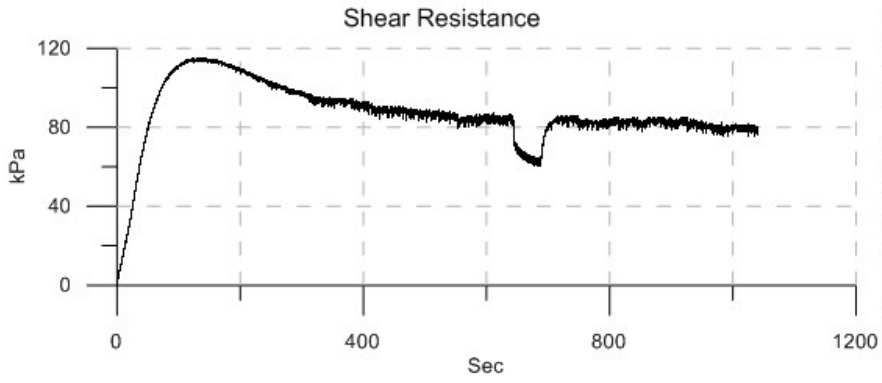

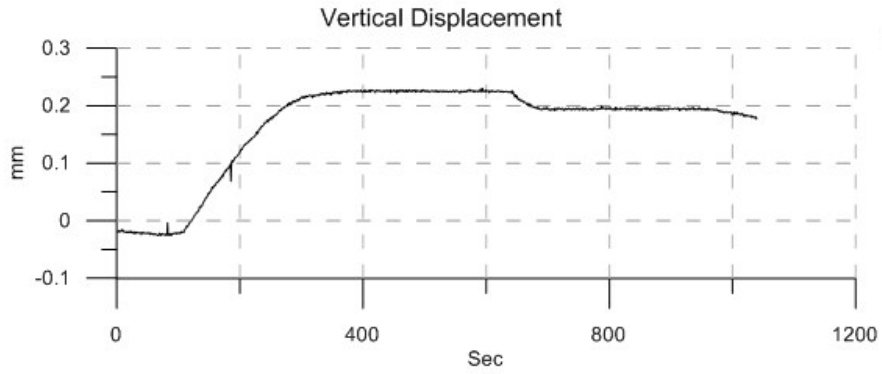

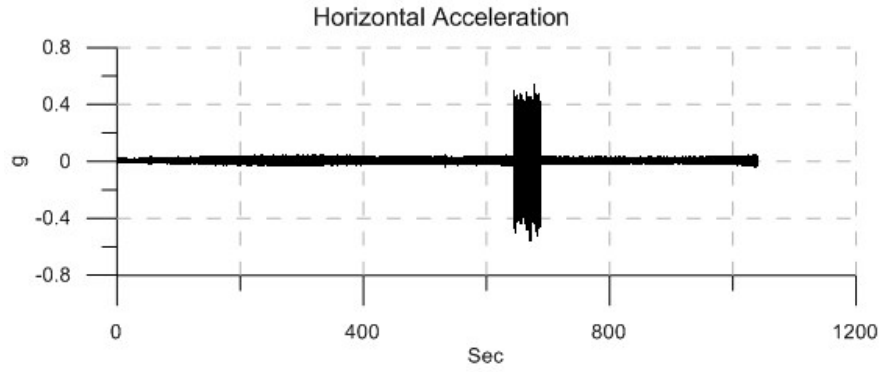

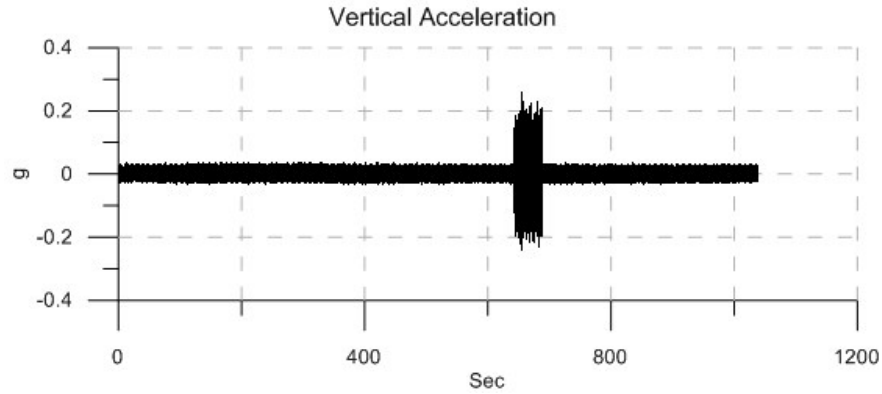

Material:	Glass Beads
Size:	0.55 mm
Normal Stress:	200 kPa
Vibration Frequency:	140 Hz
Vibration Force:	7.14 N
Vibration Duration:	44 sec
Horizontal Acceleration:	0.38 g
Vertical Acceleration:	0.14 g
Horizontal Amplitude:	4.8×10^{-3} mm
Vertical Amplitude:	1.8×10^{-3} mm
Peak Strength:	114.5 kPa
Residual Strength:	85 kPa
Post-Vibrational Strength:	85 kPa

No shearing during vibration

Shear rate: 0.61 mm/min

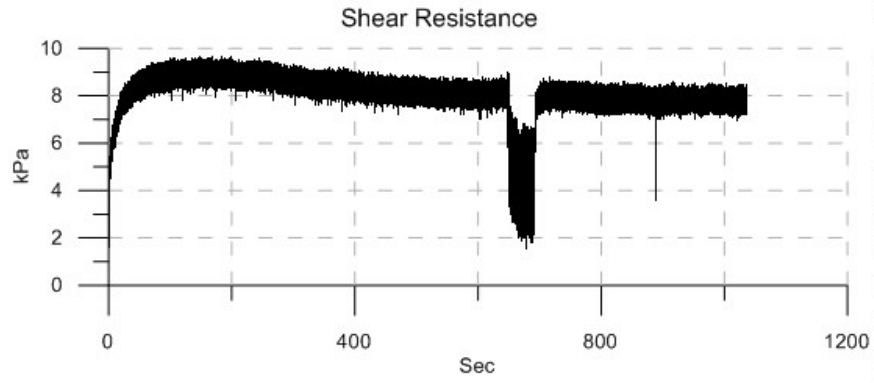

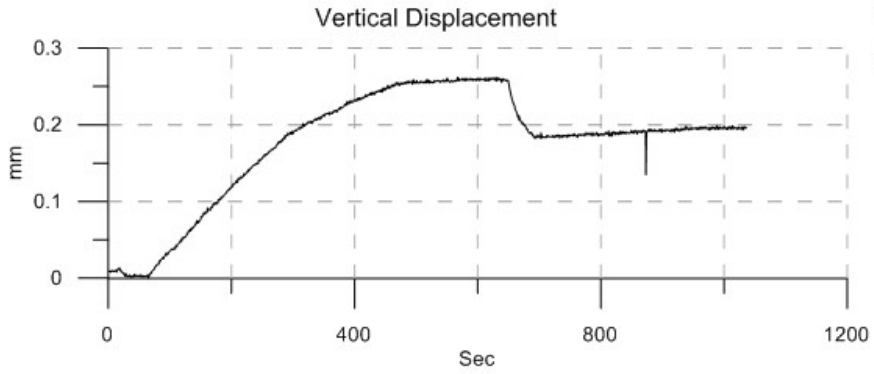

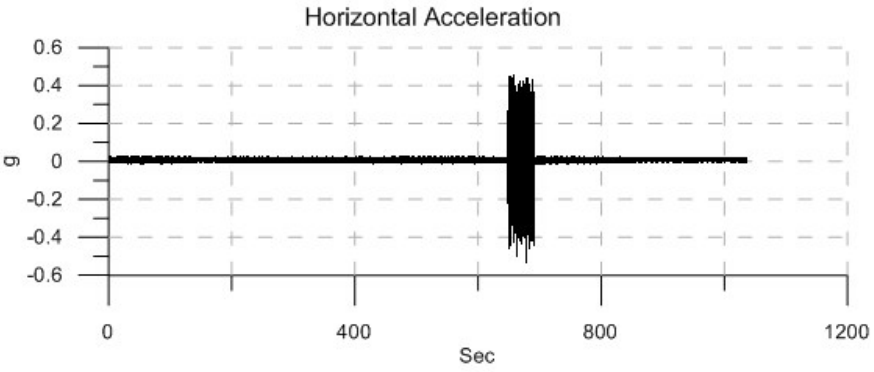

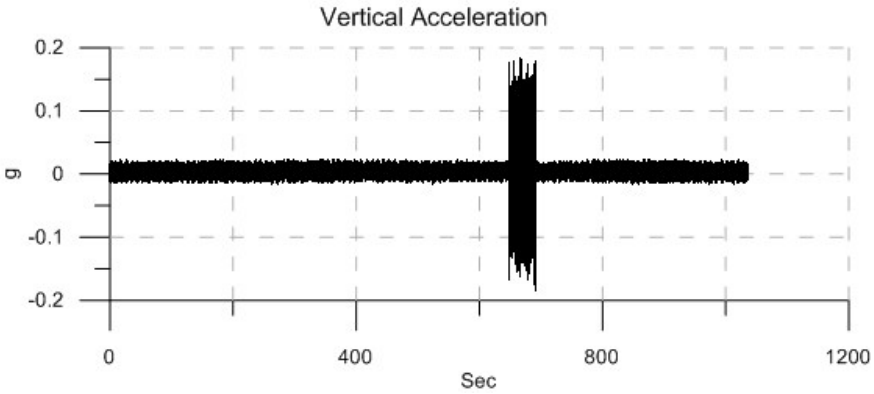

Material:	Glass Beads (Loose)
Size:	0.55 mm
Normal Stress:	8 kPa
Vibration Frequency:	140 Hz
Vibration Force:	7.14 N
Vibration Duration:	42 sec
Horizontal Acceleration:	0.36 g
Vertical Acceleration:	0.13 g
Horizontal Amplitude:	4.6×10^{-3} mm
Vertical Amplitude:	1.6×10^{-3} mm
Peak Strength:	9 kPa
Residual Strength:	8 kPa
Post-Vibrational Strength:	8 kPa

No shearing during vibration

Shear rate: 0.61 mm/min

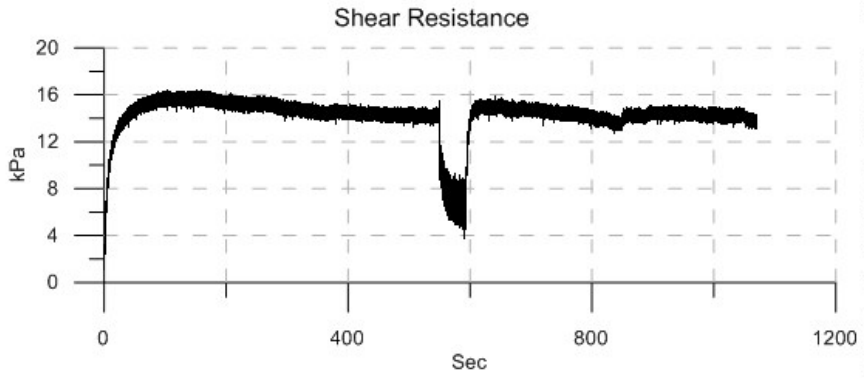

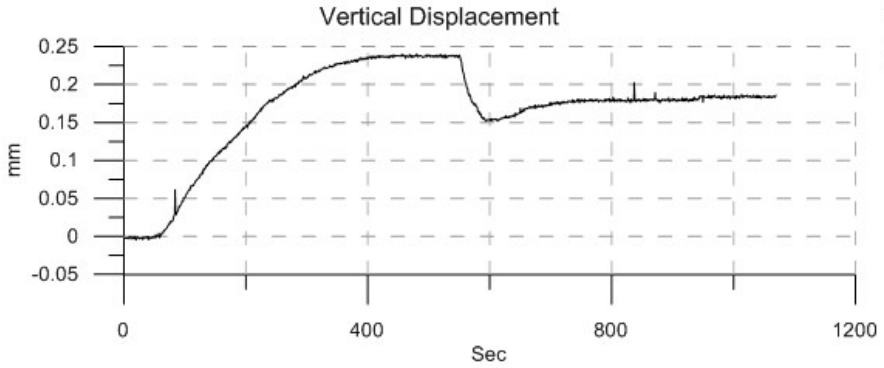

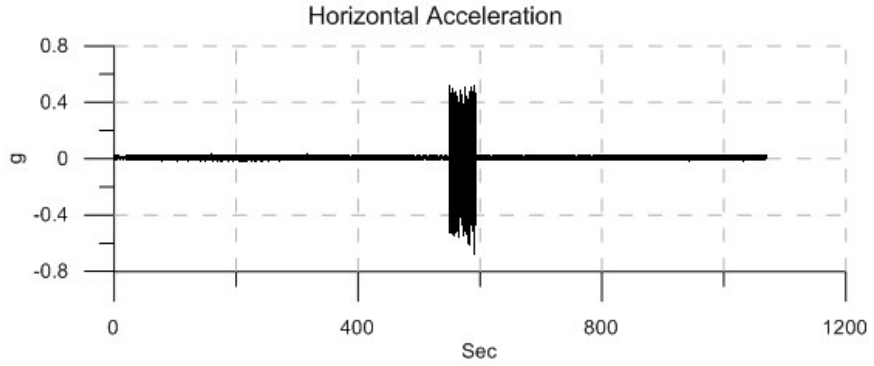

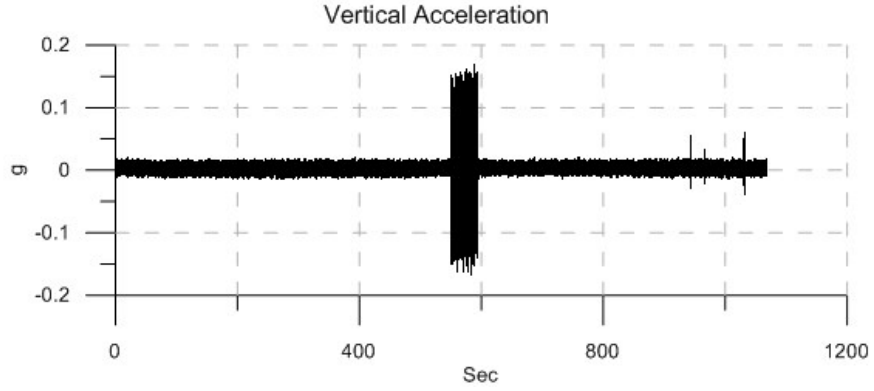

Material:	Glass Beads (Loose)
Size:	0.55 mm
Normal Stress:	23 kPa
Vibration Frequency:	140 Hz
Vibration Force:	7.14 N
Vibration Duration:	42 sec
Horizontal Acceleration:	0.41 g
Vertical Acceleration:	0.13 g
Horizontal Amplitude:	5.2×10^{-3} mm
Vertical Amplitude:	1.6×10^{-3} mm
Peak Strength:	16 kPa
Residual Strength:	14.5 kPa
Post-Vibrational Strength:	15 kPa

No shearing during vibration

Shear rate: 0.61 mm/min

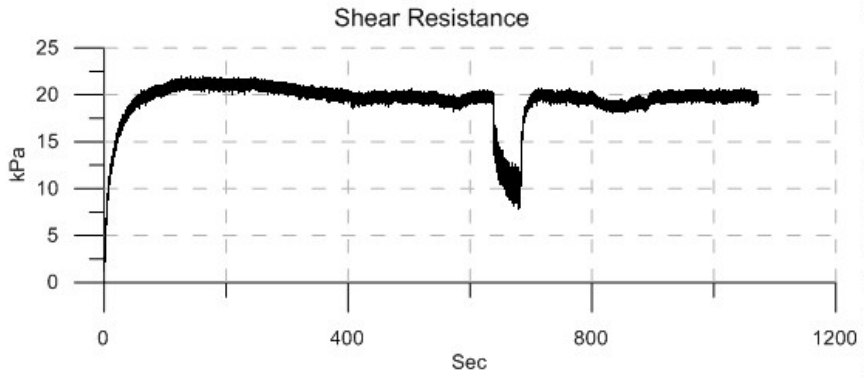

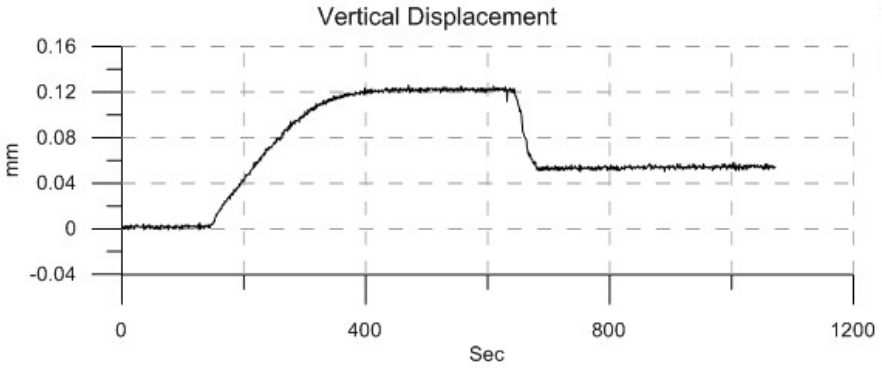

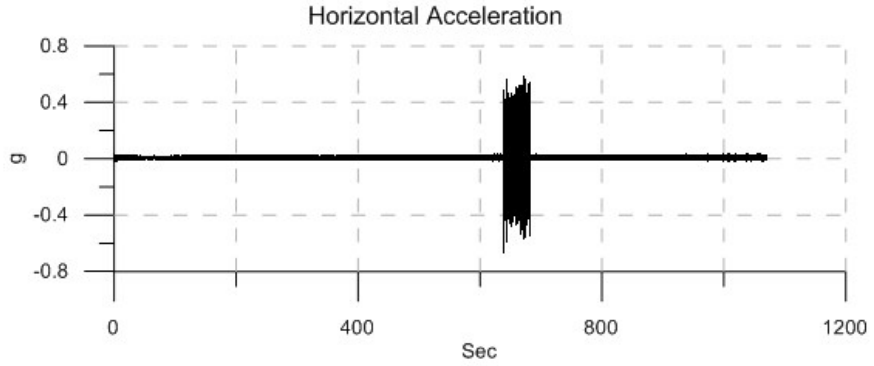

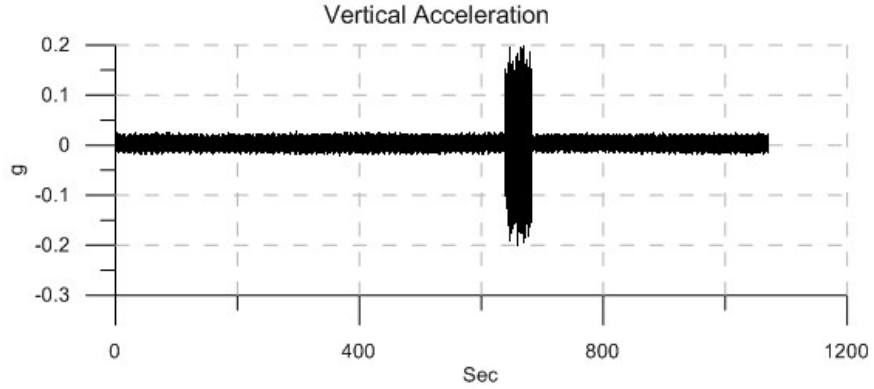

Material:	Glass Beads (Loose)
Size:	0.55 mm
Normal Stress:	36 kPa
Vibration Frequency:	140 Hz
Vibration Force:	7.14 N
Vibration Duration:	43 sec
Horizontal Acceleration:	0.41 g
Vertical Acceleration:	0.13 g
Horizontal Amplitude:	5.2×10^{-3} mm
Vertical Amplitude:	1.6×10^{-3} mm
Peak Strength:	21.5 kPa
Residual Strength:	20 kPa
Post-Vibrational Strength:	20 kPa

No shearing during vibration

Shear rate: 0.61 mm/min

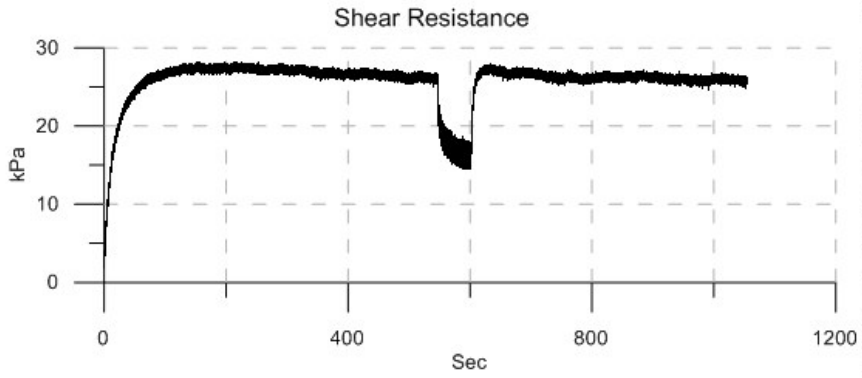

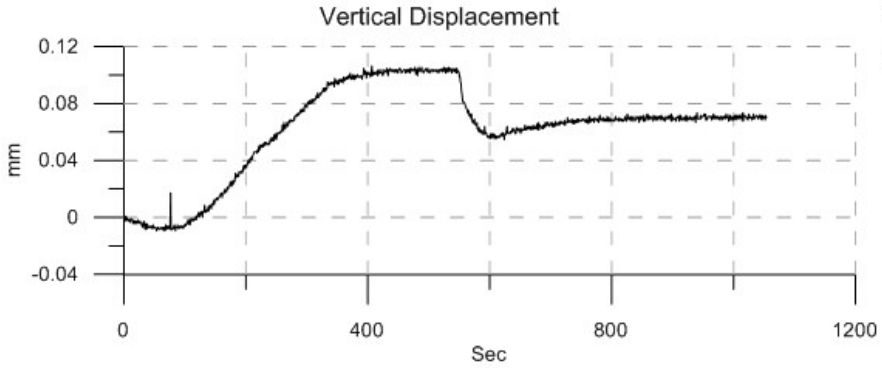

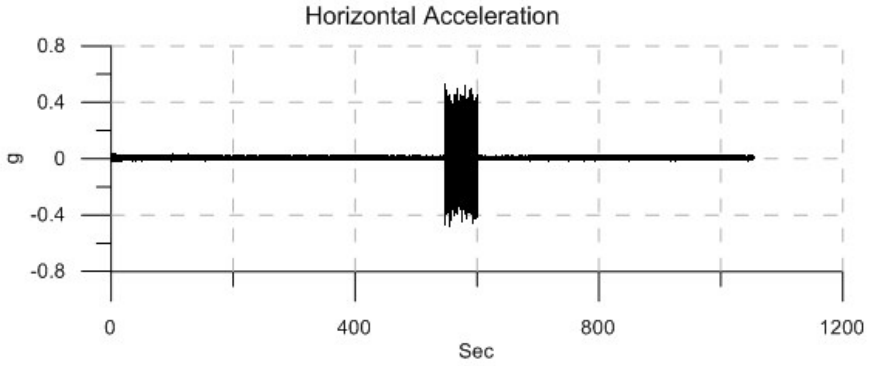

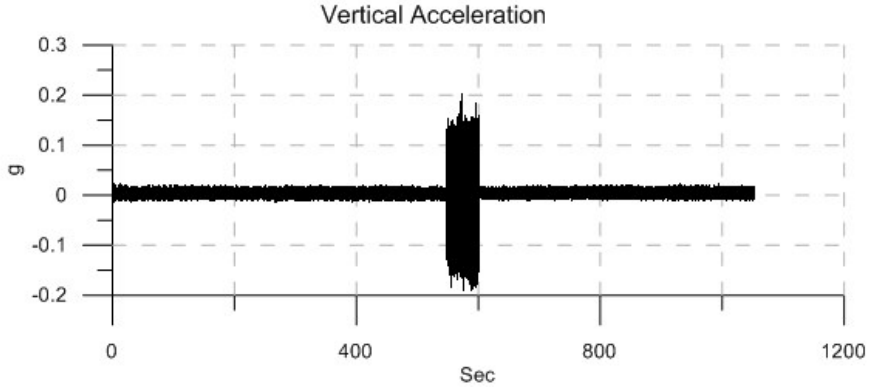

Material:	Glass Beads (Loose)
Size:	0.55 mm
Normal Stress:	50 kPa
Vibration Frequency:	140 Hz
Vibration Force:	7.14 N
Vibration Duration:	53 sec
Horizontal Acceleration:	0.35 g
Vertical Acceleration:	0.13 g
Horizontal Amplitude:	4.4×10^{-3} mm
Vertical Amplitude:	1.6×10^{-3} mm
Peak Strength:	27.5 kPa
Residual Strength:	26 kPa
Post-Vibrational Strength:	27 kPa

No shearing during vibration

Shear rate: 0.61 mm/min

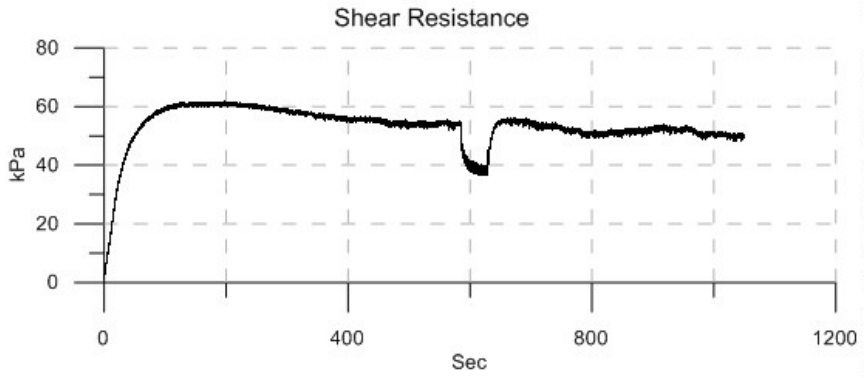

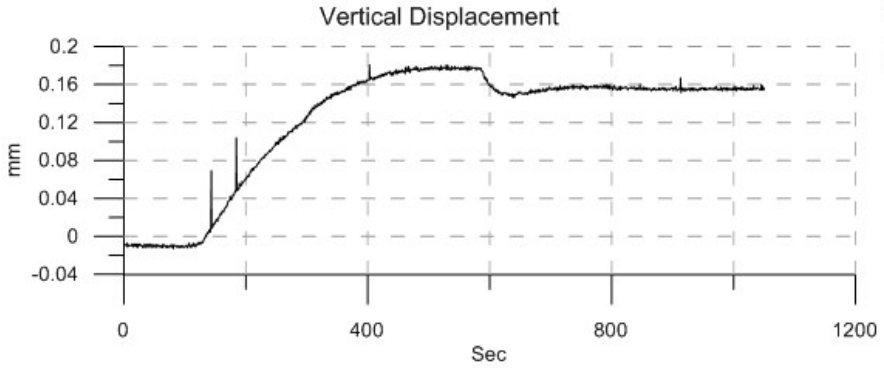

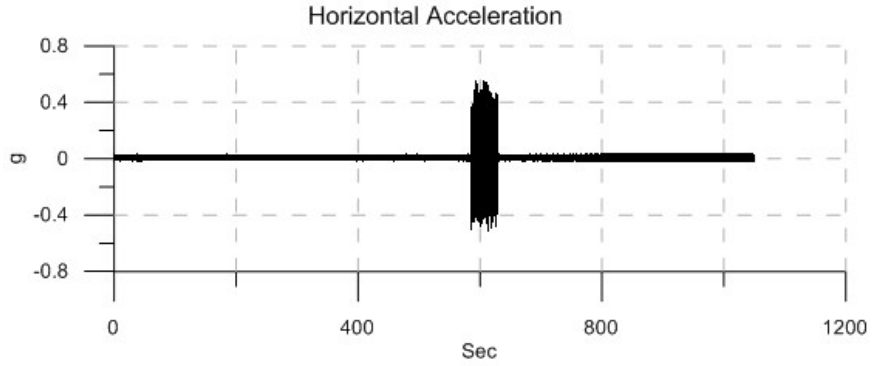

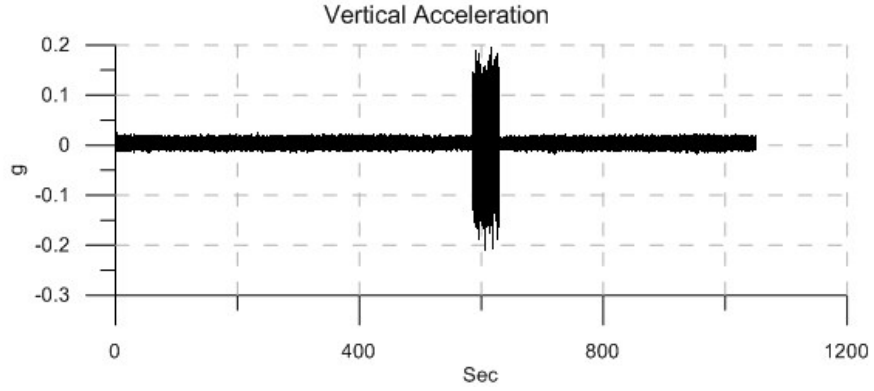

Material:	Glass Beads (Loose)
Size:	0.55 mm
Normal Stress:	118 kPa
Vibration Frequency:	140 Hz
Vibration Force:	7.14 N
Vibration Duration:	43 sec
Horizontal Acceleration:	0.38 g
Vertical Acceleration:	0.13 g
Horizontal Amplitude:	4.8×10^{-3} mm
Vertical Amplitude:	1.6×10^{-3} mm
Peak Strength:	61 kPa
Residual Strength:	54 kPa
Post-Vibrational Strength:	55 kPa

No shearing during vibration

Shear rate: 0.61 mm/min

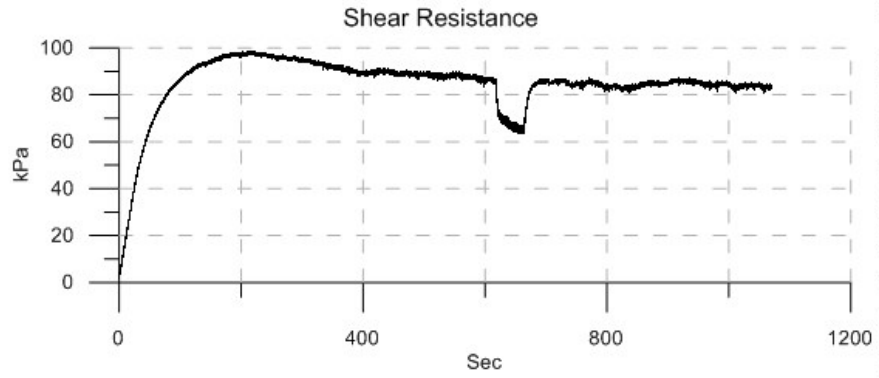

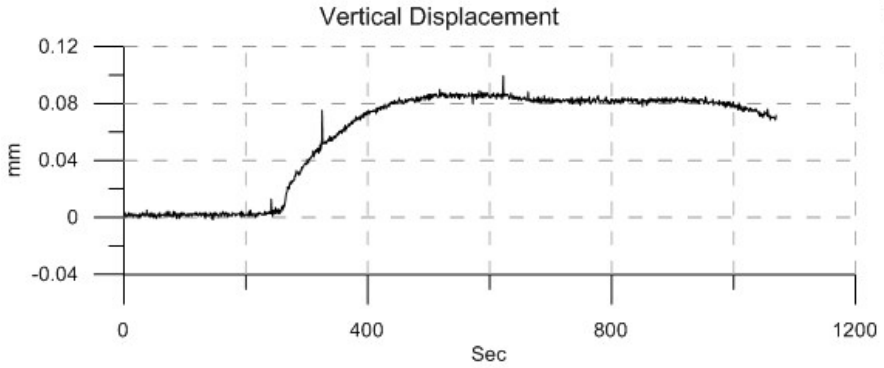

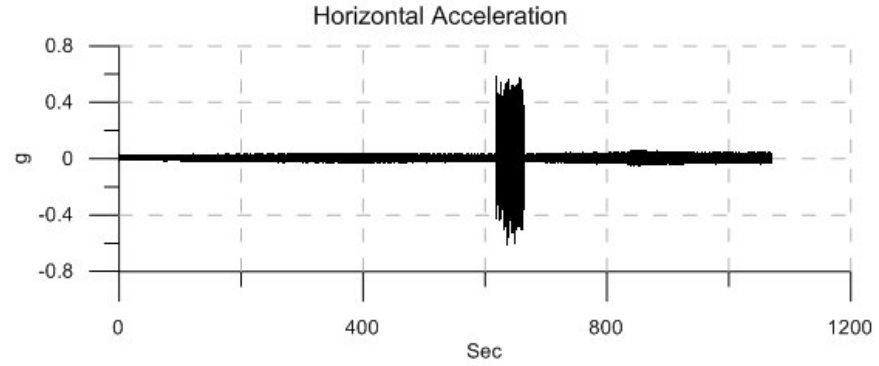

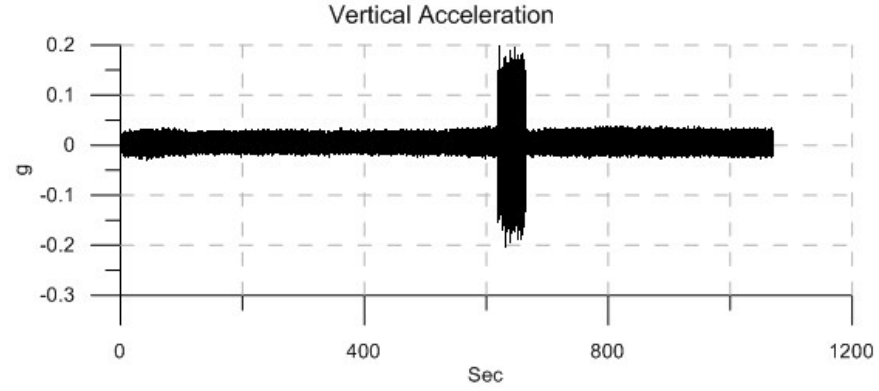

Material:	Glass Beads (Loose)
Size:	0.55 mm
Normal Stress:	200 kPa
Vibration Frequency:	140 Hz
Vibration Force:	7.14 N
Vibration Duration:	45 sec
Horizontal Acceleration:	0.39 g
Vertical Acceleration:	0.13 g
Horizontal Amplitude:	4.9×10^{-3} mm
Vertical Amplitude:	1.6×10^{-3} mm
Peak Strength:	98 kPa
Residual Strength:	86.5 kPa
Post-Vibrational Strength:	86.5 kPa

No shearing during vibration

Shear rate: 0.61 mm/min

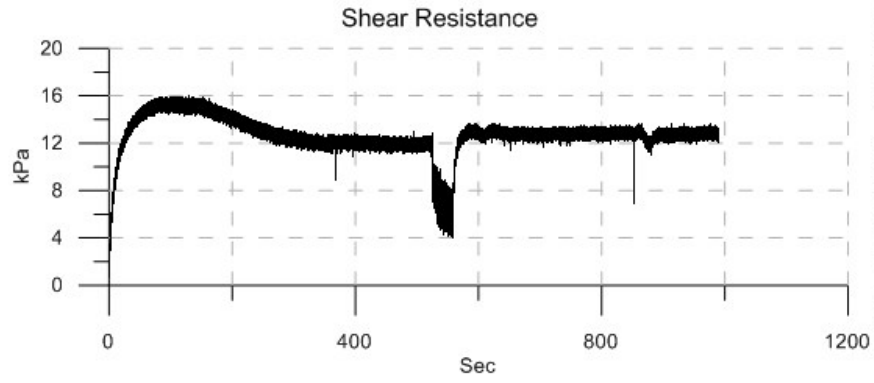

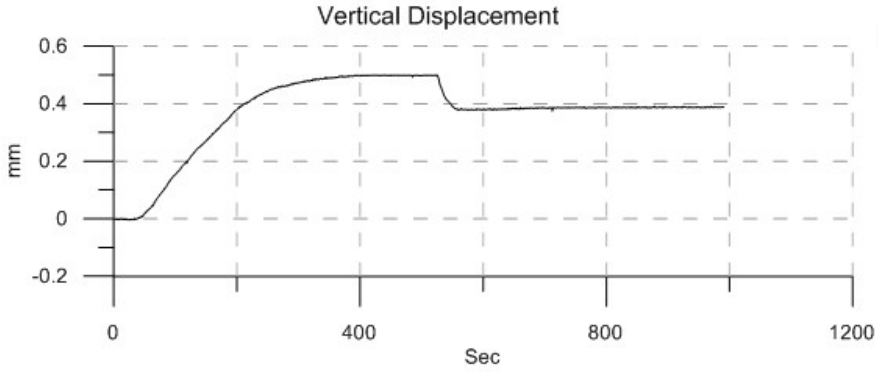

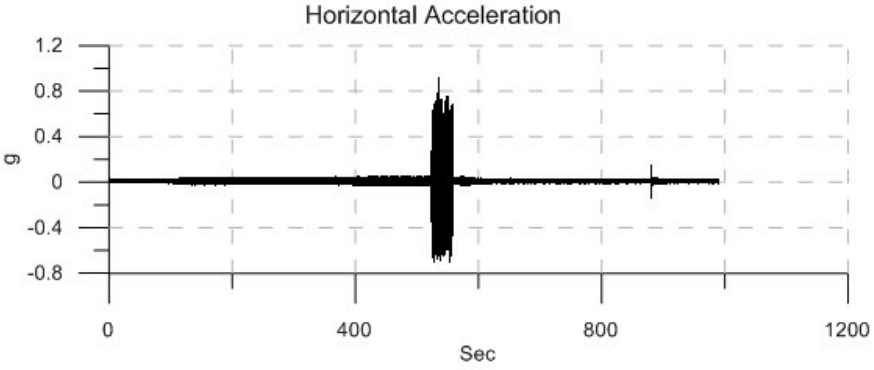

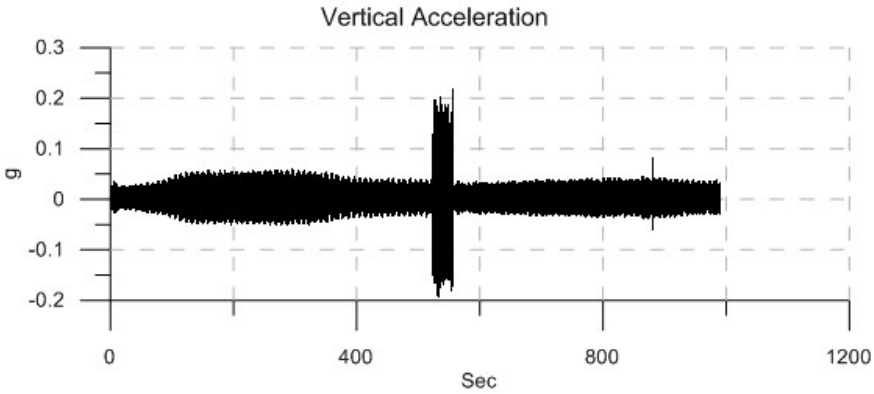

Material:	Sand
Size:	Fine
Normal Stress:	8 kPa
Vibration Frequency:	140 Hz
Vibration Force:	7.14 N
Vibration Duration:	33 sec
Horizontal Acceleration:	0.5 g
Vertical Acceleration:	0.15 g
Horizontal Amplitude:	6.3×10^{-3} mm
Vertical Amplitude:	1.9×10^{-3} mm
Peak Strength:	15.5 kPa
Residual Strength:	12 kPa
Post-Vibrational Strength:	13 kPa

No shearing during vibration

Shear rate: 0.61 mm/min

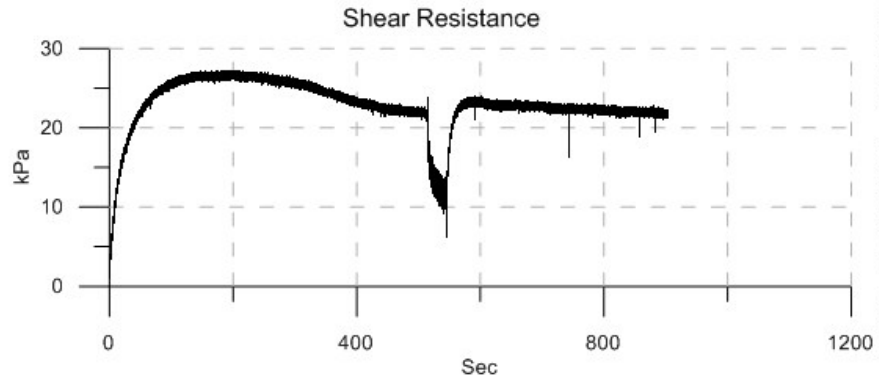

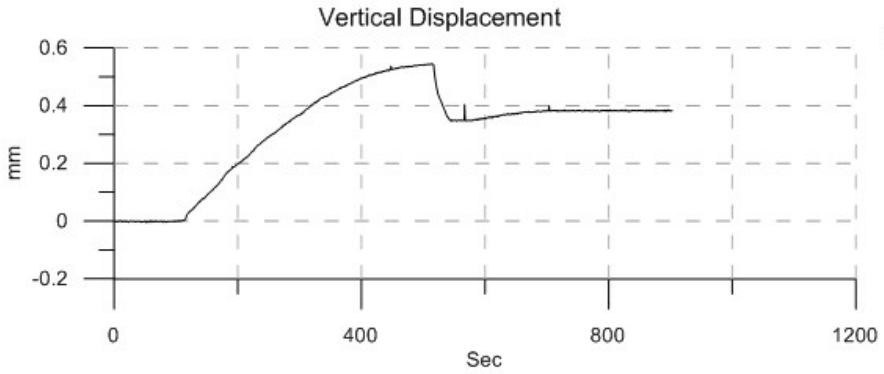

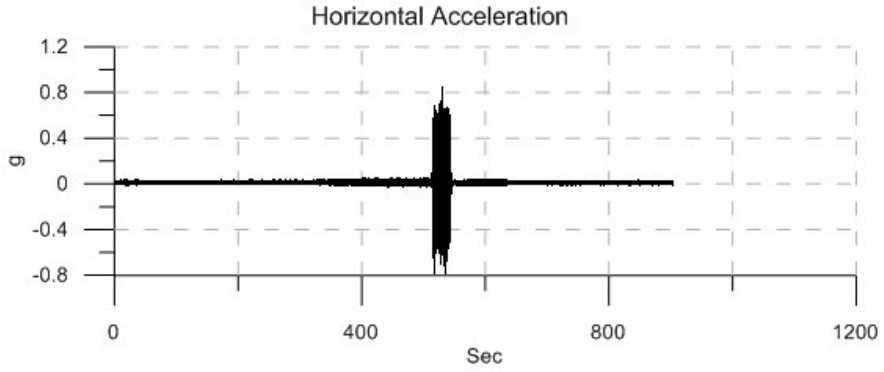

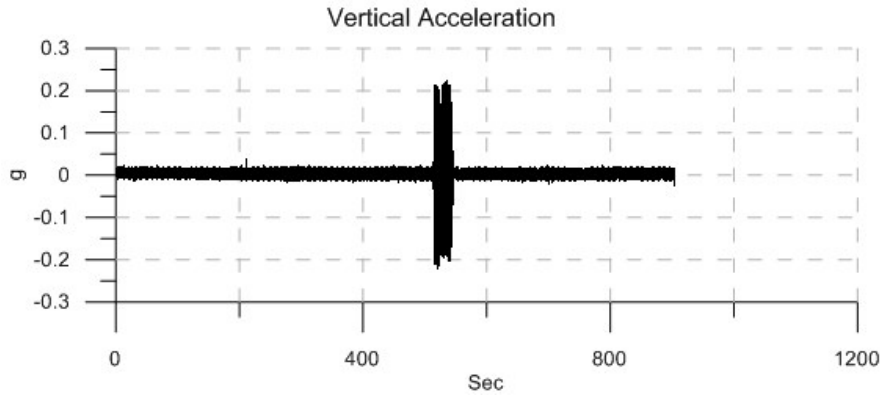

Material:	Sand
Size:	Fine
Normal Stress:	23 kPa
Vibration Frequency:	140 Hz
Vibration Force:	7.14 N
Vibration Duration:	27 sec
Horizontal Acceleration:	0.5 g
Vertical Acceleration:	0.15 g
Horizontal Amplitude:	6.3×10^{-3} mm
Vertical Amplitude:	1.9×10^{-3} mm
Peak Strength:	27 kPa
Residual Strength:	22 kPa
Post-Vibrational Strength:	23.5 kPa

No shearing during vibration

Shear rate: 0.61 mm/min

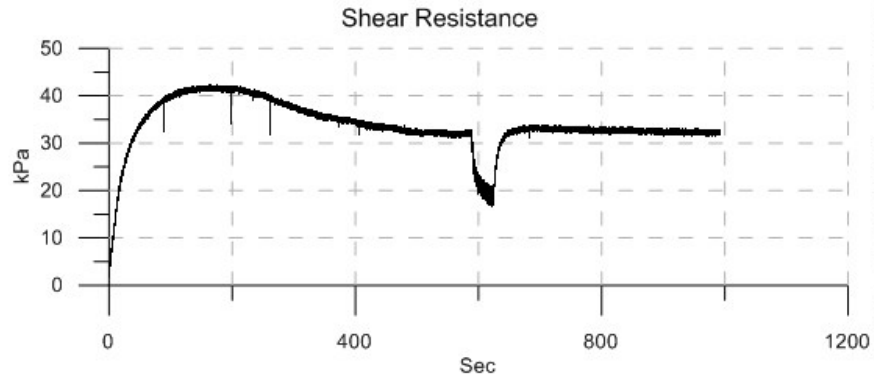

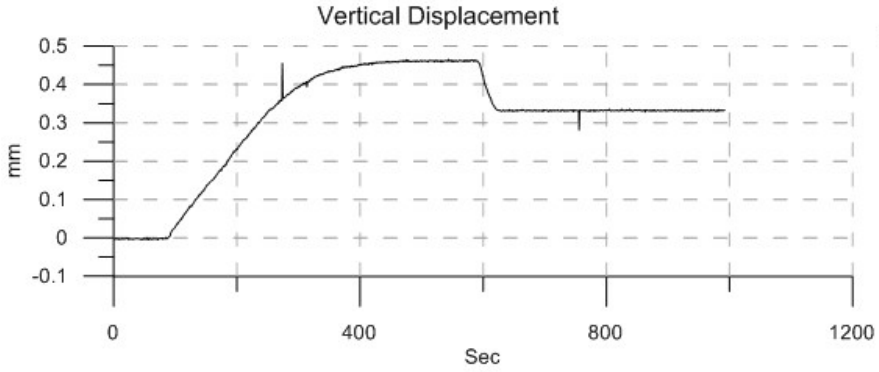

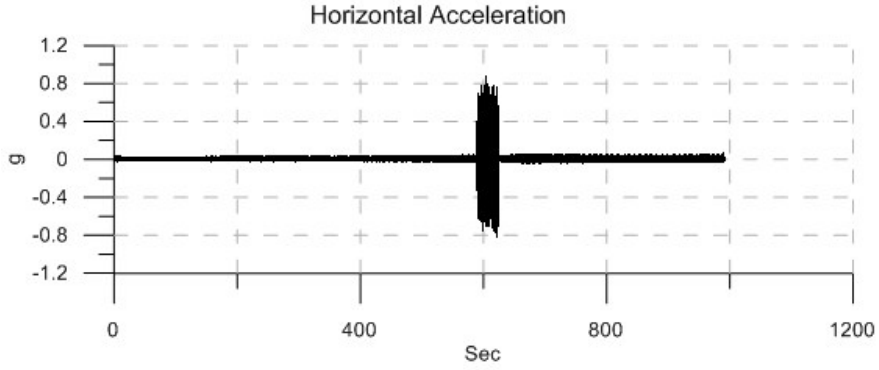

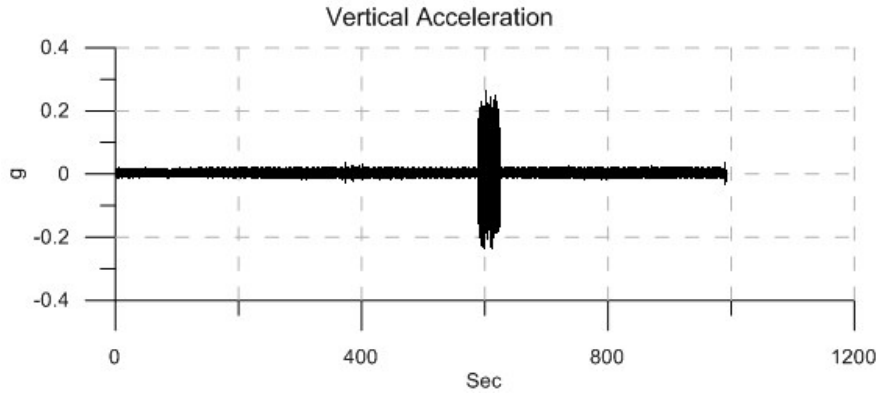

Material:	Sand
Size:	Fine
Normal Stress:	36 kPa
Vibration Frequency:	140 Hz
Vibration Force:	7.14 N
Vibration Duration:	34 sec
Horizontal Acceleration:	0.52 g
Vertical Acceleration:	0.15 g
Horizontal Amplitude:	6.6×10^{-3} mm
Vertical Amplitude:	1.9×10^{-3} mm
Peak Strength:	41.5 kPa
Residual Strength:	32 kPa
Post-Vibrational Strength:	33 kPa

No shearing during vibration

Shear rate: 0.61 mm/min

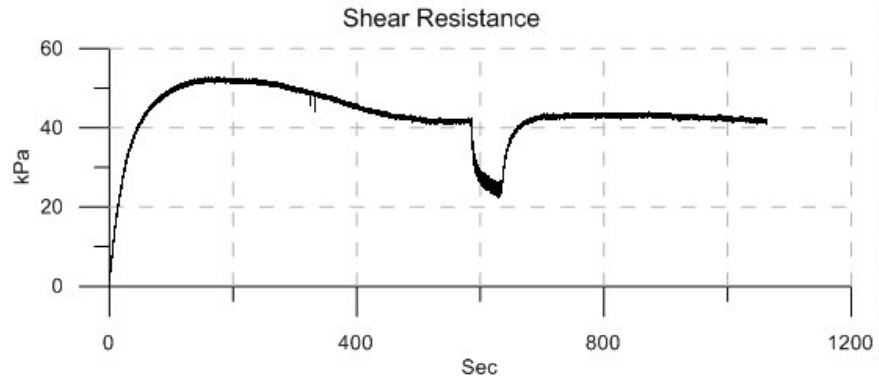

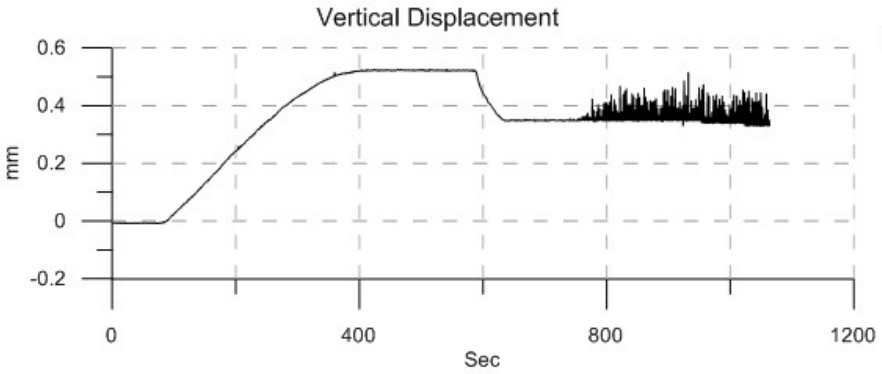

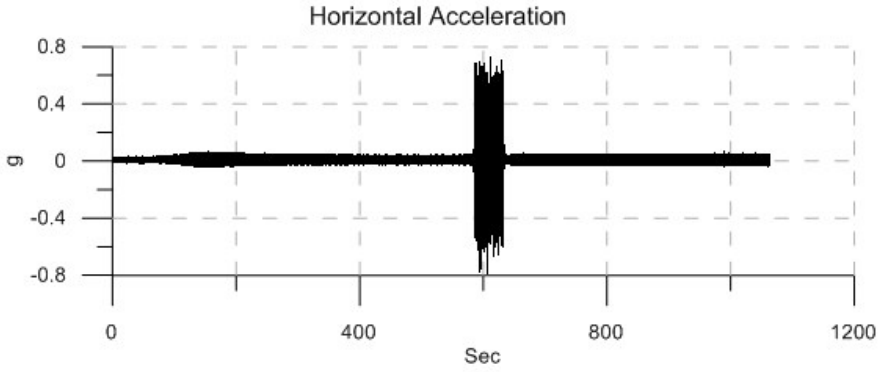

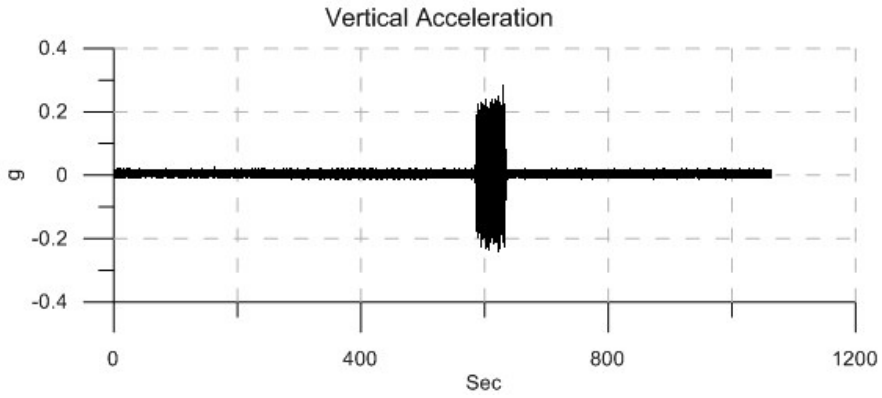

Material:	Sand
Size:	Fine
Normal Stress:	50 kPa
Vibration Frequency:	140 Hz
Vibration Force:	7.14 N
Vibration Duration:	46 sec
Horizontal Acceleration:	0.49 g
Vertical Acceleration:	0.17 g
Horizontal Amplitude:	6.2×10^{-3} mm
Vertical Amplitude:	2.2×10^{-3} mm
Peak Strength:	52.5 kPa
Residual Strength:	42 kPa
Post-Vibrational Strength:	43.5 kPa

No shearing during vibration

Shear rate: 0.61 mm/min

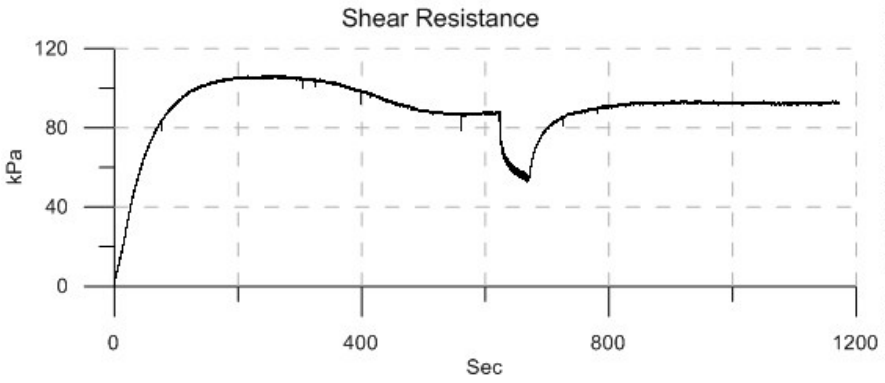

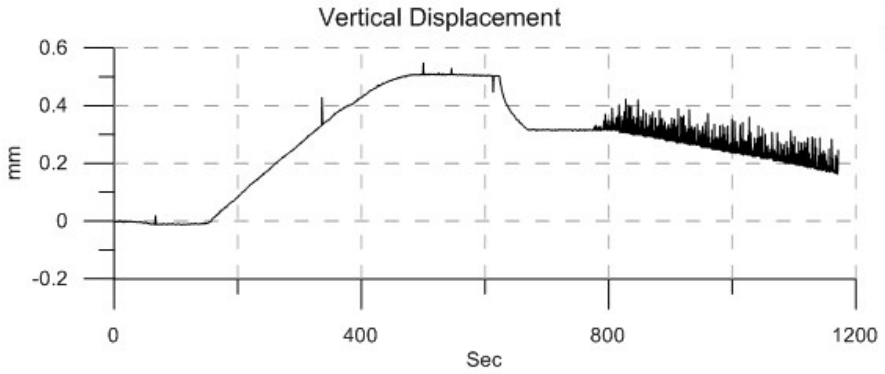

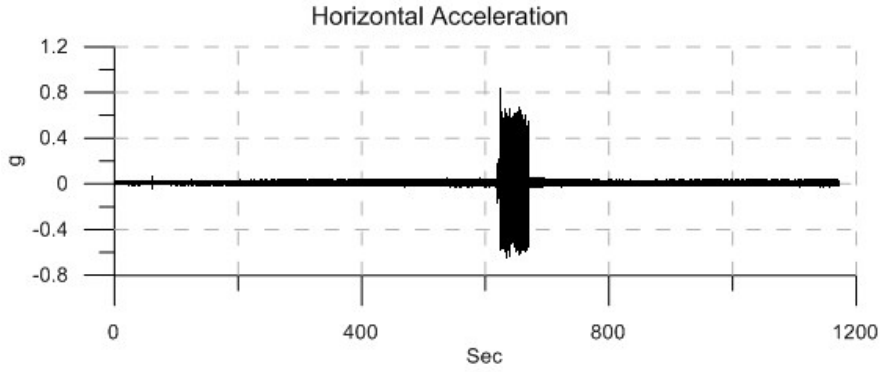

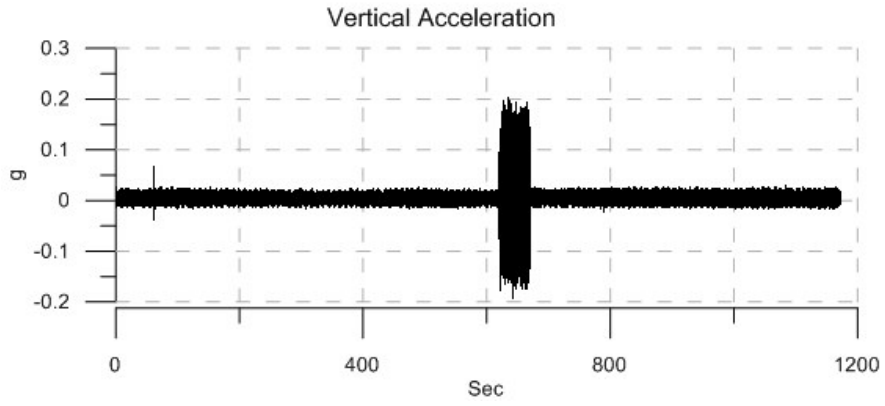

Material:	Sand
Size:	Fine
Normal Stress:	118 kPa
Vibration Frequency:	140 Hz
Vibration Force:	7.14 N
Vibration Duration:	46 sec
Horizontal Acceleration:	0.48 g
Vertical Acceleration:	0.15 g
Horizontal Amplitude:	6.1×10^{-3} mm
Vertical Amplitude:	1.9×10^{-3} mm
Peak Strength:	106 kPa
Residual Strength:	87.5 kPa
Post-Vibrational Strength:	93 kPa

No shearing during vibration

Shear rate: 0.61 mm/min

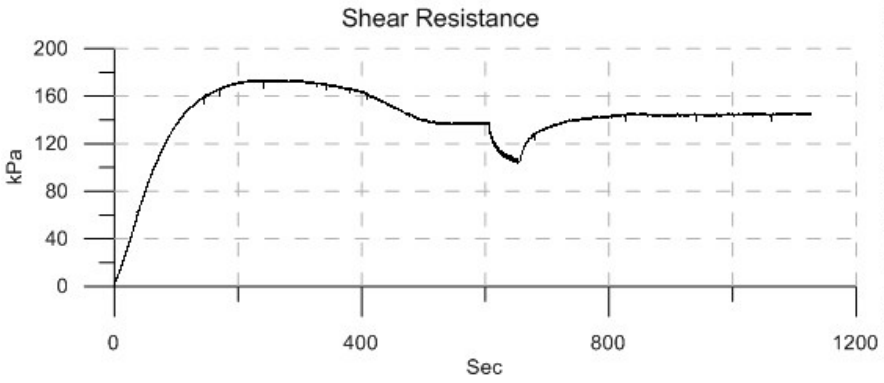

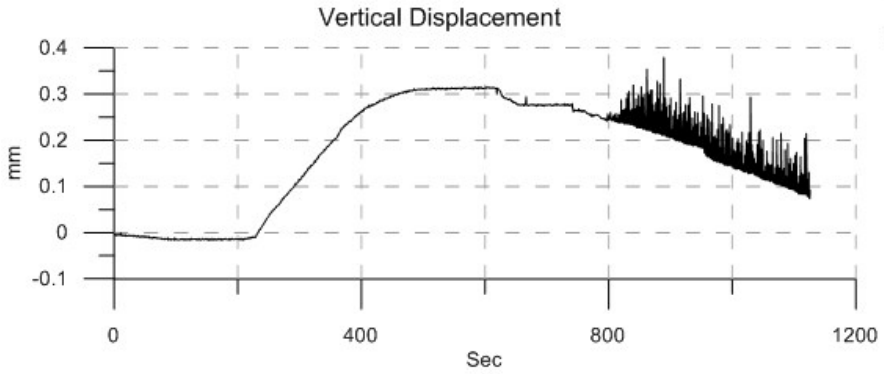

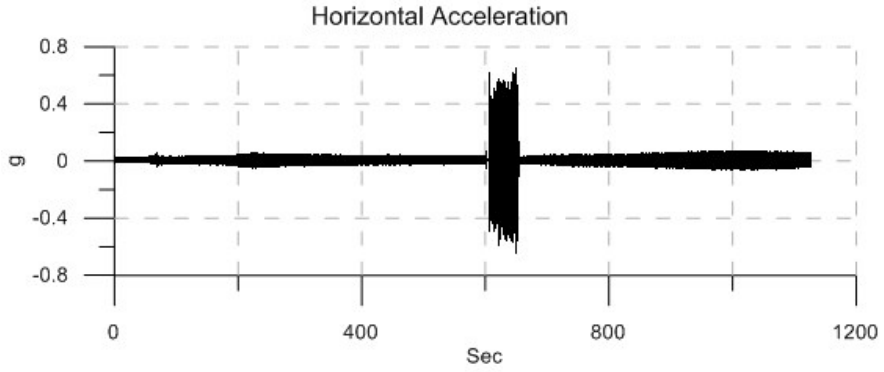

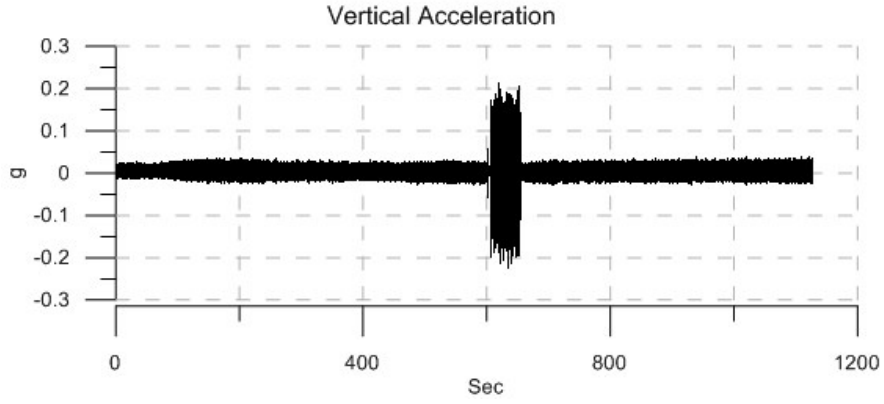

Material:	Sand
Size:	Fine
Normal Stress:	200 kPa
Vibration Frequency:	140 Hz
Vibration Force:	7.14 N
Vibration Duration:	46 sec
Horizontal Acceleration:	0.43 g
Vertical Acceleration:	0.15 g
Horizontal Amplitude:	5.5×10^{-3} mm
Vertical Amplitude:	1.9×10^{-3} mm
Peak Strength:	173 kPa
Residual Strength:	137 kPa
Post-Vibrational Strength:	145.5 kPa

No shearing during vibration

Shear rate: 0.61 mm/min

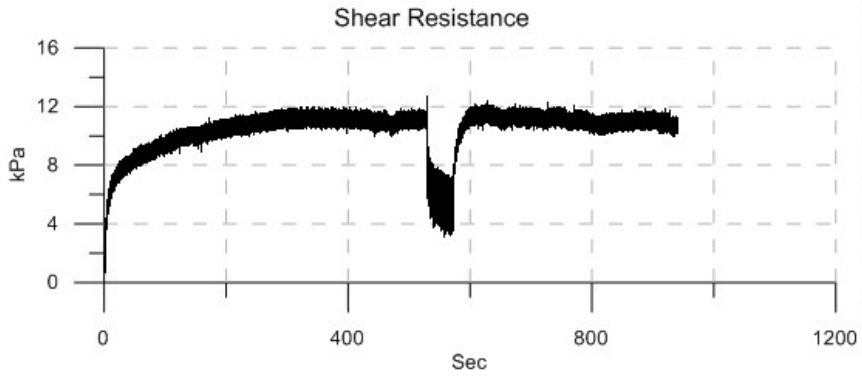

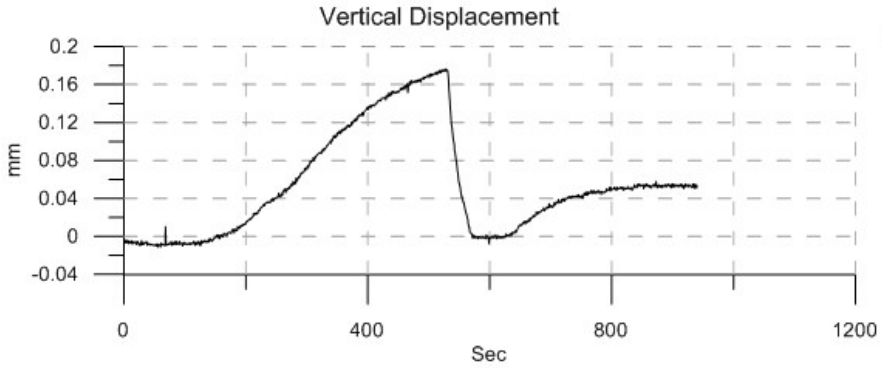

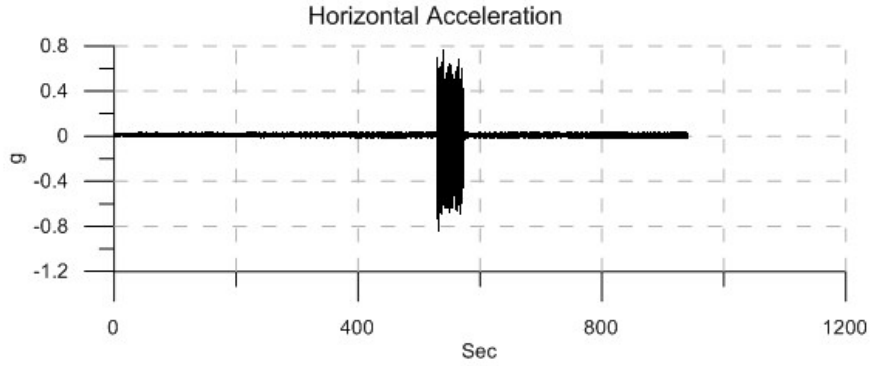

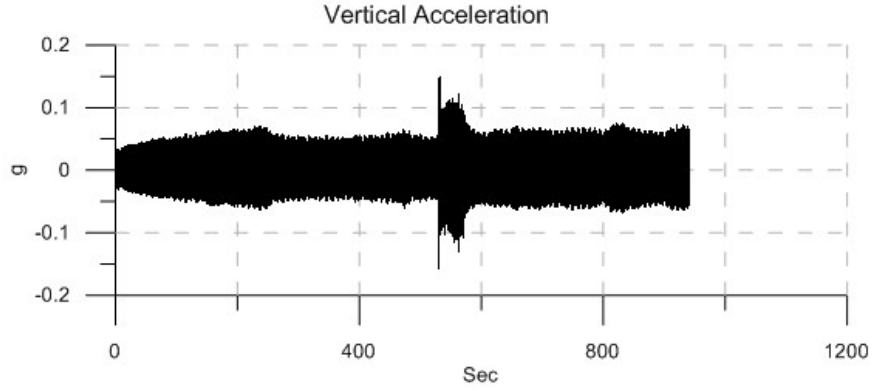

Material:	Sand (Loose)
Size:	Fine
Normal Stress:	8 kPa
Vibration Frequency:	140 Hz
Vibration Force:	7.14 N
Vibration Duration:	42 sec
Horizontal Acceleration:	0.47 g
Vertical Acceleration:	0.09 g
Horizontal Amplitude:	6.0×10^{-3} mm
Vertical Amplitude:	1.1×10^{-3} mm
Peak Strength:	-
Residual Strength:	11.5 kPa
Post-Vibrational Strength:	11.5 kPa

No shearing during vibration

Shear rate: 0.61 mm/min

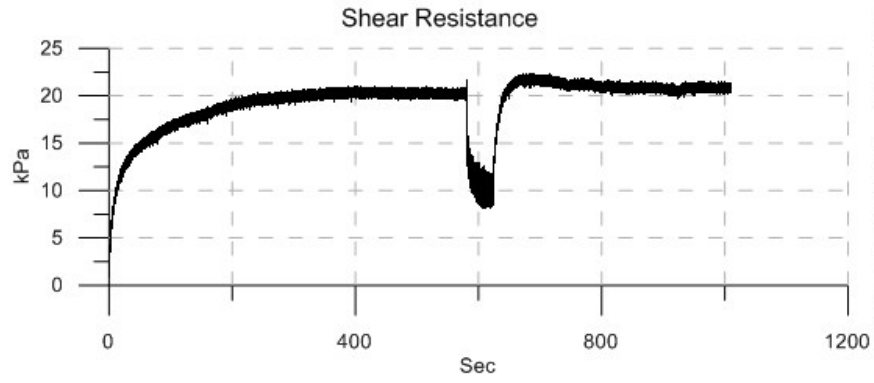

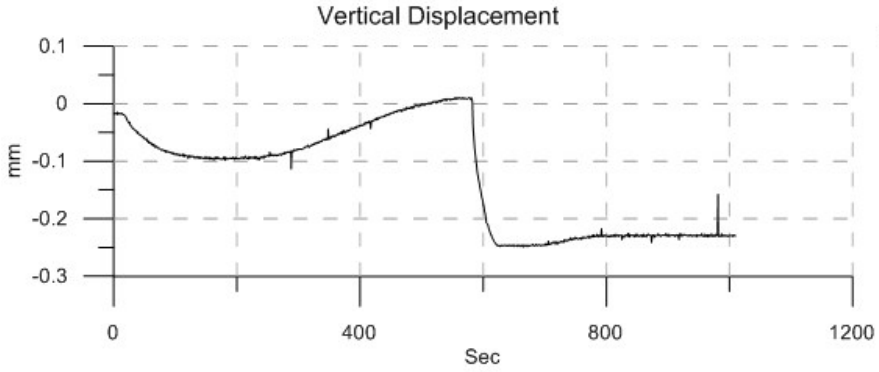

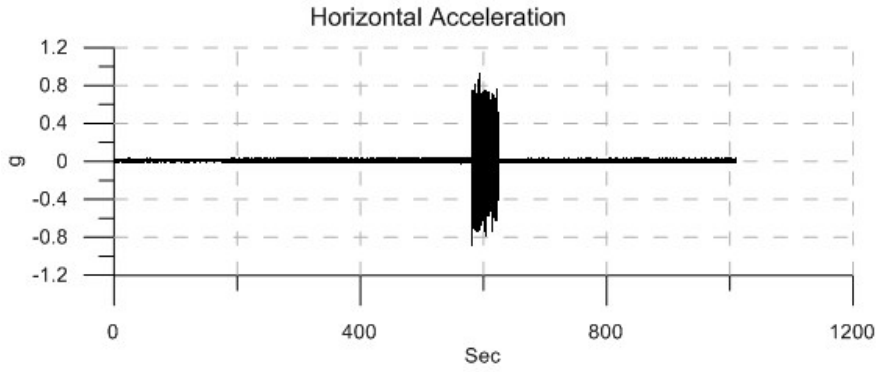

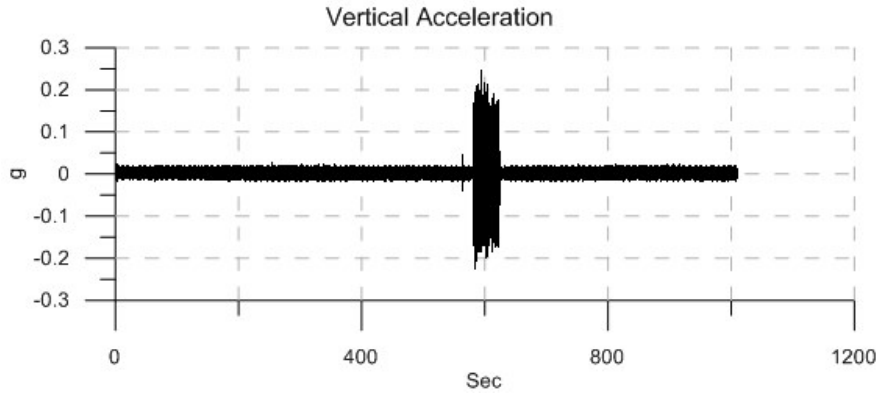

Material:	Sand (Loose)
Size:	Fine
Normal Stress:	23 kPa
Vibration Frequency:	140 Hz
Vibration Force:	7.14 N
Vibration Duration:	42 sec
Horizontal Acceleration:	0.5 g
Vertical Acceleration:	0.15 g
Horizontal Amplitude:	6.3×10^{-3} mm
Vertical Amplitude:	1.9×10^{-3} mm
Peak Strength:	-
Residual Strength:	20.5 kPa
Post-Vibrational Strength:	22 kPa

No shearing during vibration

Shear rate: 0.61 mm/min

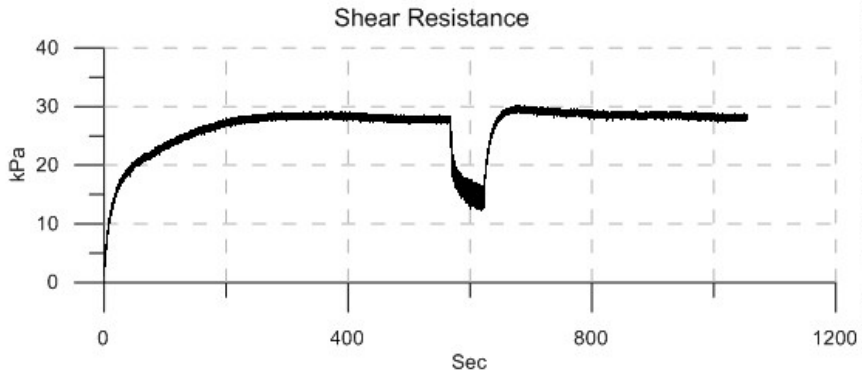

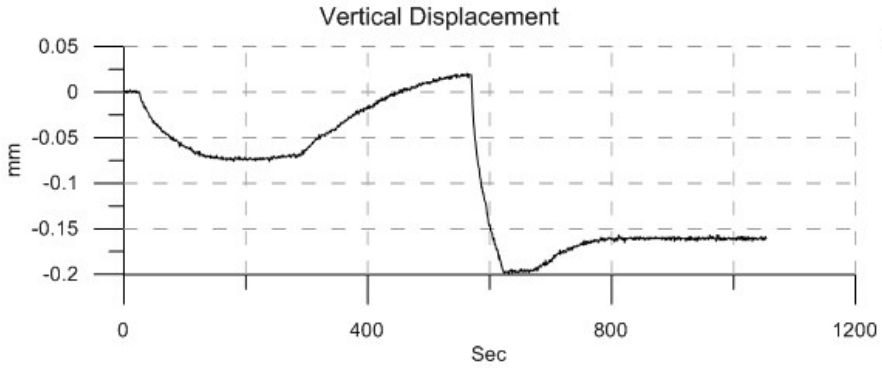

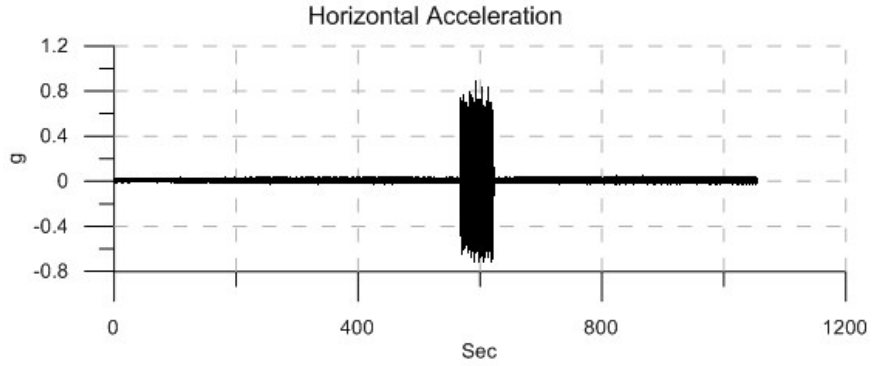

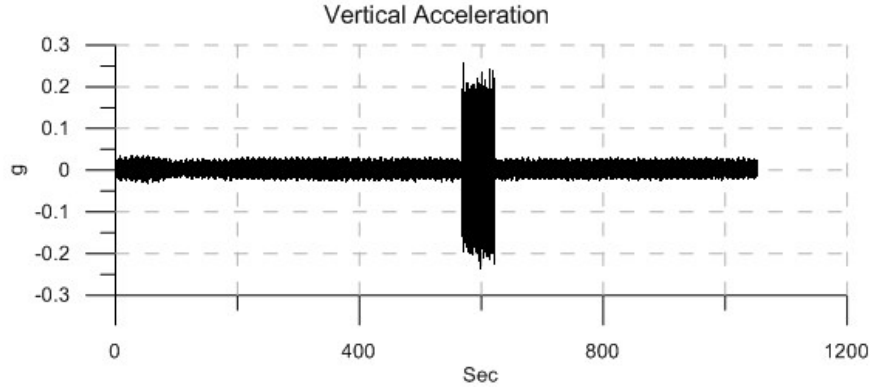

Material:	Sand (Loose)
Size:	Fine
Normal Stress:	36 kPa
Vibration Frequency:	140 Hz
Vibration Force:	7.14 N
Vibration Duration:	54 sec
Horizontal Acceleration:	0.53 g
Vertical Acceleration:	0.15 g
Horizontal Amplitude:	6.7×10^{-3} mm
Vertical Amplitude:	1.9×10^{-3} mm
Peak Strength:	28.5 kPa
Residual Strength:	28 kPa
Post-Vibrational Strength:	29.5 kPa

No shearing during vibration

Shear rate: 0.61 mm/min

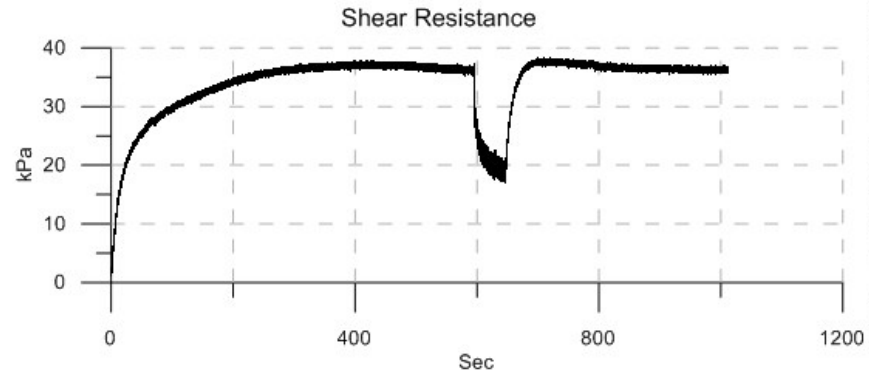

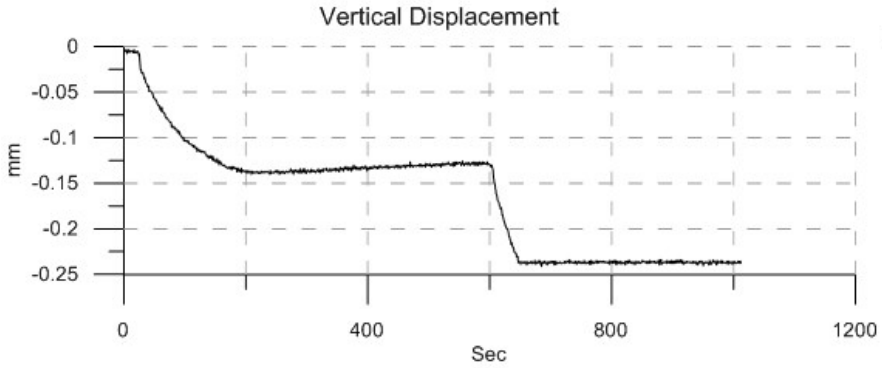

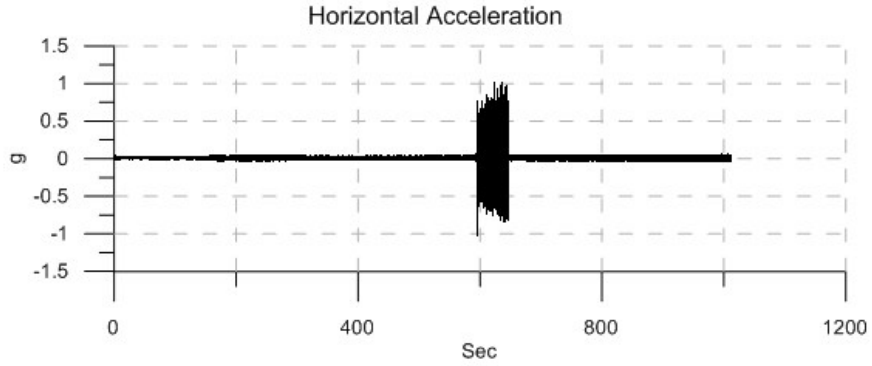

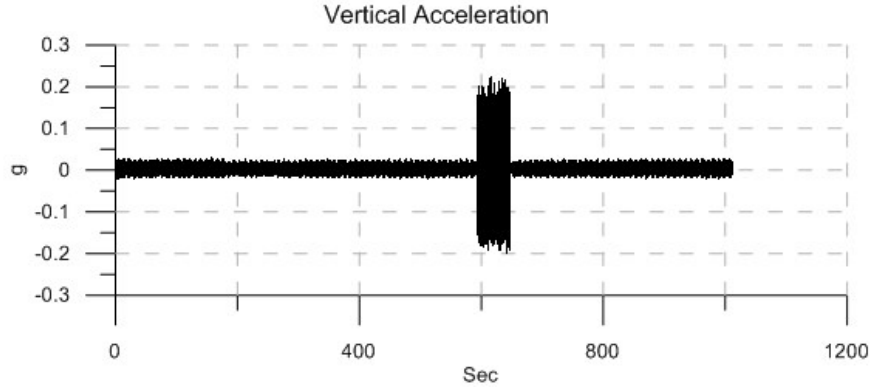

Material:	Sand (Loose)
Size:	Fine
Normal Stress:	50 kPa
Vibration Frequency:	140 Hz
Vibration Force:	7.14 N
Vibration Duration:	53 sec
Horizontal Acceleration:	0.55 g
Vertical Acceleration:	0.15 g
Horizontal Amplitude:	7.0×10^{-3} mm
Vertical Amplitude:	1.9×10^{-3} mm
Peak Strength:	37.5 kPa
Residual Strength:	36.5 kPa
Post-Vibrational Strength:	38 kPa

No shearing during vibration

Shear rate: 0.61 mm/min

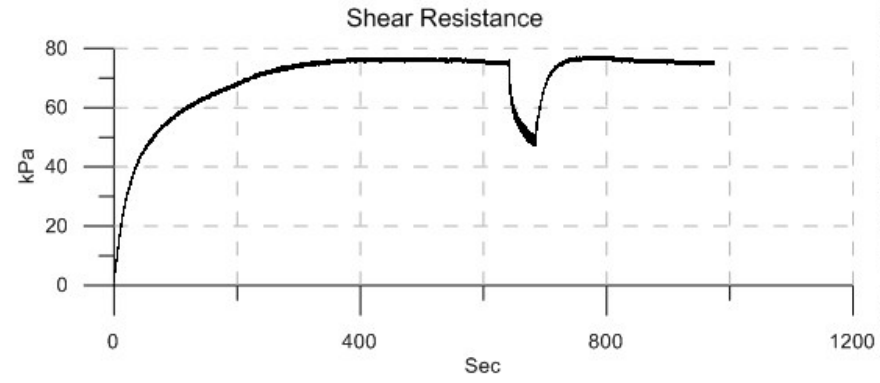

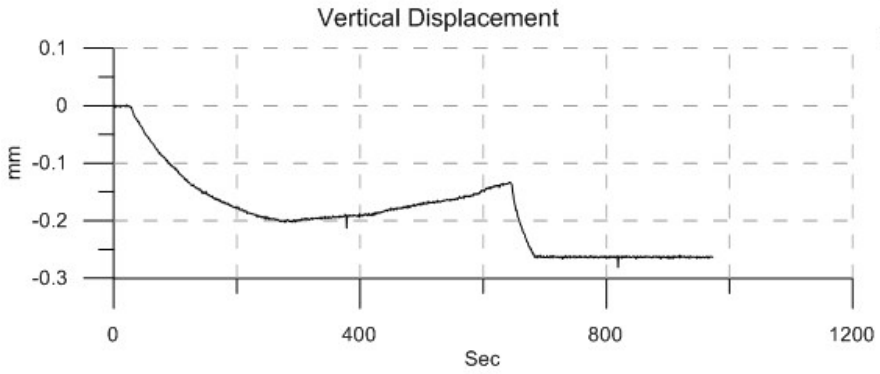

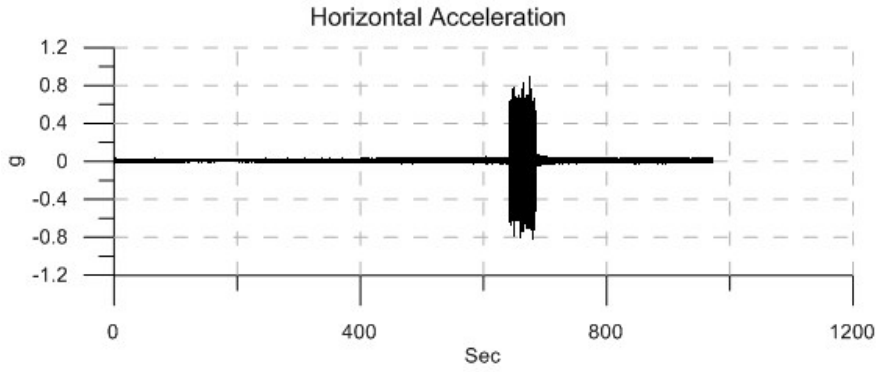

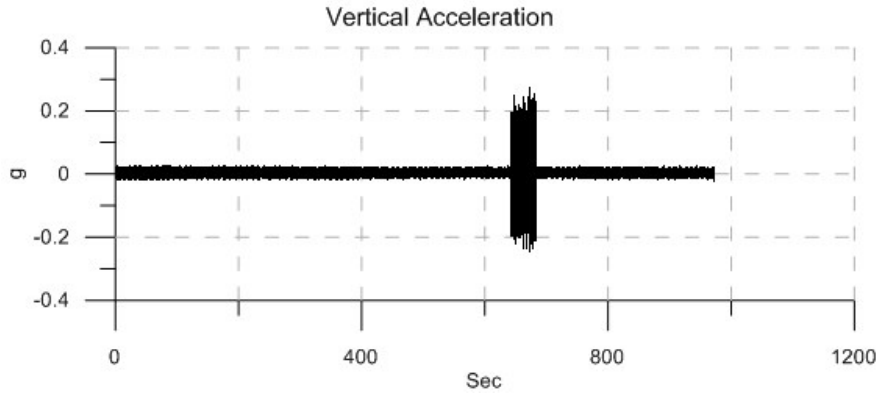

Material:	Sand (Loose)
Size:	Fine
Normal Stress:	118 kPa
Vibration Frequency:	140 Hz
Vibration Force:	7.14 N
Vibration Duration:	42 sec
Horizontal Acceleration:	0.55 g
Vertical Acceleration:	0.16 g
Horizontal Amplitude:	7.0×10^{-3} mm
Vertical Amplitude:	2.0×10^{-3} mm
Peak Strength:	76.5 kPa
Residual Strength:	75.5 kPa
Post-Vibrational Strength:	77 kPa

No shearing during vibration

Shear rate: 0.61 mm/min

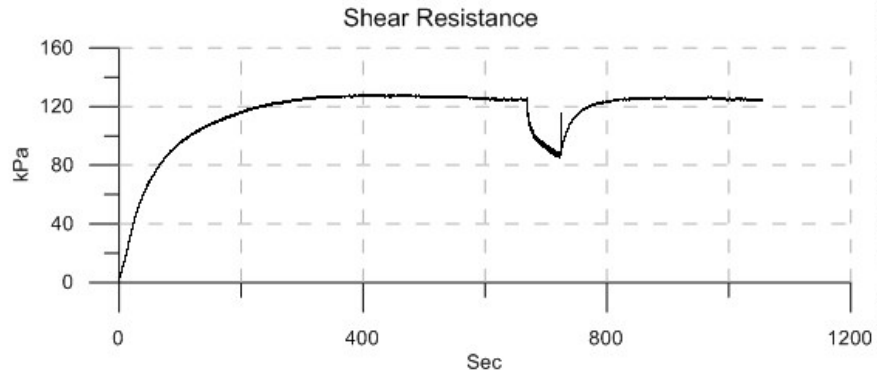

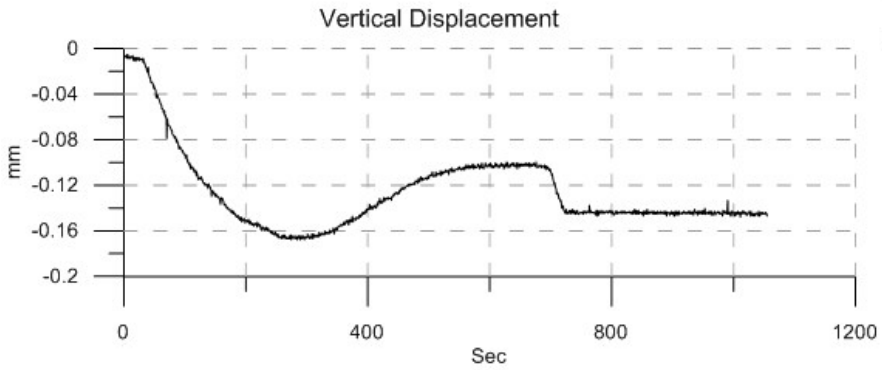

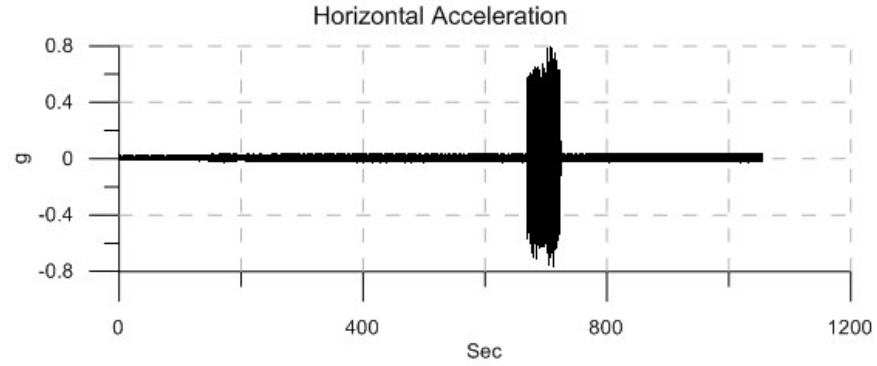

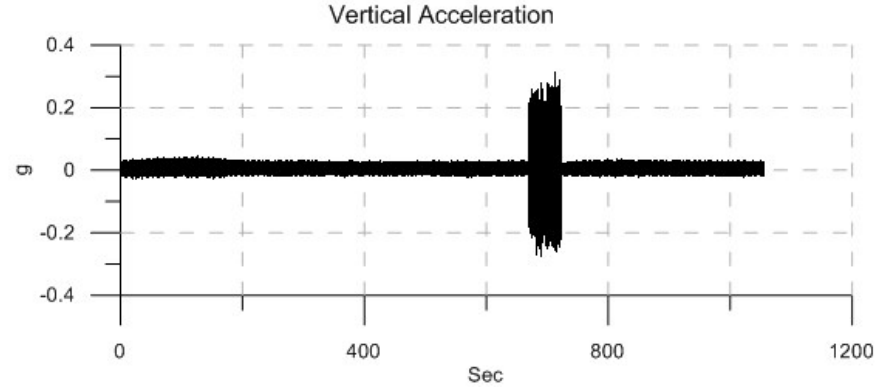

Material:	Sand (Loose)
Size:	Fine
Normal Stress:	200 kPa
Vibration Frequency:	140 Hz
Vibration Force:	7.14 N
Vibration Duration:	54 sec
Horizontal Acceleration:	0.53 g
Vertical Acceleration:	0.2 g
Horizontal Amplitude:	6.7×10^{-3} mm
Vertical Amplitude:	2.5×10^{-3} mm
Peak Strength:	127.5 kPa
Residual Strength:	125 kPa
Post-Vibrational Strength:	126 kPa

No shearing during vibration

Shear rate: 0.61 mm/min